UNIVERSITÉ DE GENÈVE

Archive ouverte UNIGE
https://archive-ouverte.unige.ch

Thèse 1999

Open Access

This version of the publication is provided by the author(s) and made available in accordance with the copyright holder(s).

Mineralogical and geochemical changes of copper flotation tailings in relation to their original composition and climatic setting : implications for acid mine drainage and element mobility

Dold, Bernhard Stefan

How to cite

DOLD, Bernhard Stefan. Mineralogical and geochemical changes of copper flotation tailings in relation to their original composition and climatic setting : implications for acid mine drainage and element mobility. Doctoral Thesis, 1999. doi: 10.13097/archive-ouverte/unige:98275

This publication URL: https://archive-ouverte.unige.ch/unige:98275
Publication DOI: 10.13097/archive-ouverte/unige:98275

© This document is protected by copyright. Please refer to copyright holder(s) for terms of use.

UNIVERSITÉ DE GENÈVE
Département de minéralogie
Institut F. - A. Forel

FACULTÉ DES SCIENCES
Professeur L. Fontboté
Professeur W. Wildi

Mineralogical and Geochemical Changes of Copper Flotation Tailings in Relation to their Original Composition and Climatic Setting – Implications for Acid Mine Drainage and Element Mobility

THÈSE

présentée à la Faculté des sciences de l'Université de Genève pour obtenir le grade de Docteur ès sciences, mention sciences de la Terre

par
Bernhard DOLD
de
Konstanz (Allemagne)

Thèse N° 3125

GENÈVE
1999

La Faculté des sciences, sur le préavis de Messieurs W. WILDI, professeur ordinaire (Institut F.-A. Forel) et L. FONTBOTÉ, professeur ordinaire (Département de minéralogie) codirecteurs de thèse, H.-R. PFEIFER, professeur (Université de Lausanne – Centre d'analyse minérale) et C.N. ALPERS, docteur (U.S. Geological Survey- Sacramento, USA), autorise l'impression de la présente thèse, sans exprimer d'opinion sur les propositions qui y sont énoncées.

Genève, le 6 décembre 1999

Thèse - 3125 -

Le Doyen, Jacques WEBER

Dold, B.: Mineralogical and Geochemical Changes of Copper Flotation Tailings in Relation to their Original Composition and Climatic Setting – Implications for Acid Mine Drainage and Element Mobility.

Terre et Environment, vol. 18, xiii + 230 pp. (1999)

ISBN 2-940153-17-5
Section des Sciences de la Terre, Université de Genève, 13 rue des Maraîchers, CH-1211 Genève 4, Suisse
Téléphone: ++41-22-702-6111, Téléfax: ++41-22-320-5732
e-mail: berthoud@sc2a.unige.ch

TABLE OF CONTENTS

* This chapter "Introduction and summary of the results" is written in French in accordance with the instructions for publications of Ph.D. theses of the Faculté des Sciences, Université de Genève.

CHAPTER 2

CHAPTER 3

CHAPTER 4

CHAPTER 5

CHAPTER 6

ACKNOWLEDGMENTS

I would like to thank very much Prof. L. Fontboté and Prof. W. Wildi, who made it possible to carry out this project. I am very thankful for their support, supervision, suggestions and the constructive discussions.

I am particularly indebted to Prof. H.-R. Pfeifer, Dr. C.N. Alpers, and Prof. B.M. Thomson for critical reading and improvement of the manuscript.

I would like to thank several specialist in different disciplines; without their help and constructive discussions this work would not have been possible. I would especially like to thank Prof. U. Schwertmann, Dr. H. Stanjek, Dr. J. Friedl (University München) for providing the samples for the dissolution kinetic tests, analytical support and extensive discussions on schwertmannite. Prof. Bigham (Ohio State University), Prof. D.W. Blowes (University of Waterloo), Dr. Jambor (Leslie Investments LTD), Dr. C.N. Alpers (USGS), Prof. A.J. Monhemius (Imperial College, London), Prof. H.L. Ehrlich (Rensselaer Polytechnic Institute, New York), Dr. G.M. Ritcey, Dr. Ingar Walder (SARB Consutlting. INC.), Dr. K.A. Morin and Dr. N.M. Hutt (Minesite Drainage Assessment Group) provided significant ideas and suggestions. I am specially indebted to C. Weatherell (MEND program – CANMET) who provided me with essential literature.

For their support in Chile in the field work, sampling, sample preparation, and analytical approaches, I would like thank to Dr. G. Cáceres, Dr. K. Eppinger, W. Silva, D. Guzman, and the technical staff of the IDICTEC, University of Atacama, Prof. S. Elgueta (Geological Department, University of Chile, Santiago), Prof. B. Escobar, Prof. J. Wiertz, and Dr. J. Casas (Chemical Department, Biometallurgy, University of Chile, Santiago), R. Troncoso, A. Hauser, C. Reuschmann, C. Espejo, E. Fonseca, W. Vivallio, I. Aguirre (Servicio Nacional de Geología y Minería SERNAGEOMIN), Dr. W. Eberle, and Dr. H.W. Müller (Bundesanstalt für Geowissenschaften und Rohstoffe BGR).

I would like to give special recognition to the management, the geologists and all staff of all the mining companies, without their support, interest and the access to their properties this work would not have been possible. In particular I would like to thank A. Puig (Exploration Division, CODELCO), L. Serrano, R. Vargas, C. Aguila, C. Castillo, M. Bustos (Division Andina, CODELCO), F. Celhay, A. Morales (Division Teniente, CODELCO), J. Blondel, R. Novajas (Division Salvador, CODELCO), E.Klohn (Cía. Minera Disputada de las Condes S.A.), F. Villanueva, R. Ceron (Cía. Minera El Soldado), B. Zamora (Cía. Minera Sali Hochschild. S.A.), and W. Rojas (Cía. Minera Ojos del Salado S.A.).

Completing this research project was only possible with considerable help from many friends and colleagues at the University of Geneva and Lausanne, which is gratefully acknowledged. The thin and polished sections were prepared by J.-M. Boccard. The X-ray diffraction analyses for clay minerals were carried out with the help of Dr. P. Thelin, Dr. François Girod, and L. Dufresne (University of Lausanne). F. Capponi and J.C. Lavanchy helped me with the coulometric titration analyses. The ICP-AES analyses for the dissolution kinetics studies were carried out with the help of Dr. Dubois (EPFL Lausanne) and Dr. P. Voldet (University of Geneva). Preliminary analytical tests with ICP-MS were carried out with the help

of Dr. P.Y. Favarger and P. Arpagaus (F. -A. Forel Institute, University of Geneva). The dissolution kinetic studies were carried out in the laboratories of Prof. H.-R. Pfeifer in Lausanne. I would like to thank Dr. R. Martini for her patience in the SEM-EDS work. Microprobe analyses were carried out with the help of Dr. M. Chirardia, Dr. A. Marzoli, and Dr. M. Streck. For encouraging discussions I would like to thank Prof. Pfeifer, Dr. P. Thelin, Dr. R. Marschik, Dr. M. Chirardia, Dr. C. Adusumalli, Dr. A. Marzoli, Dr. J. Spangenberg, Dr. I. Walder, Dr. R. Moritz, Dr. Fidel Costa, Dr. U. Neumeier, Dr. W. Halter, J. Metzger, T. Ton-That, P. Rosset. For language improvement I would like to thank Dr. J. Barclay and Dr. L. Webb. Special thanks are due to Mercè Ferrés Hernàndez for the translation of the "Introduction et résumé des résultats" into French.

I would like to thank J. Berthoud, G. Overeny, and N. Rihs (University of Geneva) for their help.

The financial support by the Deutsche Akademischer Austauschdienst (DAAD) and the Swiss National Science Foundation, grant No. 21-50778.97 is gratefully acknowledged.

I would like to thank all my friends all over the world for their support and stimulation. Last but not least, I deeply thank Patricia as well as my parents and my brother for their patience and constant support.

ABSTRACT

In the present work six flotation tailings impoundments at five flotation plants located in different climatic zones of Chile were selected to investigate the mineralogical and geochemical changes taking place in copper flotation tailings subsequent to sulfide oxidation, especially the formation of acid mine drainage and element mobility. For this study two economically important and mineralogical different types of copper ore deposits were selected. The first one are porphyry copper deposits related to the Upper Cretaceous-Tertiary magmatism. They show ore paragenesis less rich in pyrite, typically with abundant hydrothermal clay minerals and low or nonexistant carbonate content (tailings impoundments Piuquenes, Cauquenes, and Salvador No.1 at the giant porphyry copper deposits of La Andina, El Teniente, and El Salvador, respectively). The second type includes the Fe-oxide (Cu-Au) deposits of the Punta del Cobre-Candelaria belt, south of Copiapó, northern Chile, characterized by a paragenesis relatively rich in pyrite and magnetite with moderate presence of clay minerals, and with calcite as a significant gangue mineral (Ojancos and P. Cerda tailings impoundments). The selected tailings impoundments occur in different climatic zones ranging from humid to hyper-arid along the strongly N-S elongated Chilean geography. This situation allows to use the studied tailings as open-air laboratories in which variable parameters of ore mineralogy, climate, and flotation process are compared.

To study the geochemical and mineralogical changes in copper sulfide tailings due to sulfide oxidation 29 drill cores and more than 370 samples were taken. A 7-step extraction sequence was developed by dissolution kinetic tests and detection of dissolved phases by X-ray diffraction (XRD) and differential X-ray diffraction (DXRD) in the different dissolution steps (chapter 3). The selectivity of the leaches and the dissolution kinetics of schwertmannite and ferrihydrite is discussed in detail (chapter 4).

Based on the obtained results following models for element cycling in relation to climatic conditions for porphyry copper tailings are proposed (chapter 5). In humid to Mediterranean climates (e.g., Piuquenes/Andina and Cauquenes/Teniente) sulfide oxidation and/or dissolution of primary sulfates (e.g., jarosite in El Salvador No. 1) leads to the liberation of bivalent cations as Fe^{2+}, Cu^{2+}, Zn^{2+}, Mn^{2+}, oxyanions as $HMoO_4^-$, $H_2AsO_4^-$, and SO_4^{2-} as well as protons (H^+). Fe^{3+} may take over the role of the principle sulfide oxidant or hydrolyses to secondary phases as jarosite, schwertmannite, ferrihydrite, goethite or others Fe(III)hydroxides, depending on pH and activity of e.g. Fe^{3+}, SO_4^{2-}, Cl^-, and K^+. Oxidation of molybdenite is lethal for *Thiobacillus ferrooxidans* and seems to limit the microbial mediated Fe^{2+} oxidation to Fe^{3+} if present in higher concentrations (e.g., El Salvador, chapter 5). Hydrolysis is the main proton producing process. The produced protons react with neutralizing minerals as carbonates and silicates. These neutralization reactions result in the control of the pH and the formation of secondary minerals as for example vermicultite-type mixed-layer minerals under liberation of cations as e.g. Al^{3+}, Ca^{2+}, K^+, Na^+, Mg^{2+}. These cations play an important role in the formation of the secondary mineralogy as for example K for jarosite. Bivalent cations are very mobile under acid conditions and are leached out of the oxidation zone by rainfall. Below, with increasing pH sorption processes fix these elements. With increasingly reducing conditions (below the water

table) and in pH conditions, where the relevant metals are mobile, replacement processes, as documented by the transformation of chalcopyrite to covellite, may take place (Piuquenes, Cauquenes, and Ojancos). Oxyanions are mainly adsorbed under low pH in the oxidation zone to the secondary ferric minerals (chapter 7). Nevertheless, changes in their oxidation state (e.g., arsenate to arsenite) may increase their mobility and may lead to downwards enrichment. With increasingly evaporation the water-flow direction changes to upwards migration via capillary forces (Cauquenes in summer, El Salvador). The mobilized elements are transferred to mainly oxidizing conditions. Saturation and/or supersaturation controls the precipitation of the mainly water-soluble efflorescent salts (e.g., bonattite, chalcanthite, halotrichite, hexahydrite, pickeringite, and magnesioauberite in El Salvador No.1). Hydrolysis and replacement processes are less important. Due to the high ionic activity in the oxidation zone, increased substitution as Al in secondary jarosite, or Cu and Zn in biotite can be observed (Cauquenes).

Carbonate-rich mineral (P. Cerda, chapter 6) assemblage neutralizes the produced acid in the sulfide oxidation process, leading to neutral pH conditions. High pH increases the adsorption of liberated elements, limiting their mobility and preventing the upwards migration via capillary force in arid climates and so the availability of heavy metals as water-soluble efflorescent salts. Low water content in coarser horizons possibly reduces additionally pyrite oxidation rates in arid climates. The construction of a valley dam impoundment upstream of an older downstream tailings impoundment may lead to downwards transport of liberated metal ions as acid or neutral mine drainage. Change in geochemical conditions encountered in the downstream tailings (e.g., calcite-rich layers or more reducing conditions) lead to hydrolysis and/or precipitation of secondary minerals (e.g., higher ordered ferrihydrite, goethite, jarosite, and covellite), resulting in strong secondary enrichment in the downstream tailings (P. Cerda and Ojancos, chapter 6).

RÉSUMÉ

Six bassins de rejet de cinq installations de flottation, situés dans de différentes zones climatiques du Chili, ont été sélectionnés afin d'évaluer les changements minéralogiques et géochimiques qui ont lieu dans les rejets de flottation de minerais de cuivre après l'oxydation des sulfures, en particulier la formation de "drainage minier acide" et la mobilité des éléments. Pour cette étude, deux types de gisements de cuivre économiquement importants et de composition minéralogique distincte ont été sélectionnés. Le premier type comprend les porphyres cuprifères associés au magmatisme qui a lieu du Crétacé Supérieur au Tertiaire. La paragenèse du minerai n'est pas riche en pyrite, les minéraux de l'argile hydrothermaux sont abondants et la teneur en carbonates est faible ou nulle (bassins de rejet de Piuquenes, Cauquenes et Salvador N° 1 des gisements de porphyres cuprifères géants de La Andina, El Teniente et El Salvador, respectivement). Le second type de gisement comprend les dépôts d'oxydes de Fe (Cu-Au) de la ceinture de Punta del Cobre-Candelaria, au Sud de Copiapó, Nord du Chili. Ces gisements se caractérisent par une paragenèse relativement riche en pyrite et en magnétite, par un développement modéré des minéraux de l'argile et par la présence de calcite comme minéral de gangue important (bassins de rejet d'Ojancos et P. Cerda). La morphologie très allongée du Chili suivant la direction N-S favorise une répartition des bassins de rejet sélectionnés tels qu'ils se trouvent dans des zones climatiques de caractéristiques différentes, humide à extrêmement aride. Cette répartition permet d'utiliser les bassins de rejet étudiés comme des laboratoires à ciel ouvert dans lesquels il est possible de comparer des paramètres variables concernant la minéralogie du gisement, le climat et les processus de flottation.

Pour étudier les changements minéralogiques et géochimiques qui ont lieu dans les rejets de flottation de minerais de cuivre, suite à l'oxydation des sulfures, 29 carottes et plus de 370 échantillons ont été prélevés. Une séquence d'extraction à 7-étapes a été mise au point à partir de la réalisation de tests de cinétique de dissolution et de la détermination des phases dissoutes à chaque étape par diffraction de rayons-X (XRD) et par diffraction différentielle de rayons-X (DXRD). Les différentes étapes de la séquence d'extraction et la cinétique de dissolution de la schwertmannite et de la ferrihydrite sont discutées de façon détaillée (chapitre 4).

A partir des résultats obtenus, des modèles sont proposés pour expliquer le cycle des éléments dans les bassins de rejet de porphyres cuprifères, en fonction des conditions climatiques (chapitre 5). Dans des climats humides à Méditerranéen (Piuquenes/Andina et Cauquenes/Teniente), l'oxydation des sulfures et/ou la dissolution des sulfates primaires (par exemple, la jarosite à El Salvador n° 1) produit la libération de cations bivalents tels que Fe^{2+}, Cu^{2+}, Zn^{2+}, Mn^{2+}, d'oxyanions comme par exemple $HMoO_4^-$, $H_2AsO_4^-$ et SO_4^{2-}; ainsi que de protons (H^+). Le cation Fe^{3+} peut jouer le rôle du principal oxydant des sulfures, ou bien être hydrolysé pour former des phases secondaires telles que la jarosite, la schwermannite, la ferrihydrite, la goethite ou d'autres hydroxydes de Fe(III), en fonction du pH et de l'activité des ions Fe^{3+}, SO_4^{2-}, Cl^- et K^+, par exemple. L'oxydation de la molibdénite est létale pour les bactéries *Thiobacillus ferrooxidans*. Ainsi, l'oxydation microbienne du Fe^{2+} en Fe^{3+} par *Thiobacillus ferrooxidans* serait limitée en présence d'une concentration élevée de molibdénite (El Salvador, chapitre 5). L'hydrolyse est le principal processus pour la production de protons. Ceux-ci réagissent avec les minéraux à potentiel de neutralisation tels que les carbonates et les

silicates. Ces réactions de neutralisation contrôlent le pH et libèrent des cations tels que Al^{3+}, Ca^{2+}, K^{+}, Na^{+}, Mg^{2+} , qui jouent un rôle important pour la formation de minéraux secondaires, par exemple des minéraux de type vermiculite à couches mixtes. Le K est particulièrement important pour la formation de jarosite. Les cations bivalents sont très mobiles en milieu acide et ils sont lessivés de la zone d'oxydation suite à un apport d'eau par des pluies. En dessous de la zone d'oxydation, au fur et à mesure que le pH augmente, des processus de sorption fixent ces éléments. Dans des conditions de plus en plus réductrices (en dessous du niveau phréatique) et telles que le pH permet encore la mobilité des métaux relevant, les processus de remplacement peuvent avoir lieu, tels que la transformation observée de la chalcopyrite en covellite (Piuquenes, Cauquenes et Ojancos). Dans la zone d'oxydation, les oxyanions sont principalement adsorbés par les minéraux de fer secondaires dans des conditions de faible pH (chapitre 7). Cependant, un changement de leur état d'oxydation (par exemple, arséniate à arséniure) peut favoriser leur mobilité ce qui pourrait conduire à un enrichissement vers les zones situées en aval. Quand l'évaporation est importante, la direction du flux de l'eau s'inverse et il se produit une migration vers le haut par capillarité (Cauquenes en été, El Salvador). Les éléments mobilisés sont essentiellement transférés vers des zones oxydantes. La saturation et/ou la supersaturation contrôle la précipitation des principaux sels efflorescents solubles dans l'eau (bonattite, chalcanthite, halotrichite, hexahydrite, pickeringite et magnésioaubérite à El Salvador n° 1). L'hydrolyse et les processus de remplacement sont moins importants. Dans la zone d'oxydation, une activité ionique élevée favorise l'entrée de l'Al dans la jarosite ou du Cu et du Zn dans la biotite (Cauquenes).

Une paragenèse riche en carbonates (P. Cerda, chapitre 6) neutralise l'acide produit par les processus d'oxydation des sulfures, ce qui neutralise le pH. Un pH élevé favorise l'adsorption des éléments libérés. Ceci limite leur mobilité et, dans les climats arides, empêche leur migration vers le haut par capillarité et donc la concentration de métaux lourds formant des sels efflorescents solubles dans l'eau. Dans les zones à climat aride, la faible teneur en eau des horizons à grain grossier peut faire diminuer le taux d'oxydation de la pyrite. Dans une vallée, la construction d'un barrage pour retenir les rejets de flottation, en amont d'un barrage similaire plus ancien, peut conduire à un transport vers le barrage situé en aval des drainages miniers acides ou neutres contenant les ions métalliques libérés. Ceux-ci, dans les nouvelles conditions géochimiques du bassin de rejet situé en aval (présence de couches riches en calcite ou conditions plus réductrices) seront hydrolysés ou précipiteront sous forme de minéraux secondaires (ferrihydrite d'ordre élevé, goethite, jarosite et covellite), générant ainsi un fort enrichissement secondaire dans l'ancien bassin (P. Cerda et Ojancos, chapitre 6).

RESUMEN

El propósito de este trabajo consiste en determinar los cambios mineralógicos y geoquímicos que tienen lugar en los desechos de flotación de minerales de cobre, en particular la formación de aguas ácidas y la mobilidad de los elementos. Para ello, se han seleccionado seis tranques de relaves de cinco instalaciones de flotación, situadas en diferentes zonas climáticas de Chile, que corresponden a dos variedades de yacimientos de cobre económicamente importantes y de composición mineralógica distinta. El primer tipo de yacimientos son pórfidos cupríferos que están asociados al magmatismo del Cretácico Superior al Terciario. La paragénesis de la mena no presenta pirita en abundancia, los minerales de la arcilla hidrotermales son abundantes y el contenido en carbonatos es bajo o nulo (tranques de relaves de Piuquenes, Cauquenes y El Salvador n.° 1 de los yacimientos de pórfidos cupríferos gigantes de La Andina, El Teniente y El Salvador, respectivamente). El segundo tipo de yacimientos son los depósitos de Fe (Cu-Au) de la cintura de Punta del Cobre-Candelaria, en el Sur de Copiapó, Norte de Chile. Se caracterizan por una paragénesis relativamente rica en pirita y en magnetita, por una moderada abundancia de los minerales de la arcilla y por la presencia de calcita como mineral de ganga importante (tranques de relaves de Ojancos y P. Cerda). La morfología de Chile, alargada según la dirección N-S, hace que los yacimientos seleccionados se hallen en zonas de clima húmedo a hiperárido. Esta distribución permite utilizar a los tranques de relaves estudiados como laboratorios a cielo abierto entre los que se pueden comparar parámetros variables referentes a la mineralogía del yacimiento, al clima y a los procesos de flotación.

Con el fin de estudiar los cambios mineralógicos y geoquímicos que tienen lugar después de la oxidación de los sulfuros en los tranques de relaves de plantas de flotación de minerales de cobre, se han tomado 29 testigos y más de 370 muestras. Una secuencia de extracción de siete etapas se ha puesto a punto (capítulo 3) a partir de ensayos de cinética de disolución y de la determinación por difracción de rayos-X (XRD) y difracción diferencial de rayos-X (DXRD) de las fases disueltas en cada etapa. Las diferentes etapas de dicha secuencia de extracción, así como la cinética de disolución de la schwertmannita y de la ferrihidrita, se presentan de forma detallada (capítulo 4).

A partir de los resultados obtenidos se proponen varios modelos para explicar el ciclo de los elementos en los tranques de relaves de pórfidos cupríferos, en función de las condiciones climáticas (capítulo 5). En clima húmedo o mediterráneo (Piuquenes/Andina y Cauquenes/Teniente), la oxidación de los sulfuros y/o la disolución de los sulfatos primarios (por ejemplo, la jarosita en El Salvador n.° 1) produce la liberación de cationes bivalentes como Fe^{2+}, Cu^{2+}, Zn^{2+}, Mn^{2+}; de oxianiones como $HMoO_4^-$, $H_2AsO_4^-$ y SO_4^{2-}; así como de protones (H^+). El catión Fe^{3+} puede actuar como oxidante principal de los sulfuros o bien hidrolizarse y formar fases secundarias como la jarosita, la schwertmannita, la ferrihidrita, la goetita, u otros hidróxidos de Fe(III), en función del pH y de la actividad de los iones Fe^{3+}, SO_4^{2-}, Cl^- y K^+, por ejemplo. La oxidación de la molibdenita es letal para las bacterias *Thiobacillus ferrooxidans,* con lo que la oxidación microbiana del Fe^{2+} en Fe^{3+} por *Thiobacillus ferrooxidans* quedaría limitada en presencia de una concentración elevada de molibdenita (El Salvador, capítulo 5). La hidrólisis es el principal proceso generador de protones. Éstos reaccionan con los minerales que, como los carbonatos y los silicatos, presentan cierto potencial de neutralización. Las reacciones de

neutralización controlan el pH y liberan cationes como Al^{3+}, Ca^{2+}, K^{+}, Na^{+}, Mg^{2+}, los cuales desempeñan un papel importante para la formación de minerales secundarios, como por ejemplo minerales de tipo vermiculita de capas mixtas. El K es particularmente importante para la formación de jarosita. En medio ácido, los cationes bivalentes son extremadamente móbiles, con lo que el agua de las lluvias puede lixiviarlos de la zona de oxidación. Por debajo de la zona de oxidación, a medida que aumenta el pH, estos mismos cationes quedan fijados por sorpción. En condiciones cada vez más reductoras (por debajo del nivel freático) y en condiciones tales que el pH permite aún la mobilidad de los metales de interés, pueden ocurrir procesos de reemplazo como la transformación observada de calcopirita en covelita (Piuquenes, Cauquenes y Ojancos).

En la zona de oxidación, en condiciones de pH ácido, los oxianiones son principalmente adsorbidos por los minerales de hierro secundarios (capítulo 7). Sin embargo, un cambio de su estado de oxidación (como por ejemplo, transformación de arseniato en arseniuro) puede favorecer su mobilidad, lo cual podría llevar a un enriquecimiento de las zonas subyacentes. Cuando la evaporación es importante, la dirección del flujo del agua se invierte, y se produce una migración hacia arriba por capilaridad (Cauquenes en verano, El Salvador). Los elementos mobilizados migran esencialmente hacia las zonas oxidantes. La saturatión y/o supersaturación controla la precipitación de las principales sales eflorescentes solubles en agua (bonattita, calcantita, halotriquita, hexahidrita, piqueringita y magnesioauberita en El Salvador n.°1). La hidrólisis y los procesos de reemplazo son menos importantes. En la zona de oxidación, una actividad iónica elevada favorece la entrada de Al en la jarosita o de Cu y Zn en la biotita (Cauquenes).

Una paragénesis rica en carbonatos (P. Cerda, capítulo 6) neutraliza el ácido producido por los procesos de oxidación de los sulfuros, y genera así unas condiciones de pH neutro. Un pH elevado favorece la adsorción de los elementos liberados, lo cual limita su mobilidad y, en climas áridos, impide su migración hacia arriba por capilaridad. Ello inhibe la concentración de metales pesados formando sales eflorescentes solubles en agua. En las zonas de clima árido, el bajo contenido en agua de los horizontes de grano grueso puede hacer disminuir el grado de oxidación de la pirita. En un valle, si para retener los desechos de flotación se construye una presa río arriba con respecto a otra presa más antigua, puede que se produzca un transporte, de la nueva presa hacia la presa situada río abajo, de las aguas ácidas o neutras que contienen los iones metálicos liberados. Estos iones, al encontrarse con las condiciones geoquímicas distintas que corresponden a la antigua presa (presencia de capas ricas en calcita o condiciones más reductoras) serán hidrolizados o precipitarán en forma de minerales secundarios (ferrihidrita de alto orden, goetita, jarosita y covelita), lo cual puede generar un enriquecimiento secundario importante en la presa antigua (P. Cerda y Ojancos, capítulo 6).

I Introduction et résumé des résultats*

I.1 Objectifs

L'objectif de cette étude est d'évaluer les changements minéralogiques et géochimiques qui ont lieu à l'interface entre la zone d'oxydation et la zone primaire (à sulfures) dans les rejets de flottation de minerais de cuivre, afin de comprendre les processus qui agissent après l'oxydation des sulfures, en particulier la formation de "drainage minier acide" et la mobilité des éléments. Divers paramètres concernant le climat et la composition minéralogique originelle ont été considérés.

Plus concrètement, cette étude essaie de caractériser (1) les possibles mécanismes de formation et de migration ultérieure de la zone d'oxydation, (2) la précipitation de minéraux secondaires, (3) les processus de fixation secondaire par sorption et par précipitation, et (4) les processus d'enrichissement et de mobilisation des éléments qui sont importants économiquement ou qui posent des problèmes environnementaux. L'objectif final est de modéliser l'évolution minéralogique et géochimique des rejets par rapport à leur composition minéralogique primaire et aux conditions climatiques données.

Dans ce but, six rejets de flottation situés dans de différentes zones climatiques du Chili ont été sélectionnés. Le Chili a été choisi par sa situation géographique et géologique singulière. Pendant le Mésozoïque et le Cénozoïque, l'histoire géologique du Chili est contrôlée par l'évolution d'un arc magmatique de direction Nord-Sud qui migre vers l'Est. Pendant le Crétacé Inférieur à "moyen", cet arc magmatique est à l'origine de la formation de différents types de gisements. Pour cette étude, deux types de gisements de cuivre économiquement importants et de composition minéralogique distincte ont été sélectionnés. Le premier type comprend les porphyres cuprifères associés au magmatisme qui a lieu du Crétacé Supérieur au Tertiaire, et qui sont donc généralement situés à l'Est du premier type de gisement décrit (Ruiz et Peebles, 1998). La paragenèse du minerai est moins riche en pyrite et, souvent, les minéraux de l'argile hydrothermaux sont abondants et la teneur en carbonates est faible ou nulle (gisements de porphyres cuprifères géants de La Andina, El Teniente et El Salvador). Le second type de gisement comprend les gisements d'oxydes de Fe (Cu-Au) de la ceinture de Punta del Cobre-Candelaria.Ces gisements se caractérisent par une paragenèse relativement riche en pyrite et en magnétite, par un développement modéré des minéraux de l'argile et par la présence de calcite comme minéral de gangue important (bassins de rejet d'Ojancos et P. Cerda). Les bassins de rejet sélectionnés (Fig. 1) se trouvent dans des zones climatiques de caractéristiques différents, humide à extrêmement aride, suivant la direction N-S, ce qui est dû à la morphologie très allongée du Chili selon cette direction. Cette répartition permet d'utiliser les bassins de rejet étudiés comme des laboratoires à ciel ouvert dans lesquels il est possible de comparer des paramètres variables concernant le climat, la minéralogie du gisement et les processus de flottation.

---

* This chapter "Introduction and summary of the results" is written in French in accordance with the instructions for publication of Ph.D. theses of the Faculté des Sciences, Université de Genève.

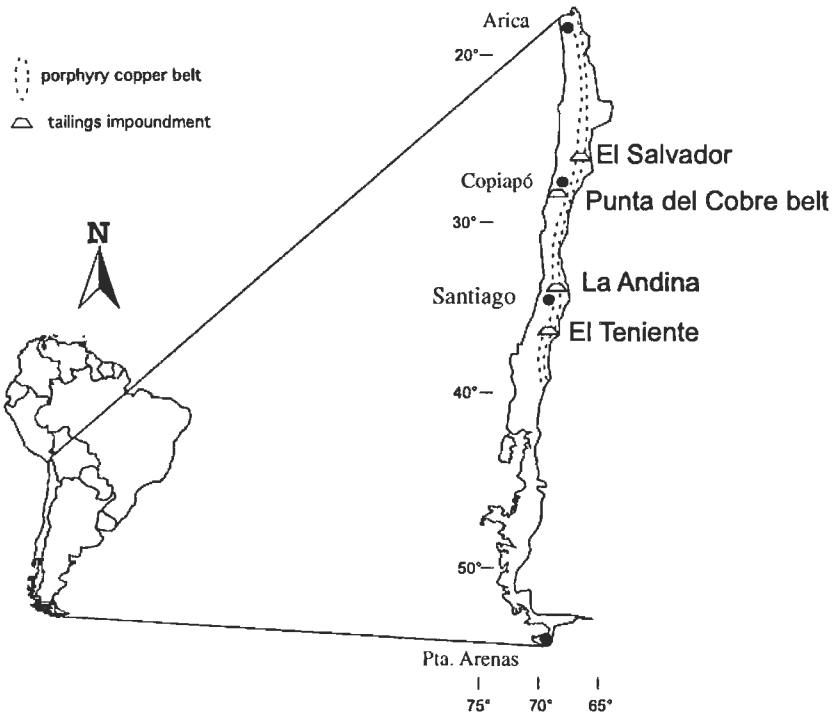

Fig. 1: Distribution des bassins de rejet étudiés au Chili. Les trois porphyres cuprifères géants (La Andina, El Teniente et El Salvador) sont associés à l'arc magmatique de direction N-S d'âge Crétacé Supérieur – Tertiaire. Les mines de La Andina, El Teniente et El Salvador sont situées dans des zones à climat alpin, méditerranéen et hyper aride, respectivement. Les bassins de rejet d'Ojancos et P. Cerda sont situés dans des zones climatiques hyper arides mais subissent un apport d'eau anthropiquement contrôlé.

I.2 Plan du travail

Le travail présenté est structuré en sept chapitres. Le premier chapitre est une introduction générale. Le deuxième introduit les notions de base de géochimie de l'environnement appliquée aux déchets des mines de sulfures. Les chapitres 3 et 4 décrivent les procédures méthodologiques, les chapitres 5 et 6 comparent les études menées sur les différents types de gisements sélectionnés et le chapitre 7 résume les principales conclusions obtenues concernant la rétention des métaux par des phases de fer. Les chapitres 4 à 7 sont présentés sous forme de manuscrits prêts à être soumis ou déjà soumis à des périodiques scientifiques.

Le chapitre 3 s'intitule "Méthodologie utilisée pour l'extraction séquentielle appliquée à l'étude géochimique des rejets de mines de sulfures en combinant la cinétique de dissolution et le contrôle minéralogique des phases dissoutes par diffraction de rayons-X (XRD) et par diffraction différentielle de rayons-X (DXRD)". Ce chapitre présente la procédure méthodologique qui a été suivie afin de développer une séquence d'extractions adéquate à l'étude des processus géochimiques des bassins de rejet de mines de sulfures de cuivre. Le

chapitre 4 étudie la cinétique de dissolution de la schwertmannite et de la ferrihydrite dans le but de distinguer ces deux phases secondaires. Le chapitre 5, "Cycles des éléments et minéralogie secondaire dans les bassins de rejet des porphyres cuprifères en fonction du climat, de la minéralogie primaire et du traitement du minerai" (Dold et Fontboté, *Journal of Geochemical Exploration*, Special Issue "Geochemical Studies of Mining and Environment", soumis) compare les rejets de flottation des trois porphyres cuprifères étudiés par rapport à la minéralogie secondaire et à la direction de mobilisation, tout en considérant la minéralogie primaire et les différentes conditions climatiques. Le chapitre 6 "Bassins de rejet des gisements d'oxydes de Fe Cu-Au de la ceinture de Punta del Cobre, Nord du Chili – influence de la minéralogie primaire riche en carbonates sur la mobilisation et de la construction des bassins de rejet sur les processus secondaires d'enrichissement" présente un cas d'étude de rejets riches en carbonates. Le chapitre 7 "Rétention sélective des métaux par des oxyhydroxydes de fer et par des sulfates d'oxyhydroxydes dans les rejets de mines de sulfures et leur contribution à la production d'acide" se concentre sur l'étude du rôle des mineraux de fer secondaires dans la mobilisation des éléments et dans la production d'acide par hydrolyse. Les appendices 1 à 4 fournissent les données analytiques non inclues dans les autres parties du travail.

I.3 Méthodes

I.3.1 Echantillonnage et méthodes de terrain

Le travail sur le terrain s'est réalisé en collaboration avec l' "Instituto de Investigaciones Científicas y Tecnológicas" (IDITEC) de l'Université d'Atacama (Copiapó), le Département de Géologie de l'Université du Chili (Santiago) et le "Servicio Nacional de Geología y Minería" (SERNAGEOMIN, Santiago) qui ont offert leur support logistique lors des campagnes sur le terrain menées en 1996 et en 1997. Les échantillons solides ont été prélevés en surface et jusqu'à 10 m de profondeur (fente d'échantillonnage de 100 x 2 x 2 cm) en utilisant une perforatrice à percussion. Les échantillons d'eau ont été prélevés des effluents.

Plus de 370 échantillons ont été prélevés de six bassins de rejet des mines La Andina, El Teniente et El Salvador ainsi que des bassins de rejet de flottation d'Ojancos et P. Cerda qui ont traité le minerai de la ceinture de Punta del Cobre (Tableau 1).

Les échantillons prélevés et les données géochimiques obtenues lors d'une recherche antérieure menée sur les bassins de rejet d'Ojancos sont aussi inclus dans ce travail.

Après avoir pris note des caractéristiques minéralogiques et de la couleur des échantillons solides, estimé la taille des grains et mesuré leur pH (avec un pH-mètre WTW ® ; lors de la campagne sur le terrain de 1997, une électrode pH qui avait originellement été conçue pour effectuer des contrôles de qualité sur de la viande a été utilisée avec beaucoup de succès pour réaliser des mesures *in situ* du pH des sédiments humides des rejets), les échantillons ont été conservés dans des sacs en plastique et stockés dans un glacière. Puis, ils ont été immédiatement transportés dans les laboratoires des mines afin d'être séchés (<35°C) et en déterminer la teneur en eau. Une fois secs, les échantillons ont été homogénéisés et stockés dans des flacons en polyéthylène (PET) pour être conservés à température ambiante.

Tableau 1: *Récapitulatif des données sur les bassins de rejet des mines de sulfures de cuivre étudiés.*

Mine	Type de dépôt	Bassin de rejet	Climat	Processus de flottation	sondage	Echan-tillons
La Andina	Porphyre cuprifère	Piuquenes	Alpin	circuit alcalin pH 10.5	5	87
El Teniente	Porphyre cuprifère	Cauquenes	Méditerranéen	circuit acide pH 4.5	5	78
El Salvador	Porphyre cuprifère	Salvador n°. 1	Hyper aride	circuit alcalin pH 10.5	4	37
Ceinture de Punta del Cobre	Oxydes de Fe Cu-Au	P. Cerda n°. 4 and 6	Hyper aride	circuit alcalin pH 10.5	4	44
Ceinture de Punta del Cobre	Oxydes de Fe Cu-Au	Ojancos n°. 2	Hyper aride	circuit alcalin pH 11	11	124

Les échantillons d'eau ont été filtrés en utilisant des filtres d'acétate de sodium de 0.45 µm. La température, la conductivité, le pH et la teneur en oxygène ont été mesurés sur le terrain. Les échantillons d'eau ont été séparés en deux aliquots, un sans traitement pour analyser les anions et l'autre conservé à pH 2 (obtenu par addition de HNO_3 suprapur) pour analyser les cations. Tous ces échantillons ont été réfrigérés jusqu'au moment d'effectuer les analyses.

I.3.2 Méthodes analytiques

Le pourcentage en poids d'humidité de tous les échantillons des rejets a été obtenu en calculant la différence de leur poids mesuré avant et après sèchage dans les laboratoires des mines. La distribution de la taille des particules de quelques échantillons sélectionnés a été obtenue en effectuant des mesures avec les analyseurs de taille de particules au laser Coulter® et Fritsch Analysette® à l'Institut F.-A. Forel de l'Université de Genève et au Département de Minéralogie de l'Université de Lausanne, respectivement.

Afin d'étudier la minéralogie du minerai, des sections polies et des lames minces polies ont été préparées à partir des échantillons des rejets et des échantillons non altérés des sédiments. Tous les échantillons ont été analysés par diffraction de rayons-X (XRD) en utilisant un diffractomètre Philips® 3020 au Département de Minéralogie de l'Université de Genève. Pour la détermination des minéraux de l'argile, des échantillons orientés prélevés de la fraction < 2 µm ont été analysés en utilisant un diffractomètre Rigaku® Rotaflex au Département de Minéralogie et de Pétrographie de l'Université de Lausanne. Les hydroxydes de Fe(III) peu cristallisés, comme la ferrihydrite et la schwertmannite, ont été détectés par diffraction différentielle de rayons-X (DXRD). Les éléments adsorbés par la schwertmannite et la biotite ont été étudiés à la microsonde électronique en utilisant un instrument CAMECA SX50 à l'Université de Lausanne. La morphologie des minéraux et la composition chimique qualitative des précipités à partir des "drainages miniers acides" ont été étudiées à l'aide d'un microscope électronique de balayage JOEL® JSM 6400 muni d'un système dispersif d'énergie (SEM-EDS).

Les tests de cinétique de dissolution de la schwertmannite et de la ferrihydrite ont été réalisés en utilisant de l'oxalate d'ammonium 0.2M à pH 3.0 et dans le noir au Centre d'Analyse Minérale (CAM) de l'Université de Lausanne. Les teneurs en Fe et en S des solutions obtenues ont été déterminées par ICP-AES en utilisant un instrument Perkin-Elmer Plasma-2000 à l'Institut des Sciences du Sol de l'EPFL, à Lausanne.

Les extractions séquentielles et les analyses multi-élémentaires par ICP-ES ont été réalisés aux "X-Ray Assay Laboratories" (XRAL) de Toronto, au Canada. La teneur totale en soufre, nécessaire pour la détermination acide-base, a été obtenue en utilisant un four Leco®. Pour déterminer la teneur en soufre présent en forme de sulfates, une attaque chimique à chaud dans de l'acide oxalique 0.2M pendant 2 h a été réalisée (étape 4 de la séquence B, chapitre 3), puis la teneur en soufre a été obtenue par ICP-ES aux XRAL. Le carbone total et minéral a été analysé par titrage coulométrique (Ströhlein CS 702®) au Centre d'Analyse Minérale de l'Université de Lausanne.

Pour l'étude micro-biologique, un aliquot non traitée de chaque échantillon a été maintenu à 5°C dans des glacière. Lors de la campagne sur le terrain de 1996, peu de temps après l'échantillonnage, 10 échantillons ont été sélectionnés et envoyés au laboratoire du groupe bio-métallurgique du Département de Génie Chimique de l'Université du Chili (Santiago). Le nombre total de cellules (comptage microscopique direct; compteur Phyroff-Hauser) ainsi que l'activité d'oxydation (taux d'oxydation du Fe(II)) ont été déterminés; et une culture de *Thiobacillus ferrooxidans* a été réalisée (comptage sur plaque).

I.4 Méthodologie utilisée pour l'extraction séquentielle appliquée à l'étude géochimique des rejets de mines de sulfures en combinant la cinétique de dissolution et le contrôle minéralogique des phases dissoutes par diffraction de rayons-X (XRD) et par diffraction différentielle de rayons-X (DXRD)

Les tests de cinétique de dissolution réalisés sur les échantillons prélevés dans les rejets des mines étudiées, en combinaison avec le contrôle par diffraction de rayons-X (XRD) et par diffraction différentielle de rayons-X (DXRD) des phases dissouts lors des extractions séquentielles, indiquent quels sont les minéraux qui sont dissous à chaque étape. Cette information est indispensable pour interpréter les données géochimiques obtenues à partir de l'analyse des extractions séquentielles ainsi que pour améliorer le degré de sélection de la séquence. Des tests préliminaires basés sur des techniques communes de dissolution ont permis de mettre au point une séquence en sept étapes adaptée particulièrement à la minéralogie primaire et secondaire des rejets des mines des gisements de sulfures étudiés, porphyres cuprifères et dépôts d'oxydes de Fe avec Cu et Au. Cette séquence à sept pas est la suivante. Le premier étape attaque la fraction soluble dans l'eau (1.0 g d'échantillon dans H_2O déionisée agité pendant 1h). Le gypse et les sels de métaux sont dissouts (p. ex., la bonattite ($CuSO_4 \cdot 3H_2O$), la chalcanthite ($CuSO_4 \cdot 5H_2O$), la pickeringite ($MgAl_2(SO_4)_4 \cdot 22H_2O$). Le deuxième étape (acétate d'ammonium 1M, pH 4.5, agité pendant 2 h) libère la fraction interchangeable qui se trouve sous forme d'ions adsorbés, mais dissout aussi la calcite et désintègre un minéral secondaire du type vermiculite à couches mixtes typique de la zone d'oxydation à faible pH. Le troisième étape

(oxalate d'ammonium 0.2M, pH 3, agité dans le noir pendant 1h, à température ambiante) vise la fraction à oxyhxdroxydes de Fe(III), et dissout la schwertmannite, la ferrihydrite à deux lignes, les hydroxydes de Mn et en partie la jarosite secondaire. Le quatrième étape (oxalate d'ammonium 0.2M, pH 3.0, chauffé au bain-marie à 80°C pendant 2h) s'occupe de la fraction à oxydes de Fe(III) et dissout tous les minéraux de Fe secondaires, c'est à dire la ferrihydrite d'ordre élevé (à six lignes), la goethite, la jarosite primaire et secondaire, la natrojarosite, l'hématite primaire et, en partie, la magnétite hypogène. Cette extraction est proposée afin de séparer le soufre oxydé dans les sulfates du soufre réduit dans les sulfures pour la détermination acide-base. Lors du cinquième étape, moyennant une attaque avec H_2O_2 (H_2O_2 35%, chauffé au bain-marie pendant 1h), les conditions réductrices changent et deviennent oxydantes, ce qui dissout la matière organique et les sulfures de cuivre supergènes comme la covellite et la chalcocite-digénite. Le sixième étape ($KClO_3$ et HCl puis HNO_3 4M en ébullition) dissout les sulfures primaires et le septième étape (HCl, HF, $HClO_4$, HNO_3) la fraction résiduelle (les silicates).

I.5 Cinétique de dissolution de la schwertmannite et de la ferrihydrite

Un test de dissolution avec de l'oxalate d'ammonium 0.2M à pH 3.0 dans le noir a été réalisé sur neuf échantillons de schwertmannite et de ferrihydrite naturelles et synthétiques. Plus précisément, quatre schwertmannites naturelles et une de synthétique, deux ferrihydrites à deux lignes naturelles et une de synthétique ainsi qu'une ferrihydrite à six lignes synthétique ont été utilisées. Un échantillon additionnel a été préparé en mélangeant de la schwertmannite et de la ferrihydrite à deux lignes suivant une proportion en poids de 1:1. Les échantillons ont été caractérisés par diffraction de rayons-X (XRD) et par diffraction différentielle de rayons-X (DXRD). Les teneurs en Fe et en SO_4 dissous ont été déterminées par ICP-AES. La morphologie des minéraux aux différentes étapes de la dissolution a été contrôlée en utilisant un microscope électronique à balayage (SEM). Les courbes dissolution-temps ont été déterminées en utilisant des équations de vitesse.

La cinétique de dissolution de la schwertmannite naturelle et synthétique dans de l'oxalate d'ammonium 0.2M à pH 3.0 et dans le noir est très rapide (>94% en 60 min). La ferrihydrite à deux lignes naturelle montre une cinétique de dissolution comparable (>85% après 60 min), tandis que la ferrihydrite synthétique se dissout plus lentement (16% et 42% après 60 min).
Les courbes de dissolution de la schwertmannite obtenues, la morphologie du minéral contrôlée par microscopie électronique de balayage (SEM) et les rapports Fe/S molaires mesurés des fractions dissoutes montrent qu'il est possible de distinguer deux variétés morphologiques de schwertmannite (sphérique ou type oursin et type maille) qui indiquent des cinétiques de dissolution distinctes. L'effondrement des agrégats de la schwertmannite sphérique (type oursin) semble contrôler la cinétique de dissolution du minéral. Quant à la schwertmannite de type maille, des molécules de SO_4^{2-} intra-cristallin pourraient jouer un rôle prédominant sur la stabilité de la structure. La modélisation des courbes de dissolution de la ferrihydrite ne fourni pas d'indications claires concernant sa morphologie.

Ces résultats suggèrent que pour dissoudre de façon sélective ces oxyhydroxydes de fer, schwertmannite et ferrihydrite à deux lignes, l'attaque pourrait consister en une dissolution dans de l'oxalate d'ammonium à pH 3.0 dans le noir et pendant 60 min. Ces conditions maximisent la dissolution de la schwertmannite et de la ferrihydrite à deux lignes, tandis qu'elles minimisent la dissolution d'autres phases susceptibles d'être réduites, comme la jarosite, l'hématite, la magnétite et la goéthite. Néanmoins, la réalisation de cette attaque sur des échantillons de la zone d'oxydation des rejets de mines de sulfures a montré qu'une fraction de jarosite secondaire se dissout aussi, mais plus lentement que la schwertmannite et la ferrihydrite de bas ordre. Pour ne dissoudre que la schwertmannite (p. ex., pour une détermination par DXRD), une attaque de 15 min est préférable afin d'obtenir une meilleure sélection.

I.6 Cycles des éléments et minéralogie secondaire dans les bassins de rejet des porphyres cuprifères en fonction du climat, de la minéralogie primaire et du traitement du minerai

Cet chapitre présente une étude géochimique, minéralogique et micro-biologique comparative de trois bassins derejets des mines des porphyres cuprifères La Andina, El Teniente et El Salvador, au Chili. L'objectif principal est d'étudier les changements minéralogiques et chimiques qui ont lieu à l'interface entre la zone d'oxydation et la zone primaire dans les bassins de rejet de flottation de minerais de cuivre. Les différents critères qui ont été considérés pour choisir les rejets étudiés comprennent la connaissance de l'origine du minerai (pour une mine seulement), le climat, les processus de flottation, et l'absence d'altération anthropique (par apport d'eau ou de nouveaux rejets) après que les activités aient cessé. Ainsi, l'influence du climat, des processus de flottation et de la minéralogie du gisement peuvent être étudiés qualitativement. Deux modèles schématiques concernant la mobilité des éléments dans des rejets de mines de sulfures contrôlée par les conditions climatiques sont présentés.

En utilisant les méthodes de diffraction de rayons-X (XRD) et de diffraction différentielle de rayons-X (DXRD), les phases secondaires, c'est-à-dire la essentiellement jarosite, la schwertmannite et un minéral de type vermiculite à couches mixtes, ont été détectées dans la zone d'oxydation. La jarosite et la schwertmannite jouent un rôle important pour la rétention d'oxyanions (p. ex., $HMoO_4^-$, $H_2AsO_4^-$ et SO_4^{2-}) dans les zones d'oxydation à faible pH, ce qui a été prouvé en utilisant la méthode des extractions séquentielles (puis analyse des éléments par ICP-ES) et par microscopie électronique à balayage (SEM-EDS) et/ou par des analyses à la microsonde électronique. Les cations bivalents sont lessivés des zones d'oxydation dans des climats où les précipitations sont dominantes. En dessous de cette zone, l'augmentation du pH contrôle l'adsorption des cations bivalents à travers des adsorbants, comme les hydroxydes secondaires de Mn(II), de Fe(III), ou les minéraux de l'argile. En dessous du niveau phréatique, dans des conditions de plus en plus réductrices, des processus de remplacement contrôlés par le pH ont lieu, tel qu'il est montré par la transformation de la chalcopyrite en covellite, ce qui mène à des enrichissements secondaires en Cu qui pourraient être économiquement intéressants.

Dans les climats arides avec forte évaporation, la direction du flux de l'eau change. Il se produit une migration vers le haut par capillarité. L'hydrolyse et les processus de remplacement

des sulfures sont moins importants. En conditions oxydantes, les éléments mobilisés sont transférés vers la partie supérieure des rejets. La saturation et/ou la supersaturation contrôle la précipitation de sulfates secondaires principalement solubles dans l'eau et le fort enrichissement qui se produit dans la partie supérieure des rejets. Dans la zone d'oxydation à faible pH, de par leur force ionique élevée certains éléments mobiles deviennent des éléments de substitution dans certaines phases secondaires. C'est le cas de l'Al dans la jarosite ou du Cu et du Zn qui substituent le K dans la biotite.

De façon surprenante, à El Salvador seulement de faibles quantités de minéraux de fer secondaires ont été trouvés par rapport à la grande abondance de pyrite (6.2 %). Une très faible activité d'oxydation lors des tests micro-biologiques ainsi que des teneurs en Mo 3 à 5 fois supérieures à celles mesurées à Piquenes et à Cauquenes suggèrent que ce phénomèn serait dû, au moins en partie, à un empoisonnement des bactéries *Thiobacillus ferroxidians* par du Mo. On remarque que la forte acidité mesurée dans les rejets d'El Salvador (pH 2.0-3.5) est due à une oxydation inorganique lente de pyrite en combinaison avec un stockage d'acidité dans la jarosite supergène et à un potentiel nul de neutralisation par les carbonates.

I.7 Influence d'une minéralogie primaire riche en carbonates et de la construction de bassins sur la mobilité des éléments et sur les processus d'enrichissement secondaire dans des bassins de rejet de sulfures – exemples des dépôts d'oxydes de Fe Cu-Au de la ceinture de Punta del Cobre, Nord du Chili

L'étude géochimique et minéralogique de deux bassins de rejet de flottation de gisements d'oxydes de Fe Cu-Au de la ceinture de Punta del Cobre (Ojancos et P. Cerda, au Sud de Copiapó, Nord du Chili), montre l'influence d'une minéralogie riche en carbonates et de la construction de bassins de rejet sur la mobilité des éléments et sur les processus d'enrichissement dans des climats arides. Contenus par des barrages, les rejets d'Ojancos et P. Cerda n° 2 et n° 4, respectivement) ont comblé des vallées. Après que les activités aient cessé, de nouveaux rejets ont été déposés en amont (Ojancos "2H" et P. Cerda n° 6). Les rejets d'Ojancos se caractérisent par l'alternance de couches de plusieurs mètres d'épaisseur à potentiel de neutralisation élevé (environ 40% de calcite et 2% de pyrite) et de couches à potentiel acide élevé (environ 3 % de calcite et 4% de pyrite). Par contre, le bassin de P. Cerda montre une répartition plus homogène du potentiel de neutralisation, qui l'emporte généralement sur le potentiel acide (environ 10% de calcite et jusqu'à 2.5% de pyrite).

L'étude réalisée dans le bassin de rejet n° 2 d'Ojancos a permis de distinguer les processus primaires qui ont affecté le minerai pendant son traitement et les processus secondaires surimposés qui sont à l'origine d'un enrichissement associé aux processus d'oxydation des sulfures. L'observation de sections polies, l'étude par diffraction de rayons-X (XRD), diffraction différentielle de rayons-X (DXRD), microscopie électronique à balayage (SEM-EDS), ainsi que des analyses par ICP-ES d'extractions séquentielles à 7 étapes, ont été entreprises afin de distinguer la minéralogie primaire des phases secondaires. La partie supérieure du bassin n° 2 d'Ojancos comprend une zone primaire (pH 7-8), gris foncé, d'environ trois mètres d'épaisseur, qui s'est formée à partir d'une déposition récente synchrone aux rejets "2H", localisé plus en

amont. En dessous de la zone primaire, une zone neutre riche en calcite qui a anciennement été une zone d'oxydation, montre une alternance d'horizons à peine oxydés, gris foncé, à grain grossier, et de couches oxydées dans des tons rouges, bruns et ocres, à grain fin. Les deux derniers mètres du carottage témoignent d'une zone homogène cimentée, acide (pH 4), brun-rougeâtre, à faible perméabilité, riche en gypse ainsi qu'en ferrihydrite d'ordre élevé (5 lignes à 6 lignes) et en goethite, avec localement de la jarosite en traces, et à faible teneur en sulfures. Les rejets 2H qui ont été récemment déposés en amont ont un potentiel acide élevée. Ceci génère la formation d'un drainage minier acide qui est mis en évidence par la présence d'effluents acides avec précipitation de schwertmannite (pH 3.15) et chalcoalumite (pH 4.9) au contact entre les rejets 2H et le bassin n° 2. Ce drainage minier acide est à l'origine de la formation de la zone cimentée à faible pH (pH 4) dans le bassin n° 2, plus ancien et situé en aval. Celui-ci se caractérise par l'hydrolyse lente des hydroxydes de Fe (III) (ferrihydrite à 5-6 lignes) et par l'enrichissement associé important en métaux lourds, détectés surtout dans les fractions à ions interchangeables de la séquence d'extraction, ainsi qu'en oxydes et hydroxydes de Fe (III) et en sulfures de cuivre secondaires (covellite).

Le potentiel de neutralisation (calcite et dolomite) des rejets de P. Cerda est suffisamment élevé pour maintenir un pH neutre. Néanmoins, la pyrite s'oxyde, ce qui est mis en évidence par la formation d'une zone d'oxydation avec précipitation d'hydroxydes secondaires de Fe (III), surtout dans les horizons à grain fin, tel qu'il est observé dans la zone d'oxydation du bassin n°2 d'Ojancos. Le fait que les horizons à grain plus grossier et plus riches en sulfures ne soient pas considérablement oxydés suggère que leur capacité de rétention d'eau est trop faible pour permettre une oxydation effective dans les conditions, extrêmement arides, qui prédominent. Dans la partie supérieure des bassins de rejet de P. Cerda, l'absence totale de sels secondaires efflorescents indique que le pH neutre, tamponné par les carbonates, inhibe la migration vers le haut (induite par le climat) des éléments libérés pendant l'oxydation des sulfures, en favorisant leur adsorption.

I.8 Rétention sélective des métaux par des oxyhydroxydes de fer et par des sulfates d'oxyhydroxydes dans les rejets de mines de sulfures et leur contribution à la production d'acide

Les oxyhydroxydes de Fe(III) ont la capacité de fixer les métaux lourds, ce qui est dû à leurs groupes fonctionnels et à leur grande surface. La méthode de la diffraction différentielle de rayons-X, a permis de détecter de la schwertmannite (idéalement comprise entre $Fe_8O_8(OH)_6SO_4$ et $Fe_{16}O_{16}(OH)10(SO_4)_3$) dans la zone d'oxydation de deux bassins de rejet des mines de sulfures de La Andina et El Terniente (Chili). La schwertmannite se trouve comme phase secondaire importante avec les principaux minéraux secondaires, la jarosite ($KFe_3(SO_4)_2(OH)_6$) et un minéral de type vermiculite à couches mixtes. Un test de cinétique de dissolution sur huit échantillons de schwertmannite naturelle et synthétique et de ferrihydrite a été réalisé en utilisant de l'oxalate d'ammonium à pH 3.0 dans le noir (NH_4-OxD) afin d'étudier la possibilité de discriminer un de ces deux minéraux en fonction de leur cinétique de dissolution. Les résultats obtenus lors du test ont été utilisés pour établir une extraction séquentielle adaptée à la

minéralogie secondaire des rejets de mine étudiés. Les variations des rapports Fe/S molaires dans la solution de l'attaque à NH_4-OxD suggèrent que la schwertmannite n'est présente que dans la zone d'oxydation avec la jarosite, et que l'oxyhydroxyde de fer prédominant dans les zones sous-jacentes est probablement la ferrihydrite. Des teneurs plus hautes en Mo, As et SO_4 des échantillons attaqués en provenance de la zone d'oxydation, ainsi que des analyses ponctuelles à la microsonde, indiquent que la schwertmannite et la jarosite jouent un rôle important dans l'adsorption d'oxyanions par échange de ligands dans des conditions acides. Par contre, les cations bivalents (p. ex. Cu^{2+}, Mn^{2+}, Zn^{2+}) ne sont pas adsorbés par ces minéraux, ce qui serait dû à une adsorption concurrentielle de protons par les groupes OH^-. En dessous de la zone d'oxydation, la ferrihydrite et d'autres adsorbants (p.ex. minéraux de l'argile, oxydes de Mn) jouent un rôle principal dans l'adsorption contrôlée par le pH de cations bivalents de la zone d'oxydation qui sont mobilisés vers le bas. Pour les déterminations acide-base, on présume que la phase $Fe(OH)_3(s)$ ou la ferrihydrite s'hydrolysent dans la solution en produisant 3 moles de H^+ pour 1 mole de Fe^{3+} hydrolysé. L'hydrolyse de la jarosite ne produit que 2 moles de H^+ et celle de la schwertmannite entre 2.625 et 2.750. Les résultats obtenus suggèrent que cette différence doit être tenue en compte pour calculer la quantité d'acide produit, puisque l'hydrolyse des phases de fer secondaires est le principal mécanisme de production d'acide lors de l'oxydation des sulfures. Néanmoins, lors du calcul de l'acide potentiel lors d'un traitement de carbonates, il est important de considérer l'augmentation du pH qui produira de la ferrihydrite ou de la goethite, ce qui conduira à une production de 3 moles de H^+ par mol de Fe^{3+} hydrolysé.

CHAPTER 1

1 Introduction

1.1 Purpose

The general aim of the present work is to investigate the mineralogical and geochemical changes occurring at the interface between the oxidation and the primary (sulfide) zone in copper flotation tailings in order to understand the processes taking place subsequent to sulfide oxidation, especially the formation of acid mine drainage and element mobility. Parameters of climate and original mineralogical composition are taken into account.

In particular, the study intends to characterize (1) possible mechanisms of formation and subsequent migration of the oxidation zone, (2) precipitation of secondary minerals, (3) secondary fixing processes through sorption and precipitation, (4) mobilization and enrichment processes of elements that are significant from an economic and environmental perspective. The final goal is to model the mineralogical and geochemical behavior of tailings in relation to their primary mineralogical composition and climatic settings.

For this purpose, six flotation tailings impoundments at five flotation plants located in different climatic zones of Chile were selected. Chile was chosen for this study because of its unique geological and geographical situation. The Mesozoic-Cenozoic geological history of Chile was controlled by a West-East migrating magmatic arc. During Lower to "middle" Cretaceous times the magmatic arc induced the formation of different types of ores. For this study two economically important and mineralogical different types of copper ore deposits were selected. The first one are the porphyry copper deposits related to the Upper Cretaceous-Tertiary magmatism, and, therefore, generally located farther to the east (Ruiz and Peebles, 1988). They show ore paragenesis less rich in pyrite, typically with abundant hydrothermal clay minerals and low or nonexistant carbonate content (the selected tailings impoundments at the giant porphyry copper deposits of La Andina, El Teniente, and El Salvador). The second type includes Fe-oxide (Cu-Au) deposits of the Punta del Cobre-Candelaria belt (Marschik and Fontboté, 1996; Marschik et al., 1997) characterized by a paragenesis relatively rich in pyrite and magnetite with moderate development of clay minerals, and with calcite as a significant gangue mineral (Ojancos and P. Cerda tailings impoundments). The selected tailings impoundments (Fig.1) occur in different climatic zones ranging from humid to hyper-arid along the strongly N-S elongated Chilean geography. This situation allows to use the studied tailings as open-air laboratories in which we can compare variable parameters of climate, ore mineralogy, and flotation process.

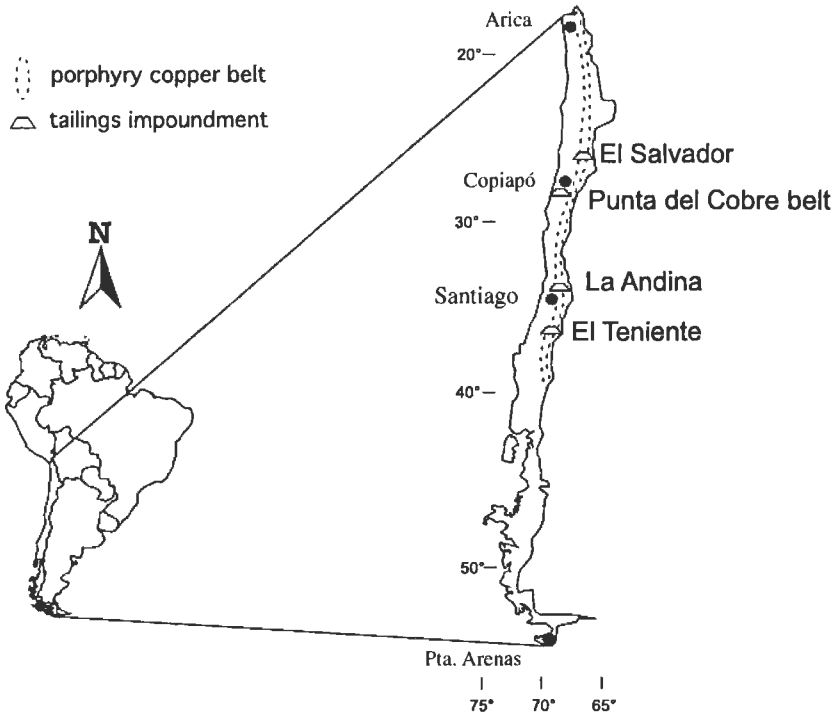

Fig.1: *Distribution of the selected mine tailings impoundments in Chile. The three giant porphyry copper deposits La Andina, El Teniente, and El Salvador are associated with the N-S trending Upper Cretaceous-Tertiary magmatic arc (Ruiz and Peebles, 1988). La Andina, El Teniente, and El Salvador are located in alpine, Mediterranean, and hyper-arid climates, respectively. The tailings impoundments of Ojancos and P. Cerda, located in the Punta del Cobre belt, are situated in hyper-arid conditions, but with an anthropogenetic controlled water input.*

Table 1: *Overview of the studied Cu-sulfide mine tailings impoundments.*

Mine	Deposit type	Impoundment	Climate	Flotation process	Drill cores	samples
La Andina	porphyry copper	Piuquenes	alpine	alkaline circuit pH 10.5	5	87
El Teniente	porphyry copper	Cauquenes	Mediterranean	acid circuit pH 4.5	5	78
El Salvador	porphyry copper	Salvador No. 1	hyper-arid	alkaline circuit pH 10.5	4	37
Punta del Cobre belt	Fe-oxide Cu-Au	P. Cerda No. 4 and 6	hyper-arid	alkaline circuit pH 10.5	4	44
Punta del Cobre belt	Fe-oxide Cu-Au	Ojancos No. 2	hyper-arid	alkaline circuit pH 11	11	124

1.2 Plan of the work

The present work is structured in seven chapters. The first chapter is a general introduction. The second chapter introduces the reader to the basic concepts in environmental geochemistry of sulfide mine-waste. Chapters 3 and 4 describe methodological aspects, chapter 5 and 6 compare case studies of the different selected ore deposit types, and chapter 7 summarizes the main findings in respect to metal retention by secondary ferric phases. Chapter 4 to 7 are presented in form of manuscripts ready to submit or already submitted to scientific journals.

Chapter 3 is entitled "methodology used for sequential extraction applied to geochemical investigations of sulfidic mine tailings by combination of dissolution kinetics and mineralogical control of dissolved phases by X-ray diffraction (XRD) and differential X-ray diffraction (DXRD)" and presents the methodological approach followed in this study to develop a sequence of extractions applied to the geochemical processes in Cu-sulfide mine tailings. Chapter 4 studies the "dissolution kinetics of schwertmannite and ferrihydrite" with the purpose of discriminating between these secondary phases. Chapter 5 "Element cycling and secondary mineralogy in porphyry copper tailings as a function of climate, primary mineralogy, and mineral processing" (Dold, B. and Fontboté, L., Journal of Geochemical Exploration, Special Issue "Geochemical studies of Mining and Environment", in review) compares the three studied porphyry copper tailings with respect to differences in secondary mineralogy and mobilization direction considering their different climatic conditions and primary mineralogy. Chapter 6 "Influence of carbonate-rich primary mineralogy and of impoundment construction on element mobility and secondary enrichment processes in sulfide tailings impoundments from the Fe-oxide Cu-Au deposits from the Punta del Cobre belt, northern Chile" is a case study of carbonate-rich tailings and the impoundment construction to mobilization and enrichment processes. Chapter 7 "Selective metal retention by ferric oxyhydroxides and oxyhydroxide sulfates in sulfide mine tailings and their importance to acid production" focuses on the role of the secondary ferric mineralogy to element cycling and their role in acid production via hydrolysis. Appendix 1 – 4 list all relevant analytical data not included in the other parts of the work.

1.3 Methods

1.3.1 Sampling and field methods

The field work was realized in collaboration with the "Instituto de Investigaciones Cientificas y Technologicas" (IDICTEC) University of Atacama, Copiapó, the Geological Department of the University of Chile, Santiago, and the "Servicio Nacional de Geología y Minería" (SERNAGEOMIN), Santiago, Chile, which have collaborated with logistic support during the field work in 1996 and 1997. Percussion drilling, which was used to reach depths of 10 m and surface sampling were applied to obtain solid samples. Water samples were collected from effluents.

More than 370 samples were collected from 6 tailings impoundments from the mines La Andina, El Teniente, and El Salvador, and from the impoundments of the flotation plants Ojancos and P. Cerda which treated ore from the Punta del Cobre belt.

Samples and geochemical data from a previously conducted study of the Ojancos tailings impoundment No. 2 (Dold, 1994; Dold et al., 1996) are also included.

The solid samples were sealed in plastic bags and stored in an ice-packed cool box. Previously, the description of mineralogical characteristics, color and grain size estimation, and pH measurement was noted (paste pH according to MEND, 1991 using a WTW® pH-meter; in the 1997 field campaign a pH-electrode which was originally developed for quality control in meat, was successfully used for in situ pH-measurement in the moist tailings sediment). The samples were transported immediately to local mine laboratories for drying (< 35°C) and water content determination. The dry samples were homogenized and packed into polyethylene (PET) containers for storage at room temperature.

Water samples were filtered with 0.45 µm sodium acetate filters. Temperature, conductivity, pH, and dissolved oxygen were measured in the field. Every water sample was separated into two aliquots, one untreated for anion analysis, and the other conserved at pH 2 (obtained by addition of suprapure HNO_3) for cation analysis. The water samples were refrigerated until analysis.

1.3.2 Analytical methods

The wt.% of moisture of all tailings samples was measured using sample weight before and after drying in the mine laboratories. The particle size distribution of selected samples were measured by a Coulter® and a Fritsch Analysette® laser particle size analyzer at the Institute F.-A. Forel, University of Geneva and the Mineralogical and Petrography Department of the University of Lausanne, respectively.

Polished and polished thin sections were prepared from bulk samples and undisturbed sediment samples to study the ore mineralogy. All samples were analyzed as bulk sample by X-ray diffraction (XRD), using a Philips® 3020 diffractometer at the Mineralogical Department of the University of Geneva. Oriented samples of the fraction < 2µm for clay minerals determination were analyzed by a Rigaku® Rotaflex diffractometer at the Mineralogical and Petrography Department of the University of Lausanne. The poorly crystalline Fe(III) hydroxides such as ferrihydrite and schwertmannite were detected by differential X-ray diffraction (DXRD). Trace elements associated with schwertmannite and biotite were studied by a CAMECA SX50 electron microprobe at the University of Lausanne. The mineral morphology and the qualitative element composition of acid mine drainage precipitates was studied by a scanning electron microscope (SEM-EDS) JOEL® JSM 6400 at the Geological Department, University of Geneva.

The dissolution kinetics of schwertmannite and ferrihydrite in 0.2M NH_4-oxalate, pH 3, under exclusion of light, were performed in the "Centre d'Analyse Minérale" (CAM), University of Lausanne. The extracted solutions were analyzed for Fe and S by ICP-AES Perkin-Elmer Plasma-2000 at the Soil Science Institute, EPFL, Lausanne.

The sequential extractions with multi-element analyses by ICP-ES were performed by the X-Ray Assay Laboratories (XRAL) of Toronto, Canada. Total sulfur necessary for acid base accounting was measured, using a Leco® furnace. For measurement of the sulfate sulfur the 0.2 M oxalic acid hot 2h leach (step 4 in sequence B, chapter 3) was used. Sulfur was determined by ICP-ES, performed at XRAL. Total and mineral carbon has been analyzed by coulometric titration (Ströhlein CS 702®) at the Centre d'Analyse Minérale, University of Lausanne.

For the microbiological study a separate aliquot of each sample was taken and maintained at a temperature of 5°C untreated in ice-packed coolers. Ten samples were selected and delivered 1996 shortly after sampling to the laboratory of the biometallurgical group of the Chemical Engineering Department of the University of Chile, Santiago de Chile. The samples were analyzed for total number of cells (direct microscopic counting; Phyroff-Hauser counting chamber), *Thiobacillus ferrooxidans* cultivation (plate counting), and oxidizing activity (Fe(II) oxidation rate).

CHAPTER 2

2 Basic concepts in environmental geochemistry of sulfide mine-waste

2.1 Mining and the environment

As minerals, which are essential to industrial economies, are presently not in short supply, nor do they seem to be for the next several generations, mining and mineral processing can no longer be presumed to be the best of all possible uses for land; it must compete with compelling demands for alternative uses. Environmental protection and rehabilitation are fast becoming high priorities throughout the world, no longer confined to industrialized countries. Environmental regulations in the developed countries are one of the main reasons for the departure of metal mining companies to less developed nations in the last few decades. Low labor costs, exploration potential, and lax or no existing environmental policies, reinforced this process (Hodges, 1995). While industrialized countries started to formulate environmental reports and to implement environmental framework laws in the 1970's (e.g., USA, Central Europe, Japan), developing countries started this process only recently in the 1990's (e.g., Chile, Peru, Korea, Nigeria), as reported in Jänicke and Weidner (1997). A main task for the future will be to build a body of local experts in these countries, which will be able to implement the environmental laws. Increasing world population together with economic growth in developing countries will increase the demand for minerals in the near future and the associated environmental assessment.

2.2 Mining and extraction processes

Once the exploration of an ore body is successful, exploitation begins. The extraction of the ore can take place in an open pit or underground. The ore is then transported to stockpiles or directly to the milling process, where crushing and grinding decrease the grain size for the benefaction process. The ore grinding must be optimized with respect to the leaching, roast-leaching, or possible benefaction circuits as tabling, flotation, high intensity magnetic separation, heavy media, and others. Liberation of the mineral by the process is governed by the grain size and the mineral complexity of the ore (e.g., Ritcey, 1989).

Flotation is the only concentration process used to generate the mine tailings impoundments studied in the present work. Flotation circuits are systems of cells and auxiliary equipment arranged to yield optimal results from an ore in creating a concentrate following grinding and reagent treatment (Fig. 2). Froth flotation involves the aggregation of air bubbles and mineral particles in an aqueous medium with subsequent levitation of the aggregates to the surface and transfer to a froth phase. Whether or not bubble attachment and aggregation occur is determined by the degree to which a particle's surface is wetted by water. When a solid surface shows little affinity for water, the surface is said to be hydrophobic, and an air bubble will attach to the surface. Coal and molybdenite are the most important hydrophobic minerals. For sulfides except molybdenite, and possibly stibnite, as well as non-sulfide minerals, the surface condition required for flotation is obtained by specific reagents called collectors. Furthermore, complex

ores require a complex combination of conditioning, collecting, and depressing necessary for optimal mineral extraction (Weiss, 1985). After the extraction of the economically interesting minerals by flotation, the residual material (in copper mines typically 95-99% of the treated material) is transported in the form of a suspension to tailings impoundments for final deposition. In practice the recovery of sulfide minerals is less than 100%, and pyrite flotation is generally suppressed by lime addition, so the tailings resulting from sulfide ores contain certain percentage of sulfides, mostly pyrite.

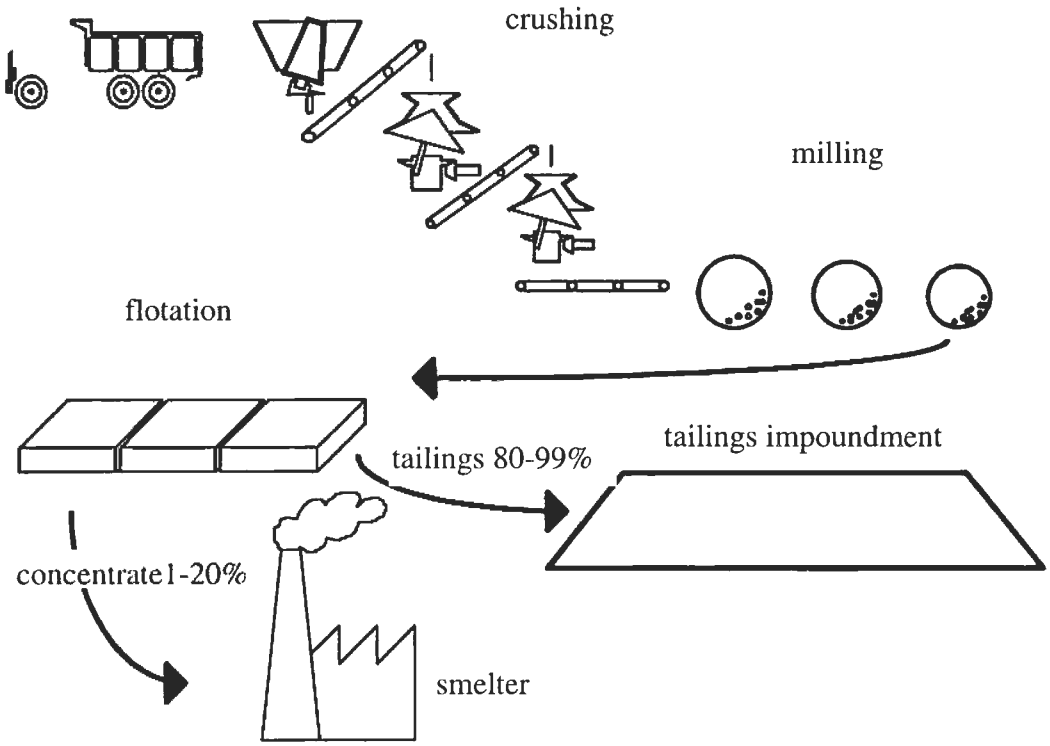

Fig. 2: The ore flow-path from the mine, through crushing and milling, to flotation. The concentrate is refined in the smelter, while the main part of the treated material will be deposited on the tailings impoundments. Tailings and concentrate proportions may differ from the given percentages.

2.3 Tailings impoundment design and deposition techniques

The most economic and most commonly used tailings deposition technique is wet deposition nearby the mine site. In this technique a water-sediment slurry is pumped in nearby topographic depressions, lakes or drainage basins (Robertson, 1994). Other techniques are a semi-dry subaerial method, thickened discharge, and deep-water disposal (Ritcey, 1989).

In countries with pronounced topography (e.g., Chile), most of the tailings impoundments are designed as valley dam impoundments. This type of design is provided by placing an embankment across the valley at the head end of drainage. The most common dam construction methods are the downstream and the upstream methods (Robertson 1984 and 1994). In the wet deposition method, the tailings slurry is thickened to 35-40% solids and discharged by either

point or line discharge. Often a discharge point is moved periodically. As a result of a periodical move of the discharge point and gravimetrical grain size separation occurring in the tailings, a general trend of coarser to finer grain size from the tailings discharge point to the pond can be observed (Fig. 3). Additionally, inhomogeneous layering of fine sand with silt and clay horizons makes the hydrological situation in the tailings material very complex. In general, it must be assumed that the coarser horizons are responsible for water permeability, and that they are connected aquifers. This should be taken into account in sampling and the calculation of permeability coefficients. As the horizons have thickness in the range of centimeters to decimeters, frequently, bulk samples lead to too low permeability coefficients.

In case of Chile, the combination of valley dam impoundments with high potential energy, the extremely high seismic activity, and the fact that this country is very rich in mining resources makes the stability of the tailings dam construction the largest apparent problem. In addition, as the tailings material is generally fine-grain sized material, it retains well moisture also in arid climates, and the process of liquefaction during seismic activity is a very important issue (Byrne, 1991 and 1997). In contrast, the geochemical instability of tailings and waste rocks in general is still not in the focus of interest and the present work is devoted to this aspect.

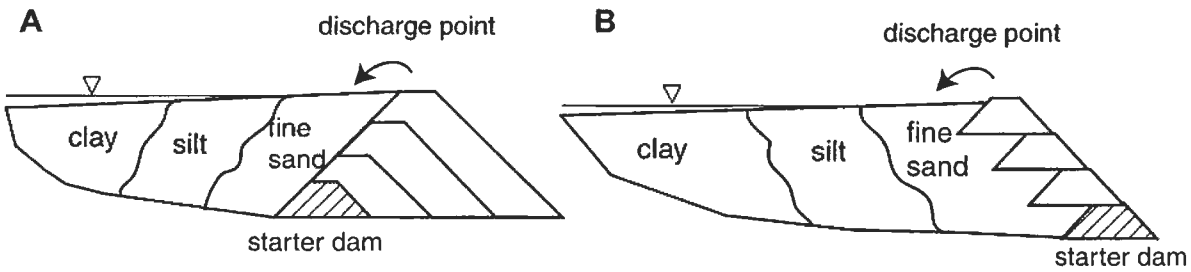

Fig. 3: Downstream (A) and upstream (B) deposition technique of tailings dam construction and the resulting grain-size separation.

2.4 Secondary processes in sulfide mine tailings - a review

2.4.1 Terminology

For the description of the tailings mineralogy the classification proposed by Jambor (1994) is used. The term "primary" is used to designate the complete ore mineralogy, i.e. "hypogene" and "supergene". "Secondary" minerals are minerals formed within the tailings impoundment as the products of weathering processes. "Tertiary" minerals form after the sample has been removed from the tailings environment.

2.4.2 *Sulfide oxidation in mine tailings*

The problem of sulfide oxidation (mainly pyrite oxidation) and the associated acid mine drainage (AMD), or more generally acid rock drainage (ARD), as well as the solution and precipitation processes of metals and minerals, has been a major focus of investigation over the last 40 years (Sato, 1960; Bryner et al., 1967; Nordstrom, 1977 and 1982; Nordstrom et al., 1979; Ritcey, 1989; Jambor and Blowes, 1994; Alpers and Blowes, 1994; Morin and Hutt, 1997; Jambor and Blowes, 1998; Nordstrom and Alpers, 1999). There has been less interest in the mineralogical and geochemical interactions taking place within the tailings itself (Jambor, 1994), yet this is an essential aspect to understand the parameters controlling acid mine drainage formation and to develop effective prevention methods. The primary mineralogical composition has possibly a strong, but at the moment poorly understood, influence on the oxidation processes. This has been best illustrated by Rimstidt et al. (1994) showing that reaction rates display significant differences depending on the sulfides being oxidized by Fe(III). Kinetic-type weathering experiments indicate the importance of trace element composition in the stability of individual sulfides. Where different sulfides are in contact with each other, electrochemical processes are likely to occur and influence the reactivity of sulfides (Kwong, 1993).

Most mining operations are surrounded by piles of impoundments containing pulverized material or waste from the benefaction process, which are known as tailings, stockpiles. Waste rock dumps contain generally material with low ore grade, which is mined but not milled. These materials commonly contain large concentrations of sulfide minerals, which may undergo oxidation, producing a major source of metal and acid contamination. The complex microbiological, hydrological, mineralogical, and geochemical post-depositional processes and their coupled interaction in mine waste environment are not yet completely understood. In the following section the focus is on the acid producing sulfide minerals, other acid producing processes, and the acid neutralizing processes.

2.4.2.1 *Acid producing sulfide minerals*

2.4.2.1.1 Pyrite (FeS_2)

The most common sulfide mineral is pyrite (FeS_2). Oxidation of pyrite takes place in several steps including the formation of the metastable secondary products ferryhydrite ($5Fe_2O_3 \cdot 9H_2O$), schwertmannite (between $Fe_8O_8(OH)_6SO_4$ and $Fe_{16}O_{16}(OH)_{10}(SO_4)_3$), and goethite (FeO(OH)), as well the more stable secondary jarosite ($KFe_3(SO_4)_2(OH)_6$), and hematite (Fe_2O_3) depending on the geochemical conditions (Nordstrom, 1979 and 1982; Sato, 1992; Jambor, 1994; Bigham, 1994; Bigham et al., 1996; Schwertmann et al., 1995; Kesler, 1997; Nordstrom and Alpers, 1999). Oxidation of pyrite may be considered to take place in three major steps: (1) oxidation of sulfur (equation 1); (2) oxidation of ferrous iron (equation 2); and (3) hydrolysis and precipitation of ferric complexes and minerals (equation 4). The kinetics of each reaction are different and depend on the conditions prevailing in the tailings.

$$FeS_2 + {}^7/_2O_2 + H_2O \rightarrow FeSO_4 + SO_4^{2-} + 2H^+ \quad (1)$$

$$Fe^{2+} + {}^1/_4O_2 + H^+ \Leftrightarrow Fe^{3+} + H_2O \quad (2)$$

reaction rates strongly increased by
microbial activity (e.g.,*Thiobacillus ferrooxidans*)

$$FeS_2 + 14\,Fe^{3+} + 8H_2O \rightarrow 15\,Fe^{2+} + 2SO_4^{2-} + 16H^+ \quad (3)$$

Equation (1) describes the initial step of pyrite oxidation in the presence of atmospheric oxygen. Once ferric iron is produced by oxidation of ferrous iron, oxidation which may be, especially at low pH conditions, strongly accelerated by microbiological activity (equation 2), ferric iron will be the primary oxidant (equation 3) of pyrite (Nordstrom, 1979; Moses et al., 1987; Ehrlich, 1996). Under abiotic conditions the rate of oxidation of pyrite by ferric iron is controlled by the rate of oxidation of ferrous iron, which decreases rapidly with decreasing pH. Below about pH 3 the oxidation of pyrite by ferric iron is about ten to a hundred times faster than by oxygen (Ritchie, 1994).

It has been known for nearly 30 years that microorganisms like *Thiobacillus ferrooxidans* obtain energy by oxidizing Fe^{2+} to Fe^{3+} from sulfides by catalyzing this reaction (Bryner et al., 1967) and this may increase the rate of reaction (2) up to the factor 10^5 over abiotic oxidation (Singer and Stumm, 1970). More recent results suggest that a complex microorganism fauna is responsible for sulfide oxidation (Norris, 1989; Rossi, 1990; Gould et al., 1994; Ehrlich, 1996; Nordstrom & Southam, 1997; Blowes et al., 1998). Nordstrom and Southam (1997) states that the initiating step of pyrite oxidation does not require an elaborated sequence of different geochemical reactions that dominate at different pH ranges. *Thiobacillus spp.* form nanoenvironments (nanometer scale) to grow on sulfide mineral surfaces. These nanoenvironments can develop thin layers of acidic water that do not affect the bulk pH of the water chemistry. With progressive oxidation, the nanoenvironments may change to microenvironments (micrometer scale). Evidence of acidic microenvironments in the presence of near neutral pH for the bulk water can be inferred from the presence of jarosite (this mineral forms only under pH < 3) in certain soil horizons where the current water pH is neutral (Carson et al., 1982). Barker et al. (1998) observed microbial colonization of biotite and measured pH in microenvironments in the surroundings of living microcolonies. The solution pH decreased from near neutral at the mineral surface to 3-4 around microcolonies living within confined spaces at interior colonized cleavage planes.

When the acid mine water, rich in ferric iron, reaches the surface it will fully oxidize, hydrolyze and may precipitate to ferrihydrite (fh), schwertmannite (sh), goethite (gt), or jarosite (jt) depending on pH-Eh conditions (Fig. 4), and availability of key elements such as potassium and sulfur (Nordstrom et al., 1979; Bigham et al., 1996). Jarosite, schwertmannite and ferrihydrite are meta-stable with respect to goethite (Bigham et al., 1996).

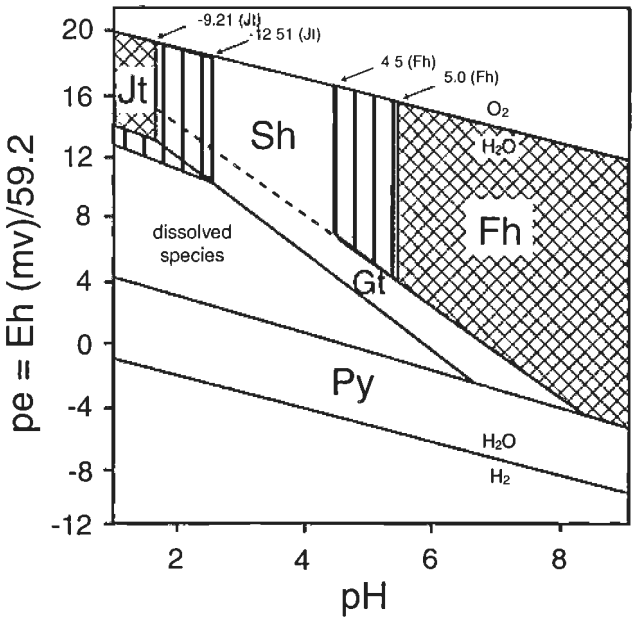

Fig. 4: pe-pH diagram for Fe-S-K-O-H system at 25°C where pe = Eh(mV)/59.2; total log activities of Fe^{2+} = -3.47; Fe^{3+} = 3.36 or –2.27; SO_4^{2-} = -2.32; K^+ = -3.78; log Kso values for solid phases for Gt = goethite, Jt = K-jarosite, Fh = ferrihydrite, Sh = schwertmannite are 1.40, -12.51, 5.0 and 18.0, respectively. Py = pyrite. Line equations are: Gt (pe = 19.22-2.6 pH); Jt (pe = 16.21-2 pH); Fh (pe = 21.50-3 pH); Sh (pe 19.22-2.6 pH), and Py (pe = 5.39-1.14 pH). Fields of metastability are shown by dashed lines. Single-hatched areas demonstrate expansion of K-jarosite and ferrihydrite fields if lower Kso's are selected. Mean composition of the schwertmannites used for the development of this pe-pH diagram was $Fe_8O_8(OH)_{4.8}(SO_4)_{1.6}$. From Bigham et al. (1996).

The hydrolysis and precipitation of iron hydroxides (and to a lesser degree, jarosite) will produce most of the acid in this process. If pH is less than about 3.5, $Fe(OH)_3$ is not stable and Fe^{3+} remains in solution:

$$Fe^{3+} + 3\ H_2O \quad \Leftrightarrow \quad Fe(OH)_{3(s)} \quad + 3H^+ \qquad (4)$$

Note that the net reaction of complete oxidation of pyrite, hydrolysis of Fe^{3+} and precipitation of iron hydroxide (sum of reactions 1, 2 and 4) produces $4H^+$ per mol of pyrite (in case of $Fe(OH)_3$ formation, see equation 5, i.e., pyrite oxidation is the most efficient producer of acid of the common sulfide minerals (net reaction 5; Table 2). Nevertheless, it is important to be aware that the hydrolysis of $Fe(OH)_3$ is the main acid producer ($^3/_4$ of H^+ per mol pyrite). Acid production via hydrolysis will be discussed in chapter 7.

$$FeS_2 + {}^{15}/_4O_2 + {}^7/_2H_2O \rightarrow \quad Fe(OH)_3 + 2SO_4^{2-} + 4H^+ \qquad (5)$$

Evangelou and Zhang (1995) reported increased oxidation rates of pyrite by addition of HCO_3^- due to the formation of pyrite surface Fe(II)-CO_3 complexes. This means that the frequent applied limestone treatment for mine waste management must be discussed critically,

because if it is able to neutralize the acid produced, it can also increase the kinetic of pyrite oxidation.

Marcasite, the orthorhombic dimorph of pyrite, may also abundantly occur as a primary mineral in sulfidic tailings, mainly from sediment-hosted base metal deposits and as primary alteration product of pyrrhotite. Marcasite has the same formula as pyrite and leads to the same amount of acid production via oxidation. Direct observation (e.g. the Zn-Pb deposit of Reocín, Spain) suggest that its oxidation kinetics should be faster than that of pyrite, perhaps as a result of its typical twinned morphology and finer grain size, which offers more surface to oxidation than pyrite. In the tailings studied in the present work, marcasite was not identified. Additional, Jambor (1994) reports the presence of marcasite as a secondary alteration product of pyrrhotite in zonal patterns in oxidizing mine tailings.

2.4.2.1.2 Pyrrhotite($Fe_{(1-x)}S$)

Wastes from sulfide ores often contain pyrrhotite associated with pyrite. The general formula of pyrrhotite is $Fe_{(1-x)}S$, where x can vary from 0.125 (Fe_7S_8) to 0.0 (FeS, troilite). The oxidation rates and weathering products of pyrite are well known, but only a few investigations have focused the oxidation of pyrrhotite. Nicholson and Scharer (1994) propose for the oxidation of pyrrhotite the following equation:

$$Fe_{(1-x)}S + (2-x/2)O_2 + xH_2O \rightarrow (1-x)Fe^{2+} + SO_4^{2-} + 2xH^+ \qquad (6)$$

in which the stoichiometry of the pyrrhotite affects the relative production of acid. At one extreme, if x = 0 and the formula is FeS, no H+ will be produced in the oxidation reaction; at the other extreme, the maximum amount of acid will be produced by the iron-deficient Fe_7S_8 phase. The main part of acid is produced by the oxidation of ferrous iron (equation 2) and the subsequent hydrolysis of ferric hydroxides (equation 4). In conclusion, the role of pyrrhotite in the acidifying process is similar to that of pyrite, but it is very important at early weathering stages because its oxidation rate is 20 to 100 times higher than that of pyrite in atmospheric concentrations of O_2 and at 22°C (Nicholson and Scharer, 1994).

The oxidation of pyrrhotite can also involve the formation of elemental sulfur (Ahonen and Tuovinen, 1994), marcasite (Jambor, 1994), or the formation of pyrite (Burns and Fischer, 1990). They are acid-consuming reactions.

2.4.2.1.3 Chalcopyrite ($CuFeS_2$)

Complete oxidation of chalcopyrite may be written as:

$$2CuFeS_2 + 4O_2 \rightarrow 2Cu^{2+} + Fe^{2+} + SO_4^{2-} \qquad (7)$$

without acid production (Walder and Schuster, 1998). Nevertheless, the combination of ferrous iron oxidation and ferrihydrate hydrolysis will be again the main acid producing process.

$$2CuFeS_2 + 17/2O_2 + 5\ H_2O \rightarrow 2Cu^{2+} + 2Fe(OH)_3 + 4SO_4^{2-} + 4H^+ \qquad (8)$$

Chalcopyrite, together with molybdenite, is known as one of the most resistant sulfides to oxidation (Plumlee, 1999). Rimstidt et al. (1994) reported that the oxidation rate of chalcopyrite increases with increasing ferric iron concentration, but with an oxidation rate of 1-2 orders of magnitude less than pyrite.

2.4.2.1.4 Arsenopyrite (FeAsS)

Arsenopyrite (FeAsS) may be oxidized by the following reaction path (Mok and Wai, 1994):

$$4FeAsS + 13O_2 + 6H_2O \rightarrow 4Fe^{2+} + 4SO_4^{2-} + 4H_2AsO_4^- + 4H^+ \qquad (9)$$

Combined with ferrous iron oxidation and ferrihydrate precipitation, the overall arsenopyrite oxidation reaction can be written as follow:

$$FeAsS + {}^7/_2O_2 + 6H_2O \rightarrow Fe(OH)_3 + SO_4^{2-} + H_2AsO_4^- + 3H^+ \qquad (10)$$

If ferric iron is the oxidant, the oxidation rate of arsenopyrite is similar to the oxidation rate of pyrite. If it is oxygen, the oxidation rate of arsenopyrite is somewhat lower than that of pyrite (Mok and Wai, 1994).

Table 2: *Hydrogen ions per mole produced by oxidation via O_2 of some frequent minerals in mine tailings (Walder and Schuster, 1998; Plumlee, 1999) and some laboratory reaction rate data from Rimstidt et al. (1994). However, Jambor (1994) suggested the relative resistance of sulfide in oxidizing tailings environment to follow the increasing order pyrrhotite → sphalerite-galena → pyrite-arsenopyrite → chalcopyrite → magnetite:*

Mineral	Mole H^+/Mole Mineral	Relative wt % H^+/Mole mineral	Reaction with Fe(III)[1)]
Pyrite	4	0.03	2.7×10^{-7}
Marcasite	4	0.03	1.5×10^{-7}
Arsenopyrite	2	0.018	1.7×10^{-6}
Chalcopyrite	2	0.011	9.6×10^{-9}
Pyrrhotite	2-0	0.022	-
Enargite	1	0.002	-

[1)] $m_{Fe^{3+}} = 10^{-3}$ and pH = 2.5 at 25°C; mol $m^{-2}s^{-1}$; - = not studied by Rimstidt et al. (1994)

2.4.2.2 *Non-acid producing sulfide minerals*

2.4.2.2.1 Sphalerite (ZnS) and galena (PbS)

Sphalerite and galena are the most important base metal bearing minerals. Though Zn is toxic only at very high concentrations, sphalerite may contain environmentally dangerous amounts of Cd and Thallium (Tl). In addition, Fe may significally substitute for Zn, in cases up to 15 mole %, in sphalerite. If iron substitutes for zinc, sphalerite will be an acid generator in a similar way as pyrrhotite (Walder and Schuster, 1998), due to hydrolysis of ferric phases. Galena is the main source of Pb contamination in mine areas. The common result of the wet oxidation of sphalerite is a leach rich in dissolved Zn, and sulfate, with variable Cd amounts, while that of galena is secondary anglesite ($PbSO_4$) in equilibrium with a Pb^{2+} and SO_4^{2-} solution according to the following equations:

$$ZnS + 2O_2 \rightarrow Zn^{2+} + SO_4^{2-} \quad (11)$$

$$PbS + 2O_2 \rightarrow Pb^{2+} + SO_4^{2-} \quad (12)$$

Secondary anglesite coating on galena may increase the apparent resistance because anglesite has a low solubility and protects the sulfides from direct contact with oxidizing reagents (Jambor and Blowes, 1998). The oxidation process does not give rise to acidity when oxidation from O_2 is considered, as it is also in case of the Cu-sulfide minerals covellite, chalcocite, digenite and djurleite which may occur as hypogene, supergene, as well as secondary phases. In the presence of Fe^{3+}, the oxidation of MeS (where Me = divalent metal) produces acidity according to reaction schemes where part of the oxidation capacity of the system is derived from Fe^{3+} as, e.g.

$$2MeS + 4Fe^{3+} + 3O_2 + 2H_2O \rightarrow 2Me^{2+} + 4Fe^{2+} + 2SO_4^{2-} + 4H^+ \quad (13)$$

Plumlee (1999) pointed out that the oxidation of sulfide minerals by aqueous ferric iron generates significantly greater quantities of acid than the oxidation by oxygen (e.g., equation 3 and 13). This is correct in the case that ferric iron is added to the system (e.g., in form of primary ferric minerals). However, if we consider that the ferric iron is produced by the oxidation from ferrous iron in the system (e.g., microbiologically catalyzed pyrite oxidation), for every mole of ferric iron produced one mole of protons is consumed (equation 2). This leads to the same overall produced quantity of two protons per mole pyrite oxidized as in case of pyrite oxidation via O_2 (compare equations 1, 2, and 3). Additionally, in case of oxidation via ferric iron no acidity can be produced via the hydrolysis of the ferric phases, the main acid producing process in sulfide oxidation (see equation 4 this chapter and chapter 7). Thus, the sulfide oxidation by ferric iron has faster kinetics and is able to oxidize sulfide minerals in the absence of oxygen, but it does not produce more acid as the oxidation via oxygen.

Table 2 shows a summary of the hydrogen ions produced by some common sulfide minerals by the oxidation via O_2. There are important differences and therefore exact knowledge

of the sulfide minerals contained in waste rocks or tailings is crucial for adequate acid-base accounting (ABA).

2.4.2.3 *Secondary Fe(III) hydroxides, oxyhydroxides, and oxyhydroxide sulfates*

As explained in 2.4.1, the acid production processes can be split into two parts. The first is the oxidation of sulfide minerals by oxygen and ferric iron. The second is the hydrolysis of Fe(III) and subsequent precipitation of ferric oxyhydroxides or oxyhydroxide sulfates.

The process of hydrolysis of Fe(III) has been reviewed by Sylva (1972), Flynn (1984), Schneider and Schwyn (1987), Stumm and Morgan (1996), and Cornell and Schwertmann (1996). Metal ions undergo hydrolysis because coordinated water is a stronger acid than free water. This results from the effect that the metal-oxygen bond weakens the O-H bonds in a way that in aqueous systems the free water molecules behave as proton acceptors. So the hydrolysis of metal ions is the result of the deprotonation of the coordinated water molecules (Sylva, 1972).

The hydrolysis, i.e. deprotonation of Fe(III), starts with the hexa-aquo ion (Fe(III) is hydrated by 6 water molecules), except at very low pH, where Fe^{3+} is stable. Initially, low molecular weight species such as $Fe(OH)^{2+}$ and $Fe(OH)_2^{1+}$ form rapidly. The following dissolved species will be stable depending on pH (see also Fig. 6 and Table 3): Fe^{3+}, $Fe(OH)^{2+}$, $Fe(OH)_2^{1+}$, $Fe(OH)_{3\,(aq)}$, $Fe(OH)_4^-$, $Fe_2(OH)_2^{4+}$, and $Fe_3(OH)_4^{5+}$ (Stumm and Morgan, 1996). By "aging" increasingly complex polymers, Fe(III) oxides, oxyhydroxides, or oxyhydroxide sulfates are formed.

Table 3: *Hydrolysis reactions of Fe(III) species and the associated protons produced (from Stumm and Morgan, 1996).*

Species	Equation	Fe^{3+}	H^+	log *K* (I = 3 M)
Fe^{3+}		1	0	0
$Fe(OH)^{2+}$	$Fe^{3+} + H_2O \Leftrightarrow Fe(OH)^{2+} + H^+$	1	-1	-3.05
$Fe(OH)_2^+$	$Fe^{3+} + 2H_2O \Leftrightarrow Fe(OH)_2^+ + 2H^+$	1	-2	-6.31
$Fe(OH)_{3\,(aq)}$	$Fe^{3+} + 3H_2O \Leftrightarrow Fe(OH)_{3\,(aq)} + 3H^+$	1	-3	-13.8
$Fe(OH)_4^-$	$Fe^{3+} + 4H_2O \Leftrightarrow Fe(OH)_4^- + 4H^+$	1	-4	-22.7
$Fe_2(OH)_2^{4+}$	$2Fe^{3+} + 2H_2O \Leftrightarrow Fe_2(OH)_2^{4+} + 2H^+$	2	-2	-2.91
$Fe_3(OH)_4^{5+}$	$3Fe^{3+} + 4H_2O \Leftrightarrow Fe_3(OH)_4^{5+} + 4H^+$	3	-4	-5.77

Depending on the secondary phases precipitated, considerably different amounts of protons are produced. This will be discussed in chapter 7.

2.4.3 *Neutralization Processes*

The acid produced in the processes presented in chapters 2.4.2.1 and 2.4.2.3 may result in pH in the range of 1.5 – 4 in mine tailings. This acid together with Fe(III), are able to dissolve minerals and mobilize elements in the tailings (Al et al., 1994; Dold et al., 1997). In their

pathway, the acid produced and the elements mobilized react with acid-neutralizing minerals such as carbonates or silicates. Acid-neutralizing reactions result in an increase in the pore-water pH. This increase in pH is frequently accompanied by precipitation of metal-bearing oxyhydroxide and oxyhydroxide sulfate minerals that remove dissolved metals from the water migrating within the tailing pores. These secondary minerals act in a certain pH range as buffers so that a sequence of pH buffering reactions can be observed in the tailings environment (Blowes and Ptacek, 1994).

2.4.3.1 Carbonates

Dissolution of carbonates releases alkaline earth and metal cations, including Ca, Mg, Fe, and Mn. These cations participate in the formation of secondary solids, including simple hydroxide solids, which in some cases can later dissolve and contribute to acid neutralization. The ability of carbonates to neutralize acid by fast reaction makes them an important part of the mineralogical assemblage for ARD prediction and prevention.

2.4.3.1.1 Calcite ($CaCO_3$)

Calcite is the most common carbonate mineral and the fastest reacting. Its solubility depends on the proton concentration as shown in the following equations:

$$CaCO_3 + H^+ \Leftrightarrow Ca^{2+} + HCO_3^- \quad (14)$$

This reaction will buffer at near neutral pH (6.5 - 7), while in more acidic environments the following equation can be written:

$$CaCO_3 + 2H^+ \Leftrightarrow Ca^{2+} + CO_2 + H_2O \quad (15)$$

Carbonate speciation is pH dependent (Fig. 5) and the dissolution of calcite increases the amount of carbonate in solution, increasing therefore the neutralization potential of the solution. It is important to mention that calcite buffers the pH to neutral values and at pH 7 HCO_3^- is the dominant specie (Fig. 5). Thus, for the neutralization of 1 mol H^+ 1 mol calcite is necessary as shown in equation (14). Most acid-base accounting procedures (ABA) assume that H_2CO_3 is the dominant specie. This is the case at lower pH and doubles the buffer capacity of calcite (equation 15), what may lead to an overestimation of the neutralization potential at neutral pH. When neutralization proceeds and pH increases, calcite may precipitate as a secondary mineral.

2.4.3.1.2 Siderite ($FeCO_3$)

Siderite may act under certain conditions as a neutralizer, and under other conditions as an acid producer. The following dissolution reaction may take place (Walder and Schuster, 1998):

$$FeCO_3 + H^+ \Leftrightarrow Fe^{2+} + HCO_3^- \quad (16)$$

Combined with ferrous iron oxidation and ferrihydrate precipitation, the overall siderite oxidation reaction is:

$$4FeCO_3 + O_2 + 10H_2O \Leftrightarrow 4HCO_3^- + 4Fe(OH)_3 + 4H^+ \quad (17)$$

This indicates that under elevated pH, where bicarbonate is stable, the total reaction from dissolution of siderite to the precipitation of ferrihydrate gives a net acid production of one mole hydrogen ion per mol siderite dissolved. However, under more acidic conditions, where carbonic acid is stable, there will be no net acid production (Walder and Schuster, 1998).

If ferrous iron is present in a solution containing bicarbonate, the formation of siderite may occur by the following reaction:

$$Fe^{2+} + HCO_3^- \Leftrightarrow FeCO_3 + H^+ \quad (18)$$

This reaction buffers the pH at around 5 - 5.5. This reaction path may be an alternative to ferrous to ferric iron oxidation and the consecutive precipitation of Fe(III)oxyhydroxides. Geochemical studies by several authors have shown that in tailing impoundmends and AMD affected aquifers the waters are frequently close to saturation or even oversaturated with respect to siderite (Morin and Cherry, 1986; Blowes et al., 1991; Blowes and Ptacek, 1994).

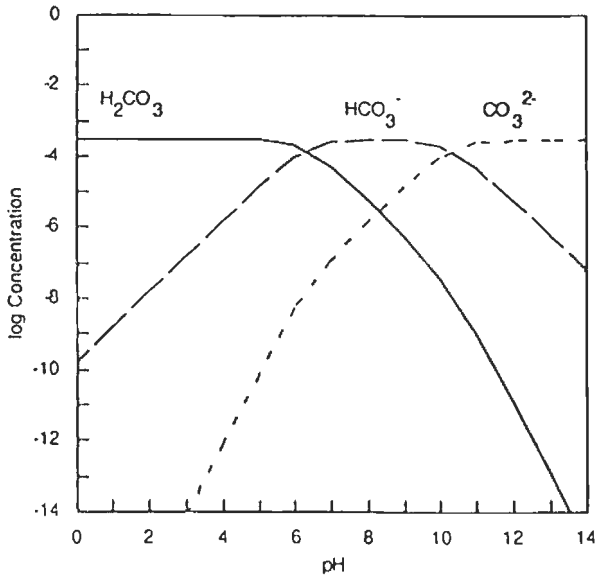

Fig. 5: Distribution of solute species in the aqueous carbonate system. Log concentration vs. pH for $10^{-3.5}$ M solution of dissolved CO_2 in closed system (Thomson, 1998).

2.4.3.1.3 Lime ($Ca(OH)_2$)

Lime is a common agent in the flotation circuit to depress the flotation of pyrite by the increase of the pH to 10.5.

$$Ca(OH)_2 + 2H^+ \Leftrightarrow Ca^{2+} + 2H_2O \quad (19)$$

$$Ca(OH)_2 \Leftrightarrow Ca^{2+} + 2OH^- \quad (20)$$

Lime has high solubility in water and may be washed out. In this case, the role in neutralizing the acid produced in the tailings may be minor.

2.4.3.2 Metal hydroxides dissolution

As a result of neutralization and pH increase, the precipitation of metal hydroxides or hydroxide sulfates is favored, as gibbsite, amorphous $Al(OH)_3$, amorphous $Fe(OH)_3$, ferrihydrite, goethite, or schwertmannite. Some of the reactions can be described as follows:

$$Al(OH)_3 + 3H^+ \Leftrightarrow Al^{3+} + 3H_2O \quad \text{this reaction buffers the pH to 4.0 - 4.3} \quad (21)$$

$$Fe(OH)_{3(s)} + 3H^+ \Leftrightarrow Fe^{3+} + 3H_2O \quad \text{this reaction buffers the pH to below 3.5} \quad (22)$$

$$FeO(OH)_{(s)} + 3H^+ \Leftrightarrow Fe^{3+} + 3H_2O \quad \text{this reaction buffers the pH to below 3.5} \quad (23)$$

These reactions complement an ideal neutralization sequence which starts with calcite (pH 6.5 - 7.5) followed by siderite (pH 5.0 - 5.5). When all carbonates are consumed the next neutralizer is gibbsite (pH 4.0 - 4.3), followed by Fe(III)hydroxides as goethite (pH below 3.5). This leads to a typical pH profile as shown in Fig. 6.

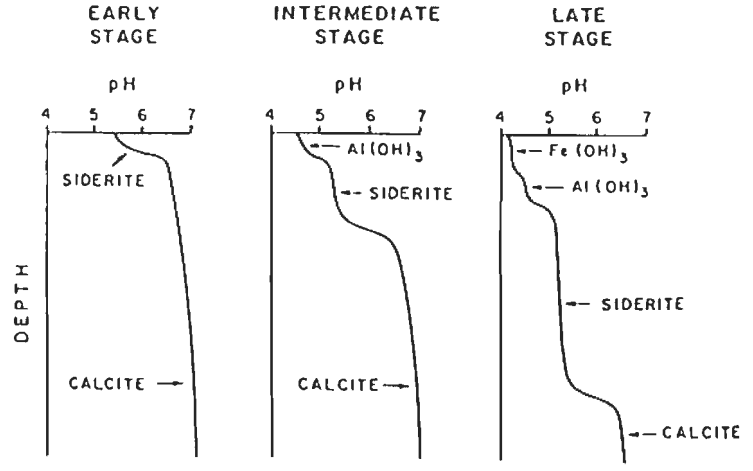

Fig. 6: *Development of pH buffering zones during early, intermediate, and late stages of sulfide oxidation in tailings impoundments (from Blowes and Ptacek, 1994).*

2.4.3.3 Silicates

Dissolution of most aluminosilicate minerals also consumes H^+ ions and contribute base cations (Ca, Mg, Fe(II)), alkali elements (Na, K) and dissolved Si and Al to the tailing pore water (Blowes and Ptacek, 1994). Though, dissolution of aluminosilicate minerals is slower than of metal hydroxides and much slower than that of carbonates. Feldspar weathering is mainly controlled by pH, silica, Na, K, and Ca concentrations. One possible reactions path is:

K-feldspar -> kaolinite -> gibbsite

Reactions 24 and 25 illustrate this path.

$$2KAlSiO_3O_8 + 9H_2O + 2H^+ \rightarrow Al_2Si_2O_5(OH)_4 + 2K^+ + 4H_4SiO_4 \quad (24)$$
K-feldspar kaolinite

In this reaction, K and Si enter the solution, while protons are consumed. The solubility of feldspar increases when proton activity increases or the removal of K or Si is fast, e.g. by secondary mineral formation. Secondary kaolinite may dissolve to form gibbsite, a reaction that does not neutralize acid:

$$AlSi_2O_5(OH)_4 + 5H_2O \rightarrow 2Al(OH)_3 + 2H_4SiO_4 \quad (25)$$
kaolinite gibbsite

Higher pH and K concentrations can lead theoretically to sericite formation instead of kaolinite as secondary mineral of feldspar weathering:

$$3KAlSiO_3O_8 + 12H_2O + 2H^+ \rightarrow KAl_2(AlSi_3O_{10})(OH)_2 + 2K^+ + 6H_4SiO_4 \quad (26)$$
K-feldspar sericite

and sericite reacts forming gibbsite:

$$KAl_2(AlSi_3O_{10})(OH)_2 + 9H_2O + H^+ \rightarrow 2Al(OH)_3 + 3H_4SiO_4 + K^+ \quad (27)$$
sericite gibbsite

However, these reactions have to be seen as a strong simplification of the very complex clay mineral group and their formation processes. In the case of plagioclase, the weathering path is similar to that of K-feldspar and is accompanied by the release of sodium and/or calcium. Under low pH conditions plagioclase will react to form kaolinite, while under higher pH smectite will be formed (Walder and Schuster, 1998).

Nesbitt and Jambor (1998) have shown the fundamental role of mafic minerals in neutralization of the Waite-Amulet tailings. As in the weathering of feldspar, the weathering of felsic minerals leads to the formation of clay minerals. Muscovite, pyroxene, and amphibole alter to chlorite. By decreasing pH, chlorite alters to sericite, kaolinite or Mg-montmorillonite. The products of biotite alteration are hydrobiotite, a regularly interstratified biotite-vermiculite phase, vermiculite, and kaolinite (Acker and Bricker, 1992; Malmström and Banwart, 1997). Direct conversion of biotite to kaolinite has also been described (e.g., Acker and Bricker, 1992). The alteration from biotite to vermiculite may be written as:

$$3K_2(Mg_3Fe_3)Al_2Si_6O_{20})(OH)_4 + 5H_2O + 12H_2CO_3 + 6H^+ + 3/2\ O_2 \rightarrow$$
$$2[(Mg_3Fe_3)\ Al_3Si_5O_{20}(OH)_4 \cdot 8\ H_2O] + 6K^+ + 3Mg^{2+} + 3Fe^{2+} + 8SiO_2 + 12HCO_3^- \qquad (28)$$

Malmström and Banwart (1997) studied the pH dependence of dissolution rate and stoichiometry of biotite at 25°C. They found that the release of the interlayer K is relatively fast and becomes diffusion controlled within a few days. The release of framework ions (Mg, Al, Fe, Si) is much slower. Strömberg and Banwart (1994) suggested that, in the absence of carbonates, primary minerals, particularly biotite, provide the major sink for acidity in drainage from mine waste rock (see equation 28).

Table 4: Acid-neutralization capacity of minerals (in Jambor and Blowes, 1998, after Sverdrup, 1990).

Group	Typical Minerals	Relative Reactivity (pH5)
1. Dissolving	calcite, dolomite, magnesite, aragonite, brucite	1.0
2. Fast weathering	anorthite, olivine, garnet, diopside, wollastonite, jadeite, nepheline, leucite, spodumene	0.6
3.Intermediate weathering	enstatite, augite, hornblende, tremolite, actinolite, biotite, chlorite, serpentine, talc, epidote, zoisite, hedenbergite, glaucophane, anthophyllite	0.4
4. Slow weathering	plagioclase (Ab_{100}-Ab_{30}), kaolinite, vermiculite, montmorillonite, gibbsite	0.02
5. Very slow weathering	K-feldspar, muscovite	0.01
6. Inert	quartz, rutile, zircon	0.004

2.4.4 Dissolution

Dissolution is mainly controlled by surface complexation of protons or organic ligands such as the organic acids acetate, oxalate, or citrate. Organic acids are widely used in studies of dissolution kinetics and the solubility of secondary oxides and hydroxides, especially in soil

science and acid mine drainage (Schwertmann, 1964; Bigham et al., 1990 and 1996; Cornell and Schwertmann, 1996). For example, the dissolution rates of Fe(III)hydroxides by oxalate (Fig. 7) are increased photochemically (Schwertmann 1964), by higher acidity and temperature, and by the presence of Fe(II) in the system (Suter et al., 1988). Reduction also increases dissolution kinetics because Fe(II) has a greater atomic radius (0.76 Å) than Fe(III) (0.64 Å), so Fe(II) does not fit any more in the crystalline system of the ferric minerals and the detachment of the ferrous ion is facilitated (Stumm and Sulzberger, 1992).

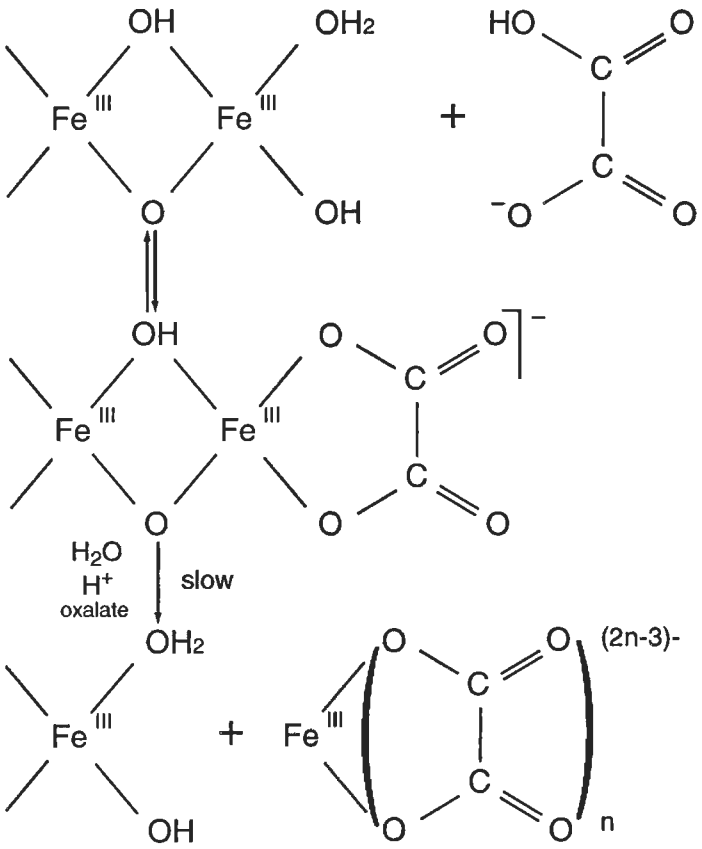

Fig. 7: Dissolution of Fe(III) hydroxide by bidentate chelate complex formation (e.g., oxalate). Dissolution is controlled by acidity, photochemical activity, temperature, and Fe(II) acts as a catalyst. Reduction additionally increases dissolution kinetics (after Stumm and Sulzberger, 1992).

2.4.4.1 Dissolution of iron sulfate minerals

Iron sulfate minerals are the most common secondary minerals found in the oxidizing environment of the mine waste, due to the wide distribution of pyrite and pyrrhotite as a sulfur source. They are also common in the oxidized portions of weathering zones from ore deposits (e.g., gossans). They may be composed of Fe(II), Fe(II) + Fe(III), or only Fe(III). Examples are melanterite, roemerite, and coquimbite, respectively. A detailed overview of these secondary minerals is given in Alpers et al. (1994) and Nordstrom and Alpers (1999). In general they have a high solubility, whereas supergene jarosite shows relatively low dissolution kinetics. Baron

and Palmer (1996) conducted a series of dissolution experiments with jarosite under 4-35°C and at pH values between 1.5 and 3. Equilibrium was established in the experiment after approximately 3 to 4 months.

An extended group of highly water-soluble sulfates, as for example gypsum or chalcanthite ($CuSO_4 \cdot 5H_2O$), formed under oxidizing conditions and high evaporation rates, can release significant amounts of metals and acid with rain. This mineral group is an important factor leading to seasonal fluctuations in contamination levels of ground and surface waters, especially in semi-arid and arid climates (Alpers et al., 1994).

2.4.5 Prediction - Acid-Base Accounting (ABA)

It has been shown in the above sections that there are minerals able of producing acid (Acid Potential - AP) and those which are able to neutralize acid (Neutralizing Potential - NP) in mine waste. Understanding the relative influence of these two parameters can lead to an estimation of the net acid-producing potential (NAPP) or net neutralizing potential (NNP). It is important to be able to predict if or if not a geological unit has the capacity of generating acid, and is a deciding factor for further treatment strategies of the material. Depending on the complexity of the mineral assemblage, it is a major task to understand all the interactions and processes taking place and to calculate the acid-base accounting (ABA). A review of the used static and kinetic test procedures is given in Morin and Hutt (1997). A simple ABA would be to measure the total sulfur and total carbon contents in a sample and assume that the total sulfur value represents the pyrite content and the total carbon the calcite content. More elaborated methods try to take into account the different sulfur-bearing phases and to record the complexity of the acid-neutralizing mineral assemblage.

In contrast, there is a need for simple and standardized tests to enable legislatory agencies to develop outlines for waste rock characterization. It is obvious that these tests cannot take into account the complexity of every specific mineral assemblage. The lack of accuracy of the ABA determination is in some environmental policies compensated by high security reserves in terms of high acid-neutralization /acid-production ratios. This may simplify the problem, but in cases may lead to unnecessary expenses (reaching up to several millions of US$) for treatments which could have been saved by an accurate ABA.

2.4.6 Mobility and sorption processes

The liberation of elements from minerals depends mainly on the solubility of minerals, which act as hosts of the metals or other elements. Once the element is liberated, its mobility is controlled by the complex-species stability at the existing pH, redox and other geochemical conditions, and the surface charge of the adsorbents, which is also pH dependent. The hydroxides and clay minerals are characterized by their small grain size and high surface area combined with a net surface charge; they are therefore effective adsorbents (Parks, 1990).

2.4.6.1 Complexation

Stumm and Morgan (1996) define complex formation as follows: Coordination or complex formation is referred to as any combination of cations with molecules or anions containing free pairs of electrons (bases). This combination can be electrostatic, covalent, or a mixture of both. The metal cation will be called the central atom, and the anions are ligands. Two type of complex species can be distinguished: the ion pairs and the complexes. Ions of opposite charge that approach within a critical distance effectively form an ion pair and are no longer electrostatically effective. In contrast, most stable entities that result from the formation of largely covalent bonds between a metal ion and an electron-donating ligand are called complexes.

2.4.6.2 Stability of complex species

Chemical speciation and species refer to the actual form in which a molecule or ion is present in solution. If a metal cation is liberated into solution it will be on the search for a partner. As a result, metal cations will tend to form in water aquo or hydroxo-complexes. This process is called hydrolysis and was discussed in the example of ferric hydroxide formation (2.4.2.3). Fig. 8 illustrates the predominant complex species of Fe(III) depending on the pH of the oxidation state of the central atom and of the solution.

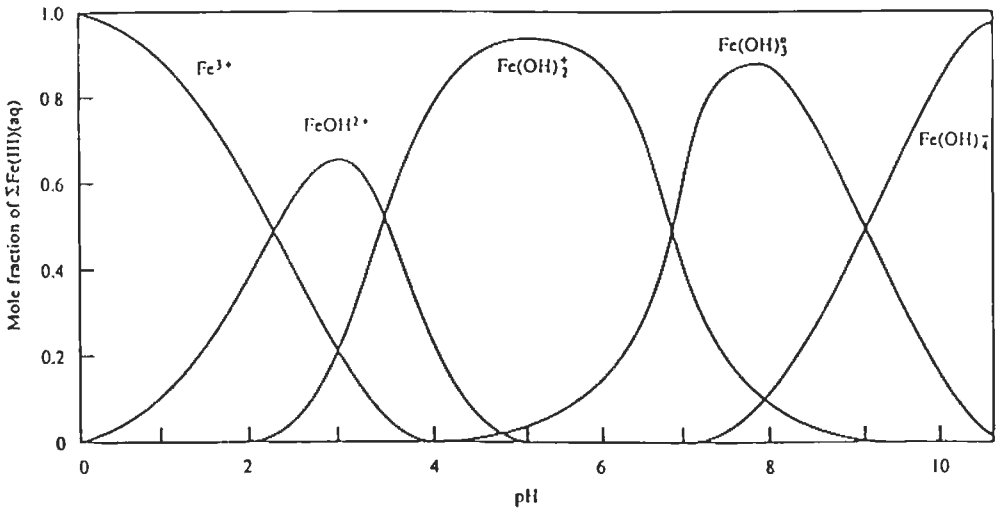

Fig. 8: Mole fraction of total dissolved Fe(III) present as Fe^{3+} and Fe(III)-OH complexes as a function of pH in pure water at 25°C (from Langmuir, 1997).

Equilibrium in hydrolysis reactions is usually established fast, as the hydrolysis species are simple. The "aging" of the solution and the associated formation of polynuclear complexes is a slower process and can be seen as the intermediate state to the solid precipitate. Hence, hydrolysis species are thermodynamically unstable or meta-stable (Stumm and Morgan, 1996).

Complexes with monodenate ligants are usually less stable than those with multidenate ligands. More important is the fact that the degree of complexation decreases more strongly with dilution for monodenate complexes than for multidenate complexes (chelates).

2.4.6.3 Redox reactions

The stability of species depends strongly on the reduction-oxidation (redox) reaction taking place between the ions. In a similar way that acids and bases are interpreted as proton donors and proton acceptors, reductants and oxidants are defined as electron donors and electron acceptors. Because there are no free electrons in nature, every oxidation is accompanied by a reduction, or in other words, an oxidant is a substance that causes oxidation to occur while being reduced itself.

$$O_2 + 4H^+ + 4e^- \Leftrightarrow 2H_2O \quad \text{reduction} \quad (29)$$

$$4Fe^{2+} \Leftrightarrow 4Fe^{3+} + 4e^- \quad \text{oxidation} \quad (30)$$

$$O_2 + 4Fe^{2+} + 4H^+ \Leftrightarrow 4Fe^{3+} + 2H_2O \quad \text{redox reaction} \quad (31)$$

The combination of redox condition (expressed as Eh or pe) and pH makes it possible to predict which species are dominant under the specific geochemical conditions. These stability fields are made visible in the Eh-pH diagrams largely used in geochemistry (e.g., Fig. 4 this chapter and Brookins, 1988).

2.4.6.4 Sorption

Sorption is a general name for adsorption, absorption, and ion exchange. Sorption also includes surface precipitation and element diffusion. The sorption processes take place at the mineral-water interface and are controlled by the reactivity of surface functional groups. Surface functional groups are the surface mineral atoms that may form chemical reactions with species in solution, forming mineral-species complexes.

Whether or not a mobilized element will be adsorbed depends on the redox conditions resulting from specific speciation of the metal complexes and on the pH dependent reactivity of the surface functional groups of the absorbent. Oxides, oxyhydroxides and silicates surfaces in contact with water typically are electrically charged because of ionization of the functional groups. The magnitude and sign of this surface charge vary with the solution pH (Parks, 1990).

Adsorption and absorption processes of metal ions on iron hydroxides, clay minerals, and calcite have been well investigated in laboratory research (Davis and Leckie, 1978; Leckie et al., 1980; Gerth and Brümmer, 1981 and 1983; Davis et al., 1987; Donnert et al., 1990; Dzomback and Morel, 1990; Hsia et al., 1992). Adsorption of metal ions on Fe(III)hydroxides is a function of pH, temperature, surface area of sorbent, dissolved metal concentrations, and reaction time

(Dzomback and Morel, 1990; Gerth and Brümmer, 1981; Stumm and Morgan, 1996). Long-term studies show that metal ions may be incorporated by diffusion into the crystalline systems of secondary ferric hydroxides (Gerth and Brümmer, 1983; Davis et al., 1986; Donnert et al., 1990). This process, where the adsorbate becomes incorporated in the crystal structure of the adsorbent, including the formation of solid solution by co-precipitation or solid-state diffusion, is referred to as absorption (Brown et al., 1995). Adsorption can be differentiated into two processes. First, the specific adsorption or chemosorption, where the sorption at the mineral-water interface may involve further reactions of some ions, results in the loss of one or more waters of hydration from the adsorbate ion and the formation of a relatively strong chemical bond between adsorbate and adsorbent (ligand exchange). The adsorbed species is refered to as an inner-sphere adsorption complex. A weaker interaction may occur between the hydrated ion and the mineral surface in which waters of hydration are retained (Fig. 9). Adsorption of this type is termed non-specific, and the adsorbed species is referred to as an outer-sphere adsorption complex (Brown et al., 1995).

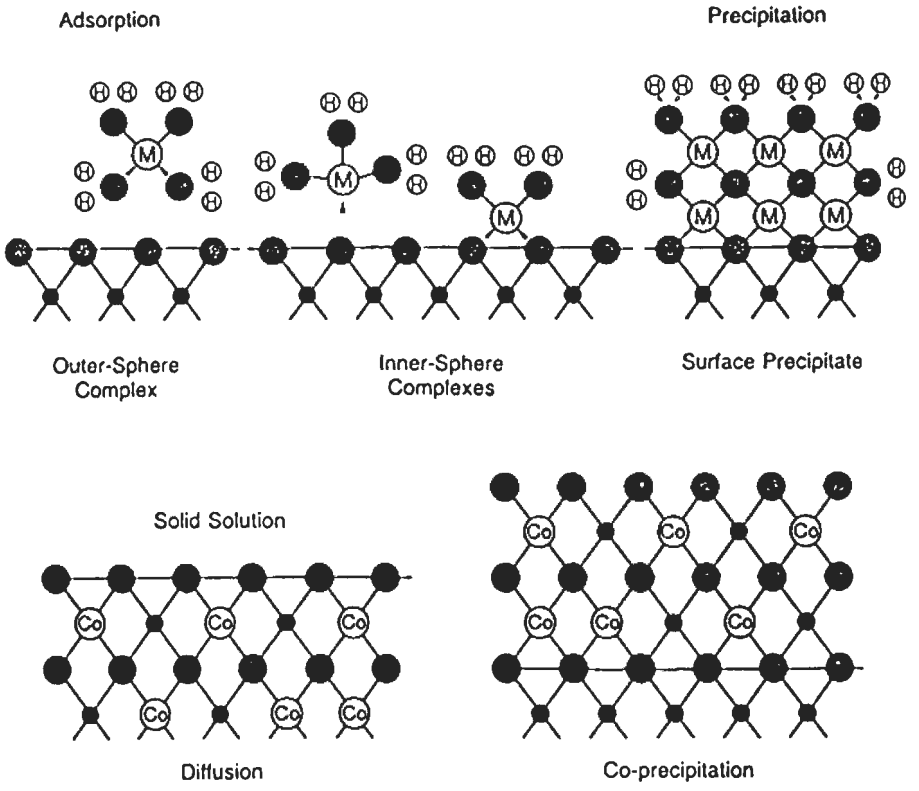

Fig. 9: Possible sorption complexes at the mineral-water interface. M represents aqueous metal ions, and H represents protons. The figures representing diffusion and co-precipitation show two possible modes of Cobalt (Co) absorption in calcite (from Brown et al., 1995).

The resulting adsorption is a function of the species stable at each pH and the net surface charge of the adsorbent at the relevant pH, e.g. for goethite is the "zero point of charge" (ZPC) at pH 8. In Fig. 10 adsorption of metal cations and oxyanions are shown with the net surface charge of the adsorbent, in this case goethite.

The underlying material of the oxidation zone in mine tailings has the function of a buffer for the acid and metal bearing solution through sorption and neutralization processes. Once the

adsorption and acid-neutralization capacity of the underlying tailing material is exceeded, the mobilized elements may lead to formation of highly metal-bearing acid mine drainage (AMD), one of the main environmental problems of the mining industry.

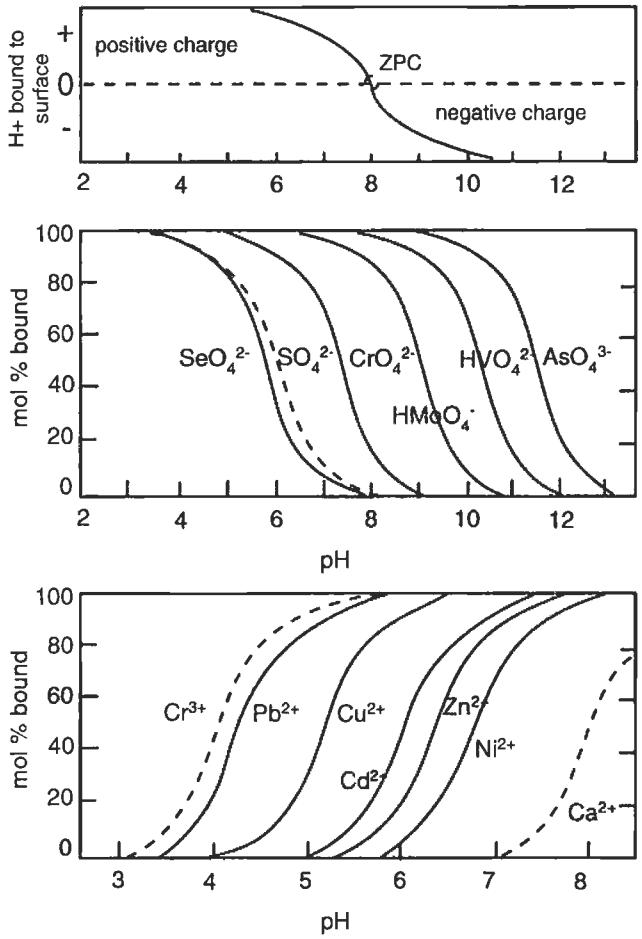

Fig. 10: Adsorption of oxyanions and bivalent cations to Fe(III)hydroxides. With decreasing pH the net surface charge becomes positive due to proton adsorption at the surface. Elements, which are stable at acidic condition as oxyanions become preferentially adsorbed. The adsorption of metals stable as cations increases with pH due to the increasing negative surface charge of the adsorbent. The dashed curves have been calculated (based on data from Dzombak and Morel, 1990; from Stumm and Morgan, 1996).

2.4.7 *Microbiological activity*

As mentioned in 2.4.2, microbiological activity acts as a catalyst for the oxidation of ferrous to ferric iron, a key process of the acid rock drainage (ARD) problem. Increasing awareness about the role of microorganism in geological processes has lead recently to a new scientific direction called geomicrobiology, e.g. Ehrlich, 1996; McIntosh and Groat, 1997; Banfield and Nealson, 1997; and Köhler and Völsgen, 1998. The microorganisms in tailings impoundments and mine waste environments are increasingly a new subject of investigation

(Gould et al., 1994; Davis, 1997, Nordstrom and Southan, 1997; Blowes et al., 1998; Mills, 1999).

As mentioned in section 2.4.2.1, *Thiobacillus ferrooxidans* has been known to play a key role in sulfide oxidation for 30 years (Singer and Stumm, 1970). This acidophilic chemolithotroph and autotroph bacteria derives cellular carbon from atmospheric CO_2 fixation via the Clavin cycle and obtains energy from the oxidation of Fe(II) or reduced S compounds (H_2S, HS, S°, $S_2O_3^{2-}$, SO_3^{2-}). This microbe is also reported to be a facultative H_2-oxidizer and is capable of surviving under anaerobic conditions by utilizing reduced S compounds as an electron donor and Fe(III) as an electron sink (Davis, 1997). *Thiobacillus ferrooxidans* is the longest known and most studied organism in acid mine drainage and mine waste environments. Nevertheless, a diverse microbial population of metal-tolerant, neutrophilic to acidophilic sulfide and sulfur-oxidizing *Thiobacilli* are known so far. *Leptospirilum ferrooxidans* seems to be the dominant genus in some acid environments as reported from Iron Mountain, California (Edwards et al., 1998). Also heterotrophic bacteria, green algae, fungi, yeasts, mycoplasma, and amoebae have all been reported from acid mine waters. Wichlacz and Unz (1981) isolated 37 acidophilic heterotrophs from acid mine drainage. In the Rum Jungle mine site, Australia, only a low number of *Thiobacillus ferrooxidans* was found in a mine waste dump, but a high number of acidophilic heterotrophs has been reported (Goodman et al., 1981). Davis (1997) reports the highest *Thiobacillus ferrooxidans* population at the oxidation front, while its heterophobic counterpart *Acidiphilum spp.* show higher population in the upper part of an aged oxidation zone of a mine tailing. Ehrlich (1996) reported several satellite microorganisms live in close association with *Thiobacillus ferrooxidans*. Barker et al. (1998) reported the increased release of cations from biotite (Si, Fe, Al) and plagioclase (Si, Al) by up to two orders of magnitude by microbial activity compared to abiotic controls. The authors also report the formation of a low pH (3-4) microenvironment associated with microcolonies of bacteria on biotite. These results suggest that in acid rock drainage, tailings and mine waste environments, a complex microbial ecosystem exists, of which the controlling parameters and interactions are poorly understood.

2.5 Conclusion

Geochemical conditions in mine waste environments change with time by the exposure of sulfide minerals to atmospheric oxygen. Sulfide oxidation is mainly controlled by oxygen and water flux, type of sulfide minerals, type of neutralizing minerals, and the microbial activity. The relation of acid producing processes and neutralizing processes determinates the geochemical Eh-pH conditions and so the mobility of the liberated elements. Thus, it is crucial to determinate the acid producing minerals (primary and secondary) and the acid neutralizing minerals in mine waste in order to predict future geochemical behavior and the hazardous potential of the material.

Summarizing, it can be stated that for accurate mine waste management assessment, a combination of detailed mineralogical, geochemical, and microbiological studies has to be performed in order to understand and predict the complex geomicrobiological interactions.

References

Acker, J.G. and Bricker, O.P. (1992): The influence of pH on biotite dissolution and alteration kinetics at low temperature. Geochimica et Cosmochimica Acta, v. 56; p. 3073-3092.

Ahonen, L. and Tuovinen, O.L. (1994): Solid-Phase Alteration and Iron Transformation in Column Bioleaching of a Complex Sulfide Ore. In: Alpers, C.N. and Blowes, D.W. (eds.): Environmental Geochemistry of Sulfide Oxidation. ACS Symposium Series, Washington, DC, v. 550, p. 79-89.

Al, T.A., Blowes, D.W. and Jambor, J.L. (1994): A geochemical study of the main tailings impoundments at the Falconbridge Limited, Kidd Creek Division Metallurgical Site, Timms, Ontario. In: Jambor, J.L. and Blowes, D.W. (eds.): Short Course Handbook on Environmental Geochemistry of Sulfide Mine Waste. Mineralogical Association of Canada, Nepean, v. 22: p. 333-364.

Allen, S.K., Allen, J.M. and Lucas, S. (1996): Concentrations of contaminants in surface water samples collected in west-central Indiana impacted by acid mine drainage. - Environmental Geology, v. 27: p. 34-37.

Alpers, C.N. and Blowes, D.W. (eds.). (1994): Environmental Geochemistry of Sulfide Oxidation. ACS Symposium Series, Washington, DC, v. 550, 661 p.

Alpers, C.N., Blowes, D.W., Nordstrom, D.K., and J.L. Jambor (1994): Secondary minerals and acid mine-water chemistry. In: Jambor, J.L. and Blowes, D.W. (eds.): Short Course Handbook on Environmental Geochemistry of Sulfide Mine Waste. Mineralogical Association of Canada, Nepean, v. 22: p. 247-270.

Alpers, C.N. and Nordstrom, D.K. (1999): Geochemical Modeling of Water-Rock Interactions in Mining Environment. In: Plumlee, G. S. and Logsdon, M.J. (Eds.), Reviews in Economic Geology, The environmental geochemistry of ore deposits. Part A: Processes, techniques, and health issues, v. 6A, p. 289-323.

Alpers, C.N., Nordstrom, D.K. and Thompson, J.M. (1994): Seasonal variations of Zn/Cu Ratios in acid mine water from Iron Mountain, California. In: Alpers, C.N. and Blowes, D.W. (eds.): Environmental Geochemistry of Sulfide Oxidation. ACS Symposium Series, Washington, DC, v. 550, p. 324-344.

Banfield, J.F. and Nealson, K.H. (1997): Geomicrobiology, Reviews in Mineralogy, Mineralogical Society of America, v. 35, 448 p.

Barker, W.W., Welch, S.A., Chu, S., and Banfield, J.F. (1998): Experimental observations of the effects of bacteria on aluminosilicate weathering. American Mineralogist, v. 83, p. 1551-1563.

Baron, D. and Palmer, C.D. (1996): Solubility of jarosite at 4-35°C. Geochimica et Cosmochimica Acta, v. 60(2), p. 185-195.

Bigham, J.M., Schwertmann, U., Carlson, L. and Murad, E. (1990): A poorly crystallized oxyhydroxysulfate of iron formed by bacterial oxidation of Fe(II) in acid mine waters. Geochimica et Cosmochimica Acta, v. 54, p. 2743-2758.

Bigham, J.M., Carlson, L. and Murad, E. (1994): Schwertmannite, a new iron oxyhydroxy-sulphate from Pyhäsalmi, Finland, and other localities. Mineralogical Magazine, v. 58, p. 641-648.

Bigham, J.M., Schwertmann, U. and Pfab, G. (1996): Influence of pH on mineral speciation in a bioreactor simulating acid mine drainage. Applied Geochemistry, v. 11, p. 845-849.

Bigham, J.M (1994): Mineralogy of ochre deposits. In: Jambor, J.L. and Blowes, D.W. (eds.): Short Course Handbook on Environmental Geochemistry of Sulfide Mine Waste. Mineralogical Association of Canada, Nepean, v. 22, p.103-131.

Bigham, J.M., Schwertmann, U., Traina, S.J., Winland, R.L. and Wolf, M. (1996): Schwertmannite and the chemical modeling of iron in acid sulfate waters Geochimica et Cosmochimica Acta, v. 60(2), p. 185-195.

Blowes, D.W., Reardon, E.J., Jambor, J.L. and Cherry, J.A. (1991): The formation and potential importance of cemented layers in inactive sulfide mine tailings. Geochimica et Cosmochimica Acta, v. 55, p. 965-978.

Blowes, D.W. (1994): Remediation and prevention of low-quality drainage from tailings impounds. In: Jambor, J.L. and Blowes, D.W. (eds.): Short Course Handbook on Environmental Geochemistry of Sulfide Mine Waste. Mineralogical Association of Canada, Nepean, v. 22, p. 365-379.

Blowes, D.W. and Ptacek, C.J. (1994): Acid-neutralization mechanisms in inactive mine tailings. In: Jambor, J.L. and Blowes, D.W. (eds.): Short Course Handbook on Environmental Geochemistry of Sulfide Mine Waste. Mineralogical Association of Canada, Nepean, v. 22, p. 271-291.

Blowes, D.W., Jambor, J.L., Hanton-Fong, C.J., Lortie, L., and Gould, W.D. (1998): Geochemical, mineralogical and microbiological characterization of sulphide-bearing carbonate-rich gold-mine tailings impoundment, Joutel, Québec. Applied Geochemistry, v. 13(6), p. 687-705.

Blum, A.E. and Stillings, L.L. (1995): Feldspar dissolution kinetics. Chemical weathering rates of silicate minerals. Reviews in Mineralogy, v.31, p. 291-342.

Brookins, D.G. (1988): Eh-pH diagrams for geochemistry. Springer, Berlin, 176 p.

Brown, G.E., Parks, G.A., and O'Day, P.A. (1995): Sorption at mineral-water interfaces: macroscopic and microscopic perspectives. In Vaughan, D.J. and Pattrick, R.A:D. (Eds.): Mineral Surfaces, Chapman and Hall, London, The Mineralogical Society Series, v. 5, p. 129-183.

Bryner, L. C., Walker, R. B. and Palmer, R. (1967): Some factors influencing the biological and non-biological oxidation of sulfide Minerals.- Transact. Soc. Minig Eng., A.I.M.E., v. 238: p. 56-65.

Burns, R.G. and Fisher, D.S. (1990): J. Geophys. Res., v. 95, p. 14415-14421.

Byrne, P.M. (1991): A model for predicting liquefaction induced displacement due to seismic loading. The Second International Conference on Recent Advances in Geoctechnical Earthquake Engeneering and Soil Dynamics, St.Louis, Missouri, Paper No.7.

Byrne, P.M., Imrie, A.S. and Morgenstern, N.R. (1994): Results and implications of seismic performance studies for Duncan Dam. Canadian Geotechnical Journal, v. 31/6, p. 979-988

Byrne, P.M. and Beaty, M. (1997): Liquefaction induced displacements. Seco e Pinto, P. S. (Ed.) 1997: Seismic behaviour of ground and geotechnical structures. -Proceeding of discussion special technical session on earthquake geotechnical engineering during fourteenth international conference on soil mechanics and foundation engineering, Balkema, Rotterdam, p. 185-195.

Camus, F. (1975): Geology of the El Teniente orebody with emphasis on wall-rock alteration. - Economic Geology, v. 70(8), p. 1341-1372.

Carson, C.D., Fanning, D.S., Dixon, J.B. (1982): Alfisols and ultisols with acid sulfate weathering features in Texas. In: Kittrick, J.A., Fanning, D.S., Hossner, L.R. (eds.): Acid sulfide weathering, Soil Science Soc. Am. Pub., Madison, Wisconsin, v. 10, p. 127-146.

Childs, C.W, Inoue, K. and Mizota, C. (1998): Natural and anthropogenetic schwertmannites from Towada-Hachimantai National Park, Honshu, Japan. Chemical Geology, v. 144, p. 81-86.

Cornell, R.M. and Schwertmann, U. (1996): The Iron oxides. VCH Verlagsgesellschaft mbH, Weinheim, 573 p.

Davis, B.S. (1997): Geomicrobiology of the oxic zone of sulfidic mine tailings. In: McIntosh, J.M. and Groat, L.A. (eds.): Short Course Handbook on Biological and Mineralogical Interactions. Mineralogical Association of Canada, Nepean, v.25, p. 93-112.

Davis, J.A. and Leckie, J.O (1978): Effect of adsorbed complexing ligants on trace metal uptake by hydrous oxides. - American Chem. Soc. v. 12(12), p. 1309-1315.

Davis, J.A., Fuller, C.C. and Cook, A.D. (1987): A model for trace metal sorption at the calcite surface: Adsorption of Cd^{2+} and subsequent solid solution formation. Geochimica et Cosmocimica Acta, v. 51, p. 1477-1490.

Dold, B. (1994): Geochemische Untersuchungen einer Flotationshalde in Copiapó/Region Atacama/Nordchile. - unpublished Diplomarbeit (Teil 2) Universität Bremen, Bremen, 91 p.

Dold, B., Eppinger, K.J. and Kölling, M. (1996a): Pyrite oxidation and the associated geochemical processes in tailings in the Atacama desert/Chile: The influence of man controlled water input after disuse. In: Sanchez, M.A., Vergara, F. and Castro, S.H., (eds.): Clean Technology for the Mining Industry, Concepción, Chile, p. 417-427.

Dold, B., Eppinger, K.J. and Kölling, M. (1996b): Element mobilization in tailings by pyrite oxidation in the Atacama desert/Chile: The influence of men controlled water input after disuse. Terra Nostra, 8/96, p 36.

Dold, B., Fontboté, L. and Wildi, W. (1997): Mobilization and secondary fixing of Fe, Cu and As in tailings from copper sulphide mines in Chile as a function of climatic conditions. European Union of Geosciences EUG9, Strasbourg, p. 286.

Dold, B., Fontboté, L. and Wildi, W. (1999a): Distribution and significance of schwertmannite, jarosite, and ferrihydrite in sulfidic mine tailings. Abstract Ecology of Post-Mining Landscape, Cottbus, p. 26.

Dold, B., Fontboté, L. and Wildi, W. (1999b): Detection and distribution of ferric oxyhydroxides and oxyhydroxide sulfates in sulfide mine tailings; their importance to selective metal retention and acid production. Mine, Water and Environment, 1999 IMWA Congress, Sevilla, Spain, v. 2, p. 525-526.

Dold, B. and Fontboté, L. (in review): Element cycling and secondary mineralogy in porphyry copper tailings as a function of climate, primary mineralogy, and mineral processing. Journal of Geochemical Exploration, Special Issue. " Geochemical studies of Mining and the Environment".

Domopoulos, G.P, Droppert, D. and Van weert, G. (1995): Production of crystalline scorodite from chloride media, - Hydrometallurgy, v. 38, p. 245-262.

Domopoulos, G.P (1996): Effluent treatment by crystallization. In Sanchez, M.A., Vergara, F. and Castro, S.H., (eds.): Clean Technology for the Mining Industry, Concepción, Chile, p. 1-13.

Donnert, D., Eberle, S.H. and Horst, J. (1990): Kinetic studies on the interaction of metal between water and clay minerals.- NATO ASI Series, Vol. G 23, Springer; Heidelberg.

Dzombak, D.A. and Morel, F.M.M. (1990): Surface complexation modeling - Hydrous ferric oxides. Wiley, New York, 393p.

Edwards, K.J., SChrenk, M.O., Hamers, R., and Banfield, J.F. (1998): Microbial oxidation of pyrite: Experiment using microorganisms from an extreme acidic environment. American Mineralogist, v. 83, p. 1444-1453.

Ehrlich, H.L. (1996): Geomicrobiology, Dekker, New York, 719 p.

Evangelou, V.P. and Zhang, Y.L. (1995): A review: Pyrite oxidation mechanisms and acid mine drainage prevention. Critical Reviews in Environmental Science and Technology, v. 25(2), p. 141-199.

Flynn, C.M. (1984): Hydrolysis of inorganic iron(III) salts. Chemical Reviews, v. 84, p. 31-41.

Fontboté, L. (1990): Stratabound ore deposits in the Andes - A review and a classification according to their geotectonic setting. In: Fontboté, L., Amstutz, G.C., Cardozo, M., Cedillo, E. and Frutos, J. (Eds.) Stratabound ore deposits in the Andes, Springer, Berlin, p. 79-110,.

Fontboté, L. Amstutz, G.C., Cardozo, M., Cedillo, E., Frutos, J. (Eds.) (1990): Stratabound Ore Deposits in the Andes. Springer, Berlin, 815 p.

Fraser, W.W. and Robertson, J.D. (1994): Subaqueous disposal of reactive mine waste: an overview and update of case studies-Mend/Canada. - United States Department of the Interior, Bureau of Mines Special Publication, Pittburgh, SP 06A-94, p. 250-259.

Fuge, R., Pearce, F.M., Pearce, J.G. and Perkins, W.T. (1994): Acid mine drainage in Wales and influence of ochre precipitation on water chemistry. In: Alpers, C.N. and Blowes, D.W. (eds.): Environmental Geochemistry of Sulfide Oxidation. ACS Symposium Series, Washington, DC, v. 550, p. 261-275.

Georgopoulou, Z.J., Fytas, K., Soto, H. and Evangelou, B. (1996): Feasibility and cost of creating an iron-phosphate coating on pyrrhotite to prevent oxidation. Environmental Geology, v. 28(2), p. 61-69.

Gerth, J. and Brümmer, G. (1981): Einfluß von Temperatur und Reaktionszeit auf die Adsorption von Nickel, Zink und Cadmium durch Goethit.- Mitteilgn. Dtsch. Bodenkundl. Gesellsch., v. 32, p. 229-238.

Gerth, J. and Brümmer, G. (1983): Adsorption und Festlegung von Nickel, Zink und Cadmium durch Goethit (α-FeOOH).- Fresenius Z. Anal. Chem., v. 316, p. 616-620.

Goodman, A.E., Khalid, A.M., Ralph, B.J. (1981): Microbial ecology of Rum Jungle. Part 1. Environmental study of sulphidic overburden dumps, environmental heap-leach piles and tailings dam area. Australian AEC AAEC/E531.

Gould, W.D., Bechard, G. and Lortie, L. (1994): The nature and the role of microorganisnms in the tailings environment. In: Jambor, J.L. and Blowes, D.W. (eds.): Short Course Handbook on Environmental Geochemistry of Sulfide Mine Waste. Mineralogical Association of Canada, Nepean, v. 22, p. 185-199.

Gustafson, L.B. and Hunt, J.P. (1975): The porphyry copper deposit at El Salvador, Chile. Economic Geology, v. 70, p. 857-912.

Hamer, K. (1993): Entwicklung von Laborversuchen als Grundlage für Modellierung des Transportverhaltens von Arsenat, Blei, Cadmium und Kupfer in wassergesättigten Säulen.- Berichte aus dem Fachbereich Geowissenschaften der Universität Bremen Nr. 39, Bremen, 147 p.

Hamman, P.F. and Vernon, P.N. (1987): The re-use of tailings dam water at a large mine in the Naminb Desert in Namibia. Water Supply 5: SS21/3-SS21/4.

Hodges, C.A. (1995): Mineral resources, environmental issues, and land use. Science, v. 268, p. 1305-1312.

Hsia, T.H., Lo, S.L. and Lin, C.F (1992): As(V) adsorption on amorphous iron oxide: triple layer modeling. Chemosphere v. 25, p. 1825-1837.

Ingeneria y Geotecnia LTDA (1990): Levantamiento castral de los tranques de relaves en Chile. SERNAGEOMIN, Santiago.

Jambor, J.L. and Blowes, D.W. (eds.). (1994): Short Course Handbook on Environmental Geochemistry of Sulfide Mine-Wastes. Mineralogical Association of Canada, Nepean, v. 22, 438p.

Jambor, J.L. (1994): Mineralogy of sulfide-rich tailings and their oxidation products. In: Jambor, J.L. and Blowes, D.W. (eds.): Short Course Handbook on Environmental Geochemistry of Sulfide Mine Waste. Mineralogical Association of Canada, Nepean, v. 22, p. 59-102.

Jambor, J.L. and Blowes, D.W. (1998): Theory and applications of mineralogy in environmental studies of sulfide-baring mine waste. In: Cabri, L. J. and Vaughan, D.J. (eds.): Short Course Handbook on Ore and Environmental Mineralogy. Mineralogical Association of Canada, Nepean, v. 27, p. 367-401.

Jänicke, M. and Weidner, H. (Eds.). (1997): National environmental policies. A comparative study of capacity-building. Springer, Berlin, 320 p.

Jones, C.E. and Wong, J.Y. (1994): Shotcrete as a cementitious cover for acid generating waste rock piles. United States Department of the Interior, Bureau of Mines Special Publication, Pittburgh, SP 06B-94, p. 104-112.

Kesler, S. E. (1997): Acid mine drainage, unpublished lecture notes, course GS425, University of Michgan at Ann Arbor, p. 79-91.

Klohn, E., Holmgren, C. and Ruge, H. (1990): El Soldado, a stratabound copper deposit associated with alkaline volcanism in the central coastal range. In: Fontboté, L. Amstutz, G.C., Cardozo, M., Cedillo, E., Frutos, J. (Eds.) Stratabound Ore Deposits in the Andes, Springer, Berlin, p. 435-448.

Köhler, M. and Völsgen, F. (1998): Geomikrobiologie Wiley-VCH, Weinheim, 346 p.

Kölling, M. (1990): Modellierung geochemischer Prozesse im Sickerwasser und Grundwasser; Beispiel: die Pyritverwitterung und das Problem saurer Grubenwässer.- Berichte aus dem Fachbereich Geowissenschaften der Universität Bremen Nr.8, Bremen, 135p.

Kwong, Y.T.J. (1993): Prediction and prevention of acid rock drainage from a geological and mineralogical perspective. MEND Project 1.32.1, 47 p.

Langmuir, D. (1997): Aqueous environmental geochemistry. Prentice Hall, 600 p.

Lapakko, K.A. (1994): Subaqueous disposal of mine waste: laboratory investigation. - United States Department of the Interior, Bureau of Mines Special Publication, Pittburgh, SP 06A-94, p. 270-278.

Leckie, J.O., Benjamin, M.M., Hayes, K., Kaufman, G. and Altman, S. (1980): Adsorption and coprecipitation of trace elements from water with iron oxyhydroxides. Stanford University.

McIntosh, J.M. and Groat, L.A. (Eds.). (1997): Biological - mineralogical interactions. Mineralogical Association of Canada, Nepean, v.25, 239 p.

Malmström, M. and Banwart, S. (1997): Biotite dissolution at 25°C. the pH dependence of dissolution rate and stoichometry. Geochimica et Cosmochimica Acta, v. 61, p. 2779-2799.

Marschik, R. (1996): Cretaceous Cu(-Fe) mineralization in the Punta del Cobre belt, northern Chile. Ph.D. thesis. Terre et Environnement, Université de Genève, v. 5, 200 p.

Marschik, R. and Fontboté, L. (1996): Copper(-iron) mineralization and superposition of alteration events in the Punta del Cobre belt, northern Chile. Economic Geology, Special Publication, No. 5, p. 171-189.

Marschik, R., Singer, B.S., Munizaga, F., Tassinari, C., Moritz, R., and Fontboté, L. (1997): Age of Cu(-Fe)-Au mineralization and thermal evolution of the Punta del Cobre district, Chile. Mineralium Deposita, v. 32, p. 531-546.

Marschik, R. and Fontboté, L. (in review): Geology of the Punta del Cobre-Candelaria area, Chile: The Jurassic(?) to pre-Valanginian Punta del Cobre Formation. GSA Bulletin.

MEND, Mine Environment Neutral Drainage Program (1991): Acid rock drainage prediction manual, Report 1.16.1b. CANMET, Dept. Natural Recources Canada, Ottawa.

MEND (1991b): New methods for determination of key minerals species in acid generation prediction by acid-accounting, Report 1.16.1c. CANMET, Dept. Natural Recources Canada, Ottawa.

MEND (1991c): Study on metals recovery/recycling from acid mine drainage, Report 3.21.1a CANMET, Dept. Natural Recources Canada, Ottawa.

MEND (1993): Evaluation of techniques for preventing acidic rock drainage: First Milestone Report, Report 2.35.2a.CANMET, Dept. Natural Recources Canada, Ottawa.

MEND (1993b): Prediction and prevention of acid rock drainage from a geological and mineralogical perspective, Report 1.32.1. CANMET, Dept. Natural Recources Canada, Ottawa.

MEND (1994): Separation of sulphides from mill tailings phase I, Report 2.45.1a. CANMET, Dept. Natural Recources Canada, Ottawa.

MEND (1995): Metal removal from acid mine drainage by ion exchange, Report 3.21.1b CANMET, Dept. Natural Recources Canada, Ottawa.

Mercado, M.W. (1978): Hojas Chañaral y Potrerillos, Region Atacama Escala 1 : 250.000. - Mapas Geologicos Preliminares de Chile, Instituto de Investigaciones Geologicas, Santiago.

McNutt, R.H. et al. (1975): Initial 87Sr/86Sr ratio of plutonic and volcanic rocks of the Central Andes between latitudes 26° and 29° South. Earth and Planetary Science Letters, v. 27, p. 305-313.

Mills, A.L. (1999): The role of bacteria in environmental geochemistry. In: Plumlee, G. S. and Logsdon, M.J. (Eds.), Reviews in Economic Geology, The environmental geochemistry of ore deposits. Part A: Processes, techniques, and health issues, v. 6A, p. 125-132.

Mok, W.M. and Wai, C.M. (1994): Mobilization of arsenic in contaminated river waters. In: Nriagu, J.O. (Ed.): Arsenic in the environment. Part I Cycling and characterization. John Wiley Interscience, New York, p. 99-108.

Morin, A.K. and Cherry, J.A. (1986): Trace amounts of siderite near a uranium-tailings impoundments, Elliot Lake, Ontario, and its implications in controlling contaminant migration in a sand aquifer. Chemical Geology (Isotope Geoscience Section), v. 56, p.117-134.

Morin, A.K. and Hutt, N.M. (1997): Environmental geochemistry of minesite drainage. Practical theory and case studies. MDAG Publishing, Vancouver, 333 p.

Moses, C.O., Nordstrom, D.K., Herman, J.S. and Mills, A.L. (1987): Aqueous pyrite oxidation by dissolved oxygen and by ferric iron. - Geochimica et Cosmocimica Acta, v. 51, p. 1561-1571.

Nesbitt, H.W. and Jambor, J.L. (1998): Role of mafic minerals in neutralizing ARD, demonstrated using a chemical weathering methology. In: Cabri, L. J. and Vaughan, D.J. (eds.): Short Course Handbook on Ore and Environmental Mineralogy. Mineralogical Association of Canada, Nepean, v. 27, p. 403-421.

Nicholson, R.V. and Scharer, J.M. (1994): Laboratory studies of pyrrhotite oxidation kinetics. In: Alpers, C.N. and Blowes, D.W. (eds.): Environmental Geochemistry of Sulfide Oxidation. ACS Symposium Series, Washington, DC, v. 550, p. 14-30.

Nordstrom, D. K. (1977): Hydrogeochemical and microbiological factors affecting the heavy metal chemistry of an acid mine drainage system. Diss. Stanford University, Standford, Calif., 190 p.

Nordstrom, D. K., Jenne, E.A. and Ball, J.W. (1979): Redox equilibria of iron in acid mine waters. In: Jenne, E.A. (Ed.): Chemical modeling in aqueous systems. Am. Chem. Soc. Symp. Washington, D.C., Series 93, p. 51-79;

Nordstrom, D. K. (1982): Aqueous pyrite oxidation and the consequent formation of secondary iron minerals. In: Kittrick, J.A.; Fanning, D.S., L.R. (Eds.): Acid sulfate weathering. Soil Sci. Soc. of Amerika, p. 37-56

Nordstrom, D.K. and Southam, G. (1997): Geomicrobiology of sulfide mineral oxidation. In: Banfield, J.F. and Nealson, K.H. (Eds.) Geomicrobiology; Reviews in Mineralogy, v. 35, p. 361-390.

Nordstrom, D.K. and Alpers, C.N. (1999): Geochemistry of acid mine waste. In: Plumlee, G. S. and Logsdon, M.J. (Eds.), Reviews in Economic Geology, The environmental geochemistry of ore deposits. Part A: Processes, techniques, and health issues, v. 6A, p. 133-160.

Norris, P.R. (1989): Mineral-oxidizing bacteria: metal-organism interactions. In: R.K. Poole and G.M. Gadd (Eds.) Metal Microbe Interactions. The Society for General Microbiology by IRL Press at Oxford University Press, Oxford, Chapter 7, p. 99-117.

Parks, G.A. (1990): Surface energy and adsorption at mineral-water interfaces: an introduction. In: Hochella, M.F. and White, A.F. (Eds.) Mineral-Water Interface Geochemistry, Reviews in Mineralogy, v.23, p. 133-175.

Plumlee, G.S. (1999): The environmental geology of mineral deposits. In: Plumlee, G. S. and Logsdon, M.J. (Eds.) Reviews in Economic Geology, The environmental geochemistry of ore deposits. Part A: Processes, Techniques, and Health Issues, v. 6A, p. 71-116.

Plumlee, G. S. and Logsdon, M.J. (Eds.) (1999): The environmental geochemistry of ore deposits. Part A: Processes, techniques, and health issues. Reviews in Economic Geology, v. 6A.

Pratt, A.R., Muir, I.J. and Nesbitt, H.W. (1994): X-ray photoelectron and auger electron spectroscopic studies of pyrhotite and mechanisms of air oxidation. Geochimica et Cosmocimica Acta, v. 58, p. 827-842.

Rahn, P.H, Davis, A.D, Webb, C.J. and Nichols, A.D. (1996): Water quality impacts from mining in the Black Hills, South Dakota, USA. - Environmental Geology v. 27, p. 38-53

Rampe, J.J. and Runnells, D.D. (1989): Contamination of water and sediment in a desert stream by metals from abandoned gold mine and mill, Eureka District, Arizona, U.S.A..- Appl. Geochem. V. 4(5), p. 445-54.

Reutter, K.-J. and Scheuber, E. (1988): Relation between tectonics and magmatism in the Andes of northern Chile and adjacent areas between 21° and 25°. - V Congreso Geologico Chileno, Santiago, Tomo 1, A345-A363.

Ribet, I., Ptacek, C.J., Blowes, D.W. and Jambor, J.L. (1995): The potential for metal release by reductive dissolution of weathered mine tailings. Journal of Contaminant Hydrology, v. 17(3), p. 239-273.

Rimstidt, J.D., Chermak, J.A. and Gagen, P.M. (1994): Rates of reaction of galena, sphalerite, chalcopyrite and arsenopyrite with Fe(III) in acidic solutions. In: Alpers, C.N. and Blowes, D.W. (eds.): Environmental Geochemistry of Sulfide Oxidation. ACS Symposium Series, Washington, DC, v. 550, p.2-13

Ritcey, G.M. (1989): Tailings management. Elsevier Science Publ, New York, p. 969.

Ritchie, A.I.M. (1994): The waste-rock environment. In: Jambor, J.L. and Blowes, D.W. (eds.): Short Course Handbook on Environmental Geochemistry of Sulfide Mine Waste. Mineralogical Association of Canada, Nepean, v. 22, p. 133-161.

Robertson, A. and Mac,G. (1984): Design of uranium tailings impoudments. Short course on Extractive Metallurgy of Uranium, Elliot Lake, Ontario.

Robertson, W.D. (1994): The physical hydrology of mill-tailings impoundments. In: Jambor, J.L. and Blowes, D.W. (eds.): Short Course Handbook on Environmental Geochemistry of Sulfide Mine Waste. Mineralogical Association of Canada, Nepean, v. 22, p. 1-17.

Rossi, G.(1990): BioHydroMetallurgy., McGraw-Hill, Germany.

Ruiz, C. and Peebles, F. (1988): Geología, distribución y génesis de los yacimientos metalíferos Chilenos; Santiago.

Sato, M. (1960): Oxidation of sulfide orebodies, II. Oxidation mechanisms of sulfide minerals at 25°C. - Economic Geology, v. 55, p. 1202-1231.

Sato, M. (1992): Persistency-field Eh-pH diagrams for sulfides and their application to supergene oxidation and enrichment of sulfide ore bodies. Geochimica et Cosmochimica Acta, v. 56, p. 3133-3156.

Schneider, W. and Schwyn, B. (1987): The hydrolysis of iron in synthetic, biological, and aquatic media. In: Stumm, W. (Ed.): Aquatic surface chemistry, Wiley-Interscience Publication, New York, p.167-196.

Schwertmann, U. (1964): Differenzierung der Eisenoxide des Bodens durch Extraktion mit Ammoniumoxalat Lösung. Zeitschrift für Pflanzenernährung und Bodenkunde, v. 105, p. 194-202.

Schwertmann, U. (1984): The influence of aluminium on iron oxides: IX. dissolution of Al-goethites in 6 M HCl. Clay Minerals, v. 19, p. 9-19.

Schwertmann, U. and Cornell, R.M. (1991): Iron oxides in the laboratory. VCH Verlagsgesellschaft mbH, Weinheim, 137 p.

Schwertmann, U., Bigham, J.M. and Murad, E. (1995): The first occurrence of schwertmannite in a natural stream environment. European Journal of Mineralogy, v. 7, p. 547-552.

Schwertmann, U., Friedl, J., and Stanjek, H. (1999): From Fe(III) ions to ferrihydrite and then to hematite. Journal of Colloid and Interface Science, v. 209, p. 215-223.

Singer, P.C. and Stumm, W. (1970): Acid mine drainage: the rate determinating step. Science v. 167, p. 1121-1123.

Stambuk, V., Blondel, J. and Serrano, L. (1982): Geología del yacimineto Río Blanco, Santiago. Actas III Congreso Geologico Chileno, Concepción, Chile, T.II, p. 419-442.

Strömberg, B. and Banwart, S. (1994): Kinetic modelling of geochemical processes at Aitik mining waste rock site in northern Sweden. Applied Geochemistry. v. 9, p. 583-595.

Stumm, W. and Sulzberger, B. (1992): The cycling of iron in natural environments: Considerations based on laboratory studies of heterogeneous redox processes. Geochimica et Cosmochimica Acta, v. 56, p. 3233-3257.

Stumm, W. and Morgan, J.J. (1996): Aquatic chemistry (3rd Edition). New York, Wiley, 1022 p.

St.Arnaud, L. (1994): Water covers for the decommissionig of sulfidic mine tailings impoundments.- United States Department of the Interior, Bureau of Mines Special Publication, Pittburgh, SP 06A-94, p. 279-287.

Suter, D., Siffert, C., Sulberger, B., and Stumm, W. (1988): Catalytic dissolution of iron(III)(hydr)oxides by oxalic acid in the presence of Fe(II). Naturwiss., v. 75, p. 571-573.

Suter, D., Banwart, S., and Stumm, W. (1991): The dissolution of hydrous iron(III) oxides by reductive mechanisms. Langmuir, v. 7, p. 809-813.

Sylva, R.N. (1972): The hydrolyse of iron(III). Rev. Pure and Appl. Chem., v. 22, p. 115-132.

Tayler, B.E. and Wheeler, M.C. (1994): Sulfur- and oxygen-isotope geochemistry of acid mine drainage in the Western United States. In: Alpers, C.N. and Blowes, D.W. (eds.): Environmental Geochemistry of Sulfide Oxidation. ACS Symposium Series, Washington, DC, v. 550, p. 481-515.

Thompson, B. (1998): Metal removal technology: Precipitation processes. In: SARB Consulting, Inc. Environmental geochemistry of ore deposits and mining activities. Short course Notes, Albuquerque, New Mexico,

Walder, I. and Schuster, P. (1998): Acid Rock Drainage. In: SARB Consulting, Inc. Environmental geochemistry of ore deposits and mining activities. Short course Notes, Albuquerque, New Mexico,

Webster, J.G., Nordstrom, D.K. and Smith, K.S. (1994): Transport and natural attentuation of Cu, Zn, As and Fe in the acid mine drainage of Leviathan and Bryant Creeks. In: Alpers, C.N. and Blowes, D.W. (eds.): Environmental Geochemistry of Sulfide Oxidation. ACS Symposium Series, Washington, DC, v. 550, p. 244-260.

Weiss, N.L. (ed.) (1985): SME mineral processing handbook. SME, 2144 p.

Wichlacz, P.L. and Unz, R.F. (1981): Acidophilic, heterotrophic bacteria of acid mione drainage waters. Appl. Environ. Microbiol., v. 41, p. 1254-1261.

Yu, J.-Y., Heo, B., Chang, H.-W. (1998): Stability of schwertmannite and ferrihydrite in the stream waters of Imgok and Osheep Creek polluted by acid mine drainage. Goldschmidt Conference Proceedings, Toulouse, p. 1675-1676.

CHAPTER 3

3 Methodology used for sequential extraction applied to geochemical investigations of sulfidic mine tailings by combination of dissolution kinetics and mineralogical control of dissolved phases by X-ray diffraction (XRD) and differential X-ray diffraction (DXRD)

Abstract

The application of dissolution kinetic tests and the control of dissolved phases in sequential extraction by X-ray diffraction (XRD) and differential X-ray diffraction (DXRD) from samples of the studied mine tailings indicate which minerals are dissolved in each leach. This information is crucial for the interpretation of geochemical data obtained from sequential extractions and to increase the selectivity of the sequence applied. Preliminary tests based on commonly used dissolution techniques have allowed the development of a seven-step sequence adapted to the secondary and primary mineralogy of the studied sulfidic mine tailings from Cu-sulfide ores, both from porphyry copper and from Fe-oxide Cu-Au deposits. It must be stated that sequential extractions are operationally defined (Hall et al., 1996), i.e. the selectivity depends on factors as chemicals employed, the time and nature of contact, sample to volume ratio. The solubility of certain minerals of interest may differ also importantly, due to their formation conditions (see chapter 5). However, sequential extractions are a very useful tool to understand geochemical processes, if they are combined with mineralogical analyses.

The applied seven-step sequence is the following: Step 1 liberates the *water-soluble fraction* (1.0 g sample into 50 ml deionized H_2O shake for 1 h at room temperature; RT) which dissolves gypsum and metal salts (e.g., bonattite ($CuSO_4 \cdot 3H_2O$), chalcanthite ($CuSO_4 \cdot 5H_2O$), pickeringite ($MgAl_2(SO_4)_4 \cdot 22H_2O$). Step 2 liberates the *exchangeable fraction* (1M NH_4-acetate, pH 4.5, shaken for 2 hrs, RT) as adsorbed ions, but also dissolves calcite and breaks down a typical secondary vermiculite-type mixed-layer minerals from the low pH oxidation zone. Step 3 addresses the *Fe(III) oxyhydroxides* fraction (0.2 M NH_4-oxalate, pH 3.0, shaken for 1 h. in darkness, RT) and dissolves schwertmannite, 2-line ferrihydrite, Mn-hydroxides, and partly also secondary jarosite. Step 4 contains the *Fe(III) oxides* fraction (0.2 M NH_4-oxalate, pH 3.0, heat in water bath 80°C for 2 h.) and dissolves all secondary ferric minerals occurring as higher ordered ferrihydrite (6-line), goethite, primary and secondary jarosite, natrojarosite, and primary hematite. Hypogene magnetite is partly dissolved. This extraction is proposed for acid-base accounting purposes to separate sulfate sulfur from sulfide sulfur. Step 5 consists in a change from reducing to oxidizing condition and is performed by a 35% H_2O_2 leach (35% H_2O_2 heat in water bath for 1 hour), which dissolves *organic matter* and *supergene Cu-sulfides* such as covellite and chalcocite-digenite. Step 6 ($KClO_3$ and HCl, followed by 4 M HNO_3 boiling) dissolves *primary sulfides* and step 7 (HCl, HF, $HClO_4$, HNO_3) the *residual* fraction (silicates).

3.1 Introduction

It is generally accepted that pyrite oxidation, or more generally sulfide oxidation, is the main source of heavy metal loaded acid effluents called acid rock drainage (ARD). As pyrite is the most abundant sulfide mineral, the sulfide oxidation is typically accompanied by the formation of secondary Fe(III) hydroxide minerals. In quantity, these minerals are minor phases in bulk samples from mine tailings or waste dumps, but are the major phases in the secondary mineral assemblage. This makes the identification and detection of these minerals difficult, as the X-ray diffraction (XRD) detection limit for a mineral in a bulk sample is about 5%. It will be therefore necessary to apply techniques to enrich or separate the minerals. Selective dissolution is a technique which may be characteristic for secondary Fe(III) hydroxides and other secondary minerals. This chapter summarizes the methodology and special focus will be given to secondary Fe(III) hydroxides because of their important role in the cycling pathway of mobilized elements, due to functional groups and high surface areas, and which have received great attention from the scientific community (see reviews in Dzombak & Morel, 1990 and Cornell & Schwertmann, 1996).

Since Tamm (1922, 1932), the bidentate organic complex-former oxalate, known as the Tamm's reagent, has been widely used to characterize secondary ferric phases by dissolution, mainly in soil environments. Schwertmann (1964) applied the influence of light and UV radiation to the dissolution kinetics of Fe(III) hydroxides for selective dissolution of the "amorphous Fe(III) hydroxides". Stumm & Sulzberger (1992) discussed the dissolution kinetics of secondary ferric minerals by organic complex formers (e.g., oxalate) as a function of concentration, acidity, Eh conditions, temperature, UV radiation, and Fe(II) as catalyst. Many studies have investigated the complex dissolution mechanisms and their controlling parameters (Stone, 1987; Suter et al., 1991; Cornell and Schwertmann, 1996; Nesbitt et al., 1998; this work, chapter 4) and tried to enhance the selectivity of the dissolution leaches (Schwertmann, 1964; Fischer, 1976, Reyes and Torrent, 1997).

The knowledge of dissolution kinetics is important for mineral separation (Czamanske and Ingamells, 1970; Chao and Sanzolone, 1977), for the determination of secondary phases (especially Fe, Al, and Mn hydrous oxides) by differential X-ray diffraction DXRD (Schulze, 1981, 1994), and to study their role in element retention by sequential extractions. Sequential extractions are widely used for exploration purposes and to study element speciation in systems such as soil and sediments (Tessier et al., 1979; Sondag, 1981; Chao & Zhou, 1983; Chao, 1984; Cardoso Fonseca & Martin, 1986; Hall et al., 1996; Hall & Bonham-Carter, 1998). Recently, sequential extractions have been increasingly applied in the mine waste environment to study the complex processes of sulfide oxidation and the retention of mobilized elements by secondary phases via precipitation and sorption processes (Ribet et al., 1995; McGregor et al., 1995; Fanfani et al., 1997; McCarty et al., 1998; this work).

Due to the wide range of possible secondary phases in these systems, the selectivity of the dissolution has been the focus of criticism (Hall et al., 1996; McCarty et al., 1998). As Fe(II) catalyses the release of Fe(III) in the presence of oxalate (Suter et al., 1991; Stumm and Sulzberger, 1992), Chao and Zhou (1983) found that the 0.175 M NH_4-oxalate, pH 3.2, dark

leach was only selective to the amorphous Fe(III) oxyhydroxides in the absence of magnetite. It must also be assumed that siderite ($FeCO_3$) and ankerite ($Ca(Fe,Mg)(CO_3)_2$) influence the dissolution kinetics by the liberation of Fe(II). Due to the complexity of the iron system in mine tailings, finding a more selective leach to each mineral or mineral group was not attempted in this study. Instead, the dissolution kinetics of secondary Fe(III) minerals subjected to common leaches was studied. These results were then used for interpretation of the results of the present work (chapter 5, 6, and 7). By using the leach steps listed below, the achieved results show that more than one mineral is dissolved in every leach step and that some minerals survive some leaches partly. To ensure appropriate geochemical interpretation it is crucial to combine detailed mineralogical studies with the application of sequential extractions. To reach this goal, dissolution kinetics tests and sequential extractions were applied to representative samples of the studied mine tailings and an adapted leach sequence for the specific secondary mineralogy was established.

The results have shown that it is possible, combining selective leaches by careful mineralogical studies, to detect which minerals are dissolved at which step. This provides an improved understanding of the retention behavior of mobile elements by specific secondary minerals or mineral groups.

3.2 Materials and methods

Two types of sequential extraction procedures were applied and compared. The first phase of the study utilized a slightly modified 6-step sequential extractions after Tessier et al. (1979) and Sondag (1981) shown in Table 1 (Sequence A). The extractions were applied to one drill core of every studied tailings impoundment in order to acquire preliminary information regarding the element distribution and the presence of possible secondary phases.

In the second phase of the study the sequence was modified and adapted to the secondary mineralogy of the studied tailings. Fig. 1 summarizes the techniques applied for the development of the 7-step sequential extractions applied in this study (Table 1, Sequence B). This adaptation increases the selectivity and is based on the following changes: 1.) The application of a water leach as first step allows discrimination between gypsum as secondary product of sulfide oxidation and calcite as primary neutralization potential, an important indicator of neutralization reactions in mine tailings. Additionally, the water-soluble fraction is important in arid climates so that for the selectivity of the exchangeable fraction (i.e. step 2, sequence B it is important to release the water-soluble fraction first. 2.) Because calcite dissolved in the NH_4-acetate leach completely, the Na-acetate leach was found to be unnecessary (step 2, sequence A). 3.) Due to very low Mn concentrations, the hydroxylamine leach (step 3, sequence A) was also left out in the sequence B, as this leach has also shown to dissolve parts of the ferric hydroxides. 4.) Instead of these two leaches (step 2 and 3, sequence A) a study was conducted to investigate the dissolution kinetics of the secondary ferric phases schwertmannite and ferrihydrite (chapter 4) which were detected by DXRD in the studied tailings. The dissolution kinetics of iron phases in 0.2 M NH_4-oxalate (pH 3.0) heated using water bath 80°C for 2 hours was also tested at samples from the tailings. The resulting two dissolution steps (step 3 & 4, sequence B) permits one to

discriminate between secondary ferric phases and the primary iron oxides, which is necessary to study their role in element retention. 5.) The application of steps 5 and 6 in Sequence B permits one to discriminate between supergene and hypogene Cu-sulfides, as primary and secondary Cu enrichment processes are also important in mine tailings.

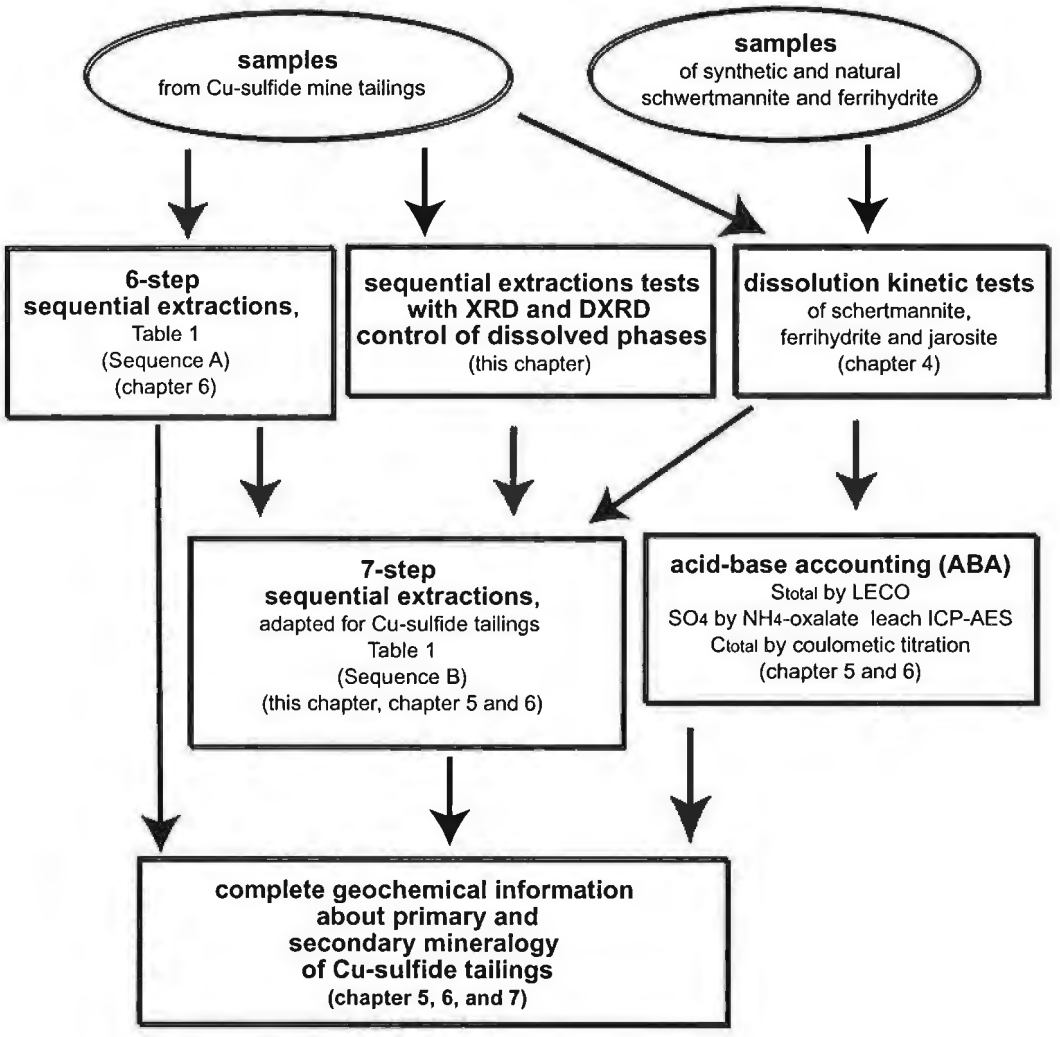

Fig. 1: Flow chart of the development of the 7-step sequential extractions for Cu-sulfide mine tailings used in this study.

To study the dissolution of the secondary mineralogy in the sulfidic mine tailings and to test the dissolution sequence B, representative samples from the following environments: 1. From the studied porphyry copper tailings impoundments Piuquenes (La Andina, "A" and "AS"), Cauquenes (El Teniente, "T" and "TS"), and El Salvador No.1 ("E") discussed in detail in chapter 5. 2. Samples from cementation zones ("hard pan") from two tailings impoundments

from the Fe-oxide Cu-Au deposits in the Punta del Cobre belt, Copiapó district, northern Chile (Ojancos, "H" and "S" and P. Cerda (Ojos del Salado), "O", both discussed in chapter 6). The selected samples were subjected to dissolution kinetic tests and sequential extractions with X-ray diffraction (XRD) and differential X-ray diffraction (DXRD) control of the dissolved phases.

Six tailings samples (oxidation zone: AS3/016, T4/010, E1/350, TS1/003, cementation zone: H1/860, and O3/500) were subjected to dissolution kinetic tests by freshly prepared 0.2 M ammonium oxalate solution brought to pH 3.00 by 0.2 M oxalic acid under exclusion of light and with light (Schwertmann 1964), as well as at 80°C. The dissolution-time curves were developed by shaking 2.5g of sample in 250 ml oxalate solution and taking 10 ml sub-samples with syringes at 5, 15, 30, 60, 75, 110, 140, 180, 185, 195, 220, 240, 300, and 360 min. During the first 60 min the sample is protected by aluminum foil from light, then the same sample is exposed 60 min to light, followed by heating the sample to 80°C in a water bath. The samples were continuously shaken during each step. The solution samples were filtered instantaneously with a 0.2 μm Teflon inline filter for syringes. Dissolved Fe and SO_4 (as S) were measured in triplicate by inductively coupled plasma - atomic emission spectroscopy (ICP-AES).

Ten representative samples from the oxidation (A4/035, T4/010, E1/050, E1/170) neutralization (A4/200), and primary zones (A4/800), as well as from a cementation zone (H1/760, H1/1000), and a hematite rich sediment (A4/010), were submitted to the first four steps of the extraction sequence B. After every leach the samples were air dried and analyzed by XRD to control which minerals went into solution in each step. As the detection limit of XRD is about 5%, to detect minor phases like ferrihydrite and schwertmannite differential X-ray diffraction (DXRD) was applied. DXRD consists of the difference of a XRD scan before and after treatment. As in the treatment minerals are dissolved, the concentration relation of the remaining phases change during the treatment, what makes an intensity correction necessary (k factor). The samples were characterized with XRD, using a Philips diffractometer 3020 with CuKα (λ = 1.54056 Å) and monochromator. Diffractometer settings were: 40 kV, 30 mA, 3-80°2θ, step scanning with 0.02° 2θ step size and 2s counting time per step. For the detection of the Fe(III) oxyhydroxides 3–80° 2θ, step scanning with 0.05° 2θ step size and 20 s counting time per step was applied as used by Bigham et al. (1990, 1994) and Schwertmann et al. (1995) for detection of schwertmannite and ferrihydrite.

The extractions sequence B was applied to the group of ten samples: 1) 3g of sample were shaken with 150 ml deionized water for 1h, filtered, and air-dried. 2) Liberation of the exchangeable fraction and/or adsorbed ions in 1M NH_4-acetate. 3) Dissolution of the secondary easily reducible Fe(III) oxyhydroxides as low ordered ferrihydrite, schwertmannite, and parts of secondary jarosite in 0.2M NH_4-oxalate pH 3.0 1 h in darkness. 4) Dissolution of the remaining secondary jarosite together with primary jarosite and iron oxides, which may be secondary or primary, in 0.2M NH_4-oxalate, pH 3.0, 80°C, 2h. Heavy metals liberated in the latter two steps are interpreted as incorporated in the mineral lattice by co-precipitation, adsorption by ligand exchange (e.g., oxyanions As and Mo), diffusion or replacement processes.

Table 1: *Sequential extractions applied in this study.*

Sequence A	References	Sequence B	References
(1) exchangeable fraction: 1.0 g sample into 20 ml 1M NH_4-acetate pH 4.5 shake for 2 hrs	Gatehouse et al., 1977; Sondag, 1981; Cardoso Fonseca et al., 1986	(1) Water soluble fraction: 1.0 g sample into 50 ml deionizied H_2O shake for 1h.	Ribet et al., 1995; Fanfani et al., 1997
(2) adsorbed, carbonates: 1M Na-acetate pH 5 shake for 2 hrs	Tessier et al., 1979	(2) exchangeable fraction: 1M NH_4-acetate pH 4.5 shake for 2 hrs	Dold, this study; Gatehouse et al., 1977; Sondag, 1981; Fonseca and Martin, 1986
(3) Mn oxides: 0.1 M NH_2OH-HCl pH 2 shake for 2 h	Chao, 1972; Cardoso Fonseca et al., 1986	(3) Fe(III) oxyhydroxides: 0.2 M NH_4-oxalate pH 3.0 shake for 1 h. in darkness, at RT	Dold et al., in prep.; Schwertmann, 1964; Stone, 1987
(4) Fe(III)oxides: 0.1 M NH_4-oxalate pH 3.3 heat in water bath 80°C for 2 hours	Fonseca and Martin, 1986	(4) Fe(III)oxides: 0.2 M NH_4-oxalate pH 3.0 heat in water bath 80°C for 2 hours	Dold, this study
(5) organics and sulfides: 35% H_2O_2 heat in water bath for 1 hour	Sondag, 1981	(5) organics and secondary Cu-sulfides: 35% H_2O_2 heat in water bath for 1 hour	Sondag, 1981; Dold, this study
(6) residual: HNO_3, HF, $HClO_4$, HCl digestion	Tessier et al., 1979; Hall et al., 1996; Dold et al., 1996	(6) primary sulfides: Combination of $KClO_3$ and HCl, followed by 4 M HNO_3 boiling	Chao & Sanzolone, 1977; Hall et al., 1996
		(7) residual: HNO_3, HF, $HClO_4$, HCl digestion	Tessier et al., 1979; Hall et al., 1996; Dold et al., 1996

3.3 Results and discussion of the Extraction Sequence B

3.3.1 Step 1: water-soluble fraction (1 g sample into 50ml deionized H2O shake for 1h)

Gypsum was identified with XRD as the main water-soluble phase in samples from the oxidation zone of El Salvador (Fig. 2), in the Piuquenes tailings (A4/200, A4/800), and in samples from a cementation zone ("hardpan") of the Ojancos tailings H1/1000 (Fig. 3), and H1/760.

Chalcanthite was identified as a secondary water-soluble mineral on the surface of tailings located in a Mediterranean climate (Cauquenes, central Chile). A wide range of water-soluble secondary sulfate minerals could be identified by XRD in samples of the evaporite zone from the

El Salvador tailings No.1, hyper-arid climate, northern Chile (Fig. 4). The dissolved minerals are identified as bonattite ($CuSO_4 \cdot 3H_2O$), chalcanthite ($CuSO_4 \cdot 5H_2O$), pickeringite ($MgAl_2(SO_4)_4 \cdot 22H_2O$), and magnesioaubertite ($(Mg,Cu)Al(SO_4)_2Cl \cdot 14H_2O$). The element concentrations in the water-soluble fraction of this sample are Cu = 5.0%; Al = 3.1%; Mg = 1.45%; Ca = 0.2%; Fe = 0.17%; Mn = 0.05%; Zn = 0.01%. Hand picked mineral specimen were identified as chalcanthite, halotrichite ($FeAl_2(SO_4)_4 \cdot 22H_2O$), and hexahydrite ($MgSO_4 \cdot 6H_2O$).

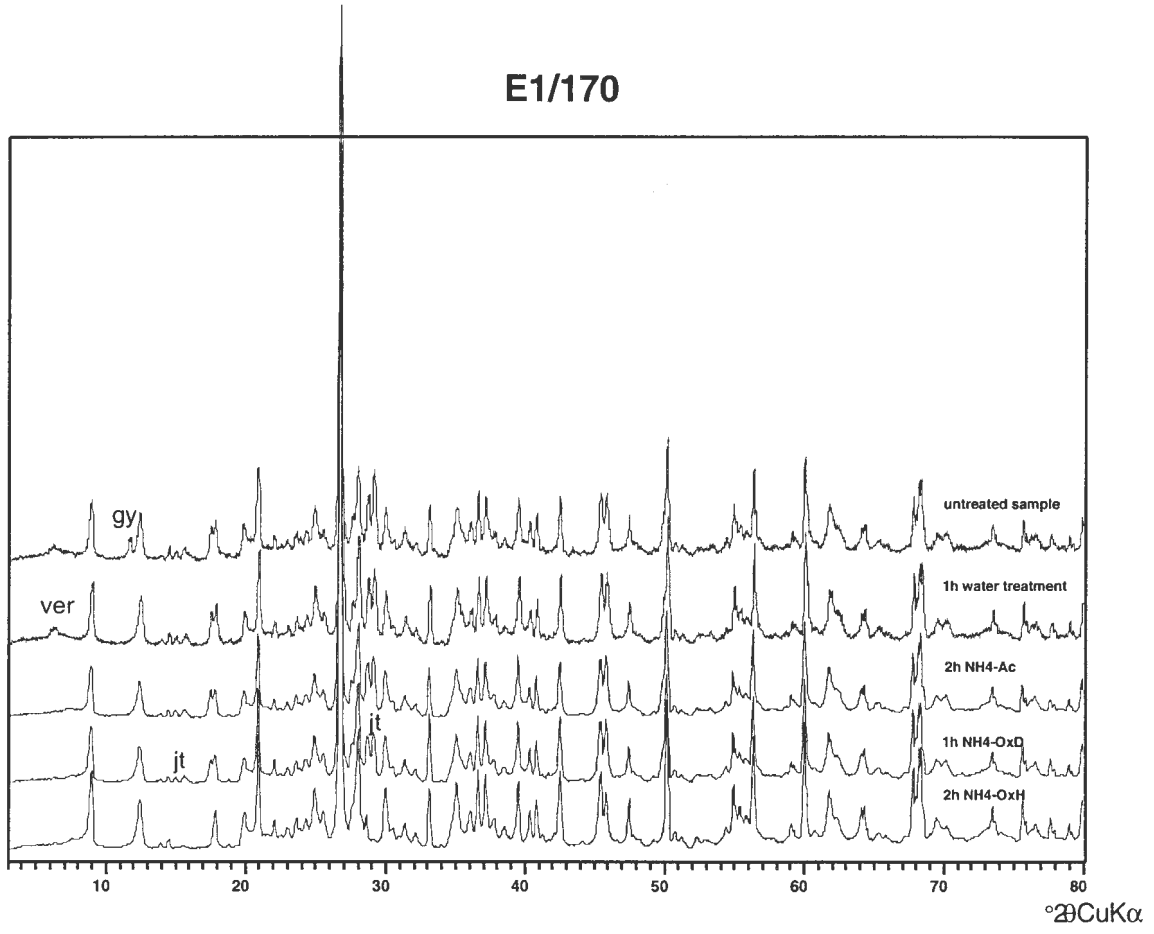

Fig. 2: *XRD results illustrating the effect of the first four steps of the extraction sequence B on a sample (E1/170) from a Fe(III)hydroxide rich layer from the El Salvador No.1 tailings impoundment, northern Chile. Gypsum dissolves in the water treatment (step 1), a vermiculite-type mixed-layer mineral breaks down in the NH4-acetate leach (step 2), and jarosite dissolves in the NH4-oxalate, hot, leach (step 4). Abbreviations: gy = gypsum; jt = jarosite; ver = vermiculite-type mixed-layer; NH_4-Ac = ammonium acetate; NH_4-OxD = ammonium oxalate, darkness; NH_4-OxH = ammonium oxalate, 80°C.*

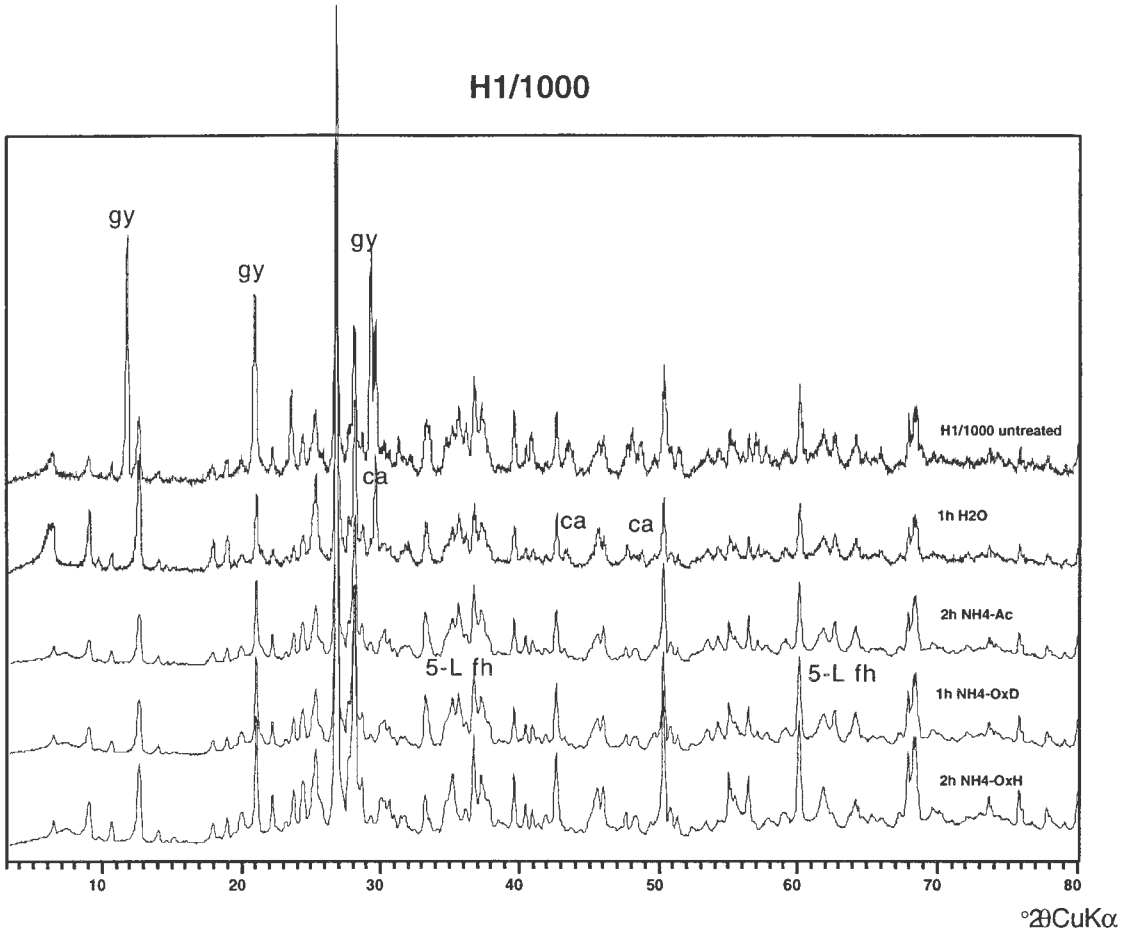

Fig. 3: XRD results illustrating the effect of the first four steps of the extraction sequence B on a sample (H1/1000) from the cemented layer of the Ojancos No.2 tailings impoundment, Copiapó, northern Chile. Gypsum (gy) dissolves in the water treatment (step 1), calcite (ca) dissolves in the NH4-acetate leach (step 2), and a 5-line ferrihydrite (5L fh) is dissolved in the NH4-oxalate, hot, leach (step 4). Abbreviations: gy = gypsum; ca = calcite; 5-L fh = 5-line ferrihydrite; NH_4-Ac = ammonium acetate; NH_4-OxD = ammonium oxalate, darkness; NH_4-OxH = ammonium oxalate, 80°C.

3.3.2 Step 2: exchangeable fraction (1M NH_4-acetate, pH 4.5, shaken for 2 hrs)

The NH_4-acetate leach is widely used for the determination of the exchangeable elements (Gatehouse et al., 1977; Sondag, 1981; Cardoso Fonseca & Martin, 1986). It is known that calcite may go into solution in this leach, well documented by the XRD control in the sample H1/1000 (Fig. 3).

A vermiculite-type mixed-layer mineral is a typical secondary mineral in the low pH oxidation zone of sulfide mine tailings, resulting from the alteration of biotite, which is a principal K source for the formation of jarosite (Acker and Bricker, 1992; Farquhar et al., 1997; Malmström and Banwart, 1997). XRD control on the solid residuals of step 2 shows that this secondary mineral is broken down in the NH_4-acetate leach (Fig. 2 and Fig. 6) or in the NH_4-oxalate leach, if no NH_4-acetate leach was used previously (Fig. 5).

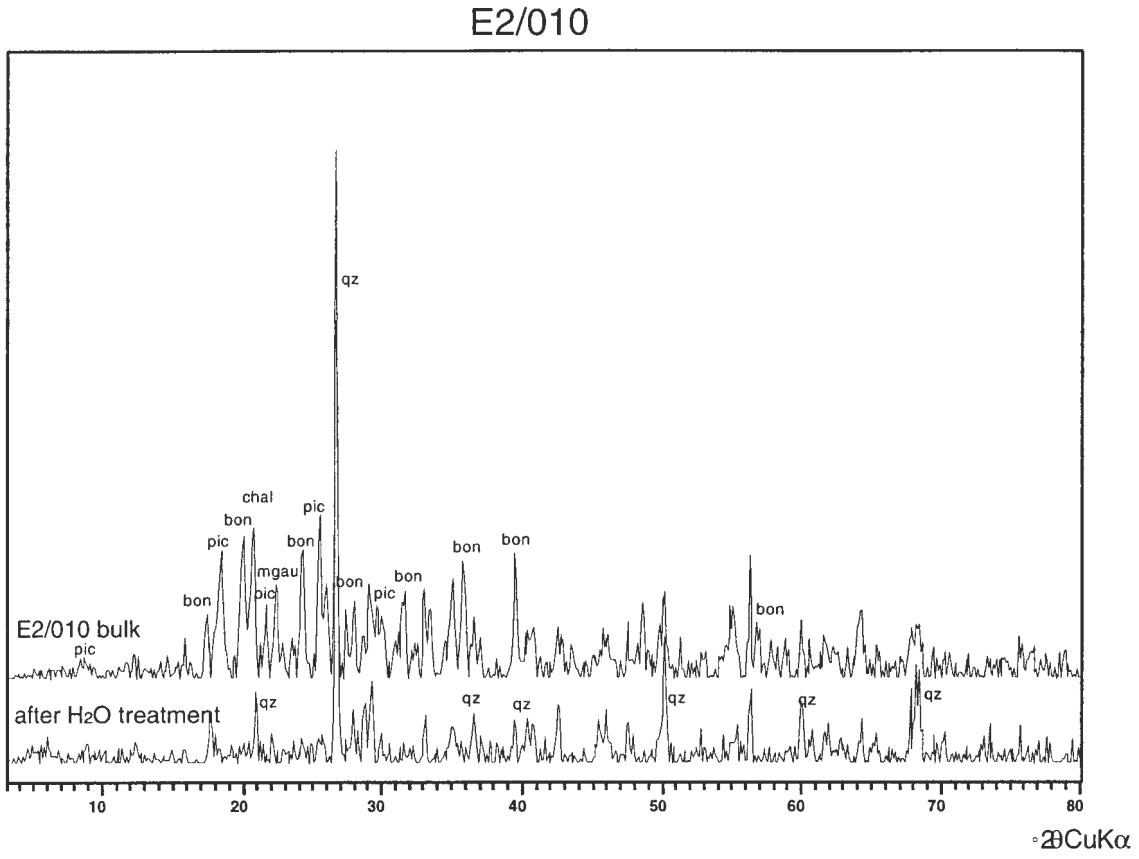

Fig. 4: Dissolution of bonattite (bon), chalcanthite (chal), pickeringite (pic), and magnesioaubertite (mgau) in the water treatment (step 1) shown by XRD on sample E2/010 from the top of the evaporite zone of the El Salvador No. 1 tailings impoundment, northern Chile. Abbreviations: bon = bonattite; chal = chalcanthite; pic = pickeringite; mgau = magnesioaubertite; qz = quartz

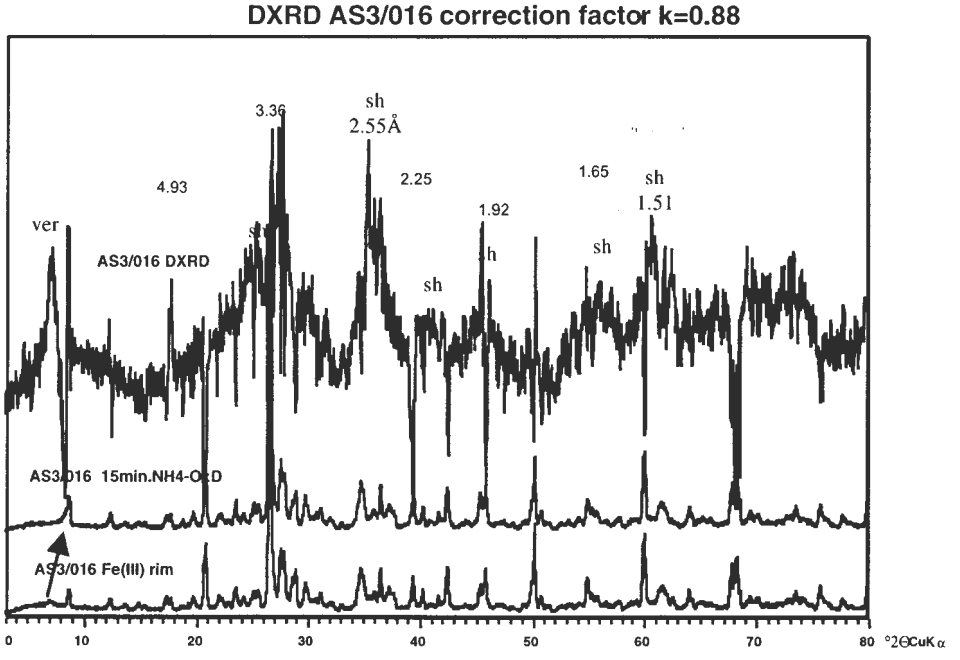

Fig. 5: DXRD of schwertmannite (sh) after 15 min treatment with NH4-OxD of a hand selected, Fe(III) oxyhydroxide-rich sample AS3 /016 from the oxidation zone from the Piuquenes tailings impoundment, La Andina mine, central Chile. The peak of the vermiculite-type mixed-layer (ver) mineral (d-value of 12.6Å) disappears with the NH4-OxD treatment (step 3) and at the higher flank of the mica peak 10.1Å a new peak appears, as shown more clearly in the DXRD by a negative peak. Abbreviations: sh = schwertmannite; ver = vermicultie-type mixed-layer; NH4-OxD = 0.2M ammonium oxalate, pH 3, darkness.

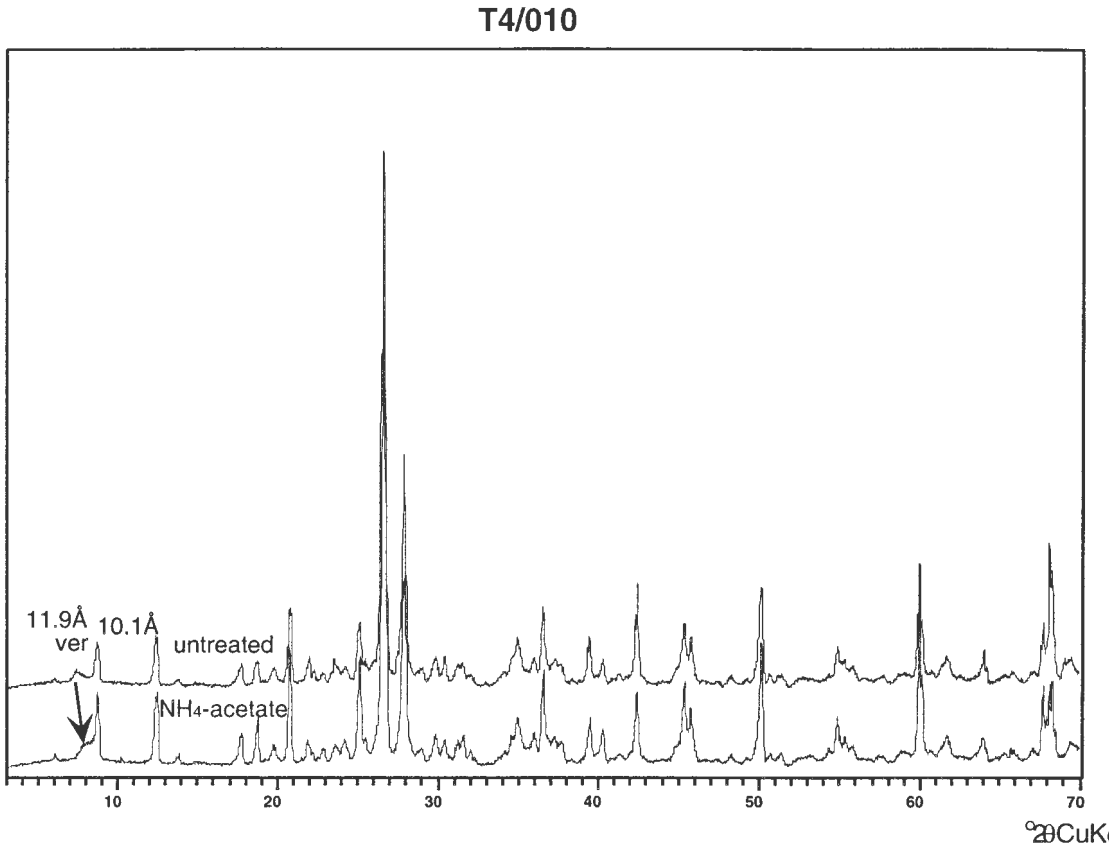

Fig. 6: Change of the position of the vermiculite-type mixed-layer mineral from 11.9Å to the flank of the mica peak of 10.1Å after the NH4-acetate leach (step 2) on the sample T4/010 from the oxidation zone from the Cauquenes tailings impoundment from El Teniente mine, central Chile. This is interpreted as an effect of the release of interlayer cations by the monodentate complex-former acetate. Abbreviations: ver = vermiculite-type mixed-layer, NH4-acetate = ammonium acetate leach

With the disappearance of the broad peaks at 11.7 – 14.5 Å a new peak at the flank of the illite peak (10.1 Å) to higher d-values can be observed after NH_4-acetate leach (Fig. 6). With this mineralogical change, which is not a complete dissolution, incorporated interlayer cations as Cu and Zn (Farquhar et al., 1997, Dold, chapter 5) may be released from this vermiculite-type mixed-layer mineral from samples in the low pH oxidation zone (chapter 5). It must be taken into account that these concentrations are not interpreted as adsorbed Cu, as at pH < 4 no significant Cu adsorption on Fe(III) hydroxides takes place (Dzombak & Morel, 1990; Webster et al., 1998). It is important to apply the NH_4-acetate leach before the NH_4-oxalate leach, as the latter also breaks down the vermiculite-type mixed-layer mineral. This would lead to a misinterpretation of the trace metal retention behavior of the secondary ferric phases.

3.3.3 Step 3: Fe(III) oxyhydroxides leach (0.2 M NH_4-oxalate, pH 3.0, 1 h in darkness, RT)

Schwertmannite and 2-line ferrihydrite dissolve completely, and secondary jarosite and higher ordered ferrihydrites (e.g., 6-line) dissolve partly in this leach. A detailed discussion of the dissolution kinetics of schwertmannite and ferrihydrite in 0.2M NH_4-oxalate, pH 3.0, in darkness, is presented in chapter 4. The study has shown that it is not possible to discriminate unequivocally these minerals by their dissolution kinetics. Based on the results of chapter 4 the

dissolution time of 1h was chosen for the sequential extractions to ensure the complete dissolution of schwertmannite and 2-line ferrihydrite. Dissolution kinetic tests and XRD control of the sample AS3/016 from the oxidation zone of a porphyry copper tailings impoundment show that after 15 min contact time schwertmannite went into solution (chapter 4, Fig. 8). After 1h secondary jarosite was partly dissolved, as is proven by XRD and also reflected by a decrease of the Fe/S mol ratio. The application of only 15 min contact time has shown to be selective for the detection of schwertmannite by DXRD in samples from the mine tailings (Fig. 5). The results show that it is impossible to restrict the dissolution to one secondary ferric phase. However, the application of one hour of 0.2M NH_4-oxalate, pH 3.0, darkness leach ensures that only the secondary ferric phases as schwertmannite and jarosite go into solution in samples from the oxidation zone.

Mineralogical detection of Mn-hydroxides by DXRD failed, due to low Mn concentration (< 1000 ppm). Mn-hydroxides may also be reduced by oxalate (Stone, 1987) and may have an important role in adsorption processes at higher concentrations.

3.3.4 Step 4: Fe(III) oxides leach (0.2 M NH_4-oxalate, pH 3.0, 80°C for 2 h.)

All secondary ferric minerals occurring as higher ordered ferrihydrite (6-line), goethite (Fig. 3), primary and secondary jarosite, natrojarosite (Fig. 2), and primary hematite go into solution in this leach. The study of a polished section of T4/010 after 1h attack shows that only some residual grains of magnetite survived this leach. Dissolution kinetic tests show that the sulfur values in samples of the oxidation zone reached the plateau after 15 and after 30 min, indicating that secondary and primary jarosite dissolve completely within 30 min, in this leach. This is confirmed by the visual control of the disappearance of the yellow color of jarosite (Fig. 7 & Table 2). Samples from the cementation zones show after 15 and after 50 min the complete dissolution of the secondary Fe(III) hydroxides, also indicated by the color change from red to gray. The application of this leach and the control of the dissolved phases by DXRD on samples from the cementation zone show that a higher ordered ferrihydrite (5-line and 6-line) together with goethite are the ferric phases present. This explains why ferrihydrite was not possible to detect in the 3rd dissolution step, due to its slow dissolution kinetics. This leach has shown to be very effective in the dissolution of the secondary sulfates such as jarosite and schwertmannite and is applied in chapter 5 and 6 for the separation of sulfate and sulfide sulfur for acid-base accounting (ABA). As shown by Chao and Sanzolone (1977), the oxalic acid dissolution method is not effective in dissolving any of the nine sulfides tested in their study. This is supported by the constant sulfur concentration after the dissolution of jarosite in the dissolution kinetic test of the sample E1/350 which contains still 6.8 wt. % of pyrite (Fig. 7).

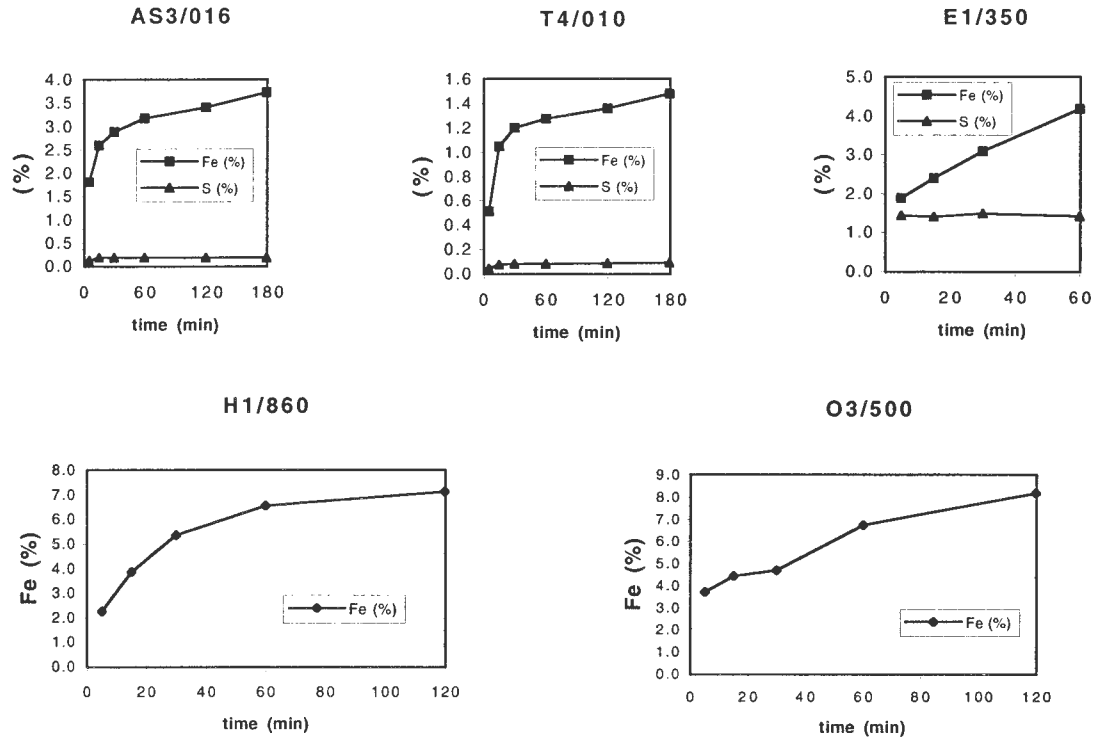

Fig. 7: Dissolution of jarosite (sample AS3/016, T4/010, and E1/350) and higher ordered ferrihydrite (H1/860 and O3/500) in NH4-oxalate hot leach (step 4). The three samples containing jarosite are from oxidation zones of porphyry copper tailings, Chile. The samples containing ferrihydrite are from cemented layers from carbonate-rich Fe-oxide Cu-Au tailings, Punta del Cobre belt, northern Chile.

3.3.5 Step 5: organics and secondary Cu-sulfides (35% H_2O_2 heat in water bath for 1 hour)

Results of sequential extraction together with mineralogical studies indicate that this leach seems to be selective to secondary Cu-sulfides such as covellite and chalcocite-digenite (chapter 5 & 6). The sulfide content in the studied tailings samples was too low for detection of the dissolved phases by DXRD. Further studies of the dissolution kinetics of supergene Cu-sulfides could enhance the selectivity of the 35% H_2O_2 leach.

Increased values of Mo in this leach in samples from the oxidation zone was observed in the three porphyry copper tailings. As 35% H_2O_2 is an oxidizing leach, the possibility that secondary Mo-sulfides are formed in the oxidation zone can be excluded. This supports the interpretation that Mo is fixed by bacteria cell material (chapter 5). Results for El Salvador (chapter 5) suggest that less stable pyrite varieties may partly dissolve in this leach.

Table 2: Data from the dissolution kinetic tests with 0.2 M NH4-oxalate, pH 3.0, heat in water bath 80°C for 2h, of the selected tailings samples. The sulfur concentrations represent the dissolved jarosite.

time (min)	5	15	30	60	120	180
AS3/016 Fe (%)	1.804	2.593	2.885	3.174	3.414	3.720
AS3/016 S (%)	0.124	0.179	0.182	0.180	0.180	0.185
T4/010 Fe (%)	0.513	1.047	1.198	1.273	1.360	1.480
T4/010 S (%)	0.044	0.074	0.080	0.079	0.084	0.090
E1/350 Fe (%)	1.886	2.396	3.078	4.174		
E1/350 S (%)	1.441	1.406	1.482	1.419		
H1/860 Fe (%)	2.252	3.859	5.354	6.544	7.121	
O3/500 Fe (%)	3.722	4.437	4.677	6.740	8.171	

3.3.6 Step 6: primary sulfides ($KClO_3$ and HCl, followed by 4 M HNO_3 boiling)

Chao and Sanzalone (1977) found that the $KClO_3$, HCl, HNO_3 leach is the most effective at dissolving pyrite, chalcopyrite, molybdenite, galena, sphalerite, tennantite-tetrahedrite, stibnite, cinnabar, and orpiment, but may attack some silicates along edges, corners, and surfaces. This leach is used in this study to separate the hypogene sulfide mineralogy from the residual silicate fraction. Due partly to the low sulfide content in the tailings material no mineralogical control of the dissolved phases was applied.

3.3.7 Step 7: residual silicates (HCl, HF, $HClO_4$, HNO_3)

This commonly used mixed acid leach was applied by Dold et al. (1996) to tailings samples from the Ojancos tailings impoundment No.2 and has shown to be very destructive to the silicate minerals. Only in some samples, in which primary minerals such as tourmaline, beryl, chromite and sphenes are present, a small amount of residuum may survive this attack (Hall et al., 1996; Dold, unpublished data).

3.4 Conclusions

The results of applying a 7-step sequential extraction to Cu-sulfide mine tailings and the dissolved phases in the different steps of the sequential extractions are summarized in table 3. The application of dissolution kinetic tests and the control of dissolved phases in sequential extraction by XRD and DXRD from samples of the studied mine tailings indicate which mineral is dissolved in each leach step. This information is crucial for interpretation of geochemical data obtained from sequential extractions.

It has been shown that the water-soluble fraction (step 1) may play an important role in the mine tailings environments, especially in climates with extensive evaporation (Mediterranean to hyper-arid) by dissolving secondary salts (e.g., bonattite, chalcanthite, pickeringite, hexahydrite).

It is strongly recommended to use the water-soluble fraction as the first step in sequential extractions for mine tailings.

In the NH_4-acetate leach (step 2), which liberates the exchangeable fraction (adsorbed), calcite is also dissolved, and a vermiculite-type mixed-layer mineral is broken down as well. This mineral is a typical secondary product in the oxidation zone of sulfidic mine tailings, resulting from the alteration of biotite by the release of K; it may liberate Cu and Zn in the NH_4-acetate leach, previously replacing K in the original biotite lattice.

The application of the 1h, 0.2 M NH_4-oxalate, pH 3.0 in darkness leach (step 3) ensures the complete dissolution of schwertmannite (chapter 3), but secondary jarosite also dissolves in samples from the oxidation zone. However, only secondary ferric minerals dissolve in this leach and minimize the dissolution of other iron phases. The application of one hour is long enough to dissolve 2-line ferrihydrite (chapter 3), but mineralogical and geochemical results indicate that in the mine tailings higher ordered ferrihydrite (5-line or 6-line) are dominant, indicating slow hydrolysis kinetics (Schwertmann et al., 1999). Thus, only parts of higher ordered ferrihydrite in the neutralization and primary zone of sulfide mine tailings will dissolve in the 1h 0.2 M NH_4-oxalate, pH 3.0, in darkness leach (step 3).

The residual of the secondary ferric minerals (jarosite and higher ordered ferrihydrite) dissolve in the following 0.2M NH_4-oxalate, pH 3.0, 80°C, 2h leach (step 4) together with the primary iron oxides. In this leach all secondary and primary ferric oxides, oxyhydroxides, and oxyhydroxide sulfates are dissolved. Only some hypogene magnetite may survive this leach. Chao and Sanzolone (1977) have shown that oxalic acid is not effective in dissolving sulfide minerals, as is confirmed by the dissolution kinetic tests. Thus, the 0.2M NH_4-oxalate, pH 3.0, 80°C, 2h leach (step 4) is proposed for differentiation of sulfate and sulfide sulfur for acid-base accounting (ABA) for mine waste. The total sulfur content of a sample can be measured by a LECO® furnace. Then the sample is attacked by the 0.2M NH_4-oxalate, pH 3.0, 80°C, 2h leach and the sulfur content may be measured by ICP-AES in the solution representing the sulfate content of the sample. The difference of the total sulfur and the sulfate sulfur leads to the sulfide sulfur content.

The two applied leaches for the sulfide fractions (35% H_2O_2 in step 5 and HCl, HF, $HClO_4$, HNO_3, in step 6) permit a semi-quantitative differentiation between hypogene and supergene Cu-sulfides in the studied tailings. However, further studies of the dissolution kinetics of supergene and hypogene Cu-sulfides in 35% H_2O_2 could enhance the selectivity of this leach. A detailed mineralogical study should accompany every geochemical study of mine waste to enhance the accuracy of the geochemical interpretations.

Table 3: *Extraction sequence "B" applied in this study and minerals preferentially dissolved in each step (abbreviations: bn: bornite; ca: calcite; cb: cinnabar; cc: chalcocite; cp: chalcopyrite; cv: covellite; dg: digenite; fh: ferrihydrite);gn: galena; gt: goethite; gy: gypsum; hm: hematite; ilm: ilmenite; jt: jarosite; mb: molybdenite; mt: magnetite; Na-jt: natrojarosite; op: orpiment; py: pyrite; sh: schwertmannite; sl: sphalerite; stb: stibnite tn: tennantite; tt: tetrahedrite).*

Leach	Preferentially dissolved minerals	References
(1) Water soluble fraction 1.0 g sample into 50ml deionizied H_2O shake for 1 h.	secondary sulfates, e.g., bonattite, chalcanthite, gy, pickeringite, magnesioauberite	Dold, this study; Ribet et al., 1995; Fanfani et al., 1997
(2) exchangeable fraction 1M NH_4-acetate pH 4.5 shake for 2 hrs	ca, vermiculite-type-mixed-layer, adsorbed and exchangeable ions	Dold, this study; Gatehouse et al., 1977; Sondag, 1981; Cardoso Fonseca et al., 1986
(3) Fe(III) oxyhydroxides 0.2 M NH_4-oxalate pH 3.0 shake for 1 h. in darkness	sh, 2-line fh, secondary jt, MnO_2	Schwertmann, 1964; Stone, 1987; Dold, chapter 4
(4) Fe(III)oxides 0.2 M NH_4-oxalate pH 3.0 heat in water bath 80°C for 2 hours	gt, jt, Na-jt, hm, mt, higher ordered fh's (6-line fh)	Dold, this study.
(5) organic and secondary Cu-sulfides 35% H_2O_2 heat in water bath for 1 hour	organic , cv, cc-dg	Sondag, 1981; Dold, chapter 5
(6) primary sulfides Combination of $KClO_3$ and HCl, followed by 4 M HNO_3 boiling	py, cp, bn, sl, gn, mb, tn-tt, cb, op, stb	Chao & Sanzolone, 1977; Hall et al., 1996
(7) residual HNO_3, HF, $HClO_4$, HCl digestion	Silicates, residual	Hall et al., 1996; Dold et al., 1996

Acknowledgments

I am grateful to Prof. L. Fontboté and Prof. W. Wildi for the support and the helpful suggestions. I thank also Prof. H.-R. Pfeiffer, J.-C. Lavanchy, and C. Schlegel for the facilities and discussions in the laboratory of the Centre d'Analyse Minerale, Université de Lausanne. Thanks to Dr. Dubois from Soil Science Institute of the EPFL, Lausanne for the ICP analysis. The project is supported by the German Academic Exchange Service (DAAD) and the Swiss National Science Foundation project No. 21-50778.97.

References

Acker, J.G., Bricker, O.P. (1992): The influence of pH on biotite dissolution and alteration kinetics at low temperature. Geochimica et Cosmochimica Acta, v. 56; p. 3073-3092.

Bigham, J.M., Schwertmann, U., Carlson, L., Murad, E. (1990): A poorly crystallized oxyhydroxysulfate of iron formed by bacterial oxidation of Fe(II) in acid mine waters. Geochimica et Cosmochimica Acta, v. 54, p. 2743-2758.

Bigham, J.M., Carlson, L., Murad, E. (1994): Schwertmannite, a new iron oxyhydroxy-sulphate from Pyhäsalmi, Finland, and other localities. Mineralogical Magazine, v. 58, p. 641-648.

Bigham, J.M., Schwertmann, U., Traina, S.J., Winland, R.L., Wolf, M. (1996): Schwertmannite and the chemical modeling of iron in acid sulfate waters. Geochimica et Cosmochimica Acta, v. 60, No. 2, p. 185-195.

Cardoso Fonseca, E., Martin, H. (1986): The selective extraction of Pb and Zn in selected mineral and soil samples, application in geochemical exploration (Portugal). Journal of Geochemical Exploration, v. 26, p. 231-248.

Chao, T.T., (1984): Use of partial dissolution techniques in geochemical exploration. Journal of Geochemical Exploration, v. 20, p. 101-135.

Chao, T.T., Sanzolone, R.F. (1977): Chemical dissolution of sulfide minerals. Journal of Research U.S. Geol.Survey, v. 5, p. 409-412.

Chao, T.T., Zhou, L. (1983): Extraction techniques for selective dissolution of amorphous iron oxides from soils and sediments. Journal of Soil Sci. Soc. Am. Proc., v. 47, p. 225-232.

Cornell, R.M., Schwertmann, U. (1996): The Iron oxides. VCH Verlagsgesellschaft mbH, Weinheim.

Czamanske, G.K., Ingamells, C.O. (1970): Selective chemical dissolution of sulfide minerals: a method of mineral separation. American Mineralogist, v. 55, p. 2131-2134.

Dold, B., Eppinger, K.J., Kölling, M. (1996): Pyrite oxidation and the associated geochemical processes in tailings in the Atacama desert/Chile: The influence of men controlled water input after disuse. Clean technology for the mining industry, Santiago, p. 417 - 427.

Dold, B., (1999): Mineralogical and geochemical changes of copper flotation tailings in relation to their climatic settings and original composition - Implications for acid mine drainage and element mobility. Ph.D thesis, University of Geneva.

Dzombak, D.A., Morel, F.M.M. (1990): Surface complexation modeling - Hydrous ferric oxides, Wiley, New York.

Fanfani, L., Zuddas, P., Chessa, A. (1997): Heavy metals speciation analysis as a tool for studying mine tailings weathering. Journal of Geochemical Exploration, v. 58, p. 241-248.

Farquhar, M.L., Vaughan, D.J., Hughes, C.R., Charnock, J.M., England, K.E.R. (1997): Experimental studies of the interaction of aqueous metal cations with mineral substrates: Lead, cadmium, and copper with perthitic feldspar, muscovite, and biotite. Geochimica et Cosmochimica Acta, v. 61; p. 3051-3064.

Fischer, W.R. (1976): Differenzierung oxalatlösllicher Eisenoxide. Zeitschrift für Pflanzenernährung und Bodenkunde, v. 139, p. 641-646.

Gatehouse, S., Roussel, D.W., Van Moort, J.C. (1977): Sequential soil analysis in exploration analysis. Journal of Geochemical Exploration, v. 8, p. 483-494.

Hall, G.E.M., Vaive, J.E., Beer, R., Hoashi, M. (1996): Selective leaches revisited, with emphasis on the amorphous Fe oxyhydroxide phase extraction. Journal of Geochemical Exploration, v. 56, p. 59-78.

Hall, G.E.M., Bonham-Carter, G.F. (eds) (1998): Special Issue: Selective Extractions. Journal of Geochemical Exploration, v. 61.

Malmström, M., Banwart, S. (1997): Biotite dissolution at 25°C. the pH dependence of dissolution rate and stoichiometry. Geochimica et Cosmochimica Acta, v. 61; p. 2779-2799.

McCarty, D.K., Moore, J.N., Marcus, W.A. (1998): Mineralogy and trace element association in an acid mine drainage iron oxide precipitate; comparison of selective extractions. Applied Geochemistry, v.13, p. 165-176.

McGregor, R.G., Blowes, D.W., Robertson, W.D. (1995): The application of chemical extractions to sulphide tailings at the Copper Cliff tailings area, Sudbury, Ontario. Sudbury '95 Proceedings, v. 3, p. 1133-1142.

Nesbitt, H.W., Canning, G.W., Bancroft, G.M. (1998): XPS study of reductive dissolution of 7Å-birnessite by H_3AsO_3 with constraints on reaction mechanism. Geochimica et Cosmochimica Acta, v. 62(12), p. 2097-2110.

Reyes, I., Torrent,J. (1997): Citrate-ascorbate as a highly selective extractant for poorly crystalline iron oxides. Soil Science Society of America Journal, v. 61, p. 1647-1654.

Ribet, I., Ptacek, C.J., Blowes, D.W., Jambor, J.L. (1995): The potential for metal release by reductive dissolution of weathered mine tailings. Journal of Contaminant Hydrology, v. 17(3), p. 239-273.

Schulze, D.G. (1981): Identification of soil iron oxides minerals by differential x-ray diffraction. Soil Sci. Soc. Am. J., v. 45, p. 437-440.

Schulze, D.G. (1994): Differential x-ray diffraction analysis of soil material. In: Quantitative methods in soil mineralogy, SSSA Miscellaneous Publication, p. 412-429.

Schwertmann, U., Schulze, D.G., Murad, E. (1982): Identification of ferrihydrite in soils by dissolution kinetics, differencial x-ray diffraction, and Mössbauer Spectroscopy. Soil Sci. Soc. Am. J., v. 46, p. 869-875.

Schwertmann, U. (1964): Differenzierung der Eisenoxide des Bodens durch Extraktion mit Ammoniumoxalat Lösung. Zeitschrift für Pflanzenernährung und Bodenkunde, v. 105, p. 194-202.

Schwertmann, U., Bigham, J.M., Murad, E. (1995): The first occurrence of schwertmannite in a natural stream environment. European Journal of Mineralogy, v. 7, p. 547-552.

Schwertmann, U., Friedl, J., Stanjek, H. (1999): From Fe(III) ions to ferrihydrite and then to hematite. Journal of Colloid and Interface Science, v. 209, p. 215-223.

Sondag, F. (1981): Selective extraction procedures applied to geochemical prospecting in an area contaminated by old mine workings. Journal of Geochemical Exploration, v. 15, p. 645-652.

Stone, A.T. (1987) Microbial metabolites and the reductive dissolution of manganese oxides: Oxalate and pyruvate. Geochimica et Cosmochimica Acta, v. 51; p. 919-925.

Stumm, W., Sulzberger, B. (1992): The cycling of iron in natural environments: Considerations based on laboratory studies of heterogeneous redox processes. Geochimica et Cosmochimica Acta, v. 56; p. 3233-30257.

Suter, D., Banwart, S., and Stumm, W. (1991): The dissolution of hydrous iron(III) oxides by reductive mechanisms. Langmuir, v. 7, p. 809-813.

Tamm, O. (1922): Eine Methode zur Bestimmung der anorganischen Komponenten des Gelkomplexes im Boden. Medd. Statens skogsförsökanstalt, v. 19, p. 385-404.

Tamm, O. (1932): Über die Oxalatmethode in der chemischen Bodenanalyse. Medd. Statens skogsförsökanstalt, v. 27, p. 1-20.

Tessier, A., Campbell, P.G.C., Bisson, M. (1979): Sequential extraction procedure for speciation of particulate trace metals. Analytical Chemistry, v. 51, p. 844-851.

Webster, J.G., Swedlund, P.J., Webster, K.S. (1998): Trace metal adsorption onto an acid mine drainage iron(III) oxyhydroxy sulfate. Environmental Science & Technology, v. 32(10), p. 1362-1368.

CHAPTER 4

4 Dissolution kinetics of schwertmannite and ferrihydrite.

Abstract

A dissolution test with nine natural and synthetic schwertmannite and ferrihydrite samples was performed with 0.2M ammonium oxalate at pH 3.0 under exclusion of light (dark). Four natural and one synthetic schwertmannite samples and two natural and one synthetic samples of 2-line ferrihydrite, as well as one synthetic 6-line ferrihydrite were used. An additional sample was prepared by mixing schwertmannite and 2-line ferrihydrite 1:1 weight. Samples were characterized by X-ray diffraction (XRD) and differential X-ray diffraction (DXRD). Dissolved Fe and SO_4 was measured by inductively coupled plasma-atomic emission spectroscopy (ICP-AES). The mineral shape at different dissolution stages was monitored by scanning electron microscopy (SEM-EDS). The dissolution-time curves were modeled with rate equations.

Dissolution kinetics of natural and synthetic schwertmannite in 0.2 M ammonium oxalate, pH 3, dark, is very fast (> 94% in 60 min). Natural 2-line ferrihydrite has a similar dissolution kinetics (> 85% after 60 min), whereas synthetic ferrihydrite dissolves slower (16 and 42% after 60 min).

Modeling of schwertmannite dissolution curves, control of mineral shape by SEM, and Fe/S mole ratios of the dissolved fractions indicate that two different schwertmannite shapes (spherical and web-like) with different dissolution kinetics can be distinguished. The collapse of the spherical shaped (sea-urchin) schwertmannite aggregates seems to control its dissolution kinetics. In case of web-like schwertmannite, structural fixed SO_4^{2-} may have a predominant effect on the stability of the structure. No relationship was found between ferrihydrite shape and dissolution curves.

The results suggest that a selective leach for the ferric oxyhydroxides schwertmannite and lower ordered (2-line) ferrihydrite should be dissolution with 0.2 M ammonium oxalate pH 3, dark, during 60 min. These conditions maximize dissolution of schwertmannite and 2-line ferrihydrite, while minimizing the dissolution of other reducible phases like jarosite, hematite, magnetite, and goethite. Nevertheless, application of this attack to samples from the oxidation zone of sulfidic mine tailings has shown that a fraction of secondary jarosite dissolves too, although at a slower rate than schwertmannite and lower ordered ferrihydrite. If only schwertmannite is of interest (e.g., determination by DXRD), a 15 min attack should be preferred to increase selectivity.

4.1 Introduction

In 1992, the Commission on New Minerals and Mineral Names accepted the name "schwertmannite" for a ferric oxyhydroxide sulfate previously known as "acid mine drainage mineral" with the ideal formula between $Fe_8O_8(OH)_6SO_4$ and $Fe_{16}O_{16}(OH)_{10}(SO_4)_3$ (Bigham et al., 1990, 1994, and 1996a). Schwertmannite (sh) forms at pH conditions intermediate between jarosite and ferrihydrite. Jarosite (jt) $KFe_3(SO_4)_2(OH)_6$ occurs under strongly acidic conditions

(pH < 3), schwertmannite in the pH range of pH 2.8-4, and ferrihydrite (fh) $5Fe_2O_3 \cdot 9H_2O$ is stable at pH > 4. Schwertmannite and ferrihydrite are meta-stable relative to jarosite and goethite (Schwertmann et al., 1995; Bigham et al., 1996a).

Schwertmannite is one of the so called "poorly crystalline" or "X-ray amorphous" minerals with X-ray diffraction (XRD) patterns showing broad peaks similar to those of ferrihydrite (Fig. 1). The broad low intensity peaks in XRD patterns, close stability fields, meta-stability, and sometimes low concentrations in mine tailings makes the detection and discrimination of both minerals difficult. Because of their reactivity and large surface area, schwertmannite and ferrihydrite play an important role in the adsorption or incorporation of mobilized elements in surface and groundwater systems, such as soils and mine tailings impoundment (Davis and Kent, 1990; Dold et al., 1999).

Schwertmannite has been identified at several locations around the world as a precipitate in heavy metal and high sulfate drainage systems (Bigham et al., 1990, 1994, and 1996a; Schwertmann et al., Childs et al., 1998; 1995; Yu et al., 1998). Dold et al. (1999) demonstrated for the first time its presence in the oxidation zone of mine tailings, from two porphyry copper mines from Chile. This finding suggests that besides ferrihydrite, which is often mentioned as the ferric oxyhydroxide present in oxidation and precipitation zones, e.g., "hardpans" (Jambor, 1994; Ribet et al., 1995), also schwertmannite may often be present in the oxidation zone of mine tailings.

Schwertmannite is a yellowish orange-brown mineral with a high specific surface area in the range of 100-230 m^2/g. The generally proposed unit cell formula is $Fe_8O_8(OH)_6SO_4$ with a Fe/S mole ratio of 8. An average Fe/S mole ratio of 5 of many natural schwertmannites (Winland et al.1991; this study) suggest a composition close to $Fe_{16}O_{16}(OH)_{10}(SO_4)_3$. The structure proposed for this mineral is akin to that of akaganéite (FeO(OH, Cl)), with sulfate instead of chloride as a stabilizing anion in the tunnel cavities (Bigham et al., 1990, 1994). Waychunas et al. (1995) found that selenate (SeO_4^{2-}) appears to both substitute directly for sulfate within tunnels in the structure, and sorb at the surface of crystals. No disruption of the basic structure occurs with selenate substitution. Arsenate (AsO_4^{3-}) appears mainly to sorb outside of crystallites, destabilizing the structure and poisoning growth. Barham (1997) reports the transformation of schwertmannite to jarosite, hematite, and/or basic iron sulfate in laboratory experiments at room temperature. SO_4^{2-} in schwertmannite could be replaced by others anions such as CO_3^{2-}, $C_2O_4^{2-}$, CrO_4^{2-}, NO_3^-, OH^-, ClO_4^-, etc.

The rapid dissolution of schwertmannite in cold, 5 M HCl or in 0.2 M ammonium oxalate at pH 3 under exclusion of light was reported by Bigham et al. (1994). Bigham et al. (1990) reported complete dissolution of natural mine drainage samples in 0.2 M ammonium oxalate of pH 3 in the absence of light in 15 minutes. They also studied the dissolution kinetics of two natural schwertmannite samples with 0.1 M HCl. A sigmoidal shape of the Fe dissolution curve was interpreted as a change in particle morphology (e.g., dissolution cavities, break up of aggregates). A fast increase of SO_4^{2-} detected at the beginning of the dissolution process was interpreted as a "burst" of surface adsorbed SO_4^{2-}. Differences in bulk dissolution rates between the two samples were interpreted as differences in morphology. As a result of that study it was shown that SO_4^{2-} occupies sites both on the surface and within the structure of schwertmannite. In a further experiment Bigham et al. (1990) could show an essential structural role for the

remaining SO_4^{2-}. Higher SO_4^{2-} contents apparently increase the dissolution rate. This could be interpreted as an effect of destabilized structure as in the case of arsenate substitution, reported by Waychunas et al. (1995).

Ferrihydrite ($5Fe_2O_3 \cdot 9H_2O$; fh) is a red-brown, poorly crystalline, natural ferric oxyhydroxide mineral named by Chukhrov et al. (1973), with a high specific surface area, around 300 m^2/g. A series from 2-line to 6-line ferrihydrites can be differentiated on the basis of the XRD patterns with two up to six broad peaks (Cornell and Schwertmann, 1996). Recent results (Schwertmann et al., 1999) suggest that this is not a genetic series by transformation from lower to higher ordered phases. It seems more likely that every product is the result of specific conditions of crystallization mainly controlled by kinetics. These authors synthesized the whole range from the 2-line to 6-line ferrihydrite by varying the rate of hydrolysis, by change of the iron oxidation rate, or by increasing Si concentration.

The dissolution kinetics of 2-line ferrihydrite has been investigated by Fischer (1976) with three samples in 0.2 M ammonium oxalate pH 3 in the dark. He found the slowest dissolution rate for slowly precipitated samples, and the faster dissolution rates for rapidly precipitated samples. Higher crystalline or Si-bearing ferrihydrite samples dissolved more slowly. Cornell and Schwertmann (1996) suggest 2 - 4h reaction time with 0.2M ammonium oxalate, pH 3, in the dark, for ferrihydrite dissolution. The dissolution kinetics of 6-line ferrihydrite has not been investigated to date.

The purpose of the present study is to investigate the possibility of discriminating between schwertmannite and ferrihydrite on the basis of their dissolution kinetics in acid ammonium oxalate. As shown above, this should be possible, owing the existing data, which indicate longer dissolution time for ferrihydrite. It is important to be able to differentiate between schwertmannite and ferrihydrite to study their role in metal adsorption. Metal adsorption to hydrous ferric oxides (HFO) is a function of pH (Dzombak and Morel, 1990; Webster et al. 1998), and the meta-stability fields of schwertmannite and ferrihydrite are also pH controlled. Thus, in interface environments between acidic and neutral conditions, as observed in oxidizing mine tailings or acid rock drainage, these two minerals may play a very different role in metal retention. Dissolution kinetics and Fe/S mole ratios may be useful in understanding the structure of these minerals and the role of the anions in the structure.

4.2 Samples and methods

Five samples of schwertmannite, three samples of 2-line ferrihydrite, and one of 6-line ferrihydrite were used for dissolution kinetics tests (Table 1). Samples MS1, MS3, PR1, PR2, BT3 (for detailed mineralogy, see Fig. 1 and Table 1) are ochre precipitates collected from acid coal mine drainages in Ohio, USA. Chemical properties of these samples are described by Winland et al. (1991) and Bigham et al. (1996a). Sh4 is synthetic schwertmannite prepared using the method of Bigham et al. (1990). The synthetic ferrihydrites Fh-2L and Fh-6L were prepared using the methods described by Schwertmann and Cornell (1991). These eight samples were all provided by Prof. U. Schwertmann, Soil Science Department of the University of München, Germany with exception of AS3/016.

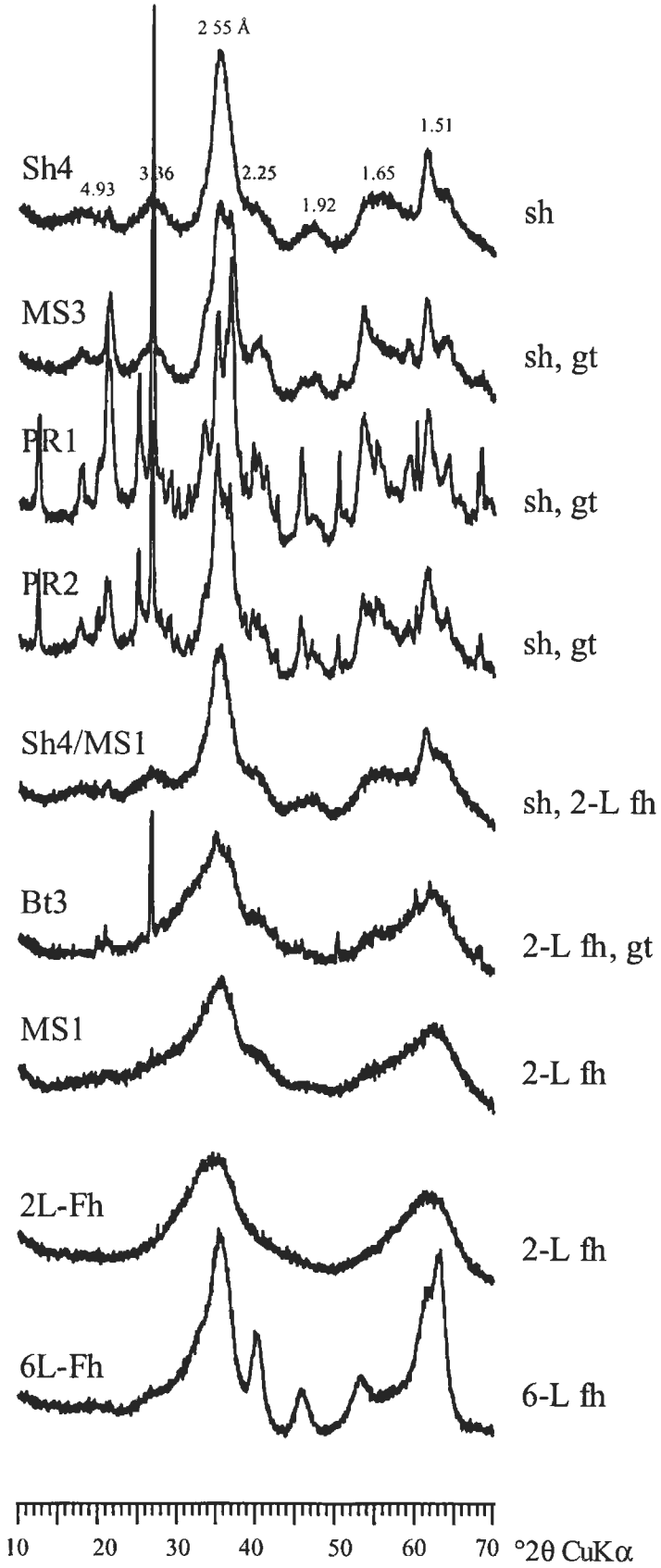

Fig. 1: *X-ray powder diffraction patterns of the 9 samples studied. More descriptive details in Table1. Abbreviations: fh = ferrihydrite, sh = schwertmannite, gt = goethite, 2L = two line, 6L = six line.*

A mechanical mixture of a synthetic schwertmannite (Sh4) and a natural 2-line ferrihydrite (MS1) 1:1 wt. % was also used. Sample MS1 was originally described by Bigham et al. (1996) as a ferrihydrite-schwertmannite mixture based on XRD patterns with features reminiscent of both ferrihydrite and schwertmannite, a low Fe/S mole ratio (9.9), and TEM observation indicating particles with morphology typical of schwertmannite (J.M. Bigham, 1998 personal communication). During the present work and based on the XRD pattern of MS1 (Fig. 1) and mineral morphology control with scanning electron microscopy (SEM), MS1 was determined to be a 2-line ferrihydrite. No indications of spherical or sea-urchin like morphology typical of schwertmannite could be found (Fig. 5). The low Fe/S mole ratio is interpreted as due to adsorbed sulfate.

Sample AS3/016 was hand-picked from a schwertmannite-containing streak from the oxidation zone of the Piuquenes tailings impoundment at the La Andina porphyry copper deposit, Central Chile (Dold et al., 1999). The mineralogy of this sample is dominated by secondary jarosite and a vermiculite-type mixed-layer. The presence of schwertmannite was ascertained by differential X-ray diffraction (DXRD, see Fig. 2). The other samples were characterized by XRD, using a Philips diffractometer 3020 with CuKα (λ = 1.54056 Å) and monochromator, at 40 kV, 30 mA. Diffractometer settings were: step scanning with 0.05° 2θ step size and 20 s counting time per step (Fig. 1) as used by Bigham et al. (1990, 1994), and Schwertmann et al. (1995).

Table 1: *Description of the natural samples used for the dissolution kinetic tests and the pH of the source waters. Fe and SO_4 of HCl-soluble fraction. Modified after Winland et al. (1991) and Bigham et al. (1996). Data for AS3/016 are from this study.*

Sample	mineralogy	pH	Fe (mole/kg)	SO_4 (mole/kg)	Fe/S mole ratio
MS3	Sh, Gt(t)	2.8	9.0	2.05	4.4
PR1	Sh, Gt(t)	3.2	8.9	1.70	5.2
PR2	Sh, Gt(t)	2.8	10.3	1.83	5.6
MS1	Fh-2L	5.8	7.0	0.71	9.9
BT3	Fh-2L	7.5	9.4	0.17	55.3
AS3/016	Sh, Jt	3.16*	0.099	0.020	4.9

fh = Ferrihydrite, 2L = two line, sh = schwertmannite, gt = goethite, jt = jarosite, (t) = trace,

** = in situ pH with a special glass electrode.*

The samples were subjected to dissolution by freshly prepared 0.2 M ammonium oxalate solution brought to pH 3.00 by 0.2 M oxalic acid under exclusion of light, at room temperature (Schwertmann, 1964). The dissolution-time curves were developed by shaking 125 mg of sample in 250 ml oxalate solution and taking 10 ml sub-samples with syringes at 3, 6, 9, 12, 15, 20, 30, 45, 60, and 120 min. The samples were filtered instantaneously with a 0.2 µm Teflon inline filter for syringes. Dissolved Fe and SO_4 (as total S) were measured in triplicate by inductively

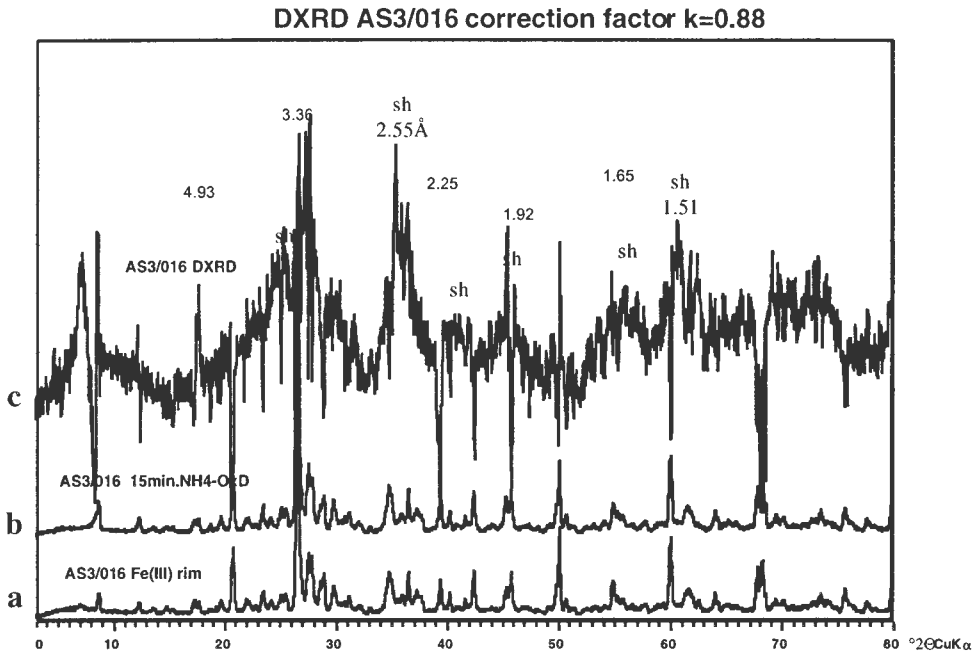

Fig. 2: X-ray powder diffraction patterns of (a) AS3/016 untreated, (b) AS3/016 treated 15 min with acid ammonium oxalate in the dark, and (c) the resulting DXRD showing schwertmannite. Abbreviations: sh = schwertmannite; NH_4-OxD = 0.2M ammonium oxalate, pH 3, darkness

coupled plasma-atomic emission spectroscopy (ICP-AES). To calculate the percentage of dissolved iron for the two synthetic phases Fh-2L and Fh-6L a sample was taken after 24 h exposure to light, representing the value for 100% dissolved (the photochemical influence to dissolution of iron oxides in acid ammonium oxalate was applied by Schwertmann, 1964). Goethite is present as a trace phase in the schwertmannite samples. Because of low, but significant solubility of goethite in ammonium oxalate pH 3 with UV light, it was not possible to obtain 100% values for schwertmannite dissolution by exposure to light. Therefore, for these samples, which reached a plateau after 60 min, it was assumed that after 120 min 100% of schwertmannite was dissolved. The dissolution curves were modeled with rate equations as outlined by Cornell and Schwertmann (1996) and curves were calculated to best fit by iteration (Table 2). Two aliquots of the samples MS3 and PR1 were subjected to dissolution 12 and 35 min, respectively 7 and 30 min with acid ammonium oxalate and filtered with a 0.45µm Na-acetate filter. The air-dried residuum was studied with SEM to determine mineral morphology and test the modeled geometric dissolution of spherical schwertmannite.

Table 2: *Rate equations used for modeling the dissolution kinetics curves (from Brown et al., 1980; Giovanoli and Brütsch, 1975; in Cornell and Schwertmann, 1996).*

Equation	Type	Physical meaning	
$(1-\alpha) = e^{-kt}$	Deceleratory	First order equation	(1)
$\alpha^2 = kt$	Deceleratory	One-dimensional diffusion	(2)
$1-(1-\alpha)^{1/3} = kt$	Geometric	Phase boundary controlled for a contracting sphere (cube root)	(3)
$1-\alpha = e^{-(kt)^a}$	Variable	No physical meaning (Kabai equation)	(4)

α = fraction dissolved at time t; a = constant; t = time; k = rate constant;

4.3 Results and discussion

The results of the dissolution kinetics tests are shown in Fig. 3a and 3b, and Table 3. Schwertmannite samples dissolve fastest (> 94% in 60 min), followed by the natural 2-line ferrihydrite samples (> 85% after 60 min) and the synthetic ferrihydrite samples (41.8% 2-line fh and 16.4% 6-line fh after 60 min), see. The following two minerals will be discussed separately.

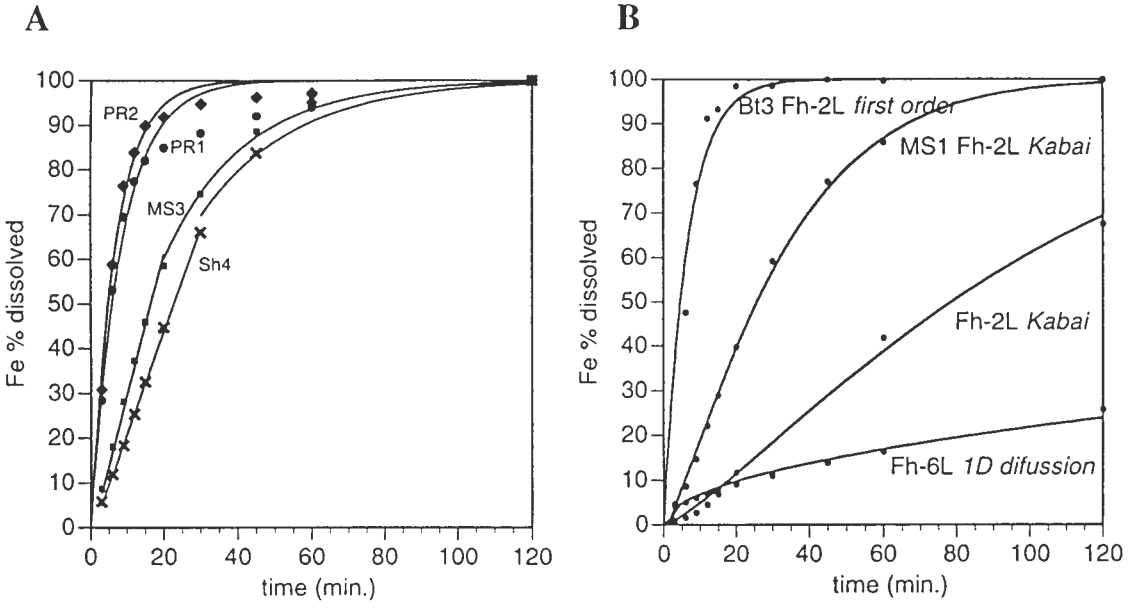

Fig. 3: (A) dissolution kinetic values (dots) and modeled curves of the schwertmannite samples MS3, Sh4, PR1, and PR2. Note that after 20 min in case of MS3 and 30 min in case of Sh4 the used model changes from contracting sphere to dissolution as a function of the remaining surface. (B) dissolution kinetic results of the ferrihydrite samples Bt3, MS1, Fh-2L, and Fh-6L.

Table 3: Fe and Fe/S mole ratios data of the dissolution tests of the studied samples.

time (min)	PR1 (Sh) Fe (% diss)	PR1 (Sh) Fe/S mole	PR2 (Sh) Fe (% diss)	PR2 (Sh) Fe/S mole	MS3 (Sh) Fe (% diss)	MS3 (Sh) Fe/S mole	Sh4 (Sh) Fe (% diss)	Sh4 (Sh) Fe/S mole	Bt3 (Fh-2L) Fe (% diss)	Fh-2L syn Fe (% diss)	Fh-6L syn Fe (% diss)	MS1 (Fh-2L) Fe (% diss)
3	28.4	2.2	30.8	3.3	8.7	2.3	5.8	2.3	-	1.0	4.2	4.7
6	53.1	2.9	58.8	4.0	18.0	3.0	11.9	3.2	47.6	1.5	5.1	8.6
9	69.5	3.3	76.4	4.6	28.2	3.4	18.3	4.0	76.6	2.7	6.1	14.7
12	77.4	3.6	83.8	4.6	37.3	3.9	25.3	4.4	91.3	4.6	6.9	22.2
15	82.0	3.7	89.8	4.8	45.9	3.9	32.5	4.9	93.3	6.9	7.9	29.0
20	84.9	3.7	91.8	4.7	58.6	3.9	44.7	5.3	98.6	11.7	9.1	39.9
30	88.2	3.7	94.7	4.5	74.6	4.4	66.0	5.4	98.7	-	11.1	59.2
45	92.0	3.9	96.2	4.8	88.6	4.3	83.7	5.2	100.0	-	13.9	77.0
60	94.0	4.0	97.2	4.7	95.1	4.5	96.0	5.2	99.8	41.8	16.4	85.8
120	100.0	4.1	100.0	5.2	100.0	4.5	100.0	5.1	100.0	67.5	25.7	100.0

Abbreviations: Sh = schwertmannite, Fh-2L = 2-line ferrihydrite, Fh-6L = 6-line ferrihydrite, % diss =% dissolved, , syn = synthetic, - = no data.

4.3.1 Schwertmannite

The shapes of the dissolution curves of the schwertmannite samples can be divided into two groups. The first group (Sh4 and MS3) shows a linear behavior at the beginning and exponential at the end (Fig. 4a and 4b). Characterization of the mineral shape with the SEM secondary electron images shows that Sh4 and MS3 have typical spherical particles with spicules, as sea-urchins (Fig. 5).

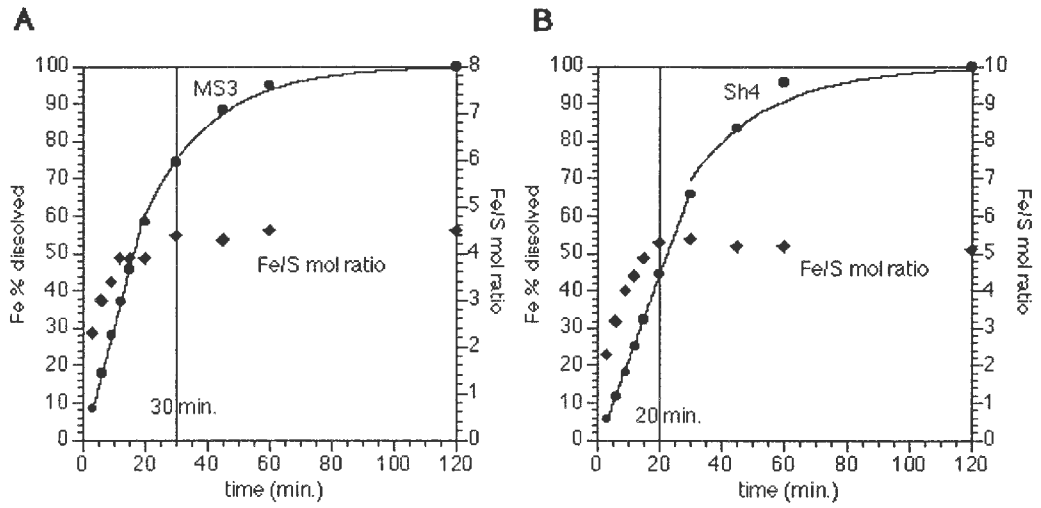

Fig. 4: (A) Dissolution curve of schwertmannite samples MS3 and (B) Sh4. Round dots are measured Fe-values, diamonds represent Fe/S mole ratio values. The line is modeled. The linear first part of the curve is modeled by the contracting sphere equation, the exponential part by the first order equation. The change in curve shape indicates when the dissolution controlling geometry of schwertmannite collapses, and the residual schwertmannite particles dissolve as a function of their remaining surface.

The first linear part of the dissolution curve can be modeled by a geometric expression with the physical meaning, that the phase boundary is controlled for a contracting sphere (Table 2, cube root). After 20 respectively 30 min, it changes to exponential behavior, described by a first order equation (Table 2), which indicates that at any time t, the dissolution rate will be a function of the remaining surface area (Cornell and Schwertmann, 1996). The change in the curve shape is thought to reflect the moment at which the spherical geometry of schwertmannite collapses, and the residual schwertmannite particles dissolve as a function of their remaining surface area. The time at which the Fe/S mole ratios stabilize does not correlate with the shape change of the dissolution curve (Fig. 4). This indicates that for the first group of schwertmannite (MS3 and Sh4) the adsorbed sulfate has no influence in the structural stability, as shown by Bigham et al. (1990).

The second group of schwertmannite samples showed slightly faster dissolution with exponential behavior and can be best modeled from the beginning by a first order equation type (PR1, PR2, Fig. 3a, and AS3/016, Fig. 8). Characterization of the mineral shape with the SEM secondary electron images shows that PR1 and PR2 have web-like, filigree structures (Fig. 5). After 12 min in case of PR1 and 15 min in case of PR2, the dissolution rate slows down.

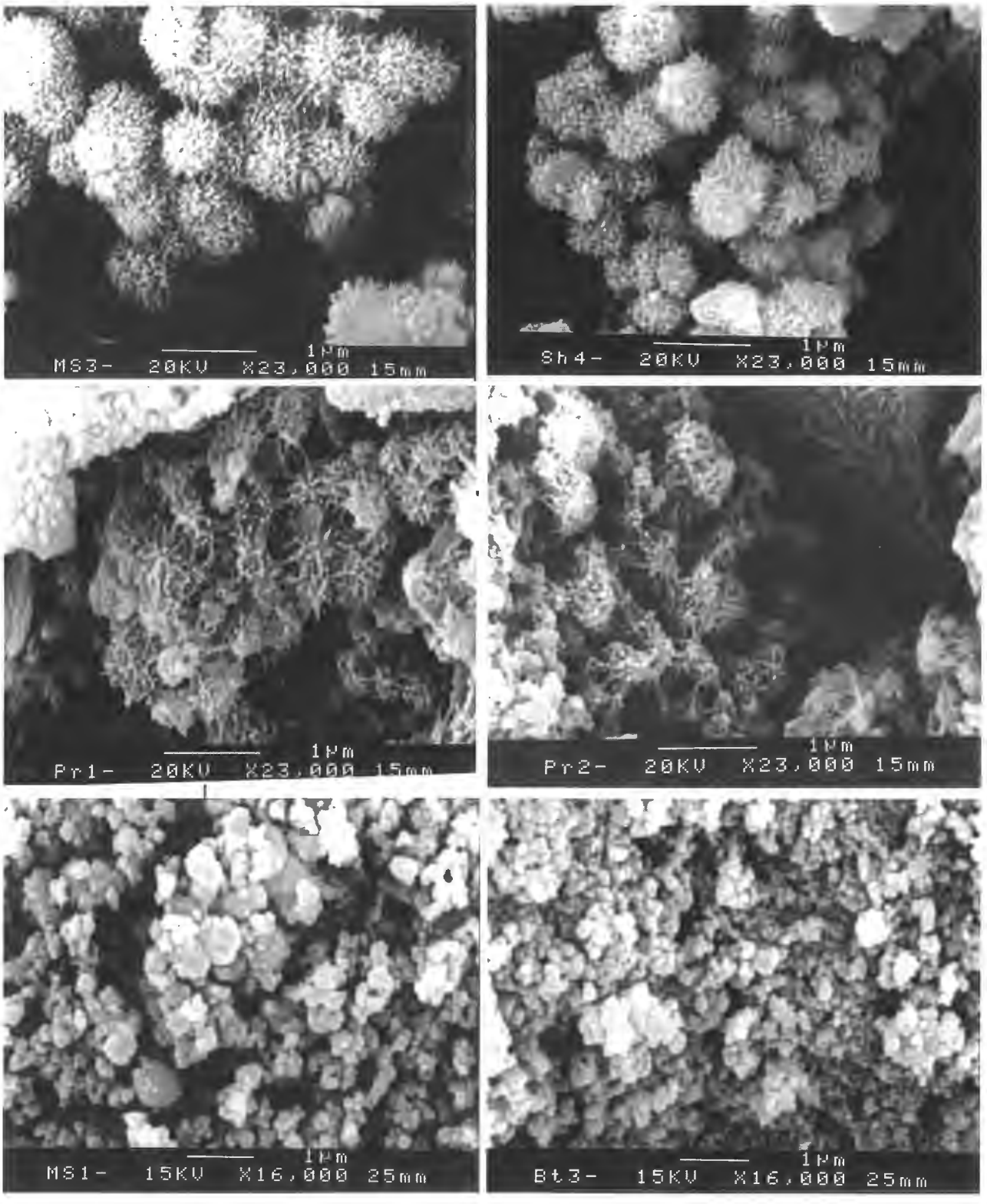

Fig. 5: *SEM images of the schwertmannite (MS3, Sh4, PR1, PR2) and ferrihydrite (MS1 and Bt3) samples for the curves shown in Fig. 4. MS3 and Sh4, which were modeled by a contracting sphere show the typical spherical particles of schwertmannite with spicules reminding sea-urchins. In contrast, the faster dissolving schwertmannite phases PR1 and PR2 show web-like, filigree structures. MS1 and Bt3 show very fine irregularly shaped particles. MS1 does not show any features of schwertmannite structures so that it was classified as a 2-line ferrihydrite.*

Replotting the data using a logarithmic scale (Fig. 6) reveal a break after 12 min, respectively 15 min appear, indicating a change in the dissolution kinetics. This corresponds to the moment, at which the Fe/S ratio reaches nearly constant values (see Table 4). The lower Fe/S mole ratios observed at the beginning of the schwertmannite dissolution, indicate a higher SO_4^{2-} release compared to Fe, possibly due to surface adsorbed SO_4^{2-}, as reported by Bigham et al. (1990). The change to stable SO_4^{2-} release corresponds to lower dissolution rates, possibly because of a stabilizing effect on the crystalline structure of the structural SO_4^{2-}.

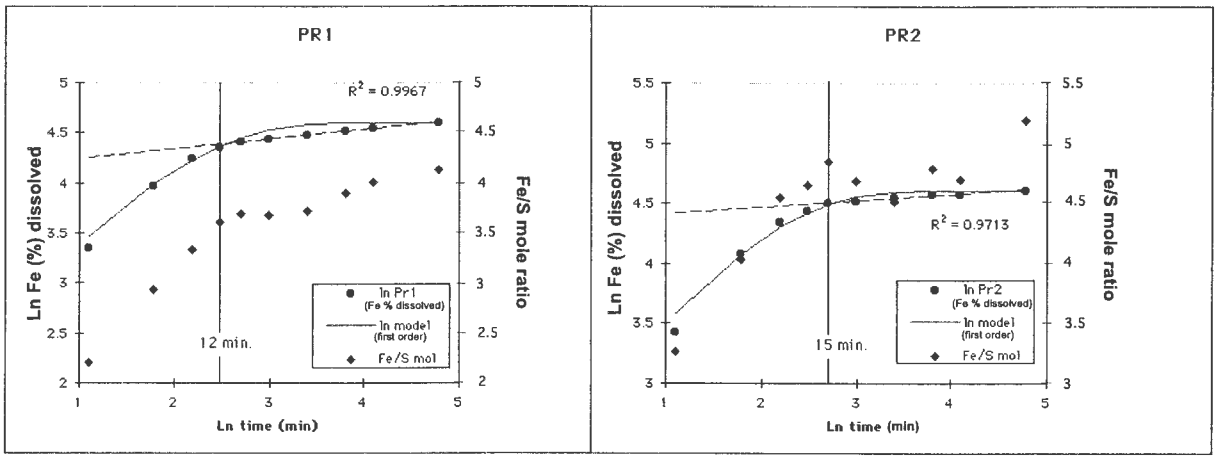

Fig. 6: *PR1 and PR2 dissolution curves and Fe/S mole ratios on logarithm scales. Dots (Fe in % dissolved) and diamonds (Fe/S) are measured values, lines are modeled by first order equation. The time at which Fe/S mole ratios reach nearly constant values (12 and 15 min, respectively) coincides with a slow down of the dissolution kinetics. This may reflect the stabilizing role of structural fixed SO_4^{2-}.*

Table 4: *Fe/S mole ratios of the dissolved fractions of schwertmannite samples, sh/fh mixture and a mine tailings bulk sample obtained in the dissolution kinetic tests. sh = schwertmannite, fh = ferrihydrite.*

time (min)	PR1 natural sh	PR2 natural sh	MS3 natural sh	Sh4 synthetic	Sh4/MS1 1:1 mix sh/fh	AS3/016 sh and jt rich tailings
3	2.2	3.3	2.3	2.3	1.9	
6	2.9	4.0	3.0	3.2	3.7	4.2
9	3.3	4.6	3.4	4.0	4.5	
12	3.6	4.6	3.9	4.4	5.3	
15	3.7	4.8	3.9	4.9	5.8	4.9
20	3.7	4.7	3.9	5.3	6.3	
30	3.7	4.5	4.4	5.4	6.6	4.8
45	3.9	4.8	4.3	5.2	7.0	
60	4.0	4.7	4.5	5.2	6.9	4.5
120	4.1	5.2	4.5	5.1	6.9	

To monitor the morphologies (spherical or web-like) which control the schwertmannite dissolution, aliquots of MS3 and PR1 were subjected to a defined time-range dissolution and the mineral morphologies were observed by SEM. Sample MS3 showed still spherical forms remaining after 12 min, while after 35 min they had disappeared (Fig.7). This is consistent with modeling as a contracting sphere for the beginning of the dissolution curve and subsequently, after the spherical structure collapses, as a first order equation. In contrast with sample MS3, sample PR1 did not show any morphological characteristics of schwertmannite after only 7 min, confirming the pertinence of the dissolution modeling as a function of the surface area of the particles left (Fig. 7).

It is not known which conditions lead to the different mineral shapes of schwertmannite. Factors that may influence mineral shape and dissolution kinetics could be SO_4^{2-} content (Bigham et al., 1990) or oxyanion substitution in schwertmannite (Waychunas et al., 1995; Barham, 1997). However, at least for samples MS3 and PR1, arsenate substitution does not seem to be responsible for the different mineral shapes and associated dissolution kinetics, as in both cases As content was < 1ppb (detection limit) in the leach. Also the Fe/S mole ratios of the schwertmannite samples do not provide any clear evidence of SO_4^{2-} controlled dissolution kinetics and shape.

4.3.2 Ferrihydrite

Dissolution curves of ferrihydrite (Fig. 3b) showed more variability than those of schwertmannite. Natural ferrihydrites dissolved faster than synthetic ones. This is possibly due to microbiological interactions during formation, as proposed by Fischer (1976). For example, sample Bt3 dissolved very fast (> 90% in 15 min) and can be modeled by a first order equation. In contrast, the dissolution curves of samples MS1 and Fh-2L showed a more sigmoidal shape (Fig. 3b). This presumably reflects a change in particle morphology (dissolution cavities, break up of aggregates, etc.) during the initial stage of dissolution (Schwertmann, 1984). The latter two curves were modeled with the Kabai equation (Table 2). This equation provides a flexible way of summarizing experimental data, but is not based on any fundamental conceptual model of the dissolution process and therefore does not provide any physical meaning for the α variable (Cornell and Schwertmann, 1996). The dissolution curve of the 6-line synthetic ferrihydrite (Fh-6L) could be best modeled with the one-dimensional diffusion model.

4.3.3 Schwertmannite/ferrihydrite mixture

XRD analyses of the 1:1 wt.% mixture of synthetic schwertmannite and a natural 2-line ferrihydrite (Sh4/MS1) show slightly lower intensities than for pure schwertmannite (Fig. 1). As the dissolution curves of samples Sh4 and MS1 are similar (Fig. 3a and 3b), the resulting dissolution curve of the mixed sample (not shown) does not allow identification of the presence of ferrihydrite. The slight intensity difference in XRD patterns of pure schwertmannite and a mixture with ferrihydrite does not permit detection of mixtures of these two phases, due to the

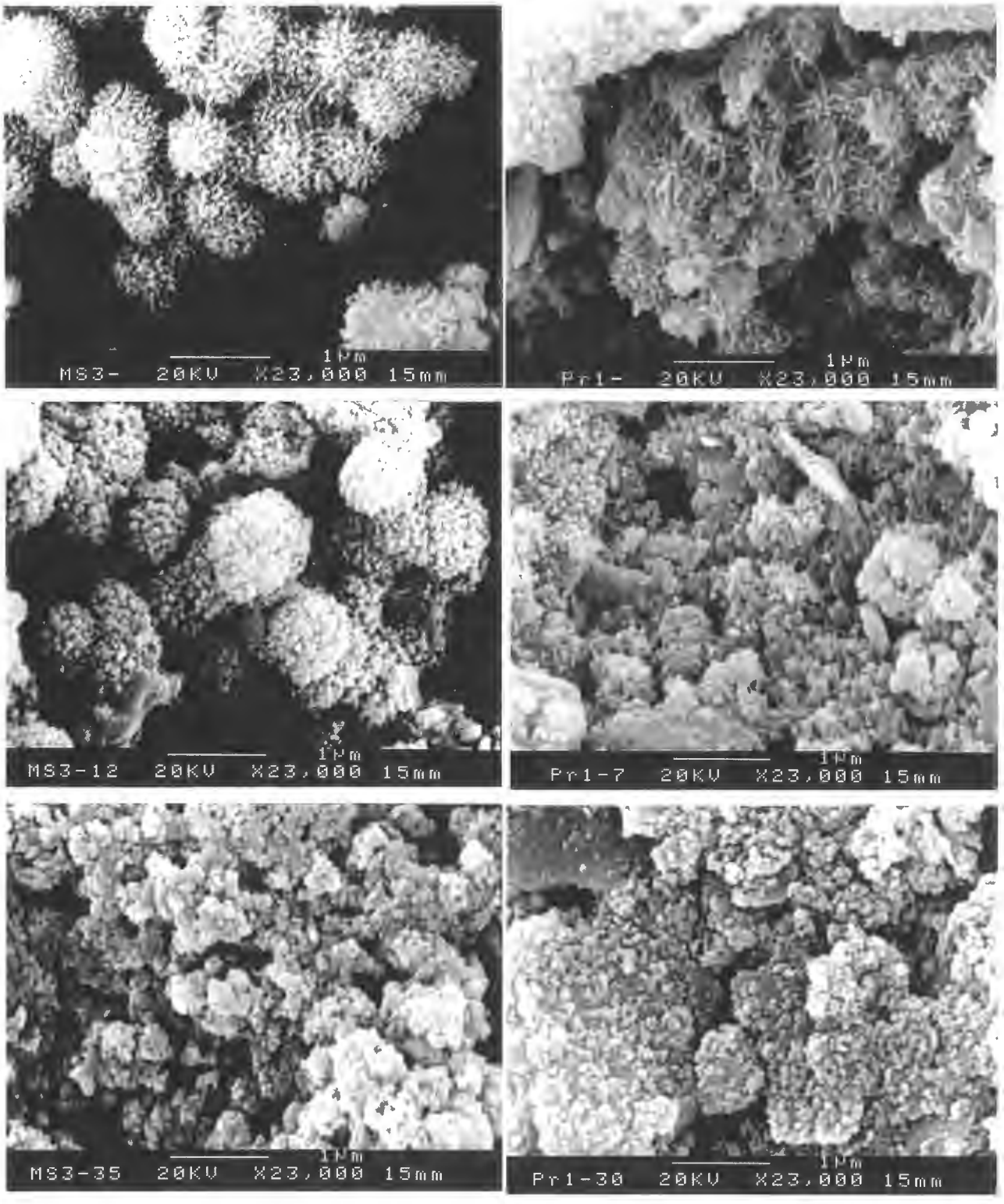

Fig. 7: *SEM images of samples MS3 and PR1. Left column, from top to bottom: MS3 after 0, 12, and 35 min acid ammonium oxalate dissolution. Right column, from top to bottom: PR1 after 0, 7, and 30 min dissolution. After 12 min dissolution MS3 still shows spherical shape as expected from the modeling of the dissolution results, whereas, after 35 min, only fine irregular particles are left, which dissolve as a function of their surface area. After 7 min PR1 shows only very fine irregular residual particles. Modeling of the dissolution kinetics tests suggest that they dissolve as a function of their surface area.*

lack of intensity studies of XRD patterns for schwertmannite. Nevertheless, the Fe/S mole ratio of the mixed sample shows a higher value (6.9) than without ferrihydrite (Table 4) so that the Fe/S mole ratio in this case is an important indicator of the presence of ferrihydrite in a schwertmannite sample. However, as long as the structural formula and so the Fe/S mole ratio of schwertmannite is not clear (5 or 8, see above), it is difficult to use the Fe/S mole ratios as a quantitative indicator to discriminate between schwertmannite and ferrihydrite.

Therefore, the variations of the Fe/S mole ratios found in samples of schwertmannite (between 5-8), which display similar dissolution kinetics and overlapping XRD patterns, could have their origin in different degrees of a mixture of schwertmannite and lower ordered ferrihydrite.

4.3.4 Test on a mine tailings sample

The results summarized in Table 5 suggest that to attain a selective dissolution of the ferric oxyhydroxides schwertmannite and 2-line ferrihydrite, 60 min attack with 0.2 M ammonium oxalate pH 3, dark should be chosen. Under these conditions > 94 % schwertmannite and > 85% 2-line ferrihydrite should dissolve, by minimizing dissolution of other reducible phases as jarosite, hematite, magnetite, and goethite. However, application of this method to mine tailings samples from the oxidation zone reveal significant dissolution of secondary jarosite after 1h, as indicated by increased potassium concentrations in the leach (Table 4 this chapter and chapter 5). An example is shown in Fig. 8, which represents a dissolution test with the schwertmannite-containing tailings bulk sample AS3/016. Iron dissolution is fast (56, 88.4, 95, and 100% after 5, 15, 30, and 60 min, respectively) and the data best fits a first-order dissolution equation, indicating that it is not a spherical schwertmannite. SEM study supports this interpretation, as no spherical, but web-like structures could be found. The Fe/S mole ratio reaches its maximum value of 4.9 after 15 min attack, to subsequently decrease down to 4.5 after 60 minutes. DXRD data (Fig. 2) indicate that after 15 min mainly schwertmannite goes into solution. A XRD scan after 60 min (data not shown), demonstrates that an easily reducible part of jarosite was also dissolved, explaining the decrease of the Fe/S mole ratio (Fig. 8) and the increased potassium values in the dissolved fraction of the Fe(III) oxyhydroxide leach in the samples from the oxidation zone (Table 5).

Table 5: *Representative K concentrations in the 1h 0.2M NH_4-oxalate, pH 3, darkness, leach of sequential extractions from the oxidation and primary zone from the studied porphyry copper tailings Piuquenes and Cauquenes, Chile (see chapter 5). Sample code e.g. A2/020 means Andina, drill No.2 in 20 cm depth.*

Samples from Piuquenes/Andina	K (%)	Samples from Cauquenes/Teniente	K (%)
Ox. Zone A2/020	0.24	Ox. Zone T4/040	0.07
Ox. Zone A2/050	0.19	Ox. Zone T4/153	0.07
Pry. Zone A2/100	0.01	Pry. Zone T4/490	0.01
Pry. Zone A2/900	0.02	Pry. Zone T4/490	0.01

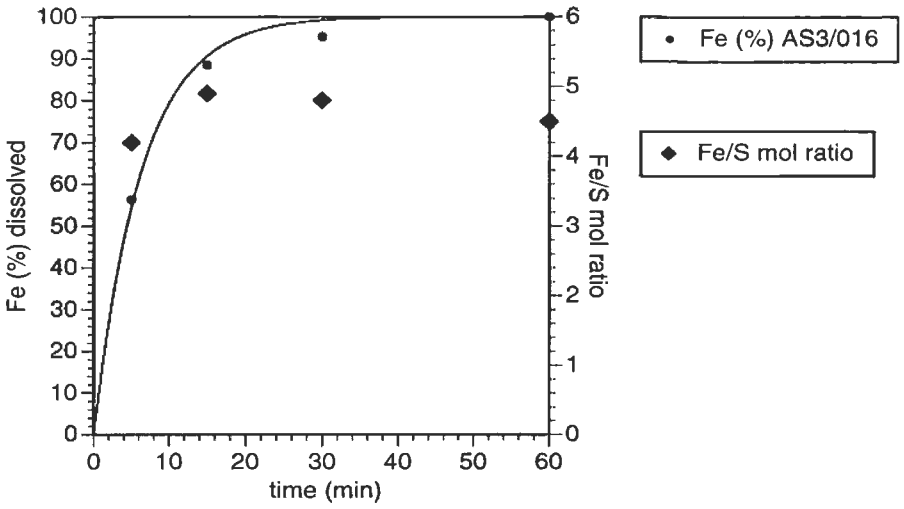

Fig. 8: Dissolution kinetics and Fe/S mole ratios of the mine tailings sample AS3/016 (Piuquenes/ La Andina). Fast dissolution of schwertmannite in 15 min is also confirmed by DXRD (Fig.2) and is indicated by the highest Fe/S mole ratio. The decrease of the Fe/S mole ratio to 4.5 in 60 min is explained by jarosite dissolution and is indicated by DXRD.

Table 6: Summary of results of the dissolution kinetic tests on schwertmannite, 2-line ferrihydrite, and 6-line ferrihydrite in 0.2 M ammonium oxalate, pH 3.0, under exclusion of light.

Mineral	Sample	dissolution equation model	dissolution control	% dissolved after 60 min
schwertmannite spherical	MS3, Sh4	contracting sphere / first order equation	Collapse of spherical form/ surface remaining	95.1, 96.0
schwertmannite web-like	PR1, PR2,	first order equation	surface remaining	94.0, 97.2
schwertmannite mine tailing	AS3/016	first order equation	surface remaining	100
2-line ferrihydrite natural	Bt3	first order equation	surface remaining	100
2-line ferrihydrite natural	MS1	Kabai - equation	no physical meaning	86.0
2-line ferrihydrite synthetic	Fh-2L	Kabai - equation	no physical meaning	42.0
6-line ferrihydrite synthetic	Fh-6L	1D-diffusion	1 D-diffusion	16.0

4.4 Conclusions

Dissolution kinetics of natural and synthetic schwertmannite and 2-line ferrihydrite in 0.2 M ammonium oxalate pH 3, dark, are fast (Table 6; > 94% and > 86% dissolved after 60 min, respectively). It is not possible to discriminate these two minerals with this extraction method. Modeling of schwertmannite dissolution curves, control of mineral shape by SEM, and Fe/S mole ratios of the dissolved fractions indicate that two different schwertmannite shapes

(spherical and web-like) with different dissolution kinetics can be distinguished. The collapse of the spherical shaped (sea-urchin) schwertmannite aggregates seems to control its dissolution kinetics. In case of web-like schwertmannite, structural SO_4^{2-} may have an effect on the stability of the structure.

Natural 2-line ferrihydrite dissolved at the same rate as schwertmannite (> 85% in 60 min), while synthetic 2-line ferrihydrite dissolved slower (41.8% after 60 min). Synthetic 6-line ferrihydrite showed a very slow dissolution rate (16.4 % after 60 min), due to its higher structural order.

In case of a mixture of schwertmannite and ferrihydrite, XRD patterns and dissolution kinetics alone do not provide a method of distinguishing these minerals. Discrimination can be achieved by combining these methods with data on the Fe/S mole ratio of the dissolved fraction.

The results suggest that a selective leach for the ferric oxyhydroxides schwertmannite and lower ordered (2-line) ferrihydrite should be dissolution with 0.2 M ammonium oxalate pH 3, dark, during 60 min. These conditions maximize dissolution of schwertmannite and 2-line ferrihydrite, while minimizing the dissolution of other reducible phases like jarosite, hematite, magnetite, and goethite. Nevertheless, application of this attack to samples from the oxidation zone of sulfidic mine tailings has shown that a part of secondary jarosite dissolves also, although at a slower rate than schwertmannite and lower ordered ferrihydrite. Therefore, if only schwertmannite is of interest (e.g., determination by DXRD), a 15 min attack should be preferred to increase selectivity. It must be also taken in account that in a ferrous iron containing system (e.g., siderite, magnetite), the dissolution kinetics of other Fe(III)hydroxides (goethite, hematite, etc.) is enhanced (Suter et al. 1988 and 1991). In conclusion, a test of crystal morphology by SEM, dissolution kinetics, and control by DXRD of the dissolved phases should be included in the studies applying sequential extractions to provide correct interpretation of geochemical data.

Acknowledgments

I would like to thank specially Prof. U. Schwertmann for supplying the samples and helpful comments and corrections. I am grateful to Prof. L. Fontboté and Prof. W. Wildi for the support and the helpful suggestions and Prof. B.M. Thompson, Prof. H.-R. Pfeifer, and Dr. C.N. Alpers for the critical reading. I thank Prof. H.-R. Pfeifer, J.-C.- Lavanchy, and C. Schlegel for the facilities and discussions in the laboratory of the Centre d'Analyse Minerale, Université de Lausanne. Thanks to Dr. Dubois from Soil Science Institute of the EPFL, Lausanne for the ICP analysis and Dr. R. Martini form the Geological Department, University of Geneva for the patient SEM work. The project is supported by the German Academic Exchange Service (DAAD) and the Swiss National Science Foundation project No. 21-50778.97.

References

Barham, R.J. (1997): Schwertmannite: A unique mineral, contains a replaceable ligand, transforms to jarosites, hematites, and/or basic iron sulfates. Journal of Material Research, v. 12, No. 10, p. 2751-2758.

Bigham, J.M., Schwertmann, U., Carlson, L. and Murad, E. (1990): A poorly crystallized oxyhydroxysulfate of iron formed by bacterial oxidation of Fe(II) in acid mine waters. Geochimica et Cosmochimica Acta, v. 54, p. 2743-2758.

Bigham, J.M., Schwertmann, U. and Carlson, L. (1992): Mineralogy of precipitates formed by the biogeochemical oxidation of Fe(II) in mine drainage. CATENA Supplement 21, Cremlingen, p. 219-232.

Bigham, J.M., Carlson, L. and Murad, E. (1994): Schwertmannite, a new iron oxyhydroxy-sulphate from Pyhäsalmi, Finland, and other localities. Mineralogical Magazine, v. 58, p. 641-648.

Bigham, J.M., Schwertmann, U., Traina, S.J., Winland, R.L. and Wolf, M. (1996a): Schwertmannite and the chemical modeling of iron in acid sulfate waters. Geochimica et Cosmochimica Acta, v. 60, No. 2, p. 185-195.

Bigham, J.M., Schwertmann, U. and Pfab, G. (1996b): Influence of pH on mineral speciation in a bioreactor simulating acid mine drainage. Applied Geochemistry, v. 11, p. 845-849.

Bigham, J.M. and Murad, E. (1997): Mineralogy of ochre deposits formed by the oxidation of iron sulfide minerals. Advances in GeoEcology, Reiskirchen, v. 30, p. 193-225.

Blowes, D.W. and Ptacek, C.J. (1994): Acid-neutralization mechanisms in inactive mine tailings. In: Jambor, J.L. and Blowes, D.W. (eds.): Short Course Handbook on Environmental Geochemistry of Sulfide Mine Waste. Mineralogical Association of Canada, Nepean, v. 22, p. 271-29.

Brown, W.E.B., Dollimore, D., and Galwey, A.K. (1980): Reactions in the solid state. In: Bamford, C.H. and Tipper, C.F.H. (eds.) Comprehensive chemical kinetics. Elsevier, Amsterdam, v. 22, p. 41-109.

Childs, C.W, Inoue, K., and Mizota, C. (1998): Natural and anthropogenetic schwertmannites from Towada-Hachimantai National Park, Honshu, Japan. Chemical Geology, v. 144, p. 81-86.

Chukhrov, F.V., Zvyagin, B.B., Gorshkov, A.I., Ermilova, L.P., and Balashova, V.V. (1973): Ferrihydrite. Izvest. Akad. Nauk, SSSR, Ser.Geol., v. 4, p.23-33.

Cornell, R.M. and Schwertmann, U. (1996): The Iron oxides. VCH Verlagsgesellschaft mbH, Weinheim, 573 p.

Davis, J.A. and Kent, D.B. (1990): Surface complexation modeling in aqueous geochemistry. In: M.F. Hochella and A.F. White, (Eds), Reviews in Mineralogy Mineral, Mineral. Soc. Amer., v. 23, p.177-260.

Dold, B., Fontboté, L. and Wildi, W. (1997): Mobilization and secondary enrichment processes in the sulfide porphyry copper tailings of Cauquenes (El Teniente) and Piuquenes (La Andina), Chile. VIII Congreso Geologico Chileno Actas, v. 2, p. 940-944.

Dold, B., Fontboté, L. and Wildi, W. (1999): Detection and distribution of ferric oxyhydroxides and oxyhydroxide sulfates in sulfide mine tailings; their importance to selective metal retention and acid production. Mine, Water and Environment; Sevilla, v. 2, p.525-526.

Fischer, W.R. (1976): Differenzierung oxalatlöslicher Eisenoxide. Zeitschrift für Pflanzenernährung und Bodenkunde, v. 139, p. 641-646.

Giovanoli, R. and Brütsch, R. (1975): Kinetics and mechanics of the dehydration of γ–FeOOH. Thermochim. Acta, v. 13, p. 15-36.

Jambor, J.L. (1994): Mineralogy of sulfide-rich tailings and their oxidations products. In: Jambor, J.L. and Blowes, D.W. (eds.): Short Course Handbook on Environmental Geochemistry of Sulfide Mine Waste. Mineralogical Association of Canada, Nepean, v. 22, p. 59-102;

Ribet, I., Ptacek, C.J., Blowes, D.W. and Jambor, J.L. (1995): The potential for metal release by reductive dissolution of weathered mine tailings. Journal of Contaminant Hydrology, v. 17(3), p. 239-273.

Schwertmann, U. (1964): Differenzierung der Eisenoxide des Bodens durch Extraktion mit Ammoniumoxalat Lösung. Zeitschrift für Pflanzenernährung und Bodenkunde, v. 105, p. 194-202.

Schwertmann, U. (1984): The influence of aluminium on iron oxides: IX. dissolution of Al-goethites in 6 M HCl. Clay Minerals, v. 19, p. 9-19.

Schwertmann, U. and Cornell, R.M. (1991): Iron oxides in the laboratory. VCH Verlagsgesellschaft mbH, Weinheim, 137 p.

Schwertmann, U., Bigham, J.M. and Murad, E. (1995): The first occurrence of schwertmannite in a natural stream environment. European Journal of Mineralogy, v. 7, p. 547-552.

Schwertmann, U., Friedl, J., and Stanjek, H. (1999): From Fe(III) ions to ferrihydrite and then to hematite. Journal of Colloid and Interface Science, v. 209, p. 215-223.

Suter, D., Siffert, C., Sulberger, B., and Stumm, W. (1988): Catalytic dissolution of iron(III)(hydr)oxides by oxalic acid in the presence of Fe(II). Naturwiss., v. 75, p. 571-573.

Suter, D., Banwart, S., and Stumm, W. (1991): The dissolution of hydrous iron(III) oxides by reductive mechanisms. Langmuir, v. 7, p. 809-813.

Waychunas, G.A., Ning Xu, Fuller, C.C., Davis, J.A., Bigham, J.M. (1995): XAS study of AsO_4^{3-} and SeO_4^{2-} substituted schwertmannites. Physica B, v. 208 and 209, p. 481-483.

Winland, R.L., Taina, S.J., Bigham, J.M. (1991): Chemical composition of ochreous precipitates from Ohio Coal Mine Drainage. J. Environ. Qual., v. 20, p. 452-460.

Yu, J-Y., Heo, B. and Chang, H-W. (1998): Stability of schwertmannite and ferrihydrite in stream waters of Imgok and Osheep Creek polluted by acid mine drainage. Goldschmidt Conference Proceedings 1998, p. 1675-1677.

CHAPTER 5

5 Element cycling and secondary mineralogy in porphyry copper tailings as a function of climate, primary mineralogy, and mineral processing.

Abstract

A comparative geochemical, mineralogical, and microbiological study of three mine tailings impoundments from the porphyry copper deposits La Andina, El Teniente, and El Salvador, Chile is presented in this paper. The main focus was on the mineralogical and geochemical changes at the interface between the oxidation zone and the primary zone in the sulfidic copper flotation tailings. The criteria used for selection of the tailings impoundments included knowledge of the origin of the mineral (from one mine only), climate, flotation process, and the absence of anthropogenic alteration (additional water or tailings input) after operation had ceased. In this way the influence of climate, flotation process, and ore mineralogy can be qualitatively studied. Two schematic models of element cycling in sulfide mine tailings controlled by climatic conditions are presented.

The secondary phases jarosite, schwertmannite, and a vermiculite-type mixed-layer mineral were detected in the oxidation zone by X-ray diffraction (XRD) and differential X-ray diffraction (DXRD). Jarosite and schwertmannite play an important role for the retention of oxyanions (e.g., $HMoO_4^-$, $H_2AsO_4^-$, and SO_4^{2-}) in the low pH oxidation zones, as proven by sequential extractions (element analysis by ICP-ES) and in-situ by scanning electron microscope (SEM-EDS) and/or electron microprobe analysis. The bivalent cations (e.g., Cu^{2+}, Zn^{2+}, Mn^{2+}) are leached out from the oxidation zones in precipitation dominated climates. Below this zone, increasing pH controls the sorption of bivalent cations through adsorbents as secondary Mn(II) hydroxides, Fe(III) hydroxides or clay minerals. Below the groundwater table, with increasingly reducing conditions, pH controlled replacement processes take place, as shown by the transformation of chalcopyrite to covellite, leading to secondary Cu enrichments of potential economic interest.

In arid climates, with strong evaporation, the water-flow direction changes to upwards migration via capillary forces. As a result the mobilized elements are transferred to oxidizing conditions at the top of the tailings. Hydrolysis and sulfide replacement processes are less important in arid climates. Saturation and/or supersaturation controls the precipitation of mainly water-soluble secondary sulfates (e.g., bonattite, chalcanthite) and strong enrichment at the top of the tailings.

In the low pH oxidation zone, due to their high ionic strength, certain mobile elements, are found to substitute into secondary phases such as Fe replacement by Al in jarosite, or K replacement by Cu and Zn in biotite.

At El Salvador only low quantities of secondary ferric oxyhydroxide minerals have been found in relation to the high pyrite (6.2 wt.%) content. A very low oxidation activity during microbiological tests and molybdenum values higher by a factor of 3 to 5 than those of Piuquenes (La Andina) and Cauquenes (El Teniente), suggest that this is due, at least in part, to molybdenum poisoning of *Thiobacillus ferrooxidans*. The, nevertheless, strong acidity at the El

Salvador tailings (pH 2 – 3.5) is seen as a result of slow inorganic pyrite oxidation in combination with acidity stored in supergene jarosite and zero carbonate neutralization potential.

5.1 Introduction

The porphyry copper and/or molybdenum sulfide deposits are the world's primary source of copper and molybdenum. This deposit type consists of disseminated and stockwork veinlet sulfide mineralization emplaced in various hostrocks that have been altered by hydrothermal solutions into roughly concentric zonal patterns (Lowell & Gilbert, 1970; Lowell, 1974; Gustafson & Hunt, 1975; Camus, 1975, Titley, 1982, Gustafson & Quiroga, 1995). Pyrite, chalcopyrite, bornite, and molybdenite are generally the dominant minerals. Minor phases are magnetite, hematite, ilmenite, rutile, enargite, cubanite, cassiterite, huebnerite, and gold. Supergene enrichment, which can make these low-grade deposits economically interesting, produces secondary hematite, goethite, alunite, jarosite, covellite, chalcocite, digenite, and native copper. During the flotation process the economically interesting Cu-Mo-sulfides are extracted, while pyrite is generally depressed from flotation, being exposed to oxidation by deposition at the tailings impoundments. It is generally accepted that sulfide oxidation, and in particular that of pyrite, is the main reason for the formation of acid rock drainage (ARD). These heavy metal loaded effluents are the principal environmental problem facing the mining industry today.

The aim of this project is to investigate the mineralogical and geochemical changes at the interface between the oxidation zone and the primary (sulfide) zone in sulfidic copper flotation tailings. For this purpose three tailings impoundments of the porphyry copper deposits La Andina, El Teniente, and El Salvador in Chile are studied. The criteria used for selection of the impoundments included knowledge of the origin of the tailings (from only one mine), climate, flotation process, and the absence of anthropogene alteration (additional water or tailings input) after operation had ceased. In this way we can qualitatively study the influence of parameters as climate, flotation process, and ore mineralogy. We focus on the processes resulting from sulfide oxidation, especially element mobility and retention by secondary minerals as well as microbial activity.

The three selected tailings impoundments represent different climates and illustrate the influence of this parameter on both mobilization direction and secondary mineralogy. The Piuquenes tailings impoundment from La Andina (alpine climate) is discussed as prime example. In the tailings of Cauquenes at El Teniente (Mediterranean climate) and El Salvador (hyper-arid) the differences with respect to Piuquenes and the controlling parameters leading to these differences will be highlighted. It will be shown that in precipitation-dominated climates (La Andina) the element mobilization direction is downwards and resulting from this, the secondary mineralogy is dominated by hydrolysis and replacement due to decreasing redox potential below the groundwater level. With increasing influence of evaporation, upwards migration becomes more important (El Teniente and El Salvador) and the secondary mineralogy consequently is dominated by water-soluble sulfates due to the increasing redox potential. The global geochemical behavior of the tailings material of each case will be presented in two schematic models of element cycling.

5.2 Terminology

For the description of the tailings mineralogy the classification proposed by Jambor (1994) is used: The term "primary" minerals is used to designate the complete ore mineralogy, i.e. "hypogene" referring to high temperature mineralization and "supergene" referring to weathering products prior to mining. "Secondary" minerals are those produced within the tailings impoundment after mining and milling as the result of weathering processes. "Tertiary" minerals form after the sample has been removed from the tailings environment.

5.3 Description of the studied tailings impoundments

The situation of the three studied tailings impoundments Piuquenes (La Andina, alpine climate, alkaline flotation circuit), Cauquenes (El Teniente, Mediterranean climate, acid flotation circuit), and El Salvador No.1 (El Salvador, hyper-arid climate, alkaline flotation circuit, strong supergene enriched ore) is shown in Fig. 1. A total of 14 drill cores were obtained from the three studied tailings impoundments (Table 1). In table 2 a summary of the main parameters is shown. A description of the ore geology, flotation processes, and climatic conditions of each site is given below.

Table 1. Sampled tailings for the present study.

	Name	Ore deposit type	Climate	Drilling	Samples
1)	La Andina Tailings Piuquenes	porphyry copper (clay mineral rich)	Alpine	A/1 to A/5	87
2)	El Teniente Tailings Cauquenes	porphyry copper (clay mineral rich)	Mediterranean	T/1 to T/5	78
3)	El Salvador Tailings No.1	porphyry copper (clay mineral rich)	Hyper-arid	E/1 to E/4	37

5.3.1 Piuquenes tailings impoundment, La Andina porphyry copper deposit, Chile

5.3.1.1 Regional geology and ore geology

The Río Blanco-Los Bronces ore body is a giant copper-molybdenum porphyry system with >50x10^6 metric tons copper with an average ore grade between 1.0 and 1.5 % (Serrano et al., 1996), located high on the west flank of the central Chilean Andes, about 50 km northeast of Santiago at 3500 to 4200 m altitude (Fig. 1). CODELCO's Andina division owns the main eastern part of the deposit. This deposit is one of three giant late Miocene to early Pliocene copper deposits in the Andes of central Chile, formed as a result of emplacement of both multiple mineralized breccias and porphyry intrusions (quartz diorite, granodiorite, quartz monzonite, and quartz monzodiorite) into early and middle Miocene plutonic rocks and Cenozoic lavas (Serrano et al., 1996). The potassic core, propylitic halo, and superimposed

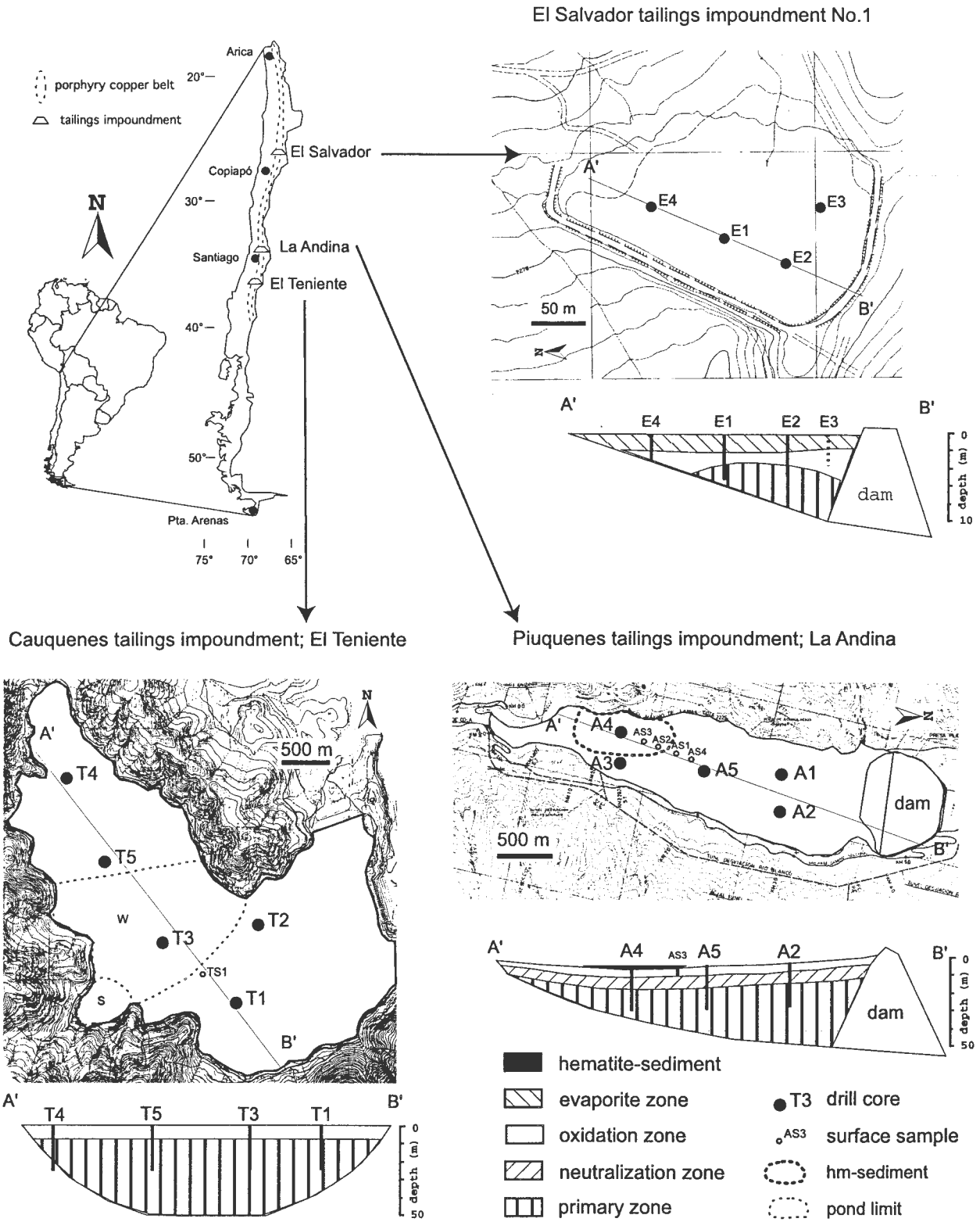

Fig. 1: *Overview of the sampled tailings impoundments and their location within the porphyry copper belt in Chile. The climate changes from hyper-arid in the Atacama desert in northern Chile to humid in the South. Note: For better visibility of the stratigraphic zonation the cross-sections are vertically exaggerated.*

Table 2: *Properties of the studied porphyry copper tailings impoundments (abbreviations: qz: quartz; al: albite; K-feld: K-feldspar; bio: biotite; ca: calcite; sid: siderite; ank: ankerite; anhy: anhydrite; gy: gypsum; tour: tourmaline; rut: rutile; ser: sericite; cl: chlorite; kaol: kaolinite; mont: monmorillonite; horn: hornblende; ap: apatite; ep: epidote; py: pyrite; cp: chalcopyrite; bn: bornite; dg: digenite; cc: chalcocite; cv: covellite; mb: molybdenite; sl: sphalerite; gn: galena; tn: tennantite; tt: tetrahedrite; cb: cinnabar; op: orpiment; stb: stibnite; mt: magnetite; hm: hematite; ilm: ilmenite; gt: goethite; jt: jarosite; Na-jt: natrojarosite; sh: schwertmannite; fh: ferrihydrite).*

Ore deposit	**La Andina**	**El Teniente**	**El Salvador**
ore deposit type	porphyry copper	porphyry copper	porphyry copper
gangue mineralogy	qz, al-K-feld, bio, ank, sid, ca, gy, ser, cl, ep, tour [1]	qz, al-K-feld, bio, ca, anhy, tour, rut, ap, ser, cl, ep, kaol, mont [2]	qz, al-K-feld, bio, anhy, rut, horn, sphene, ca [3]
hypogene ore mineralogy	py, cp, bn, mb, sl, gn, tn-tt, mt, hm [1], ilm[4]	py, cp, bn, mb, gn, tn, mt, hm[2]	py, cp, bn, mb, ilm, hm[3]
supergene mineralogy	cc, cv[1]	cc, cv[2]	cc, cv, jt, hm, gt[3], Na-jt[4]
flotation circuit	pH 10.5	pH 4.5	pH 10.5
Tailings impoundment	**Piuquenes** [5]	**Cauquenes** [6]	**El Salvador No.1**
surface	83.7 ha	640 ha	4.2 ha
volume	24 117 048 m^3	270 000 000 m^3	144 000 m^3
operation time	1970-1980	1936-1975	1959-1960
deposition technique	starter dam, downstream method	5 dams closing a natural depression	2 dams closing natural inclination
Climate (after Köppen)[7]	polar or alpine (E)	Mediterranean (Csd)	hyper-arid[8] (Bw)
altitude	2150 m	725 m	2270 m
precipitation	~ 700 mm/a	~ 540 mm/a	~ 20 mm/a
Evaporation	~ 70 mm/a	high in summer	extremely high all year

[1] Serrano et al., 1996; [2] Camus, 1975; [3] Gustafson & Hunt, 1975; [4] this study; [5] Ingeneria y Geotecnia LTDA,1990a; [6] Ingeneria y Geotecnia LTDA,1990b; [7] In: Linacre and Geerts, 1997; [8] Alpers and Brimhall, 1989.

sericitic alteration of the early stage conform to established patterns for porphyry copper deposits (Stambuk et al., 1982). Supergene enrichment is less prominent in the Andina deposit than other copper deposits in northern and central Chile, but locally supergene chalcocite and covellite double the ore grade. As the shape and depth of the enrichment zones are associated with the recent groundwater regime, it is believed that leaching and enrichment are still active (Serrano et al., 1996). The mineralization consists mainly of pyrite, chalcopyrite, chalcocite, covellite, molybdenite, sphalerite, galena, tennanite, and tetrahedrite in a gangue of ankerite, siderite, gypsum, quartz, and tourmaline.

5.3.1.2 Mining and treatment processes

CODELCO's Andina Division uses both, underground and open pit (Sur-Sur) mining. In the first step of flotation the ore is separated from the gangue by a collective Cu-Mo flotation. The mineral is conditioned by lime (pH 10.5) and the following reagents are used. Collectors: SF-323 (Isopropil Etil Tionocarbamate) 50 wt.% 15g/t, MIBC (Metil Isobutil Carbinol) 35 wt.% 10.5g/t, Diesel oil 15 wt.% 5.5g/t. Frothers: MIBC (Metil Isobutil Carbinol) 70 wt.% 11.55g/t, Pine oil 30 wt.% 4.95g/t. The tailings from this flotation step are deposited on the tailings impoundments (Division Andina, A).

5.3.1.3 History of the tailings impoundment

The Andina division has two tailings impoundments, the recently operating Los Leones and the Los Piuquenes impoundment which was in operation from 1970 to 1980. Sampling was carried out on Los Piuquenes which is located at 32°59' S and 70°15' W (UTM northing 6349000; easting 383000) at 2150 m altitude in the N-S trending valley of the river Río Blanco, 3.3 km upstream of the connection with the Los Leones River. Los Piuquenes is situated in a valley of glacial formation on Quaternary sediments with fluvial-glacial origin, mainly sandy gravels and clayey sandy gravels. They are underlain by Upper Tertiary volcanic and intrusive rocks (mainly andesites and granodiorites).

The impoundment has a surface area of 83.7 ha and a volume of 24,117,048.4 m^3 and 37,188,488.6 metric tons. The maximum height of the impoundment is 57 m and the downstream angle of the dam is 25°. Piuquenes was constructed as a valley dam impoundment with an initial starter dam after the upstream method. The soils upstream of the dam were compacted. A drainage system for effluent collection with 3 drainage lines has been installed. The discharge point of the tailings was moved periodically during operation (Ingenería y Geotecnica LTDA, 1990a; Division Andina, B). The average Cu content of the material deposited between 1970 and 1980 of the Piuquenes tailings was 0.22 % (Division Andina, 1996).

5.3.1.4 Climate

Data from two meteorological stations in the Andina region are available (Appendix. 5). One is Saladillo (32°55'55'' S and 70°16'48'' W) at 1580 m altitude. The other is Lagunitas (33°04'48'' S and 70°15'04''W) at 2765.5 m. The Piuquenes impoundment, situated at 2100 m altitude, lies in the middle in terms of altitude and distance from both meteorological stations and an average of the data from both stations was used. The climate is characterized by a rainy season from April to October followed by a very dry season from October to March. Mean precipitation can vary strongly from year to year (data available from 1958 – 1995). In Lagunitas the precipitation (rain or snow; show is calculated to rain equivalent by division by 10) varied from 212 to 1777 mm/a with an average concentration of 806 mm/a and in Saladillo from 199 up to 1209 mm/a with an average of 550 mm/a. For the Piuquenes impoundment an average precipitation of 700 mm/a is estimated. Evaporation data is only available from the Saladillo station and shows an average in the years from 1987-1995 of 71 mm/a. Calculation of the

evaporation rate after Schendel (in Hölting, 1989; E = T/H x 480 [mm/month]; where E = evaporation, T = monthly average of air temperature in °C, H = monthly average of relative moisture in %) shows that the evaporation rate for Lagunitas as well for Saladillo is around 1300 mm/a, this is nearly twenty times the measured concentration. As the relation of T and H in the Canyon of Rio Blanco is constant, this leads to similar evaporation rates along the canyon due to lower T but also lower H in Lagunitas and higher T but also higher H in Saladillo. Consequently, we assume that the evaporation rate at the Piuquenes tailings impoundment is also around 70 mm/a as measured at Saladillo. This means that precipitation exceeds evaporation by a factor of 10. The climate at Piuquenes can be classified as alpine. After the Köppen Climate Classification System the Andes are classified as E characterized by polar climate with extremely cold winters and summers (Linacre & Geerts, 1997).

5.3.2 Cauquenes tailings impoundment, El Teniente porphyry copper deposit, Chile

5.3.2.1 Regional geology and ore geology

The El Teniente copper deposit is located 67 km east of the town of Rancagua, province of O'Higgins, VI Región, Chile. The mine is owned and operated by CODELCO and represents the largest underground mine in the world and one of the giant porphyry copper systems ($48x10^6$ tons of Cu). The regional geology is characterized by a thick section of pre-mineralization volcanic rocks with intercalations of continental sediments, which are intruded by felsic to intermediate intrusive bodies. Two main stratigraphic units are the intensely folded Coya-Machalí Formation (Upper Cretaceous) and the overlying Farallones Formation (Lower Tertiary). A quartz-diorite-dacite intrusion complex to which the alteration and mineralization is related intrudes these two formations. Three main hypogene alteration assemblages and one supergene assemblage have been recognized in the ore body. The hypogene assemblages are potassic (secondary biotite, K-feldspar, anhydrite, quartz, sericite, carbonates, rutile, and apatite), quartz-sericitic (quartz, sericite, pyrite, anhydrite, tourmaline, calcite, pyrophyllite), and propylitic (chlorite, epidote, calcite, magnetite, pyrite, sericite, quartz, and anhydrite). Supergene argillic alteration is recognized by the presence of kaolinite with lesser montmorillonite and alunite. The main sulfide ore minerals are pyrite, chalcopyrite, molybdenite, sphalerite, galena and tennantite. The most important secondary mineral present in the orebody is chalcocite which occurs with minor amounts of covellite (Camus, 1975).

5.3.2.2 Treatment process

Material rich in supergene argillic alteration with high contents of kaolinite and montmorillonite inhibits flotation in an alkaline circuit. Thus the mineral is treated by an acid flotation circuit at pH 4.5 and with the following reagents (Departamento Concentrador Colón, 1973). Collectors: MINERAC-A (Amyl xanthogen, ethyl formate), Z-200 (Isopropyl ethyl, thionocarbamate). Frothers: DOW 1012 (Polypropylene glycol, methyl ether).

5.3.2.3 History of the tailings impoundment

In the long history of El Teniente mine, four tailings impoundments were built: Barahona, Cauquenes, Colihues, and Carén. The tailings impoundment Cauquenes was the best locality for sampling due to favorable age, climate and the lack of alteration by anthropogenic activity. The tailings impoundment is located at 725 m altitude, with a surface of 640 ha, 12 km southeast of Rancagua in a natural depression which is closed by five dams (Fig. 1). The impoundment was in operation from 1936 to 1975. It is situated over Upper Cretaceous rocks belonging to the Abanico formation which are overlain by younger lacustrine sediment as sands, silty clays, and clayey gravels (Ingeneria y Geotecnia LTDA., 1990b). The average Cu content of the material deposited between 1971 and 1973 on the Cauquenes tailings was 0.30 % (Departamento Concentrador Colon, 1973).

5.3.2.4 Climate

The Cauquenes tailings impoundment is situated in a region of Chile's central valley at 725 m altitude, which is classified after the Köppen Climate Classification System as Csb (Mediteranean with a marine influence, Linacre & Geerts, 1997). Data from the meteorological station Parrón in the neighborhood of the tailings impoundment are available (Appendix. 5). Mean precipitation for 24 years is 540 mm/a. No data for evaporation are available. Using the calculation scheme of Schendel gives similar evaporation rates as La Andina (E = 1074 mm/a). The T and H concentrations of the Parrón meteorological station, which is situated in a small forest, cannot be taken as representative of the open space tailings surface of 1340 ha (Cauquenes & Colihue). Thus, high evaporation rates are assumed for the summer period.

5.3.3 Tailings impoundment of the El Salvador porphyry copper deposit, Chile

5.3.3.1 Regional geology and ore geology

The El Salvador porphyry copper deposit (5.7×10^6 tons Cu) is located in the Atacama Desert about 100 km northeast of the town Copiapó, III Región, Chile. It is owned and operated by CODELCO. The formation of the porphyry copper deposit culminated volcanic activity in the Indio Muerto district. Host rocks are Cretaceous andesitic flows and sedimentary rocks overlain unconformably by Lower Tertiary volcanics. Early rhyolitic domes, with voluminous rhyolitic and andesitic volcanics, were followed by irregularly shaped subvolcanic intrusions of quartz rhyolitic and quartz porphyry, dated at about 46 m.y. (Gustafson & Hunt, 1975). Minor copper mineralization accompanied this event. A steep-walled granodioritic porphyry complex and the closely associated main center of mineralization and alteration were dated at 41 m.y. (Gustafson & Hunt, 1975). Early mineralization is characterized by distinctive quartz veins and largely disseminated K-silicate-assemblages of alkali feldspar-biotite-anhydrite-chalcopyrite-bornite or chalcopyrite-pyrite. Except at the deepest levels exposed in the younger porphyries, incipient K-silicate alteration converted hornblende phenocrysts to biotite-anhydrite-rutile, ilmenite to hematite-rutile, and sphene to rutile-anhydrite. Supergene enrichment formed the commercial ore body. Secondary Cu-sulfides (chalcocite, covellite) extensively replaced chalcopyrite and bornite

but coated pyrite with little or no replacement (Gustafson & Hunt, 1975; Gustafson & Quiroga, 1995).

5.3.3.2 *Mining and treatment processes*

The El Salvador Division is an underground mining operation. In the flotation the ore is separated from the gangue by a collective Cu-Mo flotation. The mineral is conditioned by lime (pH 10.5) and the following reagents are used. Collectors: Isopropil Na Xantate 28 g/t, Tinocarbamate 10 g/t. Frothers: DOW 1012 43 g/t, MIBC (Metil Isobutil Carbinol) 11 g/t. The tailings of this flotation step are deposited on the tailings impoundment Pampa Austral (Division Salvador, 1987).

5.3.3.3 *History of the tailings impoundment*

The Potrerillos-El Salvador mining district sent most of its flotation tailings in suspension through the El Salado River direct to the sea at the Chañaral Bay between 1926 and 1989. As a result of this activity the bay is considered as practically biologically dead. Legal action by the village Chañaral stopped deposition in the bay. Since 1989 the Pampa Austral impoundment has been the active tailings impoundment of the El Salvador mine. The present flotation plant of El Salvador started its activity in 1959. From this time there have been three small tailings impoundments halfway between the plant and El Salvador village. The largest one (tailing No.1, 4,16 ha and a maximum altitude of 8 m), which went out of operation around 1960, was sampled. The tailing is situated at 2270 m altitude, UTM 17700 N and 13100 W. The tailings impoundment was built by using two rectangular dams forming together with the natural inclination of the terrain a volume, which was filled up with the tailings material (Fig. 1). The tailings are deposited on continental clastic sediments belonging to the Potrerillos Formation, which mainly consist of gravels and sands with intercalations of rhyolitic flows (K/Ar ages between Middle and Upper Miocene). Their upper surface is called the Pediplano de Atacama (Mercado, 1978).

5.3.3.4 *Climate*

The El Salvador tailings impoundment No.1 is situated in the Andean precordillera at 2270 m altitude and the region is classified after the Köppen Climate Classification System as arid Bw (Linacre & Geerts, 1997). The Atacama Desert is known as the driest desert on earth and data from precipitation in the El Salvador region from 1962-1984 show an average of 20 mm/a as rain or snow (Dirección General de Aguas, 1996) and is classified as hyper-arid (Alpers and Brimhall, 1989). No data for evaporation and temperature are available. No vegetation is observed. High evaporation rates must be assumed throughout the whole year.

5.4 Methology

5.4.1 Sampling and field methods

A total of 14 holes were drilled and 202 samples were obtained from the three studied tailings impoundments. Percussion drilling equipment was used to reach depths of 10 m (100 x 2 x 2 cm sampling tube) in the first field campaign 1996. Up to 5 samples of 20cm length per meter were taken in the oxidation zone and at the interface between oxidation and primary zone. Three samples per meter were taken in the homogeneous primary zones. Where necessary, smaller sub-samples were taken. In a second field campaign in 1997 detailed surface sampling was undertaken in the transition to a hematite-rich sediment in the Piuquenes tailings (Fig. 1).

The 202 samples were sealed in plastic bags and stored in an ice-packed cool box. Previously, the description of mineralogical characteristics, color and grain size estimation, and pH measurement (paste pH according to MEND, 1991; WTW® pH-meter; in the second field campaign a pH-electrode for measurement in meat was successfully used for in situ pH-measurement in the moist tailings sediment) were noted. The samples were transported immediately to local mine laboratories for drying (< 35°C) and water content determination. The dry samples were homogenized and packed into polyethylene (PET) containers for storage at room temperature.

In the two impoundments which had water out-flow or ponds (Andina, Teniente) a total of four water samples were taken. The water samples were filtered with 0.45 µm sodium acetate filters. Temperature, conductivity, pH, and oxygen were measured in the field. Each water sample was separated into two aliquots, one untreated for anion analysis, and the other conserved at pH 2 (obtained by addition of suprapure HNO_3) for cation analysis. The water samples were refrigerated until analysis.

5.4.2 Physical properties

The wt.% of moisture of all tailings samples was measured using sample weight before and after drying. The particle size distribution of selected samples were measured by a Coulter® and a Fritsch Analysette® laser particle size analyzer. The hydraulic conductivity (K) was calculated after Hazen (1893, in Hölting, 1989) with the d_{10} concentrations. As the unconformity degree U = d_{60}/d_{10} was higher than five, the correction after Beyer (1964, in Hölting, 1989) was applied.

5.4.3 Mineralogical methods

Polished sections and polished thin sections were prepared from bulk samples and undisturbed sediment samples. All samples were analyzed as bulk sample by X-ray diffraction (XRD), using a Philips 3020 diffractometer with CuKα (λ = 1.54056 Å) and a monochromator. Scan settings were 3-70° 2θ, 0.02° step size, 2s count time per step. The procedure of

identification of clay minerals was used as described in Moore & Reynolds (1997), and Brindley & Brown (1980). First, the fraction < 2µm was separated by centrifugation and oriented samples were prepared on glass slides. Samples were then characterized by X-ray diffraction (XRD), with the same settings as mentioned above. The samples were analyzed before and after glycerol treatment, K & Mg-saturation and heat treatment (550°C, 1h).

The low crystalline Fe(III) hydroxides such as ferrihydrite and schwertmannite were detected by differential X-ray diffraction (DXRD) as described by Schulze (1981 & 1994). The diffractometer settings were those used by Bigham et al. (1990, 1994, and 1996), and Schwertmann et al. (1995), i.e., step scanning with 0.05° 2θ step size and 20 s counting time per step. The samples were attacked by 0.2 M ammonium oxalate, pH 3, dark, 15 min or 2h. Scans were measured before and after treatment. The treated scan was intensity corrected and then subtracted from the untreated scan. The resulting DXRD was used for mineral determination. The extraction solutions were analyzed for Fe and S by ICP-AES to calculate the Fe/S mole ratios.

5.4.4 Geochemical methods

5.4.4.1 Sequential extraction

To study the element speciation in the mine tailings a sequence of seven selective dissolution steps was established and applied to 114 samples (Tab. 3). Iron cycling is the controlling process in sulfidic mine wastes, due to acid production via pyrite oxidation and hydrolysis of Fe(III) to form oxyhydroxides and oxyhydroxide sulfates, and scavenging of mobilized elements via sorption and co-precipitation processes associated with these secondary phases. Due to the importance of the change from sulfide to oxide phases several sequential extractions were chosen to study the change from iron sulfides to ferric oxides.

The first four extractions are designed to separate the mobilized elements and the different secondary phases. Water-soluble secondary and tertiary salts are dissolved in the water extraction. In the second step, acetate, as a monodentate complex former, is believed to detach only exchangeable elements as outer-sphere complexes. The bidentate complex former oxalate dissolves the secondary phases and liberates elements which are fixed as inner-sphere complexes formed by ligand exchange (e.g., Mo and As) or by surface precipitation, diffusion, or co-precipitation in the third and forth step. The last three extractions try to discriminate the organic compounds from the sulfide and silicate phases.

In the recent literature the selectivity of sequential extractions is discussed and criticized by McCarty et al. (1998), due to the interaction of various parameters which influence the dissolution kinetics of iron minerals by widely used organic acids as oxalate, such as acidity, light, temperature, Fe(II), and reducing conditions (Stumm & Sulzberger, 1992). It will be shown that due to the complexity of the system it is crucial to correlate the geochemical data with detailed mineralogical studies for interpretation. Dissolution kinetic tests and control of the dissolved phases by XRD and DXRD evaluated the selectivity of each step at representative samples from the studied mine tailings (Dold, in prep.). DXRD analyses have shown that the vermiculite-type mixed-layer mineral disappears after the NH_4-acetate leach and a new peak at

the flank of the 001 illite peak appears. This is interpreted as a detachment of interlayer cations leading to a different structure of the mineral. Also calcite goes into solution in the NH_4-acetate leach. The dissolution of secondary ferric oyhydroxides and oyhydroxides sulfates in NH_4-oxalate is discussed in detail in chapter 3 and 4. The applied extraction scheme and the preferentially dissolved phases are summarized in Table 3. The solutions were submitted to multi-element ICP-AES analysis. The sum of all dissolution steps gives the total concentration of an element. To control the accuracy, bulk analysis of a total HNO_3, HF, $HCLO_4$, HCl digestion of every sample was done. Comparison between the sums of the sequential extraction (total) and the bulk analysis show a fair agreement (Tables 4, 6, 7, and 8).

Elemental mapping by scanning electron microscope (SEM-EDS) and/or electron microprobe analysis was used on selected polished sections and polished thin sections to detect in situ element anomalies in schwertmannite and biotite.

Table 3: *Sequential extractions applied in this study (abbreviations as in table 2).*

Leach	preferentially dissolved minerals	references
(1) Water soluble fraction 1.0 g sample into 50ml deionized H_2O shake for 1 h.	water-soluble sulfates, e.g., gy, bonattite, chalcanthite, pickeringite, magnesioaubertite	Dold, in prep.; Ribet et al., 1995; Fanfani et al., 1997
(2) exchangeable fraction 1M NH_4-acetate pH 4.5 shake for 2 hrs	ca, vermiculite-type-mixed-layer, adsorbed ions	Dold, in prep.; Gatehouse et al., 1977; Sondag, 1981; Cardoso Fonseca and Martin, 1986
(3) Fe(III)oxyhydroxides 0.2 M NH_4-oxalate pH 3.0 shake for 1 h. in darkness	sh, 2-line fh, secondary jt, MnO_2	Schwertmann, 1964; Stone, 1987; Dold et al., in prep.
(4) Fe(III) oxides 0.2 M NH_4-oxalate pH 3.0 heat in water bath 80°C for 2 hours	gt, jt, Na-jt, hm, mt, higher ordered fh (5 - 6-line)	Dold, in prep.
(5) organics and secondary Cu-sulfides H_2O_2 35% heat in water bath for 1 hour	organics , cv, cc-dg	Sondag, 1981
(6) primary sulfides Combination of $KClO_3$ and HCl, followed by 4 M HNO_3 boiling	py, cp, cc, bn, sl, gn, tt, cb, op, stb	Chao & Sanzolone, 1977; Hall et al., 1996
(7) residual HNO_3, HF, $HClO_4$, HCL digestion	silicates	Hall et al., 1996; Dold et al., 1996

5.4.4.2 Acid-Base-Accounting (ABA)

Total sulfur was measured using a Leco® furnace. For measurement of the sulfate sulfur the 0.2 M oxalic acid hot 2h leach (Iron oxides, gt, jt, hm, mt; chapter 3) was used. Sulfur was determined by ICP-AES. The differences of both results represents the sulfide sulfur content.

Total and mineral carbon has been analyzed by coulometric titration (Ströhlein CS 702®). The sulfide net neutralization potential (SNNP) was calculated in $tCaCO_3/1000t$ (Morin and Hutt, 1997).

5.4.5 Microbiological methods

For the microbiological study a separate aliquot was taken from every sample and maintained at a temperature of 5°C untreated in ice-packed coolers. The samples were delivered to the laboratory of the biometallurgical group of the Chemical Engineering Department of the University of Chile, Santiago de Chile. A total of 10 samples were analyzed from 3 drill cores (T4, A5, E1) for total number of cells (direct microscopic counting; Phyroff-Hauser counting chamber), *Thiobacillus ferrooxidans* cultivation (plate counting), and oxidizing activity (Fe(II) oxidation rate).

To determinate the number of bacteria present in the solid, 10 g of the sample was brought into contact with 100 ml of a growth medium, shaken, and centrifuged. The supernant solution was used for bacterial count (direct and plate) and measurement of pH and Eh. The medium used to grow *T. ferrooxidans* consisted of 0.4 g/l $(NH_4)_2SO_4$, 0.056 g/l $K_2HPO_4 \cdot 3H_2O$, 0.4 g/l $MgSO_4 \cdot 7H_2O$, and 33.3 g/l $FeSO_4 \cdot 7H_2O$ (modified after Tuovinen & Kelly, 1973). The pH was adjusted with H_2SO_4 to 1.6 and all material used was previously sterilized.

To determine the oxidation activity of the samples, 3 g/l Fe(II) was added to the sample solutions and shaked at 30°C. Periodically Fe(II) and Fe_{total} (colorimetrically; ferrous-o-phenanthroline complex), pH and Eh were measured. Also bacteria numbers (direct counting and plate counting) were analyzed at the beginning and the end of the experiments.

5.5 Results and Discussion

5.5.1 Piuquenes tailings impoundment, La Andina

5.5.1.1 Physical properties and mineralogy

The Piuquenes impoundment was totally dry during the first summer field campaign (1996) with groundwater levels between 2.0 (A4) and 2.6 m (A2) below the surface. In winter (1997), a pond covered the end of the impoundment (Fig. 1) and the groundwater level was 50 cm below the surface in the proximity of A2. The five drill cores (A1 – A5) reveal a very similar stratigraphy of the tailings. It is characterized by a 0.5 to 0.8 m (A1 = 0.8m; A2 = 0.5m; A3 = 0.7m; A4 = 0.65; A5 = 0.5m) thick low pH (2.1 – 3.5) *oxidation zone* at the top (Fig. 2A), followed by an underlying *neutralization zone* (pH 3.5 – 5) down to depths of 2.6 – 4.2 m (A1 = 3.2m; A2 = 3.3m; A3 = 4.2m; A4 = 2.6m; A5 = 4.3m), and below, the *primary zone* with increasing pH up to values of 8.4 was sampled down to 10 m depth. In Fig. 3 the stratigraphy, pH, and geochemical data are presented from the representative drill core A2 and will be discussed in detail in this section. In addition a *hematite-rich sediment* occurs in the pond area

and has been cut by drill core A4 (Fig. 1, Fig. 2A, and Fig. 6) and will discussed in chapter 5.5.1.6.

XRD studies show that the primary gangue is dominated by quartz, alkali-feldspar (mainly albite ± anorthoclase), and micas (muscovite, sericite, biotite). Illite, chlorite, and kaolinite are the typical minerals in the clay fraction (< 2 μm). In the oxidation zone, characterized by light gray to yellow-brown (jarosite) colors and alternating fine sandy to clayey-silty ($K = 3.1x10^{-7}$ - $1.9x10^{-8}$ m/s) horizons, disseminated jarosite and a vermiculite-type-mixed layer mineral dominate the secondary mineralogy together with schwertmannite. The orange-brown color and typical pH values (2.8-3.5) indicate in the field the presence of schwertmannite (Fig. 2B). The presence of schwertmannite was proven by DXRD (2.6 % Fe) of a hand selected schwertmannite-rich streak. Fast dissolution kinetics in NH_4-oxalate, the Fe/S mole ratio of 4.9, stoichiometric calculations, and in-situ element mapping additionally support the identification of schwertmannite (chapter 7). Schwertmannite occurs as dots or streaks in the fine grained horizons or is enriched at the interface with fine to coarse grained horizons (Fig. 2B, Fig. 6). This distribution of schwertmannite suggest that it is preferentially associated with water flow paths and that possibly dilution increases the pH to the level necessary (2.8-3.5, Bigham et al., 1996) for its formation. This is also supported by the field observation that schwertmannite is more abundant near the pond region. In contrast, jarosite is disseminated in the oxidation zone and forms possibly at lower pH in-situ, where the sulfide oxidation and liberation of potassium (mainly from biotite, resulting in the formation of a secondary vermiculite-like mixed layer mineral, 12.25 – 12.67 Å) takes place. Tertiary gypsum is associated mainly with the groundwater level and to a lesser extent the oxidation zone, where it also may be a secondary

---

***Fig. 2: A:** A layer of about 2 cm thick hematite-rich sediment (reddish-brown, pH 7.7) overlying the low pH (3.1) oxidation zone at the surface sampling point AS3, Piuquenes tailings impoundment, La Andina. **B:** Schwertmannite-rich (sh) streaks and dots in fine-grained horizon from the low pH oxidation zone shown in Fig. 2A (sample AS3/016), indicating the association of schwertmannite to water-flow paths, in this sample possible due to cracking. **C:** Low pH oxidation zone of the Cauquenes tailings impoundment, El Teniente with surface precipitation of chalcanthite (cha), and, at interfaces of layers of different grain-size, of schwertmannite. **D:** Evaporite zone of the El Salvador tailings impoundment No. 1 with a zoom showing secondary efflorescent salts (e.g., bonattite). **E:** Fractured supergene replacement of chalcopyrite (cp) by chalcocite-digenite on rims, primary zone (sample A2/900), Piuquenes tailings impoundment, La Andina. **F:** Typical chalcopyrite replacement by secondary covellite (cv) as complete rims, neutralization zone (sample A5/100), Piuquenes tailings impoundment, La Andina. Note that sphalerite (sl) does not show replacement. **G:** Fractured chalcopyrite grain (cp), showing supergene replacement of by chalcocite-digenite and minor covellite (dark blue) at the borders, primary zone (sample T1/850), Cauquenes tailings impoundment, El Teniente. **H:** Chalcopyrite replacement by Secondary covellite (cv) as thin complete rims, primary zone (sample H1/200), Cauquenes tailings impoundment, El Teniente.*

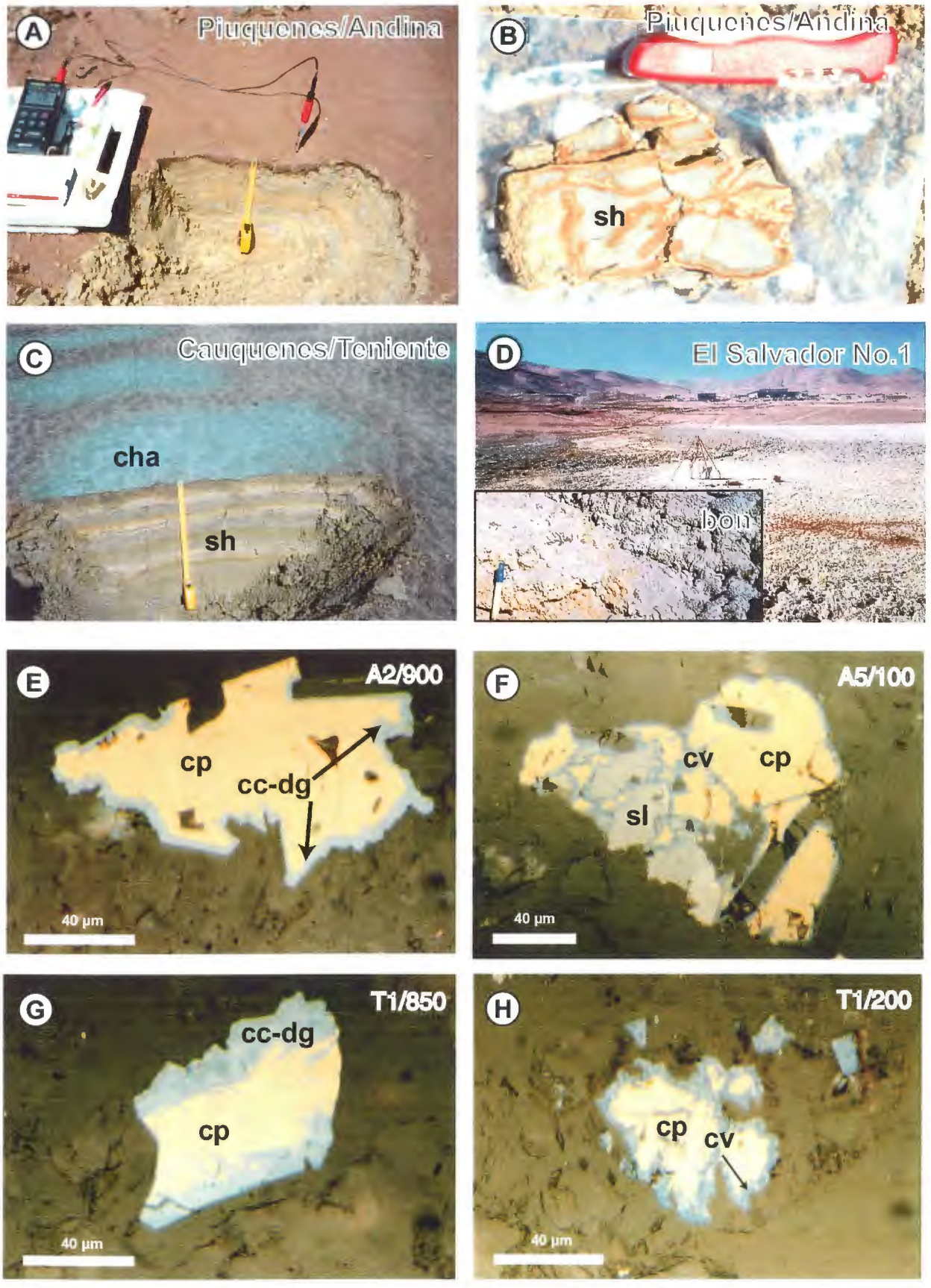

Fig. 2: *For the legend see previous page.*

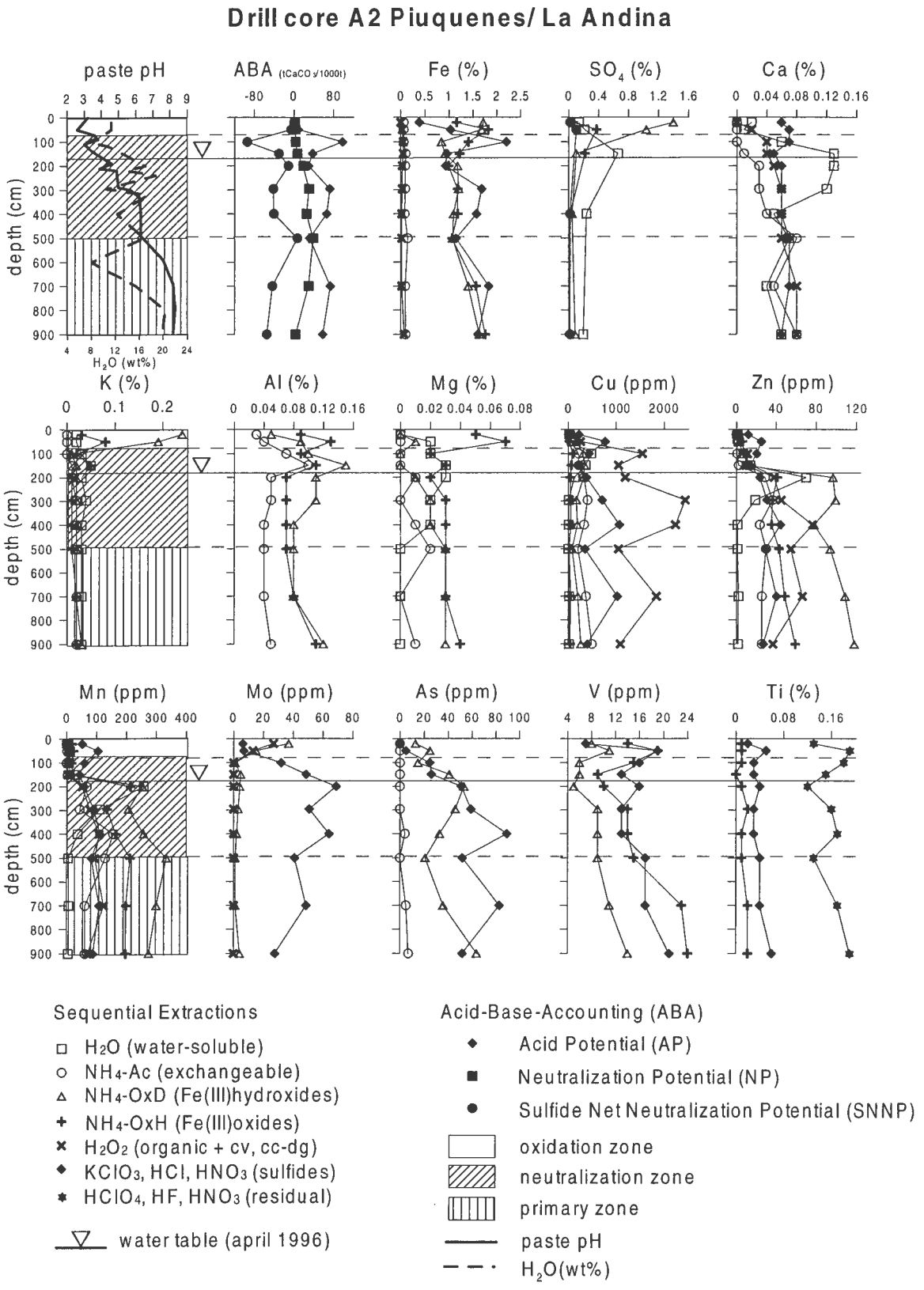

Fig. 3: *Results of sequential extractions from the representative drill core A2 from the Piuquenes tailings impoundment, La Andina, Chile. For better visibility of the changes from primary to secondary phases (mainly from sulfides to oxides or sulfates) the concentrations of the residual fraction of some major elements (Fe, K, Al, Mg, Ca) are not shown in Fig. 3, 7 and 10. For data see Tables 4, 6, 7, and 8.*

Table 4: *Drill core A2 from Piuquenes/Andina* *ICP-ES results from sequence B*

Fe (%)										
sample	depth	H_2O	NH_4-OAc	NH_4-OxD	NH_4-OxH	H_2O_2	sulfide	residual	total	bulk
A2/020	20	BDL	0.06	1.71	1.16	BDL	0.39	1.06	4.38	5.78
A2/050	50	BDL	0.06	1.68	1.82	0.03	1.03	1.68	6.3	7.87
A2/100	100	BDL	0.06	0.84	1.4	0.05	2.2	2.17	6.72	8.15
A2/150	150	BDL	0.1	0.92	1.22	0.05	0.96	1.57	4.82	6.21
A2/200	200	BDL	0.09	1.18	0.99	0.03	0.93	0.86	4.08	4.95
A2/295	295	BDL	0.09	1.2	1.18	0.03	1.68	1.51	5.69	7.3
A2/400	400	BDL	0.08	1.1	1.18	0.02	1.57	1.52	5.47	7.5
A2/500	500	BDL	0.14	1.08	1.07	0.02	1.15	0.75	4.21	5.41
A2/700	700	0.01	0.09	1.4	1.56	0.02	1.83	1.46	6.37	7.58
A2/900	900	0.01	0.1	1.64	1.75	0.07	1.61	1.36	6.54	7.42

Al (%)										
sample	depth	H_2O	NH_4-OAc	NH_4-OxD	NH_4-OxH	H_2O_2	sulfide	residual	total	bulk
A2/020	20	BDL	0.03	0.05	0.09	0.03	0.28	5.81	6.29	8.03
A2/050	50	BDL	0.04	0.09	0.13	0.05	0.66	5.77	6.74	8.27
A2/100	100	BDL	0.07	0.1	0.09	BDL	0.42	5.68	6.36	8.09
A2/150	150	BDL	0.1	0.15	0.11	BDL	0.43	6.03	6.82	8.33
A2/200	200	BDL	0.05	0.11	0.07	BDL	0.46	5.97	6.66	8.25
A2/295	295	BDL	0.05	0.11	0.07	BDL	0.46	5.9	6.59	8.55
A2/400	400	BDL	0.04	0.08	0.07	BDL	0.43	5.21	5.83	8.58
A2/500	500	BDL	0.04	0.08	0.07	BDL	0.52	5.47	6.18	8.18
A2/700	700	BDL	0.04	0.08	0.08	BDL	0.53	6.05	6.78	8.55
A2/900	900	0.01	0.05	0.12	0.11	BDL	0.69	6.12	7.1	8.24

K (%)										
sample	depth	H_2O	NH_4-OAc	NH_4-OxD	NH_4-OxH	H_2O_2	sulfide	residual	total	bulk
A2/020	20	0.02	BDL	0.24	0.03	BDL	-	3.83	4.12	5.57
A2/050	50	0.02	BDL	0.19	0.08	0.02	-	3.09	3.4	4.67
A2/100	100	0.03	BDL	0.01	0.02	BDL	-	3.2	3.26	4.59
A2/150	150	0.05	0.01	0.02	0.05	BDL	-	3.16	3.29	4.55
A2/200	200	0.03	0.01	0.02	0.01	BDL	-	3.28	3.35	4.63
A2/295	295	0.04	0.02	0.02	0.01	BDL	-	2.91	3	4.52
A2/400	400	0.03	0.02	0.02	0.01	BDL	-	3.02	3.1	4.75
A2/500	500	0.03	0.02	0.02	0.01	BDL	-	3.19	3.27	4.89
A2/700	700	0.03	0.02	0.02	0.02	BDL	-	3.35	3.44	5.01
A2/900	900	0.03	0.02	0.03	0.02	BDL	-	3.38	3.48	4.79

Mg (%)										
sample	depth	H_2O	NH_4-OAc	NH_4-OxD	NH_4-OxH	H_2O_2	sulfide	residual	total	bulk
A2/020	20	BDL	BDL	BDL	0.05	BDL	0.22	0.31	0.58	0.7
A2/050	50	0.02	BDL	0.01	0.07	0.01	0.52	0.35	0.98	1.14
A2/100	100	0.02	BDL	BDL	0.02	BDL	0.32	0.4	0.76	0.89
A2/150	150	0.03	BDL	BDL	0.03	BDL	0.32	0.31	0.69	0.81
A2/200	200	0.03	0.01	0.01	0.02	BDL	0.36	0.24	0.67	0.75
A2/295	295	0.02	BDL	0.02	0.03	BDL	0.36	0.33	0.76	0.93
A2/400	400	0.02	0.01	0.02	0.03	0.01	0.35	0.28	0.72	0.94
A2/500	500	BDL	0.02	0.03	0.03	BDL	0.41	0.2	0.69	0.8
A2/700	700	BDL	BDL	0.03	0.03	0.01	0.4	0.29	0.76	0.89
A2/900	900	BDL	0.01	0.03	0.04	BDL	0.53	0.31	0.92	0.99

Na (%)										
sample	depth	H_2O	NH_4-OAc	NH_4-OxD	NH_4-OxH	H_2O_2	sulfide	residual	total	bulk
A2/020	20	BDL	BDL	BDL	BDL	BDL	BDL	0.56	0.56	0.72
A2/050	50	BDL	BDL	BDL	BDL	BDL	BDL	0.63	0.63	0.81
A2/100	100	BDL	BDL	BDL	BDL	BDL	BDL	0.48	0.48	0.6
A2/150	150	BDL	BDL	BDL	BDL	BDL	BDL	0.79	0.79	1
A2/200	200	BDL	BDL	BDL	BDL	BDL	BDL	0.99	0.99	1.23
A2/295	295	BDL	BDL	BDL	BDL	BDL	BDL	0.67	0.67	0.86
A2/400	400	BDL	BDL	BDL	BDL	BDL	BDL	0.66	0.66	0.89
A2/500	500	BDL	BDL	BDL	BDL	BDL	BDL	0.89	0.89	1.16
A2/700	700	BDL	BDL	BDL	BDL	BDL	BDL	0.69	0.69	0.9
A2/900	900	BDL	BDL	BDL	BDL	BDL	BDL	0.72	0.72	0.86

Ca (%)										
sample	depth	H_2O	NH_4-OAc	NH_4-OxD	NH_4-OxH	H_2O_2	sulfide	residual	total	bulk
A2/020	20	0.02	BDL	0.01	BDL	BDL	0.06	0.09	0.18	0.22
A2/050	50	0.01	BDL	0.01	BDL	0.02	0.07	0.17	0.28	0.37
A2/100	100	0.06	BDL	0.01	BDL	0.04	0.07	0.08	0.26	0.29
A2/150	150	0.13	0.01	BDL	BDL	0.04	0.05	0.1	0.33	0.38
A2/200	200	0.13	0.03	BDL	0.01	0.05	0.06	0.09	0.37	0.41
A2/295	295	0.12	0.03	BDL	BDL	0.06	0.06	0.12	0.39	0.46
A2/400	400	0.05	0.04	BDL	BDL	0.06	0.06	0.09	0.3	0.39
A2/500	500	0.07	0.08	BDL	BDL	0.06	0.07	0.1	0.38	0.47
A2/700	700	0.04	0.05	BDL	BDL	0.08	0.07	0.08	0.32	0.37
A2/900	900	0.06	0.08	BDL	BDL	0.08	0.06	0.09	0.37	0.41

Tl (%)										
sample	depth	H_2O	NH_4-OAc	NH_4-OxD	NH_4-OxH	H_2O_2	sulfide	residual	total	bulk
A2/020	20	BDL	BDL	BDL	0.01	BDL	0.02	0.13	0.16	0.21
A2/050	50	BDL	BDL	BDL	0.01	BDL	0.05	0.19	0.25	0.31
A2/100	100	BDL	BDL	BDL	0.01	BDL	0.03	0.18	0.22	0.27
A2/150	150	BDL	BDL	BDL	BDL	BDL	0.03	0.15	0.18	0.23
A2/200	200	BDL	BDL	BDL	0.01	BDL	0.04	0.12	0.17	0.2
A2/295	295	BDL	BDL	BDL	0.02	BDL	0.03	0.16	0.21	0.28
A2/400	400	BDL	BDL	BDL	0.01	BDL	0.03	0.17	0.21	0.29
A2/500	500	BDL	BDL	BDL	0.01	BDL	0.04	0.13	0.18	0.24
A2/700	700	BDL	BDL	BDL	0.02	BDL	0.04	0.17	0.23	0.3
A2/900	900	BDL	BDL	BDL	0.02	BDL	0.06	0.19	0.27	0.31

Ba (ppm)										
sample	depth	H_2O	NH_4-OAc	NH_4-OxD	NH_4-OxH	H_2O_2	sulfide	residual	total	bulk
A2/020	20	BDL	BDL	53	20	BDL	12	617	702	994
A2/050	50	BDL	BDL	20	34	2	22	420	498	719
A2/100	100	1	4	11	26	BDL	16	364	422	625
A2/150	150	BDL	6	10	30	BDL	22	386	454	649
A2/200	200	1	15	13	21	1	20	405	476	679
A2/295	295	BDL	15	10	16	BDL	17	367	425	633
A2/400	400	BDL	16	7	13	BDL	15	368	419	668
A2/500	500	BDL	20	8	14	BDL	19	420	481	737
A2/700	700	1	30	8	26	1	24	446	536	777
A2/900	900	BDL	22	12	14	BDL	24	458	530	732

Cu (ppm)										
sample	depth	H_2O	NH_4-OAc	NH_4-OxD	NH_4-OxH	H_2O_2	sulfide	residual	total	bulk
A2/020	20	21.1	17.3	113	9.4	42.7	221	11.2	436	442
A2/050	50	73.3	54.2	169	24.6	260	775	13.6	1370	1360
A2/100	100	472	217	308	95.6	1550	435	103	3181	3140
A2/150	150	359	213	343	69.2	1050	217	13.1	2264	2160
A2/200	200	128	334	314	44.2	1190	382	11.5	2404	2370
A2/295	295	14.6	406	173	55.6	2440	714	60.6	3864	3850
A2/400	400	8.5	327	191	52.3	2230	1070	27.5	3906	4110
A2/500	500	5.6	206	83.3	22.5	1050	350	12.1	1730	1760
A2/700	700	18.6	368	199	59.4	1840	1030	25.6	3541	3710
A2/900	900	18.6	500	264	37.2	1090	407	12.8	2330	2250

Zn (ppm)										
sample	depth	H_2O	NH_4-OAc	NH_4-OxD	NH_4-OxH	H_2O_2	sulfide	residual	total	bulk
A2/020	20	1.2	BDL	2.7	5	BDL	12.1	11.9	32.9	43.8
A2/050	50	2.3	0.9	3.3	6.1	2.5	25	16.1	56.2	60.3
A2/100	100	7.1	0.7	10.8	7.6	11.3	20.7	18.2	76.4	68.2
A2/150	150	14	2.1	8.1	14.8	9.2	14.1	18.8	81.1	82.5
A2/200	200	70	28.5	97.1	40.7	38.1	23.5	27.3	325.2	321
A2/295	295	19.1	36.5	99.5	36.5	45	30.7	17.7	285	299
A2/400	400	1.1	23.7	77.9	35.1	76.7	44.5	18	277	308
A2/500	500	1.4	29.8	94.2	43.1	54.8	29.1	22	274.4	288
A2/700	700	2.4	25.8	109	48.8	66.5	40.4	18.9	311.8	333
A2/900	900	2	25.5	118	59.2	37.1	27.3	29.6	298.7	286

Mn (ppm)										
sample	depth	H_2O	NH_4-OAc	NH_4-OxD	NH_4-OxH	H_2O_2	sulfide	residual	total	bulk
A2/020	20	4	BDL	9	19	BDL	52	34	118	141
A2/050	50	8	2	12	24	5	104	50	205	241
A2/100	100	8	BDL	7	16	3	59	36	129	148
A2/150	150	28	3	13	21	3	44	26	138	148
A2/200	200	257	68	254	214	52	59	19	923	909
A2/295	295	111	44	207	135	77	92	30	696	750
A2/400	400	36	156	257	164	109	112	28	862	975
A2/500	500	5	128	333	211	94	82	20	873	953
A2/700	700	7	60	299	198	124	109	27	824	931
A2/900	900	5	60	275	196	70	87	28	721	727

Cr (ppm)										
sample	depth	H_2O	NH_4-OAc	NH_4-OxD	NH_4-OxH	H_2O_2	sulfide	residual	total	bulk
A2/020	20	BDL	BDL	3	5	BDL	6	3	17	8
A2/050	50	BDL	BDL	3	8	BDL	13	6	30	23
A2/100	100	BDL	BDL	3	6	BDL	8	8	25	16
A2/150	150	BDL	BDL	3	3	BDL	13	6	25	13
A2/200	200	BDL	BDL	3	3	BDL	10	3	19	8
A2/295	295	BDL	BDL	4	4	BDL	9	5	22	13
A2/400	400	BDL	BDL	4	4	BDL	8	5	21	14
A2/500	500	BDL	BDL	4	5	BDL	13	3	25	12
A2/700	700	BDL	BDL	4	7	BDL	10	6	27	21
A2/900	900	BDL	BDL	6	8	BDL	8	5	27	16

Pb (ppm)										
sample	depth	H_2O	NH_4-OAc	NH_4-OxD	NH_4-OxH	H_2O_2	sulfide	residual	total	bulk
A2/020	20	BDL	BDL	9	6	BDL	5	BDL	20	21
A2/050	50	BDL	BDL	12	BDL	BDL	3	BDL	15	25
A2/100	100	BDL	BDL	6	5	BDL	9	BDL	20	28
A2/150	150	BDL	BDL	BDL	10	BDL	8	BDL	18	33
A2/200	200	BDL	2	14	3	BDL	10	BDL	29	33
A2/295	295	BDL	3	16	5	BDL	21	BDL	45	44
A2/400	400	BDL	5	12	5	BDL	17	BDL	39	40
A2/500	500	BDL	6	8	3	BDL	9	BDL	26	34
A2/700	700	BDL	6	10	9	2	22	BDL	49	61
A2/900	900	BDL	4	17	9	BDL	26	BDL	56	50

Mo (ppm)										
sample	depth	H_2O	NH_4-OAc	NH_4-OxD	NH_4-OxH	H_2O_2	sulfide	residual	total	bulk
A2/020	20	BDL	BDL	37	3	27	6	3	76	80
A2/050	50	BDL	BDL	15	BDL	13	7	BDL	35	35
A2/100	100	BDL	BDL	1	BDL	BDL	32	5	38	35
A2/150	150	BDL	BDL	5	BDL	BDL	49	4	58	59
A2/200	200	BDL	BDL	4	BDL	BDL	69	7	80	58
A2/295	295	BDL	BDL	3	BDL	BDL	51	6	60	61
A2/400	400	BDL	BDL	2	BDL	BDL	64	9	75	64
A2/500	500	BDL	BDL	1	BDL	BDL	41	3	45	44
A2/700	700	BDL	BDL	1	BDL	BDL	49	7	57	62
A2/900	900	BDL	BDL	4	BDL	BDL	28	3	35	32

V (ppm)										
sample	depth	H_2O	NH_4-OAc	NH_4-OxD	NH_4-OxH	H_2O_2	sulfide	residual	total	bulk
A2/020	20	BDL	BDL	8	14	BDL	7	52	81	99
A2/050	50	BDL	BDL	11	19	BDL	19	70	119	149
A2/100	100	BDL	BDL	6	15	BDL	16	78	115	137
A2/150	150	BDL	BDL	6	9	BDL	13	61	89	113
A2/200	200	BDL	BDL	5	10	BDL	16	50	81	97
A2/295	295	BDL	BDL	9	14	BDL	13	68	104	133
A2/400	400	BDL	BDL	9	14	BDL	13	68	104	138
A2/500	500	BDL	BDL	9	15	BDL	17	47	88	109
A2/700	700	BDL	BDL	11	23	BDL	17	67	118	139
A2/900	900	BDL	BDL	14	24	BDL	21	66	125	141

As (ppm)										
sample	depth	H_2O	NH_4-OAc	NH_4-OxD	NH_4-OxH	H_2O_2	sulfide	residual	total	bulk
A2/020	20	BDL	BDL	13	BDL	BDL	BDL	BDL	13	38
A2/050	50	BDL	BDL	25	BDL	BDL	5	BDL	30	BDL
A2/100	100	BDL	BDL	15	BDL	BDL	25	BDL	40	33
A2/150	150	BDL	BDL	41	5	BDL	26	BDL	72	BDL
A2/200	200	BDL	BDL	53	BDL	BDL	51	BDL	104	105
A2/295	295	BDL	BDL	46	4	BDL	59	BDL	109	42
A2/400	400	BDL	4	33	3	BDL	89	BDL	129	44
A2/500	500	BDL	BDL	21	BDL	BDL	52	BDL	73	38
A2/700	700	BDL	5	36	4	BDL	83	BDL	128	119
A2/900	900	BDL	7	64	BDL	BDL	52	BDL	123	77

NH4-Ac = NH4-acetate leach
NH4-OxD =NH4-oxalate 1h dark
NH4-OxH =NH4-oxalate 2h hot
sulfide = KCLO3, HCl, HNO3 leach
residual = HClO4, HF, HNO3, HCl leach

BDL = below detection limit
- = leach interference

mineral. The primary zone is characterized by its dark gray color with some red to dark-brown horizons (indicating the presence of secondary Fe(III) hydroxides, possibly ferrihydrite).

Examination of polished sections show that in the neutralization zone and the primary zone the original sulfide paragenesis of the ore can be recognized. It is dominated by pyrite, which is partly strongly fractured, possibly due to the milling process. Chalcopyrite is present as a trace mineral and shows two types of replacement by chalcocite-digenite and/or covellite. In the primary zone, thick replacement rims mainly composed of digenite-chalcocite with some covellite (Fig. 2E) are observed and interpreted as product of supergene enrichment processes in the ore deposit as reported by Serrano et al. (1996). This primary replacement is rare and is only conserved in some grains as complete rims. In contrast, a secondary Cu replacement, found in the neutralization zone directly below the groundwater level, is characterized by complete thin rims dominated by covellite with some chalcocite-digenite replacing chalcopyrite (Fig. 2F). Most of the chalcopyrite grains show this thin replacement rim, only some chalcopyrite grains found as inclusions in silicates are protected from replacement. This replacement is interpreted as a secondary process (post-milling) which occurs in-situ and detailed discussion will follow below. Magnetite is generally present as massive grains, partly replaced by martite at the edges. Traces of enargite, molybdenite, goethite, and hematite were also found in the primary and neutralization zone.

The source for the secondary Cu enrichment is found in the oxidation zone, where extensive leaching of the supergene and hypogene Cu-sulfides occurs. Only some residual grains of pyrite and chalcopyrite are observed in the oxidation zone, no supergene Cu-sulfides are present. Pyrite grains do not show Fe(III) hydroxide coating. Magnetite with martite replacement is frequent and tabular hematite is also present.

5.5.1.2 Acid-Base Accounting

The oxidation stratification is also confirmed by the results of acid-base accounting (Fig. 3, ABA). In the primary zone the average $S_{sulfide}$ content is 0.95 wt % and the C_{tot} is 0.4 wt % leading to a sulfide net neutralization potential (SNNP) of –45.35 $tCaCO_3/1000t$, indicating that the tailings have a low acid potential (AP). Nevertheless, a well-developed oxidation – neutralization stratigraphy is observed in the tailings. In the oxidation zone the SNNP is near zero, indicating that the AP and the neutralization potential (NP) are consumed (Fig. 3). This is consistent with the pH distribution and the sulfide mineral distribution. Calculation of the pyrite content with the assumption that all sulfide sulfur is associated with pyrite, leads to an average pyrite content of 1.77 wt % in the primary zone and neutralization zone. Correction using the Cu concentrations in the sulfide fractions of sequential extractions leads to an average pyrite content of 1.66 wt %. The variation between total sulfide pyrite content and the correction accounting for the Cu-sulfides ranges between 1.7 and 11.2 % with an average variation of 6.35 %.

5.5.1.3 Sequential extractions

The results of sequential extractions reveal the mineral phase changes of the elements due to oxidation, dissolution and precipitation processes and speciation of elements under the changing geochemical conditions throughout the tailings stratigraphy. The element distribution is discussed considering first its relation to the formation of detectable secondary minerals (major elements) and then the behavior of the trace elements, which are separated by their geochemical behavior (bivalent cations and oxyanions). Data from one representative drill core (A2) are shown in Fig. 3 and Table 4. The others drill cores show all a very similar behavior (Appendix 3).

Fe. Pyrite is the main source for iron and sulfur. Iron is depleted in the sulfide fraction in the oxidation zone from 1.5 to 0.5% in the four analyzed drill cores (A2 –A5). The residual 0.5% of Fe is not necessarily from pyrite dissolution. Chao and Sanzalone (1977) reported that the $KClO_3$, HCl, HNO_3 leach may attack also the edges of silicates such as biotite and liberate additional iron. The precipitation of schwertmannite and jarosite as typical secondary minerals in the oxidation zone is reflected in an increase of the iron concentrations in the Fe(III) oxyhydroxide (from 0.5 to 1.5%) and Fe(III) oxide leach (from 1 to 2.3%) in the analyzed drill cores (Fig. 3). The sulfur concentrations in these fractions parallel these observations. The iron content of the Fe(III) oxides leach in the primary zone represents the primary hematite, magnetite, ilmenite content plus primary and/or secondary goethite. In the oxidation zone, secondary jarosite overlays this primary content additionally. The iron concentrations in the water-soluble and exchangeable fractions are negligible. The increased potassium concentrations of these two fractions in the oxidation zone confirms the dissolution kinetics and DXRD observation that part of jarosite is dissolved in the Fe(III) oxyhydroxides fraction. Stoichiometric calculations with the assumption that the potassium concentrations in the Fe(III) oxyhydroxide (3rd leach) and Fe(III) oxide (4rd leach) leach correspond to jarosite dissolution make it possible to calculate the total jarosite content. The schwertmannite content is calculated from Fe_{total} in the Fe(III) oxyhydroxide leach minus the calculated jarosite content in this extraction. Comparison of the calculated schwertmannite and jarosite concentrations with the calculated and measured sulfate concentrations in the Fe(III) oxyhydroxide leach show an good agreement (table 5) indicating that only schwertmannite and jarosite were dissolved in this leach. The difference of Fe_{total} minus the calculated jarosite content in the Fe(III) oxide leach represents the primary iron oxide content of hematite and magnetite and the primary and/or secondary goethite content. Results show that the schwertmannite content increases from 45.9 % (A2) in the dam area to 52.5 % (A4) in the pond area. This corresponds with the field observation that in the pond area more schwertmannite is formed and supports the interpretation that schwertmannite precipitation is associated with dilution via water flow.

Table 5: *Stoichiometric calculation of the sulfate content based on the Fe and K concentrations of the 3rd and 4th leach for jarosite (jt) and schwertmannite (sh; $Fe_{16}O_{16}(OH)_{10}(SO_4)_3$; Fe/S mol ratio ~ 5). The calculated sulfate concentrations are in agreement with the measured concentrations for the 3rd leach (compare bold columns), showing that only schwertmannite and jarosite were dissolved Fe(III) minerals in this leach (abbreviations as in table 2).*

sample	K 3rd	K 4th	Fe 3rd	Fe 4th	Fe jt 3rd	Fe jt 4th	Fe sh 3rd	Fe ox 4th	sh/jt	sh/sh+jt	jt SO4 3rd	sh SO4 3rd	SO4 jt+sh 3rd	SO4 3rd	SO4 jt 4th	SO4 4th
	measured (%)				calculated (%)				calc	calc (%)	calc (%)	calc (%)	calc (%)	(%)	calc (%)	(%)
A4/035	0.08	0.14	1.08	2.33	0.24	0.59	0.84	1.74	1.02	50.41	0.28	0.29	**0.57**	**0.56**	0.69	0.71
A4/065	0.17	0.07	1.42	1.25	0.62	0.30	0.80	0.95	0.88	46.75	0.72	0.28	**1.00**	**1.00**	0.35	0.17
A2/020	0.24	0.03	1.71	1.16	0.91	0.13	0.80	1.03	0.76	43.34	1.06	0.28	**1.34**	**1.39**	0.15	0.06
A2/050	0.19	0.08	1.68	1.82	0.70	0.34	0.98	1.48	0.94	48.44	0.82	0.34	**1.16**	**1.04**	0.39	0.37

calc (%) = calculated; (%) = measured concentrations.

The iron concentrations in the two fractions, which represent the secondary Fe(III) oxyhydroxides and their sulfates, decrease towards the oxidation front and in the neutralization zone, whereas in the primary zone the concentrations increase to a similar level seen in the oxidation zone (1.5-1.7%). The latter increase is interpreted to be the result of ferrihydrite precipitation. DXRD results suggest the presence of a higher ordered ferrihydrite and goethite. The interpretation is also supported by the Fe/S mole ratios, which range from values of 2.1-6.2 in the oxidation zone up to values of 14.6 - 1001 in the zones below. The fact that the Fe concentrations are similar in the two reducible fractions in the primary zone may be a result of the slower dissolution of the higher ordered (e.g., 5-line or 6-line) ferrihydrite which was clearly proven to form in a cemented layer (chapter 6). The ferrihydrite is believed to be a secondary mineral and not a tertiary product, due to the observation in the field of brown to red-brown horizons in the primary zone. A tertiary ferrihydrite should also show lower ordering (e.g., 2-line), due to faster hydrolysis (Schwertmann et al., 1999).

Ca. The distribution of Ca (Fig. 3) is an important indicator of neutralization reactions related to carbonates. Its concentrations in the water-soluble fraction reflect the distribution of gypsum, confirmed by XRD data. In some areas, an increase of what might be secondary gypsum is observed in the oxidation zone, whereas the increase in concentrations of tertiary gypsum is associated with the phreatic level, as in the drill core A2 (Fig. 3). This also correlates with the sulfur concentrations found in the water-soluble fraction. The Ca concentrations in the exchangeable fraction (NH_4-acetate leach) represent the calcite content ± adsorbed Ca. The Ca concentrations in the oxidation and neutralization zone are below the detection limit, increasing in the primary zone to average concentrations of 0.1 %, corresponding to an equivalent calcite content of 0.17 wt %. This is much less than the calculation of the calcite equivalent by using the average of 0.17 wt % total carbon in the primary zone, which would lead to a content of 1.42 wt % calcite equivalent. As the Ca concentrations show that only 0.17 wt % can be associated with calcite, it is assumed that the rest of the carbon is present as 1.44 wt % of siderite ($FeCO_3$), as this carbonate is also reported from the mine. This correlates with the pH distribution. Near neutral pH values are found in the primary zone where calcite is still present. The neutralization

zone is buffered by siderite at pH values arround 5-6. In the oxidation zone, with pH < 3.5 carbonates have been consumed (Fig. 3). This neutralization sequence is in good agreement with that described by Blowes & Ptacek (1994).

Ti. Titanium is generally considered to be an immobile element. It has low concentrations (0.01-0.03 %) in the Fe(III) oxides fraction, indicating that in this leach minor ilmenite or some Ti containing iron oxides were dissolved. Low concentrations in the sulfide leach (0.02-0.05 %) may be an indicator of the partial dissolution of rutile and/or Ti bearing silicates.

Al. Aluminium is stable as a trivalent cation under acid conditions and its source is mainly the weathering of aluminosilicates. It shows slightly increased concentrations in the oxidation zone of the Fe(III) oxyhydroxides and Fe(III) oxides fractions, possible due to co-precipitation or substitution with the secondary ferric phases. At the oxidation front the lowest concentrations are observed, while a slight increase in the primary zone is noted, possibly due to gibbsite ($Al(OH)_3$) hydrolysis, which could not be detected by XRD due to the low Al concentrations (0.1-0.5 %).

Cu. The average Cu content of the tailings deposited in the Piuquenes impoundment is 0.22% (Division Andina, 1996). Our geochemical results reflect a continuous decrease of the average Cu content in the primary zone from the dam (A2 $Cu_{primary}$ Ø = 0.25%; A5 $Cu_{primary}$ Ø = 0.22%; A3 $Cu_{primary}$ Ø = 0.17%) to the pond (A4 $Cu_{primary}$ Ø = 0.15%). This is a result of the deposition technique, where a gravimetric separation of the heavier sulfide minerals occur near the discharge point (dam area). Cu shows in all drill cores a strong total enrichment below the groundwater level (0.37% - 0.60%) mainly in the H_2O_2-leach (0.2 - 0.27%) which essentially dissolves the secondary Cu-sulfides (and/or primary supergene) as covellite and chalcocite-digenite. A slight Cu increase near the groundwater level is also found in the water-soluble fraction. The enriched Cu zone is extended to depths of 3 to 4 m where the pH reaches values of 6 and the sulfide enrichment stops, while the exchangeable fraction increases slightly. As stated above, this zone of secondary Cu enrichment is correlated to thin covellite and chalcocite-digenite rims exclusively on chalcopyrite and bornite (Fig. 2E and 2F). Jang and Wadswoth (1994) have shown in a laboratory study at hydrothermal conditions (170 – 200°C), that chalcopyrite replacement starts with covellite and changes to digenite replacement. The authors postulate that even at low temperatures the chalcopyrite will undergo enrichment to more readily leachable secondary copper sulfides. Alpers and Brimhall (1989) reported this Cu-sulfide sequence from supergene enrichment at La Escondida, northern Chile. In other tailings impoundments, where no primary supergene enrichment exist in the primary ore, the presence of secondary covellite enrichment is reported (Boorman and Watson, 1976; Blowes and Jambor, 1990; Lin and Qvarfort, 1996; Holmström et al., in review). Supergene replacement is recognized in the primary zone of the Piuquenes tailings. It only occurs occasionally as complete rims, as it is mostly fractured during milling. Supergene replacement shows thicker (> $5x10^{-3}$ mm) replacement rims than the very thin secondary rims (< $3x10^{-3}$ mm). This primary Cu enrichment mainly consists of chalcocite-digenite, while the secondary replacement consists of mainly covellite, which is in agreement with the findings of Jang and Wadsworth (1994) and Alpers and Brimhall (1989) that covellite is the first stage in replacement. The texture and mineralogy of secondary replacement and the association with the saturated neutralization zone, where more reducing conditions dominate, strongly suggest that this copper enrichment is a

secondary process taking place in-situ in the tailings impoundment. In the Piuquenes tailings this process shows a strong association with pH. Webster et al. (1998) showed that Cu adsorption at natural acid mine drainage precipitates starts at lower pH (adsorption begins at pH 4 and at pH 6 80-100% of the Cu is adsorbed) than for synthetic schwertmannite and ferrihydrite. In Piuquenes, Cu adsorption seems to be a competitive process with the Cu replacement in Cu-sulfides. In pH ranges where Cu^{2+} is mobile (< pH 5), replacement of chalcopyrite to covellite dominates, whereas with increasing pH, adsorption immobilizes Cu^{2+} and replacement decreases. The concentrations of Cu and Zn in the exchangeable fraction (adsorbed) are clearly pH dependent (Fig. 4). Cu starts adsorption at pH 3.5 and with increasing pH the Cu concentration on solids increases. Zn starts adsorption at a slightly higher pH as Cu (pH 4), confirming the results of the laboratory adsorption study by Webster et al. (1998).

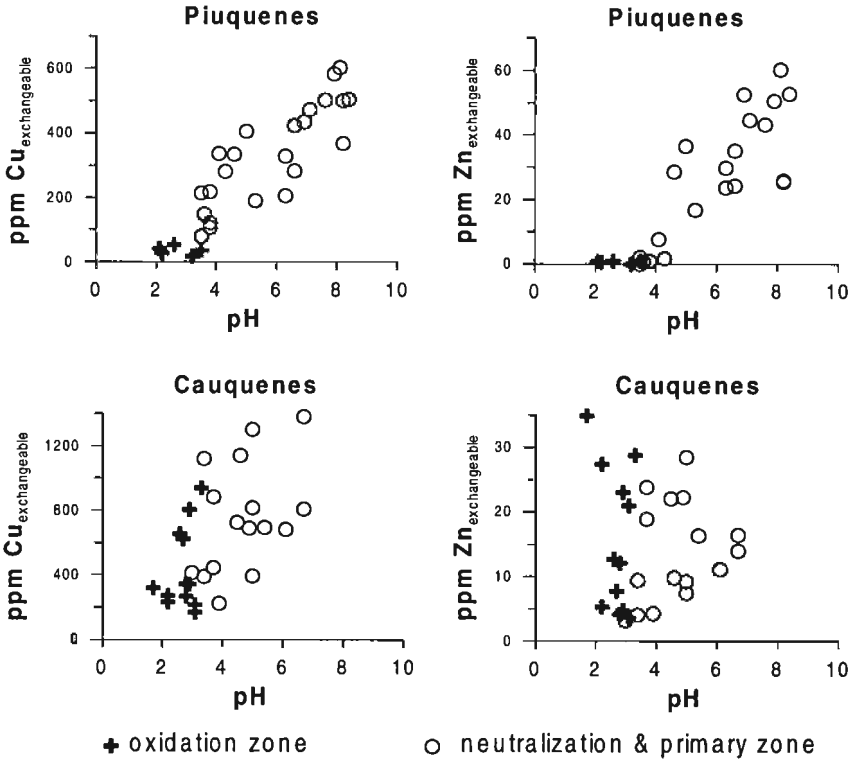

Fig. 4: Cu and Zn concentration of the exchangeable fraction (NH_4-acetate) versus the paste pH values from the Piuquenes and Cauquenes tailings. Data are from three drill cores in each tailings impoundment. For detailed discussion see the text.

Other bivalent cations. The other bivalent cations **Mg, Mn, Zn, Ba, Pb,** and **Sr** behave in a very similar way. An enrichment of these elements in the water-soluble fraction is associated with the phreatic level. The exchangeable fraction, together with the reducible fractions show nearly complete leaching in the oxidation zone and increasing concentrations downwards to the primary zone. This reflects their pH dependence with adsorption to clay minerals and secondary phases as $Fe(OH)_3$, $Al(OH)_3$, and $Mn(OH)_2$ and the diffusion into the crystalline systems and the co-precipitation with these secondary phases. The sulfide fraction is generally depleted in the oxidation zone.

Mo. In contrast to bivalent cations, which are mobile under acid conditions, oxyanions as Mo(V, VI), As(V), and V(III, IV) show increasing adsorption to HFO with decreasing pH (Dzombak & Morel, 1990). Chao & Sanzolone (1977) reported the partial dissolution of molybdenite in a H_2O_2-ascorbic acid leach. In our H_2O_2 leach the Mo concentrations were below the detection limit in the primary zone, indicating that no molybdentite was dissolved in this leach. In the Piuquenes tailings Mo is depleted in the oxidation zone in the sulfide fraction (molybdenite), due to sulfide oxidation. The liberated Mo is stable as molybdate under acid oxidizing conditions and is mainly associated with the Fe(III) oxyhydroxides fraction (schwertmannite) in the oxidation zone. An electron microprobe trans-section of a schwertmannite streak from the oxidation zone (AS3) has shown that Mo is slightly enriched, suggesting the preferentially adsorption of molybdate by schwertmannite via ligand exchange under acid conditions (chapter 7). As schwertmannite is associated with water flow paths, the enrichment of Mo in the schwertmannite streaks indicates a certain mobility under acid conditions, possibly transported as adsorbed molybdate at ferric polymers. All drill cores show increased concentrations of Mo in the sulfide fraction in the neutralization zone. When the molybdate reaches chemically reducing conditions (water-table), this oxyanion is transformed to by insoluble lower valence compounds. Thus, Mo may be incorporated into the cryptocrystalline variety of molybdenite called jordisite (Brookins, 1988). As the enrichment of Mo is probably related to the same conditions where secondary Cu replacement takes place, there is the possibility of secondary Mo enrichment by secondary sulfide precipitation or replacement. As Mo contents are low it was not possible to detect a mineral phase to explain this apparent enrichment.

A further specific feature of Mo in the oxidation zone is that it is enriched in the organic fraction. This is probably from Mo fixed in dead cell material of *Thiobacillus ferrooxidans*. *Thiobacillus ferrooxidans* is known to oxidize molybdenite but is poisoned by the resultant molybdate unless this is fixed e.g., by ferric iron (Tuovinen et al., 1971; Ehrlich, 1996).

As. Arsenic is depleted in the sulfide fraction of the oxidation zone, possibly due to oxidation of traces of enargite, tennantite and/or arsenopyrite. It is fixed in the Fe(III) hydroxide fraction with a minimum at the oxidation front (pH < 3) and a slight increase towards the oxidation as well to the primary zone. The As concentrations in the exchangeable fraction are below the detection limit in the oxidation zone and increase slightly to the primary zone. Arsenopyrite is reported to be oxidized by *Thiobacillus ferrooxidans* under the production of arsenate and arsenite and enargite with the release of cupric copper and arsenate (Ehrlich, 1996). Arsenate is strongly adsorbed at hydrous ferric oxides (HFO) under acid condition (Dzombak & Morel, 1990), reflected by the increased concentrations in the Fe(III) oxyhydroxides fraction in the oxidation zone. In-situ measurement of As by electron microprobe at the schwertmannite rim did not show any enrichment so that As is possibly fixed to jarosite. Substitution of arsenate and phosphate in jarosite as a solid solution is known (Alpers et al., 1989), but due to the low concentration of As (< 150 ppm) in the Fe(III) oxides leaches (Step 3 and 4) no mineralogical determination by XRD of possible members of the beudantite and crandallite groups was possible. Arsenite is relatively mobile at pH values below 4 and its adsorption increases with increasing pH up to concentrations of pH 8, before adsorption decreases again with increasing

pH (Dzombak & Morel, 1990). Mobilized arsenite may be an explanation for the increasing As concentrations in the primary zone.

V. Vanadium shows a similar distribution as As. In the sulfide fraction the V concentrations decrease in the oxidation zone, whereas they increase in the two reducible fractions of the oxidation and primary zone displaying the lowest concentrations at the oxidation front.

5.5.1.4 Drainage waters

Drainage water from the Piuquenes tailings showed a pH of 5.3 and very low metal concentrations. The measured metals are generally below the detection limit of the used techniques. Only Sr (0.35 mg/l), Ba (0.02 mg/l), and Cu (0.02 mg/l) could be detected. The values of Ca (62 mg/l), HCO_3 (58 mg/l), Cl (17 mg/l), and SO_4 (119 mg/l) indicate that neutralization processes are taking place in the tailings. It is predicted that when the low neutralization potential of these tailings is consumed, acidic metal-rich effluent will be produced.

5.5.1.5 Microbial activity

Three representative samples from the oxidation, neutralization, and primary zones were tested for bacterial count and oxidation activity. In all samples, high bacteria concentrations were observed by direct counting ($2.6x10^7$ – $3.4x10^8$ bact/ml). *Thiobacillus ferrooxidans* was cultivated ($3.2x10^3$ bact/ml) in the sample from the neutralization zone. Oxidizing activity tests show that the sample from the oxidation zone first starts to oxidize Fe^{2+} to Fe^{3+} after an initial or lag phase of 144 h. The lag phase is characterized by cell growth, and by the absence of cell division (Fig. 5). This good oxidation activity may indicate the presence of *Leptospirillum ferrooxidans* in the oxidation zone, as *Thiobacillus ferrooxidans* plate counting yielded no result. The sample from the neutralization zone started the oxidation activity after 240 h growth time. Once oxidation started the oxidation velocity (growth rate) was similar to the one of the sample from the oxidation zone. The sample from the primary zone showed slow oxidation starting after 336h (Fig. 5), indicating relatively low microbial oxidizing activity in the primary zone.

5.5.1.6 Hematite-rich sediment of the pond area

The maximum extent of the pond is associated with the presence of a clay-sized ($K = 8.47x10^{-9}$ m/s), intense red-brown laminated sediment with a maximum thickness in the center of the pond of 15 cm and paste pH 8 overlying the low pH (2.1 - 3.5) oxidation zone, separated by a well defined contact (Fig. 2A and Fig. 6). The transition zone of this sediment to the underlying low pH oxidation zone was sampled in detail in a second field campaign 1997 (Fig. 1, AS1 – AS4).

The thickness of this sediment decreases continuously towards the margins. Polished thin sections, as well as XRD and DXRD show that the red sediment is enriched in oriented tabular

hematite and a higher ordered ferrihydrite. The high crystallinity (results of Mössbauer spectroscopy) of the hematite in relation to pedogene hematite (Friedl, 1997, personal

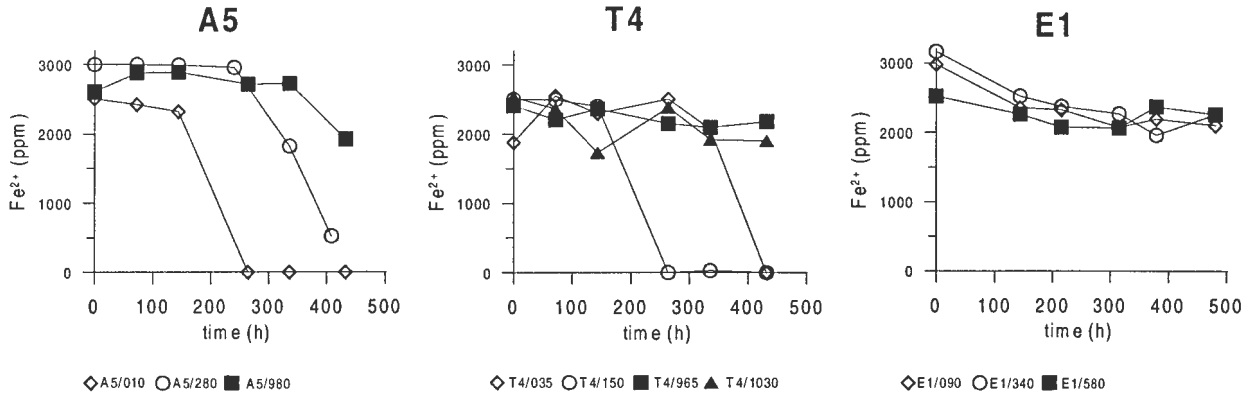

Fig. 5: *Microbial iron (Fe^{2+}) oxidation activity of representative samples from the three studied tailings. The drill core A5 is from Piuquenes (Andina), T4 from Cauquenes (Teniente), and E1 from El Salvador No.1 impoundments. Filled dots are samples from the primary zone and unfilled dots are from the oxidation or neutralization zone. As expected, samples from the oxidation zone from Piuquenes and Cauquenes start to oxidized. In contrast, none of the samples from the oxidation zone of El Salvador show important oxidation. This is interpreted as an effect of the higher molybdenite content in the Salvador tailings, which is lethal to oxidizing bacteria as Thiobacillus ferrooxidans leading to low microbial oxidation activity.*

communication) and the fact that this type of tabular hematite is also found in the primary zone of the tailings, suggest a hypogene origin. The pond pH during sampling was 7.6 and the paste pH of the sediment was between 7.6 and 8.4. The fine layering, the location at the lowest elevation of the impoundment, and the sharp contact with the low pH oxidation zone indicate that this sediment is a product of alluvial enrichment taking place on the tailings surface. The results of sequential extraction confirm this interpretation, showing strong enrichment of bivalent cations mainly in the exchangeable and Fe(III) oxyhydroxides fractions in the hematite-rich sediment, while the underlying oxidation zone is leached out with respect to these elements (Fig. 6 and Table 6). Mo is not enriched in this sediment, due to the low mobility of molybdate under acid conditions prevailing in the oxidation zone, which surrounds this sediment. Below, in the oxidation zone, Mo shows its association to the Fe(III) oyxhydroxide leach and is enriched in the organic fraction in a coarser horizon. This may indicate that in coarser material the microbial activity is higher due to better O_2 transport, resulting in higher molybdenite oxidation and increased poisoning of oxidizing bacteria as *Thiobacillus ferrooxidans*. However, coarser tailings material has generally higher sulfide contents, due to gravimetrically separation, so that higher concentration in the H_2O_2-leach could also indicate the leach of by oxidation destabilized molybdenite. This possibility is regarded as less probable as higher Mo concentrations in the El Salvador tailings are interpreted as the reason for minimal microbial oxidation activity.

At the geochemical interface between the hematite-rich sediment and the oxidation zone the different geochemical behavior of oxyanions and bivalent cations is clearly documented. The following genetic model for this hematite-sediment is proposed: Rainfall (pH 5.5) causes dilution of the acid in the oxidation zone, increases the pH, and hydroxide complexes of Fe, Al, or Mn

hydrolyze and form polymers. The latter, together with fine-grained material as clay minerals and fine tabular hematite are transported following the hydraulic surface gradient to the pond and enriched in its depression, where the particles settle. In winter, the low permeability (K =8.5x10^{-9} m/s) of the hematite-rich sediment forms a closed geochemical system, independent of the underlying low pH oxidation zone and the phreatic level. Bivalent cations are still mobile during the transport on the top of the low pH oxidation zone. But when they reach the pond with pH 7.6 they are adsorbed and ferrihydrite forms. In summer, cracking of the fine sediments permits oxygen and water flux into the underlying oxidation zone, reflected by increased concentrations of bivalent cations in the first centimeters under the hematite-sediment. The fact that the pond and the sediment have neutral pH can not only be explained by dilution with rainwater (pH 5.5). Ligand exchange of adsorbed elements with functional groups OH^- can lead to an additional increase of the pH, due to strong adsorption processes in the hematite-rich sediment. In the pond water bicarbonate is also slightly enriched to 44 mg/l possibly due to eolic input, as the surrounding oxidation zone can not be the source.

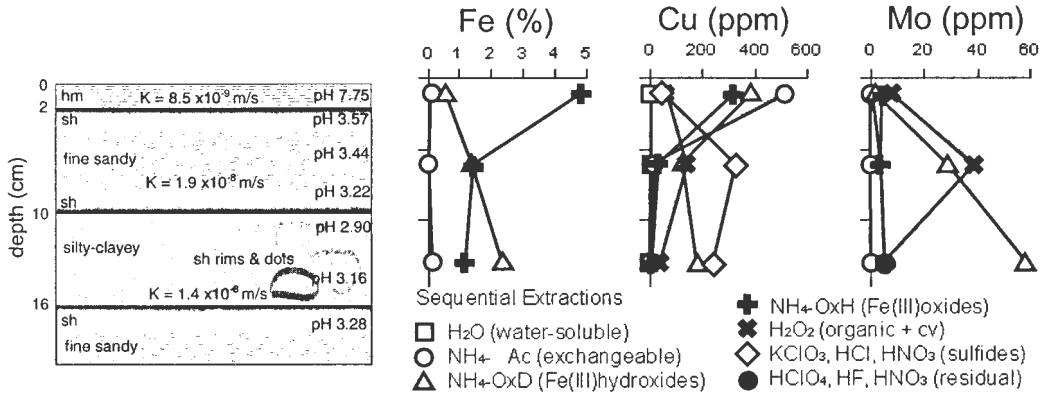

Fig. 6: *Zoom of the first 20 cm of the surface of the pond area of Piuquenes with the hematite-rich sediment and the underlying schwertmannite rich oxidation zone (sampling campaign 1997, AS3). Geochemical results from sequential extractions of Fe, Cu, and Mo from the three upper horizons are presented. The Cu distribution is representative for the behavior of bivalent cations and Mo is representative of oxyanions in the oxidation zone. K values (hydraulic conductivity) were calculated from laser grain size analyses. For detailed discussions see text. For data see Table 6.*

Table 6: *Results from sequential extraction (ICP-ES from sequence B) from the surface sampling AS3 from the Piuquenes tailings impoundment at La Andina.*

Fe (%)										
sample	depth	H_2O	NH_4-OAc	NH_4-OxD	NH_4-OxH	H_2O_2	sulfide	residual	total	bulk
AS3/002	2	BDL	0.07	0.56	4.83	0.07	0.93	0.99	7.45	8.07
AS3/010	10	BDL	0.04	1.36	1.47	0.04	0.42	1.09	4.42	5.14
AS3/016	16	BDL	0.12	2.33	1.12	0.02	0.61	1.16	5.36	6.45
Al (%)										
sample	depth	H_2O	NH_4-OAc	NH_4-OxD	NH_4-OxH	H_2O_2	sulfide	residual	total	bulk
AS3/002	2	BDL	0.07	0.18	0.58	0.3	0.68	7.28	9.09	10.1
AS3/010	10	BDL	BDL	0.04	0.15	0.03	0.26	5.35	5.83	6.43
AS3/016	16	BDL	0.02	0.05	0.18	0.06	0.45	6.22	6.98	7.86
K (%)										
sample	depth	H_2O	NH_4-OAc	NH_4-OxD	NH_4-OxH	H_2O_2	sulfide	residual	total	bulk
AS3/002	2	0.01	0.02	0.01	0.12	0.1	-	2.75	3.01	3.82
AS3/010	10	BDL	BDL	0.17	0.1	BDL	-	3.17	3.44	4.13
AS3/016	16	BDL	BDL	0.3	0.05	0.01	-	3.55	3.91	4.73
Mg (%)										
sample	depth	H_2O	NH_4-OAc	NH_4-OxD	NH_4-OxH	H_2O_2	sulfide	residual	total	bulk
AS3/002	2	BDL	0.03	0.03	0.25	0.02	0.42	0.28	1.03	1.09
AS3/010	10	BDL	BDL	BDL	0.07	BDL	0.2	0.29	0.56	0.59
AS3/016	16	BDL	BDL	0.01	0.12	BDL	0.36	0.37	0.86	0.95
Na (%)										
sample	depth	H_2O	NH_4-OAc	NH_4-OxD	NH_4-OxH	H_2O_2	sulfide	residual	total	bulk
AS3/002	2	BDL	BDL	BDL	BDL	0.01	0.01	1.19	1.21	1.53
AS3/010	10	BDL	BDL	BDL	BDL	BDL	BDL	0.81	0.81	0.94
AS3/016	16	BDL	BDL	BDL	BDL	BDL	BDL	0.76	0.76	0.91
Ca (%)										
sample	depth	H_2O	NH_4-OAc	NH_4-OxD	NH_4-OxH	H_2O_2	sulfide	residual	total	bulk
AS3/002	2	0.08	0.52	0.02	0.01	BDL	0.45	0.17	1.25	1.31
AS3/010	10	0.02	0.02	0.02	0.01	0.01	0.06	0.11	0.25	0.25
AS3/016	16	0.02	0.02	BDL	0.01	BDL	0.07	0.09	0.21	0.25
Ti (%)										
sample	depth	H_2O	NH_4-OAc	NH_4-OxD	NH_4-OxH	H_2O_2	sulfide	residual	total	bulk
AS3/002	2	BDL	BDL	BDL	0.05	0.01	0.02	0.44	0.52	0.62
AS3/010	10	BDL	BDL	BDL	0.02	BDL	0.02	0.14	0.18	0.18
AS3/016	16	BDL	BDL	BDL	0.02	BDL	0.02	0.16	0.2	0.25
Ba (ppm)										
sample	depth	H_2O	NH_4-OAc	NH_4-OxD	NH_4-OxH	H_2O_2	sulfide	residual	total	bulk
AS3/002	2	2	101	106	149	13	81	299	751	853
AS3/010	10	BDL	3	28	47	1	18	460	557	700
AS3/016	16	BDL	BDL	90	39	2	22	464	617	785

Cu (ppm)										
sample	depth	H_2O	NH_4-OAc	NH_4-OxD	NH_4-OxH	H_2O_2	sulfide	residual	total	bulk
AS3/002	2	9	513	385	322	66	52.8	8	1356	1240
AS3/010	10	9	15	124	35	140	327	14.7	665	676
AS3/016	16	10	14	183	7	34	237	7	493	486
Zn (ppm)										
sample	depth	H_2O	NH_4-OAc	NH_4-OxD	NH_4-OxH	H_2O_2	sulfide	residual	total	bulk
AS3/002	2	0.8	25.2	26.6	81.9	3.7	60.8	26.4	225.4	219
AS3/010	10	BDL	BDL	3.6	7.4	1.6	13.5	15.3	41.4	44.8
AS3/016	16	BDL	BDL	6.5	9.6	1.2	21.2	16.1	54.6	61.8
Mn (ppm)										
sample	depth	H_2O	NH_4-OAc	NH_4-OxD	NH_4-OxH	H_2O_2	sulfide	residual	total	bulk
AS3/002	2	12	333	3030	1020	16	408	69	4888	5170
AS3/010	10	BDL	BDL	9	25	3	58	33	128	139
AS3/016	16	2	BDL	17	36	BDL	91	38	184	198
Cr (ppm)										
sample	depth	H_2O	NH_4-OAc	NH_4-OxD	NH_4-OxH	H_2O_2	sulfide	residual	total	bulk
AS3/002	2	BDL	BDL	1	5	BDL	3	3	12	9
AS3/010	10	BDL	BDL	4	8	BDL	2	4	18	8
AS3/016	16	BDL	BDL	6	5	BDL	4	4	19	11
Pb (ppm)										
sample	depth	H_2O	NH_4-OAc	NH_4-OxD	NH_4-OxH	H_2O_2	sulfide	residual	total	bulk
AS3/002	2	BDL	BDL	7	25	BDL	15	BDL	47	48
AS3/010	10	BDL	BDL	9	5	BDL	4	BDL	18	27
AS3/016	16	BDL	BDL	12	6	BDL	9	BDL	27	35
Mo (ppm)										
sample	depth	H_2O	NH_4-OAc	NH_4-OxD	NH_4-OxH	H_2O_2	sulfide	residual	total	bulk
AS3/002	2	BDL	BDL	2	4	7	BDL	BDL	13	7
AS3/010	10	BDL	BDL	29	4	39	4	2	78	70
AS3/016	16	BDL	BDL	58	5	6	5	BDL	74	76
V (ppm)										
sample	depth	H_2O	NH_4-OAc	NH_4-OxD	NH_4-OxH	H_2O_2	sulfide	residual	total	bulk
AS3/002	2	BDL	BDL	6	51	6	13	82	158	174
AS3/010	10	BDL	BDL	8	19	BDL	6	48	81	87
AS3/016	16	BDL	BDL	13	16	BDL	12	61	102	116
As (ppm)										
sample	depth	H_2O	NH_4-OAc	NH_4-OxD	NH_4-OxH	H_2O_2	sulfide	residual	total	bulk
AS3/002	2	BDL	BDL	21	43	BDL	BDL	BDL	64	78
AS3/010	10	BDL	BDL	17	BDL	BDL	BDL	BDL	17	28
AS3/016	16	BDL	BDL	29	BDL	BDL	BDL	BDL	29	61

Abbreviations as in Table 4.

5.5.2 Cauquenes tailings impoundment, El Teniente

5.5.2.1 Physical properties and mineralogy

The Cauquenes impoundment was totally dry during the first summer field campaign (1996) with groundwater levels between 2.4 and 3.7 m below surface. In winter an extended pond covers the center of the impoundment (Fig. 1). A general grain-size trend from coarser grain-size at the edges (T4 ØK = 2.3×10^{-7} m/s) to finer grain-size to the center (T2 ØK = 2.8×10^{-8} m/s) of the impoundment can be observed. In the center area secondary spots of XRD determined chalcanthite occurs as secondary surface precipitates (Fig. 2C). The five drill cores (T1 – T5) show a very similar stratigraphy of the tailings (Fig. 1). The stratigraphy, pH distribution and geochemical data from the representative drill core T1 are presented in Fig. 7 and Table 7. The oxidation zone at the top reaches 1.05 to 1.65 m depth (T1 = 1.05 m; T2 = 1.65 m; T3 = 1.50 m; T4 = 1.53 m; T5 = 1.40 m), with paste-pH values of 1.72 to 4.12. The color is yellow with orange-brown horizons, streaks, and dots (Fig. 2C). The grain-size is generally smaller than in the primary zone, due to increased breakdown to clay minerals. Fine sandy and silty-clayey horizons alternate. The oxidation zone is sharply separated from the dark gray to brown-gray colored primary zone. No neutralization zone as observed at Piuquenes is developed, possibly due to the lack of carbonate neutralization potential (see acid-base accounting). Some brown horizons in the primary zone indicate the precipitation of secondary Fe(III)

oxyhydroxides. The pH increase in the primary zones generally up to maximum concentrations of 5, only in the drill core T3 neutral values are reached.

Quartz, albite, and micas (mainly biotite) dominate the gangue mineralogy, as shown by XRD. Illite, chlorite and kaolinite are the typical clay minerals. In the oxidation zone the secondary mineralogy is dominated by disseminated jarosite and a vermiculite-type mixed layer mineral (11.7 – 11.9Å) as well by schwertmannite. The latter is associated with dots or rims as well as horizon interfaces of different grain-size (Fig. 2C). The presence of schwertmannite was proven by DXRD. Gypsum is mainly associated with samples from the phreatic level and is interpreted as a tertiary mineral. The gypsum found in the oxidation zone may be secondary.

The study of polished sections show that the oxidation of the sulfides is nearly complete in the oxidation zone. Only some small residual grains of pyrite or chalcopyrite could be observed. One pyrite grain was found to be coated by ferric hydroxides and thus protected from further oxidation; in general pyrite does not show this coating. Magnetite is also present with martite replacement. Following the stratigraphy downwards to the primary zone, the original sulfide paragenesis of the ore can be observed. It is dominated by pyrite, which shows strong fracturing. In general it does not show alteration or Fe(III) hydroxide rims. Chalcopyrite is present as traces and sometimes intergrown with bornite. Both hypogene sulfides frequently show replacement to chalcocite, digenite, and covellite. As in the Piuquenes impoundment, two different generations of replacement can be differentiated. Camus (1975) reported that the most important supergene sulfide mineral present in the orebody is chalcocite, with minor proportions of covellite. Hence, the stronger digenite and chalcocite with traces of covellite replacement in the tailings is interpreted to be primary supergene enrichment, consistent with observations of fracturing and incomplete thick rims (Fig. 2G). The secondary replacement is characterized by thin, complete rims of mainly covellite and digenite also associated exclusively with chalcopyrite (Fig. 2H). The latter replacement, mainly associated with a 2-4 m thick zone below the water-level, is interpreted as secondary. Magnetite is largely found as massive grains, partly altered to martite. Traces of sphalerite, molybdenite, rutile, goethite, hematite, and galena were found.

5.5.2.2 Acid-Base Accounting

ABA results show that the C_{tot} is below the detection limit and the $S_{sulfide}$ content in the primary zone has an average of 0.59 wt % (Fig. 7). With the assumption that all $S_{sulfide}$ is associated with pyrite, this tailings yield to an average of only 1.09 wt % pyrite in the primary zone. Correcting for Cu concentrations in the sulfide fractions of sequential extractions leads to an average pyrite content of 0.99 wt %. The variation between the total sulfide pyrite content and the correction for the Cu-sulfides ranges between 4.6 and 29.3% with an average variation of 10.8 %.

The acid flotation circuit has a pH of 4.5, which explains the absence of a carbonate NP. The acid circuit is possibly also the reason for the low pyrite content, as under acid conditions a high percentage of pyrite will float and end up in the concentrate. In contrast, pyrite flotation is generally suppressed by an alkaline pH (lime addition). Low carbonate NP (0.12 & 0.16 wt.% C_{tot}) was only found in two samples of the T3 drill core. This possibly is the reason that the pH

increases up to neutral values in this drill core. It might be that in this area, material was deposited before the change from the alkaline to the acid circuit.

5.5.2.3 Sequential extractions

In the Cauquenes drill core T4 (data not shown) the element distribution is very similar to that of Piuquenes tailings. T4 is situated at the edge of the tailings impoundment (Fig. 1), where the permeability is one order of magnitude higher than in the tailings center (e.g., T2). Bivalent cations e.g. Cu, and Zn are nearly completely leached out of the oxidation zone, whereas oxyanions such as Mo and As show low mobility as reported in the Piuquenes tailings through adsorption to Fe(III) oxyhydroxide sulfates. Data from a representative drill core in the center of the impoundment (T1; Fig. 7) show that cations (Ca, K, Mg, Cu, Zn, Mn) and sulfate increase their concentrations in the water soluble-fraction to the top of the tailings. In contrast to the results of the exchangeable fraction of the Piuquenes tailings, the samples of this fraction from the Cauquenes tailings (T1, T2, T3) have elevated Cu and Zn concentration in the oxidation zone (Fig. 4). Electron microprobe analysis on biotite from the oxidation zone show that Mg and K decrease to the grain edges and Cu and Zn increase. The position of the peak of the vermiculite-type mixed-layer mineral is at lower d-values (11.7 – 11.9Å) than in the Piuquenes (Fig. 8, 12.25 – 12.67Å). DXRD control of the dissolved phases have shown that in the exchangeable fraction (NH_4-acetate) the vermiculite-type mixed-layer mineral disappears and a new peak at lower d-values at the flank of the 001 illite peak appears. Do to higher activity of Cu and Zn in the oxidation zone of the Cauquens tailings, Cu and Zn promotes the release of K of biotite as shown by Farquhar et al. (1997) and are fixed in the interlayer of the resulting vermiculite-type mixed–layer mineral, leading to the lower d-values. This mineral is broken down in the NH_4-acetate leach possibly due to detachment of the interlayer cations and the peak shift to the lower d-values, indicating that the mineral is not completely dissolved.

Fe and Al are below the detection limit in the water-soluble fraction but show increasing concentrations in the oxidation zone in the exchangeable, Fe(III) oxyhydroxide and Fe(III) oxide leaches. In the oxidation zone Mo is associated with the Fe(III) oxyhydroxide and also to Fe(III) oxide fraction possibly adsorbed to jarosite as the sh/jt ratio is below 0.5 in the Cauquenes tailings, while in Piuquenes this ratio reaches concentrations > 1. The sulfide fraction is depleted in the oxidation zone but increase to a double enrichment near the water table compared to the primary zone. This may indicate that Mo is enriched by similar processes as Cu.

The total As content is distributed in the exchangeable and reducible fraction, no As is detectable in the sulfide fractions, possibly also a result of low pH conditions in the Cauquenes tailings. V does not display significant mobilization.

Water content and geochemical data from drill cores from the center of the impoundment (T1; Fig. 7) indicate that in the upper 100 cm a significant upwards mobilization of SO_4, Ca, K, Mg, Cu, Zn, and Mn takes place during the dry season. Finer grain-size increases the water retention capacity and the capillary force, resulting in an increase of the water content at the surface and an enrichment of bivalent cations in the form of water-soluble phases, mainly sulfates (e.g., gypsum, chalcanthite), due to high evaporation rates in summer (Fig. 7).

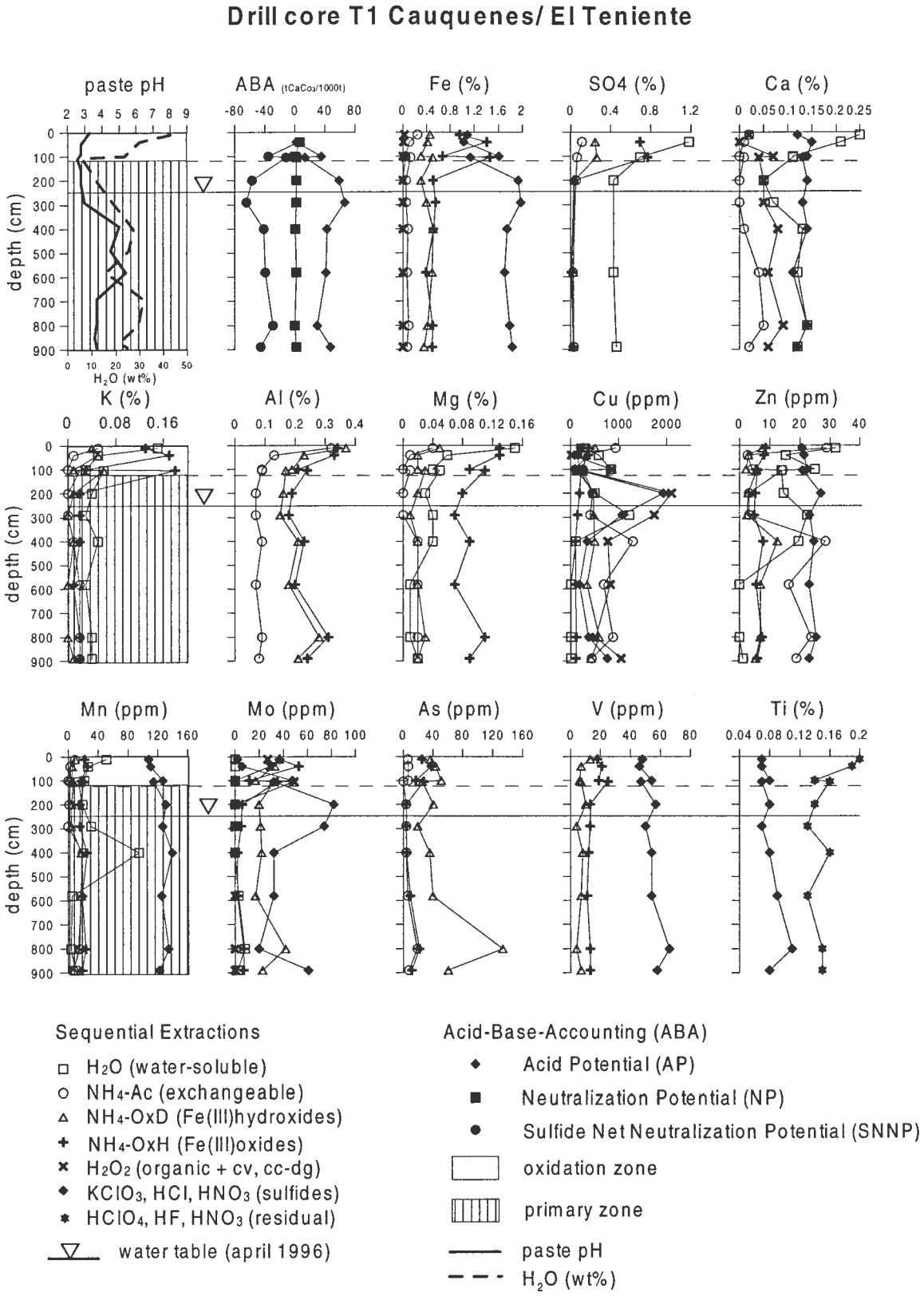

Fig. 7: Results of sequential extractions from the representative drill core T1 form the Cauquenes tailings impoundment, El Teniente, Chile. For data see Table 7.

Fe (%)										
sample	depth	H2O	NH4-OAc	NH4-OxD	NH4-OxH	H2O2	sulfide	residual	total	bulk
T1/010	10	BDL	0.25	0.46	0.96	0.03	1.09	0.91	3.7	4.3
T1/040	40	0.01	0.11	0.42	1.41	0.01	1.03	1.01	4	5.4
T1/100	100	BDL	0.04	0.31	0.67	BDL	1.61	0.93	3.56	5.03
T1/105	105	BDL	0.13	0.5	1.46	0.04	1.14	0.84	4.11	5.72
T1/200	200	BDL	0.05	0.31	0.51	BDL	1.93	0.93	3.73	5.5
T1/290	290	BDL	0.05	0.4	0.55	BDL	1.98	0.9	3.88	5.57
T1/400	400	BDL	0.09	0.51	0.52	BDL	1.75	1.01	3.88	5.42
T1/580	580	BDL	0.07	0.49	0.39	BDL	1.71	0.84	3.5	4.87
T1/800	800	BDL	0.1	0.42	0.5	BDL	1.79	0.85	3.66	5.18
T1/890	890	BDL	0.07	0.36	0.49	BDL	1.83	0.91	3.66	5.06
Al (%)										
sample	depth	H2O	NH4-OAc	NH4-OxD	NH4-OxH	H2O2	sulfide	residual	total	bulk
T1/010	10	BDL	0.32	0.37	0.34	0.03	1.2	6.44	8.7	8.31
T1/040	40	0.01	0.13	0.23	0.33	0.07	1.13	6.43	8.33	10.3
T1/100	100	0.01	0.09	0.19	0.21	BDL	1.25	5.62	7.37	9.85
T1/105	105	BDL	0.09	0.17	0.24	0.02	1.16	5.2	6.88	9.73
T1/200	200	BDL	0.07	0.16	0.19	BDL	1.28	5.49	7.19	10.2
T1/290	290	BDL	0.07	0.15	0.18	BDL	1.18	5.56	7.14	9.76
T1/400	400	BDL	0.09	0.21	0.23	BDL	1.27	5.6	7.4	10.1
T1/580	580	BDL	0.07	0.18	0.2	BDL	1.19	5.43	7.07	9.61
T1/800	800	BDL	0.09	0.28	0.31	BDL	1.54	5.15	7.37	10.2
T1/890	890	BDL	0.08	0.21	0.24	BDL	1.31	5.52	7.36	9.85
K (%)										
sample	depth	H2O	NH4-OAc	NH4-OxD	NH4-OxH	H2O2	sulfide	residual	total	bulk
T1/010	10	0.15	0.05	0.04	0.13	BDL	-	2.31	2.68	2.26
T1/040	40	0.05	0.01	0.05	0.17	0.02	-	2.23	2.53	3.73
T1/100	100	0.03	BDL	0.01	0.03	BDL	-	1.83	1.9	3.42
T1/105	105	0.06	0.02	0.06	0.18	BDL	-	1.81	2.13	3.6
T1/200	200	0.04	BDL	0.01	0.02	BDL	-	1.83	1.9	3.62
T1/290	290	0.03	BDL	BDL	0.02	BDL	-	1.84	1.89	3.48
T1/400	400	0.05	0.01	0.01	0.02	BDL	-	1.96	2.05	3.57
T1/580	580	0.03	0.02	BDL	0.01	BDL	-	1.86	1.92	3.47
T1/800	800	0.04	0.02	BDL	0.02	BDL	-	1.83	1.91	3.82
T1/890	890	0.04	0.02	0.01	0.02	BDL	-	1.86	1.95	3.51
Mg (%)										
sample	depth	H2O	NH4-OAc	NH4-OxD	NH4-OxH	H2O2	sulfide	residual	total	bulk
T1/010	10	0.15	0.04	0.05	0.13	0.02	0.94	0.61	1.94	2.4
T1/040	40	0.06	0.01	0.02	0.13	BDL	0.9	0.7	1.82	2.25
T1/100	100	0.04	BDL	0.02	0.09	BDL	0.96	0.69	1.8	2.24
T1/105	105	0.05	0.01	0.03	0.11	0.02	0.9	0.59	1.71	2.17
T1/200	200	0.03	BDL	0.02	0.08	BDL	0.99	0.65	1.77	2.3
T1/290	290	0.04	BDL	0.01	0.07	BDL	0.91	0.63	1.66	2.1
T1/400	400	0.04	0.02	0.02	0.09	0.01	0.98	0.71	1.87	2.38
T1/580	580	0.01	0.02	0.02	0.07	BDL	0.94	0.58	1.64	2
T1/800	800	0.01	0.02	0.03	0.11	0.01	1.22	0.64	2.04	2.55
T1/890	890	0.02	0.02	0.02	0.09	BDL	1.08	0.69	1.92	2.34
Na (%)										
sample	depth	H2O	NH4-OAc	NH4-OxD	NH4-OxH	H2O2	sulfide	residual	total	bulk
T1/010	10	0.01	BDL	BDL	BDL	0.02	BDL	0.03	0.86	0.92	0.96
T1/040	40	BDL	BDL	BDL	BDL	0.01	BDL	0.03	0.87	0.91	1.11
T1/100	100	BDL	BDL	BDL	BDL	0.01	BDL	0.03	0.83	0.87	1.2
T1/105	105	BDL	BDL	BDL	BDL	BDL	BDL	0.03	0.78	0.81	1.13
T1/200	200	BDL	BDL	BDL	BDL	BDL	BDL	0.03	0.85	0.88	1.28
T1/290	290	BDL	BDL	BDL	BDL	BDL	BDL	0.03	0.8	0.83	1.22
T1/400	400	BDL	BDL	BDL	BDL	BDL	BDL	0.03	0.8	0.83	1.15
T1/580	580	BDL	BDL	BDL	BDL	BDL	BDL	0.02	0.93	0.95	1.3
T1/800	800	BDL	BDL	BDL	BDL	BDL	BDL	0.03	0.72	0.75	1.13
T1/890	890	BDL	BDL	BDL	BDL	BDL	BDL	0.03	0.86	0.89	1.19
Ca (%)										
sample	depth	H2O	NH4-OAc	NH4-OxD	NH4-OxH	H2O2	sulfide	residual	total	bulk
T1/010	10	0.25	0.02	0.01	0.02	0.02	0.12	0.43	0.87	1.04
T1/040	40	0.21	0.01	0.01	0.02	BDL	0.15	0.47	0.87	1.09
T1/100	100	0.11	BDL	0.01	0.02	0.07	0.14	0.48	0.83	1.11
T1/105	105	0.11	0.01	BDL	0.01	0.04	0.13	0.46	0.76	1.08
T1/200	200	0.05	BDL	0.02	0.01	0.05	0.14	0.52	0.79	1.12
T1/290	290	0.07	BDL	BDL	0.01	0.05	0.13	0.47	0.73	1.05
T1/400	400	0.13	0.01	BDL	BDL	0.08	0.14	0.45	0.81	1.1
T1/580	580	0.12	0.04	BDL	BDL	0.06	0.11	0.46	0.79	1.08
T1/800	800	0.14	0.05	BDL	0.01	0.09	0.14	0.4	0.83	1.13
T1/890	890	0.12	0.02	BDL	0.01	0.06	0.12	0.44	0.77	1.01
Ti (%)										
sample	depth	H2O	NH4-OAc	NH4-OxD	NH4-OxH	H2O2	sulfide	residual	total	bulk
T1/010	10	BDL	BDL	BDL	BDL	BDL	0.07	0.2	0.27	0.36
T1/040	40	BDL	BDL	BDL	BDL	BDL	0.07	0.19	0.26	0.34
T1/100	100	BDL	BDL	BDL	BDL	BDL	0.08	0.14	0.22	0.31
T1/105	105	BDL	BDL	BDL	BDL	BDL	0.07	0.16	0.23	0.33
T1/200	200	BDL	BDL	BDL	BDL	BDL	0.08	0.14	0.22	0.32
T1/290	290	BDL	BDL	BDL	BDL	BDL	0.07	0.13	0.2	0.3
T1/400	400	BDL	BDL	BDL	BDL	BDL	0.08	0.16	0.24	0.32
T1/580	580	BDL	BDL	BDL	BDL	BDL	0.09	0.13	0.22	0.31
T1/800	800	BDL	BDL	BDL	BDL	BDL	0.11	0.15	0.26	0.34
T1/890	890	BDL	BDL	BDL	BDL	BDL	0.08	0.15	0.23	0.3
Ba (ppm)										
sample	depth	H2O	NH4-OAc	NH4-OxD	NH4-OxH	H2O2	sulfide	residual	total	bulk
T1/010	10	BDL	1	7	37	1	39	263	348	503
T1/040	40	BDL	BDL	2	44	2	35	256	339	465
T1/100	100	BDL	2	13	19	1	40	226	301	454
T1/105	105	BDL	BDL	9	36	2	39	205	291	437
T1/200	200	BDL	3	18	11	1	39	223	295	477
T1/290	290	BDL	2	16	13	1	35	225	292	470
T1/400	400	1	8	10	13	1	41	251	325	502
T1/580	580	BDL	11	8	11	1	42	241	314	472
T1/800	800	BDL	12	8	10	1	51	226	308	517
T1/890	890	BDL	8	8	8	1	36	208	269	406

Cu (ppm)										
sample	depth	H2O	NH4-OAc	NH4-OxD	NH4-OxH	H2O2	sulfide	residual	total	bulk
T1/010	10	298	939	510	377	212	214	14.2	2564	2330
T1/040	40	593	309	332	370	14.5	155	16.3	1790	1930
T1/100	100	847	265	260	96.1	870	175	13.8	2527	2570
T1/105	105	128	198	251	218	266	172	16	1249	1340
T1/200	200	505	463	483	189	2100	1930	62.1	5732	5970
T1/290	290	1230	414	481	145	1740	1080	40.1	5130	5240
T1/400	400	114	1300	508	99.7	778	345	16.4	3161	3260
T1/580	580	6.2	692	348	105	835	183	18.4	2188	2250
T1/800	800	3.7	882	605	123	532	378	19	2543	2650
T1/890	890	6.2	443	430	108	1060	764	27.2	2838	2830
Zn (ppm)										
sample	depth	H2O	NH4-OAc	NH4-OxD	NH4-OxH	H2O2	sulfide	residual	total	bulk
T1/010	10	31.9	28.8	7.7	8.7	1	20.7	16.2	115	104
T1/040	40	15.2	2.7	3.1	8.2	BDL	21.3	16.2	66.7	82.4
T1/100	100	25	4.2	2.2	5.7	2.1	22.3	15.8	77.3	94.6
T1/105	105	13.9	14.3	5.8	6	1.6	20.9	14.7	77.2	95.7
T1/200	200	14.6	3.2	2.9	5.3	4.5	26.9	16.3	73.7	82.5
T1/290	290	22.3	3.2	2.5	5	3.5	23.2	15.8	75.5	82.8
T1/400	400	19.5	28.5	12.6	7.8	3	24.5	18.6	114.5	139
T1/580	580	BDL	16.3	6.9	5.7	1.8	23.1	18.4	72.2	87.5
T1/800	800	BDL	23.8	6.9	7.5	1.8	25.4	17.6	83	86.7
T1/890	890	1.2	18.9	5.5	5.9	2	23.1	16	72.6	74.2
Mn (ppm)										
sample	depth	H2O	NH4-OAc	NH4-OxD	NH4-OxH	H2O2	sulfide	residual	total	bulk
T1/010	10	51	9	10	22	3	108	65	268	344
T1/040	40	27	3	6	26	BDL	111	77	250	313
T1/100	100	22	BDL	5	18	4	127	76	252	316
T1/105	105	14	3	7	21	6	115	63	229	302
T1/200	200	19	2	5	16	3	131	74	250	326
T1/290	290	31	BDL	4	16	3	127	71	252	326
T1/400	400	95	19	18	25	6	140	80	383	473
T1/580	580	6	17	18	19	3	126	66	255	318
T1/800	800	4	16	14	24	5	135	63	261	333
T1/890	890	10	7	8	19	3	123	70	240	294
Cr (ppm)										
sample	depth	H2O	NH4-OAc	NH4-OxD	NH4-OxH	H2O2	sulfide	residual	total	bulk
T1/010	10	BDL	3	1	11	BDL	20	8	43	28
T1/040	40	BDL	2	4	13	BDL	21	7	47	34
T1/100	100	BDL	1	4	10	BDL	22	7	44	26
T1/105	105	BDL	1	3	15	BDL	30	6	55	38
T1/200	200	BDL	BDL	6	7	BDL	25	8	46	29
T1/290	290	BDL	BDL	2	7	BDL	21	5	35	30
T1/400	400	BDL	1	5	7	BDL	20	7	40	30
T1/580	580	BDL	1	4	6	BDL	21	5	37	25
T1/800	800	BDL	2	3	7	BDL	28	5	45	29
T1/890	890	BDL	1	5	8	BDL	27	7	48	25
Pb (ppm)										
sample	depth	H2O	NH4-OAc	NH4-OxD	NH4-OxH	H2O2	sulfide	residual	total	bulk
T1/010	10	BDL	BDL	BDL	7	BDL	9	BDL	16	29
T1/040	40	BDL	BDL	BDL	11	BDL	4	BDL	15	27
T1/100	100	BDL	BDL	4	11	BDL	5	BDL	20	22
T1/105	105	BDL	BDL	3	5	BDL	3	BDL	11	20
T1/200	200	BDL	BDL	19	BDL	BDL	6	BDL	25	12
T1/290	290	BDL	BDL	BDL	BDL	BDL	4	BDL	4	19
T1/400	400	BDL	BDL	BDL	2	BDL	5	BDL	7	20
T1/580	580	BDL	BDL	BDL	7	BDL	6	BDL	13	14
T1/800	800	BDL	2	BDL	5	BDL	5	BDL	12	24
T1/890	890	BDL	BDL	3	3	BDL	4	BDL	10	13
Mo (ppm)										
sample	depth	H2O	NH4-OAc	NH4-OxD	NH4-OxH	H2O2	sulfide	residual	total	bulk
T1/010	10	BDL	2	37	37	27	2	BDL	105	92
T1/040	40	BDL	2	33	53	29	6	BDL	123	139
T1/100	100	BDL	BDL	17	12	BDL	48	BDL	77	87
T1/105	105	BDL	2	32	35	49	32	1	151	155
T1/200	200	BDL	1	20	6	BDL	82	10	119	143
T1/290	290	BDL	1	21	5	BDL	74	9	110	122
T1/400	400	BDL	1	22	2	BDL	32	4	61	67
T1/580	580	3	BDL	17	2	BDL	32	4	58	85
T1/800	800	8	2	42	7	BDL	20	BDL	79	84
T1/890	890	2	1	23	7	BDL	61	5	99	111
V (ppm)										
sample	depth	H2O	NH4-OAc	NH4-OxD	NH4-OxH	H2O2	sulfide	residual	total	bulk
T1/010	10	BDL	4	13	18	BDL	48	105	188	184
T1/040	40	BDL	BDL	7	21	BDL	46	107	181	222
T1/100	100	BDL	BDL	6	19	BDL	54	88	167	209
T1/105	105	BDL	BDL	7	25	BDL	47	89	168	221
T1/200	200	BDL	BDL	10	13	BDL	57	90	170	221
T1/290	290	BDL	BDL	4	13	BDL	50	83	150	204
T1/400	400	BDL	BDL	8	12	BDL	54	92	166	216
T1/580	580	BDL	BDL	7	11	BDL	54	76	148	190
T1/800	800	BDL	BDL	4	13	BDL	66	80	163	211
T1/890	890	BDL	BDL	7	13	BDL	58	88	166	211
As (ppm)										
sample	depth	H2O	NH4-OAc	NH4-OxD	NH4-OxH	H2O2	sulfide	residual	total	bulk
T1/010	10	BDL	6	37	25	BDL	BDL	BDL	68	72
T1/040	40	BDL	7	44	38	BDL	BDL	BDL	89	134
T1/100	100	BDL	7	52	17	BDL	BDL	BDL	76	96
T1/105	105	BDL	BDL	26	28	BDL	BDL	BDL	54	112
T1/200	200	BDL	4	41	4	BDL	8	BDL	57	83
T1/290	290	BDL	4	20	4	BDL	7	BDL	35	43
T1/400	400	BDL	4	36	5	BDL	BDL	BDL	45	59
T1/580	580	BDL	6	40	10	BDL	BDL	BDL	56	25
T1/800	800	BDL	19	134	22	BDL	BDL	BDL	175	202
T1/890	890	BDL	8	61	12	BDL	BDL	BDL	81	103

This upwards migration superimposes the general trend of downwards mobilization during the raining season and is conserved in the leached oxidation zone in T4 and the secondary replacement of chalcocite by covellite below the ground water table.

Stoichiometric calculation of the jarosite content leads to an overestimation of the sulfate content. An increased Al^{3+} content on the B site of the general formula of the alunite-jarosite group $AB_3(SO_4)_2(OH)_6$ or the presence of alunite could be the source for the too high calculated SO_4 contents. This is supported by increasing concentrations of Al in the Fe(III) oxyhydroxide and Fe(III) oxide leach in the oxidation zone. Detailed XRD studies of the jarosites from the Piuquenes tailings and the jarosites from the T4 core (Cauquenes), which do not show increased concentrations of Al in this leach, show peak position near synthetic jarosite (Fig. 9). In contrast, jarosites from T1 show a peak shift to lower d-values, suggesting the substitution of Fe^{3+} (ion radius 0.65Å) by the smaller Al^{3+} (0.53Å). This is supported by an increase of Al content in the Fe(III) oxide leach in samples from the oxidation zone. Correction with the Al content increases the accuracy of the stoichiometric calculation and suggests that up to 20 % of the B site of the jarosite is substituted by Al^{3+}. These findings show that the evaporation controlled upwards mobilization of elements has direct influence on the composition of the secondary minerals.

As mentioned, Cu shows in these tailings a similar enrichment below the water table by replacement of chalcopyrite by covellite as in the Piuquenes tailings. Due to the lack of carbonate NP the neutralization sequence is not as well developed as in the Piuquenes tailings and the secondary Cu enrichment is not as well defined in the stratigraphy. Ti concentrations are below the detection limit in the Fe(III) oxides leach indicating, that no ilmenite is present in the Cauquenes tailings.

5.5.2.4 Microbiology

Four representative samples from the oxidation zone and primary zone of the Cauquenes tailings were submitted to bacterial count and iron oxidation activity tests. In all samples high bacteria numbers by direct counting were observed ($3.0x10^8$ – $5.0x10^8$ bact/ml). *Thiobacillus ferrooxidans* could only be cultivated ($1.4x10^5$ bact/ml) in the sample from the oxidation front (T4/150). Oxidizing activity tests show that the sample from the oxidation front started first to oxidize Fe^{2+} to Fe^{3+} after an initial or lag phase of 144 h. This oxidation activity has to be related with the increased population of *Thiobacillus ferrooxidans* at the oxidation front. This is consistent with the findings of Davis (1997) where the highest population of *Thiobacillus ferrooxidans* was found at the oxidation front and the population of *Acidiphilium spp.* increased to the top of the oxidation zone. The sample from the upper part of the oxidation zone started the oxidation activity after 336 h growth time, indicating the lower population of active iron-oxidizing bacteria, possibly due to Mo poisoning. Once oxidation started, the oxidation velocity (growth rate) was similar. The sample from the primary zone did not start significant oxidation in the time range (432h) of the experiment (Fig. 5).

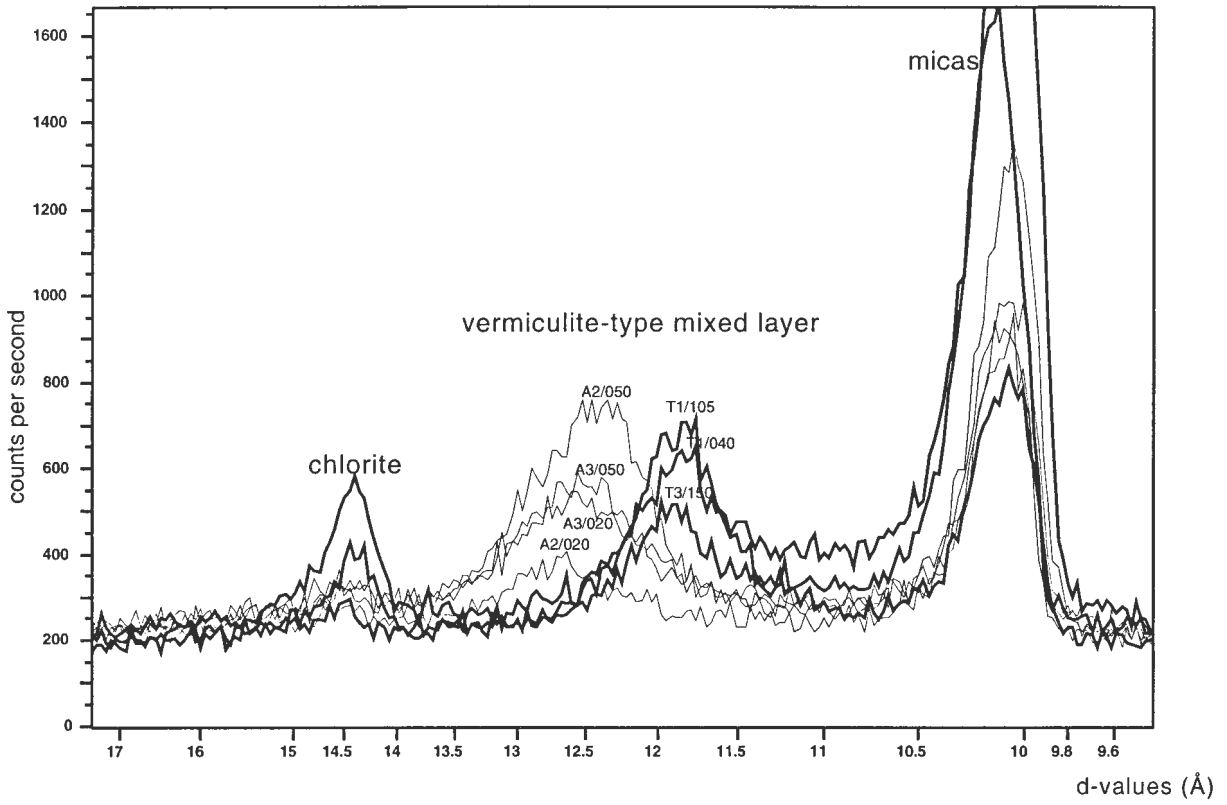

Fig. 8: Peak position (XRD results) of the vermiculite-type mixed-layer mineral in samples from the oxidation zones of Piuquenes tailings impoundment (A2/020, A2/050, A3/020, A3/050) and the Cauquenes tailings impoundment(T1/040, T1/105, T3/150). For discussion see text

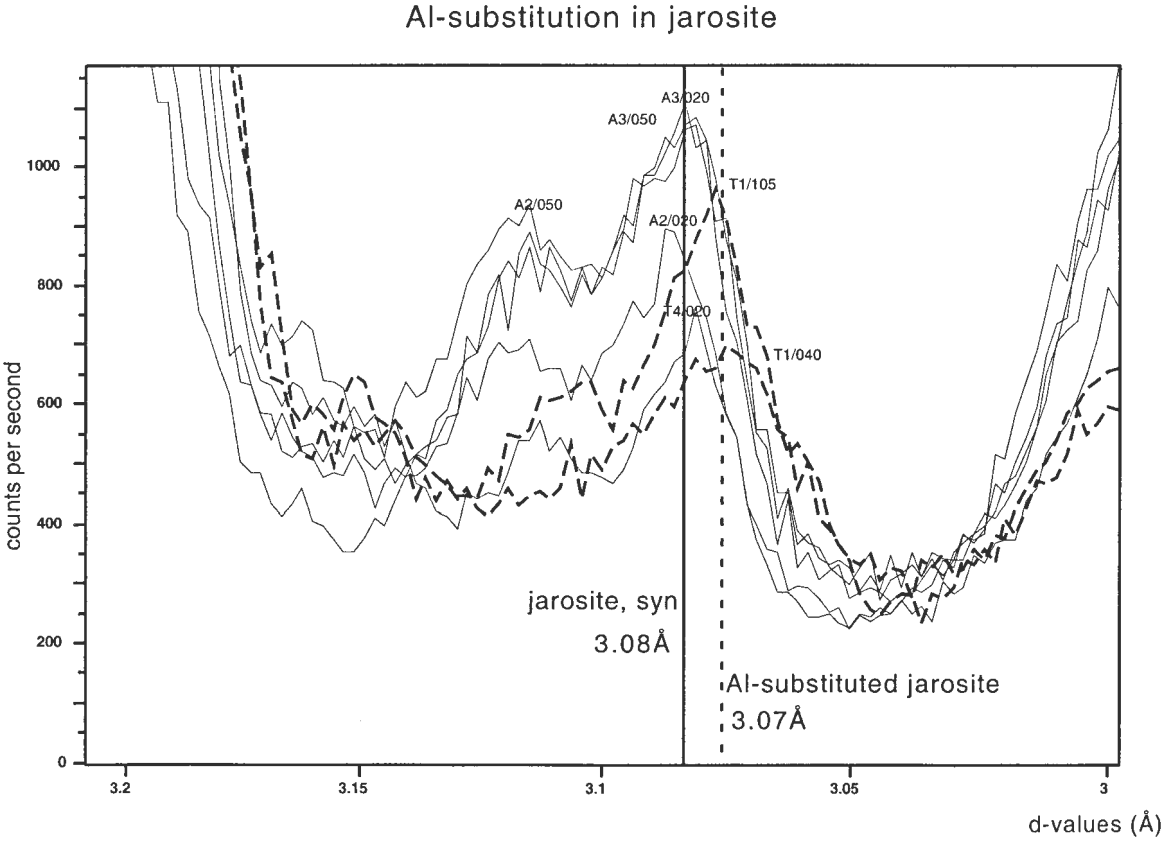

Fig. 9: Peak position (XRD results) of jarosites in samples from the oxidation zone of Piuquenes and Cauquenes tailings impoundments, indicating Al-substitution in sample T1/040 and T1/105. For discussion see text.

5.5.3 *El Salvador No.1 tailings impoundment, Chile*

5.5.3.1 Mineralogy

The four drill cores in the El Salvador No.1 tailings show that the stratigraphy is characterized by a 0.3 to 1.5m (E1 = 0.3m; E2 = 0.35m; E3 = 1.5m; E4 = 0.35m) thick *evaporite zone* at the top (Fig. 2D) with extensive blue, yellow, white and brown efflorescent salts formation (paste pH 2.00 - 3.53). Below, an *oxidation zone* with orange-brown horizons and paste pH values from 1.88 - 2.80 is observed. The *"primary zone"*, which was defined visually by its dark gray color but that, as discussed below, is significantly affected by oxidation, was intersected by two drill cores at depths of 1.7 m (E1) and 4.7 m (E2). It displays some dots and streaks of orange-brown Fe(III) hydroxides, possibly schwertmannite. In Fig. 10 and Table 8, geochemical data for the representative drill core E2 are presented. The moisture content in the evaporation zone was 0-8 wt.% and increased downwards to a constant 20 wt.%. This relative high moisture content is surprising in view of the extremely low precipitation rates (20 mm/a), the high evaporation and the age of the tailings (36 years). It should be noted, however, that similarly old tailings in hyper-arid climate (P. Cerda; chapter 6) also show moisture contents within this range.

XRD studies show that quartz, alkali-feldspar (mainly albite ± anorthoclase), biotite ± sericite, jarosite and natrojarosite dominate the primary gangue mineralogy. Kaolinite and illite are the typical clay minerals. The study of polished sections shows that pyrite is abundant (see below for amounts) in all zones and generally is still relatively fresh and even in the oxidation zone it does not show Fe(III) oxyhydroxides rims. Minor traces of covellite ± chalcocite are only observed in the primary zone in one sample (E1/030).

In the ***evaporite zone*** at the top of the tailings a wide range of water-soluble secondary efflorescent salts were identified by XRD. The dissolved minerals are identified as bonattite ($CuSO_4 \cdot 3H_2O$), chalcanthite ($CuSO_4 \cdot 5H_2O$), pickeringite ($MgAl_2(SO_4)_4 \cdot 22H_2O$), and magnesioaubertite ($(Mg,Cu)Al(SO_4)_2Cl \cdot 14H_2O$). Hand picked specimens could be identified as chalcanthite ($CuSO_4 \cdot 5H_2O$), halotrichite ($FeAl2(SO_4)_4 \cdot 22H_2O$), and hexahydrite ($MgSO_4 \cdot 6H_2O$).

In the underlying ***oxidation zone***, orange-brown ferric oxyhydroxides with the same appearance as in the Piuquenes and Cauquenes tailings, possibly schwertmannite, are enriched in some layers, but detection by DXRD failed, due to low concentrations (1.59 and 1.88 % Fe in the NH4-OxD leach). A vermiculite-type mixed layer mineral was detected in the oxidation zone in some samples by DXRD. Jarosite only was detected in the clay fraction (< 2 μm) of samples from the oxidation zone and is interpreted as secondary.

In the ***"primary zone"*** no jarosite is detected in the clay fraction, but, as mentioned before, in the bulk XRD analyses natrojarosite together with jarosite were distinguished. This suggests that jarosite and natrojarosite in this zone are primary. Additional, distinction criteria between these supergene jarosites from the primary zone and the secondary jarosite determined in the clay fraction from the oxidation zone will be discussed together with the geochemical results.

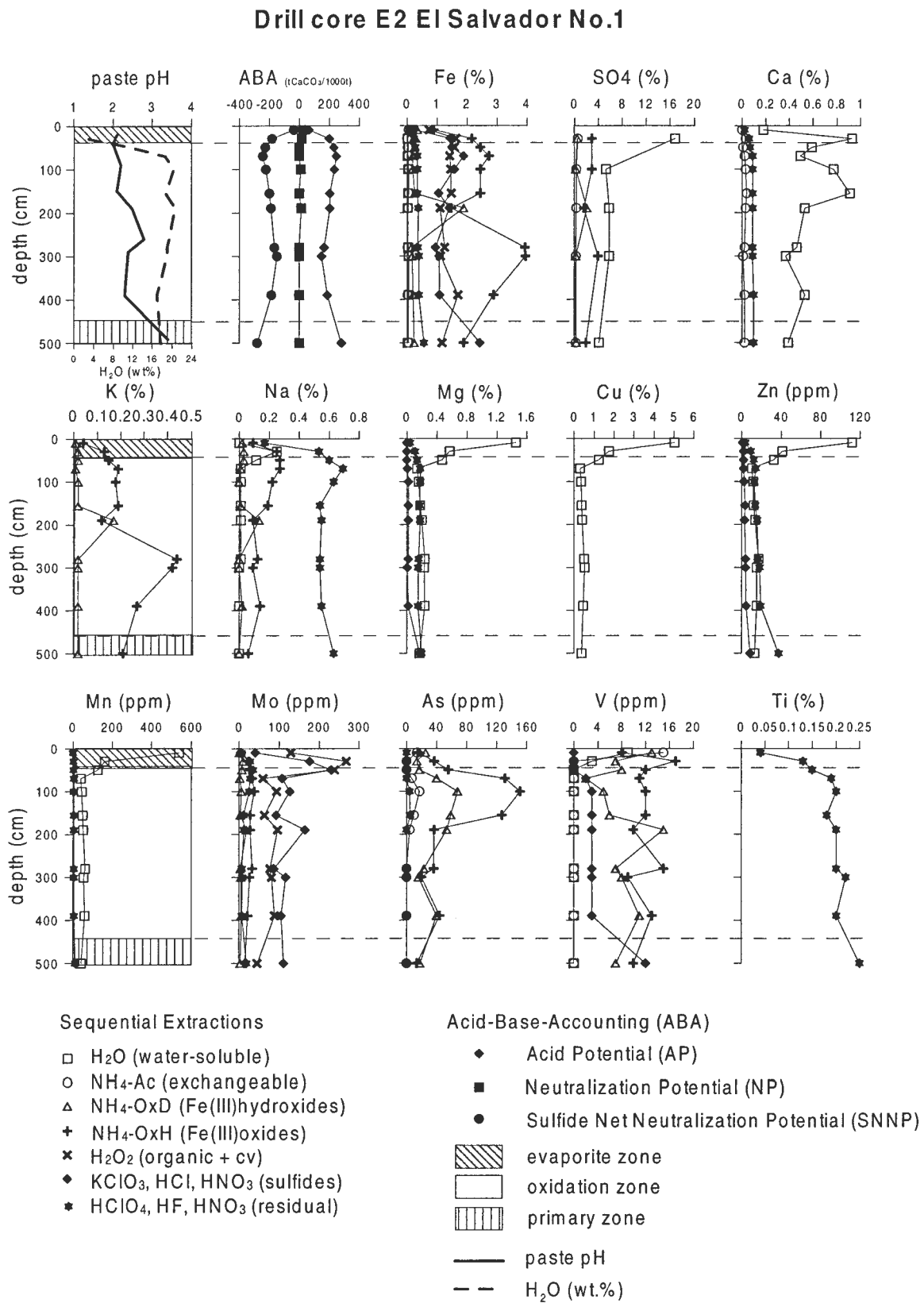

Fig. 10: *Results of sequential extractions from the representative drill core E2 form the tailings impoundment No.1, El Salvador, Chile. Note: Results of Na are shown instead of Al. Al has the same distribution as Mg, Cu, Zn, and Mn. For data see Table 8.*

Fe (%)										
sample	depth	H_2O	NH_4-OAc	NH_4-OxD	NH_4-OxH	H_2O_2	sulfide	residual	total	bulk
E2/010	10	0.17	0.06	0.34	0.88	0.73	0.23	0.07	2.48	2.89
E2/030	30	0.03	0.01	0.29	2.16	1.63	1.44	0.22	5.78	6.72
E2/050	50	0.05	0.02	0.26	2.44	1.58	1.49	0.28	6.12	6.93
E2/070	70	0.03	0.04	0.2	2.73	1.43	1.89	0.34	6.66	7.8
E2/100	100	0.04	0.06	0.2	2.45	1.46	1.58	0.35	6.14	7.23
E2/155	155	0.04	0.05	0.26	2.45	1.48	1.06	0.34	5.68	6.81
E2/190	190	0.03	0.04	1.88	1.47	1.1	1.41	0.37	6.3	7.49
E2/280	280	0.04	0.03	0.16	3.94	1.26	0.96	0.36	6.75	8.03
E2/300	300	0.05	0.05	0.18	3.96	1.13	1.07	0.39	6.83	8.36
E2/390	390	0.06	0.03	0.21	2.89	1.69	1.09	0.4	6.37	8.33
E2/500	500	0.03	0.06	0.25	1.89	1.18	2.43	0.57	6.41	8.24
Al (%)										
sample	depth	H_2O	NH_4-OAc	NH_4-OxD	NH_4-OxH	H_2O_2	sulfide	residual	total	bulk
E2/010	10	3.09	0.06	0.04	0.12	BDL	0.03	1.44	4.78	5.27
E2/030	30	1.1	0.09	0.18	0.41	0.02	0.12	4.39	6.31	7.17
E2/050	50	0.88	0.06	0.12	0.38	0.01	0.09	5.22	6.76	7.55
E2/070	70	0.25	0.06	0.1	0.33	0.01	0.11	6.36	7.22	8.9
E2/100	100	0.28	0.1	0.14	0.29	0.02	0.14	6.58	7.55	8.77
E2/155	155	0.32	0.07	0.1	0.21	0.01	0.12	6.66	7.49	8.67
E2/190	190	0.33	0.09	0.13	0.24	0.02	0.15	6.69	7.65	8.63
E2/280	280	0.39	0.13	0.19	0.34	0.03	0.18	6.21	7.47	8.68
E2/300	300	0.41	0.1	0.13	0.2	0.03	0.15	6.17	7.19	8.01
E2/390	390	0.5	0.07	0.1	0.2	0.02	0.13	6.18	7.2	8.33
E2/500	500	0.2	0.09	0.16	0.33	0.02	0.31	6.79	7.9	9.46
K (%)										
sample	depth	H_2O	NH_4-OAc	NH_4-OxD	NH_4-OxH	H_2O_2	sulfide	residual	total	bulk
E2/010	10	BDL	BDL	0.01	0.04	BDL	-	0.4	0.45	0.55
E2/030	30	BDL	BDL	0.02	0.13	BDL	-	1.32	1.47	1.83
E2/050	50	BDL	BDL	0.02	0.15	BDL	-	1.58	1.75	2.11
E2/070	70	BDL	BDL	0.01	0.19	BDL	-	2.02	2.22	2.84
E2/100	100	BDL	BDL	0.02	0.18	BDL	-	1.95	2.15	2.68
E2/155	155	BDL	BDL	0.02	0.19	BDL	-	1.83	2.04	2.48
E2/190	190	BDL	BDL	0.17	0.12	BDL	-	1.73	2.02	2.35
E2/280	280	BDL	BDL	0.02	0.44	BDL	-	1.48	1.94	2.35
E2/300	300	BDL	BDL	0.02	0.42	BDL	-	1.42	1.86	2.2
E2/390	390	BDL	BDL	0.02	0.27	BDL	-	1.56	1.85	2.28
E2/500	500	BDL	BDL	0.02	0.21	BDL	-	1.67	1.9	2.47
Mg (%)										
sample	depth	H_2O	NH_4-OAc	NH_4-OxD	NH_4-OxH	H_2O_2	sulfide	residual	total	bulk
E2/010	10	1.45	0.02	BDL	BDL	BDL	BDL	0.04	1.51	1.63
E2/030	30	0.57	0.02	BDL	BDL	BDL	BDL	0.11	0.7	0.79
E2/050	50	0.47	0.01	BDL	BDL	BDL	BDL	0.14	0.62	0.63
E2/070	70	0.14	BDL	BDL	BDL	BDL	0.01	0.18	0.33	0.45
E2/100	100	0.16	BDL	BDL	BDL	BDL	0.02	0.18	0.36	0.47
E2/155	155	0.18	BDL	BDL	BDL	BDL	0.02	0.17	0.37	0.46
E2/190	190	0.2	0.01	BDL	BDL	BDL	0.02	0.18	0.41	0.47
E2/280	280	0.24	BDL	BDL	0.01	BDL	0.02	0.16	0.43	0.5
E2/300	300	0.23	BDL	BDL	BDL	BDL	0.01	0.15	0.39	0.43
E2/390	390	0.24	BDL	BDL	BDL	BDL	0.02	0.15	0.41	0.5
E2/500	500	0.17	BDL	BDL	0.07	BDL	0.17	0.2	0.61	0.71
Na (%)										
sample	depth	H_2O	NH_4-OAc	NH_4-OxD	NH_4-OxH	H_2O_2	sulfide	residual	total	bulk
E2/010	10	BDL	BDL	0.02	0.09	BDL	BDL	0.17	0.28	0.32
E2/030	30	0.25	0.01	0.03	0.25	BDL	0.01	0.53	1.08	1.37
E2/050	50	0.11	BDL	0.03	0.27	BDL	BDL	0.6	1.01	1.22
E2/070	70	0.01	BDL	0.01	0.27	BDL	BDL	0.69	0.98	1.4
E2/100	100	0.01	BDL	BDL	0.22	BDL	BDL	0.63	0.86	1.24
E2/155	155	0.01	BDL	0.01	0.19	BDL	BDL	0.54	0.75	0.98
E2/190	190	0.01	BDL	0.13	0.09	BDL	BDL	0.55	0.78	0.89
E2/280	280	0.01	BDL	BDL	0.12	BDL	BDL	0.54	0.67	0.82
E2/300	300	BDL	BDL	BDL	0.09	BDL	BDL	0.54	0.63	0.8
E2/390	390	BDL	BDL	0.02	0.14	BDL	BDL	0.55	0.71	0.94
E2/500	500	BDL	BDL	BDL	0.06	BDL	BDL	0.63	0.69	0.93
Ca (%)										
sample	depth	H_2O	NH_4-OAc	NH_4-OxD	NH_4-OxH	H_2O_2	sulfide	residual	total	bulk
E2/010	10	0.18	BDL	BDL	BDL	BDL	BDL	0.02	0.2	0.24
E2/030	30	0.93	0.03	BDL	0.02	BDL	BDL	0.06	1.04	1.1
E2/050	50	0.59	0.01	BDL	0.01	BDL	BDL	0.07	0.68	0.66
E2/070	70	0.49	0.02	BDL	0.01	BDL	BDL	0.09	0.61	0.71
E2/100	100	0.77	0.03	BDL	0.01	BDL	BDL	0.09	0.9	0.93
E2/155	155	0.91	0.04	BDL	BDL	BDL	BDL	0.09	1.04	1.09
E2/190	190	0.53	0.03	0.01	BDL	BDL	BDL	0.09	0.66	0.68
E2/280	280	0.46	0.02	BDL	0.01	BDL	BDL	0.09	0.58	0.61
E2/300	300	0.37	0.01	BDL	BDL	BDL	BDL	0.09	0.47	0.5
E2/390	390	0.53	0.02	BDL	0.01	BDL	BDL	0.1	0.66	0.78
E2/500	500	0.39	0.02	0.01	0.01	BDL	BDL	0.1	0.53	0.63
Ti (%)										
sample	depth	H_2O	NH_4-OAc	NH_4-OxD	NH_4-OxH	H_2O_2	sulfide	residual	total	bulk
E2/010	10	BDL	BDL	BDL	BDL	BDL	BDL	0.04	0.04	0.05
E2/030	30	BDL	BDL	BDL	BDL	BDL	BDL	0.13	0.13	0.12
E2/050	50	BDL	BDL	BDL	BDL	BDL	BDL	0.15	0.15	0.14
E2/070	70	BDL	BDL	BDL	BDL	BDL	BDL	0.19	0.19	0.17
E2/100	100	BDL	BDL	BDL	BDL	BDL	BDL	0.2	0.2	0.18
E2/155	155	BDL	BDL	BDL	BDL	BDL	BDL	0.18	0.18	0.18
E2/190	190	BDL	BDL	BDL	BDL	BDL	BDL	0.2	0.2	0.19
E2/280	280	BDL	BDL	BDL	BDL	BDL	BDL	0.2	0.2	0.2
E2/300	300	BDL	BDL	BDL	BDL	BDL	BDL	0.22	0.22	0.2
E2/390	390	BDL	BDL	BDL	BDL	BDL	BDL	0.2	0.2	0.21
E2/500	500	BDL	BDL	BDL	BDL	BDL	0.01	0.25	0.26	0.28
Ba (ppm)										
sample	depth	H_2O	NH_4-OAc	NH_4-OxD	NH_4-OxH	H_2O_2	sulfide	residual	total	bulk
E2/010	10	BDL	BDL	BDL	8	BDL	2	51	61	95
E2/030	30	BDL	BDL	BDL	18	BDL	9	162	189	359
E2/050	50	BDL	BDL	BDL	22	BDL	8	187	217	383
E2/070	70	BDL	BDL	BDL	24	BDL	10	226	260	569
E2/100	100	BDL	BDL	BDL	21	BDL	10	213	244	526
E2/155	155	BDL	BDL	2	21	BDL	9	202	234	432
E2/190	190	BDL	BDL	5	21	BDL	10	199	235	353
E2/280	280	BDL	BDL	BDL	27	BDL	16	182	225	341
E2/300	300	BDL	BDL	BDL	25	BDL	26	183	234	360
E2/390	390	BDL	BDL	5	22	BDL	14	190	231	382
E2/500	500	BDL	BDL	1	17	BDL	10	216	244	383

Cu (ppm)										
sample	depth	H_2O	NH_4-OAc	NH_4-OxD	NH_4-OxH	H_2O_2	sulfide	residual	total	bulk
E2/010	10	50386	592	40.9	138	8.5	5.5	12.7	51184	48918
E2/030	30	17430	617	125	554	26	42.3	34.5	18829	20120
E2/050	50	12330	347	95.8	605	27.3	24.9	32.5	13463	12140
E2/070	70	2900	160	138	738	42	35.1	38.6	4052	3980
E2/100	100	3420	291	194	710	48.2	49.1	43.2	4756	4540
E2/155	155	3780	225	70.1	459	22.1	38.2	44.1	4639	4740
E2/190	190	4030	306	113	406	71.9	48.1	46.2	5021	5230
E2/280	280	5040	294	81	421	23.3	42.3	53.3	5955	6250
E2/300	300	5220	245	76.1	266	28.8	48.4	57.6	5942	5690
E2/390	390	4380	164	61.1	347	22.8	38.3	51.5	5065	5160
E2/500	500	3870	283	175	346	117	101	64.7	4957	5140
Zn (ppm)										
sample	depth	H_2O	NH_4-OAc	NH_4-OxD	NH_4-OxH	H_2O_2	sulfide	residual	total	bulk
E2/010	10	112	1.2	BDL	0.8	BDL	0.8	3.5	118.3	101
E2/030	30	41.1	1.1	BDL	1.6	BDL	2.1	9.2	55.1	51.5
E2/050	50	32.6	0.7	BDL	1.2	0.8	2.2	12.2	49.7	39.5
E2/070	70	10.1	BDL	BDL	1.3	BDL	2.2	14.4	28	26.2
E2/100	100	11.7	BDL	BDL	1.2	BDL	2.4	12.8	28.1	30.5
E2/155	155	12.3	BDL	BDL	0.8	BDL	3.7	14	30.8	27.9
E2/190	190	13.6	0.7	BDL	1.6	0.5	3.2	16	35.6	43.6
E2/280	280	17.2	0.5	BDL	2.1	BDL	4.2	16.7	40.7	52.1
E2/300	300	15.5	BDL	BDL	1.5	BDL	4	18.4	39.4	39.3
E2/390	390	15.5	BDL	0.5	1.8	0.5	4.5	19.4	42.2	44.6
E2/500	500	13.3	0.5	0.6	5	0.9	8.6	37.4	66.3	79.2
Mn (ppm)										
sample	depth	H_2O	NH_4-OAc	NH_4-OxD	NH_4-OxH	H_2O_2	sulfide	residual	total	bulk
E2/010	10	539	6	BDL	2	BDL	BDL	BDL	547	620
E2/030	30	161	4	BDL	7	BDL	BDL	4	176	189
E2/050	50	127	3	BDL	7	BDL	BDL	5	142	128
E2/070	70	39	BDL	BDL	4	BDL	2	7	52	52
E2/100	100	45	BDL	BDL	3	BDL	3	7	58	57
E2/155	155	50	BDL	BDL	2	BDL	3	6	61	62
E2/190	190	53	3	5	3	BDL	3	7	74	71
E2/280	280	62	BDL	BDL	4	BDL	2	7	75	73
E2/300	300	55	BDL	BDL	3	BDL	BDL	7	65	60
E2/390	390	59	BDL	BDL	2	BDL	2	7	70	73
E2/500	500	42	BDL	BDL	9	BDL	19	13	83	90
Cr (ppm)										
sample	depth	H_2O	NH_4-OAc	NH_4-OxD	NH_4-OxH	H_2O_2	sulfide	residual	total	bulk
E2/010	10	23	3	6	5	BDL	BDL	BDL	37	42
E2/030	30	5	BDL	BDL	7	BDL	1	BDL	13	6
E2/050	50	4	BDL	2	5	BDL	BDL	BDL	11	5
E2/070	70	1	1	BDL	6	BDL	BDL	BDL	8	7
E2/100	100	1	1	1	5	BDL	BDL	1	9	8
E2/155	155	BDL	1	1	4	BDL	BDL	BDL	6	6
E2/190	190	1	1	4	3	BDL	BDL	2	11	10
E2/280	280	1	1	BDL	8	BDL	BDL	2	12	11
E2/300	300	2	BDL	BDL	3	BDL	BDL	BDL	5	7
E2/390	390	2	1	3	5	BDL	1	BDL	12	9
E2/500	500	BDL	1	1	BDL	BDL	4	2	8	10
Pb (ppm)										
sample	depth	H_2O	NH_4-OAc	NH_4-OxD	NH_4-OxH	H_2O_2	sulfide	residual	total	bulk
E2/010	10	BDL	BDL	3	BDL	BDL	BDL	BDL	3	BDL
E2/030	30	BDL	BDL	2	BDL	BDL	3	5	10	8
E2/050	50	BDL	BDL	BDL	BDL	BDL	3	3	6	10
E2/070	70	BDL	BDL	BDL	BDL	BDL	4	6	10	30
E2/100	100	BDL	BDL	5	4	BDL	3	4	16	24
E2/155	155	BDL	BDL	9	BDL	BDL	4	4	17	16
E2/190	190	BDL	BDL	4	3	BDL	BDL	2	9	16
E2/280	280	BDL	BDL	3	BDL	BDL	BDL	BDL	3	21
E2/300	300	BDL	BDL	4	BDL	BDL	3	3	10	25
E2/390	390	BDL	BDL	26	2	BDL	3	6	37	21
E2/500	500	BDL	BDL	7	BDL	BDL	4	3	14	27
Mo (ppm)										
sample	depth	H_2O	NH_4-OAc	NH_4-OxD	NH_4-OxH	H_2O_2	sulfide	residual	total	bulk
E2/010	10	BDL	BDL	1	5	129	40	6	181	178
E2/030	30	3	1	10	24	268	176	28	510	502
E2/050	50	BDL	BDL	8	26	239	230	36	539	505
E2/070	70	BDL	BDL	2	33	59	108	28	230	232
E2/100	100	BDL	BDL	6	38	94	127	25	290	274
E2/155	155	BDL	BDL	4	28	63	92	11	198	197
E2/190	190	BDL	BDL	19	28	96	165	13	321	311
E2/280	280	BDL	BDL	4	33	77	88	7	209	206
E2/300	300	BDL	BDL	5	27	81	117	9	239	228
E2/390	390	BDL	BDL	6	22	89	105	8	230	229
E2/500	500	BDL	BDL	4	15	46	112	19	196	200
V (ppm)										
sample	depth	H_2O	NH_4-OAc	NH_4-OxD	NH_4-OxH	H_2O_2	sulfide	residual	total	bulk
E2/010	10	9	15	13	8	BDL	BDL	18	63	68
E2/030	30	3	BDL	7	17	BDL	BDL	57	84	102
E2/050	50	BDL	BDL	8	12	BDL	BDL	66	86	107
E2/070	70	BDL	BDL	2	11	BDL	2	80	95	124
E2/100	100	BDL	BDL	5	12	BDL	3	85	105	134
E2/155	155	BDL	BDL	6	12	BDL	3	88	109	141
E2/190	190	BDL	BDL	15	10	BDL	3	91	119	144
E2/280	280	BDL	BDL	7	15	BDL	3	84	109	140
E2/300	300	BDL	BDL	8	9	BDL	3	84	104	132
E2/390	390	BDL	BDL	11	13	BDL	3	86	113	138
E2/500	500	BDL	BDL	7	10	BDL	12	99	128	166
As (ppm)										
sample	depth	H_2O	NH_4-OAc	NH_4-OxD	NH_4-OxH	H_2O_2	sulfide	residual	total	bulk
E2/010	10	BDL	14	25	15	BDL	BDL	BDL	54	35
E2/030	30	BDL	BDL	14	37	BDL	3	BDL	54	57
E2/050	50	BDL	BDL	17	56	BDL	4	BDL	77	74
E2/070	70	BDL	7	40	131	BDL	5	BDL	183	204
E2/100	100	BDL	17	68	151	BDL	11	4	251	223
E2/155	155	BDL	10	59	127	BDL	9	5	210	229
E2/190	190	BDL	4	54	37	BDL	5	BDL	100	112
E2/280	280	BDL	BDL	23	36	BDL	5	BDL	64	51
E2/300	300	BDL	BDL	16	20	BDL	4	BDL	40	77
E2/390	390	BDL	BDL	40	44	BDL	4	BDL	88	129
E2/500	500	BDL	BDL	18	14	BDL	BDL	BDL	32	65

The low quantities of secondary ferric minerals in the El Salvador No.1 tailings are explained by the high preservation degree of pyrite with contents around 6 wt.% in the primary as well as in the oxidation zone. In spite of the low degree of sulfide oxidation at El Salvador No.1 tailings, the pH is very acidic (2 – 3.5). This may be explained as a result from acidity liberated by primary jarosites in combination with zero carbonate neutralization potential. The reason of the low pyrite oxidation in the El Salvador No.1 tailings will be discussed together with the microbiological results.

5.5.3.2 Acid-Base Accounting

The ABA reflects the high pyrite content of the El Salvador No.1 impoundment. The average sulfide content is 3.3 %, which corresponds with an average pyrite content of 6.2 %, as pyrite is nearly the only sulfide. The carbonate NP is generally at the detection limit so that the SNNP is strongly negative with an average from –183 tCaCO3/1000t (Fig. 10). A decrease of the AP at the top of the tailings impoundment is normally interpreted as a result of depletion of sulfides (e.g., pyrite) via oxidation (compare Fig. 3 and Fig. 7). In the case of El Salvador No. 1 the decrease of the AP in the evaporite zone is seen more likely as an effect of upwards mass-transfer, resulting from the extreme aridity and not as an effect of stronger pyrite oxidation in this zone. This is supported by decreasing concentrations of the immobile element Ti in the evaporite zone (0.04 %), compared to the original Ti average content of 0.2 % in the underlying tailings. Additionally, the concentrations of the metals Fe, K, and Na are also lower in the evaporite zone. The decrease of Fe, K, and Na reflects more likely a dilution of the primary jarosite and natrojarosite content and not an effect of pyrite oxidation. If the decrease of the AP in the evaporite zone would be an effect of pyrite oxidation this should be visible an increase of Fe, K, or Na in the fractions of the Fe(III) oxyhydroxides or the Fe(III) oxides as observed at Piuquenes and Cauquenes (Fig. 3 and Fig. 7).

5.5.3.3 Sequential extractions

The sequential extractions reflect a strong enrichment of SO_4, Al, Mg, Na, Cu, Zn, and Mn in the water-soluble fraction at the top of the tailings in the evaporite zone (Fig. 10). This is consistent with the abundance of the water-soluble salts described in section 3.3.1. The concentrations of Cu and Zn in the sulfide fraction are generally very low throughout the whole tailings stratigraphy (below 100 and 10 ppm, respectively), indicating that nearly all mobile elements are mobilized upwards and confirming that the "primary zone", which is defined by its dark color, has been in fact significantly affected by oxidation processes, as it is was mentioned under 3.3.1

The distribution of Fe in the oxidizing fractions (H_2O_2 and $KClO_3$-HCl-HNO_3 leaches) at El Salvador reflects a difference in the distribution and dissolution behavior of pyrite compared to the tailings of Piuquenes and Cauquenes. In the El Salvador No.1 tailings, Fe shows constant and comparable concentrations in the weakly oxidizing H_2O_2-leach and in the strong sulfide leach throughout the tailings stratigraphy (Fig. 10), whereas in the Piuquenes and Cauquenes

tailings the Fe concentrations in the H_2O_2-leach are below the detection limit and those in the sulfide leach are much higher in the primary than in the overlying zones (Fig. 3 and Fig. 7). The high Fe concentrations in the H_2O_2-leach suggest that the pyrite in the studied impoundment of El Salvador is easier to oxidize, probably because it comes from an area of the deposit submitted to strong supergene alteration.

In the tailings of Piuquenes and Cauquenes, the coupled behavior of the elements Fe, K, Na, and SO_4 has served to trace the alteration of sulfides (essentially pyrite) and silicates and formation of new secondary phases as jarosite, schwertmannite, and ferrihydrite. In addition, at El Salvador dissolution kinetics can be used to discriminate between primary and secondary jarosite. The elements Fe, K, Na, and SO_4 show a similar distribution in the two Fe(III) oxyhydroxide and Fe(III) oxide fractions (Fig. 10). The Fe(III) oxyhydroxide fraction shows a peak of these elements in the orange-brown horizons of the oxidation zone, where possibly secondary schwertmannite, natrojarosite, as well as jarosite have been formed. According to stoichiometric calculations based on Fe and SO_4 values the amount of schwertmannite is subordinated compared to those of jarosite and natrojarosite. However, it has to be taken into account that non-stoichiometry of the Fe:S ratio of the alunite-jarosite group is frequently observed (Alpers et al., 1989) and may range from 3:2 to 2.3:2. As mentioned above, in El Salvador No. 1 tailings jarosite is not exclusively restricted to the oxidation zone, but it occurs also in the primary zone and is considered to be in part of supergene origin. The jarosite found in the El Salvador No. 1 tailings is different from the secondary jarosite in the Cauquenes and Piuquenes tailings. At El Salvador, the K/Na ratio in the Fe(III) oxide leach is 1.8 indicating that jarosite is the dominant species but that natrojarosite also occurs. This is supported by XRD results. In addition, the jarosite solubility at El Salvador (less than 10 % the Fe(III) oxyhydroxide leach with exception of the schwertmannite/jarosite horizon where it is > 50 %) is lower than at the Cauquenes and Piuquenes tailings (> 50 % in the Fe(III) oxyhydroxide leach together with schwertmannite). That the natrojarosite at the El Salvador No. 1 tailings is of primary (supergene) origin is also supported by the fact that in the Cauquenes and Piuquenes tailings no secondary natrojarosite is found although as in these tailings albite as a potential source of Na exists. This may be explained by the dissolution kinetics of albite which is much lower than that of biotite (Jambor & Blowes, 1998), resulting in a preferential formation of secondary (K-rich) jarosite instead of natrojarosite.

It remains the question if a significant amount of (K-rich) jarosite is formed during weathering of the El Salvador No. 1 tailings. Biotite alteration results in a vermiculite or a vermiculite-type mixed-layer mineral (Acker & Bricker, 1992; Jambor, 1994; Malmström & Banwart, 1997, Farquar et al., 1997). Per mole of biotite 2 mole of K^+ are liberated, available for the formation of 2 moles of jarosite (chapter 2 equation 28). Biotite is the main source for K as K-feldspar as sericite have an about 40 times slower reactivity than biotite (Jambor & Blowes, 1998). If jarosite is an important secondary mineral at El Salvador No. 1 tailings, it should be found in the clay fraction as shown by Stoffregen and Alpers (1992) for secondary alunite and the formation of vermiculite or vermiculite-type mixed-layer minerals should be detectable by XRD, as it is the case of Piuquenes and Cauquenes tailings. Yet, In the El Salvador tailings, this mineral could only be identified by DXRD as a very minor secondary phase, while in the other two tailings it is a major secondary phase. These findings suggest that at El Salvador, the main

part of the jarosites, especially the natrojarosite, are primary and the tailings material possibly comes from the area where the jarosite cap overlies a pyritic sulfide zone (Gustafson and Hunt, 1975), also explaining the relatively high pyrite content of these tailings and the lack of NP.

The oxyanions show a specific behavior. Mo concentrations are 3 to 5 times higher than in the other two tailings. Mo is slightly enriched at the schwertmannite layers in the Fe(III) oxyhydroxide fraction. The concentrations in the Fe(III) oxide fraction are constant throughout the tailings stratigraphy and may represent the adsorbed Mo (ligand exchange) of the primary jarosites. The molybdenum contained in the organic fraction correlates well with that in the sulfide fraction.

Arsenic is enriched in the upper part of the oxidation zone in the exchangeable, Fe(III) oxyhydroxide, and Fe(III) oxide fractions, but is not mobile enough to be enriched in the evaporite zone. This can be explained by the fact that As adsorbs preferentially to Fe(III) hydroxides and that these secondary iron phases are scarce in the evaporite zone. V shows more mobility than Mo and As, resulting in an enrichment in the evaporite zone in the water-soluble, exchangeable and Fe(III) oxyhydroxide fractions. Nevertheless, the main part of V is associated with the Fe(III) oxyhydroxide and Fe(III) oxide leach.

5.5.3.4 Microbial activity

Three representative samples from the evaporite, oxidation and primary zones of the drill core E1 were submitted to bacterial count and oxidation activity tests. In all samples high bacteria numbers by direct counting are observed (2.0×10^7 – 1.8×10^8 bact/ml). *Thiobacillus ferrooxidans* could not be cultivated in any of the El Salvador tailings samples. The oxidizing activity tests show that all three samples behaved in a similar way. They started immediately a slow oxidation and reached a plateau after 150 h at around 2000 ppm Fe^{2+} (Fig. 5). This slight decrease of the Fe concentration is interpreted as the non-bacterial background oxidation via O_2 exchange at the water surface of the shaken sample. The very low or non-existent bacterial oxidation activity at the El Salvador No.1 contrasts with the higher oxidation activities detected in the similar microbiologic tests carried out on tailings from Piuquenes and Cauquenes (Fig. 5). This may be due to the high molybdenum contents of El Salvador (Tab.7) which are 3 to 5 times higher than in Piuquenes and Cauquenes (Tab. 4 & 6). It is known that molybdenum acts as a poison for *Thiobacillus ferrooxidans* (Tuovinen et al., 1971).

5.5.3.5 Slow pyrite oxidation and acid availability

The very low or non existent microbial oxidation at the El Salvador No.1 tailings constitutes the best explanation for the above mentioned high preservation degree of pyrite in the "primary" and oxidation zones, as non bacterial oxidation is much less efficient. Singer & Stumm (1970) have shown that microbial mediation of sulfide oxidation may accelerate the oxidation rates by a factor larger than 10^6). The low quantities of secondary ferric minerals compared to the high pyrite content are interpreted to be the result of slow inorganic pyrite oxidation. The possibility that a lack of oxygen or water is the reason of the slow pyrite

oxidation is less probable, as cracking assures availability of oxygen even in the deeper part of the tailings and the 20 wt.% of moisture content is in the range of Piuquenes and Cauquenes (Fig. 3 & 6). The association of the secondary ferric minerals (jarosite and schwertmannite) to horizons and streaks and dots reflects the mobilization of Fe^{3+}, so that the availability of Fe^{3+} is high enough also for inorganic pyrite oxidation. Thus, we see the low pyrite oxidation mainly as a result from the absence of microbial oxidation activity, possibly due to molybdate poisoning.

Some results from the sequential extractions may illustrate the role of the (lack) of microbial oxidation. At El Salvador No 1 tailings, with pyrite contents around 6.2 wt.%, all but one samples yield Fe values < 0.77 % in the Fe(III) oxyhydroxide leach (Tab. 7). In contrast, in the oxidation zone of the younger tailings of Piuquenes (Tab. 4) the original pyrite (1.66 w.% in average) has been almost completely oxidized to schwertmannite and jarosite (sh/jt ratio = 1.0). In Piuquenes the Fe(III) oxyhydroxide leaches yield Fe values in the range 0.5 to 1.5 % Fe (mainly from schwertmannite), and the Fe(III) oxide leaches in the range of the 1 to 2.3 % Fe (mainly from secondary jarosite). Similar results were obtained in the Cauquenes tailings (0.99 wt.% original pyrite) where jarosite is the dominant secondary phase with Fe content in the Fe(III) oxide leach up to 1% (Tab, , average sh/jt ratio = 0.5 except in one layer with 1.58).

Despite the fact that, possibly through molybdate poisoning, the rate of sulfide oxidation was much lower at El Salvador No.1 tailings, the combination of near zero neutralization potential with acidity available in primary jarosite leads to extreme low pH conditions in the tailings making possible a strong element mobilization which was upwards because of the extreme aridity.

5.6 Summarizing discussion and conclusions

5.6.1 Selectivity of sequential extractions

Stumm & Sulzberger (1992) discussed the dissolution kinetics of secondary ferric minerals by organic complex formers (e.g., oxalate) as a function of concentration, acidity, temperature, infra-red radiation, and Fe(II) as catalyst. Dissolution kinetics is important for the determination of secondary phases (Fe, Al, Mn) by DXRD (Schulze, 1981, 1994) and to study their role in element retention. Dissolution kinetics are also implicated in sequential extractions which are widely used to study element speciation in systems such as soil, sediments and for exploration proposes (Tessier et al., 1979; Sondag, 1981; Chao & Zhou, 1983; Chao, 1984; Cardoso Fonseca & Martin, 1986; Hall & Bonham-Carter, 1998). Recently, sequential extractions have increasingly been used in the mine waste environment to study the complex processes of sulfide oxidation and the retention of mobilized elements by secondary phases via precipitation and sorption processes (Ribet et al., 1995; McGregor et al., 1995; Fanfani et al., 1997; McCarty et al., 1998; chapter 5 and 6). Due to the wide range of possible secondary phases in these systems, the selectivity of the dissolution is the focus of some criticism (McCarty et al., 1998). This criticism is justified, as for instance our results show that in the leach of the Fe(III) oxyhydroxides (0.2 M NH_4-oxalate, pH 3, dark, 1h) schwertmannite, ferrihydrite, and secondary jarosite go into solution. This problem can be partly solved, as shown in the previous sections,

through careful mineralogical studies to detect which secondary minerals are dissolved at which step of the sequential extractions. It is even possible to estimate the concentration of the secondary phases in the solution by stoichiometric calculations. This opens the way to study the selective retention behavior of mobile elements by secondary minerals.

5.6.2 *Influence of the climate, ore mineralogy and flotation process to geochemical and mineralogical processes*

In this study the geochemical behavior of three inactive flotation tailings from the porphyry copper deposits La Andina, El Teniente, and El Salvador, Chile is compared. The hypogene sulfide assemblage of these three deposits is comparable and is dominated by pyrite, chalcopyrite, bornite, molybdenite, and minor magnetite and hematite. Differences can be found in the minor sulfide assemblage (Table. 1). The gangue mineralogy is in all three deposits dominated by quartz, alkali-felspars (albite to K-feldspar), and biotite. Carbonate contents are in all deposits low. Calcite, siderite and traces of ankerite are reported from La Andina (Serrano et al., 1996), whereas in El Teniente and El Salvador only calcite is described (Camus, 1975; Gustafson & Hunt, 1975). In the Piuquenes tailings a low average carbonate neutralization potential from 1.4 $tCaCO_3$/1000t can be detected in the primary zone, while in the tailings from Cauquenes and El Salvador No.1 the carbonate neutralization potential is zero. Supergene enrichment is weak in La Andina, moderate in El Teniente, and strong in El Salvador. The latter has developed a pronounced leached cap with the formation of supergene jarosite, hematite, and goethite. The supergene Cu-sulfide assemblage is dominated in all three deposites by chalcocite-digenite with minor covellite (Camus, 1975; Gustafson & Hunt, 1975; Serrano et al., 1996). The tailings from Piuquenes and Cauquenes are mainly from the supergene enriched zone of the two ore deposits, as in both tailings the supergene Cu-sulfide assemblage is present in the primary zone (Fig. 2E and 2G). The tailings from El Salvador No. 1 comes possibly from a pyritic sulfide zone of the orebody in contact with a jarosite cap, explaining the high pyrite content and the lack of neutralization potential reflected in the acid-base accountings.

The Piuquenes impoundment (La Andina) represents a precipitation-dominated climate (alpine), the Cauquenes impoundment (El Teniente) is situated in a Mediterranean climate with rainfall in winter and high evaporation rates in summer, whereas the El Salvador No. 1 impoundment is located in a hyper-arid climate with extreme evaporation rates all year through. La Andina and El Salvador use an alkaline flotation circuit, while the complex clay mineralogy in El Teniente makes it necessary to apply an acid flotation circuit (pH 4.5), resulting in dissolution of the carbonates. At El Salvador No.1 tailings an alkaline circuit was applied. The zero carbonate neutralization potential is explained by the primary ore assemblage containing abundant jarosite. In the Piuquenes tailings the carbonates are still stable in the primary zone and control a similar pH-buffering zonation as described in the model proposed by Blowes & Ptacek (1994). The average pyrite contents of the tailings are in Piuquenes 1.66 wt.%, in Cauquenes 0.99 wt.%, and in El Salvador 6.19 wt.%, which, in combination with the low or near zero carbonate neutralization potential yields in the Piuquenes and Cauquenes tailings to strong oxidation activities and associated element mobilization and secondary mineralogy. In the El

Salvador No.1 tailings primary jarosite is a main source of acidity leading in combination of the arid climate to strong element enrichment as water-soluble salts at the top of the tailings.

Development of secondary mineralogy is principally concentrated in the oxidation and neutralization zone, and at El Salvador, also in the evaporite zone. The Cauquenes and El Salvador No.1 tailings have no well-defined neutralization zone, due to the lack of carbonate neutralization potential. High evaporation rates in El Salvador promote an upwards mass transfer and the formation of a evaporite zone at the top of the tailings (Table 9).

Oxidation zone. The Piuquenes tailings impoundment has proved to be an ideal example to study the oxidation, mobilization and retention processes in a climate where precipitation exceeds evaporation. Results from sequential extraction in the oxidation zone from Piuquenes tailings document the element liberation by oxidation of the host minerals (sulfides) or dissolution by acidity (carbonates and silicates) produced by the oxidation of sulfides and the subsequent hydrolysis of secondary phases. The liberated elements stable as bivalent cations under acid conditions (e.g., Cu^{2+}, Zn^{2+}, and Mn^{2+}) are leached out of the oxidation zone. Mono and trivalent cations (K^{+}, Na^{+}, Fe^{3+}) together with sulfate are involved in the formation of secondary precipitates mainly in the oxidation zone (jarosite and schwertmannite, Fig. 2B). Elements which are stable as oxyanions ($HMoO_4^-$, $H_2AsO_4^-$) under acid conditions are less mobile and adsorbed at the secondary ferric minerals formed in the oxidation zone under acidic conditions (schwertmannite and jarosite). This could be detected with microprobe analyses in

Table 9: *Secondary mineralogy of the studied tailings (chalc = chalcanthite; halotr = halotrichite; hexa = hexahydrite; other abbreviations as in table 2).*

Tailings impoundment	Piuquenes	Cauquenes	Salvador No.1
pyrite content [wt%]	1.66	0.99	6.19
ABA [tCaCO3/1000t]	-28.27	-18.15; NP ≈ 0	-101.60; NP ≈ 0
evaporite zone			jt, ver, sh, gy, chalc, halotr, hexa, bonattite, pickeringite, magnesioauberite
oxidation zone	jt, ver, sh, gy	jt, ver, sh, gy, chalc, Al substituted jt	jt, ver, Na-jt, sh, gy
neutralization zone	fh*, $Mn(OH)_2$*, cv,	fh*, $Mn(OH)_2$*, cv	
primary zone	fh*, $Mn(OH)_2$*	fh*, $Mn(OH)_2$*	sh* traces

** indications, but not unequivocally proved.*

situ at a schwertmannite streak, which show slight increased Mo contents (chapter 7). Schwertmannite was be detected by DXRD and is associated with paste pH values of 2.8 – 3.5, which are found preferentially close to water flow paths, possibly due to pH increase by dilution.

Stoichiometric calculation from the Fe(III) oxyhydroxide leach show that only schwertmannite together with secondary jarosite are leached in these samples from the oxidation zone and not ferrihydrite as used in most computer models. These findings suggest that for geochemical modeling of processes affecting sulfide mine waste it is crucial to incorporate schwertmannite into the data base.

Jarosite is the main secondary mineral in the oxidation zone of Piuquenes. XRD data show peak positions near synthetic jarosite. This mineral derives Fe and sulfate from pyrite oxidation and K mainly from biotite alteration, resulting in the formation of the second important secondary phase, a vermiculite-type mixed-layer mineral. The Piuquenes tailings oxidation zone samples do not show any adsorption of Cu and Zn in the exchangeable fraction, where the vermiculite-type mixed-layer mineral is broken down and this mineral displays in the Piuquenes samples a peak position of 12.25 – 12.67Å. With increasing pH the concentrations in the exchangeable fraction increase (Fig. 4), as expected from the known pH dependence of the adsorption behavior of these metals (Dzombak and Morel, 1990, Webster et al., 1998).

The Cauquenes tailings present some differences in the secondary mineralogy of the oxidation zone compared to Piuquenes. In Cauquenes the Mediterranean climate leads to a downwards mobilization of mobile elements in the rainy season and the high evaporation rates in the dry season leads to a subordinate upwards migration. Drill core T4, situated at the margin of the Cauquenes impoundment and characterized by a coarser grain-size than in the center of the impoundment, shows the same element distribution and secondary mineralogy in the oxidation zone as Piuquenes (bivalent cations are leached out and oxyanions are adsorbed to the secondary schwertmannite and jarosite). This suggests that the capillary force is not high enough for upwards transport in the fine sandy material.

In contrast, in the center of the Cauquenes tailings (drill cores T1, T2, T3) the samples from the oxidation zone show elevated metal concentrations (e.g., Cu and Zn) in the water-soluble and the exchangeable fraction. In this area of the impoundment the grain-size is one order of magnitude lower than at the edges (silt-clay), due to the alluvial accumulation of fine material from the elevated margins of the impoundment. The metal enrichment at the top is controlled by evaporation driven upwards migration, due to the finer grain-size witch increases the capillary force and the moisture retention capacity of these tailings. It appears that one part of the upwards mobilized Cu and Zn are fixed in the vermiculite-type mixed-layer mineral (Farquhar et al., 1997) as shown through a peak shift of the d-values (Fig. 8) as well as high Cu and Zn concentrations in the exchangeable fraction (Fig. 4), and in-situ microprobe analyses of biotite.

Stoichiometric calculations of the jarosite content in the Cauquenes tailings lead to an overestimation of the sulfate proportion by about 20%. An increased Al^{3+} content on its B site (general formula $AB_3(SO_4)_2(OH)_6$) could be the source for the too high calculated SO_4 contents. This is supported by increasing Al concentrations in the Fe(III) oxyhydroxide and Fe(III) oxide leaches from the oxidation zone and by a peak-shift to lower d-values (Fig. 9) compared with peak positions near synthetic jarosite for samples from Piuquenes and from the T4 core at Cauquenes, which do not show increased Al concentrations in these leaches.

At El Salvador, where the continuous high evaporation rates result in upwards mobilization, most of the mobile elements are leached out in the oxidation zone (e.g., Cu, Zn, Mn, Mg). Only a low background level of these elements is visible mainly in the water-soluble fraction (Fig. 10). Low quantities of secondary schwertmannite, jarosite, and traces of a vermiculite-type mixed-layer mineral characterize the secondary mineralogy. Formation of secondary ferric minerals is essentially restricted to some orange-yellow horizons. The low quantities of secondary ferric minerals in the El Salvador No.1 tailings are surprising considering the high pyrite (6.2 wt.%) content. A very low oxidation activity during microbiological tests and molybdenum values higher by a factor of 3 to 5 than those of Piuquenes and Cauquenes, suggest that this is due, at least in part, to molybdenum poisoning of *Thiobacillus ferrooxidans* as described by Tuovinen et al. (1971). The lack of microbial mediated sulfide oxidation, which as shown by Singer & Stumm (1970) may accelerate the oxidation rates by a factor larger than 10^6, could account for the high preservation degree of pyrite at El Salvador No.1 impoundment. The strong acidity of these tailings (pH 2 – 3.5) is seen as a result of slow inorganic pyrite oxidation in combination with acidity stored in supergene jarosite and zero carbonate neutralization potential.

In the 0.3 m thick evaporite zone at the top of the tailings of the El Salvador No.1 impoundment (Fig. 2D), as result of the above mentioned upwards migration of metals and other mobile elements, water-soluble salts as bonattite ($CuSO_4 \cdot 3H_2O$), chalcanthite ($CuSO_4 \cdot 5H_2O$), pickeringite ($MgAl_2(SO_4)_4 \cdot 22H_2O$), magnesioaubertite $(Mg,Cu)Al(SO_4)_2Cl \cdot 14H_2O$), halotrichite ($FeAl_2(SO_4)_4 \cdot 22H_2O$), hexahydrite ($MgSO_4 \cdot 6H_2O$), and gypsum could be determined.

The behavior of Cu (Fig. 11) illustrates best the different types of migration resulting from different climatic conditions and, to a subordinate degree, grain-size. Piuquenes (A3 drill hole) and Cauquenes (T4 drill hole) exemplify the "normal" downwards mobilization to more reducing conditions tailings with the formation of secondary Cu-sulfides. The El Salvador drill holes represent the case where because of extreme aridity, the element migration is essentially upwards to more oxidizing conditions, and results in the formation of the water-soluble salts mentioned above. The drill holes T1, T2, and T3 at Cauquenes represent an intermediate case where a significant upwards migration is favored by the very fine grain-size.

Oxidation front. Microbial acitivity tests have shown that the microbial oxidation activity is highest at the oxidation front from the Cauquenes tailings. The oxidation front is also characterized by low concentrations of secondary ferric phases. Often, an increase of the secondary ferric phases at the oxidation front is observed, resulting from neutralization reactions and are conserved in cementation layers or "hard pans" (chapter 6). A further research project will test the working hypothesis of the possible influences of organic acids (e.g., pyruvate, oxalate, and acetate), produced by the increased microbial activity at the oxidation front, to solubility control of secondary Fe(III) oxyhydroxides in tailings with low neutralization potential. The controlling parameters for Fe^{3+} solubility are: (1) kinetics of the sulfide oxidation, e.g., they may control the production of acidity via hydrolysis, (2) availability of Fe^{3+} as sulfide oxidant, and (3) possible oxidation limiting processes by coating of sulfides with Fe(III) hydroxides or the formation of cemented layers. The results of the here presented study indicate that the low sulfide content of porphyry copper tailings in combination with low neutralization

potential indicate that there is less potential to the formation of a cemented layer at the oxidation front compared with tailings from massive sulfide deposits.

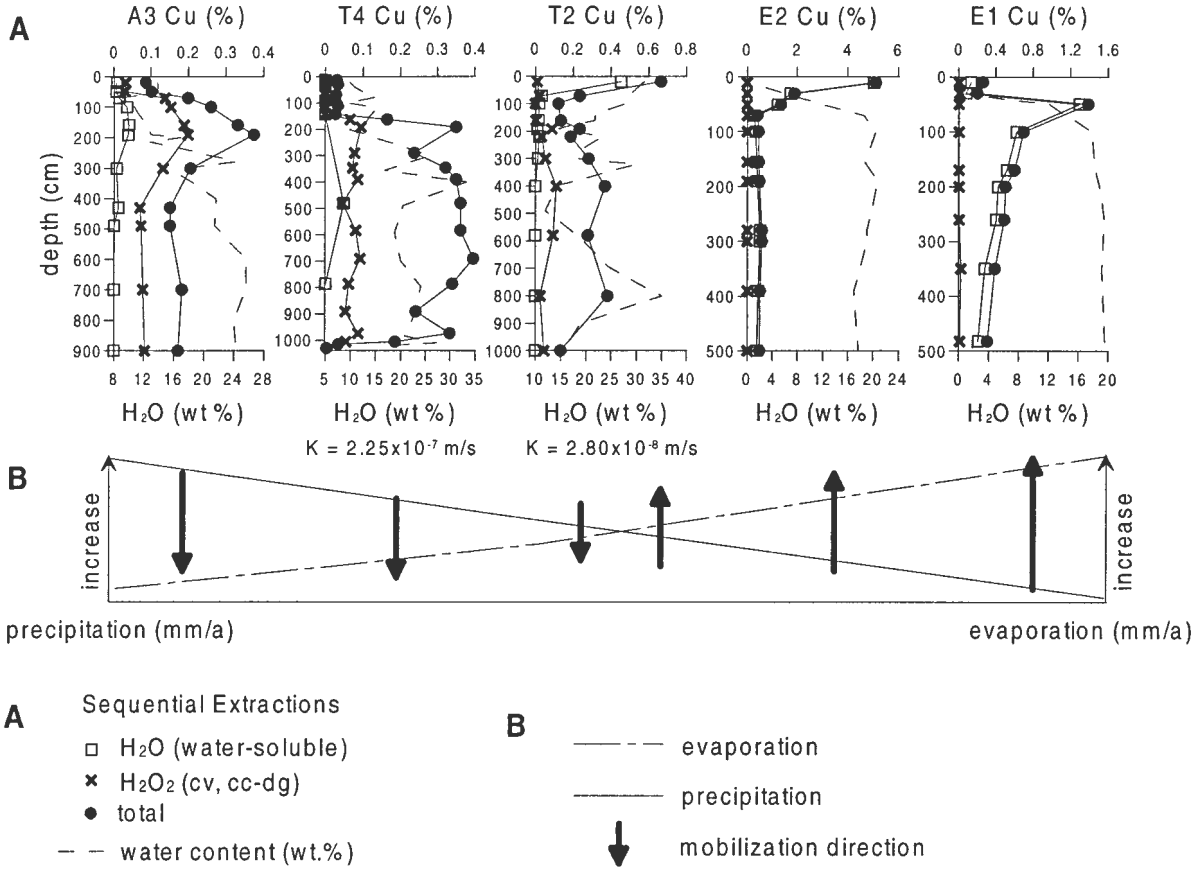

Fig. 11: *The results for Cu of five drill cores from the three studied tailings demonstrate the influence of climate, grain size and water content to the mobilization direction. In precipitation dominated climates as Piuquenes (Andina; A3) Cu is leached out from the oxidation zone and enriched below the water level mainly as secondary covellite. In the Mediterranean climate of Cauquenes (El Teniente; T4 & T2) the effect of grain size to capillary force is displayed. Coarser grain sizes (T4) lead to leaching out from the oxidation zone as in Piuquenes, whereas finer grain-size (T2) leads to a higher capillary force and consequently to a higher water content at the top, resulting in an enrichment of Cu in the water-soluble fraction. In extremely arid climates (El Salvador) moisture contents as low as 3 wt.% (E2) are enough for an enrichment of the water-soluble Cu-sulfates at the surface of the tailings. However, complete dryness in the evaporite zone of E1 (moisture = 0.002 wt.%) limits the capillary upwards migration.*

Neutralization zone. Leached Cu from the oxidation zone is mobilized downwards in the Piuquenes tailings and is enriched via replacement of chalcopyrite by covellite ± digenite-chalcocite in a well-defined neutralization zone below the groundwater level. This replacement at Piuquenes is only observed in depths with pH values below 6. At less acidic conditions the Cu^{2+} is adsorbed to adsorbents as secondary Fe- and Mn-hydroxides or clay minerals. In the Cauquenes tailings the same Cu replacement is observed, but, due to the absence of carbonate neutralization, no clear neutralization sequence is developed and pH does not limit the mobility

of Cu. In the El Salvador No.1 tailings no neutralization zone is developed due to the zero carbonate neutralization potential.

Other bivalent cations (e.g., Mn, Mg, Zn, Pb) which are leached out from the oxidation zone in Piuquenes and Cauquenes could not be XRD detected in the primary zone as secondary phases due to their low concentrations. Nevertheless, increased concentrations of Fe, Al and Mn in the Fe(III) oxyhydroxide leach suggests the probable presence of secondary Fe, Al and Mn hydroxides (e.g., ferrihydrite, $Mn(OH)_2$ and $Al(OH)_3$). Tertiary gypsum was found in samples obtained near the groundwater table as an indicator of neutralization reactions taking place. The upwards migration recognized in Cauquenes and El Salvador is reflected by increased concentrations of these element in the exchangeable and water-soluble fractions in the center of Cauquenes (T1, T2, and T3). This upwards migration in summer superposes the general downwards. In El Salvador these metals are all enriched as water-soluble salts in the evaporite zone, indicating that with increasing evaporation controlled climate the importance of hydrolysis for mineral formation decreases.

Primary zone. In the primary zone of Piuquenes and Cauquenes tailings the hypogene pyrite, chalcopyrite, bornite, and molybdenite as well as the supergene chalcocite-digenite and covellite are stable. In the Piuquenes tailings secondary Cu replacement is restricted to the neutralization zone, due to a well-developed neutralization zoning. In Cauquenes no clear pH buffering zonation is developed owing to the lack of NP so that the Cu replacement affects also the primary zone. Hydrolysis of secondary hydroxides (e.g., an average of 1.2 % Fe in the Fe(III) oxyhydroxide fraction in Piuquenes and an average of 0.5% in Cauquenes, respectively) take place in the primary zones in the Piuquenes and Cauquenes tailings. The minerals play an important role in the adsorption of bivalent cations (e.g., Cu, Zn, Mn) as well as As and V. In the extreme arid conditions of El Salvador some dots of possibly schwertmannite indicate that the primary zone is also affected by oxidation. Pyrite is relatively stable and only some residual grains of chalcopyrite-covellite assemblage can be observed in the primary zone. The covellite might also be a result of secondary replacement.

5.6.3 Implications from the ore mineralogy

The three tailings impoundments investigated in this study have a negative SNNP and a well developed low pH oxidation zone, showing clearly that they are acid producing and in the case of El Salvador that they have acid stored form the primary mineralogy. This results from the following factors with respect to ABA of porphyry copper deposits:

(1) Calc-alkaline rock types (andesite and dacite as extrusives and quarzdiorite, monzodiorite and granodiorite as intrusives) are normaly anorthite rich, but due to intense K- and Na-alteration alkali-feldspars dominate (albite to orthoclase). The latter are characterized by lower neutralizing reactivity (Jambor & Blowes, 1998).

(2) Due to the low reactivity of the silicate assemblage, the carbonate content is the main acid neutralizer. Generally this deposit type has a very low carbonate content.

(3) Supergene enrichment (El Salvador) and alteration additionally decrease the neutralization reactivity of the host rock assemblage. This has to be taken in account for waste dumps from leached cap material, which may have very low residual sulfide contents in combination with low or near zero neutralization potential, and may produce AMD.

(4) Clay mineral assemblage sometimes makes it necessary to use an acid flotation circuit (El Teniente), resulting in a NP of zero as the result of the dissolution of carbonates in the flotation process.

(5) High molybdenite contents may suppress microbial oxidation activity.

(6) As show in the example of the El Salvador No.1 tailings, low or zero microbial oxidation activity in combination with zero carbonate neutralization potential and acidity stored in primary jarosite lead also to low pH values and strong element mobilization.

(7) Low ore grade results in extensive amounts of waste material.

Summarizing, it can be pointed out that flotation tailings from porphyry copper deposits have a high potential for acid production, resulting from the relatively low sulfide contents in combination with very low neutralization potential.

5.6.4 Implications for supergene processes

The secondary mineralogy and geochemical processes detected in the tailings at Andina, El Teniente, and El Salvador show marked similarities to that described in supergene processes of porphyry coppers (e.g., Gustafson & Hunt, 1975, Alpers & Brimhall, 1989) and may help in the understanding of their formational mechanisms. In this context, the widespread occurrence of secondary schwermannite in the oxidation zones of the studied tailings, which was not known before, let us to the hypothesis that schwermannite may also occur during supergene alteration in porphyry coppers environments. The typical jarosite and goethite-hematite assemblage of leached caps, commonly referred to as "limonites" (e.g., Gustafson & Hunt, 1975; Alpers & Brimhall, 1989), may also include schwertmannite. The latter may occur preferentially in veinlets. Bigham et al. (1990, 1994, and 1996) have shown that schwertmannite is a meta-stable phase with respect to goethite and hematite. Barham (1997) showed that schwertmannite can transform to jarosite under certain conditions. Thus, the generally reported mineralogy of jarosite-goethite–hematite of leached caps from porphyry copper systems may be the stable endproduct of an original jarosite-schwertmannite±goethite mineralogy.

5.6.5 Schematic Model of element cycling in sulfidic mine tailings

The present study illustrates how climate has a direct influence on the composition of secondary minerals. The main results are summarized in two schematic models of element cycling in porphyry copper tailings (Fig. 12). The first one (Fig. 12A) deals with the case of precipitation-dominated tailings and the second one (Fig. 12B) that of evaporation-controlled tailings.

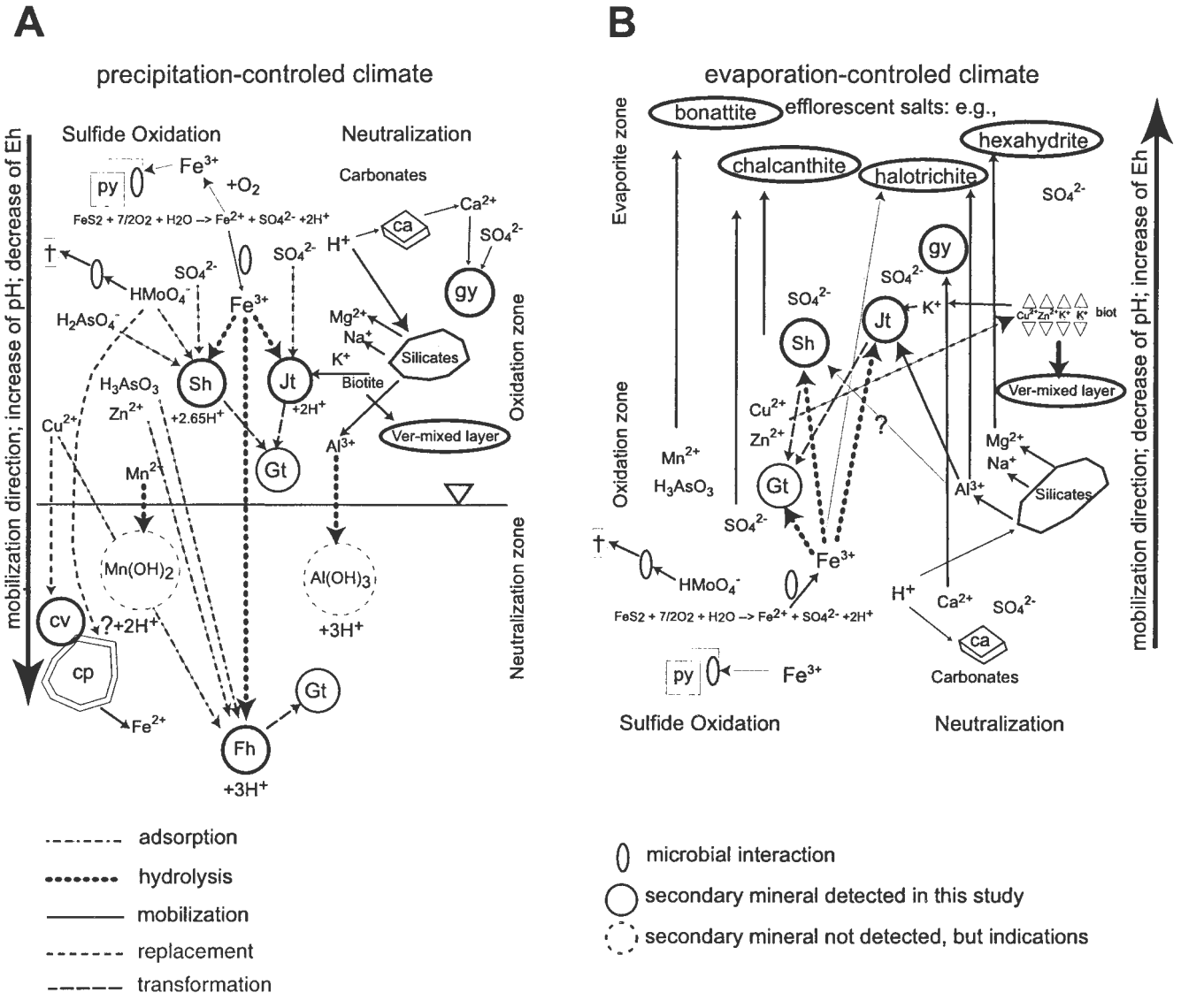

Fig. 12: The proposed schematic model for precipitation-dominated climates is shown in **A** *and applies for the Piuquenes tailings (La Andina) and the drill core T4 from Cauquenes (El Teniente). In* **B** *the model for evaporation-controlled climate is presented.* **A:** *Sulfide oxidation (e.g., equations 1, 2 and 3) leads to the liberation of bivalent cations as Fe^{2+}, Cu^{2+}, Zn^{2+}, Mn^{2+}, oxyanions as $HMoO_4^-$, $H_2AsO_4^-$, and SO_4^{2-} as well as protons (H^+). Oxidation of molybdenite is lethal for Thiobacillus ferrooxidans and may limit the microbial mediated oxidation of Fe^{2+} to Fe^{3+}. Fe^{3+} may take over the role of the principal sulfide oxidant, or may hydrolyse to secondary phases as jarosite, schwertmannite, ferrihydrite, goethite or others Fe(III) hydroxides, depending on pH and activity of Fe, SO_4, Cl, and K. The hydrolysis of Fe and Al is one of the main proton producing process. The produced protons react with neutralizing minerals as carbonates and silicates. These neutralization reactions result in the control of the pH and the formation of secondary minerals as for example gypsum and vermicultite-type minerals under liberation of cations as Al^{3+}, K^+, Na^+, Mg^{2+}. These cations play an important role in the formation of the secondary mineralogy as K for jarosite. They also may hydrolyze with concomitant liberation of protons as for the formation of gibbsite ($Al(OH)_3$). Bivalent cations are very mobile under acid conditions and are leached out of the oxidation zone. Below, with increasing pH sorption processes fix these elements. With increasingly reducing conditions (below the water table) replacement processes, as documented by the transformation of chalcopyrite to covellite may take place.*

Oxyanions are mainly adsorbed under low pH in the oxidation zone to the secondary ferric minerals. Nevertheless, changes in their oxidation state (e.g., arsenate to arsenite) may increase their mobility and may lead to enrichment. ***B:*** *With evaporation-controlled climates the water-flow direction changes to upwards migration via capillary forces. The mobilized elements are transferred to mainly oxidizing condition. Saturation and/or supersaturation controls the precipitation of the water-soluble secondary salts. Hydrolysis and replacement processes are less important. Increased substitution as Al in jarosite, or Cu and Zn in biotite can be observed.*

The model for precipitation-dominated climates (Fig. 12A) applies for the Piuquenes tailings (La Andina) and and the drill core T4 from Cauquenes (El Teniente). Sulfide oxidation (e.g., equations 1, 2 and 3) leads to the liberation of bivalent cations as Fe^{2+}, Cu^{2+}, Zn^{2+}, Mn^{2+}, oxyanions as $HMoO_4^-$, $H_2AsO_4^-$, and SO_4^{2-} as well as protons (H^+).

$$FeS_2 + {}^7/_2O_2 + H_2O \rightarrow FeSO_4 + SO_4^{2-} + 2H^+ \quad (1)$$

$$Fe^{2+} + {}^1/_4O_2 + H^+ \Leftrightarrow Fe^{3+} + H_2O \quad (2)$$

(much faster if in presence of certain bacteria, e.g.,*Thiobacillus ferrooxidans*)

$$FeS_2 + 14\,Fe^{3+} + 8H_2O \rightarrow 15\,Fe^{2+} + 2SO_4^{2-} + 16H^+ \quad (3)$$

Oxidation of molybdenite, a common mineral in porphyry coppers, is lethal for *Thiobacillus ferrooxidans* and may limit the kinetics of reaction (2). Fe^{3+} may take over the role of the principle sulfide oxidant (equation 3) or may hydrolyze to secondary phases as jarosite, schwertmannite, ferrihydrite, goethite or others Fe(III) hydroxides, depending on pH and activity of Fe, SO_4, Cl, and K. Jarosite, is formed generally at low pH (<2) conditions, is the first phase precipitating subsequently to pyrite oxidation and is limited by the availability of K and Na deriving from biotite and feldspar alteration, therefore it occurs disseminated in the oxidation zone. The ferric iron, which could not find a partner to form jarosite is mobile under the acid condition and migrates with the water-flow system. Together with the very mobile sulfate it may hydrolyze to schwertmannite when slightly higher pH (2.8 - 3.5, Bigham et al., 1996) conditions are reached, resulting in the accumulation of schwertmannite in streaks, dots, and grain-size interfaces, i.e., a different distribution than jarosite. In this step, sulfate is the limiting factor and the ferric iron may reach the neutralization zone if not enough sulfate is available, where it may hydrolyze to ferrihydrite. Equations 4 – 6 show that the hydrolysis is the main proton-producing process resulting in 3 mole protons per mole hydrolyzed Fe^{3+} for ferrihydrite, 2.625 for schwertmannite and 2 for jarosite.

Ferrihydrite: $10Fe^{3+} + 60H_2O \Leftrightarrow 5Fe_2O_3{\cdot}9H_2O + 30H^+$ (4)

Schwertmannite: $16Fe^{3+} + 3SO_4^{2-} + 26H_2O \Leftrightarrow Fe_{16}O_{16}(OH)_{10}(SO_4)_3 + 42H^+$ (5)

Jarosite: $3Fe^{3+} + K + 2SO_4^{2-} + 6H_2O \Leftrightarrow KFe_3(SO_4)_2(OH)_6 + 6H^+$ (6)

The protons produced by reactions (1) – (6) may react with neutralizing minerals as carbonates and silicates. These neutralization reactions control pH, the liberation of cations as Al^{3+}, K^+, Na^+,

Mg^{2+}, and the formation of secondary minerals as gypsum and vermiculite-type minerals. As an example the neutralization reaction of biotite resulting in the formation of vermiculite is shown in equation 7.

$$3K_2(Mg_3Fe_3)Al_2Si_6O_{20})(OH)_4 + 5H_2O + 12H_2CO_3 + 6H^+ + {}^3/_2O_2 \rightarrow$$
$$2[(Mg_3Fe_3)\ Al_3Si_5O_{20}(OH)_4 \cdot 8\ H_2O] + 6K^+ + 3Mg^{2+} + 3Fe^{2+} + 8SiO_2 + 12HCO_3^- \quad (7)$$

The liberated cations play a limiting role in the formation of secondary minerals as for example K in jarosite. They also may hydrolyze with concomitant liberation of protons as in the formation of gibbsite ($Al(OH)_3$). Bivalent cations are very mobile under acid conditions and are leached out of the oxidation zone. Below, with increasing pH, change in solubility of the mobilized element and sorption processes fix these elements. Below the water table, with increasingly reducing conditions, replacement processes, as the transformation of chalcopyrite to covellite may take place.

Oxyanions are mainly adsorbed to the secondary ferric minerals under the low pH conditions of the oxidation zone. Nevertheless, less oxidizing conditions may increase their mobility and may lead to enrichments in the neutralization zone as it is typical for As (e.g., arsenate and arsenite). As long as the underlying tailings have enough neutralization potential to control the pH distribution, the metals leached from the oxidation zone are fixed and effluents of the tailings have acceptable water quality (e.g. Piuquenes). Once the neutralization potential is consumed or was originally not available due to the primary mineralogical composition or the flotation process, the underlying material is no longer able of scavenging the mobilized elements and acid mine drainage (AMD) develops.

The model for evaporation-controlled tailings (Fig. 12B) applies to El Salvador No.1 impoundment and, with restrictions, to the central part of the Cauquenes tailing at El Teniente (T1, T2, and T3). With increasing evaporation the water-flow direction changes to upwards migration via capillary forces. Hydrolysis and sulfide enrichment processes are less important. The mobilized elements are transferred to the top of the tailings with oxidizing conditions. Saturation and/or supersaturation controls the precipitation of the water-soluble secondary salts as bonattite ($CuSO_4 \cdot 3H_2O$), chalcanthite ($CuSO_4 \cdot 5H_2O$), pickeringite ($MgAl_2(SO_4)_4 \cdot 22H_2O$), magnesioaubertite ($(Mg,Cu)Al(SO_4)_2Cl \cdot 14H_2O$), halotrichite ($FeAl_2(SO_4)_4 \cdot 22H_2O$), hexahydrite ($MgSO_4 \cdot 6H_2O$), and gypsum. Due to their high activity in the low pH oxidation zone, these mobile elements may substitute into secondary phases as Al in jarosite, or K replacement by Cu and Zn in biotite.

The availability of the mobilized metals as water-soluble phases under arid conditions makes it necessary to prevent the flush-out during seasonally strong rainfalls even in very arid conditions. The hazardous potential of such impoundment, especially if they are constructed near rivers or with connection with the groundwater, therefore should not be underestimated.

Acknowledgements

We thank the management and the geologists and all stuff involved in this project from CODELCO for their interest, the access to their properties, their logistic support and their collaboration, especially A. Piug (Exploration Division, CODELCO), L. Serrano, R. Vargas, C. Aguila, C. Castillo, and M. Bustos (Division Andina, CODELCO), F. Celhay, A. Morales (Division El Teniente, CODELCO), J. Blondel, and R. Novajas (Division Salvador, CODELCO). For their support in Chile in the field work, sampling, sample preparation, and analytical approaches we would like thank to G. Cáceres and K. Eppinger (IDICTEC – University of Atacama), S. Elqueta (Geological Department, University of Chile, Santiago), B. Escobar, J. Wiertz, and J. Casas (Chemical Department, Biometallurgy, University of Chile, Santiago), R. Troncoso, A. Hauser, C. Reuschmann, C. Espejo, E. Fonseca, W. Vivallio, I. Aguirre (Servicio Nacional de Geología y Minería SERNAGEOMIN), W. Eberle, and H.W. Müller (Bundesanstalt für Geowissenschaften und Rohstoffe BGR). The project is supported by the German Academic Exchange Service (DAAD) and the Swiss National Science Foundation project No. 21-50778.97.

References

Acker, J.G., Bricker, O.P. (1992): The influence of pH on biotite dissolution and alteration kinetics at low temperature. Geochimica et Cosmochimica Acta, v. 56, p. 3073-3092.

Alpers, C.N., Brimhall, G.H. (1989): Paleohydrologic evolution and geochemical dynamics of cumulative supergene metal enrichment at La Escondida, Atacama Desert, northern Chile. Economic Geology, v. 84, p. 229-255.

Alpers, C.N., Nordstrom, D.K. and Ball, J.W. (1989): Solubility of jarosite solid solutions precipiated from acid mine waters, Iron Mountain, California, U.S.A. Sci.Géol., Bull., Strasbourg, v. 42,4, p.281-298.

Alpers, C.N., Rye, R.O., Nordstrom, D.K., White, L.D. and King, B.-S. (1992): Chemical, crystallographic and stable isotopic properties of alunite and jarosite from acid-hypersaline Australian lakes. Chemical Geology, v. 96, p. 203-226.

Alpers, C.N., Nordstrom, D.K. and Thompson, J.M. (1994): Seasonal variations of Zn/Cu Ratios in acid mine water from Iron Mountain, California. In: Alpers, C.N. and Blowes, D.W. (eds.): Environmental Geochemistry of Sulfide Oxidation. ACS Symposium Series, Washington, DC, v. 550, p. 324-344.

Alpers, C.N., Blowes, D.W., Nordstrom, D.K., and J.L. Jambor (1994): Secondary minerals and acid mine-water chemistry. In: Jambor, J.L. and Blowes, D.W. (eds.): Short Course Handbook on Environmental Geochemistry of Sulfide Mine Waste. Mineralogical Association of Canada, Nepean, v. 22, p. 247-270.

Bigham, J.M., Schwertmann, U., Carlson, L., Murad, E. (1990): A poorly crystallized oxyhydroxysulfate of iron formed by bacterial oxidation of Fe(II) in acid mine waters. Geochimica et Cosmochimica Acta, v. 54, p. 2743-2758.

Bigham, J.M., Carlson, L., Murad, E. (1994): Schwertmannite, a new iron oxyhydroxy-sulphate from Pyhäsalmi, Finland, and other localities. Mineralogical Magazine, v. 58, p. 641-648.

Bigham, J.M., Schwertmann, U., Traina, S.J., Winland, R.L., Wolf, M. (1996): Schwertmannite and the chemical modeling of iron in acid sulfate waters. Geochimica et Cosmochimica Acta, v. 60 (2), p. 185-195.

Blowes, D.W., Jambor, J.L. (1990): The pore-water geochemistry and the mineralogy of the vadose zone of sulfide tailings, Waite Amulet, Quebec, Canada, Applied Geochemistry, v. 5, p. 327-346.

Blowes, D.W., Reardon, E.J., Jambor, J.L., Cherry, J.A. (1991): The formation and potential importance of cemented layers in inactive sulfide mine tailings. Geochimica et Cosmochimica Acta, v. 55, p. 965-978.

Blowes, D.W., Ptacek, C.J. (1994): Acid-neutralization mechanisms in inactive mine tailings. In: Jambor, J.L. and Blowes, D.W. (eds.): Short Course Handbook on Environmental Geochemistry of Sulfide Mine Waste. Mineralogical Association of Canada, Nepean, v. 22, p. 271-291.

Boorman, R.S., Watson, D.W. (1976): Chemical processes in abandoned sulphide tailings dumps and environmental implication for Northeastern New Brunswick. CIM bulletin, v. 69, p. 86-96.

Borek, S.L. (1994): Effect of humidity on pyrite oxidation. In: Alpers, C.N. and Blowes, D.W. (Eds.), Environmental Geochemistry of sulfide oxidation, ACS Symposium Series 550, Washington, D.C., p. 31-44.

Brindley, G.W., Brown, G. (1980): Crystal structures of clay minerals and other X-ray identification, Mineralogical Society, London.

Brookins, D.G. (1988): Eh-pH diagrams for geochemistry. Springer, Berlin.

Camus, F. (1975): Geology of the El Teniente orebody with emphasis on wall-rock alteration. Economic Geology, v. 70, p. 1341-1372.

Cardoso Fonseca, E., Martin, H. (1986): The selective extraction of Pb and Zn in selected mineral and soil samples, application in geochemical exploration (Portugal). Journal of Geochemical Exploration, v. 26, p. 231-248.

Chao, T.T., (1984): Use of partial dissolution techniques in geochemical exploration. Journal of Geochemical Exploration, v. 20, p. 101-135.

Chao, T.T., Sanzolone, R.F. (1977): Chemical dissolution of sulfide minerals. Journal of Research U.S. Geol.Survey, v. 5, p. 409-412.

Chao, T.T., Zhou, L. (1983): Extraction techniques for selective dissolution of amorphous iron oxides from soils and sediments. Journal of Soil Sci. Soc. Am. Proc., v. 47, p. 225-232.

Clark, A.H. (1993): Are outsize porphyry copper deposits either anatomically or environmentally distinctive? In: Whiting, B.H., Hodgon, C.J. and Mason, R. (Eds.). Giant ore deposits, Society of Economic Geologists, Special Publication, v. 2, p. 213-283.

CIMM (1994): Caracterización quimica, granulometrica y mineralogica de muestras testigos de sondajes de relaves tranque Piuquenes, Santiago, Chile.

Craig, J.R., Vaughan, D.J. (1981): Ore microscopy and ore petrography. Wiley, New York.

Davis, B.S. (1997): Geomicrobiology of the oxic zone of sulfidic mine tailings. In: McIntosh, J.M. and Groat, L.A. (eds.): Short Course Handbook on Biological and Mineralogical Interactions. Mineralogical Association of Canada, Nepean, v.25, p. 93-112.

Departamento Concentrador Colon (1973): Informe anual 1973. Sociedad Minera El Teniente, internal report CODELCO, Colon.

Dirección General de Aguas (1996): Estadisticas pluviometricas originales, periodo 1960 – 1984, Santiago.

Division Andina, A. Descripción planta concentradora. Internal report CODELCO.

Division Andina, B. Descripción del tranque Piuquenes. Internal report CODELCO.

Division Andina (1996): Valores historicos de producción. Internal report CODELCO.

Division Salvador (1987): Superintendencia Concentradora. Internal report CODELCO.

Dold, B., Fontboté, L., Wildi, W. (1997): Mobilization and secondary enrichment processes in the sulfide porphyry copper tailings of Cauquenes (El Teniente) and Piuquenes (La Andina), Chile. VIII Congreso Geologico Chileno Actas, v. 2, p. 940-944.

Dold, B., Fontboté, L., Wildi, W. (1999): Detection and distribution of ferric oxyhydroxides and oxyhydroxide sulfates in sulfide mine tailings; their importance to selective metal retention and acid production. Mine, water and Environment, 1999 IMWA Congress, Sevilla, Spain, v. 2, p. 525-526.

Dzombak, D.A., Morel, F.M.M. (1990): Surface complexation modeling - Hydrous ferric oxides Wiley, New York.

Ehrlich, H.L. (1996): Geomicrobiology, Dekker, New York.

Fanfani, L., Zuddas, P., Chessa, A. (1997): Heavy metals speciation analysis as a tool for studying mine tailings weathering. Journal of Geochemical Exploration, v. 58, p. 241-248.

Farquhar, M.L., Vaughan, D.J., Hughes, C.R., Charnock, J.M., England, K.E.R. (1997): Experiminetal studies of the interaction of aqueous metal cations with mineral substrates: Lead, cadmium, and copper with perthitic feldspar, muscovite, and biotite. Geochimica et Cosmochimica Acta, v. 61; p. 3051-3064.

Gatehouse, S., Roussel, D.W., Van Moort, J.C. (1977): Sequential soil analysis in exploration analysis. Journal of Geochemical Exploration, v. 8, p. 483-494.

Guilbert, J.M., Park, C.F. (1989): The Geology of ore deposits. Freeman, New York.

Gustafson, L.B., Hunt, J.P. (1975): The porphyry copper deposit at El Salvador, Chile. Economic Geology, v. 70, p. 857-912.

Gustafson, L.B., Quiroga, J. (1995): Patterns of mineralization and alteration below the porphyry copper orebody at El Salvador, Chile. Economic Geology, v. 90, p. 2-16.

Hall, G.E.M., Vaive, J.E., Beer, R., Hoashi, M. (1996): Selective leaches revisited, with emphasis on the amorphous Fe oxyhydroxide phase extraction. Journal of Geochemical Exploration, v. 56, p. 59-78.

Hall, G.E.M., Bonham-Carter, G.F. (Eds) (1998): Special Issue: Selective Extractions. Journal of Geochemical Exploration,v. 61.

Holmström, H., Ljungberg, J., Ekström, M., Öhlander, B. (in review): Secondary copper enrichment in tailings at the Laver mine, northern Sweden. Environmental Geology.

Hölting, B. (1989): Hydrogeologie. Enke, Stuttgart.

Ingeneria y Geotecnia LTDA, (1990a): Tranques de relaves Planta Division Andina. Levantamiento catastral de los tranques de relaves en Chile, p. 8-20.

Ingeneria y Geotecnia LTDA, (1990b): Tranques de relaves Division El Teniente de Codelco Chile. Levantamiento catastral de los tranques de relaves en Chile. P. 10-52.

Ingeneria y Geotecnia LTDA, (1990c): Tranques de relaves Pampa Austral (El Salvador). Levantamiento catastral de los tranques de relaves en Chile. p. 151-158.

Jang, H.J., Wadsworth, M.E. (1994): Kinetics of hydrothermal enrichment of chalcopyrite. In: Alpers, C.N. & Blowes, D.W. (eds.). Environmental Geochemistry of Sulfide Oxidation, ACS Symposium Series, Washington, DC, 550, p.45-58.

Jambor, J.L. (1994): Mineralogy of sulfide-rich tailings and their oxidation products. In: Jambor, J.L. and Blowes, D.W. (eds.): Short Course Handbook on Environmental Geochemistry of Sulfide Mine Waste. Mineralogical Association of Canada, Nepean, v. 22, p. 59-102.

Jambor, J.L., Blowes, D.W. (1998): Theory and applications of mineralogy in environmental studies of sulfide-baring mine waste. In: MAC Short Course, v. 27, p. 367-401.

Lin, Z., Qvarfort, U. (1996): A study of the Lilla Bredsjön tailings impoundment in mid-Sweden - a comparison of observations with RATAP model simulations. Applied Geochemistry, v. 11, p. 293-298.

Linacre, E., Geerts, B. (1997): Climates and weather explained. Routledge, London.

Lowell, J.D. (1974): Regional characteristics of porphyry copper deposits of the Southwest. Economic Geology, v. 69, p. 601-617.

Lowell; J.D., Guilbert, J.M. (1970): Lateral and vertical alteration mineralization zoning in porphyry ore deposits. Economic Geology, v. 65, p. 373-408.

Malmström, M., Banwart, S. (1997): Biotite dissolution at 25°C. the pH dependence of dissolution rate and stoichometry. Geochimica et Cosmochimica Acta, v. 61; p. 2779-2799.

McCarty, D.K., Moore, J.N., Marcus, W.A. (1998): Mineralogy and trace element association in an acid mine drainage iron oxide precipitate; comparison of selective extractions. Applied Geochemistry, v. 13, p. 165-176.

McGregor, R.G., Blowes, D.W., Robertson, W.D. (1995): The application of chemical extractions to sulphide tailings at the Copper Cliff tailings area, Sudbury, Ontario. Sudbury '95 Proceedings, v. 3, p. 1133-1142.

Mercado, M. (1978): Avance geológico de la hoja Caldera, Region de Atacama. Instituto de Investigaciones Geológicas, Mapas Geológicos Preliminares de Chile, Escala 1:25 000, N°1, Santiago de Chile.

Moore, D.M., Reynolds, R.C. (1997): X-ray diffraction and the identification and analysis of clay minerals, 2nd Ed. Oxford University Press, Oxford.

Morin, A.K., Hutt, N.M. (1997): Environmental geochemistry of minsite drainage. Practical theory and case studies. MDAG Publishing, Vancouver.

Nordstrom, D.K. and Alpers, C.N. (1999): Geochemistry of acid mine waste. In: Plumlee, G. S. and Logsdon, M.J. (Eds.)Reviews in Economic Geology, The environmental geochemistry of ore deposits. Part A: Processes, techniqoes, and health issues, v. 6A, p. 133-160.

Ribet, I., Ptacek, C.J., Blowes, D.W., Jambor, J.L. (1995): The potential for metal release by reductive dissolution of weathered mine tailings. Journal of Contaminant Hydrology, v. 17(3), p. 239-273.

Schulze, D.G. (1981): Identification of soil iron oxides minerals by differential x-ray diffraction. Soil Sci. Soc. Am. J., v. 45, p. 437-440.

Schulze, D.G. (1994): Differential x-ray diffraction analysis of soil material. In: Quantitative methods in soil mineralogy, SSSA Miscellaneous Publication, p. 412-429.

Schwertmann, U., Schulze, D.G., Murad, E. (1982): Identification of ferrihydrite in soils by dissolution kinetics, differencial x-ray diffraction, and Mössbauer Spectroscopy. Soil Sci. Soc. Am. J., v. 46, p. 869-875.

Schwertmann, U. (1964): Differenzierung der Eisenoxide des Bodens durch Extraktion mit Ammoniumoxalat Lösung. Zeitschrift für Pflanzenernährung und Bodenkunde, v. 105, p. 194-202.

Schwertmann, U., Bigham, J.M., Murad, E. (1995): The first occurrence of schwertmannite in a natural stream environment. European Journal of Mineralogy, v. 7, p. 547-552.

Schwertmann, U., Friedl, J., and Stanjek, H. (1999): From Fe(III) ions to ferrihydrite and then to hematite. Journal of Colloid and Interface Science, v. 209, p. 215-223.

Serrano, L., Vargas, R., Stambuk, V. (1996): The late Miocene to early Pliocene Rio Blanco-Los Bronces copper deposit, Central Chilean Andes. In: Camus, F., Sillitoe, R.H., Petersen, R. (Eds.): Andean copper deposits: new discoveries, mineralization, styles and metallogeny, Soc.Econ.Geol.Spec.Publ. v. 5, p. 119-130.

Singer, P.C., Stumm, W. (1970): Acid mine drainage: the rate-determining step. Science, v. 167, p. 1121-1123.

Sondag, F. (1981): Selective extraction procedures applied to geochemical prospecting in an area contaminated by old mine workings. Journal of Geochemical Exploration, v. 15, p. 645-652.

Stambuk, V., Blondel, L., Serrano, L. (1982): Geológia del yacimiento Río Blanco. Congreso Geologico Chileno, 3rd, Conception, Actas, v. 2, p. E419-E442.

Stoffregen, R.E., Alpers, C.N. (1992): Observation on the unit-cell dimensions, H_2O contents, and δD values of natural and synthetic alunite. American Mineralogist, v. 77, p. 1092-1098.

Stone, A.T. (1987): Microbial metabolites and the reductive dissolution of manganese oxides: Oxalate and pyruvate. Geochimica et Cosmochimica Acta, v. 51; p. 919-925.

Stumm, W., Sulzberger, B. (1992): The cycling of iron in natural environments: Considerations based on laboratory studies of heterogeneous redox processes. Geochimica et Cosmochimica Acta, v. 56; p. 3233-30257.

Tessier, A., Campbell, P.G.C., Bisson, M. (1979): Sequential extraction procedure for speciation of particulate trace metals. Analytical Chemistry, v. 51, p. 844-851.

Titley, S.R. (1982): Advances in geology of the porphyry copper deposits, Southwesten North America. Univ. Ariz. Press, Tucson.

Tuovinen, O.H., Niemelae, S.I., Gyllenberg, H.G. (1971): Tolerance of Thiobacillus ferrooxidans to some metals. Antonie van Leeuwenhoek, v. 37, p. 489-496.

Tuovinen, O.H., Kelley, B.C. (1973): Studies of the growth of Thiobacillus ferrooxidans. Archiv of Mikrobiologie, v. 88, p. 285-298.

Webster, J.G., Swedlund, P.J., Webster, K.S. (1998): Trace metal adsorption onto an acid mine drainage iron(III)oxyhydry sulfate. Environmental Science & Technology, v. 32,10, p. 1362-1368.

CHAPTER 6

6 Influence of carbonate-rich primary mineralogy and of impoundment construction on element mobility and secondary enrichment processes in sulfide tailings impoundments - examples from the Fe-oxide Cu-Au deposits from the Punta del Cobre belt, northern Chile

Abstract

The geochemical and mineralogical study of two flotation tailings sites (Ojancos and P. Cerda) from the Fe-oxide Cu-Au Punta del Cobre belt, south of Copiapó, northern Chile, give insight in the influence of carbonate-rich mineralogy and of impoundment construction to element mobility and to enrichment processes in arid climates. Both Ojancos and P. Cerda tailings filled valley dam impoundments (impoundment No. 2 and No. 4, respectively) and after operation ceased, new tailings were deposited upstream (Ojancos "2H" and P. Cerda No. 6). The Ojancos tailings are characterized by the alternation of several meter thick intervals with high neutralizing potential (about 40 wt.% calcite and 2 wt.% pyrite) and intervals with high acid potential (about 3 wt.% calcite and 4 wt.% pyrite), whereas in the P. Cerda impoundment the neutralization potential is more homogenously distributed and generally exceeds the acid potential (about 10 wt.% calcite and up to 2.5 wt.% pyrite).

In the study of the Ojancos tailings impoundment No. 2 it was possible to discriminate between primary differences in the ores treated during the plant history and superimposed secondary processes leading to element enrichment associated with sulfide oxidation processes. To differentiate between primary and secondary mineralogy, studies of polished sections, X-ray diffraction (XRD), differential X-ray diffraction (DXRD), and scanning electron microscopy (SEM-EDS), as well as ICP-AES analyses of 7 step sequential extractions were performed. The upper part of the Ojancos impoundment No. 2 consists of dark gray, primary zone (pH 7-8) about 3 m thick resulting from recent deposition coeval to the "2H" tailings deposited further uphill. At depth, a neutral calcite-rich "paleo" oxidation zone is characterized by alternating coarse, dark gray, mainly unoxidized horizons with fine-grained, reddish-brown to ochre oxidized layers. A homogeneous, acidic (paste pH 4), reddish-brown cementation zone, with low permeability, rich in gypsum and higher ordered ferrihydrite (5-line to 6-line), goethite, locally minor jarosite, and low sulfide contents appears in the lower 2 m of the drill cores. The "2H" tailings recently deposited uphill have high acid potential leading to the formation of AMD evidenced by the appearance of acidic effluent with the precipitation of schwertmannite (pH 3.15) and chalcoalumite (pH 4.9) at the contact of the "2H" tailings with impoundment No. 2. This AMD contributes to the formation of the cementation zone in the older downstream impoundment No. 2. The cementation zone is characterized by Fe(III) hydroxides (5 to 6-line ferrihydrite) formed by the relatively slow oxidation (and hydrolysis) of ferrous iron and associated strong enrichment of heavy metals, detected mainly in the sequential extraction fractions of exchangeable ions, Fe(III) hydroxides and oxides, and of secondary Cu-sulfides (covellite).

The neutralization potential (from calcite and dolomite) of the P. Cerda tailings is high enough to maintain pH at neutral values. Nevertheless, pyrite oxidation takes place, as shown by the formation of an oxidation zone with precipitation of secondary Fe(III) hydroxides essentially

in the fine grained horizons, similarly as in the oxidation zone from Ojancos No. 2. The fact that the coarser, more sulfide-rich horizons do not display significant oxidation suggest that their water retention capacity is too low to effectively enable oxidation under the prevailing extreme arid conditions. The total absence of secondary efflorescent salts at the top of the P. Cerda tailings impoundments indicates that the carbonate-buffered neutral pH suppresses the climate induced upwards migration of liberated elements during sulfide oxidation via adsorption.

6.1 Introduction

Two case studies of tailings impoundments of Fe-oxide Cu-Au deposits from the Punta del Cobre belt, Copiapó, northern Chile (Marschik and Fontboté, 1996, Marschik et al. 1997, Marschik and Fontboté, in review) are presented in this work (Fig. 1). Pyrite and chalcopyrite are the main sulfide minerals in the mines of the Punta del Cobre belt and calcite is locally important as gangue mineral. The aim of this study is to investigate the potential of sulfide oxidation and element mobilization in relatively carbonate-rich mine tailings under arid conditions and to compare the results to carbonate-poor porphyry copper tailings (chapter 5).

Beside the neutralizing role of carbonate minerals, there are others aspects to be considered in carbonate-rich tailings. Lapakko et al. (1997) demonstrated in laboratory studies with mixing of acid-producing tailings with limestone and Holmström et al. (1999) with carbonate-rich tailings that high carbonate content may decrease the sulfide oxidation rates. This is generally thought to be related to the coating of sulfide by secondary ferric phases. Blowes et al. (1998) reported that in high carbonate tailings (5 wt.% sulfide-S and 30 wt.% carbonate minerals) microbially mediated sulfide oxidation takes place. Evangelou and Huang (1994) suggest that CO_3 may even promote pyrite oxidation by promoting electron transfer via pyrite surface Fe(II)-CO_3 complexes.

Dold and Fontboté (in review) report the upwards migration of mobilized elements in strongly acidic porphyry copper tailings impoundments under arid conditions. These mobilized elements are mainly present in form of water-soluble efflorescent salts at the surface of the tailings. In the case of carbonate-rich tailings, the carbonates neutralize the acid produced by sulfide oxidation and pH values are much higher. One objective of this study is to evaluate whether the upwards migration of the mobilized element in arid climates also occurs in sulfidic tailings impoundments with high carbonate contents.

In addition to the influence of the primary mineralogy on sulfide oxidation and element mobilization, the influence of impoundment construction technique and history on secondary processes will be outlined. In areas with pronounced topography, valley dam construction techniques are mainly used and consist of tailings deposition upstream from a dam closing the valley. Continuos operation of the flotation plant beyond the originally planned impoundment capacity makes additional space necessary to deposit the waste material. An often-applied solution is to construct a new valley dam impoundment directly upstream of the older one. This leads to a situation where the seepage of the active tailings impoundment will infiltrate into the older tailings (Fig. 2). In this chapter, two examples will be presented in which sulfide oxidation

takes place in the upstream deposited tailings. This results in the formation of metal-rich, acidic solutions that seep downstream and lead to precipitation of secondary minerals and to metal enrichment in the older tailings impoundment.

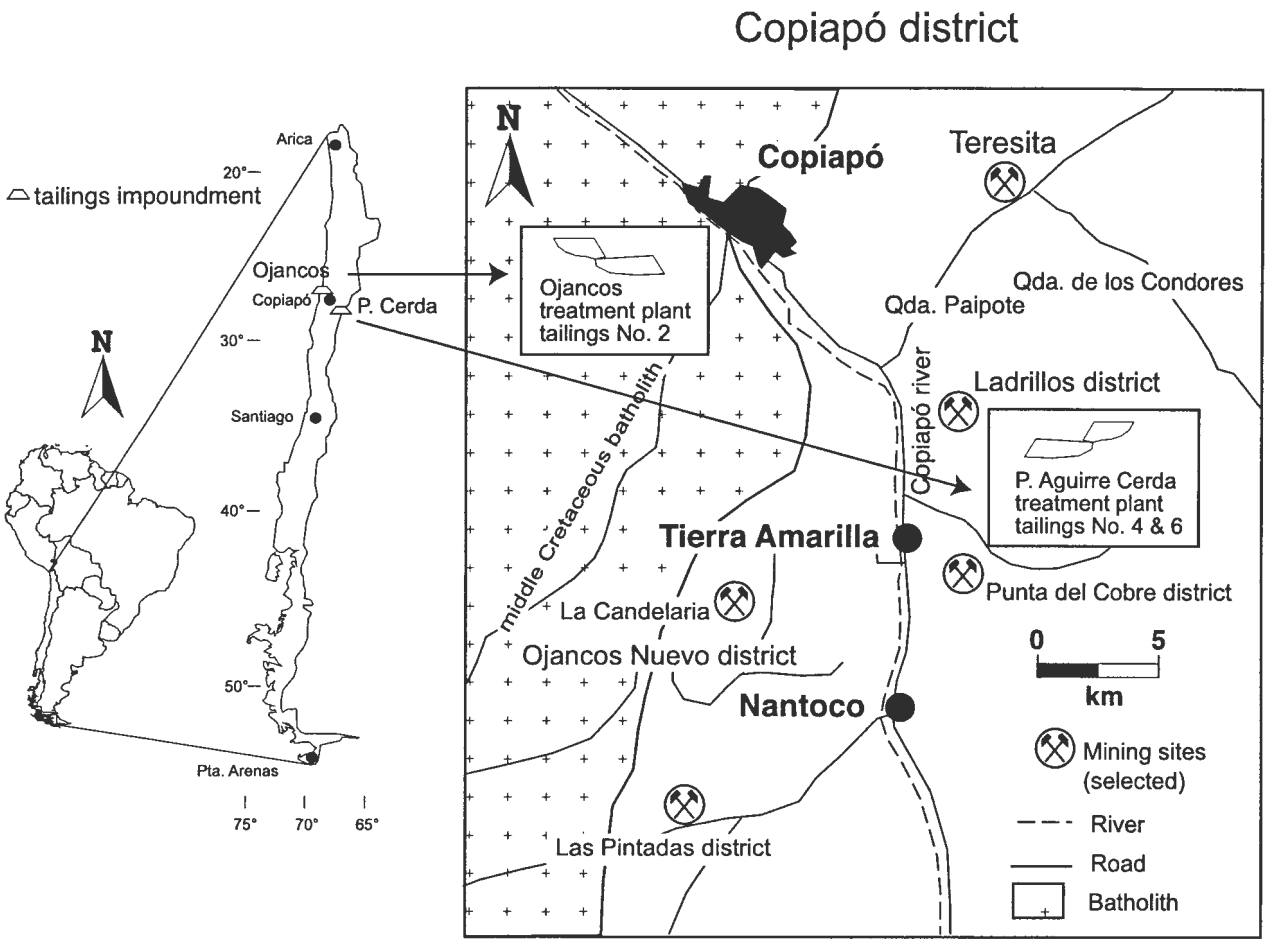

Fig. 1: Overview of the sampled tailings impoundments from the Ojancos flotation plant and the P. Cerda flotation plant, Copiapó district, northern Chile.

6.2 Regional geology and ore geology

The Cretaceous Fe-oxide Cu-Au Punta del Cobre belt, northern Chile, includes the mining districts of Punta del Cobre, Ladrillos, Las Pintadas, as well as the newly discovered giant deposit at the La Candelaria mine (Fig. 1). The area has been a traditional center of the Chilean middle-size mining industry since the early 1900s. Copper ores have been processed by flotation since 1929. Recent studies that have focused on the mineralization and alteration in the Punta del Cobre Belt include those of Hopf (1990), Schönfelder (1990), Marschik (1996), Marschik and Fontboté (1996), Ryan et al. (1995), Marschik et al. (1997), and Marschik and Fontboté (in review).

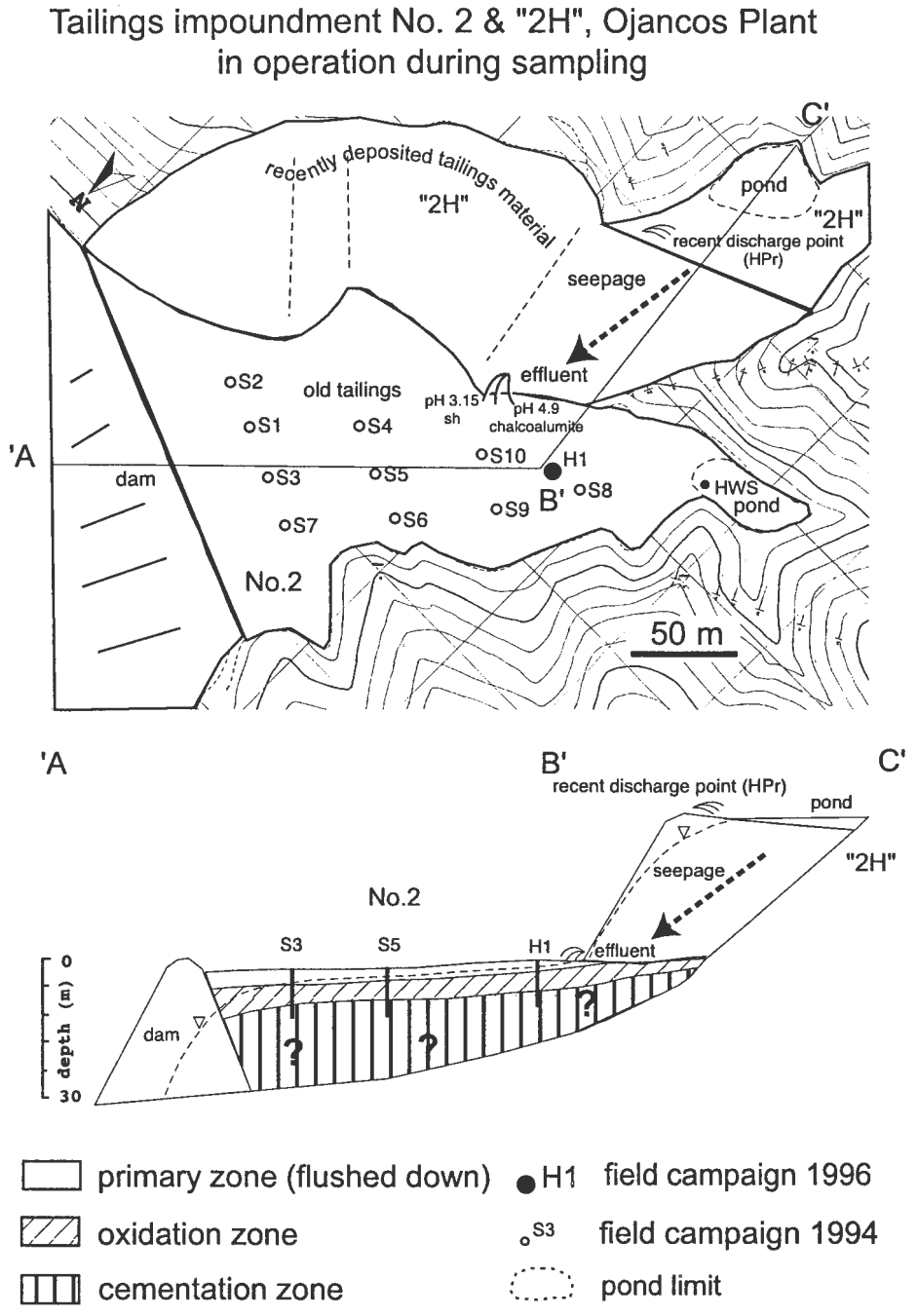

Fig. 2: Overview of the tailings impoundment No. 2 of the Ojancos flotation plant with the recent deposition of the tailings at "2H" at the hillside of impoundment No. 2. The deposition at "2H" was active during sampling.

The Punta del Cobre Formation, exposed in the core of the Tierra Amarilla anticline, consists mainly of altered volcanic and volcanoclastic rocks. It includes epiclastic breccias, sandstone, siltstone, and, in its upper part, chert and limestone. The outcrop pattern of the Punta del Cobre Formation is controlled by the N-S trending anticline and NNW- to NW-trending high angle faults.

Marschik and Fontboté (1996) differentiated five main alteration types at the Punta del Cobre belt. An early episode of hydrothermal alteration caused extensive albitization (albite-quartz-chlorite, ± sericite ± calcite) which was locally superimposed by potassic alteration (K-feldspar-quartz-chlorite/biotite ± sericite ± calcite ± tourmaline). The other three alteration types are located adjacent to the middle Cretaceous batholith in the western part of the area. They are characterized from west to east by the mineral assemblages of Ca-amphibole ± biotite ± sericite, biotite ± chlorite ± sericite ± epidote, and epidote-chlorite ± quartz ± calcite.

The mineralization at Punta del Cobre is characterized by a simple hypogene mineral assemblage including (in decreasing order of importance) pyrite, magnetite or hematite, and chalcopyrite. Sphalerite is observed locally. Gangue is dominantly calcite with minor quartz. Lens-shaped ores ("mantos"), are underlain generally by breccia bodies and veins (Marschik, 1996). A general trend of increased calcite content with greater distance from the middle Cretaceous Andean batholith is observed in the different deposits in the region. Thus, the Teresita ores (mantos emplaced in limestone) and the mines in the eastern part of the Punta del Cobre belt (e.g., Socavón Rampla, Augustina, and Bateas) higher calcite contents than the La Candelaria mine and the Las Pintadas district (Fig. 1). Additionally, the first mined upper parts of the sequence of the Punta del Cobre belt were, in general, richer in calcite than the lower, quartz-rich areas (R. Marschik, 1999; personal communication).

6.3 Climate

The Copiapó valley is located in the Atacama desert. The climate is hyper-arid with an average rainfall from 1904 – 1988 of 20,7 mm/a (Geotechnica, 1996). The averages of maximal, median and minimal absolute temperature values in the period of 1946 - 1977 are 32.1, 15.6, and –0.4 °C, respectively. The average of the relative humidity in the period from 1946 – 1977 measured at 8 a.m. was 87.5%, at 2 p.m. 51.0%, and at 8 p.m. 65.7%, reflecting the frequent presence of morning fog, which disappears generally at noon. Exceptional, strong rainfall may occur in association with the El Niño phenomenon, as in 1997. No data are available for evaporation rates. It must be assumed that the evaporation strongly exceeds the rainfall.

6.4 Description of the studied mine tailings impoundments

6.4.1 Tailings impoundment No. 2 from the Ojancos plant, Sali Hochschild S.A., Copiapó, northern Chile

6.4.1.1 Treatment processes

The Ojancos mineral treatment plant is located within the city of Copiapó directly behind the campus of the University of Atacama. This installation is owned and managed by the Compañia Minera Sali Hochschild S.A. It was the first treatment plant in the Copiapó mining district (1911) and treated during its long history copper, gold, and silver ores mainly by alkaline

flotation (pH 11), minor cyanidation, and heap leaching. The flotation plant started operation in 1936. Before 1982, all treated material was bought from external mines (Zamora, 1993). Although there are no reliable records regarding which mines the ore came, it is reasonable to assume that prior to 1982 the plant processed ore primarily from the Punta del Cobre belt, i.e. possibly mainly from the Teresita, Pintadas, Augustina, Socavón Rampla, Manto Verde, and Bateas mines. Since 1982, the Ojancos plant has treated only ore the Teresita and Las Pintadas mines (Fig. 1); plant operations shut down in 1998, due to low copper prices.

6.4.1.2 Tailings impoundment history

The Ojancos mineral treatment plant has four tailings impoundments. The present work studies tailings impoundment No. 2 which was in operation during the period of 1967 to 1977 (Fig. 2, Fig. 4A). It is situated over alluvial and fluvial alternating silty and clayey sands with gravels and conglomerate intercalations at an altitude of 100 m a.s.l. About 1987 (B. Zamora, 1996, Hochschild. S.A., Copiapó, personal communication), the Ojancos plant started the deposition of the coarse tailings fraction (separated by cyclones) of ores from the Teresita and Las Pintadas mines on the hillside upstream of impoundment No. 2 (Fig. 4A). The recent tailings at the hillside are referred to as the "2H" to differentiate them from the original "No. 2". Deposition of "2H" tailings was still active during the sampling period (1994-1997). Each month, slurry with 4000 m^3 of water was deposited on the hillside above impoundment No. 2. Due to the active operation it was not possible to sample the "2H" tailings and only one sample from the discharge point (HPr, fig. 2) could be taken. The dam for impoundment No. 2 is constructed mainly with material from heap leaching. During the original operating time of the impoundment No. 2 (1967 – 1982) cyanidation was not in operation (Zamora, 1993) so that the tailings in this impoundment are assumed to be totally from the flotation process. The fine fraction from the operations during the sampling period (1994-1997) were deposited in tailings impoundments No. 3 and No. 4, which are situated about 3 km northwest of the plant.

6.4.2 Tailings impoundments No. 4 and 6, Pedro A. Cerda treatment plant Ojos del Salado deposits, south of Copiapó.

The old tailings impoundments No. 4 and 6 of the Pedro de Aguirre Cerda treatment plant (P. Cerda), were selected due to the expected similarities in mineralogy and deposition technique with the more recent Ojancos tailings impoundment No. 2 (Fig. 3, Fig. 4D).

6.4.2.1 Treatment process

The flotation treatment plant P. Cerda is located next to the village Tierra Amarilla, about 15 km south of the town of Copiapó. It started operation in 1929 and in 1984 it was bought by the Compañia Minera Ojos del Salado. The plant uses an alkaline flotation circuit.

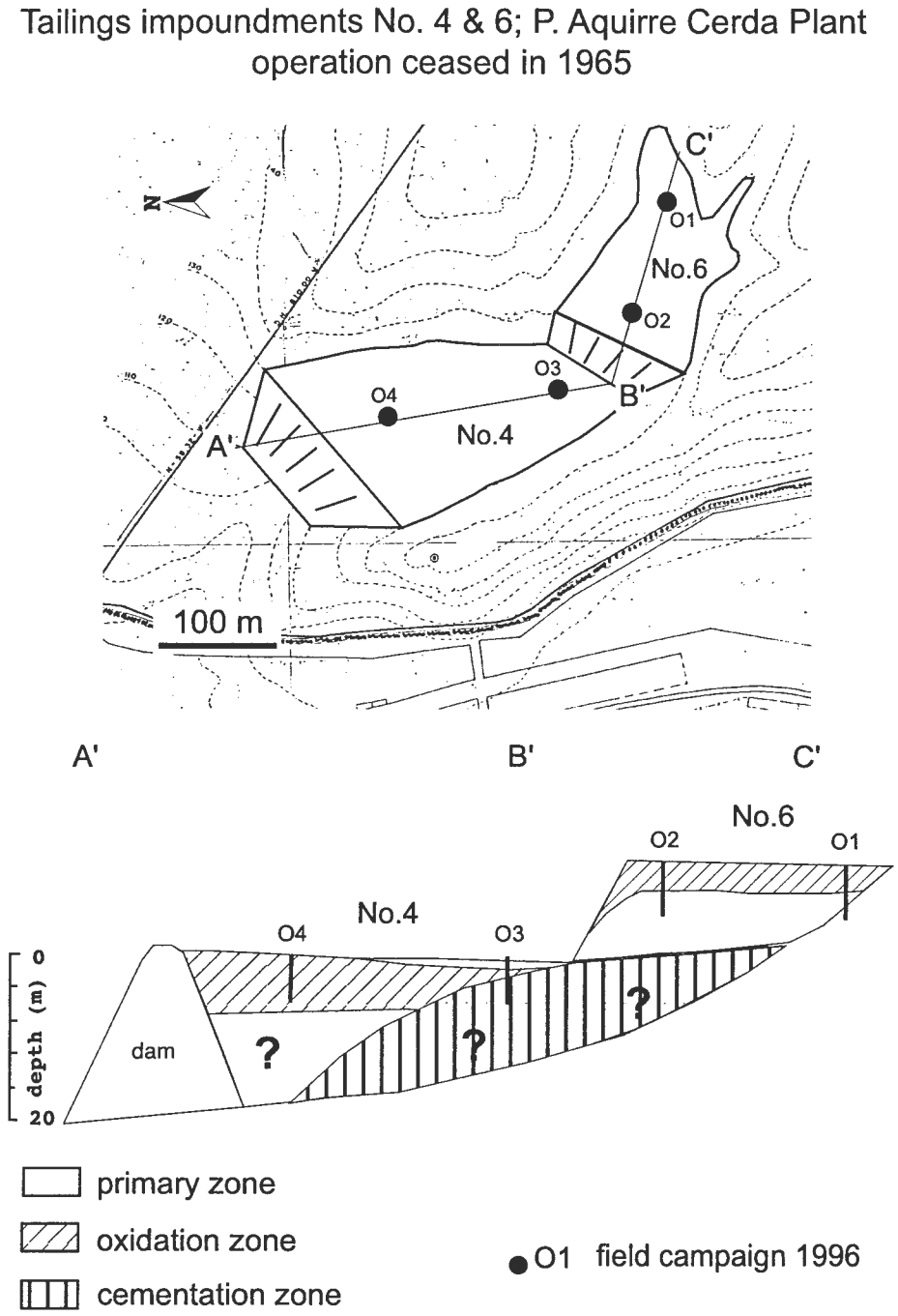

Fig. 3: Overview of the tailings impoundments No. 4 and 6 of the flotation plant P. Cerda. These tailings are out of operation since 1965.

6.4.2.2 Tailings history

The P. Cerda plant has presently one tailings impoundment in operation, situated 1.8 km northwest of the plant, and six older tailings impoundments. The old impoundments No. 4 and 6 were the best suited for sampling. The treated material has its origin in the eastern part of Punta

del Cobre belt, possibly mainly from the mines Agustina, Bateas, Manto Verde, and Socavón Rampla, which were the principal mines in operation during the filling of the impoundments No. 4 and No. 6 (Hopf, 1987). The tailings impoundment No. 4 is located in a small valley closed by a dam at an altitude of 100 m a.s.l. Tailings impoundment No. 6 is situated directly upstream of the impoundment No. 4 (Fig. 3, Fig. 4D). Tailings impoundment No. 4 stopped operation around 1965 and No. 6 was active possibly until 1975. Therefore, for an approximately ten year period, the seepage from tailings impoundment No. 6 flowed into the tailings No. 4. Both tailings are located over Atacama gravels of Miocene age.

6.5 Methology

6.5.1 Sampling and field methods

A total of 15 holes were drilled and 170 samples were obtained from the two studied tailings sites. In the first field campaign in 1994 in the Ojancos tailings impoundment No. 2, 10 holes up to depths of 8 m were drilled with percussion sampling equipment, and 101 samples were obtained with a 100 x 2 x 2 cm sampling tube. In a second field campaign in 1996, an additional drill core H1 of 10m depth was sampled from the Ojancos impoundment No. 2 and four drill cores were sampled on the Ojos del Salado tailings impoundment No. 4 and 6. Up to 5 samples of 20 cm length per meter were taken in the cementation zone and at the interface between the cementation and oxidation zones, whereas in the homogeneous primary zone only three samples were taken. In a third visit to Ojancos in 1997 eight samples of effluent precipitates at the foot of the recent coarse "2H" tailings were collected, pH was measured, and the samples were air-dried (Fig. 4B). The appearance of the effluents was associated with strong rainfalls in the El Niño year 1997, which flushed away a part of the "2H" tailings (Fig. 4B).

Fig. 4: ***A:*** *Photograph of the situation at the Ojancos impoundment No. 2 with the recently deposited tailings "2H" at the hill-site.* ***B:*** *AMD precipitates at the interface of both impoundments. HE5 with schwertmannite (sh) has pH 3.15, HE6 with chalcoalumite (chalm) has pH 4.9, and HE7 with gypsum (gy) has pH 4.54. Width of photo 100 cm.* ***C:*** *Detail of the P. Cerda tailings No. 4. The coarser layers are essentially not oxidized, whereas the fine grained horizons show precipitation of secondary Fe(III)hydroxides.* ***D:*** *Sampling on the tailings impoundment No. 6 of the P. Cerda flotation plant. Note that inspite the aridity no efflorescent salts are formed at the surface, due to neutral pH (in contrast to El Salvador tailings, chapter 5)* ***E:*** *Polished section with typical appearance of pyrite (py), magnetite (mt) and hematite (hm, specularite) in the primary zone of P. Cerda tailings impoundment No. 4 (sample O3/025).* ***F:*** *Pyrite (py) and magnetite (mt) as dominant ore minerals in the primary zone of the Ojancos tailings impoundment No. 2 (sample H1/100).* ***G:*** *Typical appearance of the fine-grained cementation zone with hematite (hm) and Fe(III) hydroxides in the P. Cerda tailings impoundment No. 4 (sample O3/300).* ***H:*** *The fine-grained cementation zone with relicts of pyrite (py), magnetite (mt), covellite (cv), and Fe(III) hydroxides in the Ojancos tailings impoundment No. 2 (sample H1/1000).*

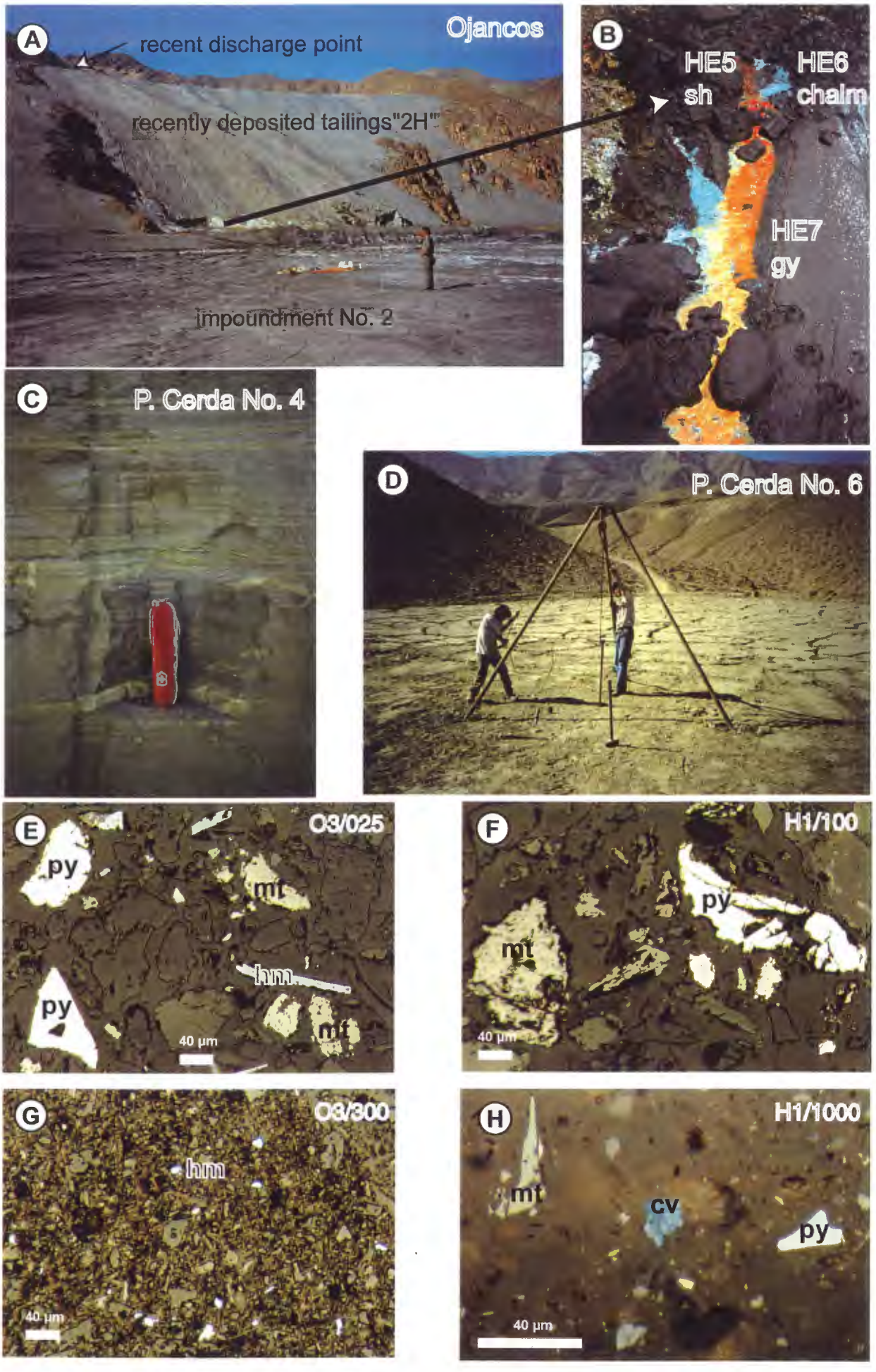
A
Ojancos
recent discharge point
recently deposited tailings"2H"
impoundment No. 2
B
HE5
sh
HE6
chalm
HE7
gy
C
P. Cerda No. 4
D
P. Cerda No. 6
E
O3/025
py
mt
hm
py
mt
40 µm
F
H1/100
py
mt
40 µm
G
O3/300
hm
40 µm
H
H1/1000
mt
cv
py
40 µm

The tailings samples were sealed in plastic bags and stored in an ice-packed cool box. Previously, the description of mineralogical characteristics, color and grain size estimation, and pH measurement (paste pH according to MEND, 1991; WTW® pH-meter) were noted. The samples were transported immediately to the IDICTEC laboratories, University of Atacama, for drying (< 35°C) and water content determination. The dry samples were homogenized and packed into polyethylene (PET) containers for conservation at room temperature.

6.5.2 *Physical properties*

The moisture content of all tailing samples was measured by the difference of sample weight before and after drying (< 35 °C). The particle size distribution of selected samples were measured by a Coulter® and a Fritsch Analysette® laser particle size analyzer. The hydraulic conductivity (K) was calculated after Hazen (1893, in Hölting, 1989) using the d_{10} concentrations. If the unconformity degree $U = d_{60}/d_{10}$ was higher than five, the correction after Beyer (1964, in Hölting, 1989) was applied.

6.5.3 *Mineralogical methods*

Polished sections and polished thin sections were prepared from selected bulk samples. Samples were analyzed as bulk sample by X-ray diffraction (XRD), using a Philips 3020 diffractometer with CuKα ($\lambda = 1.54056$ Å) and a monochromator. Scan settings were 3-70° 2θ, 0.02° step size, 2s count time per step. Procedures for identification of clay minerals were following Moore and Reynolds (1997) and Brindley and Brown (1980). First, the fraction < 2μm was separated by centrifugation and oriented samples were prepared on glass slides. Samples were then characterized by X-ray diffraction (XRD), with the same settings as given above.

The poorly crystalline Fe(III) hydroxides such as ferrihydrite were detected by differential X-ray diffraction (DXRD), following the methods described by Schulze (1981 and 1994). The samples from the cementation zone selected for DXRD were attacked by 0.2 M ammonium oxalate, pH 3, 80°C, 2h. Scans were measured before and after treatment. The treated scan was intensity corrected and then subtracted from the untreated scan. The resulting DXRD pattern was used for mineral determination. The diffractometer settings were those used by Bigham et al. (1990, 1994, and 1996), and Schwertmann et al. (1995), i.e., step scanning with 0.05° 2θ step size and 20 s counting time per step. The acid mine drainage effluents were characterized with the same settings as mentioned above. The mineral morphology and the qualitative element composition of the acid mine drainage precipitates were studied by scanning electron microscopy (SEM-EDS).

6.5.4 Geochemical methods

6.5.4.1 Mixed acid digestion (HNO_3, HF, $HClO_4$, HCl)

In a preliminary phase of the investigation, tailings samples from four representative drill cores (S1, S2, S3, S6, S7, S8, and S9) were completely digested with a mixture of HNO_3, HF, $HClO_4$, and HCl. Metal concentrations in the solutions were measured by ICP-MS and ICP-AES (Dold, 1994; Dold et al., 1996). The objective was to obtain an overall insight in the tailings composition.

6.5.4.2 Sequential extraction

The development of an extraction sequence applied to the secondary mineralogy of the studied tailings is reported in detail in chapter 3. In a first phase of the study a slightly modified 6-step sequential extraction ("sequence A", chapter 3) after Tessier et al. (1979) and Sondag (1981) was utilized: 1.) 1M NH_4-acetate, pH4.5, 2h; 2.) 0.1M Na-acetate, pH 5, 2h; 3.) 0.25M hydroxylamine-HCl, pH 2, 2h; 4.) 0.1M oxalic acid, pH 3.3, heat, 1h; 5.) H_2O_2 35%, heat 1h; 6.) HNO_3, HF, $HClO_4$, HCl. The extractions were applied to drill core H1 in order to acquire information regarding the element distribution and the presence of possible secondary phases. In a second phase of the study the sequence was modified to 7 steps ("sequence B", chapter 3) and adapted to the secondary mineralogy of the studied tailings (Table 1).

6.5.5 Acid-Base Accounting (ABA)

Total sulfur content was measured using a Leco® furnace. For measurement of the sulfate-S the 0.2 M oxalic acid hot 2h leach (iron oxides, e.g. jarosite, schwermannite, goethite, hematite, magnetite, ferrihydrite; chapter 3 and 4) was used. Sulfur was determined by ICP-ES. The differences of both results represent the sulfide-S content. Total and mineral carbon was analyzed by coulometric titration (Ströhlein CS 702®). The sulfide net neutralization potential (SNNP) was calculated in t $CaCO_3$/1000t, with the assumption that at neutral pH four moles of calcite (HCO_3^- dominant species at pH 7) are necessary for the neutralization of four moles H^+ produced by the oxidation of 1 mole of pyrite.

Table 1: *Sequential extraction "B" applied in this study (abbreviations: bn: bornite; ca: calcite; cb: cinnabar; cc: chalcocite; cv: covellite; cp: chalcopyrite; dg: digenite; fh: ferrihydrite; gn: galena; gt: goethite; gy: gypsum; hm: hematite; ilm: ilmenite; jt: jarosite; Na-jt: natrojarosite; mb: molybdenite; mt: magnetite; op: orpiment; py: pyrite; sh: schwertmannite; sl: sphalerite; stb: stibnite; tn: tennantite; tt: tetrahedrite).*

Leach	Preferentially dissolved minerals	References
(1) Water soluble fraction 1.0 g sample into 50ml deionizied H_2O shake for 1 h.	secondary sulfates, e.g., bonattite, chalcanthite, gy, pickeringite, magnesioauberite	chapter 5 and 6; Ribet et al., 1995; Fanfani et al., 1997
(2) exchangeable fraction 1M NH_4-acetate pH 4.5 shake for 2 hrs	ca, vermiculite-type-mixed-layer, adsorbed and exchangeable ions	chapter 5; Gatehouse et al., 1977; Sondag, 1981; Fonseca and Martin, 1986
(3) Fe(III) oxyhydroxides 0.2 M NH_4-oxalate pH 3.0 shake for 1 h. in darkness	sh, 2-line fh, secondary jt, MnO_2	Schwertmann, 1964; Stone, 1987; chapter 4
(4) Fe(III) oxides 0.2 M NH_4-oxalate pH 3.0 heat in water bath 80°C for 2 hours	gt, jt, Na-jt, hm, mt, higher ordered fh's (e.g., 6-line fh)	chapter 3.
(5) organics and secondary Cu-sulfides 35% H_2O_2 heat in water bath for 1 hour	organics , cv, cc-dg	Sondag, 1981;, chapter 5
(6) primary sulfides Combination of $KClO_3$ and HCl, followed by 4 M HNO_3 boiling	py, cp, bn, sl, gn, mb, tt, cb, op, stb	Chao and Sanzolone, 1977; Hall et al., 1996
(7) residual HNO_3, HF, $HClO_4$, HCL digestion	Silicates, residual	Hall et al., 1996; Dold et al., 1996

6.6 Results and discussion

6.6.1 Ojancos tailings impoundment No. 2

As mentioned above, the historical reports indicate that the flotation tailings deposited between 1967 and 1977 in the "old" Ojancos impoundment No. 2 come most likely from the Punta del Cobre belt. After 1977, there was a period of no deposition. The "2H" tailings deposited after 1987 and still being deposited during sampling at the hillside of impoundment No. 2 have their origin from the Teresita mine and the Pintadas district (Fig. 1, 2 & 4A). Thus, it has to be assumed that a mixed stratigraphy of carbonate-rich material from the Teresita mine with high neutralization potential and low-carbonate material from the Las Pintadas district with high acid potential characterize the composition of these recent tailings.

The results are presented following the present water flow path, i.e. in following order: recent discharge point (6.6.1.1), AMD effluents at the lower part of the recent coarse tailings "2H" (6.6.1.2), and the "old" impoundment No. 2, including a primary zone flushed down from the "2H" tailings and recently deposited on the top of the old tailings impoundment No. 2 (6.6.1.3).

6.6.1.1 Mineralogy and acid-base accounting of sample HPr from the recent discharge point for tailings "2H"

The present discharge point for the tailings "2H" has a pH of 11 (Fig. 2). The recently deposited tailings (sample HPr) consists mainly of quartz, alkali-feldspar (mainly albite), calcite, Ca-amphibole (magnesiohornblende), pyroxene (hedenbergite), magnetite, hematite, pyrite and minor chalcopyrite, and micas (biotite). Ca-amphibole ± sericite ± biotite is a typical alteration mineral assemblage in areas near the batholith (Marschik and Fontboté, 1996). According to available information, the source of the "2H" tailings is either the Las Pintadas district, close to the batholith, or the carbonate- hosted Teresita mine, the high pH of sample HPr appears to indicate its derivation from the Pintadas district.

ABA of the sample HPr shows a pyrite content of 3.5 wt.% and negative sulfide net neutralization potential (SNNP = -47.32 t $CaCO_3$/1000t), indicating that this material has acid-forming potential. It is assumed that others parts of the "2H" tailings have high NP, due to their reported provenance from the carbonate-hosted Teresita mine.

6.6.1.2 AMD effluents at the lower part of the recent deposited "2H" tailings

In a third site visit in November 1997, after exceptional strong rainfalls in the Copiapó valley, a small part of the "2H" tailings, directly at the contact with the old tailings impoundment No.2, was flushed away. This led to the appearance of acid effluents with the formation of orange-brown, pale blue, yellow and reddish precipitates (Fig. 4B). Three out-flows were located within a small area of 50 cm diameter. The center effluent had a pH of 3.15 with orange-brown colored precipitates. XRD patterns show typical features for schwertmannite ($Fe_8O_8(OH)_6SO_4$, with broad peaks at 1.51, 1.66, 2.28, 2.55, 3.39, and 4.86Å) and gypsum. SEM images show characteristic spherical forms of schwertmannite, 1 – 1.5 µm in size, reminiscent of sea-urchins (Fig. 2, see also chapter 4). EDS determinations reflect high iron content (Fig. 5A). The other two out-flows had pale blue precipitates and pH values of 4.90. XRD patterns with broad peaks at 4.25 and 8.5Å and SEM-EDS results indicate that the precipitate is mainly chalcoalumite ($CuAl_4(SO_4)(OH)_{12}•3H_2O$). The SEM image (Fig. 5B) shows very fine particles (< 1µm), reminiscent of dried raisins. At the confluence of the three effluents the pH was 4.54, the color changed to yellow, and the XRD detected mineral is gypsum.

The fact that the two geochemically different effluents discharge closely (20 cm distance), indicates that different geochemical conditions may co-exist in close vicinity in the tailings material and the percolation of these effluents may be seen as "acid spots", independent of the general bulk water composition.

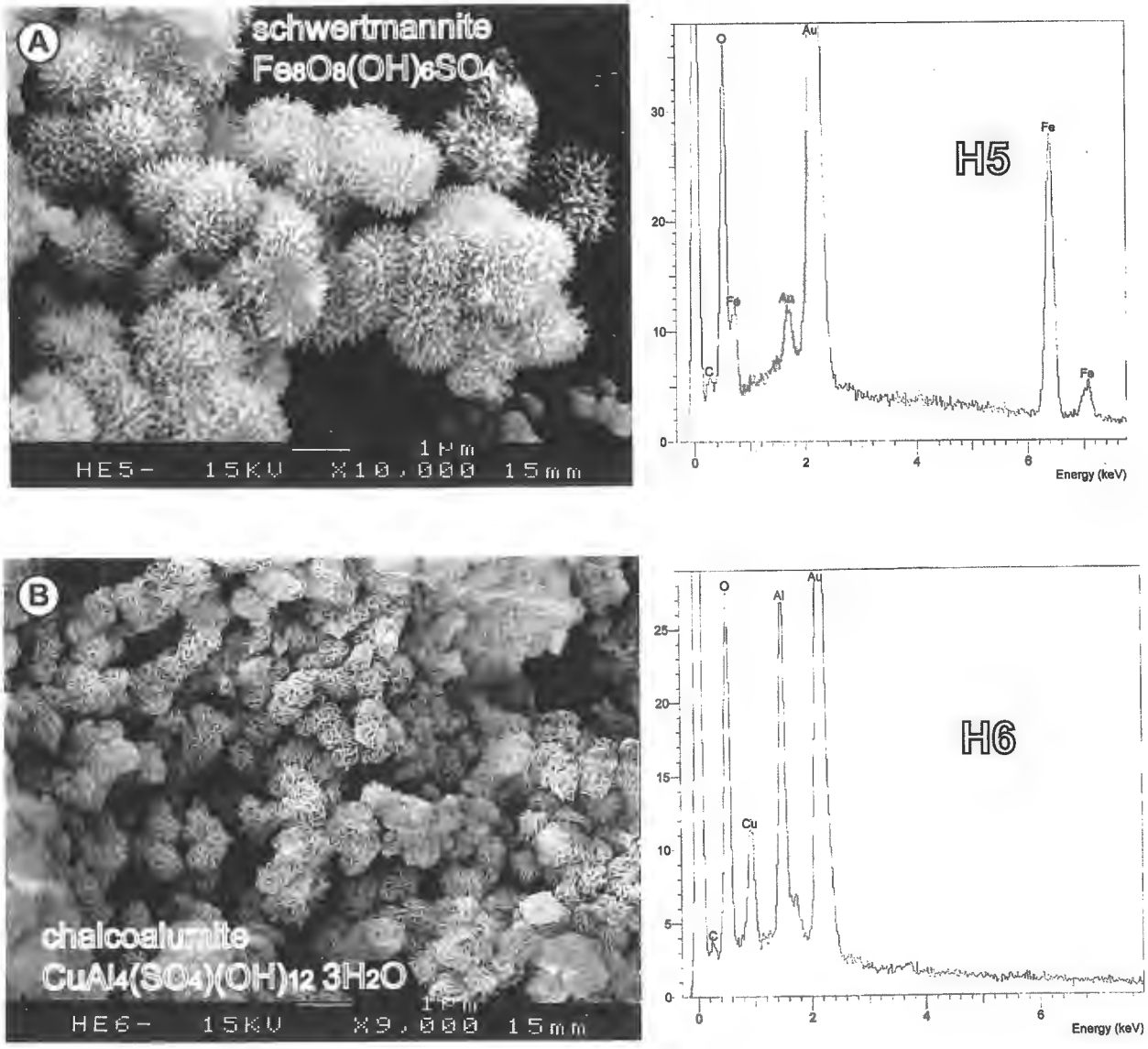

***Fig. 5**: A: SEM photograph of sample HE5 with EDS-spectrogram of schwertmannite, showing the typical spherical sea-urchin reminding morphology. B: SEM photograph with EDS of chalcoalumite (sample HE6).*

Additionally, high sulfate (formed during sulfide oxidation) and Ca (liberated by acid neutralization with calcite) concentrations in the water sample HWS, taken in 1996 from the small pond of the impoundment No. 2 (Fig. 2), which received surface seepage from "2H", indicate strong oxidation and neutralization reaction in the tailings "2H" (Results of HWS: pH = 7.55, T = 9.2 °C, conductivity = 13.61 mS/cm, O_2 = 6.7 mg/l, cations: Ca = 786 mg/l, Mg = 101 mg/l, Na = 2350 mg/l, K = 70 mg/l, Li = 0.15 mg/l, anions: SO_4 = 2836 mg/l, Cl = 3190 mg/l, HCO_3 = 109 mg/l, B = 7,2 mg/l, F = 1 mg/l, SiO_2 = 15 mg/l, metals: Cu = 0.12 mg/l, Sr = 4.6 mg/l, Mn = 0.36 mg/l, Ba = 0.04 mg/l, Mo = 0.05 mg/l, the other metals are below detection limit). The high Na concentrations may have its origin in the application of Isopropil Na-Xantate, a commonly applied collector in the flotation process.

6.6.1.3 Stratigraphy and acid-base accounting of the Ojancos tailings impoundment No.2

Ten cores were drilled in 1994 in the Ojancos tailings impoundment No. 2 to a maximum depth of 8 m. The cores revealed a similar stratigraphy with, from the top to the bottom, an about 3 m thick recent dark gray primary zone, an about 3 m thick dark gray colored oxidation zone with intercalations of oxidized horizons, and a homogeneous, reddish-brown cementation zone of which only about 2 m could be penetrated. A general dipping of the recognized zones and of the ground water level (e.g., ground water level at S8 = 1.2 m and S1 = 3.6 m) towards the dam can be recognized (Fig. 2). The stratigraphy, mineralogy and geochemistry of the Ojancos tailings impoundment No. 2 is discussed in detail using as an example, the representative drill core H1 (Fig. 9 and 10), which was sampled in 1996 to 10 m depth near drill core S8 from the 1994 campaign. Drill core H1 shows the same stratigraphy as S8 but the primary zone reaches a depth of 2.8 m, instead the 1.3 m found in S8. This indicates that in the two years between the drillings H1 and S8, 1.5 m of additional tailings material was flushed down from the "2H" tailings deposited uphill. The cementation zone starts in H1 at 8 m depth compared to 5.2 m in the nearby S8 drill hole. Change in grain-size from fine sandy-silty ($K = 1x10^{-7} - 3x10^{-7}$ m/s) in the primary and oxidation zones to clayey ($K = 3x10^{-8} - 4x10^{-8}$ m/s) in the cementation zone is observed. The moisture content graded from 15 wt.% in the primary zone to 25 wt.% in the oxidation zone and to 33 wt.% in the cementation zone.

Calculation of the pyrite content with the assumption that all sulfide sulfur is associated with pyrite, indicates pyrite contents of 3.5 - 4.8 wt.% in the primary zone, 1.5 - 2.9 wt.% in the oxidation zone, and 1 – 1.8 in the cementation zone.

The tailings of the primary zone have a SNNP of –83.4 to –158.5 t $CaCO_3$/1000t. In the oxidation zone the SNNP is positive (14.4 to 417.8 t $CaCO_3$/1000t), indicating that this material has a high neutralization potential (NP). This is consistent with abundant calcite (up to 47 wt.%) and low pyrite contents. Below the oxidation zone, and in spite of low sulfide content the ABA becomes negative again due to the decrease of calcite abundance, possibly because of neutralization reactions with down-seeping acid solutions. The stratigraphy of the Ojancos impoundment No. 2 is characterized by an interlayering of acid producing and neutralizing zones.

The drilled tailings show three intervals, which are distinguished on the basis of their primary silicate and carbonate mineralogy (Fig. 6). The first interval corresponds to the primary zone down to a depth of 2.8 m, which is dominated by quartz, alkali-feldspar (mainly albite), Ca-amphibole (magnesiohornblende), pyroxene (hedenbergite), magnetite, hematite, pyrite (Fig. 4F), and minor chalcopyrite, calcite, and micas (biotite). This mineral assemblage is very similar to that of the recent discharge point (sample HPr, section 6.6.1.1) and is also thought to derive from the Pintadas district (Fig. 1). These mineralogical data support the field observations, which indicate that the primary zone on the top of the old tailings impoundment No. 2 is being flushed down from the same recent discharge point, of the hillside tailings "2H".

Below, an interval from 2.8 to 7 m depth is characterized by abundant calcite and minor quartz, albite, magnetite and low pyrite, hematite, and mica contents. The source for this carbonate-rich zone may be the Teresita mine or another calcite-rich mine as mentioned in chapter 6.2. Below 7 m the assemblage is dominated by quartz-albite-calcite-chlorite ± epidote,

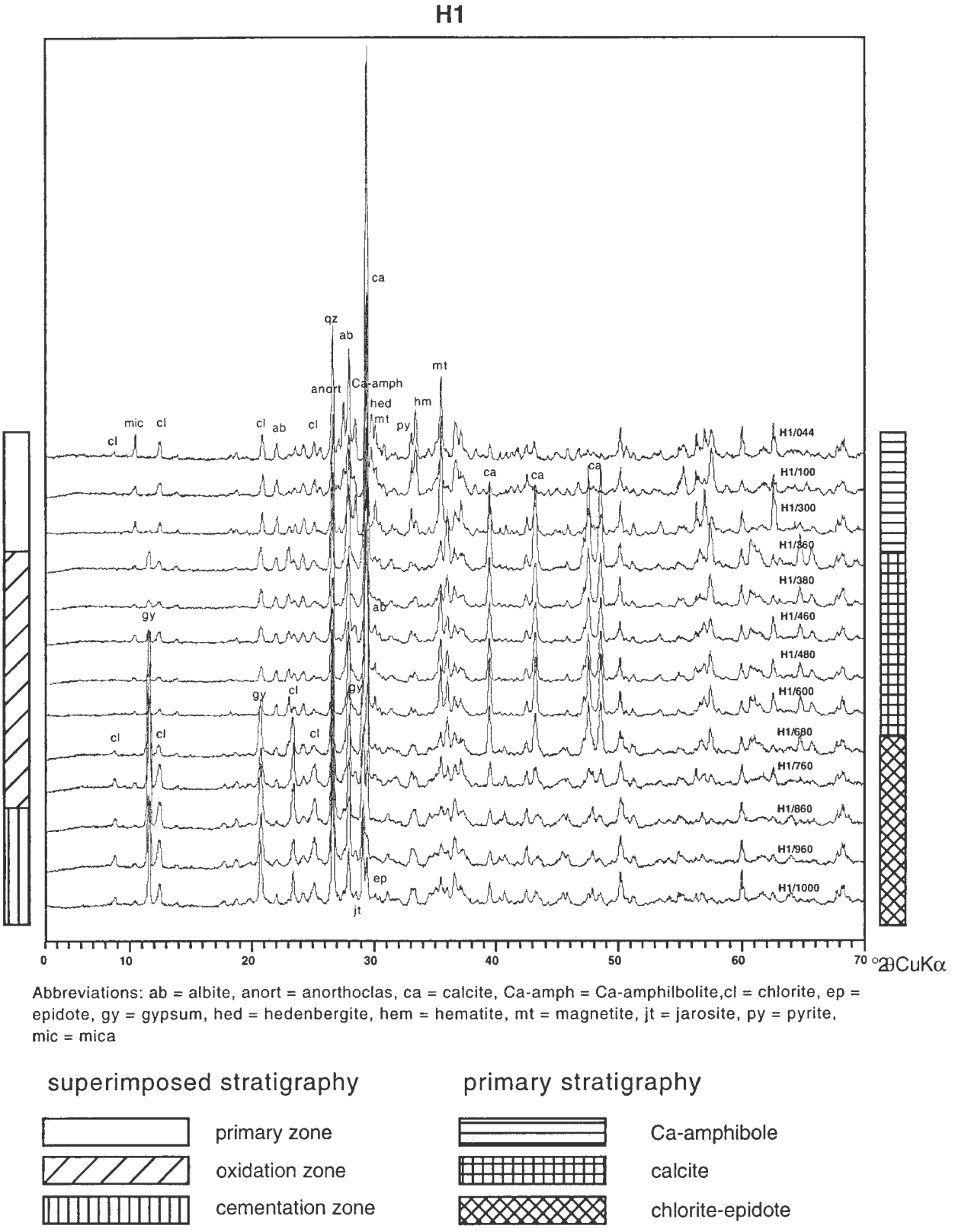

Fig. 6: Results of XRD from drill core H1 from the Ojancos impoundment No. 2. The stratigraphy and the proposed primary source of the tailings are shown.

suggesting that this material may come from a mine in the eastern part of the Punta del Cobre belt (Marschik and Fontboté, 1996).

The above described sections of the primary stratigraphy are superimposed by a secondary zonation resulting from weathering processes. Below the recent primary zone an oxidation zone follows between 2.8 to 8 m. This oxidation zone is characterized by the interlayering of coarser dark gray unoxidized layers with fine grained, Fe(III) hydroxide-rich, ochre to red-brown colored horizons. As mentioned above, the oxidation zone is calcite-rich with neutral pH values, which decrease in the lower part of the oxidation zone. The features of this oxidation zone are very similar to those found in the also carbonate-rich oxidation zone of the P. Cerda impoundments (Fig. 4C and chapter 6.6.2) and may be explained as follows. High evaporation in arid climates favors upwards migration via capillary force (chapter 5) and concentration of sulfide oxidation in fine grained horizons due to their higher water retention capacity. Generally, fine horizons are poorer in sulfides than coarser layers, because of gravity separation during deposition, so that lower sulfide contents are available for oxidation. The mobility of the liberated elements is very low due to the neutral pH values so that secondary Fe(III) hydroxides precipitate in-situ in the fine horizons, where the main sulfide oxidation takes place. This leads to a specific layering for oxidation zones of carbonate-rich tailings in arid climates.

The oxidation zone at the Ojancos impoundment No. 2 has to be seen as a "paleo"-oxidation zone, which formed in the ten years without operation (1977-1987), before operation started again uphill with the recent deposition of the "2H" tailings and the formation of the recent primary zone at the top of impoundment No. 2. It is important to mention here that this oxidation zone can not be the source of the element enrichment found in the lower part of the oxidation zone and the underlying cementation zone. A cementation zone is normally formed at the interface of a low pH oxidation zone, from where the element are mobilized, and a neutralizing primary zone, where the secondary minerals as Fe(III) hydroxides and sulfates precipitate (Blowes et al., 1991; Tassé et al., 1997, Lin, 1997). In the Ojancos No. 2 tailings, below the oxidation zone and down to the end of the drill holes (8 to 10 m) occurs a cementation zone with gypsum as the dominant phase (~ 9 wt.% gypsum equivalent), which is assumed to be mainly from tertiary origin. Subordinate 5-line and 6-line ferrihydrite (~ 4 – 5 wt.% $Fe(OH)_{3(S)}$ equivalent) together with goethite and jarosite could be determined by DXRD (Fig. 7). Pyrite, magnetite, and hematite are very minor phases and secondary covellite can be observed in the cementation zone as fine disseminated grains (Fig. 4H). The low sulfide contents can be explained because of oxidation by Fe(III). Calcite contents decrease in the lower part of the oxidation zone and are completely lacking in the cementation zone. The pH also decreases from values around 7 down to 5 in the lower part of the oxidation zone and is buffered in the cementation zone possibly by ferrihydrite to values around 4. The deepest sample H1/1000 (depth 10 m) shows again XRD detectable calcite and a pH value of 6.

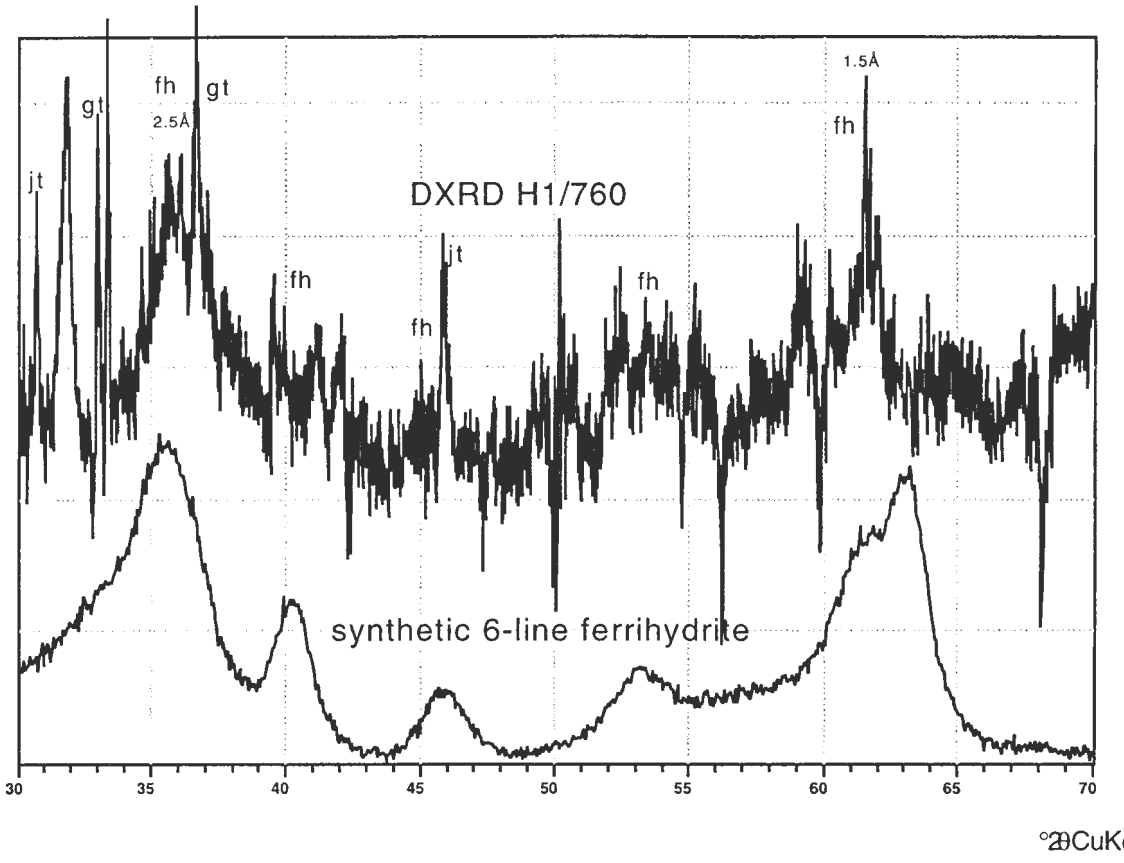

Fig. 7: *Fig. 6: DXRD of higher ordered ferrihydrite (5-line) with goethite and minor jarosite of the sample H1/760 of the cementation zone from Ojancos impoundment No. 2. For comparison a diffractogram of a synthetic 6-line ferrihydrite is shown.*

6.6.1.4 Geochemical results

As mentioned above, in a preliminary stage of this investigation, total digestion analyses were performed. The results from drill cores S1, S2, S3, S6, S7, S8, and S9 show maximum values of all heavy metals in an interval spanning the upper part of the cementation zone and the lower part of the calcite-rich oxidation zone. The intensity of the heavy metal peaks decrease with increasing distance from the seepage input as seen in Fig. 8 which shows a depth profiles for drill holes S8, S9, S6, and S7. As total digestion results give limited information about geochemical processes, they will not be discussed here in detail but data are available in appendix 4.

In this section the results of analyses of sequential extractions of the representative drill core H1 (located close to S8) are shown in Fig. 9 and Table 2 (sequence A) and in Fig. 10 and Table 3 (sequence B for some selected samples). For better visibility of the geochemical

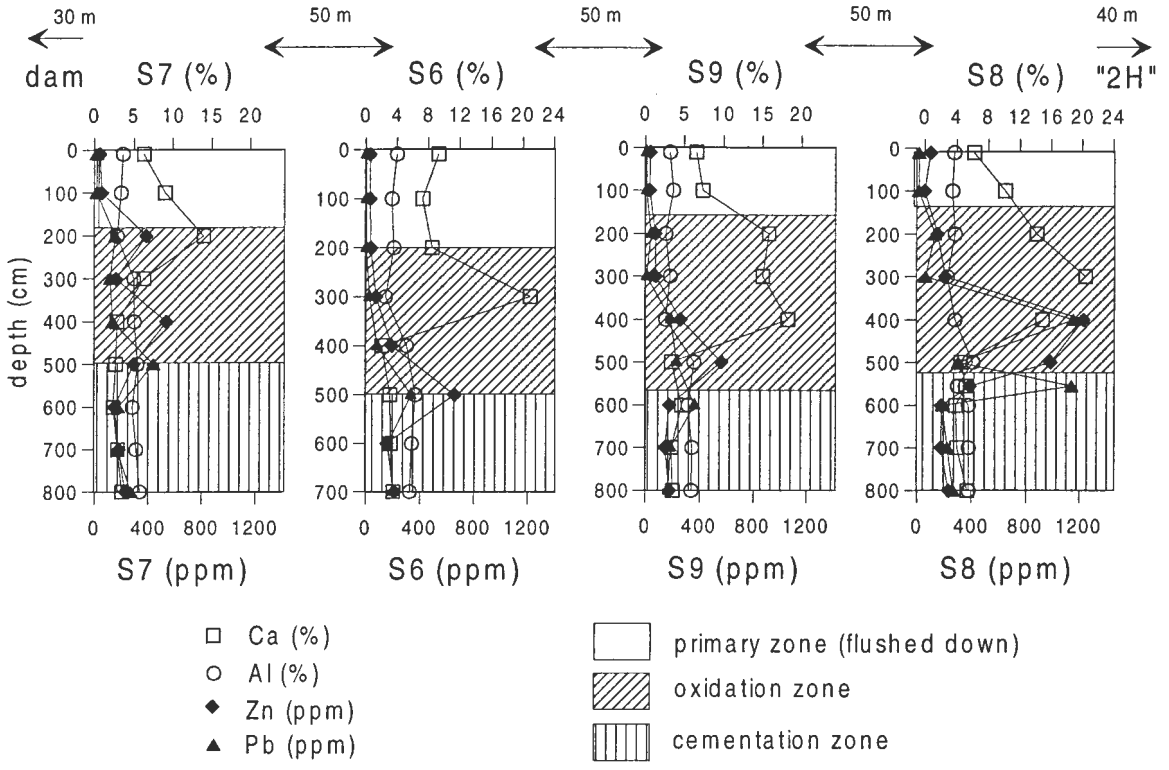

Fig. 8: Ca and Al as indicators for primary carbonate and silicate distribution in the drill cores S7, S6, S9, and S8. Zn and Pb concentrations show a peak located below the Ca peak (calcite) and above the cementation zone, indicating that the flow of metal reach solution is defined in between these two zones. Heavy metal concentrations are about three times higher near the seepage input (S8) than near the dam (S7).

fingerprints of secondary phases (e.g., jarosite), the residual fraction for some elements (e.g., Fe, K) are not presented in figures 9 and 10, but the analyses are included in Tables 2 and 3. The analytical results using extraction sequence A (Fig. 9) are be discussed in the following three groups: (1) The relatively immobile elements as Ti and Al, as well as K, that may be taken as indicators for the primary silicate minerals. (2) The elements Ca, Mn, and Mg that are indicators for the carbonate distribution. (3) Constituents that show important variations in concentration in the oxidation and cementation zones (e.g., Fe, SO_4, Cu, Zn, Pb, Mo, As, and V).

Three intervals can be distinguished according their Ti, Al, and K concentrations in the residual fraction. They coincide with those defined by mineralogical criteria (6.6.1.3). The upper part of the primary zone down to 2.8 m depth shows higher concentrations (Ti = 0.2%, Al = 4%, K = 1.2-1.8%) than in the following interval from 2.8 to 7 m depth (Ti = 0.16%, Al = 3%, K = 0.4%). Below 7 m depth, the concentrations are also higher than the interval from 2.8 to 7 m. (Ti = 0.2, Al = 5%, and K = 1.6%). Results of the first four extraction steps of the sequence B (Fig. 10) indicate that K increases in the cementation zone compared to the overlying oxidation and primary zones, indicating that K is available as water-soluble and adsorbed cation, and fixed in jarosite as indicated by XRD and DXRD.

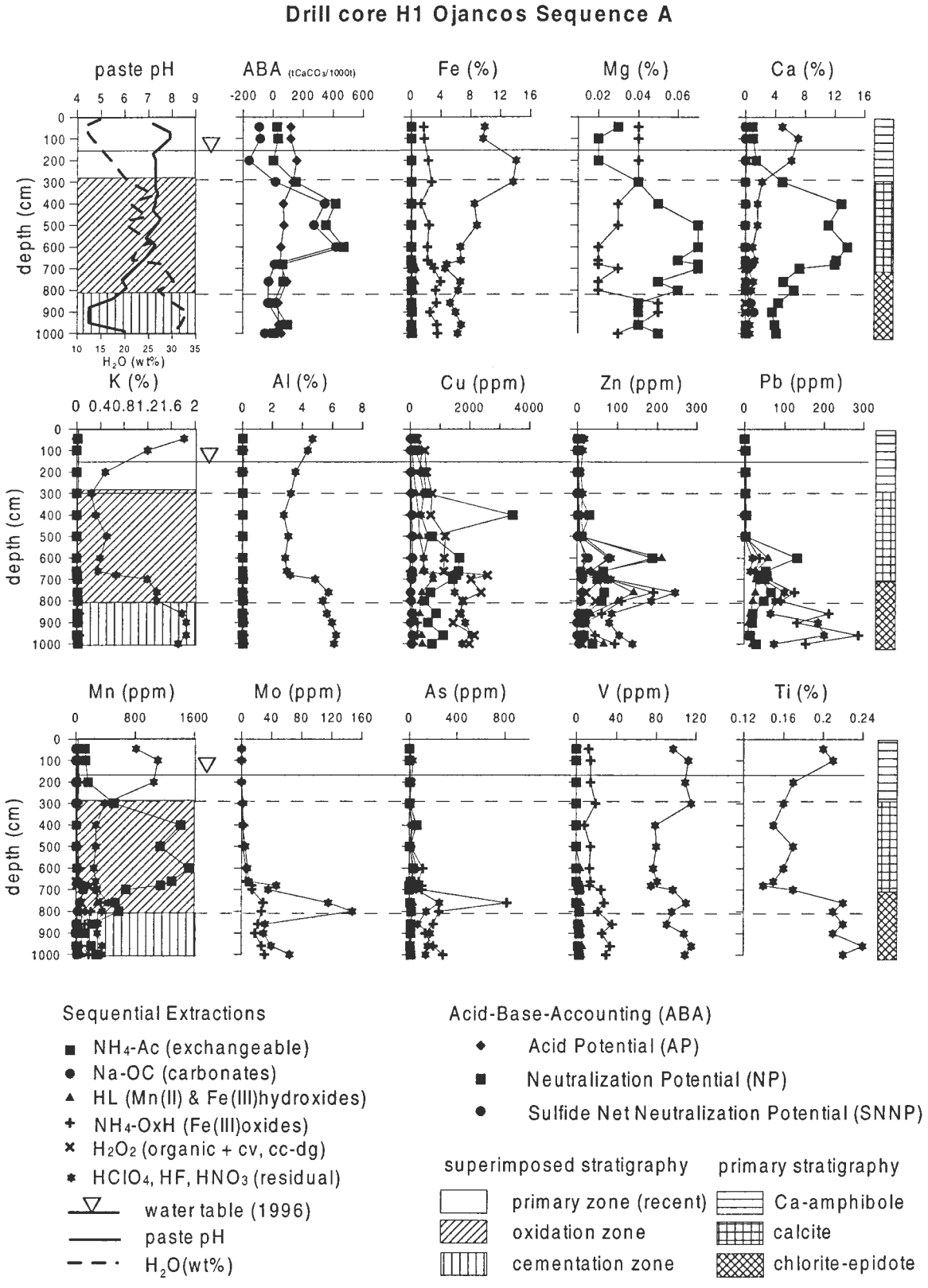

Fig. 9: Results of sequential extraction (sequence A) of drill core H1 from the Ojancos impoundment No. 2.

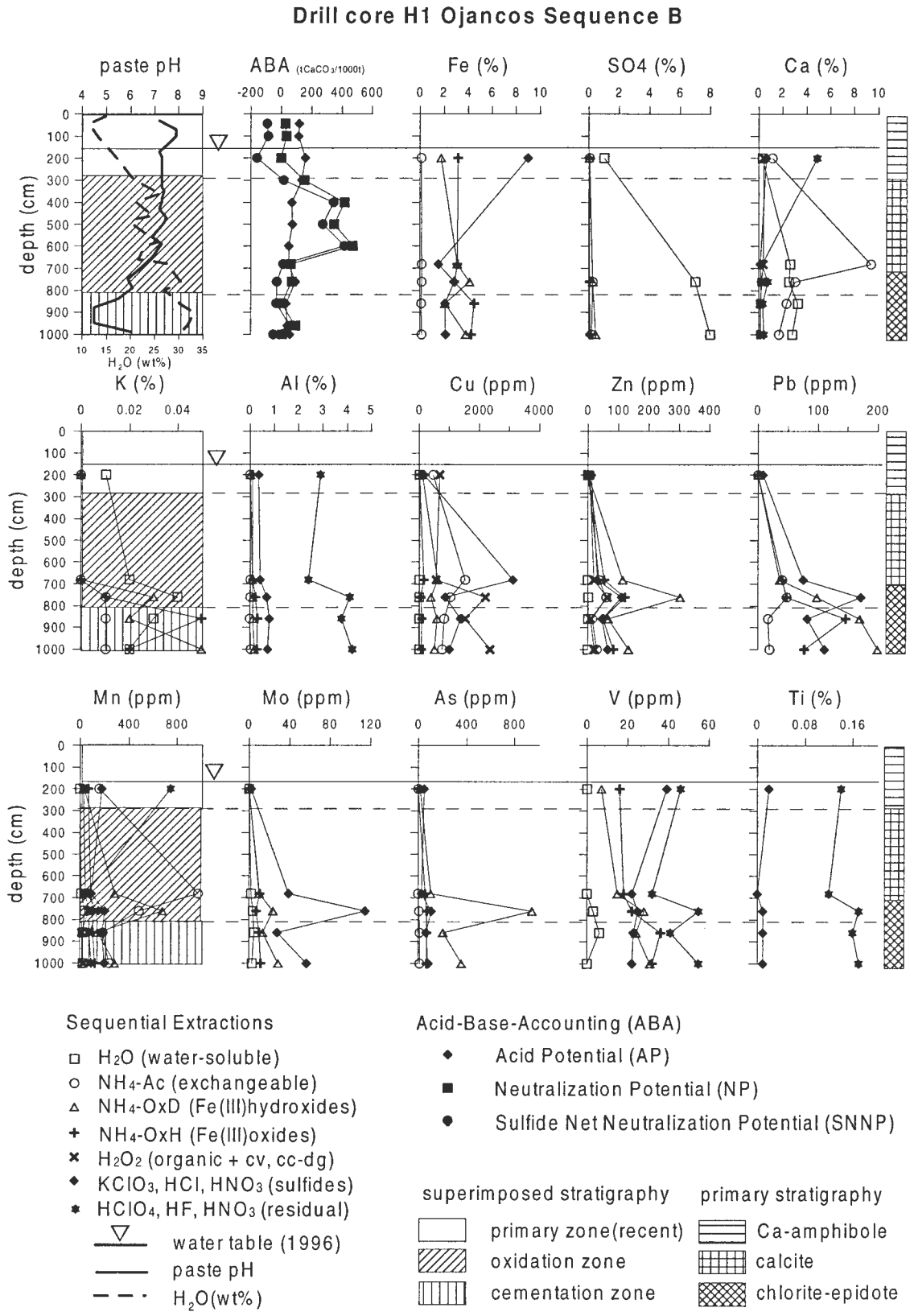

Fig. 10: *Results of sequential extractions (sequence B) of selected samples from drill core H1 from the Ojancos impoundment No. 2.*

A similar stratigraphy is described by the Ca, Mn, and Mg contents. In the residual fraction, Ca shows concentrations of about 6% in the upper 2.8 meters, and values below 2% in all deeper samples. The Ca contents in the exchangeable fraction of sequence A (Fig. 9), in which gypsum is dissolved together with calcite, show low concentrations in the upper two meters. In the section between 2.8 and 7 m depth, the Ca content increases up to 12% which is consistent with the abundant presence of calcite (XRD). Between 7 and 10 m the exchangeable Ca contents are around 4%. In the lower part of the oxidation zone calcite is scarce and in the cementation zone it was not detected by XRD. Gypsum becomes a dominant phase in the cementation zone. Application of a water leach before the exchangeable leach (sequence B, Fig. 10), permits quantitative discrimination between gypsum and calcite and shows that most of the Ca is fixed in the water-soluble fraction as gypsum, confirming the XRD results. Mn follows the same distribution as Ca in the upper seven meters. At 7.5 m depth Mn shows in Fig. 10 a peak in the fraction of the Fe(III) hydroxides, what may indicate the dissolution of secondary Mn(II) hydroxides. Mg shows a similar distribution as Ca and Mn in the exchangeable fraction, indicating that the gangue carbonates are at least in part Mg- and Mn-bearing calcites, which is typical for hydrothermal systems. The distribution of these elements confirms the mineralogical stratification of the primary tailings composition described in (6.6.1.3).

Fe, SO_4, Cu, Zn, Pb, Mo, As, and V show important concentration increases in the lower part of the oxidation zone and in the cementation zone (Fig. 9 and 10). This is explained by the precipitation of secondary sulfates, ferric hydroxide phases, and secondary sulfides, as well by strong adsorption of mobile heavy metals (Tables 2 and 3). The precipitation of secondary ferrihydrite, goethite, and jarosite in the lower part of the oxidation zone and the cementation zone is reflected in the increase of Fe concentrations in the Fe(III) oxides fraction. The strong enrichment of bivalent cations such as Cu (up to 0.65 %), Zn (up to 600 ppm), and Pb (up to 500 ppm) compared to values in the primary zone of about Cu (0.2 %), Zn (20 ppm), and Pb (13 ppm), respectively, is mainly associated with the layers below the calcite-rich tailings, where low pH (about 4) ensures the mobility of these metals. At pH values below 6, Cu precipitates mainly as covellite, whereas above pH 6, in the vicinity of the calcite-rich parts of the oxidation zone, adsorption dominates as shown in the increase in the exchangeable fraction. This pH dependence of the secondary Cu-sulfide formation is also recognized in porphyry copper tailings (chapter 5). Zn shows a concentration maximum at the top of the cementation zone mainly in the fraction of the Fe(III) hydroxides (Fig. 10). The adsorption of Zn on ferric hydroxides is pH-controlled and requires pH values of 5 or higher (Dzombak and Morel, 1990, Webster et al., 1998). This explains why, in the low-pH cementation zone, less Zn is associated with the ferric hydroxides than in the lower part of the oxidation zone, were the pH reaches values of 6. Pb adsorbs on ferric hydroxides at pH values greater than about 3.5 (Dzombak and Morel, 1990, Webster et al., 1998), which is reflected in high Pb concentrations of the Fe(III) hydroxide and Fe(III) oxide fractions over the whole cementation zone.

Fe (%)									
sample	depth	NH_4-Ac	Na-OC	HL	NH_4-OxH	H_2O_2	residual	total	bulk
H1/044	44	0.09	BDL	0.13	1.72	0.09	9.9	11.93	13.8
H1/100	100	0.07	BDL	0.09	1.79	0.03	9.73	11.71	12.5
H1/200	200	0.09	BDL	0.15	2.34	0.08	14.1	16.76	17.6
H1/300	300	0.09	BDL	0.14	2.81	0.15	13.7	16.89	17.4
H1/400	400	0.11	BDL	0.15	1.4	BDL	8.55	10.21	10.6
H1/500	500	0.08	BDL	0.13	2.46	0.04	8.87	11.58	11
H1/600	600	0.11	BDL	0.2	2.27	0.01	6.68	9.27	9.06
H1/660	660	0.11	BDL	0.21	2.23	0.02	6.7	9.27	9.29
H1/680	680	0.18	BDL	0.43	2.78	0.01	4.81	8.21	7.96
H1/700	700	0.3	BDL	0.69	3.1	0.1	4.63	8.82	8.23
H1/760	760	0.14	BDL	0.58	4	0.03	6.67	11.42	10.6
H1/800	800	0.17	BDL	0.4	3.35	0.12	6.4	10.44	9.53
H1/860	860	0.14	BDL	0.28	3.5	0.02	5.29	9.23	8.9
H1/900	900	0.21	BDL	0.28	2.57	0.02	6.08	9.16	8.22
H1/960	960	0.17	BDL	0.3	3.52	0.03	6.81	10.83	9.76
H1/1000	1000	0.19	BDL	0.38	3.6	0.05	6.3	10.52	9.65
Al (%)									
sample	depth	NH_4-Ac	Na-OC	HL	NH_4-OxH	H_2O_2	residual	total	bulk
H1/044	44	0.02	BDL	0.03	0.04	BDL	4.68	4.77	5.72
H1/100	100	0.01	BDL	0.03	0.05	BDL	4.37	4.46	5.75
H1/200	200	0.01	BDL	0.02	0.05	BDL	3.55	3.63	4.64
H1/300	300	0.02	BDL	0.03	0.04	BDL	3.26	3.35	4.33
H1/400	400	0.02	BDL	0.02	0.03	BDL	2.78	2.85	3.68
H1/500	500	0.02	BDL	0.03	0.04	BDL	3.07	3.16	3.92
H1/600	600	0.02	BDL	0.04	0.04	BDL	2.89	2.99	3.74
H1/660	660	0.02	BDL	0.03	0.05	BDL	2.97	3.07	3.8
H1/680	680	0.04	BDL	0.04	0.07	BDL	3.22	3.37	4.13
H1/700	700	0.06	BDL	0.05	0.09	BDL	4.87	5.07	6.03
H1/760	760	0.03	BDL	0.04	0.1	BDL	5.75	5.92	6.68
H1/800	800	0.05	BDL	0.07	0.1	BDL	5.37	5.59	6.05
H1/860	860	0.03	BDL	0.06	0.14	BDL	5.65	5.88	6.41
H1/900	900	0.05	BDL	0.06	0.12	BDL	6	6.23	6.49
H1/960	960	0.04	BDL	0.06	0.15	BDL	6.27	6.52	6.75
H1/1000	1000	0.06	BDL	0.08	0.13	BDL	6.12	6.39	6.56
K (%)									
sample	depth	NH_4-Ac	Na-OC	HL	NH_4-OxH	H_2O_2	residual	total	bulk
H1/044	44	0.02	BDL	0.02	BDL	BDL	1.82	1.86	2.11
H1/100	100	BDL	BDL	BDL	BDL	BDL	1.2	1.2	1.47
H1/200	200	BDL	BDL	BDL	BDL	BDL	0.49	0.49	0.61
H1/300	300	BDL	BDL	BDL	BDL	BDL	0.25	0.25	0.33
H1/400	400	BDL	BDL	BDL	BDL	BDL	0.33	0.33	0.43
H1/500	500	BDL	BDL	BDL	BDL	BDL	0.51	0.51	0.64
H1/600	600	BDL	BDL	BDL	BDL	BDL	0.4	0.4	0.51
H1/660	660	BDL	BDL	BDL	BDL	BDL	0.37	0.37	0.47
H1/680	680	0.01	BDL	0.01	BDL	BDL	0.67	0.69	0.84
H1/700	700	0.02	BDL	0.01	0.02	BDL	1.2	1.25	1.46
H1/760	760	0.02	BDL	0.01	0.03	BDL	1.36	1.42	1.54
H1/800	800	0.03	BDL	0.01	0.04	BDL	1.36	1.44	1.52
H1/860	860	0.02	BDL	BDL	0.05	BDL	1.78	1.85	2
H1/900	900	0.02	BDL	BDL	0.04	BDL	1.86	1.92	1.95
H1/960	960	0.01	BDL	BDL	0.05	BDL	1.86	1.92	1.95
H1/1000	1000	0.03	BDL	BDL	0.04	BDL	1.72	1.79	1.82
Mg (%)									
sample	depth	NH_4-Ac	Na-OC	HL	NH_4-OxH	H_2O_2	residual	total	bulk
H1/044	44	0.03	BDL	0.02	0.04	0.01	1.3	1.4	1.7
H1/100	100	0.02	BDL	0.01	0.04	BDL	1.34	1.41	1.63
H1/200	200	0.02	BDL	0.01	0.04	BDL	0.91	0.98	1.13
H1/300	300	0.04	BDL	0.01	0.04	0.01	1.27	1.37	1.55
H1/400	400	0.05	BDL	BDL	0.03	BDL	0.52	0.6	0.69
H1/500	500	0.07	BDL	0.01	0.03	BDL	0.75	0.86	0.95
H1/600	600	0.07	BDL	0.01	0.02	BDL	0.65	0.75	0.82
H1/660	660	0.06	BDL	0.01	0.02	BDL	0.77	0.86	0.95
H1/680	680	0.07	BDL	BDL	0.02	BDL	0.62	0.71	0.76
H1/700	700	0.07	BDL	0.01	0.03	BDL	0.84	0.95	0.99
H1/760	760	0.05	BDL	BDL	0.02	BDL	1.09	1.16	1.19
H1/800	800	0.06	BDL	BDL	0.02	BDL	0.88	0.96	0.96
H1/860	860	0.04	BDL	BDL	0.05	BDL	1.03	1.12	1.13
H1/900	900	0.04	BDL	BDL	0.05	BDL	1.05	1.14	1.11
H1/960	960	0.04	BDL	BDL	0.04	BDL	1.05	1.13	1.09
H1/1000	1000	0.05	BDL	BDL	0.03	BDL	1.01	1.09	1.08
Na (%)									
sample	depth	NH_4-Ac	Na-OC	HL	NH_4-OxH	H_2O_2	residual	total	bulk
H1/044	44	0.03	BDL	0.03	BDL	BDL	1.49	1.55	1.85
H1/100	100	0.02	BDL	0.08	BDL	BDL	1.35	1.45	1.92
H1/200	200	0.02	BDL	0.06	BDL	BDL	1.38	1.46	1.93
H1/300	300	0.02	BDL	0.04	BDL	BDL	1.62	1.68	2.29
H1/400	400	0.02	BDL	0.02	BDL	BDL	1.26	1.3	1.79
H1/500	500	0.02	BDL	0.06	BDL	BDL	1.36	1.44	1.87
H1/600	600	0.03	BDL	0.04	BDL	BDL	1.2	1.27	1.67
H1/660	660	0.02	BDL	0.04	BDL	BDL	1.24	1.3	1.7
H1/680	680	0.04	BDL	0.05	BDL	BDL	1.02	1.11	1.4
H1/700	700	0.04	BDL	0.06	BDL	BDL	1.13	1.23	1.49
H1/760	760	0.04	BDL	0.1	0.02	BDL	1.09	1.25	1.36
H1/800	800	0.04	BDL	0.09	0.03	BDL	1.16	1.32	1.41
H1/860	860	0.05	BDL	0.14	0.03	BDL	0.86	1.08	1.04
H1/900	900	0.04	BDL	0.12	0.02	BDL	0.75	0.93	0.85
H1/960	960	0.04	BDL	0.2	0.03	BDL	0.94	1.21	1.03
H1/1000	1000	0.04	BDL	0.14	0.02	BDL	1.01	1.21	1.09

Cu (ppm)									
sample	depth	NH_4-Ac	Na-OC	HL	NH_4-OxH	H_2O_2	residual	total	bulk
H1/044	44	163	15.5	49	6.7	248	218	700.2	794
H1/100	100	177	20.8	66.4	7.4	496	390	1157.6	1320
H1/200	200	466	37.2	131	13	559	334	1540.2	1630
H1/300	300	546	54.4	215	23.6	753	454	2046	2240
H1/400	400	3440	73.7	289	25.7	698	371	4897.4	5470
H1/500	500	755	91.7	324	43.8	1200	608	3022.5	3140
H1/600	600	1660	91.3	485	20	1160	466	3882.3	4110
H1/660	660	1640	92.4	432	23.4	1140	491	3818.8	4090
H1/680	680	1570	61	785	103	2620	1420	6559	6850
H1/700	700	1450	73.8	784	54.1	2060	1470	5892	6420
H1/760	760	695	45.5	419	25.2	2400	1510	5095	4950
H1/800	800	503	50.5	377	28.9	1790	1780	4529	4550
H1/860	860	892	69.3	338	194	1680	1710	4883	4930
H1/900	900	623	46.1	192	256	1460	1870	4447.1	4460
H1/960	960	1120	96.6	406	264	2170	2070	6127	6060
H1/1000	1000	744	66.1	432	129	2010	1770	5151	5010
Zn (ppm)									
sample	depth	NH_4-Ac	Na-OC	HL	NH_4-OxH	H_2O_2	residual	total	bulk
H1/044	44	2.7	BDL	1.2	0.9	1.3	17.1	23.2	17.1
H1/100	100	2	BDL	1.3	1.3	1.5	13.8	19.9	17
H1/200	200	3	BDL	1.6	0.8	1.4	8.6	15.4	6.8
H1/300	300	4.6	BDL	2.2	0.8	3	13.3	23.9	12.5
H1/400	400	30.1	1.4	6.2	3.7	2.8	9.9	54.1	39.7
H1/500	500	10.8	1.4	6	5.5	4.9	14.9	43.5	28
H1/600	600	189	27	212	78.3	21.5	84.3	612.1	487
H1/660	660	65.3	9	61.1	33.6	9.8	33.2	212	172
H1/680	680	52.5	13.2	67.4	65.1	11.6	64.6	274.4	224
H1/700	700	50.8	13.6	74	77	62	86	363	258
H1/760	760	67.6	13.1	142	192	22.5	246	683	589
H1/800	800	62.3	9.7	103	111	47.2	186	519	409
H1/860	860	21.6	2.9	35	61.4	10.1	87.7	219	180
H1/900	900	19.1	1.6	11.6	20.9	10.9	81.2	145.3	126
H1/960	960	17.9	1.6	16.5	45	9.8	106	197	162
H1/1000	1000	39.6	6.2	66.6	95	14	140	361	282
Mn (ppm)									
sample	depth	NH_4-Ac	Na-OC	HL	NH_4-OxH	H_2O_2	residual	total	bulk
H1/044	44	122	5	16	36	15	819	1013	1140
H1/100	100	133	4	13	39	14	1110	1313	1390
H1/200	200	166	5	12	48	18	1050	1299	1350
H1/300	300	519	5	10	32	15	395	976	994
H1/400	400	1420	16	7	17	7	275	1742	1840
H1/500	500	1140	8	10	27	10	277	1472	1400
H1/600	600	1530	25	45	56	19	248	1923	1940
H1/660	660	1300	29	32	40	13	274	1688	1740
H1/680	680	1150	102	131	116	15	175	1689	1680
H1/700	700	683	110	278	264	105	298	1738	1590
H1/760	760	536	55	295	342	76	446	1750	1650
H1/800	800	583	31	138	206	94	363	1415	1280
H1/860	860	228	9	38	127	15	306	723	682
H1/900	900	129	5	10	45	9	295	493	450
H1/960	960	211	7	19	75	13	360	685	624
H1/1000	1000	280	22	84	180	29	354	949	854
Cr (ppm)									
sample	depth	NH_4-Ac	Na-OC	HL	NH_4-OxH	H_2O_2	residual	total	bulk
H1/044	44	BDL	BDL	2	3	BDL	26	31	35
H1/100	100	BDL	BDL	BDL	3	BDL	29	32	34
H1/200	200	BDL	BDL	1	5	BDL	27	33	33
H1/300	300	1	BDL	2	5	BDL	24	32	31
H1/400	400	1	BDL	2	3	BDL	25	31	30
H1/500	500	1	BDL	2	6	BDL	25	34	31
H1/600	600	2	BDL	2	4	BDL	26	34	33
H1/660	660	2	BDL	3	5	BDL	25	35	34
H1/680	680	4	BDL	4	11	BDL	23	42	39
H1/700	700	3	BDL	2	9	BDL	23	37	33
H1/760	760	3	BDL	3	23	BDL	29	58	45
H1/800	800	4	BDL	3	16	BDL	26	49	38
H1/860	860	8	BDL	8	26	BDL	19	61	50
H1/900	900	8	BDL	8	21	1	21	59	49
H1/960	960	8	BDL	9	31	BDL	26	74	64
H1/1000	1000	8	BDL	8	22	BDL	23	61	48
Pb (ppm)									
sample	depth	NH_4-Ac	Na-OC	HL	NH_4-OxH	H_2O_2	residual	total	bulk
H1/044	44	BDL	BDL	BDL	BDL	BDL	BDL	BDL	BDL
H1/100	100	3	BDL	BDL	BDL	BDL	BDL	3	BDL
H1/200	200	2	BDL	BDL	2	BDL	4	8	8
H1/300	300	3	BDL	BDL	2	BDL	4	9	13
H1/400	400	5	BDL	3	BDL	BDL	BDL	8	10
H1/500	500	4	BDL	BDL	4	BDL	BDL	8	9
H1/600	600	133	BDL	60	38	BDL	20	251	204
H1/660	660	53	BDL	28	28	BDL	16	125	106
H1/680	680	58	BDL	33	50	BDL	32	173	144
H1/700	700	44	BDL	30	60	BDL	50	184	151
H1/760	760	68	BDL	28	126	BDL	100	322	264
H1/800	800	49	BDL	22	92	BDL	78	241	192
H1/860	860	22	BDL	16	212	BDL	66	316	278
H1/900	900	20	BDL	11	133	BDL	186	350	281
H1/960	960	15	BDL	9	287	BDL	201	512	402
H1/1000	1000	31	BDL	20	154	BDL	75	280	245

Abbreviation as in appendix. 2

Ca (%)									
sample	depth	NH_4-Ac	Na-OC	HL	NH_4-OxH	H_2O_2	residual	total	bulk
H1/044	44	0.92	BDL	0.27	BDL	0.1	4.92	6.21	6.34
H1/100	100	1.05	BDL	0.28	BDL	0.13	7.08	8.54	8.07
H1/200	200	1.46	BDL	0.28	BDL	0.17	6.18	8.09	7.61
H1/300	300	4.96	0.01	0.3	BDL	0.04	2.23	7.54	7.1
H1/400	400	12.9	0.07	0.2	BDL	0.03	1.64	14.84	14.9
H1/500	500	11.1	0.04	0.25	BDL	0.03	1.62	13.04	11.6
H1/600	600	13.7	0.04	0.2	BDL	0.01	0.93	14.88	14.5
H1/660	660	12.2	0.06	0.22	BDL	0.02	1.31	13.81	13.6
H1/680	680	12	0.9	0.21	BDL	0.01	0.42	13.54	13.1
H1/700	700	7.25	0.38	0.2	BDL	0.05	0.32	8.2	7.52
H1/760	760	5.12	0.13	0.21	BDL	0.03	1.13	6.62	5.99
H1/800	800	6.51	0.08	0.18	BDL	0.03	0.79	7.59	6.75
H1/860	860	4.43	0.74	0.19	BDL	0.02	0.53	5.91	5.33
H1/900	900	3.62	1.18	0.2	BDL	0.01	0.41	5.42	4.88
H1/960	960	3.97	0.15	0.13	BDL	0.01	0.62	4.88	4.36
H1/1000	1000	4.13	0.07	0.13	BDL	0.02	0.61	4.96	4.31
Tl (%)									
sample	depth	NH_4-Ac	Na-OC	HL	NH_4-OxH	H_2O_2	residual	total	bulk
H1/044	44	BDL	BDL	BDL	BDL	BDL	0.2	0.2	0.26
H1/100	100	BDL	BDL	BDL	BDL	BDL	0.21	0.21	0.25
H1/200	200	BDL	BDL	BDL	BDL	BDL	0.17	0.17	0.2
H1/300	300	BDL	BDL	BDL	BDL	BDL	0.16	0.16	0.19
H1/400	400	BDL	BDL	BDL	BDL	BDL	0.15	0.15	0.17
H1/500	500	BDL	BDL	BDL	BDL	BDL	0.17	0.17	0.18
H1/600	600	BDL	BDL	BDL	BDL	BDL	0.16	0.16	0.16
H1/660	660	BDL	BDL	BDL	BDL	BDL	0.15	0.15	0.16
H1/680	680	BDL	BDL	BDL	BDL	BDL	0.14	0.14	0.15
H1/700	700	BDL	BDL	BDL	BDL	BDL	0.17	0.17	0.18
H1/760	760	BDL	BDL	BDL	BDL	BDL	0.22	0.22	0.22
H1/800	800	BDL	BDL	BDL	BDL	BDL	0.21	0.21	0.19
H1/860	860	BDL	BDL	BDL	BDL	BDL	0.22	0.22	0.2
H1/900	900	BDL	BDL	BDL	BDL	BDL	0.21	0.21	0.2
H1/960	960	BDL	BDL	BDL	BDL	BDL	0.24	0.24	0.2
H1/1000	1000	BDL	BDL	BDL	BDL	BDL	0.22	0.22	0.2
P (%)									
sample	depth	NH_4-Ac	Na-OC	HL	NH_4-OxH	H_2O_2	residual	total	bulk
H1/044	44	BDL	BDL	0.12	BDL	BDL	BDL	0.12	0.1
H1/100	100	BDL	BDL	0.13	BDL	BDL	BDL	0.13	0.1
H1/200	200	BDL	BDL	0.12	BDL	BDL	BDL	0.12	0.1
H1/300	300	BDL	BDL	0.13	BDL	BDL	BDL	0.13	0.11
H1/400	400	BDL	BDL	0.08	BDL	BDL	BDL	0.08	0.07
H1/500	500	BDL	BDL	0.11	BDL	BDL	BDL	0.11	0.08
H1/600	600	BDL	BDL	0.08	0.01	BDL	BDL	0.09	0.08
H1/660	660	BDL	BDL	0.09	0.02	BDL	BDL	0.11	0.08
H1/680	680	BDL	BDL	0.04	0.04	BDL	0.02	0.1	0.08
H1/700	700	BDL	BDL	0.03	0.04	BDL	0.02	0.09	0.07
H1/760	760	BDL	BDL	0.04	0.05	BDL	0.03	0.12	0.09
H1/800	800	BDL	BDL	0.05	0.03	BDL	0.03	0.11	0.08
H1/860	860	0.02	BDL	0.06	0.07	BDL	0.02	0.17	0.13
H1/900	900	0.02	BDL	0.04	0.06	BDL	0.05	0.17	0.13
H1/960	960	0.02	BDL	0.05	0.08	BDL	0.05	0.2	0.14
H1/1000	1000	0.01	BDL	0.05	0.06	BDL	0.03	0.15	0.12
Ba (ppm)									
sample	depth	NH_4-Ac	Na-OC	HL	NH_4-OxH	H_2O_2	residual	total	bulk
H1/044	44	4	5	5	2	BDL	240	256	485
H1/100	100	4	3	4	1	BDL	276	288	362
H1/200	200	2	3	3	1	BDL	121	130	167
H1/300	300	2	4	7	2	BDL	50	65	90
H1/400	400	3	24	33	13	2	117	192	229
H1/500	500	3	6	6	3	BDL	138	156	186
H1/600	600	6	56	168	149	BDL	214	593	988
H1/660	660	4	42	123	43	BDL	184	396	458
H1/680	680	2	BDL	50	61	BDL	333	446	527
H1/700	700	3	2	72	43	1	423	544	625
H1/760	760	2	4	123	71	BDL	203	403	793
H1/800	800	5	7	155	66	BDL	47	280	560
H1/860	860	3	BDL	81	62	BDL	1580	1726	902
H1/900	900	3	BDL	51	71	BDL	1500	1625	786
H1/960	960	2	3	102	51	BDL	1140	1298	650
H1/1000	1000	4	7	170	64	BDL	129	374	719
Sr (ppm)									
sample	depth	NH_4-Ac	Na-OC	HL	NH_4-OxH	H_2O_2	residual	total	bulk
H1/044	44	7.5	BDL	1.5	BDL	0.6	89.2	98.8	125
H1/100	100	6.5	BDL	1.4	BDL	0.7	110	118.6	141
H1/200	200	8.5	BDL	1.5	BDL	0.5	76.4	86.9	103
H1/300	300	24.2	BDL	1.8	BDL	0.6	55.5	82.1	98.2
H1/400	400	44.6	0.9	2.1	BDL	0.6	68.7	116.9	138
H1/500	500	47.9	0.5	2.1	BDL	0.5	75.5	126.5	142
H1/600	600	57.6	3.3	6.9	2.1	2	60.9	132.8	155
H1/660	660	50.8	2.3	5.1	0.7	1.8	54.4	115.1	132
H1/680	680	57.7	6.1	4.3	1.8	1.6	64.2	135.7	157
H1/700	700	37.7	2.2	4.4	2.1	5.4	78.7	130.5	144
H1/760	760	26.5	1.7	6.2	2.7	2.8	140	179.9	196
H1/800	800	32	1.6	8.1	4.9	4.5	157	208.1	217
H1/860	860	23.5	4.3	4.5	11.9	5.1	129	178.3	187
H1/900	900	20.1	5.8	2.7	7.6	2.7	137	175.9	177
H1/960	960	22.4	1.2	3.3	10.5	3.1	152	192.5	193
H1/1000	1000	23.6	1.3	6.6	6.8	4.6	148	190.9	192

Mo (ppm)									
sample	depth	NH_4-Ac	Na-OC	HL	NH_4-OxH	H_2O_2	residual	total	bulk
H1/044	44	BDL	BDL	BDL	BDL	BDL	BDL	BDL	BDL
H1/100	100	BDL	BDL	BDL	BDL	BDL	BDL	BDL	BDL
H1/200	200	BDL	BDL	BDL	BDL	BDL	BDL	BDL	1
H1/300	300	BDL	BDL	BDL	1	BDL	2	3	4
H1/400	400	BDL	BDL	BDL	3	BDL	1	4	5
H1/500	500	BDL	BDL	BDL	2	BDL	5	7	6
H1/600	600	BDL	BDL	BDL	6	BDL	8	14	12
H1/660	660	BDL	BDL	BDL	6	BDL	10	16	15
H1/680	680	BDL	BDL	BDL	14	BDL	47	61	57
H1/700	700	BDL	BDL	BDL	14	BDL	36	50	43
H1/760	760	BDL	BDL	BDL	29	BDL	116	145	134
H1/800	800	BDL	BDL	BDL	27	BDL	148	175	144
H1/860	860	BDL	BDL	BDL	22	BDL	32	54	50
H1/900	900	BDL	BDL	BDL	18	BDL	30	48	43
H1/960	960	BDL	BDL	BDL	27	BDL	40	67	56
H1/1000	1000	BDL	BDL	BDL	31	BDL	64	95	85
V (ppm)									
sample	depth	NH_4-Ac	Na-OC	HL	NH_4-OxH	H_2O_2	residual	total	bulk
H1/044	44	BDL	BDL	BDL	12	BDL	97	109	130
H1/100	100	BDL	BDL	BDL	14	BDL	112	126	138
H1/200	200	BDL	BDL	BDL	14	BDL	109	123	133
H1/300	300	BDL	BDL	BDL	19	BDL	115	134	145
H1/400	400	BDL	BDL	BDL	8	BDL	79	87	99
H1/500	500	BDL	BDL	BDL	14	BDL	80	94	97
H1/600	600	BDL	BDL	4	13	BDL	77	94	98
H1/660	660	BDL	BDL	3	14	BDL	81	98	105
H1/680	680	2	BDL	4	13	BDL	75	94	97
H1/700	700	3	BDL	5	25	BDL	97	130	130
H1/760	760	BDL	BDL	5	28	BDL	110	143	141
H1/800	800	3	BDL	4	22	BDL	96	125	117
H1/860	860	2	BDL	5	36	BDL	91	134	133
H1/900	900	3	BDL	5	26	BDL	108	142	132
H1/960	960	2	BDL	6	34	BDL	116	158	147
H1/1000	1000	3	BDL	5	30	BDL	109	147	139
As (ppm)									
sample	depth	NH_4-Ac	Na-OC	HL	NH_4-OxH	H_2O_2	residual	total	bulk
H1/044	44	BDL	BDL	4	BDL	BDL	BDL	4	4
H1/100	100	BDL	BDL	4	BDL	BDL	32	36	18
H1/200	200	4	BDL	9	6	BDL	23	42	12
H1/300	300	5	BDL	8	4	BDL	BDL	17	7
H1/400	400	65	BDL	58	26	BDL	24	173	119
H1/500	500	6	BDL	12	15	BDL	6	39	17
H1/600	600	36	BDL	66	116	BDL	38	256	182
H1/660	660	14	BDL	31	81	BDL	27	153	100
H1/680	680	BDL	BDL	7	106	BDL	63	176	124
H1/700	700	3	BDL	5	106	BDL	61	175	114
H1/760	760	11	BDL	35	819	BDL	256	1121	796
H1/800	800	19	BDL	32	252	BDL	144	447	297
H1/860	860	15	BDL	27	204	BDL	74	320	242
H1/900	900	13	BDL	21	138	BDL	178	350	259
H1/960	960	10	BDL	18	206	BDL	156	390	289
H1/1000	1000	14	BDL	27	284	BDL	140	465	352
W (ppm)									
sample	depth	NH_4-Ac	Na-OC	HL	NH_4-OxH	H_2O_2	residual	total	bulk
H1/044	44	BDL	BDL	BDL	BDL	BDL	BDL	BDL	BDL
H1/100	100	BDL	BDL	BDL	BDL	BDL	BDL	BDL	BDL
H1/200	200	BDL	BDL	BDL	BDL	BDL	BDL	BDL	BDL
H1/300	300	BDL	BDL	BDL	BDL	BDL	BDL	BDL	BDL
H1/400	400	BDL	BDL	BDL	BDL	BDL	BDL	BDL	BDL
H1/500	500	BDL	BDL	BDL	BDL	BDL	BDL	BDL	BDL
H1/600	600	BDL	BDL	BDL	BDL	BDL	BDL	BDL	BDL
H1/660	660	BDL	BDL	BDL	BDL	BDL	BDL	BDL	BDL
H1/680	680	BDL	BDL	BDL	BDL	BDL	BDL	BDL	BDL
H1/700	700	BDL	BDL	BDL	BDL	BDL	BDL	BDL	BDL
H1/760	760	BDL	BDL	BDL	BDL	BDL	BDL	BDL	BDL
H1/800	800	BDL	BDL	BDL	BDL	BDL	BDL	BDL	BDL
H1/860	860	BDL	BDL	BDL	BDL	BDL	BDL	BDL	BDL
H1/900	900	BDL	BDL	BDL	BDL	BDL	BDL	BDL	BDL
H1/960	960	BDL	BDL	BDL	BDL	BDL	BDL	BDL	BDL
H1/1000	1000	BDL	BDL	BDL	BDL	BDL	BDL	BDL	BDL
La (ppm)									
sample	depth	NH_4-Ac	Na-OC	HL	NH_4-OxH	H_2O_2	residual	total	bulk
H1/044	44	2.3	0.6	3.2	BDL	1.9	31.5	39.5	50
H1/100	100	1.4	BDL	3.1	BDL	1.2	26	31.7	37.6
H1/200	200	BDL	BDL	0.8	BDL	BDL	10.1	10.9	11.7
H1/300	300	0.8	BDL	0.5	BDL	BDL	14.6	15.9	22.1
H1/400	400	1.6	BDL	BDL	BDL	BDL	1.1	2.7	4.8
H1/500	500	1.5	BDL	BDL	0.9	BDL	1.1	3.5	3.5
H1/600	600	1.8	BDL	BDL	BDL	BDL	1.9	3.7	5.5
H1/660	660	1.9	BDL	BDL	BDL	BDL	7.9	9.8	11.1
H1/680	680	2.6	BDL	0.8	BDL	BDL	15.1	18.5	23.6
H1/700	700	1.8	BDL	BDL	BDL	1	18	21	28
H1/760	760	2.1	BDL	1	BDL	BDL	22.2	25	29
H1/800	800	1.7	BDL	0.7	BDL	BDL	15.7	18	21
H1/860	860	2.9	BDL	0.6	2.8	0.8	40.8	48	53
H1/900	900	3.2	0.6	BDL	1.3	BDL	44.4	49.5	51
H1/960	960	3.4	BDL	0.5	4	0.8	67	76	79
H1/1000	1000	2.3	BDL	0.5	1	0.9	40.4	45	48

Ni (ppm)									
sample	depth	NH_4-Ac	Na-OC	HL	NH_4-OxH	H_2O_2	residual	total	bulk
H1/044	44	2	BDL	BDL	2	6	36	46	50
H1/100	100	2	BDL	BDL	3	6	44	55	54
H1/200	200	2	BDL	1	3	6	47	59	58
H1/300	300	3	BDL	1	6	6	73	89	82
H1/400	400	6	BDL	1	2	2	20	31	25
H1/500	500	4	BDL	1	4	4	24	37	26
H1/600	600	6	BDL	2	4	4	22	38	30
H1/660	660	5	BDL	2	5	4	28	44	37
H1/680	680	5	1	3	7	3	18	37	31
H1/700	700	6	2	6	8	5	19	46	34
H1/760	760	6	1	7	13	4	37	68	57
H1/800	800	6	BDL	4	8	4	31	53	41
H1/860	860	3	BDL	2	10	3	25	43	39
H1/900	900	5	BDL	BDL	6	3	29	43	37
H1/960	960	4	BDL	2	9	3	35	53	45
H1/1000	1000	4	BDL	3	10	4	32	53	47

Zr (ppm)									
sample	depth	NH_4-Ac	Na-OC	HL	NH_4-OxH	H_2O_2	residual	total	bulk
H1/044	44	BDL	BDL	BDL	2	BDL	51.8	53.8	74.1
H1/100	100	BDL	BDL	BDL	2.6	BDL	55.3	57.9	72.5
H1/200	200	BDL	BDL	BDL	2.6	BDL	46.9	49.5	60.3
H1/300	300	BDL	BDL	BDL	0.7	BDL	41	41.7	55.9
H1/400	400	BDL	BDL	BDL	1.3	BDL	31.8	33.1	42.7
H1/500	500	BDL	BDL	BDL	4.8	BDL	38.3	43.1	49
H1/600	600	BDL	BDL	BDL	1	BDL	32	33	41.1
H1/660	660	BDL	BDL	BDL	0.6	BDL	33.3	33.9	42.1
H1/680	680	BDL	BDL	BDL	0.8	BDL	32.6	33.4	42.2
H1/700	700	BDL	BDL	BDL	2.5	BDL	35.1	37.6	49
H1/760	760	BDL	BDL	BDL	1.5	BDL	39.7	41.2	51.8
H1/800	800	BDL	BDL	BDL	2.5	BDL	45.2	47.7	52.1
H1/860	860	BDL	BDL	BDL	5.5	BDL	54.9	60.4	66.9
H1/900	900	BDL	BDL	BDL	3.1	BDL	54.8	57.9	67.2
H1/960	960	BDL	BDL	BDL	3.6	BDL	50.4	54	57.1
H1/1000	1000	BDL	BDL	BDL	2.8	BDL	46.2	49	56.7

Co (ppm)									
sample	depth	NH_4-Ac	Na-OC	HL	NH_4-OxH	H_2O_2	residual	total	bulk
H1/044	44	5	BDL	1	1	16	79	102	120
H1/100	100	3	BDL	1	1	13	85	103	108
H1/200	200	11	2	5	4	25	161	208	201
H1/300	300	6	1	3	3	21	138	172	169
H1/400	400	7	BDL	2	2	7	79	97	94
H1/500	500	4	BDL	2	4	12	78	100	88
H1/600	600	7	1	4	4	12	47	75	70
H1/660	660	8	2	5	6	14	60	95	86
H1/680	680	9	5	9	19	7	37	86	74
H1/700	700	12	7	20	24	17	30	110	85
H1/760	760	10	3	13	19	11	62	118	107
H1/800	800	7	2	7	12	13	55	96	81
H1/860	860	5	1	3	19	12	32	72	65
H1/900	900	10	2	1	12	14	37	76	64
H1/960	960	10	2	3	16	18	49	98	82
H1/1000	1000	8	2	6	20	17	46	99	84

Sn (ppm)									
sample	depth	NH_4-Ac	Na-OC	HL	NH_4-OxH	H_2O_2	residual	total	bulk
H1/044	44	BDL	BDL	BDL	BDL	BDL	BDL	BDL	BDL
H1/100	100	BDL	BDL	BDL	BDL	BDL	14	14	BDL
H1/200	200	BDL	BDL	BDL	BDL	BDL	14	14	BDL
H1/300	300	BDL	BDL	BDL	BDL	BDL	15	15	BDL
H1/400	400	BDL	BDL	BDL	BDL	BDL	15	15	BDL
H1/500	500	BDL	BDL	BDL	BDL	BDL	14	14	BDL
H1/600	600	BDL	BDL	BDL	BDL	BDL	15	15	BDL
H1/660	660	BDL	BDL	BDL	BDL	BDL	14	14	BDL
H1/680	680	BDL	BDL	BDL	BDL	BDL	16	16	BDL
H1/700	700	BDL	BDL	BDL	BDL	BDL	16	16	BDL
H1/760	760	BDL	BDL	BDL	BDL	BDL	16	16	BDL
H1/800	800	BDL	BDL	BDL	BDL	BDL	18	18	BDL
H1/860	860	BDL	BDL	BDL	BDL	BDL	19	19	BDL
H1/900	900	BDL	BDL	BDL	BDL	BDL	21	21	BDL
H1/960	960	BDL	BDL	BDL	BDL	BDL	23	23	BDL
H1/1000	1000	BDL	BDL	BDL	BDL	BDL	18	18	BDL

Y (ppm)									
sample	depth	NH_4-Ac	Na-OC	HL	NH_4-OxH	H_2O_2	residual	total	bulk
H1/044	44	0.8	BDL	0.9	BDL	BDL	11.3	13	17.1
H1/100	100	0.8	BDL	0.8	BDL	BDL	16.1	17.7	21.2
H1/200	200	BDL	BDL	0.6	BDL	BDL	8.3	8.9	11.1
H1/300	300	1	BDL	1.1	BDL	BDL	8.8	10.9	13.4
H1/400	400	2.2	BDL	0.8	BDL	BDL	5.4	8.4	10.2
H1/500	500	1.8	BDL	0.9	BDL	BDL	7.2	9.9	11.4
H1/600	600	2.3	BDL	1.1	BDL	BDL	5.1	8.5	10.1
H1/660	660	2.2	BDL	1.1	BDL	BDL	6.1	9.4	11.2
H1/680	680	2.9	BDL	1.3	0.6	BDL	5.4	10.2	12
H1/700	700	2.4	BDL	1.4	1.1	BDL	6	11	13
H1/760	760	2	BDL	1.7	1.7	BDL	8.8	14	16
H1/800	800	2	BDL	1.6	1.1	BDL	8.4	13	14
H1/860	860	1.9	BDL	1	1.6	BDL	10.5	15	17
H1/900	900	1.6	BDL	0.6	1.1	BDL	12.2	15.5	18
H1/960	960	1.4	BDL	0.7	2	BDL	13.5	17	20
H1/1000	1000	1.7	BDL	1	2	BDL	11.2	16	16

Sc (ppm)									
sample	depth	NH_4-Ac	Na-OC	HL	NH_4-OxH	H_2O_2	residual	total	bulk
H1/044	44	BDL	BDL	BDL	BDL	BDL	7.9	7.9	9.5
H1/100	100	BDL	BDL	BDL	BDL	BDL	7.4	7.4	9.6
H1/200	200	BDL	BDL	BDL	BDL	BDL	5.5	5.5	7.7
H1/300	300	0.8	BDL	BDL	BDL	BDL	5.7	6.5	8.2
H1/400	400	2.1	BDL	BDL	BDL	BDL	3.7	5.8	7.5
H1/500	500	2	BDL	BDL	0.6	BDL	4.9	7.5	8.2
H1/600	600	2.2	BDL	BDL	BDL	BDL	4.6	6.8	8.4
H1/660	660	2	BDL	BDL	BDL	BDL	4.8	6.8	8.3
H1/680	680	2	BDL	BDL	BDL	BDL	4.6	6.6	8.1
H1/700	700	1.3	BDL	BDL	0.9	BDL	8	10	11
H1/760	760	0.9	BDL	BDL	1.4	BDL	8.9	11	12
H1/800	800	1.2	BDL	BDL	1.1	BDL	8.1	10	11
H1/860	860	0.9	BDL	BDL	2.5	BDL	7.9	11	12
H1/900	900	0.8	BDL	BDL	1.4	BDL	9.8	12	13
H1/960	960	0.8	BDL	BDL	2	BDL	9.8	12	13
H1/1000	1000	0.9	BDL	BDL	2	BDL	9.4	12	12

Be (ppm)									
sample	depth	NH_4-Ac	Na-OC	HL	NH_4-OxH	H_2O_2	residual	total	bulk
H1/044	44	BDL	BDL	BDL	BDL	BDL	1.1	1.1	1.4
H1/100	100	BDL	BDL	BDL	BDL	BDL	1	1	1.2
H1/200	200	BDL	BDL	BDL	BDL	BDL	1.5	1.5	1.5
H1/300	300	BDL	BDL	BDL	BDL	BDL	1.5	1.5	1.5
H1/400	400	BDL	BDL	BDL	BDL	BDL	0.7	0.7	0.7
H1/500	500	BDL	BDL	BDL	BDL	BDL	0.7	0.7	0.7
H1/600	600	BDL	BDL	BDL	BDL	BDL	0.6	0.6	0.7
H1/660	660	BDL	BDL	BDL	BDL	BDL	0.6	0.6	0.7
H1/680	680	BDL	BDL	BDL	BDL	BDL	BDL	BDL	0.7
H1/700	700	BDL	BDL	BDL	BDL	BDL	1	1	1
H1/760	760	BDL	BDL	BDL	BDL	BDL	0.8	1	1
H1/800	800	BDL	BDL	BDL	BDL	BDL	0.9	1	1
H1/860	860	BDL	BDL	BDL	BDL	BDL	0.8	1	1
H1/900	900	BDL	BDL	BDL	BDL	BDL	0.9	0.9	1
H1/960	960	BDL	BDL	BDL	BDL	BDL	0.9	1	1
H1/1000	1000	BDL	BDL	BDL	BDL	BDL	0.9	1	1

Ag (ppm)									
sample	depth	NH_4-Ac	Na-OC	HL	NH_4-OxH	H_2O_2	residual	total	bulk
H1/044	44	BDL	BDL	0.5	BDL	BDL	0.8	1.3	1.6
H1/100	100	BDL	BDL	0.3	BDL	BDL	0.8	1.1	0.9
H1/200	200	BDL	BDL	BDL	BDL	BDL	1.6	1.6	1.9
H1/300	300	BDL	BDL	BDL	BDL	BDL	3	3	3.6
H1/400	400	BDL	BDL	0.6	BDL	BDL	10.3	10.9	13.2
H1/500	500	BDL	BDL	BDL	BDL	BDL	5.1	5.1	5.7
H1/600	600	BDL	BDL	0.5	BDL	BDL	11.1	11.6	12.8
H1/660	660	BDL	BDL	0.4	BDL	BDL	8	8.4	9.2
H1/680	680	BDL	BDL	0.5	BDL	BDL	10.9	11.4	12.2
H1/700	700	BDL	BDL	0.4	BDL	BDL	9	10	10
H1/760	760	BDL	BDL	0.2	BDL	BDL	15.2	15	17
H1/800	800	BDL	BDL	0.4	BDL	BDL	23.2	24	23
H1/860	860	BDL	BDL	0.5	BDL	BDL	17.3	18	18
H1/900	900	BDL	BDL	0.3	BDL	BDL	22.8	23.1	23
H1/960	960	BDL	BDL	BDL	BDL	BDL	25.4	25	26
H1/1000	1000	BDL	BDL	0.3	BDL	BDL	22.3	23	22

Abbreviation as in appendix. 2

Fe (%)

sample	depth	H_2O	NH4-Ac	NH_4-OxD	NH_4-OxH	H_2O_2	sulfide	residual	total	bulk
H1/200	200	BDL	0.1	1.78	3.17	0.02	9.02	3.68	17.8	20
H1/680	680	BDL	0.16	3.1	3.11	BDL	1.56	0.97	8.9	9.9
H1/760	760	BDL	0.15	4.13	2.86	0.09	2.85	1.66	11.7	12.8
H1/860	860	BDL	0.12	2.08	4.51	0.01	2.08	1.14	9.94	10.3
H1/1000	1000	BDL	0.16	3.82	4.26	0.07	2.14	1.38	11.8	11.9

Al (%)

sample	depth	H_2O	NH4-Ac	NH_4-OxD	NH_4-OxH	H_2O_2	sulfide	residual	total	bulk
H1/200	200	BDL	0.01	0.03	0.1	BDL	0.36	2.9	3.4	3.78
H1/680	680	BDL	0.02	0.11	0.12	BDL	0.43	2.41	3.09	3.65
H1/760	760	BDL	0.02	0.12	0.24	BDL	0.71	4.12	5.21	5.59
H1/860	860	BDL	0.01	0.13	0.32	BDL	0.81	3.78	5.05	5.22
H1/1000	1000	BDL	0.04	0.19	0.31	BDL	0.75	4.21	5.5	5.65

K (%)

sample	depth	H_2O	NH4-Ac	NH_4-OxD	NH_4-OxH	H_2O_2	sulfide	residual	total	bulk
H1/200	200	0.01	BDL	BDL	BDL	BDL	-	0.45	0.46	0.54
H1/680	680	0.02	BDL	BDL	BDL	BDL	-	0.61	0.63	0.83
H1/760	760	0.04	0.01	0.03	0.01	BDL	-	1.13	1.22	1.45
H1/860	860	0.03	0.01	0.02	0.05	BDL	-	1.48	1.59	1.83
H1/1000	1000	0.02	0.01	0.05	0.02	BDL	-	1.46	1.56	1.76

Mg (%)

sample	depth	H_2O	NH4-Ac	NH_4-OxD	NH_4-OxH	H_2O_2	sulfide	residual	total	bulk
H1/200	200	BDL	0.01	0.02	0.05	0.01	0.3	0.57	0.96	1.07
H1/680	680	0.02	0.04	0.02	0.06	0.01	0.42	0.17	0.74	0.78
H1/760	760	0.03	0.02	0.02	0.09	0.03	0.58	0.37	1.14	1.17
H1/860	860	0.03	BDL	0.02	0.16	0.01	0.65	0.25	1.12	1.09
H1/1000	1000	0.03	0.02	0.02	0.13	0.02	0.55	0.35	1.12	1.1

Na (%)

sample	depth	H_2O	NH4-Ac	NH_4-OxD	NH_4-OxH	H_2O_2	sulfide	residual	total	bulk
H1/200	200	0.02	BDL	BDL	BDL	BDL	BDL	1.4	1.42	1.6
H1/680	680	0.03	BDL	BDL	BDL	BDL	BDL	1	1.03	1.27
H1/760	760	0.03	BDL	0.01	BDL	0.01	BDL	0.97	1.02	1.16
H1/860	860	0.04	BDL	BDL	0.02	BDL	BDL	0.72	0.78	0.86
H1/1000	1000	0.03	BDL	0.02	BDL	BDL	0.07	0.82	0.94	0.97

Ca (%)

sample	depth	H_2O	NH4-Ac	NH_4-OxD	NH_4-OxH	H_2O_2	sulfide	residual	total	bulk
H1/200	200	0.31	1.16	BDL	BDL	0.43	0.66	4.9	7.46	8.47
H1/680	680	2.64	9.37	0.01	0.01	0.41	0.16	0.31	12.9	15.5
H1/760	760	2.56	3.06	BDL	0.01	0.25	0.21	0.76	6.85	6.93
H1/860	860	3.28	2.36	0.01	0.02	0.16	0.17	0.34	6.34	6.01
H1/1000	1000	2.83	1.72	0.01	0.02	0.17	0.15	0.45	5.35	5.15

Tl (%)

sample	depth	H_2O	NH4-Ac	NH_4-OxD	NH_4-OxH	H_2O_2	sulfide	residual	total	bulk
H1/200	200	BDL	BDL	BDL	BDL	BDL	0.02	0.14	0.16	0.19
H1/680	680	BDL	BDL	BDL	BDL	BDL	BDL	0.12	0.12	0.15
H1/760	760	BDL	BDL	BDL	BDL	BDL	0.01	0.17	0.18	0.21
H1/860	860	BDL	BDL	BDL	BDL	BDL	0.01	0.16	0.17	0.2
H1/1000	1000	BDL	BDL	BDL	BDL	BDL	0.01	0.17	0.18	0.21

P (%)

sample	depth	H_2O	NH4-Ac	NH_4-OxD	NH_4-OxH	H_2O_2	sulfide	residual	total	bulk
H1/200	200	BDL	BDL	0.04	0.01	BDL	0.08	BDL	0.13	0.12
H1/680	680	BDL	BDL	0.06	BDL	BDL	0.03	BDL	0.09	0.04
H1/760	760	BDL	BDL	0.06	BDL	BDL	0.03	0.01	0.1	0.08
H1/860	860	BDL	0.02	0.09	0.02	BDL	0.02	0.01	0.16	0.12
H1/1000	1000	BDL	0.01	0.09	0.01	BDL	0.03	0.01	0.15	0.12

Ba (ppm)

sample	depth	H_2O	NH4-Ac	NH_4-OxD	NH_4-OxH	H_2O_2	sulfide	residual	total	bulk
H1/200	200	BDL	4	2	5	BDL	2	108	121	149
H1/680	680	BDL	18	108	206	1	166	117	616	523
H1/760	760	BDL	30	87	403	BDL	916	332	1768	916
H1/860	860	BDL	7	152	108	BDL	1260	381	1908	852
H1/1000	1000	BDL	31	166	336	BDL	1170	316	2019	1240

Sr (ppm)

sample	depth	H_2O	NH4-Ac	NH_4-OxD	NH_4-OxH	H_2O_2	sulfide	residual	total	bulk
H1/200	200	3.6	4.7	BDL	BDL	1.4	2.3	69.2	81.2	92.4
H1/680	680	19.2	39.5	1.1	3.7	8	9.8	47	128	147
H1/760	760	14.1	14.8	0.8	5.9	11.3	33.4	87.7	168	181
H1/860	860	15.6	11.9	7.2	10.3	10.7	40.9	70.8	167	168
H1/1000	1000	14.8	9.9	6.6	6.8	11.4	42.5	85.7	178	184

Ni (ppm)

sample	depth	H_2O	NH4-Ac	NH_4-OxD	NH_4-OxH	H_2O_2	sulfide	residual	total	bulk
H1/200	200	BDL	2	4	2	21	46	6	81	74
H1/680	680	BDL	5	12	7	5	11	3	43	40
H1/760	760	BDL	6	21	8	7	24	6	72	70
H1/860	860	BDL	2	9	12	4	16	4	47	46
H1/1000	1000	BDL	3	15	12	6	19	7	62	61

Zr (ppm)

sample	depth	H_2O	NH4-Ac	NH_4-OxD	NH_4-OxH	H_2O_2	sulfide	residual	total	bulk
H1/200	200	BDL	BDL	3.1	1.9	BDL	3.3	42.4	50.7	57.3
H1/680	680	BDL	BDL	3.1	3.8	BDL	0.8	29.3	37	43.7
H1/760	760	BDL	BDL	5.4	BDL	BDL	1.2	32.1	38.7	49.2
H1/860	860	BDL	BDL	8.7	2.5	BDL	1.1	43.5	55.8	60.8
H1/1000	1000	BDL	BDL	9.8	1.9	BDL	0.9	37.5	50.1	60.4

Co (ppm)

sample	depth	H_2O	NH4-Ac	NH_4-OxD	NH_4-OxH	H_2O_2	sulfide	residual	total	bulk
H1/200	200	BDL	10	9	2	47	169	4	241	212
H1/680	680	2	7	27	13	16	23	1	89	83
H1/760	760	3	10	33	8	24	54	2	134	116
H1/860	860	4	4	14	21	14	23	2	82	70
H1/1000	1000	BDL	8	24	18	26	34	3	113	97

Sn (ppm)

sample	depth	H_2O	NH4-Ac	NH_4-OxD	NH_4-OxH	H_2O_2	sulfide	residual	total	bulk
H1/200	200	BDL	BDL	BDL	BDL	BDL	29	BDL	29	BDL
H1/680	680	BDL	BDL	BDL	BDL	BDL	29	BDL	29	BDL
H1/760	760	BDL	BDL	BDL	BDL	BDL	27	BDL	27	BDL
H1/860	860	BDL	BDL	BDL	BDL	BDL	28	BDL	28	BDL
H1/1000	1000	BDL	BDL	BDL	BDL	BDL	26	BDL	26	BDL

Cu (ppm)

sample	depth	H2O	NH4-Ac	NH4-OxD	NH4-OxH	H2O2	sulfide	residual	total	bulk
H1/200	200	5.7	464	108	12.2	689	165	10.6	1455	1400
H1/680	680	4.1	1540	616	167	559	3120	33.4	6040	6320
H1/760	760	7.8	1050	403	57.2	2220	878	40.4	4656	4310
H1/860	860	8.4	840	608	94.2	1530	1380	122	4583	4210
H1/1000	1000	5.5	769	512	80.1	2360	1010	120	4857	4540

Zn (ppm)

sample	depth	H_2O	NH4-Ac	NH_4-OxD	NH_4-OxH	H_2O_2	sulfide	residual	total	bulk
H1/200	200	BDL	2.2	2.6	2.2	7	11.6	5.9	31.5	20.3
H1/680	680	0.6	37.7	116	53.5	20	31.7	10.8	270.3	257
H1/760	760	1.5	61.6	304	122	64	111	41.8	705.9	674
H1/860	860	0.8	15.8	68.4	51.4	10.5	46.7	22.7	216.3	205
H1/1000	1000	0.6	31	134	84.5	21.9	66.4	30.8	369.2	339

Mn (ppm)

sample	depth	H_2O	NH4-Ac	NH_4-OxD	NH_4-OxH	H_2O_2	sulfide	residual	total	bulk
H1/200	200	BDL	155	33	65	30	177	749	1209	1420
H1/680	680	12	979	284	89	45	93	50	1552	1930
H1/760	760	41	487	680	105	71	201	149	1734	1820
H1/860	860	25	186	144	105	15	182	74	731	741
H1/1000	1000	25	237	283	121	29	199	94	988	972

Cr (ppm)

sample	depth	H_2O	NH4-Ac	NH_4-OxD	NH_4-OxH	H_2O_2	sulfide	residual	total	bulk
H1/200	200	BDL	BDL	3	3	BDL	13	7	26	18
H1/680	680	BDL	3	16	4	BDL	11	4	38	33
H1/760	760	2	2	26	6	BDL	9	6	51	37
H1/860	860	3	7	28	11	BDL	8	4	61	42
H1/1000	1000	BDL	6	29	7	BDL	7	6	55	36

Pb (ppm)

sample	depth	H_2O	NH4-Ac	NH_4-OxD	NH_4-OxH	H_2O_2	sulfide	residual	total	bulk
H1/200	200	BDL	BDL	BDL	BDL	BDL	9	BDL	9	15
H1/680	680	BDL	41	37	41	4	76	BDL	199	173
H1/760	760	BDL	49	99	48	4	172	5	377	321
H1/860	860	2	17	171	147	BDL	83	8	428	326
H1/1000	1000	BDL	20	200	77	BDL	111	11	419	321

Mo (ppm)

sample	depth	H_2O	NH4-Ac	NH_4-OxD	NH_4-OxH	H_2O_2	sulfide	residual	total	bulk
H1/200	200	BDL	BDL	BDL	BDL	BDL	2	BDL	2	BDL
H1/680	680	2	BDL	10	11	BDL	39	2	64	57
H1/760	760	4	BDL	24	7	BDL	115	4	154	138
H1/860	860	5	BDL	14	10	BDL	28	1	58	50
H1/1000	1000	3	BDL	29	12	BDL	57	2	103	91

V (ppm)

sample	depth	H_2O	NH4-Ac	NH_4-OxD	NH_4-OxH	H_2O_2	sulfide	residual	total	bulk
H1/200	200	BDL	BDL	7	16	BDL	39	46	108	125
H1/680	680	BDL	BDL	15	18	BDL	22	32	87	98
H1/760	760	3	BDL	28	22	BDL	25	55	133	139
H1/860	860	6	BDL	24	36	BDL	23	41	130	126
H1/1000	1000	BDL	BDL	31	32	BDL	22	55	140	141

As (ppm)

sample	depth	H_2O	NH4-Ac	NH_4-OxD	NH_4-OxH	H_2O_2	sulfide	residual	total	bulk
H1/200	200	BDL	BDL	15	BDL	BDL	50	BDL	65	13
H1/680	680	BDL	BDL	106	57	BDL	27	BDL	190	164
H1/760	760	BDL	7	948	71	BDL	107	BDL	1133	982
H1/860	860	4	11	207	71	BDL	65	BDL	358	302
H1/1000	1000	BDL	11	359	68	BDL	82	BDL	520	453

W (ppm)

sample	depth	H_2O	NH4-Ac	NH_4-OxD	NH_4-OxH	H_2O_2	sulfide	residual	total	bulk
H1/200	200	BDL	BDL	BDL	BDL	BDL	BDL	BDL	BDL	BDL
H1/680	680	BDL	BDL	BDL	BDL	BDL	BDL	BDL	BDL	BDL
H1/760	760	BDL	BDL	BDL	BDL	BDL	BDL	BDL	BDL	BDL
H1/860	860	BDL	BDL	BDL	BDL	BDL	BDL	BDL	BDL	BDL
H1/1000	1000	BDL	BDL	BDL	BDL	BDL	BDL	BDL	BDL	BDL

La (ppm)

sample	depth	H_2O	NH4-Ac	NH_4-OxD	NH_4-OxH	H_2O_2	sulfide	residual	total	bulk
H1/200	200	BDL	0.6	2.4	1.5	BDL	4.1	13.2	21.8	11.9
H1/680	680	BDL	2.6	1.1	4.8	BDL	8.5	9.1	26.1	22.1
H1/760	760	BDL	2.2	3.7	0.7	2.9	9.6	12.8	32.1	28.2
H1/860	860	BDL	3.2	9	7.1	2.4	21	18.2	60.9	46.9
H1/1000	1000	BDL	2.1	10.1	5.9	3.4	17	19.4	57.9	45.5

Y (ppm)

sample	depth	H_2O	NH4-Ac	NH_4-OxD	NH_4-OxH	H_2O_2	sulfide	residual	total	bulk
H1/200	200	BDL	BDL	BDL	BDL	BDL	1.1	6.4	7.5	9.9
H1/680	680	BDL	2.5	BDL	BDL	0.7	2.3	2.8	8.3	11.2
H1/760	760	0.9	2	2.4	0.9	1.4	3.3	4.2	15.1	14.8
H1/860	860	1.4	2.1	2.2	1.3	BDL	3.6	5.1	15.7	15.1
H1/1000	1000	BDL	1.5	2.2	1.4	0.6	4.2	4.8	14.7	16.9

Sc (ppm)

sample	depth	H_2O	NH4-Ac	NH_4-OxD	NH_4-OxH	H_2O_2	sulfide	residual	total	bulk
H1/200	200	BDL	BDL	BDL	BDL	BDL	5	5	7.7	
H1/680	680	BDL	1.8	0.6	0.8	BDL	1	2 8	7	8.8
H1/760	760	BDL	1	1.8	0.6	BDL	1.4	5.4	10.2	12.4
H1/860	860	BDL	0.8	2.6	1.3	BDL	1.7	4.5	10.9	12.3
H1/1000	1000	BDL	0.8	2.5	1.2	BDL	1.5	5.5	11.5	13

Be (ppm)

sample	depth	H_2O	NH4-Ac	NH_4-OxD	NH_4-OxH	H_2O_2	sulfide	residual	total	bulk
03/025	25	BDL	BDL	BDL	BDL	BDL	0.5	BDL	0.5	0.8
03/070	70	BDL	BDL	BDL	BDL	BDL	BDL	BDL	BDL	0.8
03/200	200	BDL	BDL	BDL	BDL	BDL	BDL	BDL	BDL	0.8
03/300	300	BDL	BDL	BDL	BDL	BDL	BDL	BDL	BDL	0.8
03/500	500	BDL	BDL	BDL	BDL	BDL	BDL	BDL	BDL	0.8

Ag (ppm)

sample	depth	H_2O	NH4-Ac	NH_4-OxD	NH_4-OxH	H_2O_2	sulfide	residual	total	bulk
H1/200	200	BDL	BDL	BDL	BDL	0.3	1.2	0.2	1.7	BDL
H1/680	680	1	BDL	BDL	BDL	0.3	9.5	0.6	11.4	10.6
H1/760	760	3.4	BDL	BDL	0.2	0.3	12.5	1.4	17.8	13.6
H1/860	860	5.3	BDL	BDL	BDL	BDL	13.8	1.9	21	15.2
H1/1000	1000	1.7	BDL	BDL	BDL	BDL	17.3	2.2	21.2	20

The oxyanions Mo, As, and V show also peaks at in the lowest part of the oxidation zone and increased values in the cementation zone compared to the upper parts of the drill core (Figs. 9 and 10). These elements have a high affinity to ferric hydroxides under acid conditions (Dzombak and Morel, 1990). Arsenic is mainly associated with the easily reducible Fe(III) hydroxide fraction cementation zone. Vanadium enrichments are associated to the water-soluble, Fe(III) hydroxide, and Fe(III) oxide fractions (Fig. 10). Vanadium is the only heavy metal available in relevant amounts in the water-soluble fraction in the cementation zone. This may be explained by its complex geochemical speciation. Under oxidizing conditions V is stable as $H_2VO_4^-$ in the pH range between 2 and 8. Under reducing conditions it is stable as VO^{2+} up to pH values of 5 (Brookins, 1988). $H_2VO_4^-$ is possibly adsorbed under acid conditions at ferric polymers (continiuum of aqueous ferric complexes with more than one iron atom and including the collodial size fraction). Due to the recent high water input at the tailings, the ferric polymers may migrate downwards and transfer the adsorbed V to areas under reducing conditions, where it will be available as water-soluble cation VO^{2+} in the low pH cementation zone. Mo shows its highest concentrations in the sulfide leach in the lowest part of the oxidation zone (Fig. 10). This is interpreted as secondary Mo-sulfide precipitation under the slightly reducing conditions below the water level.

6.6.1.5 Conclusions Ojancos

In the study of the Ojancos tailings impoundment No. 2 it was possible to discriminate between primary differences in the ores treated during the plant history and superimposed secondary element enrichment associated to sulfide oxidation processes. The about 3 m thick primary zone at the top of the impoundment No. 2 results from recent deposition coeval to the "2H" tailings. Parts of this primary material (the "2H" tailings deposited directly uphill were flushed down and deposited on the top of impoundment No. 2 (Fig. 11C). This is supported by the similar mineralogical composition of the primary zone at the top of the impoundment No. 2 and the composition of the sample HPr from the recent discharge point at "2H". In both cases the tailings derive from an ore characterized by Ca-amphibole alteration mined at the Pintadas district. Below, there is a 4 m thick interval of calcite-rich tailings, probably derived from the Teresita mine. The lower part of the tailings impoundment No. 2 indicates that the treated ore had a chlorite-epidote alteration, typical of the eastern part of the Punta del Cobre belt (Fig. 11A).

The 5 m thick neutral oxidation zone located below the recent primary zone is interpreted as the "paleo"-oxidation zone formed during the ten years in which the impoundment No. 2 was out of operation (Fig. 11B, 1977-1987). The characteristics of this carbonate-rich (around 40 wt.% calcite and 2 wt.% pyrite), neutral oxidation zone are similar to those of the oxidation zone encountered in the carbonate-rich tailings of the P. Cerda treatment plant discussed in section 6.6.2 of this chapter. The neutral oxidation zone at Ojancos, as well as the one in P. Cerda, are characterized by low quantities of secondary ferric minerals spatially associated with fine-grained horizons and low mobility of metals due to high pH. Normally, in tailings with less carbonate minerals, the heavy metals are leached out from the oxidation zone and transported

downwards, and a cemented layer, essentially made up of by secondary ferric phases formed by hydrolysis and precipitation following ferrous iron oxidation and a pH increase, is built below the low pH oxidation zone at the interface to a neutralizing primary zone. This mechanism can not be responsible for the high amounts of secondary ferric phases with adsorbed heavy metal enrichments encountered in the underlying cementation zone of the Ojancos No. 2 impoundment, as the high calcite content of most of the oxidation zone prevents formation of low pH conditions and restricts element mobility. Additionally, the lack of water input during the ten years of oxidation (hyper-arid climate) limited the downwards element migration. It can be concluded, therefore, that the carbonate-rich oxidation zone can not be a significant source of the elements enriched in the underlying cementation zone. The lowermost part of the oxidation zone, i.e., the about 1 m thick interval developed over tailings derived from ores with chlorite-epidote alteration, could be a source of heavy metals, but high pH values limit the element mobility and suggest that the decreasing calcite values in the cementation zone with depth are an effect of neutralization reactions with acidic solutions.

The primary zone on top of impoundment No 2, which as indicated above is coeval with the "2H" tailings, does not show signs of oxidation, possibly because it is too recent and new primary tailings have been continuously flushed down (Fig. 11C). Even if any AMD was produced and seeped down it would be neutralized by the carbonate-rich oxidation zone before reaching the cementation zone and the pH increase would prevent any significant metal transport. Thus, the primary zone on top of impoundment No. 2 does not appear as potential source of elements contributing to the formation of the cemented layers.

Fig. 11: *Proposed model to explain the stratigraphy found in the Ojancos tailings impoundment No.2.* ***A:*** *Until 1977 the Ojancos treatment plant bought the ore from different mines in the Punta del cobre belt, leading to an interlayering of carbonate–rich and carbonate poor layers. During operation, the impoundment was water saturated and no oxidation took place.* ***B:*** *In 1977-1987 the operation ceased at the impoundment No. 2 and an oxidation zone in the calcite-rich upper part was formed.* ***C:*** *1987 the recent deposition at "2H" started, resulting in the coeval flush-down of primary tailings over the old oxidation zone.* ***D:*** *Simultaneously, sulfide oxidation took place at "2H" and AMD started to seep into the impoundment No. 2. Acid metal loaded solutions were neutralized at horizons with high calcite content, hydrolysis of ferric phases is initiated and the formation of a cementation zone could start. With time, this low permeability cementation zone changed the downwards water-flow to a lateral flow-path on the top of the cementation zone, leading to heavy metal enrichment in and directly above the cementation zone.* ***E:*** *The situation encountered during the sampling period shows that the cementation zone can be observed in the whole impoundment. It is not clear if the whole underlying material is cemented or primary material is still remaining.* ***F:*** *The operation stopped 1998, under the prevailing extreme arid climate the migration direction will change to upwards, the recent primary zone will start to oxidize and due to the lower neutralization potential in the primary zone and in "2H" possibly low pH conditions will develop, leading to the formation of efflorescent salts at the top of the tailings.*

Proposed model of the development of the stratigraphy found in the Ojancos tailings impoundment No. 2

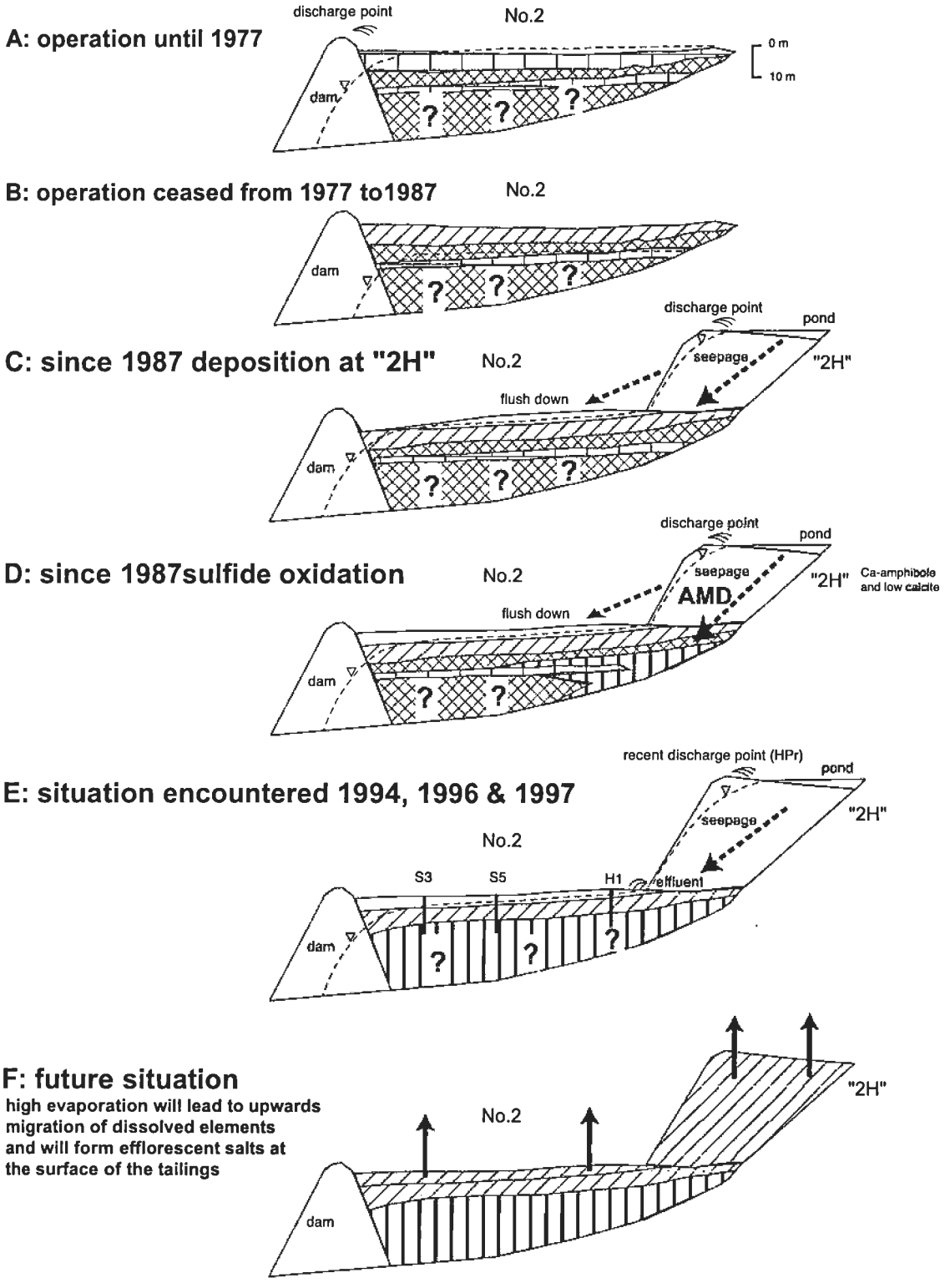

The only significant source left for the secondary metal enrichment underlying the carbonate-rich oxidation zone of the No. 2 impoundment is AMD seepage from the recently deposited tailings "2H" on the hillside upstream of impoundment No. 2 (Fig. 11D). Indeed, the appearance at the surface of low-pH AMD effluents with the precipitation of schwertmannite, chalcoalumite, and gypsum at the foot of the recently deposited "2H" tailings, indicates that extensive pyrite oxidation and neutralization reactions take place in the "2H" tailings (Fig. 11E). Layers with high neutralization potential are (most probably) present in the form of high carbonate intercalations from the Teresita mine, but the existence of low-pH seepage demonstrates that they can not prevent the formation of AMD.

The formation of the low permeable cementation zone intersected in the lower 2 m of the drillings can be explained as follows. The metal-rich solutions seep first downwards in the tailings "2H" and then laterally into the tailings impoundment No. 2 (Fig. 11D). Precipitation is initiated when the solution encounters originally calcite rich layers, as for instance the basal part of the cementation zone (still calcite-bearing and with a pH of 6). The resulting pH increase favors hydrolysis and precipitation of Fe compounds and secondary ferric phases such as higher ordered ferrihydrite, goethite, gypsum, and locally jarosite. High concentrations of Fe, Ca, K, and SO_4 in the first four steps of the sequence B in the cementation zone support indeed an abundant presence of these minerals. The high ordering of the ferrihydrite indicates slow oxidation and hydrolysis kinetics (Schwertmann et al., 1999). By precipitation of the secondary ferric phases the pore space is sealed and the low permeable cementation zone is formed with the typical mineral paragenesis of the so-called "hardpans" (Blowes et al., 1991, Tassé et al., 1997, Lin, 1997).

It can be envisaged that lateral flow is channeled within less reactive intervals between low permeability layers. In the section cut by drill hole H1, effective lateral flow appears to be restricted to an about 1 m thick interval between the homogeneous, low permeability cementation zone, found at the bottom of the drill hole and the overlying carbonate-rich oxidation zone (Fig. 11E). It is in this interval where most of the heavy metals are enriched by adsorption processes (e.g., Zn, Pb, As, and V) or by precipitation of secondary minerals (Cu, Mo, and Pb).

It can be hypothesized that, as the cementation zone progressively develops and permeability decreases, the interval with efficient lateral water flow would migrate upwards as long as supply of acid solutions exists or precipitation of ferric hydroxides do not seal the flow path. In this way, the cementation zone may equally migrate upwards, as suggested by Dold et al. (1996).

Besides this enrichment, the element speciation provides other indication for the existence of a significant water flow in this interval. The increased concentrations of V and Mo in the water-soluble fraction in the upper part of the cementation zone are consistent with the interpreted lateral water flow. Constant concentrations of Cu, Pb, and V in the cementation zone indicate that the conditions were similar during formation, leading to retention of these metals via adsorption or precipitation of secondary sulfides. The peaks at the top of the cementation zone of most metals is seen as recent retention process, due to increasing pH, by approaching the carbonate-rich oxidation zone. The decrease of the pH by increased flow of acid solutions and

hydrolysis of Fe(III) hydroxides and thus the upwards migration of the cementation zone should remobilize a part of the adsorbed elements (e.g., Cu, Zn) in the oxidation zone, making them available for sulfide precipitation (Cu and possibly Zn and Pb) or for adsorption at other places of higher pH.

In conclusion, the Ojancos tailings impoundment No. 2 constitutes an example in which a complex deposition history and impoundment construction largely influence the distribution of primary, oxidation, and cemention zones.

6.6.2 Tailings impoundments No. 4 and 6 of the Pedro A. Cerda treatment plant, Fe-oxide Cu-Au deposit Ojos del Salado, Tierra Amarilla, south of Copiapó, northern Chile

6.6.2.1 Physical properties and mineralogy P. Cerda tailings impoundments No.4 and 6.

The four holes drilled in tailings impoundments No. 4 and 6 from the P. Cerda flotation plant reached a maximum depth of 5.9 m. The paste pH in all core samples remained in the neutral range (6.9 – 8.3). Calcite content amounts to about 10 wt.% and pyrite up to 2.5 wt.%. The younger upstream impoundment No. 4 has an oxidation zone at the top with 5 m thickness in drill core O1 and 3.6 m in drill core O2 (Fig. 3). The oxidation zone is very similar to that of Ojancos impoundment No. 2 and shows alternating coarse grain-sized horizons without macroscopic indication of oxidation and fine-grained horizons of ochre to reddish brown color indicating the precipitation of secondary Fe(III) hydroxides (Fig. 4). Below the oxidized zone is a dark gray colored primary zone. The moisture content increases in core O1 from 2.7 wt.% at the top to maximum values of 22.2 wt.% at depth. In core O2, near the dam, the maximum moisture content is 5.2 wt.%.

The mineralogical composition in impoundment No. 6 is homogeneous. With decreasing abundance, the main minerals are quartz, chlorite, calcite, albite ± anorthoclase, magnetite, hematite, epidote, and gypsum. As mentioned above, the chlorite-epidote assemblage is an indicator for the alteration in the eastern part of the Punta del Cobre belt. Polished sections reveal that the pyrite is strongly fractured but does not show oxidation rims or coatings. The pyrite content varies strongly. Traces of chalcopyrite and very minor supergene replacement by chalcocite–digenite occur. Secondary covellite is detected as a trace constituent in the lower part of the primary zone. Magnetite is generally coarse-grained, in places partly martitized. Hematite dominates in form of mm-sized grains of specularite as described by Marschik (1996).

Drill core O4 at the older impoundment No. 4 shows a similar composition and the same interlayering as described for impoundment No. 6 based on drill cores O1 and O2. Differences are the higher amounts of calcite and dolomite, and less chlorite. The moisture content is also low with maximum values up to 7 %, which is consistent with its location near the dam.

The stratigraphy of drill core O3, located at the foot of impoudment No. 6 shows an important difference. From the top to the bottom the drill core intersects first a homogeneous gray- green primary zone interpreted to have flushed down from the impoundment No. 6. Below, an oxidation zone with Fe(III) hydroxide rich horizons follows to a depth of 1.8 m. Acid-base accountings show that the upper two meters have a negative SNNP (-75.9 t $CaCO_3$/1000t)

indicating a significant acid producing potential of the primary zone, while the underlying, homogeneous reddish brown, silty-glayey ($K = 3.3x10^{-8} - 3.6x10^{-8}$ m/s) cementation zone has neutralizing potential (SNNP = 24.4 t $CaCO_3$/1000t). This reddish-brown zone is similar to the cementation zone described in chapter 6.6.1 in the Ojancos impoundment No. 2. The moisture content increases in O3 from zero at the top to a constant value of 23 wt.% in the cementation zone. The mineralogy in this part of the impoundment is dominated by quartz, albite ± anorthoclase, calcite, chlorite, magnetite, hematite, epidote, pyrite, and minor gypsum. Relative to the oxidized zone, gypsum is high in the cementation zone, whereas calcite is less abundant . Polished sections show that, in the cementation zone only, some residual, very small pyrite grains remain. The reddish brown color suggests that ferrihydrite and goethite are present, but DXRD did not show conclusive results.

6.6.2.2 Geochemical results

Constant Ti values and XRD results of drill core O1 (impoundment No. 6) indicate that the upper five meters of the tailings are from similar composition, and derived from an ore with a calcite-rich gangue. Results from sequential extractions (Fig. 12, sequence A) show that the major elements Na, Fe, K, Ca, and Mg are not significantly mobilized under the near neutral pH condition prevailing in the impoundment. However, metals which under oxidizing and acid to neutral conditions are stable as bivalent cations, as Cu, Zn, and Mn, show concentrations decrease at the top of the oxidation zone and enrichments in the exchangeable fraction and in the fraction of the Fe(III) hydroxides in samples located below (Fig. 12, Table 4). Cu shows a slight increase downwards in the fraction of secondary copper sulfides (from 66 ppm at the top to 930 ppm at 5 m depth in the H_2O_2-leach), which is consistent with the presence of traces of secondary covellite. The oxyanions Mo and As show increasing values with depth mainly in the fraction of the Fe(III) hydroxides.

Results from sequential extractions (Fig. 13, Table 5, sequence B) of drill core O3 (impoundment No. 4) show slightly decreasing concentrations in the primary zone of Ti and Al, suggesting a different origin of the upper part of the tailings, which consistent with the hypothesis that they have flushed down from the younger impoundment No. 6. Fe, SO_4, Ca, Cu, Zn, Mn, Mo, and As show increased concentrations in the cementation zone in the exchangeable fraction and the fraction of the Fe(III) hydroxides (Fig. 12). The high Fe, SO_4, and Ca concentrations are consistent with abundant gypsum observed by XRD and visible Fe(III) hydroxides. The high Mn concentration, mainly in the exchangeable fraction of the cementation zone, is interpreted as a result of calcite dissolution in this leach, similarly as discussed above for Ojancos. The enrichment of the heavy metals Cu, Zn, Mo, as well as of As in the cementation zone is strongly associated to Fe(III) hydroxides and the exchangeable fraction, suggesting they are adsorbed to ferric polymers.

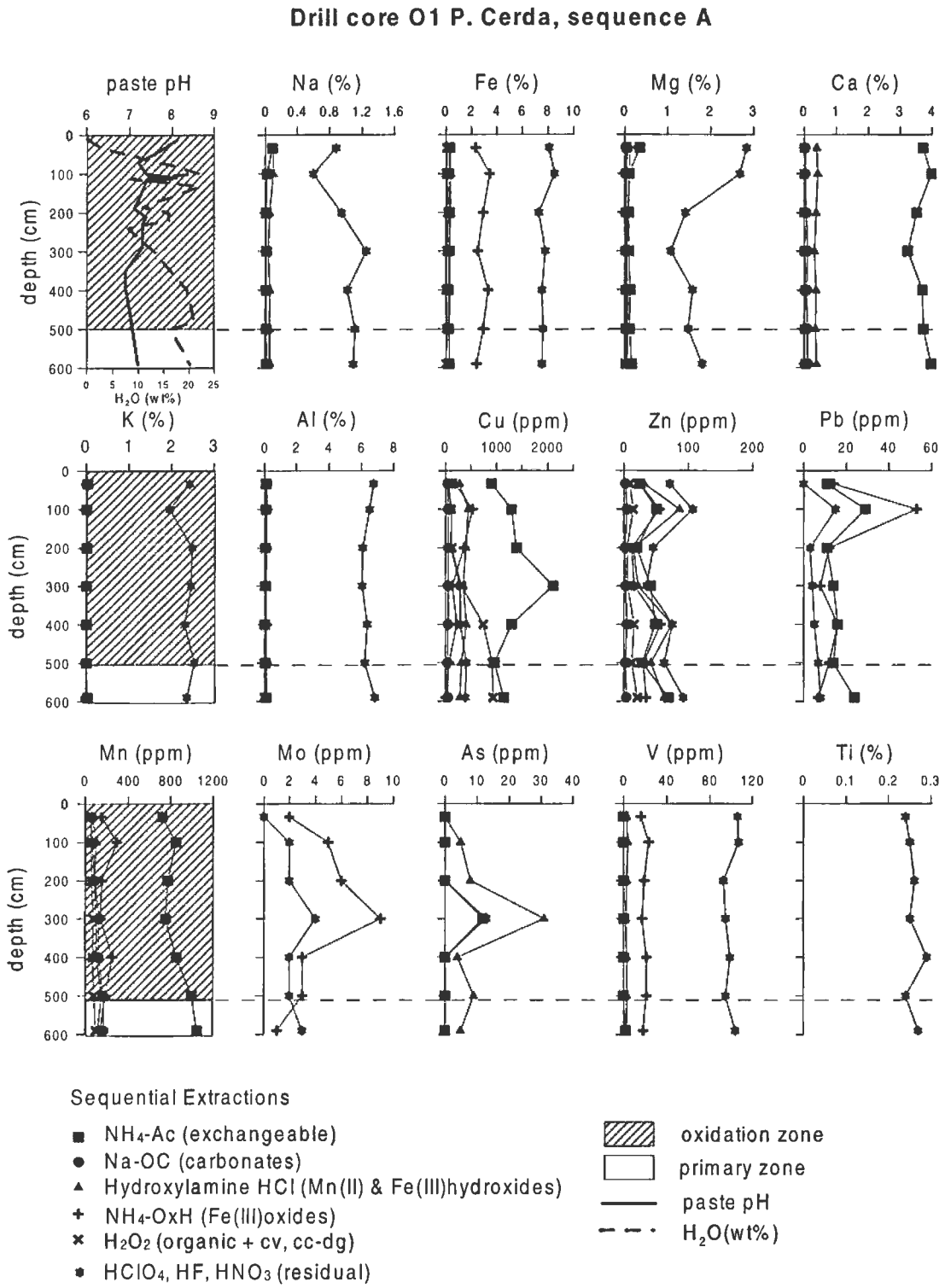

Fig. 12: Results of sequential extraction (sequence A) of drill core O1 from the P. Cerda impoundment No. 6.

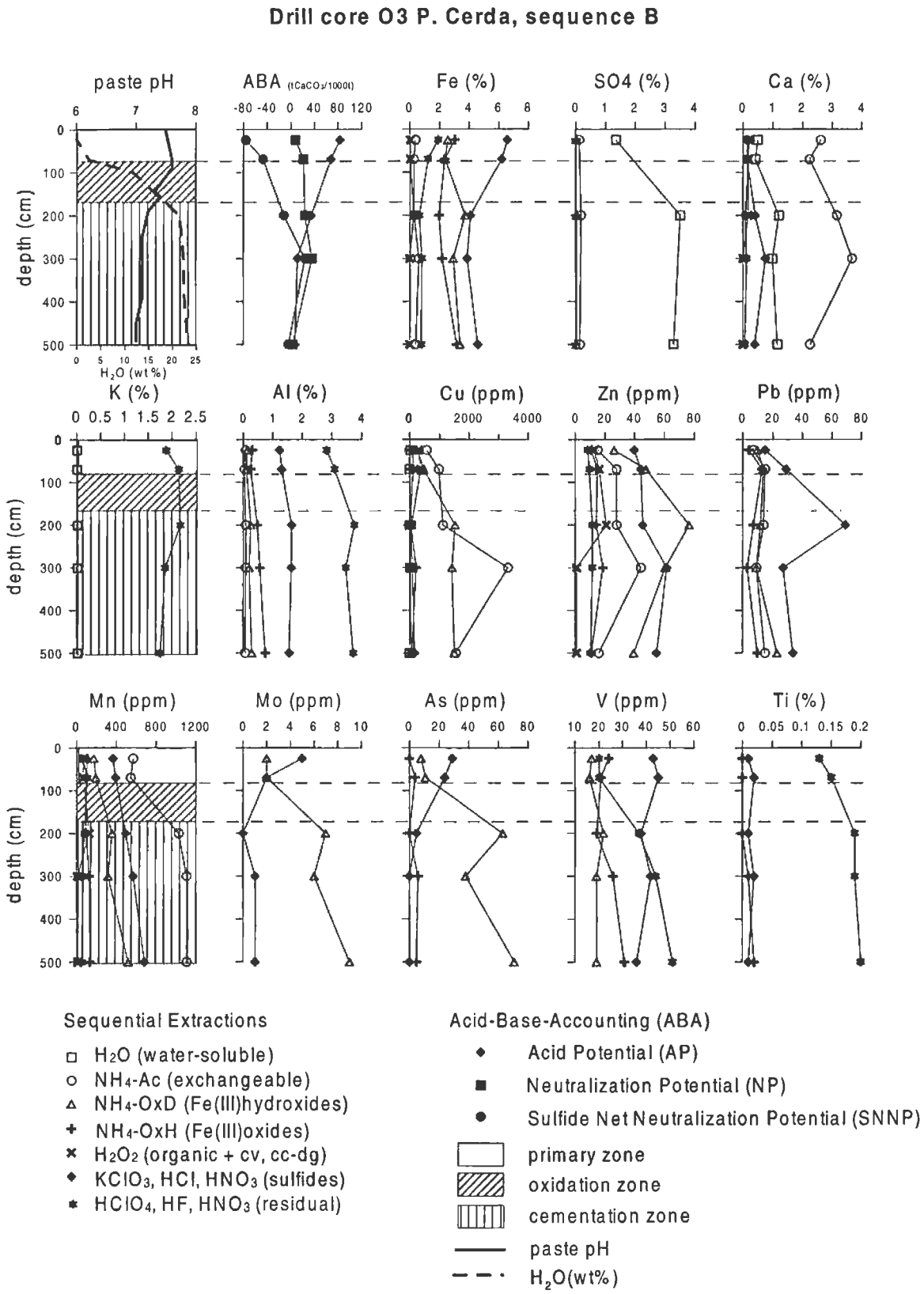

***Fig. 13**: Results of sequential extraction (sequence B) of drill core O3 from the P. Cerda impoundment No. 4.*

Fe (%)

sample	depth	NH_4-Ac	Na-OC	HL	NH_4-OxH	H_2O_2	residual	total	bulk
O1/034	34	0.3	BDL	0.36	2.33	0.08	8.12	11.19	10.5
O1/100	100	0.21	BDL	0.39	3.44	0.05	8.54	12.63	11.9
O1/200	200	0.29	BDL	0.39	2.92	0.17	7.32	11.09	11
O1/300	300	0.27	BDL	0.3	2.53	0.1	7.79	10.99	10.8
O1/400	400	0.2	BDL	0.32	3.3	0.07	7.56	11.45	11.1
O1/500	500	0.21	BDL	0.3	2.92	0.08	7.64	11.15	10.9
O1/590	590	0.31	BDL	0.32	2.43	0.07	7.54	10.67	10

Al (%)

sample	depth	NH_4-Ac	Na-OC	HL	NH_4-OxH	H_2O_2	residual	total	bulk
O1/034	34	0.09	BDL	0.09	0.15	0.02	6.73	7.08	7.16
O1/100	100	0.05	BDL	0.08	0.18	0.02	6.51	6.84	7
O1/200	200	0.06	BDL	0.06	0.12	0.02	6.1	6.36	6.9
O1/300	300	0.05	BDL	0.05	0.1	BDL	6.05	6.25	6.75
O1/400	400	0.04	BDL	0.07	0.13	0.01	6.36	6.61	6.85
O1/500	500	0.05	BDL	0.06	0.13	BDL	6.24	6.48	6.86
O1/590	590	0.1	BDL	0.09	0.12	BDL	6.84	7.15	7.16

K (%)

sample	depth	NH_4-Ac	Na-OC	HL	NH_4-OxH	H_2O_2	residual	total	bulk
O1/034	34	0.05	BDL	0.01	BDL	BDL	2.43	2.49	2.47
O1/100	100	0.02	BDL	0.02	0.01	BDL	1.96	2.01	2.18
O1/200	200	0.03	BDL	0.01	BDL	BDL	2.49	2.53	2.76
O1/300	300	0.02	BDL	0.01	BDL	BDL	2.47	2.5	2.67
O1/400	400	0.02	BDL	BDL	BDL	BDL	2.32	2.34	2.45
O1/500	500	0.02	BDL	BDL	BDL	BDL	2.55	2.57	2.72
O1/590	590	0.04	BDL	0.01	BDL	BDL	2.37	2.42	2.38

Mg (%)

sample	depth	NH_4-Ac	Na-OC	HL	NH_4-OxH	H_2O_2	residual	total	bulk
O1/034	34	0.35	0.03	0.07	0.12	0.04	2.84	3.45	3.32
O1/100	100	0.11	0.01	0.04	0.11	0.03	2.69	2.99	2.97
O1/200	200	0.1	0.02	0.03	0.07	0.02	1.42	1.66	1.72
O1/300	300	0.1	0.03	0.03	0.06	0.02	1.07	1.31	1.33
O1/400	400	0.13	0.03	0.04	0.08	0.02	1.58	1.88	1.85
O1/500	500	0.12	0.03	0.05	0.08	0.02	1.48	1.78	1.8
O1/590	590	0.17	0.04	0.05	0.06	0.02	1.81	2.15	2.08

Na (%)

sample	depth	NH_4-Ac	Na-OC	HL	NH_4-OxH	H_2O_2	residual	total	bulk
O1/034	34	0.09	BDL	0.1	BDL	BDL	0.88	1.07	0.97
O1/100	100	0.02	BDL	0.1	BDL	BDL	0.6	0.72	0.63
O1/200	200	0.01	BDL	0.05	BDL	BDL	0.95	1.01	1.05
O1/300	300	0.01	BDL	0.04	BDL	BDL	1.25	1.3	1.35
O1/400	400	0.01	BDL	0.06	BDL	BDL	1.02	1.09	1.06
O1/500	500	0.01	BDL	0.05	BDL	BDL	1.12	1.18	1.17
O1/590	590	0.02	BDL	0.06	BDL	BDL	1.1	1.18	1.11

Ca (%)

sample	depth	NH_4-Ac	Na-OC	HL	NH_4-OxH	H_2O_2	residual	total	bulk
O1/034	34	3.71	0.04	0.39	BDL	0.01	0.11	4.26	3.69
O1/100	100	3.99	0.04	0.43	BDL	0.01	0.19	4.66	4.07
O1/200	200	3.51	0.07	0.38	BDL	0.01	0.2	4.17	3.71
O1/300	300	3.23	0.1	0.32	BDL	0.02	0.2	3.87	3.36
O1/400	400	3.7	0.09	0.37	BDL	0.03	0.6	4.79	4.13
O1/500	500	3.73	0.11	0.36	BDL	0.02	0.47	4.69	4.05
O1/590	590	3.99	0.12	0.39	BDL	0.03	0.42	4.95	4.21

Tl (%)

sample	depth	NH_4-Ac	Na-OC	HL	NH_4-OxH	H_2O_2	residual	total	bulk
O1/034	34	BDL	BDL	BDL	BDL	BDL	0.24	0.24	0.19
O1/100	100	BDL	BDL	BDL	BDL	BDL	0.25	0.25	0.21
O1/200	200	BDL	BDL	BDL	BDL	BDL	0.26	0.26	0.2
O1/300	300	BDL	BDL	BDL	BDL	BDL	0.25	0.25	0.21
O1/400	400	BDL	BDL	BDL	BDL	BDL	0.29	0.29	0.23
O1/500	500	BDL	BDL	BDL	BDL	BDL	0.24	0.24	0.22
O1/590	590	BDL	BDL	BDL	BDL	BDL	0.27	0.27	0.22

P (%)

sample	depth	NH_4-Ac	Na-OC	HL	NH_4-OxH	H_2O_2	residual	total	bulk
O1/034	34	BDL	BDL	0.14	0.04	BDL	0.01	0.19	0.13
O1/100	100	BDL	BDL	0.13	0.06	BDL	0.01	0.2	0.15
O1/200	200	BDL	BDL	0.12	0.05	BDL	BDL	0.17	0.13
O1/300	300	BDL	BDL	0.1	0.02	BDL	BDL	0.12	0.1
O1/400	400	BDL	BDL	0.11	0.05	BDL	0.01	0.17	0.12
O1/500	500	BDL	BDL	0.11	0.03	BDL	0.01	0.15	0.11
O1/590	590	BDL	BDL	0.14	0.02	BDL	0.01	0.17	0.12

Ba (ppm)

sample	depth	NH_4-Ac	Na-OC	HL	NH_4-OxH	H_2O_2	residual	total	bulk
O1/034	34	5	31	131	44	BDL	596	807	814
O1/100	100	4	28	139	88	BDL	676	935	945
O1/200	200	6	34	83	22	BDL	573	718	785
O1/300	300	5	31	51	14	BDL	588	689	738
O1/400	400	3	21	91	28	BDL	532	675	705
O1/500	500	6	36	86	20	BDL	615	763	796
O1/590	590	11	38	78	14	BDL	528	669	672

Sr (ppm)

sample	depth	NH_4-Ac	Na-OC	HL	NH_4-OxH	H_2O_2	residual	total	bulk
O1/034	34	34.9	4	6	1	1	53	99	102
O1/100	100	26	3	6	2	1	58	96	98
O1/200	200	20	2	4	1	1	48	75	81
O1/300	300	19	2	3	1	1	61	86	91
O1/400	400	23	2	5	1	1	58	89	92
O1/500	500	21	2	4	BDL	1	69	96	104
O1/590	590	25	2	4	BDL	1	67	98	99

Ni (ppm)

sample	depth	NH_4-Ac	Na-OC	HL	NH_4-OxH	H_2O_2	residual	total	bulk
O1/034	34	6	BDL	2	3	7	18	36	30
O1/100	100	6	BDL	3	9	6	19	43	36
O1/200	200	8	BDL	3	7	9	23	50	44
O1/300	300	6	BDL	2	4	5	20	37	33
O1/400	400	6	BDL	4	13	7	24	54	42
O1/500	500	5	BDL	3	6	6	22	42	35
O1/590	590	4	BDL	1	3	6	21	35	30

Cu (ppm)

sample	depth	NH_4-Ac	Na-OC	HL	NH_4-OxH	H_2O_2	residual	total	bulk
O1/034	34	907	44.4	279	195	66	55	1547	1550
O1/100	100	1290	58.5	450	533	107	116	2555	2600
O1/200	200	1390	54.3	406	359	132	103	2444	2540
O1/300	300	2110	55.3	352	138	324	290	3269	3290
O1/400	400	1290	59	413	229	743	298	3032	3050
O1/500	500	966	44.5	321	73	920	415	2740	2750
O1/590	590	1150	57.9	288	13	935	393	2837	2800

Zn (ppm)

sample	depth	NH_4-Ac	Na-OC	HL	NH_4-OxH	H_2O_2	residual	total	bulk
O1/034	34	24	2	31	25	9	71	163	130
O1/100	100	50	5	86	55	15	106	316	266
O1/200	200	20	1	15	13	4	46	99	80
O1/300	300	41	2	22	15	6	35	122	99
O1/400	400	49	5	74	57	15	75	276	231
O1/500	500	28	2	42	30	13	63	178	144
O1/590	590	69	4	63	34	21	92	283	227

Mn (ppm)

sample	depth	NH_4-Ac	Na-OC	HL	NH_4-OxH	H_2O_2	residual	total	bulk
O1/034	34	726	56	68	150	58	691	1749	1570
O1/100	100	853	71	110	291	56	974	2355	2160
O1/200	200	773	92	82	154	62	523	1686	1620
O1/300	300	754	127	108	145	78	500	1712	1580
O1/400	400	859	122	105	253	72	793	2204	2060
O1/500	500	996	170	156	186	84	659	2251	2010
O1/590	590	1050	169	120	138	103	757	2337	2110

Cr (ppm)

sample	depth	NH_4-Ac	Na-OC	HL	NH_4-OxH	H_2O_2	residual	total	bulk
O1/034	34	1	BDL	2	3	BDL	17	23	18
O1/100	100	BDL	BDL	2	5	BDL	18	25	19
O1/200	200	BDL	BDL	1	3	BDL	13	17	17
O1/300	300	BDL	BDL	1	2	BDL	11	14	12
O1/400	400	BDL	BDL	1	5	BDL	14	20	20
O1/500	500	1	BDL	1	5	BDL	16	23	16
O1/590	590	2	BDL	BDL	4	BDL	16	22	23

Pb (ppm)

sample	depth	NH_4-Ac	Na-OC	HL	NH_4-OxH	H_2O_2	residual	total	bulk
O1/034	34	11	BDL	9	14	BDL	BDL	34	29
O1/100	100	29	BDL	29	53	BDL	15	126	95
O1/200	200	11	BDL	7	12	BDL	3	33	28
O1/300	300	14	BDL	7	8	BDL	4	33	24
O1/400	400	16	BDL	10	16	BDL	5	47	36
O1/500	500	14	BDL	6	12	BDL	7	39	31
O1/590	590	24	BDL	6	7	BDL	8	45	39

Mo (ppm)

sample	depth	NH_4-Ac	Na-OC	HL	NH_4-OxH	H_2O_2	residual	total	bulk
O1/034	34	BDL	BDL	BDL	2	BDL	BDL	2	3
O1/100	100	BDL	BDL	BDL	5	BDL	2	7	5
O1/200	200	BDL	BDL	BDL	6	BDL	2	8	8
O1/300	300	BDL	BDL	BDL	9	BDL	4	13	11
O1/400	400	BDL	BDL	BDL	3	BDL	2	5	6
O1/500	500	BDL	BDL	BDL	3	BDL	2	5	4
O1/590	590	BDL	BDL	BDL	1	BDL	3	4	5

V (ppm)

sample	depth	NH_4-Ac	Na-OC	HL	NH_4-OxH	H_2O_2	residual	total	bulk
O1/034	34	BDL	BDL	3	16	BDL	106	125	122
O1/100	100	BDL	BDL	4	23	BDL	107	134	130
O1/200	200	BDL	BDL	3	19	BDL	93	115	121
O1/300	300	BDL	BDL	2	17	BDL	95	114	118
O1/400	400	BDL	BDL	3	21	BDL	99	123	123
O1/500	500	BDL	BDL	3	21	BDL	95	119	121
O1/590	590	2	BDL	3	18	BDL	104	127	122

As (ppm)

sample	depth	NH_4-Ac	Na-OC	HL	NH_4-OxH	H_2O_2	residual	total	bulk
O1/034	34	BDL	BDL	BDL	13	BDL	BDL	13	BDL
O1/100	100	BDL	BDL	5	34	BDL	BDL	39	20
O1/200	200	BDL	BDL	8	47	BDL	BDL	55	42
O1/300	300	12	BDL	31	63	BDL	13	119	89
O1/400	400	BDL	BDL	4	44	BDL	BDL	48	37
O1/500	500	BDL	BDL	9	57	BDL	BDL	66	36
O1/590	590	BDL	BDL	5	10	BDL	BDL	15	BDL

W (ppm)

sample	depth	NH_4-Ac	Na-OC	HL	NH_4-OxH	H_2O_2	residual	total	bulk
O1/034	34	BDL	BDL	BDL	BDL	BDL	BDL	BDL	BDL
O1/100	100	BDL	BDL	BDL	BDL	BDL	BDL	BDL	BDL
O1/200	200	BDL	BDL	BDL	BDL	BDL	BDL	BDL	BDL
O1/300	300	BDL	BDL	BDL	BDL	BDL	12	12	BDL
O1/400	400	BDL	BDL	BDL	BDL	BDL	14	14	BDL
O1/500	500	BDL	BDL	BDL	BDL	BDL	BDL	BDL	BDL
O1/590	590	BDL	BDL	BDL	BDL	BDL	BDL	BDL	BDL

La (ppm)

sample	depth	NH_4-Ac	Na-OC	HL	NH_4-OxH	H_2O_2	residual	total	bulk
O1/034	34	4	BDL	4	BDL	2	77	87	91
O1/100	100	5	BDL	5	1	2	86	98	98
O1/200	200	5	BDL	5	2	3	39	53	59
O1/300	300	4	BDL	2	1	1	35	43	48
O1/400	400	4	BDL	4	2	1	46	57	57
O1/500	500	5	BDL	6	1	2	65	79	91
O1/590	590	6	1	5	BDL	2	63	76	79

Y (ppm)

sample	depth	NH_4-Ac	Na-OC	HL	NH_4-OxH	H_2O_2	residual	total	bulk
O1/034	34	3	BDL	3	BDL	BDL	6	12	13
O1/100	100	3	BDL	3	1	BDL	7	14	15
O1/200	200	3	BDL	3	1	BDL	7	14	15
O1/300	300	3	BDL	2	1	BDL	7	13	14
O1/400	400	3	BDL	3	1	BDL	9	15	17
O1/500	500	3	BDL	2	1	BDL	7	14	15
O1/590	590	4	BDL	2	1	BDL	7	14	15

Abbreviations as in appendix. 2

Zr (ppm)									
sample	depth	NH_4-Ac	Na-OC	HL	NH_4-OxH	H_2O_2	residual	total	bulk
O1/034	34	BDL	BDL	BDL	2	BDL	74	76	76
O1/100	100	BDL	BDL	BDL	4	BDL	64	67	66
O1/200	200	BDL	BDL	BDL	5	BDL	66	70	73
O1/300	300	BDL	BDL	BDL	3	BDL	61	64	72
O1/400	400	BDL	BDL	BDL	6	BDL	75	81	85
O1/500	500	BDL	BDL	BDL	4	BDL	62	66	75
O1/590	590	BDL	BDL	BDL	2	BDL	65	67	79
Co (ppm)									
sample	depth	NH_4-Ac	Na-OC	HL	NH_4-OxH	H_2O_2	residual	total	bulk
O1/034	34	8	BDL	3	3	12	10	36	33
O1/100	100	9	BDL	7	13	11	14	54	47
O1/200	200	17	1	7	11	16	24	76	71
O1/300	300	13	BDL	4	4	10	24	55	50
O1/400	400	11	2	8	18	14	21	74	65
O1/500	500	7	BDL	5	8	12	24	56	51
O1/590	590	4	BDL	1	3	12	20	40	37
Sn (ppm)									
sample	depth	NH_4-Ac	Na-OC	HL	NH_4-OxH	H_2O_2	residual	total	bulk
O1/034	34	BDL	BDL	BDL	BDL	BDL	BDL	BDL	BDL
O1/100	100	BDL	BDL	BDL	BDL	BDL	BDL	BDL	BDL
O1/200	200	BDL	BDL	BDL	BDL	BDL	11	11	BDL
O1/300	300	BDL	BDL	BDL	BDL	BDL	13	13	BDL
O1/400	400	BDL	BDL	BDL	BDL	BDL	12	12	BDL
O1/500	500	BDL	BDL	BDL	BDL	BDL	12	12	BDL
O1/590	590	BDL	BDL	BDL	BDL	BDL	10	10	BDL

Sc (ppm)									
sample	depth	NH_4-Ac	Na-OC	HL	NH_4-OxH	H_2O_2	residual	total	bulk
O1/034	34	1.7	BDL	BDL	1	BDL	9.1	11.8	11.8
O1/100	100	1.4	BDL	BDL	1.3	BDL	9.5	12.2	12.1
O1/200	200	1.7	BDL	BDL	1.2	BDL	6.8	9.7	10.3
O1/300	300	1.4	BDL	BDL	1	BDL	5.9	8.3	9
O1/400	400	1.7	BDL	BDL	1.7	BDL	8	11.4	11.8
O1/500	500	1.6	BDL	BDL	1.3	BDL	6.7	9.6	10.4
O1/590	590	2	BDL	BDL	1	BDL	8.5	11.5	11.9
Be (ppm)									
sample	depth	NH_4-Ac	Na-OC	HL	NH_4-OxH	H_2O_2	residual	total	bulk
O1/034	34	BDL	BDL	BDL	BDL	BDL	0.7	0.7	1
O1/100	100	BDL	BDL	BDL	BDL	BDL	0.8	0.8	1.2
O1/200	200	BDL	BDL	BDL	BDL	BDL	0.8	0.8	1.2
O1/300	300	BDL	BDL	BDL	BDL	BDL	0.9	0.9	1.1
O1/400	400	BDL	BDL	BDL	BDL	BDL	0.8	0.8	1.2
O1/500	500	BDL	BDL	BDL	BDL	BDL	0.8	0.8	1.3
O1/590	590	BDL	BDL	BDL	BDL	BDL	0.8	0.8	1.1
Ag (ppm)									
sample	depth	NH_4-Ac	Na-OC	HL	NH_4-OxH	H_2O_2	residual	total	bulk
O1/034	34	BDL	BDL	1.4	BDL	BDL	2	3	3
O1/100	100	BDL	BDL	2	BDL	BDL	2	4	4
O1/200	200	BDL	BDL	1	BDL	BDL	2	3	2
O1/300	300	BDL	BDL	1	BDL	BDL	2	3	3
O1/400	400	BDL	BDL	0	BDL	BDL	3	4	3
O1/500	500	BDL	BDL	BDL	BDL	BDL	3	3	3
O1/590	590	BDL	BDL	0.2	BDL	BDL	3	3	3

6.6.2.3 Conclusion P. Cerda impoundments

The neutralization potential of the P. Cerda tailings is high enough to maintain pH at neutral values and show high calcite contents. Nevertheless, and in despite of the high carbonate environment, pyrite oxidation takes place, as shown by the formation of an oxidation zone with precipitation of secondary Fe(III) hydroxides essentially in the fine grained horizons, similarly as in Ojancos (Fig. 4C).

Due to high water input during operation, a constant water flow downstream is assumed for the P. Cerda impoundment No 6, as observed presently in the case of Ojancos. Calcite distribution is homogeneous, whereas the pyrite content varies strongly, leading to locally strong differences in the ABA. Acidic, metal rich solutions may migrate and form "acid spots" or "channels" as shown by the Ojancos effluents, or if the pH is buffered to neutral, ferric polymers will hydrolyze.

In this case, the neutral pH will have the effect that the liberated metal cations and anions will adsorb to the polymers and may be transported downstream to the older impoundment No. 4. This would explain the metals enrichments in the cementation zone.

When operation of the mineral processing plant stopped, it is assumed that under the extreme arid conditions of this area, an upwards water migration by capillary force as reported by Dold and Fontboté (in review) could develop, resulting in tailings with low neutralizing potential, to the formation of water-soluble efflorescent salts at the top of the tailings. The lack of water in the upper part of the tailings may decrease the sulfide oxidation rates and the high carbonate content of the studied oxidation zone of the tailings impoundments of P. Cerda maintain the pH at a neutral level, favoring the adsorption of liberated elements, and decreasing their mobility. The total absence of secondary efflorescent salts at the top of the P. Cerda tailings impoundments indicates that the carbonate buffered pH suppresses the upwards migration of liberated element during sulfide oxidation. Thus, it can be stated that the P. Cerda tailings impoundments No. 4 and 6 do not present a hazardous potential of water contamination by metal-rich seepage. Nevertheless, restart of operation could increase oxidation rates via water input and enhance metal mobility. Also aeolian transport of heavy metal containing tailings should be prevented by a simple cover of inert waste-rock.

Fe (%)										
sample	depth	H_2O	NH4-Ac	NH_4-OxD	NH_4-OxH	H_2O_2	sulfide	residual	total	bulk
03/025	25	BDL	0.37	2.54	3.04	0.05	6.58	1.92	14.5	16
03/070	70	BDL	0.27	2.39	2.33	0.03	6.23	1.24	12.5	13.2
03/200	200	BDL	0.32	3.72	1.99	0.29	4.12	0.66	11.1	11.9
03/300	300	BDL	0.63	2.92	2.19	0.01	3.87	0.81	10.4	11.5
03/500	500	BDL	0.42	3.38	3.16	0.02	4.62	0.8	12.4	12.9

Al (%)										
sample	depth	H_2O	NH4-Ac	NH_4-OxD	NH_4-OxH	H_2O_2	sulfide	residual	total	bulk
03/025	25	BDL	0.09	0.14	0.3	0.01	1.24	2.82	4.6	4.75
03/070	70	BDL	0.05	0.12	0.25	BDL	1.31	3.1	4.83	4.76
03/200	200	BDL	0.08	0.26	0.48	0.02	1.64	3.76	6.24	6.58
03/300	300	BDL	0.08	0.2	0.55	0.02	1.62	3.47	5.94	6.51
03/500	500	BDL	0.07	0.28	0.75	0.03	1.56	3.73	6.42	6.25

K (%)										
sample	depth	H_2O	NH4-Ac	NH_4-OxD	NH_4-OxH	H_2O_2	sulfide	residual	total	bulk
03/025	25	0.02	0.01	BDL	BDL	BDL	-	1.88	1.91	2.34
03/070	70	0.02	BDL	BDL	BDL	BDL	-	2.14	2.16	2.43
03/200	200	0.03	0.01	BDL	BDL	BDL	-	2.18	2.22	2.7
03/300	300	0.03	0.01	BDL	BDL	BDL	-	1.86	1.9	2.37
03/500	500	0.03	0.02	BDL	0.02	BDL	-	1.75	1.82	2.04

Mg (%)										
sample	depth	H_2O	NH4-Ac	NH_4-OxD	NH_4-OxH	H_2O_2	sulfide	residual	total	bulk
03/025	25	0.03	0.1	0.09	0.15	0.07	0.99	0.14	1.57	1.53
03/070	70	0.02	0.07	0.08	0.14	0.06	1.1	0.17	1.64	1.53
03/200	200	0.05	0.11	0.11	0.18	0.19	1.3	0.2	2.14	2.14
03/300	300	0.06	0.22	0.21	0.23	0.1	1.48	0.24	2.54	2.56
03/500	500	0.05	0.13	0.11	0.16	0.1	1.04	0.2	1.79	1.65

Na (%)										
sample	depth	H_2O	NH4-Ac	NH_4-OxD	NH_4-OxH	H_2O_2	sulfide	residual	total	bulk
03/025	25	0.02	BDL	BDL	BDL	BDL	BDL	0.89	0.91	1.04
03/070	70	0.02	BDL	BDL	BDL	BDL	BDL	0.96	0.98	1.03
03/200	200	0.02	BDL	BDL	BDL	BDL	BDL	0.62	0.64	0.74
03/300	300	0.02	BDL	BDL	BDL	BDL	BDL	0.66	0.68	0.81
03/500	500	0.02	BDL	BDL	BDL	BDL	BDL	0.37	0.39	0.41

Ca (%)										
sample	depth	H_2O	NH4-Ac	NH_4-OxD	NH_4-OxH	H_2O_2	sulfide	residual	total	bulk
03/025	25	0.5	2.61	BDL	BDL	0.2	0.14	0.19	3.64	3.79
03/070	70	0.41	2.24	BDL	0.01	0.18	0.13	0.18	3.15	3.05
03/200	200	1.2	3.15	BDL	0.01	0.17	0.41	0.08	5.02	4.84
03/300	300	0.99	3.68	BDL	0.02	BDL	0.75	0.12	5.56	5.78
03/500	500	1.16	2.26	BDL	0.01	BDL	0.39	0.07	3.89	3.62

Ti (%)										
sample	depth	H_2O	NH4-Ac	NH_4-OxD	NH_4-OxH	H_2O_2	sulfide	residual	total	bulk
03/025	25	BDL	BDL	BDL	BDL	BDL	0.01	0.13	0.14	0.16
03/070	70	BDL	BDL	BDL	BDL	BDL	0.02	0.15	0.17	0.17
03/200	200	BDL	BDL	BDL	BDL	BDL	0.01	0.19	0.2	0.24
03/300	300	BDL	BDL	BDL	BDL	BDL	0.02	0.19	0.22	0.25
03/500	500	BDL	BDL	BDL	0.02	BDL	0.01	0.2	0.23	0.24

P (%)										
sample	depth	H_2O	NH4-Ac	NH_4-OxD	NH_4-OxH	H_2O_2	sulfide	residual	total	bulk
03/025	25	BDL	BDL	0.05	BDL	BDL	0.06	BDL	0.11	0.11
03/070	70	BDL	BDL	0.05	BDL	BDL	0.05	BDL	0.1	0.09
03/200	200	BDL	BDL	0.15	BDL	BDL	0.05	BDL	0.2	0.19
03/300	300	BDL	BDL	0.08	0.02	BDL	0.04	BDL	0.14	0.12
03/500	500	BDL	BDL	0.09	BDL	BDL	0.02	BDL	0.11	0.1

Ba (ppm)										
sample	depth	H_2O	NH4-Ac	NH_4-OxD	NH_4-OxH	H_2O_2	sulfide	residual	total	bulk
03/025	25	2	60	119	187	1	73	467	909	940
03/070	70	2	61	68	135	2	67	577	912	994
03/200	200	BDL	42	120	176	2	74	408	822	851
03/300	300	BDL	34	77	121	1	55	322	610	644
03/500	500	BDL	47	156	338	2	88	284	915	761

Sr (ppm)										
sample	depth	H_2O	NH4-Ac	NH_4-OxD	NH_4-OxH	H_2O_2	sulfide	residual	total	bulk
03/025	25	6.3	13.2	0.7	2.2	3.9	3.3	36.4	66	72.9
03/070	70	4.1	12	BDL	1.7	3.1	3.1	48	72	75.9
03/200	200	10.6	17.8	0.6	2.1	2.6	9.8	44.5	88	97.3
03/300	300	9.6	16.9	BDL	0.5	BDL	11	50.4	88.4	103
03/500	500	10.7	14	0.9	3.2	BDL	11.3	41.4	81.5	83.3

Ni (ppm)										
sample	depth	H_2O	NH4-Ac	NH_4-OxD	NH_4-OxH	H_2O_2	sulfide	residual	total	bulk
03/025	25	BDL	3	4	2	10	30	1	50	54
03/070	70	BDL	3	5	3	9	28	2	50	46
03/200	200	BDL	9	15	3	11	18	2	58	57
03/300	300	BDL	8	10	2	1	18	4	43	41
03/500	500	BDL	5	9	2	BDL	11	2	29	27

Zr (ppm)										
sample	depth	H_2O	NH4-Ac	NH_4-OxD	NH_4-OxH	H_2O_2	sulfide	residual	total	bulk
03/025	25	BDL	BDL	4.8	2	BDL	1.4	52.1	60.3	69.8
03/070	70	BDL	BDL	4.4	3.3	BDL	2	51.2	60.9	68.8
03/200	200	BDL	BDL	8	0.7	BDL	2	52.4	63.1	77.4
03/300	300	BDL	BDL	10	BDL	BDL	1.8	57.1	68.9	83.2
03/500	500	BDL	BDL	9.4	1.4	BDL	1	68.8	80.6	96.1

Co (ppm)										
sample	depth	H_2O	NH4-Ac	NH_4-OxD	NH_4-OxH	H_2O_2	sulfide	residual	total	bulk
03/025	25	BDL	3	4	BDL	16	43	BDL	66	60
03/070	70	BDL	4	6	3	15	37	BDL	65	53
03/200	200	BDL	12	23	2	17	11	BDL	65	61
03/300	300	BDL	12	14	3	BDL	14	BDL	43	43
03/500	500	BDL	8	16	2	BDL	9	BDL	35	32

Sn (ppm)										
sample	depth	H_2O	NH4-Ac	NH_4-OxD	NH_4-OxH	H_2O_2	sulfide	residual	total	bulk
03/025	25	BDL	BDL	BDL	BDL	BDL	27	BDL	27	BDL
03/070	70	BDL	BDL	BDL	BDL	BDL	20	BDL	20	BDL
03/200	200	BDL	BDL	BDL	BDL	BDL	21	BDL	21	14
03/300	300	BDL	BDL	BDL	BDL	BDL	19	BDL	19	BDL
03/500	500	BDL	BDL	BDL	BDL	BDL	20	BDL	20	13

Cu (ppm)										
sample	depth	H2O	NH4-Ac	NH4-OxD	NH4-OxH	H2O2	sulfide	residual	total	bulk
03/025	25	27.3	575	264	11.7	303	106	4.8	1292	1260
03/070	70	2.7	979	483	20.6	373	119	7.8	1985	1820
03/200	200	6.2	1130	1530	58.7	64	36.5	5.7	2831	2650
03/300	300	14.8	3330	1430	220	14.8	114	4.8	5128	5200
03/500	500	3.8	1570	1520	94.2	78.9	177	6.5	3450	3150

Zn (ppm)										
sample	depth	H_2O	NH4-Ac	NH_4-OxD	NH_4-OxH	H_2O_2	sulfide	residual	total	bulk
03/025	25	BDL	15.3	26.4	10.7	12.6	39.9	8.5	113.4	107
03/070	70	BDL	28.1	47.7	14.7	16.2	44.4	9.4	160.5	148
03/200	200	BDL	27.9	76.6	14.2	20.8	45.7	11.3	196.5	187
03/300	300	0.5	44.2	60.5	18.4	0.8	61.5	11.5	197.4	198
03/500	500	BDL	15.7	39.5	10.8	0.9	54.6	10.4	131.9	121

Mn (ppm)										
sample	depth	H_2O	NH4-Ac	NH_4-OxD	NH_4-OxH	H_2O_2	sulfide	residual	total	bulk
03/025	25	2	570	173	107	76	367	61	1356	1430
03/070	70	BDL	548	197	99	69	392	111	1416	1400
03/200	200	4	1030	360	98	132	495	80	2199	2230
03/300	300	11	1110	318	132	12	573	69	2225	2410
03/500	500	9	1110	521	135	15	683	52	2525	2560

Cr (ppm)										
sample	depth	H_2O	NH4-Ac	NH_4-OxD	NH_4-OxH	H_2O_2	sulfide	residual	total	bulk
03/025	25	BDL	BDL	4	2	BDL	7	2	15	6
03/070	70	BDL	BDL	4	5	BDL	15	2	26	10
03/200	200	BDL	BDL	3	3	BDL	8	2	16	6
03/300	300	BDL	2	5	6	BDL	11	1	25	12
03/500	500	BDL	BDL	3	5	BDL	7	2	17	9

Pb (ppm)										
sample	depth	H_2O	NH4-Ac	NH_4-OxD	NH_4-OxH	H_2O_2	sulfide	residual	total	bulk
03/025	25	BDL	7	10	4	BDL	15	BDL	36	35
03/070	70	BDL	15	14	13	BDL	29	BDL	71	56
03/200	200	BDL	14	12	7	BDL	69	BDL	102	103
03/300	300	BDL	9	9	3	BDL	27	BDL	48	48
03/500	500	BDL	15	23	10	BDL	34	BDL	82	66

Mo (ppm)										
sample	depth	H_2O	NH4-Ac	NH_4-OxD	NH_4-OxH	H_2O_2	sulfide	residual	total	bulk
03/025	25	1	BDL	2	BDL	BDL	5	BDL	8	3
03/070	70	BDL	BDL	2	1	BDL	2	BDL	5	1
03/200	200	1	BDL	7	BDL	BDL	BDL	BDL	8	8
03/300	300	1	BDL	6	2	2	1	BDL	12	9
03/500	500	1	BDL	9	BDL	BDL	1	BDL	11	5

V (ppm)										
sample	depth	H_2O	NH4-Ac	NH_4-OxD	NH_4-OxH	H_2O_2	sulfide	residual	total	bulk
03/025	25	BDL	BDL	17	24	BDL	43	20	104	111
03/070	70	BDL	BDL	16	21	BDL	45	20	102	101
03/200	200	BDL	BDL	22	19	BDL	38	37	116	130
03/300	300	BDL	BDL	19	26	BDL	42	44	131	139
03/500	500	BDL	BDL	19	31	BDL	36	51	137	135

As (ppm)										
sample	depth	H_2O	NH4-Ac	NH_4-OxD	NH_4-OxH	H_2O_2	sulfide	residual	total	bulk
03/025	25	BDL	BDL	8	BDL	BDL	29	BDL	37	BDL
03/070	70	BDL	BDL	11	4	BDL	24	BDL	39	51
03/200	200	BDL	BDL	63	BDL	BDL	5	BDL	68	97
03/300	300	BDL	BDL	38	6	BDL	BDL	BDL	44	47
03/500	500	BDL	BDL	71	5	BDL	BDL	BDL	76	100

W (ppm)										
sample	depth	H_2O	NH4-Ac	NH_4-OxD	NH_4-OxH	H_2O_2	sulfide	residual	total	bulk
03/025	25	BDL	BDL	BDL	BDL	BDL	BDL	BDL	BDL	BDL
03/070	70	BDL	BDL	BDL	BDL	BDL	BDL	BDL	BDL	BDL
03/200	200	BDL	BDL	BDL	BDL	BDL	BDL	BDL	BDL	BDL
03/300	300	BDL	BDL	11	BDL	BDL	BDL	BDL	11	BDL
03/500	500	BDL	BDL	15	19	BDL	BDL	11	45	BDL

La (ppm)										
sample	depth	H_2O	NH4-Ac	NH_4-OxD	NH_4-OxH	H_2O_2	sulfide	residual	total	bulk
03/025	25	BDL	3.6	3.6	4.6	2.9	11.8	32.4	58.9	50.3
03/070	70	BDL	3.2	2.5	4.9	1.5	9.7	34.1	55.9	48.4
03/200	200	BDL	5.2	4.1	8.1	1.5	43.7	17.3	79.9	72.5
03/300	300	BDL	5.5	7.2	BDL	BDL	61.2	15.6	89.5	82.6
03/500	500	BDL	3.2	6.8	3.4	BDL	26.5	7.4	47.3	33.9

Y (ppm)										
sample	depth	H_2O	NH4-Ac	NH_4-OxD	NH_4-OxH	H_2O_2	sulfide	residual	total	bulk
03/025	25	BDL	2.4	1.1	BDL	0.7	1.4	3.9	9.5	10.6
03/070	70	BDL	2.1	0.9	1.4	0.5	1.5	3.7	10.1	9.6
03/200	200	BDL	3.2	0.7	1.1	BDL	4.4	3.2	12.6	15
03/300	300	BDL	4.9	1.6	1	BDL	5	3.5	16	17
03/500	500	BDL	2.7	1.9	1.2	BDL	3.1	5.3	14.2	14.6

Sc (ppm)										
sample	depth	H_2O	NH4-Ac	NH_4-OxD	NH_4-OxH	H_2O_2	sulfide	residual	total	bulk
03/025	25	BDL	1.2	0.7	0.8	BDL	1.4	3	7.1	8.2
03/070	70	BDL	1.2	0.7	0.8	BDL	1.7	3.2	7.6	8.3
03/200	200	BDL	1.7	1.4	0.8	BDL	1.9	4.1	9.9	12.1
03/300	300	BDL	2.5	1.7	0.8	BDL	2.3	3.9	11.2	14
03/500	500	BDL	1.8	1.9	1.4	BDL	1.4	5.1	11.6	12.3

Be (ppm)										
sample	depth	H_2O	NH4-Ac	NH_4-OxD	NH_4-OxH	H_2O_2	sulfide	residual	total	bulk
03/025	25	BDL	BDL	BDL	BDL	BDL	0.5	BDL	0.5	0.8
03/070	70	BDL	BDL	BDL	BDL	BDL	BDL	BDL	BDL	0.8
03/200	200	BDL	BDL	BDL	BDL	BDL	BDL	BDL	BDL	0.8
03/300	300	BDL	BDL	BDL	BDL	BDL	BDL	BDL	BDL	0.8
03/500	500	BDL	BDL	BDL	BDL	BDL	BDL	BDL	BDL	0.8

Ag (ppm)										
sample	depth	H_2O	NH4-Ac	NH_4-OxD	NH_4-OxH	H_2O_2	sulfide	residual	total	bulk
03/025	25	0.4	BDL	BDL	BDL	BDL	1.8	BDL	2.2	1
03/070	70	BDL	BDL	BDL	1.7	BDL	2.4	BDL	4.1	1.4
03/200	200	0.6	BDL	BDL	BDL	BDL	3.1	BDL	3.7	2.7
03/300	300	0.4	BDL	BDL	BDL	BDL	3.7	BDL	4.1	2.7
03/500	500	0.8	BDL	BDL	BDL	BDL	2.5	0.2	3.5	1.6

6.7 Summary and conclusions

The geochemical and mineralogical study of two sulfide-rich flotation tailings sites from the Fe-oxide Cu-Au Punta del Cobre belt has given insight in the influence of carbonate-rich mineralogy on element mobility in arid climates, and the role of impoundment construction with regard to enrichment processes.

Sequential extractions in combination with mineralogical studies have proven to be an important tool to discriminate between primary and secondary mineralogy and the associated geochemical processes. This is important, because the origin of the tailings and their potential acid production and neutralization may vary strongly, as in the here presented case studies. It has been shown that the adapted 7-step extraction sequence B (chapter 3) supports detailed information about primary and secondary differences in the Cu-sulfide tailings.

The selected tailings impoundments include, in the case of Ojancos, old material (impoundment No. 2 ceased operation 1977) and recently deposited material ("2H" tailings). In the case of P. Cerda, the older impoundment No. 4 has been out of operation since 1965 and the younger No. 6 since 1975. In both cases the older tailings filled a valley dam impoundment and after operation ceased (Ojancos No. 2 and P. Cerda No. 4), new tailings were deposited upstream (Ojancos "2H" and P. Cerda No. 6). The Ojancos tailings are characterized by a stratification of intervals rich in calcite (about 40 wt.% calcite and 2 wt.% pyrite) and therefore with high neutralizing potential and sections with high acid potential (about 3 wt.% calcite and 4 wt.% pyrite), whereas in the P. Cerda tailings, the neutralization potential is more homogenous distributed and generally exceeds the acid potential (about 10 wt.% calcite and up to 2.5 wt.% pyrite). Nevertheless, it is assumed that also in P. Cerda locally the acid potential may exceed the neutralization potential, as average calcite contents are about 10 wt.% and maximum pyrite contents about 2.5 wt.%, what gives sulfide net neutralization potential of about 10 t $CaCO_3$/1000t. A NP/AP mol ratio of 4 is necessary to neutralize the 4 moles of protons produced by 1 mole of pyrite with calcite with the assumption that at pH 7 HCO_3^- is the stable carbonate specie. This suggests that the P. Cerda tailings are from the ABA point of view at the limit of acid producing conditions.

The carbonate-rich tailings show clear indications of pyrite oxidation. Blowes et al. (1998) reported the formation of an oxidation zone in a sulfide-baring carbonate-rich gold-mine tailings impoundment, Joutel, Québec, Canada. The oxidation and cementation zones of the Ojancos and P. Cerda tailings impoundments show similar features (Table 6). The oxidation zones are characterized by an alternating layering of coarse, dark gray, un-oxidized horizons with fine-grained, reddish-brown to ochre oxidized horizons. The less-oxidized, coarser horizons are generally richer in pyrite than the finer horizons, possibly due to gravity separation during tailings deposition. The lower oxidation degree results possibly from their lower moisture retention capacity. This suggests that the arid climate limits in part pyrite oxidation due to the lack of water as reactant and that this can not counter-balance the reputed increase of the pyrite oxidation rate in presence of carbonate (Evangelou and Zhang, 1995).

The cementation zones are homogeneous, low in permeability, reddish-brown, rich in Fe(III) hydroxides, mainly higher ordered ferrihydrite and goethite due to pH values above 4,

low sulfide contents, and develop preferentially in areas closer to seepage input coming from the new recently deposited tailings, what is confirmed in Ojancos and P. Cerda by higher heavy metals concentrations found in drill cores at the foot of the "2H" tailings (H1 and S8) and in impoundment No. 4 (O3), respectively.

Table 6: *Mineralogical characteristics of the oxidation and cementation zone of the tailings impoundments Ojancos No. 2 and P. Cerda No. 4.*

	Ojancos No. 2		P. Cerda No. 4	
	primary	secondary	primary	Secondary
oxidation zone	dark gray, mt (up to 10%), ca-rich (~40 wt.%), py (1.5–2.9 wt.%)	Reddish-brown to ochre horizons Fe(III) hydroxides (fh, gt)*	dark gray, mt (up to 10%), ca-rich (~ 10 wt.%), py (~1 wt.%), chl-ep alteration	Reddish-brown to ochre horizons Fe(III) hydroxides (fh, gt)*
cementation zone	chl - ep alteration	Homogeneous reddish-brown, 5-6 line fh, gt, jt, gy°, decrease of ca, $K = 3.2x10^{-8} - 4.4x10^{-8}$ m/s, < 1.7 wt.% py[a]	chl-ep alteration	Homogeneous reddish-brown, fh*, gt*, gy°, decrease of ca $K = 3.3x10^{-8} - 3.6x10^{-8}$ m/s, < 0.34 wt.% py

*Abbreviation as in Table 1, chl = chlorite, ep = epidote, K = permeability, *indications but not unequivocally proved, °tertiary mineral, [a]the calculation is based on the S-sulfide content, but secondary sulfide precipitation (cv) in this zone suggest that the effective pyrite content is lower supported by microscopic results.*

Two main possibilities of downwards transport of the liberated heavy metals are recognized in these carbonate-containing tailings.

1.) If the carbonate is not homogeneously distributed in the tailings material, but following randomly distributed intercalations as in the case of the Ojancos "2H" tailings, acid mine drainage will form and seeps downwards. If these acid solutions get in contact with oxidizing conditions as those prevailing at the tailings surface, acid mine drainage precipitates may form. Its composition will depend on the chemical composition of the effluent and this can vary strongly at small scale (e.g., schwertmannite at a pH 3.15 and chalcoalumite at a pH 4.90 precipitate a few cm apart at Ojancos, Fig. 4B), and indicate that the effluents may form their own solution flow path protected from reactive host rocks. If these acid solutions seep, without getting in contact with oxidizing conditions into the downstream impoundment, the hydrolysis of secondary ferric phases (e.g., ferrihydrite, goethite, and locally jarosite detected by DXRD) may be initiated by pH increase, for example due to carbonate-rich layers. Higher ordering of the 5 to 6-line ferrihydrite (detected by DXRD, Fig. 7), presumed to form because of formation by slow oxidation and hydrolysis (Schwertmann et al., 1999) and is in contrast to the normally lower ordered ferrihydrites (2- to 4- line) encountered in acid mine drainage environment (Nordstrom and Alpers, 1999). As the cementation zone is located below the water table slightly reducing

conditions prevail. It has to be assumed that the main oxidation from ferrous to ferric iron takes place in the "2H" tailings as microbial oxidation tests (data not shown) do not show important oxidation of Fe^{2+} in a sample from the cementation zone. These indications lead to the interpretation that the oxidation rate is high in the "2H" tailings and iron seeps as Fe^{3+} in low pH solution (< 3) into the tailings impoundment No. 2, where a slow hydrolysis, initiated by the slight pH increase to 4 with contact at the cementation zone will form higher ordered ferrihydrite.

Heavy metals may be adsorbed by secondary ferric phases as shown by the results of sequential extractions. Bivalent Cu mobilized under acid conditions may precipitate as secondary covellite under slightly reducing conditions (Boorman and Watson, 1976; Blowes and Jambor, 1990; Lin and Qvarfort, 1996; Holmström et al., in review), as those encountered below the ground water level, documented by an increase in the H_2O_2-leach of sequential extraction and by microscopic study. With increasing pH values > 4 the adsorption of Cu increases, shown by the exchangeable fraction of sequential extractions, and the precipitation of secondary Cu-sulfides decreases. Mo and Pb may precipitate as secondary sulfide minerals.

2.) If high neutralizing potential maintains pH near neutral values, the mobility of the liberated metals depends essentially on the adsorption behavior of these elements under neutral conditions. Bivalent cations as well as oxyanions are adsorbed at neutral pH on ferric hydroxides (Dzombak and Morel, 1990; Webster et al., 1998). These ferric polymers will hydrolyze soon after their formation and are available as adsorbant for the liberated heavy metals. With a high water input during the operation of an upstream impoundment these metal-rich polymers may be transported downwards, leading to enrichment in the older downstream impoundment. This mechanism is suggested in the case of the P. Cerda impoundments as geochemical data from the cementation zone shows only enrichment in heavy metals in the adsorbed fraction and the fraction of the Fe(III) hydroxides. If the metals would have been transported as acid solutions as in case of Ojancos, some indications of secondary sulfide formation may be found at least in the lower part of the cementation zone, where the enrichment in heavy metals are strong and reducing conditions may prevail.

The enrichment of liberated elements observed in the downstream tailings is, under the prevailing extreme arid conditions, strictly associated to the high water input (4000 m^3/month in case of Ojancos) on the upstream tailings during operation. Once this water input ceased, the migration should have changed to upwards, similarly as described by Dold and Fontboté (in review) for other tailings located under Mediterranean to arid conditions. However, and in contrast to the enrichment of mobile elements as water-soluble salts observed at the top of the El Salvador tailings impoundment in a evaporation zone (Dold and Fontboté, in review), no enrichment in water-soluble form of any analyzed element can be observed at the top of the P. Cerda impoundments No. 4 and 6. The reason has to be seen in the neutral pH condition throughout the whole tailings, which increase adsorption and decrease mobility of the liberated elements. The ferric polymers do not seem to be able to migrate upwards via capillary force, as already shown by in the acid tailings impoundment at El Salvador. The element distribution documented in the P. Cerda tailings impoundments indicates relatively immobility under the present conditions and element mobilization has not to be expected even in case of one of the

strong periodic rainfalls occurring in this area, as no metals are available in form of water-soluble phases. However, new water input through the restarting of operation would increase the pyrite oxidation rates. This has to be seen critical, as the ABA of the tailings of P. Cerda is at the limit to acid generation and acid mine drainage may be formed. To prevent aeolian transport of the tailings a simple cover with inert waste rock would be sufficient.

As a results of the hydrogeologic setting of two valley dam tailings impoundments in Ojancos and P. Cerda, and in particular high metal concentrations in the cementation zones (e.g., Cu, Zn, and Pb), it is suggested that this type of impoundment construction leads to an enrichment of heavy metals in the downstream, older impoundment in the area near the seepage inflow (Fig. 14). This enrichment may be economically interesting and, in certain cases, could make a re-treatment of the tailings feasible. Adequate impoundment construction may profit from these enrichment processes. It must be pointed out that an application of this enrichment process at industrial scale must be controlled by several security implementations, including exact knowledge of the hydrological parameters, and liners to prevent infiltration of AMD to underlying aquifers. Additionally, it has to be ensured that in the downstream tailings, enough neutralization potential is available for the acid produced upstream.

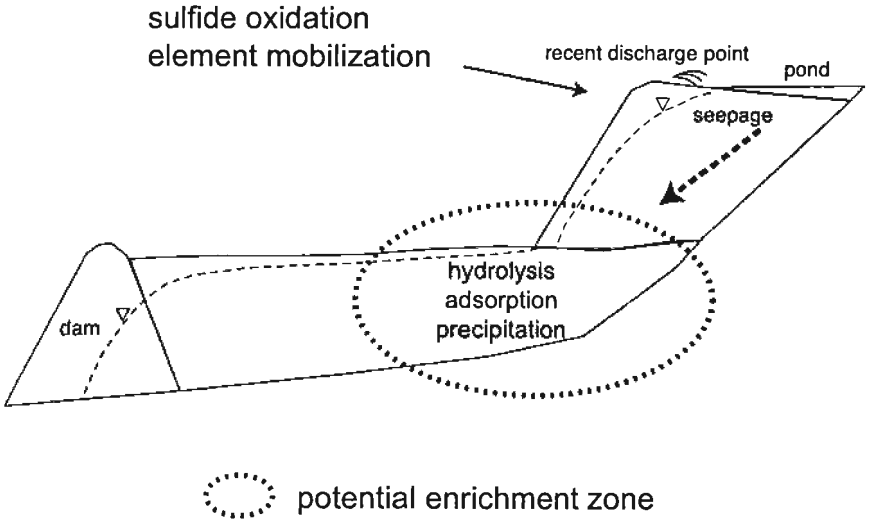

Fig. 14: Proposed model of secondary enrichment processes as a result of impoundment construction with the potential enrichment zone.

Acknowledgements

I thank the management and all staff involved in this project from Cía. Minera Sali Hochschild S.A. and Cía. Minera Ojos del Salado S.A. for their interest, the access to their properties, their logistic support and their collaboration, especially B. Zamora (Planta Ojancos, Compañia Minera Sali Hochschild S.A.), W. Rojas (Compañia Minera Ojos del Salado). For their support in Chile in the field work, sampling, sample preparation, and analytical approaches

I would like thank to G. Cáceres, K. Eppinger and their staff (IDICTEC – University of Atacama), S. Elqueta (Geological Department, University of Chile, Santiago), B. Escobar, J. Wiertz, and J. Casas (Chemical Department, Biometallurgy, University of Chile, Santiago), R. Troncoso, A. Hauser, C. Reuschmann, C. Espejo, E. Fonseca, W. Vivallio, I. Aguirre (Servicio Nacional de Geología y Minería, SERNAGEOMIN), W. Eberle, and H.W. Müller (Bundesanstalt für Geowissenschaften und Rohstoffe BGR). The project is supported by the German Academic Exchange Service (DAAD) and the Swiss National Science Foundation project No. 21-50778.97.

References

Acker, J.G., Bricker, O.P. (1992): The influence of pH on biotite dissolution and alteration kinetics at low temperature. Geochimica et Cosmochimica Acta, v. 56, p. 3073-3092.

Alpers, C.N., Blowes, D.W., Nordstrom, D.K., and J.L. Jambor (1994): Secondary minerals and acid mine-water chemistry. In: Jambor, J.L. and Blowes, D.W. (eds.): Short Course Handbook on Environmental Geochemistry of Sulfide Mine Waste. Mineralogical Association of Canada, Nepean, v. 22: p. 247-270.

Alpers, C.N., Nordstrom, D.K. and Thompson, J.M. (1994): Seasonal variations of Zn/Cu ratios in acid mine water from Iron Mountain, California. In: Alpers, C.N. and Blowes, D.W. (eds.): Environmental Geochemistry of Sulfide Oxidation. ACS Symposium Series, Washington, DC, v. 550, p. 324-344.

Bigham, J.M., Schwertmann, U., Carlson, L., Murad, E. (1990): A poorly crystallized oxyhydroxysulfate of iron formed by bacterial oxidation of Fe(II) in acid mine waters. Geochimica et Cosmochimica Acta, v. 54, p. 2743-2758.

Bigham, J.M., Carlson, L., Murad, E. (1994) Schwertmannite, a new iron oxyhydroxy-sulphate from Pyhäsalmi, Finland, and other localities. Mineralogical Magazine, v. 58, p. 641-648.

Bigham, J.M., Schwertmann, U., Traina, S.J., Winland, R.L., Wolf, M. (1996): Schwertmannite and the chemical modeling of iron in acid sulfate waters. Geochimica et Cosmochimica Acta, v. 60 (2), p. 185-195.

Blowes, D.W., Jambor, J.L. (1990): The pore-water geochemistry and the mineralogy of the vadose zone of sulfide tailings, Waite Amulet, Quebec, Canada, Applied Geochemistry, v. 5, p. 327-346.

Blowes, D.W., Reardon, E.J., Jambor, J.L., Cherry, J.A. (1991): The formation and potential importance of cemented layers in inactive sulfide mine tailings. Geochimica et Cosmochimica Acta, v. 55, p. 965-978.

Blowes, D.W. and Ptacek, C.J. (1994): Acid-neutralization mechanisms in inactive mine tailings. In: Jambor, J.L. and Blowes, D.W. (eds.): Short Course Handbook on Environmental Geochemistry of Sulfide Mine Waste. Mineralogical Association of Canada, Nepean, v. 22, p. 271-291.

Blowes, D.W.,Jambor, J.L. , Hanton-Fong, C.J., Lortie, L., Gould, W.D. (1998): Chemical, mineralogical and microbiological characterization of a sulphide-bearing carbonate-rich gold-mine tailings impoundment, Joutel, Québec. Applied Geochemistry, v. 13, p. 687-705.

Boorman, R.S., Watson, D.W. (1976): Chemical processes in abandoned sulphide tailings dumps and environmental implication for Northeastern New Brunswick. CIM bulletin, 69, 86-96.

Borek, S.L. (1994): Effect of humidity on pyrite oxidation. In: Alpers, C.N. and Blowes, D.W. (Eds.), Environmental Geochemistry of sulfide oxidation, ACS Symposium Series 550, Washington, D.C., p. 31-44.

Brindley, G.W., Brown, G. (1980): Crystal structures of clay minerals and other X-ray identification, Mineralogical Society, London.

Brookins, D.G. (1988): Eh-pH diagrams for geochemistry. Springer, Berlin.

Cardoso Fonseca, E., Martin, H. (1986): The selective extraction of Pb and Zn in selected mineral and soil samples, application in geochemical exploration (Portugal). Journal of Geochemical Exploration, v. 26, p. 231-248.

Chao, T.T., Sanzolone, R.F. (1977): Chemical dissolution of sulfide minerals. Journal of Research U.S. Geol.Survey, v. 5, p. 409-412.

Davis, B.S. (1997): Geomicrobiology of the oxic zone of sulfidic mine tailings. In: McIntosh, J.M. and Groat, L.A. (eds.): Short Course Handbook on Biological and Mineralogical Interactions. Mineralogical Association of Canada, Nepean, v.25, p. 93-112.

Dold, B. (1994): Geochemische Untersuchungen einer Flotationshalde in Copiapo / Region Atacama/ Nordchile. Diplom-thesis, unpublished, University Bremen, Bremen.

Dold, B., Eppinger, K.J., Kölling, M.(1996): Pyrite oxidation and the associated geochemical processes in tailings in the Atacama desert/Chile: The influence of men controlled water input after disuse. Clean technology for the mining industry, Santiago, p. 417 - 427.

Dold, B., Fontboté, L., Wildi, W. (1997): Mobilization and secondary enrichment processes in the sulfide porphyry copper tailings of Cauquenes (El Teniente) and Piuquenes (La Andina), Chile. VIII Congreso Geologico Chileno Actas, v. 2, p. 940-944.

Dold, B., Fontboté, L., Wildi, W. (1999): Detection and distribution of ferric oxyhydroxides and oxyhydroxide sulfates in sulfide mine tailings; their importance to selective metal retention and acid production. Mine, Water and Environment, 1999 IMWA Congress, Sevilla, Spain, v. 2, p. 525-526.

Dold, B., Fontboté, L. (in review): Element cycling and secondary mineralogy in porphyry copper tailings as a function of climate, primary mineralogy and mineral processing. Special Issue: Geochemical studies of mining and the environment, Journal of Geochemical Exploration.

Dzombak, D.A., Morel, F.M.M. (1990): Surface complexation modeling - Hydrous ferric oxides, Wiley, New York.

Evangelou, V.P. , Huang, X. (1994): Infrared spectroscopy evidence of an iron(II)-carbonate complex on the surface of pyrite. Spectrochimica Acta, v. 50A, p. 1333.

Evangelou, V.P. , Zhang, Y.L. (1995): A review: Pyrite oxidation mechanisms and acid mine drainage prevention. Critical Reviews in Environmental Science and Technology, v. 25(2), p. 141-199.

Fanfani, L., Zuddas, P., Chessa, A. (1997): Heavy metals speciation analysis as a tool for studying mine tailings weathering. Journal of Geochemical Exploration, v. 58, p. 241-248.

Farquhar, M.L., Vaughan, D.J., Hughes, C.R., Charnock, J.M., England, K.E.R. (1997): Experiminetal studies of the interaction of aqueous metal cations with mineral substrates: Lead, cadmium, and copper with perthitic feldspar, muscovite, and biotite. Geochimica et Cosmochimica Acta, v. 61; p. 3051-3064.

Gatehouse, S., Roussel, D.W., Van Moort, J.C. (1977): Sequential soil analysis in exploration analysis. Journal of Geochemical Exploration, v. 8, p. 483-494.

Geotechnica (1996): Sociedad Punta de Cobre S.A. – Estudio de Impacto Ambiental, Proyecto Pucobre. Santiago.

Hall, G.E.M., Vaive, J.E., Beer, R., Hoashi, M. (1996): Selective leaches revisited, with emphasis on the amorphous Fe oxyhydroxide phase extraction. Journal of Geochemical Exploration, v. 56, p. 59-78.

Hall, G.E.M., Bonham-Carter, G.F. (eds.) (1998): Special Issue: Selective Extractions. Journal of Geochemical Exploration, v. 61.

Holmström, H., Ljungberg, J., Ekström, M., Öhlander, B. (in review): Secondary copper enrichment in tailings at the Laver mine, northern Sweden. Environmental Geology.

Holmström, H., Ljungberg, J., Öhlander, B. (1999): Role of carbonates in mitigation of metal release from mining waste. Evidence from humidity cells tests. Environmental Geology, v. 37(4), p. 267-280.

Hölting, B. (1989): Hydrogeologie. Enke, Stuttgart.

Hopf, S. (1990): The Agustina Mine, a volcanic-hosted copper deposit in northern Chile. In: L.Fontboté, G.C.Amstutz, M.Cardozo, E.Cedillo, J.Frutos (Eds.) Stratabound ore deposits in the Andes. Springer, Berlin-Heidelberg-New York, p. 421-434.

Ingeneria y Geotecnia LTDA (1990a): Tranques de relaves Planta Ojancos. Levantamiento catastral de los tranques de relaves en Chile, p. 188-195.

Ingeneria y Geotecnia LTDA (1990b): Tranques de relaves Planta Pedro. A. Cerda. Levantamiento catastral de los tranques de relaves en Chile, p. 235-242.

Jang, H.J., Wadsworth, M.E. (1994): Kinetics of hydrothermal enrichment of chalcopyrite. In: Alpers, C.N. and Blowes, D.W. (eds.). Environmental Geochemistry of Sulfide Oxidation, ACS Symposium Series, Washington, DC, v. 550, p. 45-58.

Jambor, J.L. (1994): Mineralogy of sulfide-rich tailings and their oxidations products. In: Jambor, J.L. and Blowes, D.W. (eds.): Short Course Handbook on Environmental Geochemistry of Sulfide Mine Waste. Mineralogical Association of Canada, Nepean, v. 22, p. 59-102.

Jambor, J.L. and Blowes, D.W. (1998): Theory and applications of mineralogy in environmental studies of sulfide-baring mine waste. In: Cabri, L. J. and Vaughan, D.J. (eds.): Short Course Handbook on Ore and Environmental Mineralogy. Mineralogical Association of Canada, Nepean, v. 27, p. 367-401.

Lapakko, K., Antonson, D.A., Wagner, J.R. (1997): Mixing of limestone with finely-crushed acid producing rock. 4th Internationl Conference on Acid Rock Drainage '97, Vancouver, BC, v. 3, p. 1345-1360.

Lin, Z., Qvarfort, U. (1996): A study of the Lilla Bredsjön tailings impoundment in mid-Sweden - a comparison of observations with RATAP model simulations. Applied Geochemistry, v. 11, p. 293-298.

Lin, Z. (1997): Mobilization and retention of heavy metals in mill-tailings from Garpenberg sulfide mines, Sweden. The Science of the Total Environment, Elsevier, v. 198, p. 13-31.

Malmström, M., Banwart, S. (1997): Biotite dissolution at 25°C. the pH dependence of dissolution rate and stoichiometry. Geochimica et Cosmochimica Acta, v. 61; p. 2779-2799.

Marschik, R. (1996) Cretaceous Cu(-Fe) mineralization in the Punta del Cobre belt, northern Chile. Ph.D. thesis. Terre et Environnement, Université de Genève, v. 5, 200 p.

Marschik, R., Fontboté, L. (1996): Copper(-iron) mineralization and superposition of alteration events in the Punta del Cobre belt, northern Chile. Economic Geology, Special Publication, No. 5, p. 171-189.

Marschik, R., Singer, B.S., Munizaga, F., Tassinari, C., Moritz, R., Fontboté, L. (1997): Age of Cu(-Fe)-Au mineralization and thermal evolution of the Punta del Cobre district, Chile. Mineralium Deposita, v. 32, p. 531-546.

Marschik, R., Fontboté, L. (in review): Geology of the Punta del Cobre-Candelaria area, Chile: The Jurassic(?) to pre-Valanginian Punta del Cobre Formation. GSA Bulletin.

McCarty, D.K., Moore, J.N., Marcus, W.A. (1998): Mineralogy and trace element association in an acid mine drainage iron oxide precipitate; comparison of selective extractions. Applied Geochemistry, v. 13, p. 165-176.

McGregor, R.G., Blowes, D.W., Robertson, W.D. (1995): The application of chemical extractions to sulphide tailings at the Copper Cliff tailings area, Sudbury, Ontario. Sudbury '95 Proceedings, v. 3, p. 1133-1142.

MEND, Mine Environment Neutral Drainage Program (1991): Acid rock drainage prediction manual, Report 1.16.1b. CANMET, Dept. Natural Resources Canada, Ottawa.

Moore, D.M., Reynolds, R.C. (1997): X-ray diffraction and the identification and analysis of clay minerals, 2nd Ed. Oxford University Press, Oxford.

Morin, A.K., Hutt, N.M. (1997): Environmental geochemistry of minesite drainage. Practical theory and case studies. MDAG Publishing, Vancouver.

Nordstrom, D.K. and Alpers, C.N. (1999): Geochemistry of acid mine waters. In: Plumlee, G. S. and Logsdon, M.J. (Eds.), The environmental geochemistry of ore deposits. Part A: Processes, techniqoes, and health issues, Littleton , Colo., Society of Economic Geologists, Reviews in Economic Geology , v. 6A, p. 133-160.

Ribet, I., Ptacek, C.J., Blowes, D.W., Jambor, J.L. (1995): The potential for metal release by reductive dissolution of weathered mine tailings. Journal of Contaminant Hydrology, v. 17(3), p. 239-273.

Ryan, P.J., Lawrence, A.I., Jenkins, R.A., Matthews, J.P., Zamora, J.C., and Marino, E., and Urqueta, I. (1995): The Candelaria copper-gold deposit, Chile. In: Pierce, F.W. and Bolm, J.G., (Eds.). Porphyry copper deposits of the American Cordillera: Arizona Geological Society Digest, v. 20, p. 625-645.

Tessier, A., Campbell, P.G.C., Bisson, M. (1979): Sequential extraction procedure for speciation of particulate trace metals. Analytical Chemistry, v. 51, p. 844-851.

Schulze, D.G. (1981): Identification of soil iron oxides minerals by differential x-ray diffraction. Soil Sci. Soc. Am. J., v. 45, p. 437-440.

Schulze, D.G. (1994): Differential x-ray diffraction analysis of soil material. In: Quantitative methods in soil mineralogy, SSSA Miscellaneous Publication, p. 412-429.

Schwertmann, U., Schulze, D.G., Murad, E. (1982): Identification of ferrihydrite in soils by dissolution kinetics, differential x-ray diffraction, and Mössbauer Spectroscopy. Soil Sci. Soc. Am. J., v. 46, p. 869-875.

Schwertmann, U. (1964): Differenzierung der Eisenoxide des Bodens durch Extraktion mit Ammoniumoxalat Lösung. Zeitschrift für Pflanzenernährung und Bodenkunde, v. 105, p. 194-202.

Schwertmann, U., Bigham, J.M., Murad, E. (1995): The first occurrence of schwertmannite in a natural stream environment. European Journal of Mineralogy, v. 7, p. 547-552.

Schwertmann, U., Friedl, J., and Stanjek, H. (1999): From Fe(III) ions to ferrihydrite and then to hematite. Journal of Colloid and Interface Science, v. 209, p. 215-223.

Schönfelder, H. (1990): Die Kupferlagerstätte Punta del Cobre, Nord-Chile: Eine Analyse der geochemisch-petrographischen Umwandlungszonierung und der vulkano-sedimentären Serie im Hangenden. Diplomarbeit (unpubl.), Univ. Heidelberg, Heidelberg.

Singer, P.C., Stumm, W. (1970): Acid mine drainage: the rate-determining step. Science, v. 167, p. 1121-1123.

Sondag, F. (1981): Selective extraction procedures applied to geochemical prospecting in an area contaminated by old mine workings. Journal of Geochemical Exploration, v. 15, p. 645-652.

Stone, A.T. (1987): Microbial metabolites and the reductive dissolution of manganese oxides: Oxalate and pyruvate Geochimica et Cosmochimica Acta, v. 51; p. 919-925.

Stumm, W., Sulzberger, B., 1992. The cycling of iron in natural environments: Considerations based on laboratory studies of heterogeneous redox processes. Geochimica et Cosmochimica Acta, v. 56, p.3233-3257.

Tassé, N., Germain, D., Dufour, C., Tremblay, R. (1997): Hard-pan formation in the Canadian Malartic tailings: implication for the reclamation of the abandoned impoundment. 4th Internationl Conference on Acid Rock Drainage '97, Vancouver, BC, v. 4, p. 1797-1812.

Webster, J.G., Swedlund, P.J., Webster, K.S. (1998): Trace metal adsorption onto an acid mine drainage iron(III)oxyhydroxy sulfate. Environmental Science and Technology, v. 32(10), p. 1362-1368.

Zamora, B. (1993): Antecedentes para monografia de Compañia Minera y Comercial Sali Hochschild S.A., internal report, Copiapó..

CHAPTER 7

7 Selective metal retention by ferric oxyhydroxides and oxyhydroxide sulfates in sulfide mine tailings and their importance to acid production

Abstract

Fe(III) oxyhydroxides are well known for their ability to scavenge heavy metals, due to their functional groups and high surface areas. During the present investigation, the application of differential X-ray diffraction (DXRD) to detected schwertmannite (ideally between $Fe_8O_8(OH)_6SO_4$ and $Fe_{16}O_{16}(OH)_{10}(SO_4)_3$) in the oxidation zone of two sulfidic mine tailings from the porphyry copper mines of La Andina and El Teniente (Chile) as a minor phase in bulk samples. Schwertmannite occurs as a significant secondary phase together with the main secondary minerals jarosite ($KFe_3(SO_4)_2(OH)_6$) and a vermiculite-type mixed layer. A dissolution kinetic test with eight natural and synthetic schwertmannite and ferrihydrite ($5Fe_2O_3 \cdot 9H_2O$) samples was performed using 0.2 M ammonium oxalate at pH 3 under exclusion of light (NH_4-OxD) to study the possibility of discrimination of one of these minerals by its dissolution kinetics. The results of the dissolution kinetic test were taken into account for the design of a sequential extraction procedure adapted to the secondary mineralogy of the studied mine tailings. The variations of Fe/S mole ratios in the NH_4-OxD leach suggest that schwertmannite together with jarosite is limited to the oxidation zone and that the predominant ferric oxyhydroxide in the zones below is possibly ferrihydrite. Higher values of Mo, As and SO_4 in the NH_4-OxD leach in samples from the oxidation zone and in situ microprobe analysis indicate that schwertmannite and jarosite play an important role in oxyanion adsorption by ligand exchange under acidic conditions or possible coprecipitation (and solid solution). In contrast, bivalent cations (e.g., Cu^{2+}, Mn^{2+}, Zn^{2+}) are not adsorbed by these minerals, because of competitive proton adsorption at outstanding OH^- groups. Below the oxidation zone, ferrihydrite together with other adsorbents (clay minerals, Mn-oxides) plays a major role in the pH-controlled adsorption of bivalent cations mobilized downwards from the oxidation zone.

For acid-base accounting it is assumed in general that $Fe(OH)_{3(s)}$ or ferrihydrite hydrolyses from solution with the production of 3 moles H^+/mole Fe^{3+} hydrolyzed. The hydrolysis of jarosite produce only 2 moles of H^+ and schwertmannite between 2.625 and 2.75, respectively per mole of Fe^{3+}. The results suggest that this difference must be taken into account by calculation of the quantity of acid produced, as hydrolysis of the secondary ferric phases is the main acid producing process in sulfide oxidation. Nevertheless, it is important to be aware that for calculation of the acid potential in case of carbonate treatment, due to increased pH values, ferrihydrite or goethite will be produced, leading to the production of 3 moles H^+/mole Fe^{3+}.

7.1 Introduction

Three tailings impoundments of the giant porphyry copper deposits El Teniente, La Andina, and El Salvador, Chile were studied. The aim of this project was to investigate the mineralogical and geochemical changes at the interface between the oxidation zone and the

primary (sulfide) zone in sulfidic copper flotation tailings as a contribution to understanding processes taking place subsequent to sulfide oxidation, specially element mobility and sorption to secondary phases. The tailings impoundments are seen as open-air laboratory and we focus in this paper on the role of the secondary mineralogy to metal retention by sorption processes and the influence of climate to metal mobility. Detailed discussion of element mobilization in these tailings are described in chapter 5 and 6.

The stratigraphy of an oxidizing sulfidic mine tailing is usually divided into an oxidation zone at the top (pH 1.5 -3.5, high sulfate contents), followed by a neutralization zone below (pH 3.5 - 5) and an underlying primary zone with near-neutral pH (Fig. 3). The formation of secondary Fe(III) minerals depends essentially on pH and element activity. Jarosite and goethite are reported as common secondary ferric oxyhydroxides or oxyhydroxide sulfates in sulfide-rich tailings. Ferrihydrite, lepidocrocite, akagan ite, and maghemite are other identified secondary ferric phases in this environment (Jambor and Blowes, 1998).

Schwertmannite (ideally $Fe_8O_8(OH)_6SO_4$ or $Fe_{16}O_{16}(OH)_{10}(SO_4)_3$) has been reported from several locations around the world, as precipitate in heavy metal and sulfate loaded drainage systems (Bigham et al. 1990, 1994, 1996; Childs et al. 1998; Schwertmann et al. 1995, Yu et al. 1998). Webster et al. (1998) studied the adsorption behavior of Cu, Zn, Pb, and Cd with a natural acid mine drainage precipitate, a synthetic schwertmannite, and a synthetic 2-line ferrihydrite. Jamieson et al. (1995) reported an oxyhydroxysulfate, which they reported that is possibly schwertmannite on the basis of electron microprobe analysis from Geco tailings, Ontario, Canada. However, electron microprobe analysis is not sufficient to identify schwertmannite, due to the possibility that the SO_4 content leading to the stoichiometric composition of schwertmannite may only be adsorbed as oxyanion at low pH conditions to Fe(III) hydroxides. Lin (1996) reported the presence of schwertmannite and ferrihydrite in the Rudolfsgruvan mine waste rock dump, central Sweden. The presented XRD do not show a clear identification of these minerals. In the present study we could determine the presence of schwertmannite in the oxidation zone of two sulfide mine tailings impoundments at the La Andina and El Teniente mines (Chile) by differential X-ray diffraction (DXRD) and study its role to selective adsorption of oxyanions.

7.2 Material and methods

Polished sections, polished thin sections, X-ray diffraction (XRD), differential X-ray diffraction (DXRD), SEM-EDS, and electron microprobe was used for the mineralogical study. Dissolution kinetics tests with eight natural and synthetic schwertmannite and ferrihydrite ($5Fe_2O_3 \cdot 9H_2O$; fh) samples were performed using 0.2 M ammonium oxalate at pH 3 under exclusion of light (NH_4-OxD) to study the possibility of discrimination of one of these secondary minerals by its dissolution kinetics (chapter 4). The results of the dissolution kinetics tests were used to detect these secondary ferric phases by DXRD and have been taken into account for the design of the sequential extractions applied in this study (chapter 3; Table 1). The solutions were submitted to multi-element ICP-ES analysis. To control the accuracy an analysis of a total HNO_3, HF, $HCLO_4$ digestion of every sample was done.

Table 1: *Sequential extraction B applied in this study (abbreviations: bn: bornite; ca: calcite; cb: cinnabar; cc: chalcocite; cv: covellite; cp: chalcopyrite; dg: digenite; fh: ferrihydrite; gn: galena; gt: goethite; gy: gypsum; hm: hematite; ilm: ilmenite; jt: jarosite; Na-jt: natrojarosite; mb: molybdenite; mt: magnetite; op: orpiment; py: pyrite; sh: schwertmannite; sl: sphalerite; stb: stibnite; tn: tennantite; tt: tetrahedrite).*

Leach	Preferentially dissolved minerals	References
(1) Water soluble fraction 1.0 g sample into 50ml deionizied H_2O shake for 1 h.	secondary sulfates, e.g., bonattite, chalcanthite, gy, pickeringite, magnesioauberite	chapter 5 and 6; Ribet et al., 1995; Fanfani et al., 1997
(2) exchangeable fraction 1M NH_4-acetate pH 4.5 shake for 2 hrs	ca, vermiculite-type-mixed-layer, adsorbed and exchangeable ions	chapter 5; Gatehouse et al., 1977; Sondag, 1981; Fonseca and Martin, 1986
(3) Fe(III) oxyhydroxides 0.2 M NH_4-oxalate pH 3.0 shake for 1 h. in darkness	sh, 2-line fh, secondary jt, MnO_2	Schwertmann, 1964; Stone, 1987; chapter 4
(4) Fe(III) oxides 0.2 M NH_4-oxalate pH 3.0 heat in water bath 80¡C for 2 hours	gt, jt, Na-jt, hm, mt, higher ordered fh s (e.g., 6-line fh)	chapter 3.
(5) organics and secondary Cu-sulfides 35% H_2O_2 heat in water bath for 1 hour	organics , cv, cc-dg	Sondag, 1981;, chapter 5
(6) primary sulfides Combination of $KClO_3$ and HCl, followed by 4 M HNO_3 boiling	py, cp, bn, sl, gn, mb, tt, cb, op, stb	Chao and Sanzolone, 1977; Hall et al., 1996
(7) residual HNO_3, HF, $HClO_4$, HCL digestion	Silicates, residual	Hall et al., 1996; Dold et al., 1996

7.3 Results and discussion

Dissolution kinetics tests using 0.2 M ammonium oxalate at pH 3 under exclusion of light (NH_4-OxD) indicate that it is not possible to discriminate schwertmannite and ferrihydrite (2-line) by their dissolution kinetics (Fig. 1). Schwertmannite dissolves fastest (> 94% in 60 min), followed by the natural 2-line ferrihydrites (> 85% after 60 min) and the synthetic ferrihydrites (41.8% 2-line fh and 16.4% 6-line fh after 60 min). However, it is possible to distinguish these minerals by combining the dissolution results with their Fe/S mole ratios. This allows selective leaching of schwertmannite and ferrihydrite and minimizes the dissolution of other reducible phases (e.g., hematite, magnetite, goethite, and jarosite). Nevertheless, higher potassium values in NH_4-OxD leach of samples from the oxidation zone and DXRD control have shown that an

easily reducible part of jarosite is also dissolved after 1h in this step. For detailed discussion of the dissolution kinetics see chapter 4.

The application of DXRD (Fig. 2) has detected schwertmannite (sh) in the oxidation zone of two sulfidic mine tailings as a minor phase in bulk samples (Piuquenes tailings impoundment of the La Andina porphyry copper deposit, humid-alpine climate, and the Cauquenes tailings impoundment of the El Teniente porphyry copper deposit, semi-arid climate, both located in central Chile). The orange-brown to brown schwertmannite occurs as dots or streaks in the fine grained horizons and is enriched at the interface of fine to coarser grained horizons, due to capillary barrier controlled water flow. This distribution of schwertmannite indicates that it is preferentially associated with water flow paths, possibly because through dilution pH is increased to a sufficient value for its precipitation (2.8-3.5, Bigham et al. 1996). Schwertmannite occurs as a significant secondary phase together with the main secondary minerals jarosite ($KFe_3(SO_4)_2(OH)_6$) and a vermiculite-type mixed layer.

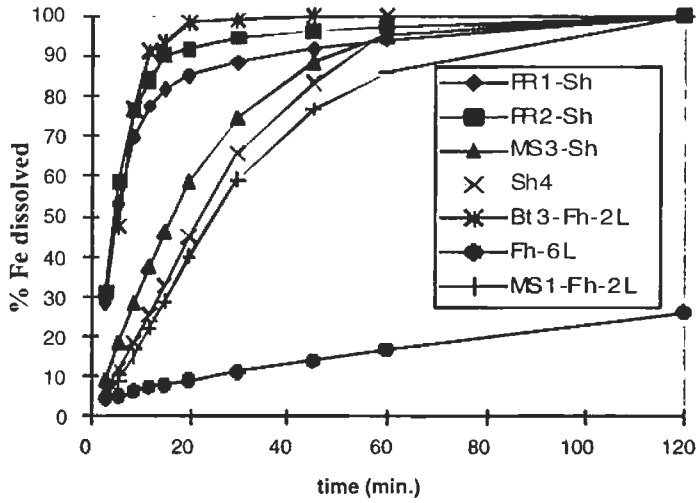

Fig. 1: *Dissolution kinetic curves of three natural sh (PR1, PR2, MS3) and one synthetic sh (Sh4), two natural 2-line fh (MS1, Bt3), and one synthetic 6-line fh (Fh-6L) performed with 0.2 M NH4-oxalate pH 3, dark. Mineral abbreviations as in Table 1.*

The variations of Fe/S mole ratios in the NH_4-OxD leach (Fig. 3) and XRD results suggest that schwertmannite together with jarosite is limited to the oxidation zone and that the predominant ferric oxyhydroxide in the zones below is possibly ferrihydrite. The pH-controlled distribution of these minerals in the tailings stratigraphy is consistent with observations made by Schwertmann et al. (1995) in a natural stream environment showing that ferrihydrite is stable at less acidic conditions (pH > 4) than schwertmannite (pH 3-4) and jarosite (pH < 3).

In the Piuquenes tailings impoundment, the higher values of Mo, As and SO_4 in the NH_4-OxD leach in samples from the oxidation zone and in situ microprobe analysis (Fig. 5) indicate that schwertmannite and jarosite play an important role for the oxyanion adsorption by ligand exchange under acidic conditions. In contrast, bivalent cations (e.g., Zn^{2+}, Mn^{2+}, Pb^{2+}) are not

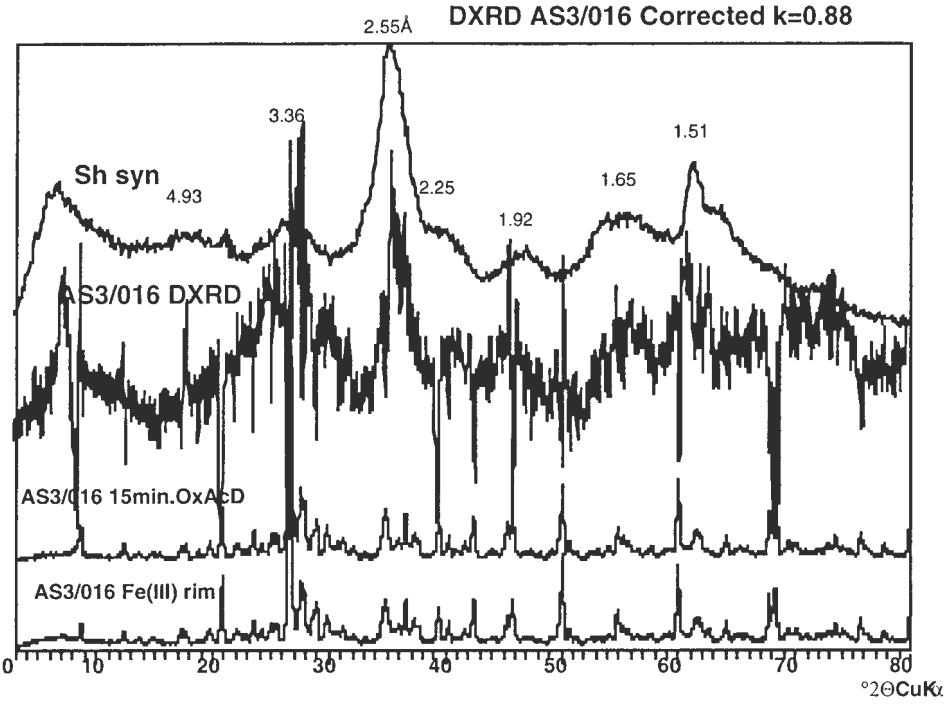

Fig. 2: DXRD of a hand selected schwertmannite rich sample from the Piuquenes tailings (AS3/016) after 15 min. treatment with NH4-oxalate pH 3 under exclusion of light compared to a XRD scan of a synthetic schwertmannite sample (Sh syn). AS3/016 Fe(III)streak and AS3/016 15min.OxAcD shows the diffractograms before and after treatment, respectively. The Fe/S mole ratio in solution is 4.9 and the iron content is 2.6 %. A dissolution test with the schwertmannite containing tailings sample AS3/016 shows fast dissolution of this iron phase (88.4% after 15 min).

adsorbed (at pH < 4) by these minerals, because of competitive proton adsorption at outstanding OH^- groups. Below the oxidation zone, ferrihydrite together with other adsorbents (clay minerals, Mn-oxides) plays a major role in the pH controlled adsorption of bivalent cations mobilized downwards from the oxidation zone (Fig. 3).

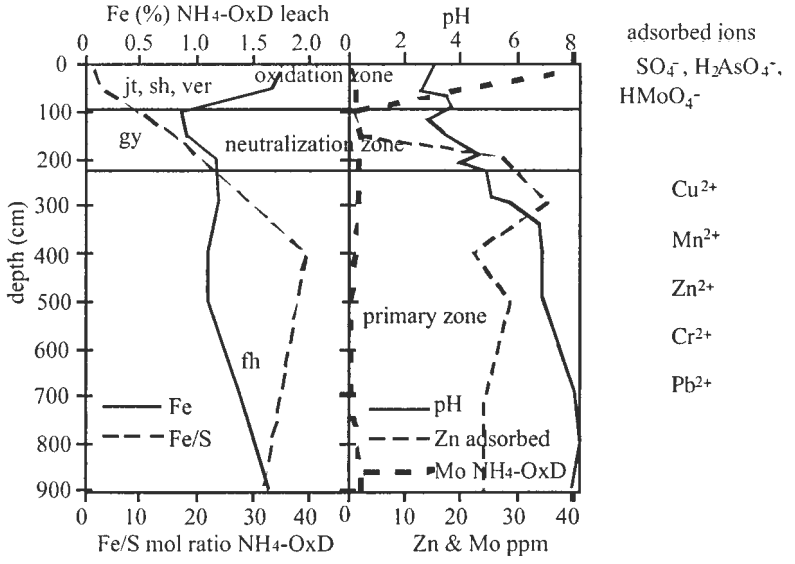

Fig. 3: *Typical porphyry copper tailings stratigraphy (e.g. Piuquenes A2) with secondary mineralogy (jarosite = jt, schwertmannite = sh, vermiculite-type mixed layer clay mineral = ver, gypsum = gy, ferrihydrite = fh), pH, and Fe, and Fe/S mole ratio variation in the ferric oxyhydroxide leach (NH4-OxD). Adsorbed Zn values are from the 1M NH4-acetate leach. The general trend of adsorbed ion species is shown at the right.*

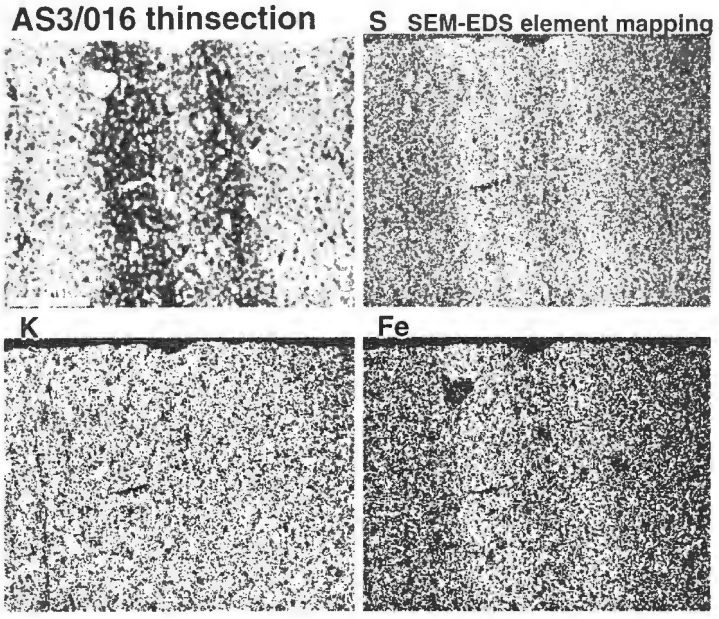

Fig. 4: *Undisturbed samples of tailing sediments rich in Fe(III) oxyhydroxide streaks from the Piuquenes impoundment were impregnated with epoxy resin and a thin section of this sediment was prepared. SEM-EDS element mapping for major elements show that Fe and S, the major elements of schwertmannite, are enriched at the streaks of fluid paths. Sulfur could also be adsorbed as sulfate to goethite and/or ferrihydrite if present. Potassium as a tracer for jarosite, shows no relationship to the streak.*

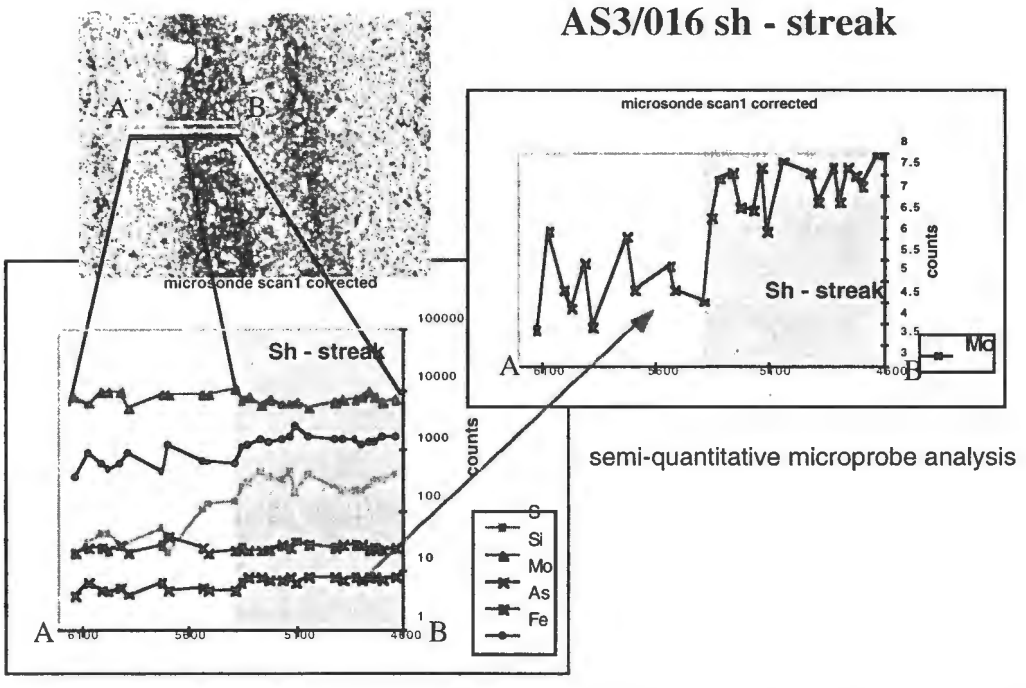

Fig. 5: *Semi-quantitative microprobe analysis of schwertmannite streaks (sh-streak) of sample AS3/016 (Piuquenes) showing increasing concentrations of Fe, S and Mo. The higher content of Mo in the sh-streak suggest the adsorption of molybdate at sh under low pH (2.5-3.5). The slight enrichment of Mo in the sh-streak indicates a certain mobility of this element, possibly transported as adsorbed oxyanion at ferric polymers. Arsenic does not show increased values in the sh-streak, this may indicate that arsenate is less mobile and possibly adsorbed at disseminated or coprecipitated with jarosite.*

In the Cauquenes tailings impoundment (semi-arid climate), the adsorption behavior is similar, but in places the very mobile elements Cu and Zn are enriched in the oxidation zone as water soluble secondary minerals (e.g., chalcanthite $CuSO_4 \cdot 5H_2O$, see chapter 5). This superposition is induced by capillary-upwards migration which is controlled by high evaporation, finer grain size, and higher moisture conditions prevailing mainly in the center of the impoundment. In hyper-arid conditions (El Salvador; Atacama desert, Northern Chile) copper is enriched up to 5 % in the upper part of the tailings stratigraphy as water soluble fraction (mainly chalcanthite).

Results have shown that the main secondary ferric phases in the oxidation zone are jarosite and schwertmannite in the Piuquenes and Cauquenes tailings. For acid-base accounting in general it is assumed that $Fe(OH)_{3(s)}$ or ferrihydrite hydrolyzes from solution with the production of 3 moles H^+/mole Fe^{3+} hydrolyzed. The hydrolysis of jarosite produces only 2 moles H^+ and that of schwertmannite between 2.625 and 2.75 (Table. 1). This difference must be taken into account into the calculation of the quantity of acid produced, as hydrolysis of the secondary ferric phases is the main acid producing process in sulfide oxidation. Nevertheless, it is important to point out that for calculation of the acid potential (AP) in case of lime or carbonate treatment, due to increased pH values, ferrihydrite or goethite will be produced, leading to the production of 3 moles H^+/mole Fe^{3+}.

Table 1: *Amount of protons produced by the hydrolysis of the different secondary Fe(III) phases.*

Phase	Equation	moles H^+/mole Fe^{3+}hydrolyzed
amp. $Fe(OH)_{3(s)}$	$Fe^{3+} + 3H_2O \Leftrightarrow Fe(OH)_{3(s)} + 3H^+$	3
ferrihydrite	$10\ Fe^{3+} + 60H_2O \Leftrightarrow 5Fe_2O_3 \cdot 9H_2O + 30H^+$	3
goethite	$Fe^{3+} + 2H_2O \Leftrightarrow FeO(OH) + 3H^+$	3
hematite	$2Fe^{3+} + 3H_2O \Leftrightarrow Fe_2O_3 + 6H^+$	3
schwertmannite	$8Fe^{3+} + SO_4^{2-} + 14H_2O \Leftrightarrow Fe_8O_8(OH)_6SO_4 + 22H^+$	2.75
	$16Fe^{3+} + 3SO_4^{2-} + 26H_2O \Leftrightarrow Fe_{16}O_{16}(OH)_{10}(SO_4)_3 + 42H^+$	2.625
jarosite	$3Fe^{3+} + K + 2SO_4^{2-} + 6H_2O \Leftrightarrow KFe_3(SO_4)_2(OH)_6 + 6H^+$	2

Plumlee (1999) pointed out that the oxidation of sulfide minerals by aqueous ferric iron generates significantly greater quantities of acid than the oxidation by oxygen (see equations 1, 3 and 4). This is correct in the case that ferric iron is added to the system (e.g., in form of primary ferric minerals or as reported in chapter 6, where ferric iron is produced upstream and seeps downstream into an older tailings impoundment as acid mine drainage).

$$FeS_2 + {}^7/_2O_2 + H_2O \rightarrow FeSO_4 + SO_4^{2-} + 2H^+ \quad (1)$$

$$Fe^{2+} + {}^1/_4O_2 + H^+ \Leftrightarrow Fe^{3+} + H_2O \quad (2)$$

reaction rates strongly increased by

microbial activity (e.g., *Thiobacillus ferrooxidans*)

$$FeS_2 + 14\ Fe^{3+} + 8H_2O \rightarrow 15\ Fe^{2+} + 2SO_4^{2-} + 16H^+ \quad (3)$$

$$2MeS + 4Fe^{3+} + 3O_2 + 2H_2O \rightarrow 2Me^{2+} + 4Fe^{2+} + 2SO_4^{2-} + 4H^+ \quad (4)$$

In contrast, if it is considered that the ferric iron is produced by the oxidation from ferrous iron in the system (e.g., microbiologically catalyzed pyrite oxidation), for every mole of ferric iron produced one mole of protons is consumed (equation 2). This leads to the same overall produced quantity of two protons per mole pyrite oxidized as in case of pyrite oxidation via O_2 (compare equations 1, 2, and 3). The overall net pyrite oxidation via oxygen with hydrolysis of ferric hydroxides produces 4 moles of H^+ per mole pyrite oxidized (equation 5). The overall net pyrite oxidation via ferric iron with hydrolysis of ferric hydroxides produces 6 moles of H^+ per mole pyrite oxidized (equation 6). But, in equation 6 it has to be considered that before the two moles of $Fe(OH)_{3(s)}$ can hydrolyze, 2 moles of protons will be consumed by the oxidation of the 2 moles of ferrous iron resulting from the left half reaction of equation 6 to the ferric iron (equation 2). Thus, effectively 4 moles of protons are produced by the pyrite oxidation via ferric iron, the same amount as by the oxidation via oxygen.

$$FeS_2 + {}^{15}/_4O_2 + {}^{7}/_2H_2O \rightarrow \quad Fe(OH)_3 + 2SO_4^{2-} + 4H^+ \qquad (5)$$

$$FeS_2 + \quad Fe^{3+} + \quad 6H_2O \rightarrow \quad 2Fe(OH)_3 + 2SO_4^{2-} + 6H^+ \qquad (6)$$

Additionally, it has to be taken in account that in case of oxidation via ferric iron no acidity can be produced via the hydrolysis of the ferric phases (equation 3), the main acid producing process in sulfide oxidation (see equation 4 this chapter and Table 1). Thus, the sulfide oxidation by ferric iron has faster kinetics (Moses et al., 1987) and is able to oxidize sulfide minerals in the absence of oxygen, but it does not produce more acid as the oxidation via oxygen if it is considered that ferric iron is formed in the system.

7.4 Conclusions

The presence of schwertmannite in the oxidation zone of two tailings (Piuquenes from La Andina and Cauquenes from El Teniente) was determined by DXRD and is also supported by SEM-EDS element mapping, fast dissolution kinetics in NH_4-oxalate, Fe/S mole ratio of 4.9, typical pH from 2.8 to 3.5, and its orange brown color.

Schwertmannite occurs as dots or streaks in the fine grained horizons or is enriched at the interface of fine to coarser grained horizons, due to capillary barrier controlled water flow. This distribution of schwertmannite indicates that it is preferentially associated with water flow paths and possibly dilution effects increase the pH to the level necessary (2.8-3.5) for its precipitation.

Schwertmannite, together with jarosite plays an important role in the adsorption of oxyanions in the oxidation zone. Bivalent cations (e.g., Cu^{2+}, Zn^{2+}, Mn^{2+}, Pb^{2+}) are leached out of the oxidation zone and enriched stratigraphically below by adsorption processes to Fe(III) hydroxides as ferrihydrite or other adsorbents (clay minerals, Mn-oxides), replacement of sulfides (in case of Cu^{2+} only), and co-precipitation processes. These enrichments are guided by neutralization processes which increase the pH in the underlying zones and control the pH-dependent adsorption of these elements.

Climate plays an important role in the mobilization direction of the very mobile element as Cu and Zn. High evaporation rates may lead to significant enrichment of water-soluble efflorescent salts of these metals in the upper part of the tailings. In contrast, in humid climates a downwards mobilization is typical.

For acid-base accounting it is assumed in general that $Fe(OH)_{3(s)}$ or ferrihydrite hydrolyzes from solution with the production of 3 moles H^+/mole Fe^{3+} hydrolyzed. The hydrolysis of jarosite produce only 2 moles H^+ and schwertmannite between 2.625 and 2.75, respectively. Results suggest that this difference must be taken into account by calculation of the quantity of acid produced and for geochemical modeling, as hydrolysis of the secondary ferric phases is the main acid producing process in sulfide oxidation. Nevertheless, it is important to be aware that for calculation of the acid potential in case of carbonate treatment, due to increased pH values, ferrihydrite or goethite will be produced, leading to the production of 3 moles H^+/mole Fe^{3+}.

Oxidation of sulfides via ferric iron produces importantly higher amounts of acidity if the ferric iron is added to system (e.g., ferric minerals or acid seepage). But, in case that the ferric iron is produced in the process of sulfide oxidation, the net acid production of pyrite oxidation with the hydrolysis of ferric hydroxides via oxygen or ferric iron is the same (oxidation from ferrous to ferric iron is a proton consuming process). Thus, for an overall estimation of the acid potential of mine waste it has also to be considered if ferric iron is produced in the system or added to the system.

These results illustrate the importance of secondary mineralogy to the adsorption properties in mine tailings and the production of acidity. The distribution of schwertmannite, jarosite, and ferrihydrite is mainly controlled by pH and the activity of Fe, K, and SO_4. Their selective adsorption behavior is essentially pH-controlled.

Acknowledgements

I would like to thank the management and the geologists and all stuff involved in this project from CODELCO for their interest, the access to their properties, their logistic support and their collaboration, especially A. Piug (Exploration Division, CODELCO), L. Serrano, R. Vargas, C. Aguila, C. Castillo, and M. Bustos (Division Andina, CODELCO), F. Celhay, A. Morales (Division El Teniente, CODELCO), J. Blondel, and R. Novajas (Division Salvador, CODELCO). For their support in Chile in the field work, sampling, sample preparation, and analytical approaches I would like thank to G. C ceres and K. Eppinger (IDICTEC —University of Atacama), S. Elqueta (Geological Department, University of Chile, Santiago), B. Escobar, J. Wiertz, and J. Casas (Chemical Department, Biometallurgy, University of Chile, Santiago), R. Troncoso, A. Hauser, C. Reuschmann, C. Espejo, E. Fonseca, W. Vivallio, I. Aguirre (Servicio Nacional de Geolog a y Miner a SERNAGEOMIN), W. Eberle, and H.W. M ller (Bundesanstalt f r Geowissenschaften und Rohstoffe BGR). I thank also Prof. R. Pfeiffer and his group for the facilities and discussions in the laboratory of the Centre de Analyse de Mineralogie, Universit de Lausanne. Thanks to Dr. Dubois from Soil Science Institute of the EPFL, Lausanne for the ICP analysis and Dr. R. Martini from the Geological Department , University of Geneva for the patient SEM work and to Dr. M. Streck, Mineralogical Department, University of Geneva, for

the help with the microprobe analyses. The project is supported by the German Academic Exchange Service (DAAD) and the Swiss National Science Foundation project No. 21-50778.97.

References

Bigham, J.M., Schwertmann, U., Carlson, L. and Murad, E. (1990): A poorly crystallized oxyhydroxysulfate of iron formed by bacterial oxidation of Fe(II) in acid mine waters. Geochimica et Cosmochimica Acta, v. 54, p. 2743-2758.

Bigham, J.M., Carlson, L. and Murad, E. (1994): Schwertmannite, a new iron oxyhydroxy-sulphate from Pyh salmi, Finland, and other localities. Mineralogical Magazine, v. 58, p. 641-648.

Bigham, J.M., Schwertmann, U., Traina, S.J., Winland, R.L. and Wolf, M. (1996): Schwertmannite and the chemical modeling of iron in acid sulfate waters. Geochimica et Cosmochimica Acta, v. 60, No. 2, p. 185-195.

Cardoso Fonseca, E. and Martin, H. (1986): The selective extraction of Pb and Zn in selected mineral and soil samples, application in geochemical exploration (Portugal). Journal of Geochemical Exploration, v. 26, p. 231-248.

Chao, T.T. and Sanzolone, R.F. (1977): Chemical dissolution of sulfide minerals. Journal of Research U.S. Geol.Survey, v. 5 p.409-412.

Childs, C.W, Inoue, K. and Mizota, C. (1998): Natural and anthropogenetic schwertmannites from Towada-Hachimantai National Park, Honshu, Japan. Chemical Geology, v. 144, p. 81-86.

Dold, B., Eppinger, K.J. and K lling, M. (1996): Pyrite oxidation and the associated geochemical processes in tailings in the atacama desert/Chile: The influence of men controlled water input after disuse. Clean technology for the mining industry, Santiago, p. 417 - 427.

Dold, B., Fontbot , L. and Wildi, W. (1999): Detection and distribution of ferric oxyhydroxides and oxyhydroxide sulfates in sulfide mine tailings; their importance to selective metal retention and acid production. Mine, Water and Environment, 1999 IMWA Congress, Sevilla, Spain, v. 2, p. 525-526.

Fanfani, L., Zuddas, P., Chessa, A. (1997): Heavy metals speciation analysis as a tool for studying mine tailings weathering. Journal of Geochemical Exploration, v. 58, p. 241-248.

Gatehouse, S., Roussel, D.W., Van Moort, J.C. (1977): Sequential soil analysis in exploration analysis. Journal of Geochemical Exploration, v. 8, p. 483-494.

Hall, G.E.M., Vaive, J.E., Beer, R., Hoashi, M. (1996): Selective leaches revisited, with emphasis on the amorphous Fe oxyhydroxide phase extraction. Journal of Geochemical Exploration, v. 56, p. 59-78.

Lin, Z. (1996): Leachate chemistry and precipitates mineralogy of Rudolfsgruvan mine waste rock dump in Central Sweden. Wat.Sci.Tech., v. 33, No. 6, p. 163-171.

Jambor, J.L. and Blowes, D.W. (1998): Theory and applications of mineralogy in environmental studies of sulfide-baring mine waste. In: Cabri, L. J. and Vaughan, D.J. (eds.): Short Course Handbook on Ore and Environmental Mineralogy. Mineralogical Association of Canada, Nepean, v. 27, p. 367-401.

Jamieson, H.E., Shaw, S.C., Clark, A.H. (1995): Mineralogical factors controlling metal release from tailings at Geco, Manitouwadge, Ontario. In: Hynes, T.P. and Blanchette, M.C., (Eds.), Proceedings Sudbury '95 - Mining and the Environment, CANMET, Ottawa, v. 1, p. 405-413.

Moses, C.O., Nordstrom, D.K., Herman, J.S. and Mills, A.L. (1987): Aqueous pyrite oxidation by dissolved oxygen and by ferric iron. Geochimica et Cosmochimica Acta, v. 51, p. 1561-1571.

Plumlee, G.S. (1999): The environmental geology of mineral deposits. In: Plumlee, G. S. and Logsdon, M.J. (Eds.) Reviews in Economic Geology, The environmental geochemistry of ore deposits. Part A: Processes, Techniques, and Health Issues, v. 6A, p. 71-116.

Ribet, I., Ptacek, C.J., Blowes, D.W. and Jambor, J.L. (1995): The potential for metal release by reductive dissolution of weathered mine tailings. Journal of Contaminant Hydrology, v. 17(3), p. 239-273.

Tessier, A., Campbell, P.G.C., Bisson, M. (1979): Sequential extraction procedure for speciation of particulate trace metals. Analytical Chemistry, v. 51, p. 844-851.

Schwertmann, U. (1964): Differenzierung der Eisenoxide des Bodens durch Extraktion mit Ammoniumoxalat L sung. Zeitschrift f r Pflanzenern hrung und Bodenkunde, v. 105, p. 194-202.

Schwertmann, U., Bigham, J.M. and Murad, E. (1995): The first occurrence of schwertmannite in a natural stream environment. European Journal of Mineralogy, v. 7, p. 547-552.

Sondag, F. (1981): Selective extraction procedures applied to geochemical prospecting in an area contaminated by old mine workings. Journal of Geochemical Exploration, v. 15, p.645-652.

Stone, A.T. (1987): Microbial metabolites and the reductive dissolution of manganese oxides: Oxalate and pyruvate. Geochimica et Cosmochimica Acta, v. 51; p. 919-925.

Webster, J.G., Swedlund, P.J., and Webster, K.S. (1998): Trace metal adsorption onto an acid mine drainage iron(III)oxyhydroxy sulfate. Environmental Science and Technology, v. 32,10, p. 1362-1368.

Yu, J-Y., Heo, B. and Chang, H-W. (1998): Stability of schwertmannite and ferrihydrite in stream waters of Imgok and Osheep Creek polluted by acid mine drainage. Goldschmidt Conference Proceedings 1998, p. 1675-1677.

APPENDIX. 1

Results of Acid-Base Accounting (ABA)

Analytical conditions

The calculation of the sulfide acid potential (SAP) is based on the total sulfur (S_{tot}) contents obtained by LECO® furnace and the total sulfate (SO_{4tot}) content obtained by the attack of the sample with 0.2M NH_4-oxalate, pH 3.0, 80°C for 2h (step 4 in chapter 3) and measuring the sulfur concentrations in the leach by ICP-ES. The difference of the two concentrations represent the S-sulfide content of the sample. These analyses were performed by the X-Ray Assay Laboratories (XRAL) of Toronto, Canada.

The calculation of the carbonate neutralization potential (CaNP) is based on the total carbon (C_{tot}) content obtained by coulometric titration (Ströhlein CS 702®) at the Centre d'Analyse Minérale, University Lausanne.

Calculation

The calculation of the acid-base accounting (ABA) is based on the following assumptions:

1. S-sulfide is available only in form of pyrite.
2. ferric iron hydrolyses as $Fe(OH)_3$, leading to the production of four mol protons per mol of oxidized pyrite.
3. The pH is neutralized by calcite to values of 7 leading to the stability of HCO_3^- so that 1 mol of calcite is necessary to neutralize one mol of protons.

These assumptions lead to a factor of 62.5 to which has to be multiplied with the S-sulfide value to obtain the calcite equivalent necessary to neutralize the amount of acid produced by sulfide oxidation. The factor 62.5 is obtained as followed: $4(H^+)$ x 100(molar weight of calcite)/32(molar weight of sulfur) x $2(FeS_2)$ = 6.25. Multiplying by 10 leads SAP in t $CaCO_3$/1000 t, resulting in the applied factor of 62.5 for the SAP.

The CaNP is calculated with the total carbon content in molar wt.% calcite equivalent multiplied by the factor 8.33 (mol weight 100 for calcite/12 carbon = 8.33) and also multiplied by 10 to obtain in t $CaCO_3$/1000 t, resulting in the factor 88.3. The sulfide net neutralization potential (SNNP) is obtained by the subtraction of the SAP from the CaNP. Negative values indicate that the SAP is higher than the CaNP and the material is most likely acid producing. If the value is positive the CaNP is higher than the SAP and able to neutralize the produced acid. The paste pH of the samples, calculated pyrite content (wt.%) and the zonation of each sample is given (XY/ZZZ, where X = impoundment, Y = core No, Z = sample depth in cm).

Table A1.1: Acid-Base Accounting (ABA) with paste pH and location of each sample in the tailings stratigraphy

ABA from the Piuquenes tailings impoundment/ La Andina

Sample	zone	pH	Stot	SO4 tot	S (SO4)	S sulfide	S pyrite	SAP (Sulfide Acid Pot)	Ctot	CaNP (Carbonat NP)	SNNP (Sulfide Net NP)
			%	%	%	%	%	t CaCO3/1000t	%	t CaCO3/1000t	t CaCO3/1000t
A2/020	ox	3.2	0.55	1.524	0.508	0.042	0.078	2.63	0.03	2.56	-0.06
A2/050	ox	2.6	0.64	1.46	0.487	0.153	0.285	9.58	0.04	3.42	-6.17
A2/100	neutr	3.8	1.73	0.493	0.164	1.566	2.911	97.85	0.04	3.42	-94.44
A2/150	neutr	3.5	0.91	0.896	0.299	0.611	1.137	38.21	0.09	7.68	-30.52
A2/200	neutr	4.6	0.68	0.603	0.201	0.479	0.891	29.94	0.23	18.78	-11.15
A2/295	neutr	5	1.3	0.433	0.144	1.156	2.149	72.23	0.37	30.74	-41.49
A2/400	pri	6.3	1.13	0.218	0.073	1.057	1.966	66.08	0.31	25.61	-40.47
A2/500	pri	6.3	0.55	0.148	0.049	0.501	0.931	31.29	0.46	38.42	7.13
A2/700	pri	8.2	1.22	0.137	0.046	1.174	2.184	73.40	0.36	29.88	-43.51
A2/900	pri	8.2	1.01	0.223	0.074	0.936	1.740	58.48	0.04	3.42	-55.06
A4/010	hm	8.4	0.15	0.179	0.060	0.090	0.168	5.65	0.03	2.56	-3.08
A4/035	ox	5.4	0.78	1.327	0.442	0.338	0.628	21.10	0.03	2.56	-18.54
A4/065	ox	3.5	0.74	1.213	0.404	0.336	0.624	20.98	0.03	2.56	-18.42
A4/100	neutr	3.8	1.01	0.487	0.162	0.848	1.576	52.98	0.00	0.17	-52.81
A4/125	neutr	3.8	1.14	0.982	0.327	0.813	1.511	50.79	0.03	2.56	-48.23
A4/200	neutr	4.1	1.11	0.428	0.143	0.967	1.799	60.46	0.09	7.68	-52.77
A4/260	neutr	5	1.29	0.326	0.109	1.181	2.197	73.83	0.08	6.83	-67.00
A4/400	pri	6.6	1.2	0.274	0.091	1.109	2.061	69.29	0.22	17.93	-51.36
A4/600	pri	7.1	1.29	0.262	0.087	1.203	2.236	75.17	0.19	16.22	-58.94
A4/800	pri	8.4	0.84	0.235	0.078	0.762	1.416	47.60	0.19	16.22	-31.38
A4/1000	pri	7.9	1.06	0.267	0.089	0.971	1.805	60.69	0.41	34.15	-26.53
A5/020	ox	2.8	0.7	1.235	0.412	0.288	0.536	18.02	0.17	14.52	-3.51
A5/050	ox	3.5	1.28	0.841	0.280	1.000	1.859	62.48	0.06	5.12	-57.36
A5/140	neutr	3.9	1.23	0.667	0.222	1.008	1.874	62.98	0.00	0.00	-62.98
A5/500	pri	7	1	0.232	0.077	0.923	1.716	57.67	0.00	0.00	-57.67
A5/900	pri	7.8	0.85	0.222	0.074	0.776	1.443	48.50	0.07	5.98	-42.52

ABA from the Cauquenes tailings impoundment/ El Teniente

Sample	zone	pH	Stot	SO4 tot	S (SO4)	S sulfide	S pyrite	SAP (Sulfide Acid Pot)	Ctot	CaNP (Carbonat NP)	SNNP (Sulfide Net NP)
Unit			%	%	%	%	%	t CaCO3/1000t	%	t CaCO3/1000t	t CaCO3/1000t
T1/040	ox	2.8	0.66	1.90	0.63	0.03	0.05	1.69	0.08	6.83	5.14
T1/100	ox	2.8	0.84	0.83	0.28	0.56	1.05	35.29	0.00	0.00	-35.29
T1/105	ox	2.8	0.7	1.46	0.49	0.21	0.39	13.25	0.02	1.71	-11.54
T1/200	pri	2.8	1.08	0.42	0.14	0.94	1.75	58.67	0.02	1.71	-56.96
T1/290	pri	3	1.26	0.59	0.20	1.06	1.98	66.44	0.02	1.71	-64.73
T1/400	pri	5	0.9	0.65	0.22	0.68	1.27	42.67	0.01	0.85	-41.81
T1/580	pri	5.4	0.77	0.34	0.11	0.66	1.22	41.08	0.02	1.71	-39.38
T1/800	pri	3.7	0.61	0.41	0.14	0.47	0.88	29.58	0.00	0.00	-29.58
T1/890	pri	3.7	0.89	0.42	0.14	0.75	1.40	46.98	0.02	1.71	-45.27
T2/020	ox	2.7	1.05	2.85	0.95	0.10	0.19	6.33	0.07	5.98	-0.36
T2/070	ox	2.6	0.56	1.38	0.46	0.10	0.19	6.29	0.02	1.71	-4.58
T2/100	ox	2.3	0.52	1.32	0.44	0.08	0.15	5.08	0.01	0.85	-4.23
T2/160	ox	1.7	0.54	1.29	0.43	0.11	0.21	6.98	0.02	1.71	-5.27
T2/190	pre	2.2	0.6	0.38	0.13	0.47	0.88	29.67	0.00	0.00	-29.67
T2/220	pre	2.8	0.5	0.72	0.24	0.26	0.48	16.27	0.04	3.42	-12.86
T2/300	pre	3.4	0.7	0.68	0.23	0.47	0.88	29.58	0.00	0.34	-29.24
T2/400	pri	4.5	0.78	0.32	0.11	0.67	1.25	42.06	0.00	0.26	-41.81
T2/580	pri	4.9	0.74	0.33	0.11	0.63	1.17	39.29	0.03	2.56	-36.73
T2/800	pri	4.6	0.44	0.67	0.22	0.22	0.40	13.48	0.04	3.42	-10.06
T2/1000	pri	3.9	0.52	0.81	0.27	0.25	0.47	15.71	0.04	3.42	-12.29
T3/020	ox	2.9	0.56	1.49	0.50	0.06	0.12	4.00	0.16	13.66	9.66
T3/060	ox	2.9	0.34	0.73	0.24	0.10	0.18	5.96	0.00	0.26	-5.70
T3/100	ox	3.1	0.61	0.77	0.26	0.35	0.65	22.00	0.03	2.56	-19.44
T3/150	ox	3.1	0.52	1.13	0.38	0.14	0.27	8.92	0.03	2.56	-6.36
T3/170	pri	3.4	1.49	0.36	0.12	1.37	2.55	85.69	0.12	10.25	-75.44
T3/300	pri	5	0.59	0.32	0.11	0.48	0.90	30.23	0.02	1.71	-28.52
T3/400	pri	6.1	0.6	0.26	0.09	0.51	0.96	32.15	0.01	0.85	-31.29
T3/595	pri	6.7	0.73	0.33	0.11	0.62	1.16	38.85	0.02	1.71	-37.15
T3/800	pri	6.7	0.43	0.50	0.17	0.26	0.49	16.42	0.03	2.56	-13.86
T3/1000	pri	5	0.54	1.02	0.34	0.20	0.37	12.50	0.04	3.42	-9.08
T4/010	ox	4.12	0.21	0.59	0.20	0.02	0.03	0.94	0.03	2.56	1.62
T4/040	ox	3.8	0.27	0.78	0.26	0.01	0.02	0.60	0.04	3.42	2.81
T4/100	ox	2.9	0.33	0.97	0.32	0.01	0.01	0.44	0.01	0.85	0.42
T4/153	ox	3	0.27	0.71	0.24	0.04	0.07	2.19	0.00	0.34	-1.85
T4/490	pri	3.7	0.84	0.49	0.16	0.68	1.26	42.21	0.04	3.42	-38.79
T4/795	pri	5.3	0.76	0.27	0.09	0.67	1.25	41.88	0.01	0.85	-41.02

Table A1.1: *Acid-Base Accounting (ABA) with paste pH and location of each sample in the tailings stratigraphy*

ABA from the El Salvador impoundment No.1

Sample	zone	pH	Stot	SO4 tot	S (SO4)	S sulfide	S pyrite	SAP (Sulfide Acid Pot)	Ctot	CaNP (Carbonat NP)	SNNP (Sulfide Net NP)
			%	%	%	%	%	t CaCO3/1000t	%	t CaCO3/1000t	t CaCO3/1000t
E1/010	ev		6.51	4.022	1.341	5.169	9.612	323.08	0.08	6.66	-316.42
E1/030	ev	3.5	6.8	3.491	1.164	5.636	10.480	352.27	0.15	12.50	-339.78
E1/050	ev	2.6	7.37	11.4	3.800	3.570	6.638	223.13	0.1	8.33	-214.80
E1/100	ev	2.3	5.19	8.126	2.709	2.481	4.614	155.08	0.05	4.17	-150.92
E1/170	ox	2.3	5.81	8.704	2.901	2.909	5.408	181.79	0	0.00	-181.79
E1/200	ox	2.2	6.08	8.635	2.878	3.202	5.953	200.10	0	0.00	-200.10
E1/260	pri	2.5	5.87	7.748	2.583	3.287	6.112	205.46	0	0.00	-205.46
E1/350	pri	2.5	6.83	9.52	3.173	3.657	6.799	228.54	0	0.00	-228.54
E1/482	pri	3.5	8.44	7.719	2.573	5.867	10.909	366.69	0.08	6.66	-360.02
E2/010	ev		13.2	36.6	12.200	1.000	1.859	62.50	0.3	24.99	-37.51
E2/030	ev	2.1	9.39	18.6	6.200	3.190	5.931	199.38	0.2	16.66	-182.72
E2/050	ox	2	7.86	12.6	4.200	3.660	6.805	228.75	0	0.00	-228.75
E2/070	ox	2.1	6.26	6.985	2.328	3.932	7.310	245.73	0	0.00	-245.73
E2/100	ox	2.2	6.15	7.237	2.412	3.738	6.950	233.60	0.1	8.33	-225.27
E2/155	ox	2.1	6.12	8.701	2.900	3.220	5.987	201.23	0	0.00	-201.23
E2/190	ox	2.5	6.05	8.447	2.816	3.234	6.014	202.15	0.14	11.66	-190.48
E2/280	ox	2.8	5.82	9.459	3.153	2.667	4.959	166.69	0	0.00	-166.69
E2/300	ox	2.4	6.06	11	3.667	2.393	4.450	149.58	0	0.00	-149.58
E2/390	ox	2.3	6.78	11.4	3.800	2.980	5.541	186.25	0	0.00	-186.25
E2/500	pri	3.4	6.14	4.859	1.620	4.520	8.405	282.52	0	0.00	-282.52
E3/010	ev		6.44	3.605	1.202	5.238	9.740	327.40	0.22	18.33	-309.07
E3/030	ev	2.4	6.75	3.798	1.266	5.484	10.197	342.75	0.4	33.32	-309.43
E3/100	ev	3.5	7.1	11.1	3.700	3.400	6.322	212.50	0.77	64.14	-148.36
E3/150	ev	3.3	7.97	10.9	3.633	4.337	8.063	271.04	1.12	93.30	-177.75
E3/170	ox	2.4	10.2	18.2	6.067	4.133	7.685	258.33	0.8	66.64	-191.69
E3/200	ox	2.5	6.49	9.94	3.313	3.177	5.907	198.54	1.1	91.63	-106.91
E3/250	ox	2.2	6.41	10.7	3.567	2.843	5.287	177.71	0.92	76.64	-101.07
E3/270	ox	2.2	7.1	13.2	4.400	2.700	5.020	168.75	0.6	49.98	-118.77
E3/300	ox	2.2	8.35	12.5	4.167	4.183	7.778	261.46	1.85	154.11	-107.35
E3/386	ox	2.5	7.6	8.863	2.954	4.646	8.638	290.35	1.66	138.28	-152.08
E3/400	soil	3.9	0.59	1.185	0.395	0.195	0.363	12.19	0.16	13.33	1.14
E4/010	ev		10.7	26.7	8.900	1.800	3.347	112.50	0.22	18.33	-94.17
E4/040	ev	2	9	18.5	6.167	2.833	5.268	177.08	0.25	20.83	-156.26
E4/080	ox	2	5.62	8.237	2.746	2.874	5.344	179.65	0	0.00	-179.65
E4/100	ox	1.9	5.18	8.454	2.818	2.362	4.392	147.63	0	0.00	-147.63
E4/120	ox	2.1	5.52	11.1	3.700	1.820	3.384	113.75	0.32	26.66	-87.09
E4/140	ox	2.2	6.32	7.939	2.646	3.674	6.831	229.60	0.3	24.99	-204.61
E4/200	ox	2.5	6.53	7.984	2.661	3.869	7.193	241.79	0	0.00	-241.79
E4/250	ox	2.5	6.01	9.038	3.013	2.997	5.573	187.33	0	0.00	-187.33
E4/270	soil	3.3	1.5	3.507	1.169	0.331	0.615	20.69	0	0.00	-20.69

ABA from the Ojancos No. 2 impoundment

Sample	zone	pH	Stot	SO4 tot	S (SO4)	S sulfide	S pyrite	SAP (Sulfide Acid Pot)	Ctot	CaNP (Carbonat NP)	SNNP (Sulfide Net NP)
			%	%	%	%	wt.%	t CaCO3/1000t	%	t CaCO3/1000t	t CaCO3/1000t
HPr	pri	11	1.92	0.09	0.03	1.89	3.51	118.13	0.85	70.81	-47.32
H1/044	pri	7.2	1.97	0.20	0.07	1.90	3.54	118.96	0.33	27.49	-91.47
H1/100	pri	7.9	1.93	0.19	0.06	1.87	3.47	116.67	0.4	33.32	-83.35
H1/200	pri	7.3	2.8	0.71	0.24	2.56	4.77	160.23	0.02	1.71	-158.52
H1/300	pri	7.3	2.42	0.71	0.24	2.18	4.06	136.46	1.84	153.27	16.81
H1/400	ox	7.3	1.36	0.73	0.24	1.12	2.08	69.79	5	416.50	346.71
H1/500	ox	7.4	1.41	0.61	0.20	1.21	2.24	75.42	4.21	350.69	275.28
H1/600	ox	7.3	1.28	1.35	0.45	0.83	1.54	51.88	5.65	470.65	418.77
H1/680	ox	6.6	3.1	6.90	2.30	0.80	1.49	50.02	0.77	64.46	14.44
H1/760	ox	5.9	3.55	6.05	2.02	1.53	2.85	95.81	0.84	69.67	-26.14
H1/860	cem	5.5	3.73	9.46	3.15	0.58	1.08	36.15	0.06	4.61	-31.54
H1/960	cem	4.5	3.66	9.07	3.02	0.64	1.18	39.79	1.16	96.63	56.84
H1/1000	cem	6	3.33	7.20	2.40	0.93	1.73	58.10	0.07	6.15	-51.96

ABA from the P. Cerda No. 4 impoundment

Sample	zone	pH	Stot	SO4 tot	S (SO4)	S sulfide	S pyrite	SAP (Sulfide Acid Pot)	Ctot	CaNP (Carbonat NP)	SNNP (Sulfide Net NP)
			%	%	%	%	wt.%	t CaCO3/1000t	%	t CaCO3/1000t	t CaCO3/1000t
03/025	pri	7.5	1.7	1.09	0.363	1.337	2.485	83.54	0.09	7.60	-75.94
03/070	pri	7.6	1.35	0.778	0.259	1.091	2.028	68.17	0.26	21.43	-46.74
03/200	ox	7.2	1.36	2.381	0.794	0.566	1.053	35.40	0.29	23.82	-11.57
03/300	cem	7.1	0.84	1.973	0.658	0.182	0.339	11.40	0.43	35.78	24.38
03/500	cem	7	0.92	2.423	0.808	0.112	0.209	7.02	0.04	3.24	-3.78

Abbreviations: pri = primary zone, ox = oxidation zone, cem = cemented zone, ev = evaporate zone, neutr = neutralization zone, hm = hematite rich sediment

APPENDIX. 2

Results of the extraction sequence A

Applied sequence A:

Sequence A	References
(1) exchangeable fraction; 1.0 g sample into 20 ml 1M NH_4-acetate pH 4.5 shake for 2 hrs	Gatehouse et al., 1977; Sondag, 1981; Cardoso Fonseca et al., 1986
(2) adsorbed, carbonates 1M Na-acetate pH 5 shake for 2 hrs	Tessier et al., 1979
(3) Mn oxides 0.1 M NH_2OH-HCl pH 2 shake for 2 h	Chao, 1984; Cardoso Fonseca et al., 1986
(4) Fe(III)oxides 0.1 M NH_4-oxalate pH 3.3 heat in water bath 80°C for 2 hours	Fonseca and Martin, 1986
(5) organic and sulfides H_2O_2 35% heat in water bath for 1 hour	Sondag, 1981
(6) residual HNO_3, HF, $HCLO_4$, HCl digestion	Tessier et al., 1979; Hall et al., 1996; Dold et al., 1996

Analytical conditions

Multi-element (31 elements) analyses were performed in the leach by ICP-ES. The analyses were performed by the X-Ray Assay Laboratories (XRAL) of Toronto, Canada. Accuracy of the analyses was controlled by a bulk analysis of every sample with the HNO_3, HF, $HCLO_4$, HCL digestion.

Abbreviations:

NH_4-Ac	= 1. Step: 1 M ammonium acetate, pH 4.5 leach
Na-Oc	= 2. Step: 1M Na-acetate, pH 5 leach
HL	= 3. Step: 0.1 M NH_2OH-HCl, pH 2 leach
NH_4-OxH	= 4. Step: 0.1M ammonium oxalate, pH 3, heat leach
H_2O_2	= 5. Step: 35 % peroxide leach
residual	= 6. Step: HNO_3, HF, $HCLO_4$, HCL leach
total	= sum of step 1 to step 6
bulk	= control analysis of a bulk sample with the HNO_3, HF, $HCLO_4$, HCL leach
BDL	= below detection limit

References

Cardoso Fonseca, E., Martin, H. (1986): The selective extraction of Pb and Zn in selected mineral and soil samples, application in geochemical exploration (Portugal). Journal of Geochemical Exploration, v. 26, p. 231-248.

Chao, T.T., (1984): Use of partial dissolution techniques in geochemical exploration. Journal of Geochemical Exploration, v. 20, p. 101-135.

Dold, B., Eppinger, K.J., Kölling, M. (1996): Pyrite oxidation and the associated geochemical processes in tailings in the Atacama desert/Chile: The influence of men controlled water input after disuse. Clean technology for the mining industry, Santiago, p. 417 - 427.

Gatehouse, S., Roussel, D.W., Van Moort, J.C. (1977): Sequential soil analysis in exploration analysis. Journal of Geochemical Exploration, v. 8, p. 483-494.

Hall, G.E.M., Vaive, J.E., Beer, R., Hoashi, M. (1996): Selective leaches revisited, with emphasis on the amorphous Fe oxyhydroxide phase extraction. Journal of Geochemical Exploration, v. 56, p. 59-78.

Sondag, F. (1981): Selective extraction procedures applied to geochemical prospecting in an area contaminated by old mine workings. Journal of Geochemical Exploration, v. 15, p. 645-652.

Tessier, A., Campbell, P.G.C., Bisson, M. (1979): Sequential extraction procedure for speciation of particulate trace metals. Analytical Chemistry, v. 51, p. 844-851.

Fe (%)								
sample	depth	NH_4-Ac	Na-OC	HL	NH_4-OxH	H_2O_2	residual	total
A5/020	20	0.07	BDL	0.09	1.39	0.01	3.11	4.66
A5/035	35	0.08	BDL	0.08	1.49	0.01	2.91	4.56
A5/050	50	0.08	BDL	0.12	0.71	0.10	3.48	4.49
A5/100	100	0.05	BDL	0.08	0.43	0.04	3.69	4.29
A5/120	120	0.05	BDL	0.07	0.52	0.02	3.45	4.11
A5/140	140	0.05	BDL	0.08	0.67	0.02	3.95	4.78
A5/200	200	0.07	BDL	0.12	0.73	0.01	5.63	6.56
A5/220	220	0.09	BDL	0.13	0.75	0.03	5.15	6.16
A5/260	260	0.12	BDL	0.14	0.54	0.04	4.89	5.73
A5/300	300	0.06	BDL	0.10	0.64	0.03	3.28	4.12
A5/360	360	0.08	BDL	0.12	0.60	0.06	2.31	3.17
A5/400	400	0.06	BDL	0.13	0.62	0.05	3.97	4.83
A5/500	500	0.10	0.02	0.16	0.78	0.10	3.95	5.11
A5/600	600	0.12	0.02	0.18	0.83	0.08	3.14	4.36
A5/700	700	0.11	0.02	0.23	0.90	0.10	3.11	4.48
A5/800	800	0.15	0.03	0.25	1.04	0.12	3.53	5.12
A5/900	900	0.14	0.02	0.20	1.10	0.06	4.32	5.85
A5/1000	1000	0.15	0.03	0.22	1.19	0.07	4.57	6.23

Al (%)								
sample	depth	NH_4-Ac	Na-OC	HL	NH_4-OxH	H_2O_2	residual	total
A5/020	20	0.03	BDL	0.02	0.13	BDL	7.06	7.24
A5/035	35	0.02	BDL	0.01	0.06	BDL	6.51	6.60
A5/050	50	0.07	BDL	0.03	0.07	0.01	7.24	7.42
A5/100	100	0.05	BDL	0.02	0.04	BDL	6.11	6.22
A5/120	120	0.04	BDL	0.02	0.04	BDL	6.32	6.42
A5/140	140	0.05	BDL	0.02	0.06	BDL	6.70	6.83
A5/200	200	0.02	BDL	0.02	0.04	BDL	7.07	7.14
A5/220	220	0.04	BDL	0.02	0.05	BDL	6.27	6.38
A5/260	260	0.01	BDL	0.01	0.05	BDL	6.89	6.96
A5/300	300	0.01	BDL	0.01	0.08	BDL	6.46	6.56
A5/360	360	0.01	BDL	0.02	0.10	BDL	4.65	4.77
A5/400	400	0.01	BDL	0.02	0.07	BDL	6.72	6.81
A5/500	500	0.01	BDL	0.02	0.10	BDL	6.94	7.07
A5/600	600	0.01	BDL	0.02	0.08	BDL	6.99	7.10
A5/700	700	0.02	BDL	0.03	0.08	BDL	6.98	7.11
A5/800	800	0.02	BDL	0.03	0.11	BDL	6.83	6.99
A5/900	900	0.01	BDL	0.02	0.14	BDL	7.37	7.54
A5/1000	1000	0.02	BDL	0.02	0.17	BDL	7.47	7.68

K (%)								
sample	depth	NH_4-Ac	Na-OC	HL	NH_4-OxH	H_2O_2	residual	total
A5/020	20	BDL	BDL	BDL	0.20	BDL	4.06	4.26
A5/035	35	BDL	BDL	BDL	0.21	BDL	3.79	4.00
A5/050	50	BDL	BDL	BDL	0.06	BDL	4.25	4.31
A5/100	100	BDL	BDL	BDL	0.01	BDL	3.50	3.51
A5/120	120	BDL	BDL	BDL	0.04	BDL	3.63	3.67
A5/140	140	BDL	BDL	0.01	0.05	BDL	3.77	3.82
A5/200	200	0.01	BDL	0.01	0.01	BDL	4.12	4.14
A5/220	220	0.01	BDL	0.01	0.02	BDL	3.49	3.52
A5/260	260	0.01	BDL	0.01	0.02	BDL	3.90	3.94
A5/300	300	0.01	BDL	0.01	0.02	BDL	3.34	3.38
A5/360	360	0.02	BDL	0.01	0.02	BDL	2.40	2.45
A5/400	400	0.02	BDL	0.01	0.02	BDL	3.60	3.64
A5/500	500	0.03	BDL	0.01	0.03	BDL	3.56	3.63
A5/600	600	0.03	BDL	0.01	0.02	BDL	3.73	3.79
A5/700	700	0.03	BDL	0.01	0.02	BDL	3.91	3.97
A5/800	800	0.03	0.01	0.01	0.03	BDL	3.64	3.73
A5/900	900	0.03	0.01	0.01	0.04	BDL	3.94	4.03
A5/1000	1000	0.03	0.01	0.01	0.05	BDL	3.96	4.06

Mg (%)								
sample	depth	NH_4-Ac	Na-OC	HL	NH_4-OxH	H_2O_2	residual	total
A5/020	20	0.01	BDL	BDL	0.02	BDL	0.75	0.78
A5/035	35	0.01	BDL	BDL	0.01	BDL	0.64	0.66
A5/050	50	0.02	BDL	BDL	0.01	BDL	0.78	0.81
A5/100	100	0.01	BDL	BDL	BDL	BDL	0.63	0.64
A5/120	120	0.01	BDL	BDL	0.01	BDL	0.64	0.66
A5/140	140	0.02	BDL	BDL	0.01	BDL	0.81	0.84
A5/200	200	0.01	BDL	BDL	0.01	BDL	0.93	0.95
A5/220	220	0.01	BDL	BDL	0.01	BDL	0.81	0.83
A5/260	260	0.02	BDL	0.01	0.02	0.01	0.84	0.89
A5/300	300	0.02	BDL	BDL	0.01	BDL	0.64	0.67
A5/360	360	0.03	BDL	BDL	0.01	BDL	0.46	0.50
A5/400	400	0.02	BDL	BDL	0.01	BDL	0.65	0.68
A5/500	500	0.03	BDL	0.01	0.02	0.01	0.70	0.76
A5/600	600	0.01	BDL	0.01	0.02	0.01	0.66	0.71
A5/700	700	0.01	BDL	0.01	0.02	0.01	0.68	0.73
A5/800	800	0.01	BDL	0.01	0.03	0.01	0.70	0.76
A5/900	900	0.01	BDL	0.01	0.03	0.01	0.81	0.86
A5/1000	1000	0.02	BDL	0.01	0.03	0.01	0.98	1.04

Na (%)								
sample	depth	NH_4-Ac	Na-OC	HL	NH_4-OxH	H_2O_2	residual	total
A5/020	20	BDL	BDL	0.07	0.01	BDL	0.85	0.93
A5/035	35	BDL	BDL	0.06	0	BDL	0.83	0.90
A5/050	50	BDL	BDL	0.05	BDL	BDL	0.78	0.83
A5/100	100	BDL	BDL	0.06	BDL	BDL	0.58	0.64
A5/120	120	BDL	BDL	0.06	BDL	BDL	0.63	0.69
A5/140	140	BDL	BDL	0.05	BDL	BDL	0.64	0.69
A5/200	200	BDL	BDL	0.05	BDL	BDL	0.57	0.62
A5/220	220	BDL	BDL	0.04	BDL	0.03	0.55	0.61
A5/260	260	BDL	BDL	0.07	BDL	BDL	0.60	0.67
A5/300	300	BDL	BDL	0.08	BDL	BDL	0.91	0.99
A5/360	360	BDL	BDL	0.06	BDL	BDL	0.62	0.68
A5/400	400	BDL	BDL	0.06	BDL	BDL	0.88	0.94
A5/500	500	BDL	BDL	0.08	BDL	BDL	0.91	0.99
A5/600	600	BDL	BDL	0.06	BDL	BDL	1.01	1.07
A5/700	700	BDL	BDL	0.11	BDL	BDL	1.00	1.11
A5/800	800	BDL	BDL	0.10	0.01	BDL	0.88	0.98
A5/900	900	BDL	BDL	0.09	0.01	BDL	0.97	1.07
A5/1000	1000	0.01	BDL	0.14	0.01	BDL	1.03	1.19

Cu (ppm)								
sample	depth	NH_4-Ac	Na-OC	HL	NH_4-OxH	H_2O_2	residual	total
A5/020	20	70	4	10	166	454	462	1166
A5/035	35	74	3	7	118	322	296	820
A5/050	50	349	16	41	82	463	622	1573
A5/100	100	303	42	105	61	1260	1260	3031
A5/120	120	237	35	60	64	1490	1460	3346
A5/140	140	377	29	68	107	1240	1130	2950
A5/200	200	560	81	313	165	1750	3150	6019
A5/220	220	519	48	160	182	796	2090	3795
A5/260	260	357	39	65	26	1000	1650	3138
A5/300	300	171	29	58	54	672	1060	2043
A5/360	360	179	28	42	33	415	709	1406
A5/400	400	202	30	57	25	932	2170	3415
A5/500	500	206	40	51	44	506	1030	1877
A5/600	600	170	26	48	35	435	860	1574
A5/700	700	327	36	76	92	476	557	1565
A5/800	800	323	40	67	99	438	617	1584
A5/900	900	233	41	63	51	836	1050	2274
A5/1000	1000	247	27	58	51	565	716	1663

Zn (ppm)								
sample	depth	NH_4-Ac	Na-OC	HL	NH_4-OxH	H_2O_2	residual	total
A5/020	20	2	BDL	1	8	2	52	64
A5/035	35	3	BDL	1	5	1	33	42
A5/050	50	7	1	1	8	4	44	65
A5/100	100	5	1	2	10	12	50	79
A5/120	120	5	1	2	7	11	50	75
A5/140	140	7	BDL	3	6	7	50	73
A5/200	200	15	2	6	25	18	69	135
A5/220	220	11	1	3	13	7	52	85
A5/260	260	49	3	13	26	27	91	209
A5/300	300	49	4	11	39	28	85	218
A5/360	360	85	7	22	55	28	66	264
A5/400	400	49	8	20	45	41	111	275
A5/500	500	30	9	21	68	47	124	299
A5/600	600	35	10	27	77	55	125	329
A5/700	700	37	9	26	80	34	97	283
A5/800	800	56	14	40	115	51	125	401
A5/900	900	51	12	29	106	65	145	408
A5/1000	1000	50	12	33	116	47	162	419

Mn (ppm)								
sample	depth	NH_4-Ac	Na-OC	HL	NH_4-OxH	H_2O_2	residual	total
A5/020	20	5	BDL	5	15	BDL	142	167
A5/035	35	5	BDL	5	11	BDL	105	126
A5/050	50	12	BDL	7	11	3	129	162
A5/100	100	13	BDL	12	37	11	133	206
A5/120	120	12	BDL	8	26	8	126	180
A5/140	140	19	BDL	7	15	4	158	203
A5/200	200	45	4	18	62	21	170	320
A5/220	220	30	BDL	9	21	7	134	201
A5/260	260	160	10	50	114	89	251	674
A5/300	300	138	8	41	138	78	261	664
A5/360	360	424	21	62	172	64	172	915
A5/400	400	230	27	69	177	87	322	912
A5/500	500	172	51	93	212	93	260	881
A5/600	600	136	41	107	250	103	285	922
A5/700	700	105	41	97	228	80	241	792
A5/800	800	179	60	143	285	114	256	1037
A5/900	900	159	43	99	268	117	336	1022
A5/1000	1000	146	43	102	265	95	325	976

Cr (ppm)								
sample	depth	NH_4-Ac	Na-OC	HL	NH_4-OxH	H_2O_2	residual	total
A5/020	20	BDL	BDL	1	5	BDL	13	19
A5/035	35	BDL	BDL	BDL	4	BDL	11	15
A5/050	50	3	BDL	1	4	BDL	15	23
A5/100	100	1	BDL	BDL	2	BDL	13	16
A5/120	120	2	BDL	BDL	3	BDL	15	20
A5/140	140	1	BDL	BDL	3	BDL	19	23
A5/200	200	BDL	BDL	BDL	3	BDL	25	28
A5/220	220	BDL	BDL	BDL	3	BDL	22	25
A5/260	260	BDL	BDL	BDL	3	BDL	15	18
A5/300	300	BDL	BDL	BDL	3	BDL	13	16
A5/360	360	BDL	BDL	BDL	3	BDL	11	14
A5/400	400	BDL	BDL	BDL	3	BDL	16	19
A5/500	500	1	BDL	BDL	3	BDL	13	17
A5/600	600	1	BDL	BDL	3	BDL	14	18
A5/700	700	2	BDL	1	4	BDL	14	21
A5/800	800	2	BDL	BDL	4	BDL	13	19
A5/900	900	1	BDL	BDL	5	BDL	17	23
A5/1000	1000	2	BDL	BDL	5	BDL	23	30

Pb (ppm)								
sample	depth	NH_4-Ac	Na-OC	HL	NH_4-OxH	H_2O_2	residual	total
A5/020	20	BDL	BDL	BDL	10	BDL	11	21
A5/035	35	BDL	BDL	BDL	8	BDL	8	16
A5/050	50	BDL	BDL	BDL	9	BDL	6	15
A5/100	100	BDL	BDL	BDL	6	BDL	4	10
A5/120	120	BDL	BDL	BDL	7	BDL	4	11
A5/140	140	BDL	BDL	BDL	7	BDL	4	11
A5/200	200	BDL	BDL	BDL	10	BDL	8	18
A5/220	220	BDL	BDL	BDL	10	BDL	11	21
A5/260	260	BDL	BDL	BDL	6	BDL	8	14
A5/300	300	BDL	BDL	2	15	BDL	17	34
A5/360	360	BDL	BDL	2	7	BDL	10	19
A5/400	400	BDL	BDL	2	8	BDL	10	20
A5/500	500	5	BDL	3	10	BDL	15	33
A5/600	600	7	BDL	3	9	BDL	12	31
A5/700	700	9	BDL	2	11	BDL	20	42
A5/800	800	10	BDL	3	13	BDL	18	44
A5/900	900	6	BDL	2	13	BDL	18	39
A5/1000	1000	5	BDL	3	14	BDL	29	51

Ca (%)

sample	depth	NH_4-Ac	Na-OC	HL	NH_4-OxH	H_2O_2	residual	total
A5/020	20	0.01	BDL	0.06	BDL	BDL	0.13	0.20
A5/035	35	0.01	BDL	0.06	BDL	BDL	0.15	0.23
A5/050	50	0.10	BDL	0.08	BDL	BDL	0.12	0.30
A5/100	100	0.01	BDL	0.07	BDL	BDL	0.11	0.19
A5/120	120	0.01	BDL	0.06	BDL	BDL	0.11	0.18
A5/140	140	0.04	BDL	0.07	BDL	BDL	0.17	0.27
A5/200	200	0.08	BDL	0.10	BDL	BDL	0.08	0.25
A5/220	220	0.06	BDL	0.10	BDL	BDL	0.10	0.25
A5/260	260	0.07	BDL	0.10	BDL	0.01	0.09	0.26
A5/300	300	0.12	BDL	0.08	BDL	0.01	0.17	0.38
A5/360	360	0.15	BDL	0.07	BDL	BDL	0.10	0.32
A5/400	400	0.15	BDL	0.08	BDL	0.01	0.12	0.36
A5/500	500	0.20	0.01	0.10	BDL	0.01	0.14	0.46
A5/600	600	0.24	0.01	0.11	BDL	0.01	0.17	0.53
A5/700	700	0.22	BDL	0.09	BDL	0.01	0.11	0.43
A5/800	800	0.30	0.01	0.12	BDL	0.02	0.12	0.56
A5/900	900	0.18	BDL	0.12	BDL	0.02	0.15	0.46
A5/1000	1000	0.24	0.01	0.13	BDL	0.02	0.20	0.59

Ti (%)

sample	depth	NH_4-Ac	Na-OC	HL	NH_4-OxH	H_2O_2	residual	total
A5/020	20	BDL	BDL	BDL	BDL	BDL	0.17	0.17
A5/035	35	BDL	BDL	BDL	BDL	BDL	0.15	0.15
A5/050	50	BDL	BDL	BDL	BDL	BDL	0.16	0.16
A5/100	100	BDL	BDL	BDL	BDL	BDL	0.12	0.12
A5/120	120	BDL	BDL	BDL	BDL	BDL	0.12	0.12
A5/140	140	BDL	BDL	BDL	BDL	BDL	0.17	0.17
A5/200	200	BDL	BDL	BDL	BDL	BDL	0.21	0.21
A5/220	220	BDL	BDL	BDL	BDL	BDL	0.19	0.19
A5/260	260	BDL	BDL	BDL	BDL	BDL	0.2	0.2
A5/300	300	BDL	BDL	BDL	BDL	BDL	0.16	0.16
A5/360	360	BDL	BDL	BDL	BDL	BDL	0.11	0.11
A5/400	400	BDL	BDL	BDL	BDL	BDL	0.16	0.16
A5/500	500	BDL	BDL	BDL	BDL	BDL	0.18	0.18
A5/600	600	BDL	BDL	BDL	BDL	BDL	0.18	0.18
A5/700	700	BDL	BDL	BDL	BDL	BDL	0.18	0.18
A5/800	800	BDL	BDL	BDL	BDL	BDL	0.2	0.2
A5/900	900	BDL	BDL	BDL	BDL	BDL	0.23	0.23
A5/1000	1000	BDL	BDL	BDL	BDL	BDL	0.27	0.27

P (%)

sample	depth	NH_4-Ac	Na-OC	HL	NH_4-OxH	H_2O_2	residual	total
A5/020	20	BDL	BDL	0.02	0.04	BDL	0.02	0.07
A5/035	35	BDL	BDL	0.02	0.03	BDL	0.02	0.07
A5/050	50	0.01	BDL	0.03	0.02	BDL	0.02	0.08
A5/100	100	BDL	BDL	0.03	0.01	BDL	0.02	0.06
A5/120	120	BDL	BDL	0.02	0.01	BDL	0.02	0.06
A5/140	140	BDL	BDL	0.02	0.02	BDL	0.02	0.07
A5/200	200	BDL	BDL	0.03	0.03	BDL	0.03	0.08
A5/220	220	BDL	BDL	0.02	0.03	BDL	0.02	0.08
A5/260	260	BDL	BDL	0.04	0.01	BDL	0.03	0.08
A5/300	300	BDL	BDL	0.03	0.02	BDL	0.02	0.07
A5/360	360	BDL	BDL	0.03	0.01	BDL	0.01	0.05
A5/400	400	BDL	BDL	0.03	0.01	BDL	0.02	0.07
A5/500	500	0.01	BDL	0.04	0.01	BDL	0.02	0.09
A5/600	600	0.01	BDL	0.04	0.01	BDL	0.02	0.08
A5/700	700	0.01	BDL	0.04	0.01	BDL	0.02	0.08
A5/800	800	0.01	BDL	0.05	0.02	BDL	0.02	0.09
A5/900	900	0.01	BDL	0.05	0.02	BDL	0.03	0.10
A5/1000	1000	0.01	BDL	0.05	0.02	BDL	0.03	0.11

Ba (ppm)

sample	depth	NH_4-Ac	Na-OC	HL	NH_4-OxH	H_2O_2	residual	total
A5/020	20	BDL	BDL	2	24	2	616	644
A5/035	35	BDL	BDL	4	19	2	587	612
A5/050	50	3	5	11	14	2	304	339
A5/100	100	3	7	8	5	2	97	122
A5/120	120	2	4	7	8	2	187	210
A5/140	140	2	2	5	9	2	322	342
A5/200	200	5	7	6	1	2	181	202
A5/220	220	3	7	7	5	2	239	263
A5/260	260	6	8	7	2	2	259	284
A5/300	300	4	8	6	3	2	438	461
A5/360	360	5	10	7	3	2	305	332
A5/400	400	4	7	7	2	2	440	462
A5/500	500	8	10	10	4	2	466	500
A5/600	600	9	10	10	4	2	533	568
A5/700	700	11	10	14	4	2	464	505
A5/800	800	13	16	22	5	2	465	523
A5/900	900	14	17	21	7	3	539	601
A5/1000	1000	13	11	17	6	2	530	579

Sr (ppm)

sample	depth	NH_4-Ac	Na-OC	HL	NH_4-OxH	H_2O_2	residual	total
A5/020	20	BDL	BDL	1	4.5	BDL	94.8	100.3
A5/035	35	BDL	BDL	1.1	5.1	BDL	98.3	104.5
A5/050	50	BDL	BDL	1.5	2.8	BDL	94.8	99.1
A5/100	100	BDL	BDL	1.4	1.8	BDL	76.6	79.8
A5/120	120	BDL	BDL	1.1	2.3	BDL	81.3	84.7
A5/140	140	BDL	BDL	1.2	3.5	BDL	80.5	85.2
A5/200	200	BDL	BDL	1.6	BDL	BDL	48.8	50.4
A5/220	220	BDL	BDL	1.6	1.7	BDL	51.2	54.5
A5/260	260	0.5	BDL	1.7	0.6	BDL	61.6	64.4
A5/300	300	0.9	BDL	1.4	0.9	BDL	95.6	98.8
A5/360	360	1.7	BDL	1.3	0.8	BDL	59.1	62.9
A5/400	400	1.9	0.8	1.5	0.8	BDL	78.7	83.7
A5/500	500	4.9	0.6	2.1	1.1	0.6	85.6	94.9
A5/600	600	4.6	BDL	2	0.8	BDL	104	111.4
A5/700	700	5.1	0.5	1.9	0.8	BDL	84.1	92.4
A5/800	800	6	0.8	2.5	0.9	0.7	75.2	86.1
A5/900	900	4	0.7	2.3	1.2	0.8	78.3	87.3
A5/1000	1000	5.2	0.5	2.3	1.3	0.7	83.7	93.7

Mo (ppm)

sample	depth	NH_4-Ac	Na-OC	HL	NH_4-OxH	H_2O_2	residual	total
A5/020	20	BDL	BDL	BDL	30	15	49	94
A5/035	35	BDL	BDL	BDL	45	20	46	111
A5/050	50	BDL	BDL	BDL	7	BDL	83	90
A5/100	100	BDL	BDL	BDL	4	BDL	130	134
A5/120	120	BDL	BDL	BDL	8	BDL	81	89
A5/140	140	BDL	BDL	BDL	5	BDL	83	88
A5/200	200	BDL	BDL	BDL	BDL	BDL	63	63
A5/220	220	BDL	BDL	BDL	2	BDL	36	38
A5/260	260	BDL	BDL	BDL	BDL	BDL	44	44
A5/300	300	BDL	BDL	BDL	3	BDL	73	76
A5/360	360	BDL	BDL	BDL	2	BDL	36	38
A5/400	400	BDL	BDL	BDL	3	BDL	70	73
A5/500	500	BDL	BDL	BDL	3	BDL	49	52
A5/600	600	BDL	BDL	BDL	2	BDL	39	41
A5/700	700	BDL	BDL	BDL	3	BDL	45	48
A5/800	800	BDL	BDL	BDL	3	BDL	31	34
A5/900	900	BDL	BDL	BDL	3	BDL	36	39
A5/1000	1000	BDL	BDL	BDL	3	BDL	35	38

V (ppm)

sample	depth	NH_4-Ac	Na-OC	HL	NH_4-OxH	H_2O_2	residual	total
A5/020	20	BDL	BDL	2	9	BDL	93	104
A5/035	35	BDL	BDL	2	9	BDL	87	98
A5/050	50	BDL	BDL	BDL	7	BDL	94	101
A5/100	100	BDL	BDL	BDL	4	BDL	80	84
A5/120	120	BDL	BDL	BDL	5	BDL	81	86
A5/140	140	BDL	BDL	BDL	6	BDL	100	106
A5/200	200	BDL	BDL	BDL	6	BDL	139	145
A5/220	220	BDL	BDL	BDL	7	BDL	120	127
A5/260	260	BDL	BDL	BDL	6	BDL	121	127
A5/300	300	BDL	BDL	BDL	6	BDL	89	95
A5/360	360	BDL	BDL	BDL	6	BDL	65	71
A5/400	400	BDL	BDL	BDL	6	BDL	100	106
A5/500	500	BDL	BDL	BDL	7	BDL	103	110
A5/600	600	BDL	BDL	BDL	7	BDL	94	101
A5/700	700	BDL	BDL	BDL	8	BDL	96	104
A5/800	800	BDL	BDL	BDL	10	BDL	104	114
A5/900	900	BDL	BDL	BDL	11	BDL	118	129
A5/1000	1000	BDL	BDL	BDL	13	BDL	128	141

As (ppm)

sample	depth	NH_4-Ac	Na-OC	HL	NH_4-OxH	H_2O_2	residual	total
A5/020	20	BDL	BDL	BDL	27	BDL	BDL	27
A5/035	35	BDL	BDL	BDL	14	BDL	BDL	14
A5/050	50	BDL	BDL	BDL	8	BDL	BDL	8
A5/100	100	BDL	BDL	BDL	6	BDL	BDL	6
A5/120	120	BDL	BDL	BDL	9	BDL	BDL	9
A5/140	140	BDL	BDL	BDL	10	BDL	BDL	10
A5/200	200	BDL	BDL	BDL	8	BDL	6	14
A5/220	220	BDL	BDL	BDL	11	BDL	4	15
A5/260	260	BDL	BDL	BDL	BDL	BDL	BDL	BDL
A5/300	300	BDL	BDL	BDL	21	BDL	10	31
A5/360	360	BDL	BDL	BDL	18	BDL	12	30
A5/400	400	BDL	BDL	4	18	BDL	35	57
A5/500	500	BDL	BDL	5	27	BDL	32	64
A5/600	600	BDL	BDL	4	22	BDL	44	70
A5/700	700	BDL	BDL	4	24	BDL	13	41
A5/800	800	4	BDL	6	36	BDL	44	90
A5/900	900	BDL	BDL	5	30	BDL	46	81
A5/1000	1000	BDL	BDL	4	33	BDL	44	81

W (ppm)

sample	depth	NH_4-Ac	Na-OC	HL	NH_4-OxH	H_2O_2	residual	total
A5/020	20	BDL	BDL	BDL	BDL	BDL	21	21
A5/035	35	BDL	BDL	BDL	BDL	BDL	22	22
A5/050	50	BDL	BDL	BDL	BDL	BDL	27	27
A5/100	100	BDL	BDL	BDL	BDL	BDL	26	26
A5/120	120	BDL	BDL	BDL	BDL	BDL	23	23
A5/140	140	BDL	BDL	BDL	BDL	BDL	19	19
A5/200	200	BDL	BDL	BDL	BDL	BDL	15	15
A5/220	220	BDL	BDL	BDL	BDL	BDL	16	16
A5/260	260	BDL	BDL	BDL	BDL	BDL	16	16
A5/300	300	BDL	BDL	BDL	BDL	BDL	12	12
A5/360	360	BDL	BDL	BDL	BDL	BDL	BDL	BDL
A5/400	400	BDL	BDL	BDL	BDL	BDL	14	14
A5/500	500	BDL	BDL	BDL	BDL	BDL	14	14
A5/600	600	BDL	BDL	BDL	BDL	BDL	11	11
A5/700	700	BDL	BDL	BDL	BDL	BDL	13	13
A5/800	800	BDL	BDL	BDL	BDL	BDL	15	15
A5/900	900	BDL	BDL	BDL	BDL	BDL	14	14
A5/1000	1000	BDL	BDL	BDL	BDL	BDL	18	18

La (ppm)

sample	depth	NH_4-Ac	Na-OC	HL	NH_4-OxH	H_2O_2	residual	total
A5/020	20	BDL	BDL	BDL	BDL	BDL	10	10
A5/035	35	BDL	BDL	BDL	BDL	BDL	9	9
A5/050	50	BDL	BDL	BDL	BDL	BDL	10	10
A5/100	100	BDL	BDL	BDL	BDL	BDL	6	6
A5/120	120	BDL	BDL	BDL	BDL	BDL	8	8
A5/140	140	BDL	BDL	BDL	BDL	BDL	8	8
A5/200	200	BDL	BDL	BDL	BDL	BDL	7	7
A5/220	220	BDL	BDL	BDL	BDL	BDL	7	7
A5/260	260	BDL	BDL	BDL	BDL	BDL	8	8
A5/300	300	BDL	BDL	BDL	BDL	BDL	9	9
A5/360	360	BDL	BDL	BDL	BDL	BDL	6	6
A5/400	400	BDL	BDL	BDL	BDL	BDL	8	8
A5/500	500	BDL	BDL	BDL	BDL	BDL	9	9
A5/600	600	BDL	BDL	BDL	BDL	BDL	10	10
A5/700	700	BDL	BDL	BDL	BDL	BDL	9	9
A5/800	800	BDL	BDL	BDL	BDL	BDL	9	9
A5/900	900	BDL	BDL	BDL	BDL	BDL	11	11
A5/1000	1000	BDL	BDL	BDL	BDL	BDL	12	12

Ni (ppm)

sample	depth	NH_4-Ac	Na-OC	HL	NH_2-OxH	H_2O_2	residual	total
A5/020	20	BDL	BDL	BDL	BDL	BDL	11	11
A5/035	35	BDL	BDL	BDL	BDL	BDL	10	10
A5/050	50	BDL	BDL	BDL	BDL	BDL	13	13
A5/100	100	BDL	BDL	BDL	BDL	BDL	11	11
A5/120	120	BDL	BDL	BDL	BDL	BDL	13	13
A5/140	140	BDL	BDL	BDL	BDL	BDL	16	16
A5/200	200	BDL	BDL	BDL	BDL	BDL	19	19
A5/220	220	BDL	BDL	BDL	BDL	BDL	18	18
A5/260	260	1	BDL	BDL	BDL	1	18	20
A5/300	300	BDL	BDL	BDL	BDL	BDL	10	10
A5/360	360	2	BDL	BDL	BDL	BDL	10	12
A5/400	400	BDL	BDL	BDL	BDL	BDL	13	13
A5/500	500	BDL	BDL	BDL	BDL	1	14	15
A5/600	600	BDL	BDL	BDL	BDL	BDL	13	13
A5/700	700	BDL	BDL	BDL	BDL	BDL	14	14
A5/800	800	1	BDL	BDL	BDL	BDL	13	14
A5/900	900	BDL	BDL	BDL	BDL	2	14	16
A5/1000	1000	BDL	BDL	BDL	BDL	1	21	22

Zr (ppm)

sample	depth	NH_4-Ac	Na-OC	HL	NH_2-OxH	H_2O_2	residual	total
A5/020	20	BDL	BDL	BDL	BDL	BDL	8.2	8.2
A5/035	35	BDL	BDL	BDL	BDL	BDL	15.5	15.5
A5/050	50	BDL	BDL	BDL	BDL	BDL	14.6	14.6
A5/100	100	BDL	BDL	BDL	0.5	BDL	7.7	8.2
A5/120	120	BDL	BDL	BDL	BDL	BDL	9.9	9.9
A5/140	140	BDL	BDL	BDL	BDL	BDL	7.2	7.2
A5/200	200	BDL	BDL	BDL	BDL	BDL	14.4	14.4
A5/220	220	BDL	BDL	BDL	BDL	BDL	13.1	13.1
A5/260	260	BDL	BDL	BDL	BDL	BDL	6.2	6.2
A5/300	300	BDL	BDL	BDL	0.9	BDL	11.5	12.4
A5/360	360	BDL	BDL	BDL	BDL	BDL	6.8	6.8
A5/400	400	BDL	BDL	BDL	0.7	BDL	15.6	16.3
A5/500	500	BDL	BDL	BDL	BDL	BDL	18.7	18.7
A5/600	600	BDL	BDL	BDL	BDL	BDL	7.4	7.4
A5/700	700	BDL	BDL	BDL	BDL	BDL	19.1	19.1
A5/800	800	BDL	BDL	BDL	BDL	BDL	12.4	12.4
A5/900	900	BDL	BDL	BDL	BDL	BDL	18.7	18.7
A5/1000	1000	BDL	BDL	BDL	BDL	BDL	17.7	17.7

Co (ppm)

sample	depth	NH_4-Ac	Na-OC	HL	NH_2-OxH	H_2O_2	residual	total
A5/020	20	BDL	BDL	BDL	BDL	BDL	5	5
A5/035	35	BDL	BDL	BDL	BDL	BDL	4	4
A5/050	50	2	BDL	BDL	BDL	2	10	14
A5/100	100	1	BDL	BDL	BDL	1	12	14
A5/120	120	BDL	BDL	BDL	BDL	1	10	11
A5/140	140	2	BDL	BDL	BDL	1	10	13
A5/200	200	BDL	BDL	BDL	BDL	2	12	14
A5/220	220	BDL	BDL	BDL	BDL	1	12	13
A5/260	260	2	BDL	BDL	BDL	2	10	14
A5/300	300	2	BDL	BDL	BDL	BDL	6	8
A5/360	360	4	BDL	BDL	BDL	2	5	11
A5/400	400	2	BDL	BDL	BDL	BDL	6	8
A5/500	500	1	BDL	BDL	1	2	8	12
A5/600	600	BDL	BDL	BDL	BDL	2	6	8
A5/700	700	1	BDL	BDL	BDL	2	7	10
A5/800	800	1	BDL	BDL	1	2	8	12
A5/900	900	1	BDL	BDL	BDL	2	8	11
A5/1000	1000	1	BDL	BDL	1	2	9	13

Sn (ppm)

sample	depth	NH_4-Ac	Na-OC	HL	NH_2-OxH	H_2O_2	residual	total
A5/020	20	BDL	BDL	BDL	BDL	BDL	BDL	BDL
A5/035	35	BDL	BDL	BDL	BDL	BDL	BDL	BDL
A5/050	50	BDL	BDL	BDL	BDL	BDL	BDL	BDL
A5/100	100	BDL	BDL	BDL	BDL	BDL	BDL	BDL
A5/120	120	BDL	BDL	BDL	BDL	BDL	BDL	BDL
A5/140	140	BDL	BDL	BDL	BDL	BDL	BDL	BDL
A5/200	200	BDL	BDL	BDL	BDL	BDL	BDL	BDL
A5/220	220	BDL	BDL	BDL	BDL	BDL	BDL	BDL
A5/260	260	BDL	BDL	BDL	BDL	BDL	BDL	BDL
A5/300	300	BDL	BDL	BDL	BDL	BDL	BDL	BDL
A5/360	360	BDL	BDL	BDL	BDL	BDL	BDL	BDL
A5/400	400	BDL	BDL	BDL	BDL	BDL	BDL	BDL
A5/500	500	BDL	BDL	BDL	BDL	BDL	BDL	BDL
A5/600	600	BDL	BDL	BDL	BDL	BDL	BDL	BDL
A5/700	700	BDL	BDL	BDL	BDL	BDL	BDL	BDL
A5/800	800	BDL	BDL	BDL	BDL	BDL	BDL	BDL
A5/900	900	BDL	BDL	BDL	BDL	BDL	BDL	BDL
A5/1000	1000	BDL	BDL	BDL	BDL	BDL	BDL	BDL

Y (ppm)

sample	depth	NH_4-Ac	Na-OC	HL	NH_2-OxH	H_2O_2	residual	total
A5/020	20	0.2	BDL	0.8	0.7	BDL	2.4	4.1
A5/035	35	0.2	BDL	0.8	0.4	BDL	2.2	3.6
A5/050	50	0.2	BDL	1	0.8	BDL	2.5	4.5
A5/100	100	0.1	BDL	0.8	0.4	BDL	2	3.3
A5/120	120	0.1	BDL	0.6	0.4	BDL	2.3	3.4
A5/140	140	0.2	BDL	0.9	0.5	BDL	2.5	4.1
A5/200	200	1	BDL	1.4	0.3	BDL	2.6	5.3
A5/220	220	0.5	BDL	1.3	0.4	BDL	2.5	4.7
A5/260	260	1.1	BDL	1.3	0.3	BDL	2.3	5
A5/300	300	0.3	BDL	1	0.6	BDL	2.3	4.2
A5/360	360	0.3	BDL	0.9	0.4	BDL	1.9	3.5
A5/400	400	0.2	BDL	1	0.4	BDL	3	4
A5/500	500	0.3	BDL	1.2	0.6	BDL	2.8	5
A5/600	600	0.4	BDL	1.3	0.4	BDL	2.7	5
A5/700	700	0.5	BDL	1.2	0.7	BDL	2.7	5
A5/800	800	0.5	BDL	1.4	0.7	0.1	3	5.7
A5/900	900	0.4	BDL	1.5	1	0.1	3.1	6
A5/1000	1000	0.5	BDL	1.7	1	0.2	3.8	7

Sc (ppm)

sample	depth	NH_4-Ac	Na-OC	HL	NH_2-OxH	H_2O_2	residual	total
A5/020	20	BDL	BDL	BDL	BDL	BDL	5.9	5.9
A5/035	35	BDL	BDL	BDL	BDL	BDL	5.3	5.3
A5/050	50	BDL	BDL	BDL	BDL	BDL	5.7	5.7
A5/100	100	BDL	BDL	BDL	BDL	BDL	4.4	4.4
A5/120	120	BDL	BDL	BDL	BDL	BDL	4.7	4.7
A5/140	140	BDL	BDL	BDL	BDL	BDL	6.7	6.7
A5/200	200	BDL	BDL	BDL	BDL	BDL	9.8	9.8
A5/220	220	BDL	BDL	BDL	BDL	BDL	8.4	8.4
A5/260	260	BDL	BDL	BDL	BDL	BDL	8.8	8.8
A5/300	300	BDL	BDL	BDL	BDL	BDL	6	6
A5/360	360	BDL	BDL	BDL	BDL	BDL	4.4	4.4
A5/400	400	BDL	BDL	BDL	BDL	BDL	7	7
A5/500	500	BDL	BDL	BDL	BDL	BDL	7.1	7
A5/600	600	BDL	BDL	BDL	BDL	BDL	6.6	7
A5/700	700	BDL	BDL	BDL	BDL	BDL	6.4	6
A5/800	800	BDL	BDL	BDL	BDL	BDL	7.1	7.1
A5/900	900	BDL	BDL	BDL	BDL	BDL	8.1	8
A5/1000	1000	BDL	BDL	BDL	BDL	BDL	9.3	9

Be (ppm)

sample	depth	NH_4-Ac	Na-OC	HL	NH_2-OxH	H_2O_2	residual	total
A5/020	20	BDL	BDL	BDL	BDL	BDL	1.1	1.1
A5/035	35	BDL	BDL	BDL	BDL	BDL	1.1	1.1
A5/050	50	BDL	BDL	BDL	BDL	BDL	1.2	1.2
A5/100	100	BDL	BDL	BDL	BDL	BDL	1.1	1.1
A5/120	120	BDL	BDL	BDL	BDL	BDL	1.1	1.1
A5/140	140	BDL	BDL	BDL	BDL	BDL	1.1	1.1
A5/200	200	BDL	BDL	BDL	BDL	BDL	1.3	1.3
A5/220	220	BDL	BDL	BDL	BDL	BDL	1.1	1.1
A5/260	260	BDL	BDL	BDL	BDL	BDL	1.3	1.3
A5/300	300	BDL	BDL	BDL	BDL	BDL	1.1	1.1
A5/360	360	BDL	BDL	BDL	BDL	BDL	0.9	0.9
A5/400	400	BDL	BDL	BDL	BDL	BDL	1	1
A5/500	500	BDL	BDL	BDL	BDL	BDL	1.2	1
A5/600	600	BDL	BDL	BDL	BDL	BDL	1.2	1
A5/700	700	BDL	BDL	BDL	BDL	BDL	1.1	1
A5/800	800	BDL	BDL	BDL	BDL	BDL	1.2	1.2
A5/900	900	BDL	BDL	BDL	BDL	BDL	1.3	1
A5/1000	1000	BDL	BDL	BDL	BDL	BDL	1.3	1

Ag (ppm)

sample	depth	NH_4-Ac	Na-OC	HL	NH_2-OxH	H_2O_2	residual	total
A5/020	20	BDL	BDL	BDL	0.3	BDL	0.6	0.9
A5/035	35	BDL	BDL	BDL	0.3	BDL	0.6	0.9
A5/050	50	BDL	BDL	BDL	0.2	BDL	0.8	1
A5/100	100	BDL	BDL	BDL	BDL	BDL	1	1
A5/120	120	BDL	BDL	BDL	BDL	BDL	1.1	1.1
A5/140	140	BDL	BDL	BDL	0.2	BDL	0.9	1.1
A5/200	200	BDL	BDL	BDL	BDL	BDL	1.3	1.3
A5/220	220	BDL	BDL	BDL	0.2	BDL	0.9	1.1
A5/260	260	BDL	BDL	BDL	BDL	BDL	0.9	0.9
A5/300	300	BDL	BDL	BDL	0.6	BDL	0.8	1.4
A5/360	360	BDL	BDL	BDL	BDL	BDL	0.6	0.6
A5/400	400	BDL	BDL	BDL	BDL	BDL	1	1
A5/500	500	BDL	BDL	BDL	0.3	BDL	1	1
A5/600	600	BDL	BDL	BDL	BDL	BDL	0.9	1
A5/700	700	BDL	BDL	BDL	BDL	BDL	0.9	1
A5/800	800	BDL	BDL	BDL	BDL	BDL	1	1
A5/900	900	BDL	BDL	BDL	0	BDL	1.3	2
A5/1000	1000	BDL	BDL	BDL	0	BDL	1.1	1

Fe (%)

sample	depth	NH_4-Ac	Na-OC	HL	NH_4-OxH	H_2O_2	residual	total
T4/020	20	0.0161	BDL	0.019	0.943	0.037	2.24	3.2553
T4/040	40	0.016	BDL	0.0171	0.997	0.035	2.27	3.3351
T4/080	80	0.04	BDL	0.05	0.69	0.03	2.82	3.62
T4/100	100	0.02	BDL	0.03	0.94	0.03	2.74	3.75
T4/120	120	0.04	BDL	0.05	0.91	0.03	3.07	4.11
T4/153	153	0.04	BDL	0.04	0.75	0.02	2.64	3.48
T4/170	170	0.02	BDL	0.03	0.31	0.04	3.15	3.54
T4/200	200	0.01	BDL	0.02	0.27	0.01	3.72	4.04
T4/300	300	0.04	BDL	0.06	0.25	0.01	3.32	3.67
T4/355	355	0.04	BDL	0.04	0.25	0.01	3.11	3.45
T4/400	400	0.12	BDL	0.13	0.31	0.01	3.63	4.20
T4/490	490	0.09	BDL	0.06	0.30	0.02	3.21	3.69
T4/591	591	0.04	BDL	0.04	0.27	0.02	3.84	4.21
T4/700	700	0.05	BDL	0.04	0.27	0.01	4.02	4.39
T4/795	795	0.08	BDL	0.10	0.25	0.01	3.76	4.20
T4/900	900	0.05	BDL	0.06	0.26	0.01	3.34	3.71
T4/985	985	0.04	BDL	0.05	0.19	0.01	3.51	3.80
T4/1010	1010	0.11	BDL	0.14	0.44	0.11	3.99	4.79
T4/1020	1020	0.05	BDL	0.05	0.46	0.10	4.39	5.05
T4/1040	1040	0.06	BDL	0.03	0.19	0.13	2.78	3.19

Al (%)

sample	depth	NH_4-Ac	Na-OC	HL	NH_4-OxH	H_2O_2	residual	total
T4/020	20	0.02	BDL	0.03	0.08	0.06	7.16	7.35
T4/040	40	0.02	BDL	0.02	0.07	0.06	7.34	7.51
T4/080	80	0.03	BDL	0.04	0.10	0.07	7.63	7.86
T4/100	100	0.02	BDL	0.03	0.07	0.04	7.33	7.49
T4/120	120	0.03	BDL	0.04	0.10	0.06	7.94	8.17
T4/153	153	0.02	BDL	0.03	0.06	0.04	7.33	7.49
T4/170	170	0.04	BDL	0.03	0.10	0.01	7.45	7.64
T4/200	200	0.04	BDL	0.03	0.08	BDL	7.69	7.84
T4/300	300	0.08	BDL	0.05	0.16	0.01	8.17	8.46
T4/355	355	0.05	BDL	0.03	0.10	BDL	7.60	7.78
T4/400	400	0.10	BDL	0.06	0.23	0.01	9.39	9.79
T4/490	490	0.03	BDL	0.04	0.10	0.01	7.61	7.79
T4/591	591	0.02	BDL	0.03	0.09	0.01	7.99	8.14
T4/700	700	0.03	BDL	0.04	0.11	BDL	8.17	8.34
T4/795	795	0.05	BDL	0.06	0.20	0.01	8.32	8.63
T4/900	900	0.03	BDL	0.04	0.15	0.01	7.57	7.79
T4/985	985	0.02	BDL	0.03	0.13	BDL	8.15	8.34
T4/1010	1010	0.02	BDL	0.04	0.34	0.02	7.53	7.96
T4/1020	1020	0.04	BDL	0.03	0.15	0.34	8.17	8.72
T4/1040	1040	0.01	BDL	0.01	0.10	0.46	9.12	9.70

K (%)

sample	depth	NH_4-Ac	Na-OC	HL	NH_4-OxH	H_2O_2	residual	total
T4/020	20	0.01	BDL	BDL	0.15	0.02	2.26	2.43
T4/040	40	0.01	BDL	BDL	0.15	0.02	2.31	2.49
T4/080	80	0.01	BDL	BDL	0.10	0.02	2.58	2.71
T4/100	100	0.01	BDL	BDL	0.15	0.01	2.40	2.58
T4/120	120	0.01	BDL	0.01	0.15	0.02	2.73	2.92
T4/153	153	0.01	BDL	0.01	0.11	0.01	2.44	2.57
T4/170	170	0.01	BDL	BDL	0.01	BDL	2.57	2.59
T4/200	200	0.01	BDL	0.01	0.01	BDL	2.66	2.68
T4/300	300	0.01	BDL	0.01	0.01	BDL	2.95	2.98
T4/355	355	0.01	BDL	0.01	0.01	BDL	2.73	2.75
T4/400	400	0.02	BDL	0.02	0.01	BDL	3.52	3.57
T4/490	490	0.02	BDL	0.01	0.01	BDL	2.72	2.76
T4/591	591	0.02	BDL	0.01	0.01	BDL	2.95	2.98
T4/700	700	0.02	BDL	0.01	0.01	BDL	2.91	2.95
T4/795	795	0.02	BDL	0.02	0.01	BDL	3.18	3.23
T4/900	900	0.02	BDL	0.01	0.01	BDL	2.77	2.81
T4/985	985	0.02	BDL	0.01	0.01	BDL	2.98	3.01
T4/1010	1010	0.02	BDL	0.01	0.02	BDL	1.88	1.92
T4/1020	1020	0.04	BDL	BDL	BDL	0.01	0.34	0.38
T4/1040	1040	0.01	BDL	BDL	BDL	0.01	0.25	0.27

Mg (%)

sample	depth	NH_4-Ac	Na-OC	HL	NH_4-OxH	H_2O_2	residual	total
T4/020	20	BDL	BDL	BDL	0.01	0.01	1.59	1.61
T4/040	40	BDL	BDL	BDL	0.01	0.01	1.65	1.67
T4/080	80	BDL	BDL	BDL	0.01	0.01	1.81	1.83
T4/100	100	BDL	BDL	BDL	0.01	0.01	1.73	1.75
T4/120	120	BDL	BDL	BDL	0.01	0.01	1.93	1.95
T4/153	153	BDL	BDL	BDL	0.01	0.01	1.69	1.70
T4/170	170	BDL	BDL	BDL	0.01	BDL	1.69	1.70
T4/200	200	BDL	BDL	BDL	0.01	BDL	1.70	1.71
T4/300	300	BDL	BDL	BDL	0.02	BDL	1.99	2.01
T4/355	355	BDL	BDL	BDL	0.01	BDL	1.67	1.68
T4/400	400	0.02	BDL	BDL	0.03	0.01	2.33	2.38
T4/490	490	0.02	BDL	BDL	0.01	BDL	1.74	1.77
T4/591	591	0.01	BDL	BDL	0.01	BDL	1.77	1.79
T4/700	700	0.01	BDL	BDL	0.01	BDL	1.95	1.97
T4/795	795	0.01	BDL	0.01	0.02	BDL	2.13	2.16
T4/900	900	0.01	BDL	BDL	0.01	BDL	1.94	1.96
T4/985	985	0.01	BDL	BDL	0.01	BDL	2.07	2.08
T4/1010	1010	0.03	BDL	BDL	0.02	BDL	1.32	1.37
T4/1020	1020	0.05	BDL	BDL	BDL	BDL	0.11	0.16
T4/1040	1040	0.06	BDL	BDL	BDL	0.01	0.10	0.16

Cu (ppm)

sample	depth	NH_4-Ac	Na-OC	HL	NH_4-OxH	H_2O_2	residual	total
T4/020	20	58	4	12	141	6	76	297
T4/040	40	62	5	13	171	5	81	336
T4/080	80	53	4	14	118	4	85	279
T4/100	100	33	3	9	113	4	105	267
T4/120	120	51	4	15	137	6	124	337
T4/153	153	73	6	13	92	3	88	275
T4/170	170	196	34	73	68	651	612	1634
T4/200	200	236	59	174	71	949	2010	3499
T4/300	300	530	88	221	137	778	608	2362
T4/355	355	332	61	234	88	725	1780	3221
T4/400	400	1520	171	322	222	860	419	3514
T4/490	490	1920	130	375	104	447	648	3624
T4/591	591	447	77	309	73	819	1900	3625
T4/700	700	450	80	279	73	935	2150	3967
T4/795	795	897	128	436	170	616	1150	3397
T4/900	900	488	73	359	108	531	856	2415
T4/985	985	242	57	255	87	876	1820	3337
T4/1010	1010	261	37	136	214	556	662	1866
T4/1020	1020	69	5	30	36	73	140	353
T4/1040	1040	10	1	4	7	3	27	52

Zn (ppm)

sample	depth	NH_4-Ac	Na-OC	HL	NH_4-OxH	H_2O_2	residual	total
T4/020	20	3	BDL	BDL	2	1	46	53
T4/040	40	3	BDL	BDL	2	1	43	49
T4/080	80	4	BDL	BDL	1	1	51	58
T4/100	100	6	BDL	BDL	2	1	47	55
T4/120	120	6	BDL	BDL	2	1	49	58
T4/153	153	11	1	BDL	1	1	43	58
T4/170	170	4	BDL	BDL	2	3	47	55
T4/200	200	4	BDL	1	1	3	54	63
T4/300	300	6	BDL	1	3	3	57	69
T4/355	355	7	BDL	2	3	3	55	69
T4/400	400	14	1	3	5	3	72	97
T4/490	490	36	3	5	5	3	61	113
T4/591	591	13	1	4	4	5	62	88
T4/700	700	9	1	2	3	3	62	81
T4/795	795	10	1	3	4	2	61	81
T4/900	900	10	1	2	2	2	51	69
T4/985	985	7	1	2	2	3	58	73
T4/1010	1010	14	2	5	5	5	45	76
T4/1020	1020	16	1	2	2	1	16	38
T4/1040	1040	2	BDL	1	1	1	14	19

Mn (ppm)

sample	depth	NH_4-Ac	Na-OC	HL	NH_4-OxH	H_2O_2	residual	total
T4/020	20	BDL	BDL	4	4	BDL	180	188
T4/040	40	BDL	BDL	4	4	BDL	183	191
T4/080	80	BDL	BDL	5	4	BDL	229	238
T4/100	100	BDL	BDL	5	4	BDL	220	229
T4/120	120	BDL	BDL	5	4	BDL	236	245
T4/153	153	BDL	BDL	6	3	BDL	217	226
T4/170	170	BDL	BDL	5	3	BDL	221	229
T4/200	200	BDL	BDL	5	2	BDL	225	232
T4/300	300	BDL	BDL	6	4	BDL	251	261
T4/355	355	BDL	BDL	5	3	BDL	218	226
T4/400	400	7	BDL	6	6	2	298	319
T4/490	490	31	2	12	8	3	231	287
T4/591	591	12	4	14	8	2	237	277
T4/700	700	14	4	10	6	BDL	260	294
T4/795	795	19	3	10	7	2	244	285
T4/900	900	8	BDL	7	4	BDL	214	233
T4/985	985	10	BDL	6	5	BDL	230	251
T4/1010	1010	25	2	7	8	3	193	238
T4/1020	1020	12	BDL	BDL	3	BDL	60	75
T4/1040	1040	7	BDL	BDL	2	3	45	57

Cr (ppm)

sample	depth	NH_4-Ac	Na-OC	HL	NH_4-OxH	H_2O_2	residual	total
T4/020	20	BDL	BDL	BDL	5	1	21	27
T4/040	40	BDL	BDL	BDL	5	1	24	30
T4/080	80	1	BDL	BDL	5	1	27	34
T4/100	100	BDL	BDL	BDL	5	1	26	32
T4/120	120	1	BDL	1	5	1	37	45
T4/153	153	BDL	BDL	BDL	5	1	28	34
T4/170	170	2	BDL	BDL	4	BDL	27	33
T4/200	200	BDL	BDL	BDL	4	BDL	33	37
T4/300	300	2	BDL	1	4	BDL	32	39
T4/355	355	2	BDL	BDL	4	BDL	33	39
T4/400	400	3	BDL	2	5	BDL	35	45
T4/490	490	1	BDL	1	5	BDL	27	34
T4/591	591	BDL	BDL	BDL	4	BDL	30	34
T4/700	700	1	BDL	1	4	BDL	35	41
T4/795	795	2	BDL	2	3	BDL	34	41
T4/900	900	1	BDL	1	3	BDL	29	34
T4/985	985	BDL	BDL	BDL	2	BDL	31	33
T4/1010	1010	1	BDL	BDL	3	1	43	48
T4/1020	1020	BDL	BDL	BDL	2	3	12	17
T4/1040	1040	BDL	BDL	BDL	1	2	11	14

Na (%) sample	depth	NH_4-Ac	Na-OC	HL	NH_4-OxH	H_2O_2	residual	total
T4/020	20	BDL	BDL	0.12	BDL	0.01	1.24	1.37
T4/040	40	BDL	BDL	0.17	BDL	0.01	1.32	1.50
T4/080	80	BDL	BDL	0.10	BDL	BDL	0.94	1.04
T4/100	100	BDL	BDL	0.11	BDL	BDL	0.98	1.09
T4/120	120	BDL	BDL	0.09	0	BDL	1.05	1.15
T4/153	153	BDL	BDL	0.11	BDL	BDL	0.94	1.05
T4/170	170	BDL	BDL	0.05	BDL	BDL	0.95	1.00
T4/200	200	BDL	BDL	0.05	BDL	BDL	1.02	1.07
T4/300	300	BDL	BDL	0.06	BDL	BDL	0.88	0.94
T4/355	355	BDL	BDL	0.05	BDL	BDL	0.97	1.02
T4/400	400	BDL	BDL	0.07	BDL	0.01	0.84	0.91
T4/490	490	BDL	BDL	0.09	BDL	BDL	1.10	1.19
T4/591	591	BDL	BDL	0.05	BDL	BDL	1.10	1.15
T4/700	700	BDL	BDL	0.08	BDL	BDL	1.12	1.20
T4/795	795	0.01	BDL	0.07	BDL	BDL	0.94	1.01
T4/900	900	BDL	BDL	0.07	BDL	BDL	0.96	1.03
T4/985	985	BDL	BDL	0.06	BDL	BDL	1.02	1.08
T4/1010	1010	0.01	BDL	0.15	0.01	0.01	1.04	1.22
T4/1020	1020	0.08	BDL	0.20	0.01	0.01	1.13	1.43
T4/1040	1040	0.04	BDL	0.25	0.01	0.01	1.05	1.36

Ca (%) sample	depth	NH_4-Ac	Na-OC	HL	NH_4-OxH	H_2O_2	residual	total
T4/020	20	0.04	BDL	0.08	BDL	BDL	0.63	0.75
T4/040	40	0.04	BDL	0.08	BDL	BDL	0.66	0.78
T4/080	80	0.03	BDL	0.09	BDL	BDL	0.63	0.75
T4/100	100	0.08	BDL	0.09	BDL	BDL	0.73	0.89
T4/120	120	0.14	BDL	0.10	BDL	BDL	0.67	0.91
T4/153	153	0.08	BDL	0.11	BDL	BDL	0.63	0.82
T4/170	170	0.16	BDL	0.11	BDL	BDL	0.65	0.92
T4/200	200	0.10	BDL	0.10	BDL	BDL	0.68	0.88
T4/300	300	0.19	BDL	0.12	BDL	BDL	0.58	0.89
T4/355	355	0.16	BDL	0.10	BDL	BDL	0.67	0.92
T4/400	400	0.19	BDL	0.11	BDL	0.01	0.48	0.79
T4/490	490	0.14	BDL	0.11	BDL	BDL	0.62	0.86
T4/591	591	0.15	BDL	0.08	BDL	BDL	0.63	0.86
T4/700	700	0.25	0.01	0.09	BDL	0.01	0.74	1.09
T4/795	795	0.19	BDL	0.10	BDL	0.01	0.62	0.91
T4/900	900	0.17	BDL	0.11	BDL	0.01	0.64	0.92
T4/985	985	0.08	BDL	0.08	BDL	0.01	0.79	0.95
T4/1010	1010	0.25	0.01	0.06	BDL	0.01	0.43	0.76
T4/1020	1020	0.24	0.01	BDL	BDL	BDL	0.15	0.40
T4/1040	1040	0.24	BDL	BDL	BDL	BDL	0.15	0.39

Ti (%) sample	depth	NH_4-Ac	Na-OC	HL	NH_4-OxH	H_2O_2	residual	total
T4/020	20	BDL	BDL	BDL	BDL	BDL	0.19	0.19
T4/040	40	BDL	BDL	BDL	BDL	BDL	0.2	0.2
T4/080	80	BDL	BDL	BDL	BDL	BDL	0.23	0.23
T4/100	100	BDL	BDL	BDL	BDL	BDL	0.22	0.22
T4/120	120	BDL	BDL	BDL	BDL	BDL	0.23	0.23
T4/153	153	BDL	BDL	BDL	BDL	BDL	0.2	0.2
T4/170	170	BDL	BDL	BDL	BDL	BDL	0.19	0.19
T4/200	200	BDL	BDL	BDL	BDL	BDL	0.19	0.19
T4/300	300	BDL	BDL	BDL	BDL	BDL	0.22	0.22
T4/355	355	BDL	BDL	BDL	BDL	BDL	0.19	0.19
T4/400	400	BDL	BDL	BDL	BDL	BDL	0.24	0.24
T4/490	490	BDL	BDL	BDL	BDL	BDL	0.21	0.21
T4/591	591	BDL	BDL	BDL	BDL	BDL	0.22	0.22
T4/700	700	BDL	BDL	BDL	BDL	BDL	0.24	0.24
T4/795	795	BDL	BDL	BDL	BDL	BDL	0.26	0.26
T4/900	900	BDL	BDL	BDL	BDL	BDL	0.23	0.23
T4/985	985	BDL	BDL	BDL	BDL	BDL	0.25	0.25
T4/1010	1010	BDL	BDL	BDL	BDL	BDL	0.43	0.43
T4/1020	1020	BDL	BDL	BDL	BDL	BDL	0.42	0.42
T4/1040	1040	BDL	BDL	BDL	BDL	BDL	0.39	0.39

P (%) sample	depth	NH_4-Ac	Na-OC	HL	NH_4-OxH	H_2O_2	residual	total
T4/020	20	0.01	BDL	0.03	0.04	BDL	0.01	0.10
T4/040	40	0.01	BDL	0.04	0.04	BDL	0.01	0.09
T4/080	80	0.01	BDL	0.04	0.04	BDL	0.02	0.11
T4/100	100	0.01	BDL	0.03	0.04	BDL	0.02	0.10
T4/120	120	0.01	BDL	0.04	0.05	BDL	0.02	0.12
T4/153	153	0.01	BDL	0.05	0.04	BDL	0.02	0.11
T4/170	170	0.02	BDL	0.05	0.03	BDL	0.02	0.11
T4/200	200	0.01	BDL	0.04	0.02	BDL	0.02	0.10
T4/300	300	0.02	BDL	0.05	0.04	BDL	0.02	0.13
T4/355	355	0.01	BDL	0.04	0.02	BDL	0.02	0.10
T4/400	400	0.03	BDL	0.05	0.06	BDL	0.03	0.17
T4/490	490	0.02	BDL	0.05	0.02	BDL	0.02	0.11
T4/591	591	0.01	BDL	0.03	0.02	BDL	0.02	0.09
T4/700	700	0.02	BDL	0.04	0.02	BDL	0.03	0.11
T4/795	795	0.02	BDL	0.04	0.04	BDL	0.03	0.14
T4/900	900	0.01	BDL	0.04	0.03	BDL	0.02	0.11
T4/985	985	0.01	BDL	0.03	0.03	BDL	0.02	0.09
T4/1010	1010	0.01	BDL	0.02	0.04	BDL	0.04	0.11
T4/1020	1020	BDL	BDL	BDL	0.01	BDL	0.03	0.04
T4/1040	1040	BDL	BDL	BDL	BDL	BDL	0.02	0.02

Pb (ppm) sample	depth	NH_4-Ac	Na-OC	HL	NH_4-OxH	H_2O_2	residual	total
T4/020	20	BDL	BDL	BDL	8	BDL	7	15
T4/040	40	BDL	BDL	BDL	6	BDL	6	12
T4/080	80	BDL	BDL	BDL	4	BDL	BDL	4
T4/100	100	BDL	BDL	BDL	3	BDL	BDL	3
T4/120	120	BDL	BDL	BDL	5	BDL	9	14
T4/153	153	BDL	BDL	BDL	4	BDL	7	11
T4/170	170	BDL	BDL	BDL	3	BDL	7	10
T4/200	200	BDL	BDL	BDL	3	BDL	8	11
T4/300	300	BDL	BDL	BDL	4	BDL	11	15
T4/355	355	BDL	BDL	BDL	4	BDL	6	10
T4/400	400	BDL	BDL	BDL	5	BDL	14	19
T4/490	490	BDL	BDL	BDL	3	BDL	3	6
T4/591	591	BDL	BDL	BDL	3	BDL	5	8
T4/700	700	BDL	BDL	BDL	BDL	BDL	6	6
T4/795	795	BDL	BDL	BDL	BDL	BDL	7	7
T4/900	900	BDL	BDL	BDL	3	BDL	5	8
T4/985	985	BDL	BDL	BDL	BDL	BDL	3	3
T4/1010	1010	BDL	BDL	BDL	2	BDL	3	5
T4/1020	1020	BDL	BDL	BDL	BDL	BDL	2	2
T4/1040	1040	BDL	BDL	BDL	2	BDL	BDL	2

Mo (ppm) sample	depth	NH_4-Ac	Na-OC	HL	NH_4-OxH	H_2O_2	residual	total
T4/020	20	1	BDL	BDL	77	26	12	116
T4/040	40	1	BDL	BDL	66	33	16	116
T4/080	80	3	BDL	1	55	37	20	116
T4/100	100	BDL	BDL	BDL	44	53	13	110
T4/120	120	1	BDL	BDL	55	41	19	116
T4/153	153	BDL	BDL	BDL	32	26	18	76
T4/170	170	BDL	BDL	BDL	18	BDL	64	82
T4/200	200	BDL	BDL	BDL	14	BDL	92	106
T4/300	300	2	BDL	BDL	26	BDL	48	76
T4/355	355	1	BDL	BDL	19	BDL	77	97
T4/400	400	2	BDL	BDL	31	BDL	37	70
T4/490	490	BDL	BDL	BDL	18	BDL	40	58
T4/591	591	2	BDL	BDL	14	BDL	71	87
T4/700	700	3	BDL	BDL	17	BDL	82	102
T4/795	795	10	1	1	45	BDL	47	104
T4/900	900	6	BDL	1	34	BDL	33	74
T4/985	985	18	3	3	29	BDL	79	132
T4/1010	1010	2	1	BDL	25	BDL	37	65
T4/1020	1020	BDL	BDL	BDL	2	2	1	5
T4/1040	1040	BDL	BDL	BDL	BDL	BDL	BDL	BDL

V (ppm) sample	depth	NH_4-Ac	Na-OC	HL	NH_4-OxH	H_2O_2	residual	total
T4/020	20	BDL	BDL	BDL	11	BDL	151	162
T4/040	40	BDL	BDL	BDL	11	BDL	155	166
T4/080	80	BDL	BDL	BDL	7	BDL	177	184
T4/100	100	BDL	BDL	BDL	9	BDL	172	181
T4/120	120	BDL	BDL	BDL	8	BDL	189	197
T4/153	153	BDL	BDL	BDL	8	BDL	167	175
T4/170	170	BDL	BDL	BDL	6	BDL	167	173
T4/200	200	BDL	BDL	BDL	6	BDL	176	182
T4/300	300	BDL	BDL	BDL	4	BDL	191	195
T4/355	355	BDL	BDL	BDL	6	BDL	168	174
T4/400	400	BDL	BDL	BDL	4	BDL	220	224
T4/490	490	BDL	BDL	BDL	7	BDL	166	173
T4/591	591	BDL	BDL	BDL	6	BDL	180	186
T4/700	700	BDL	BDL	BDL	6	BDL	189	195
T4/795	795	BDL	BDL	BDL	4	BDL	194	198
T4/900	900	BDL	BDL	BDL	4	BDL	172	176
T4/985	985	BDL	BDL	BDL	4	BDL	183	187
T4/1010	1010	3	BDL	BDL	7	BDL	140	150
T4/1020	1020	BDL	BDL	BDL	6	3	83	92
T4/1040	1040	BDL	BDL	BDL	3	3	80	86

As (ppm) sample	depth	NH_4-Ac	Na-OC	HL	NH_4-OxH	H_2O_2	residual	total
T4/020	20	6	BDL	8	79	3	BDL	96
T4/040	40	5	BDL	7	81	BDL	BDL	93
T4/080	80	9	BDL	11	43	BDL	BDL	63
T4/100	100	BDL	BDL	6	39	BDL	BDL	45
T4/120	120	9	BDL	11	54	BDL	BDL	74
T4/153	153	8	BDL	10	50	BDL	BDL	68
T4/170	170	10	BDL	11	38	BDL	11	70
T4/200	200	6	BDL	9	25	BDL	9	49
T4/300	300	12	BDL	14	41	BDL	BDL	67
T4/355	355	6	BDL	9	26	BDL	BDL	41
T4/400	400	12	BDL	15	53	BDL	BDL	80
T4/490	490	4	BDL	7	21	BDL	BDL	32
T4/591	591	4	BDL	5	18	BDL	BDL	27
T4/700	700	12	BDL	10	44	BDL	5	71
T4/795	795	29	BDL	27	109	BDL	7	172
T4/900	900	19	BDL	25	90	BDL	BDL	134
T4/985	985	14	BDL	19	88	BDL	25	146
T4/1010	1010	21	BDL	19	110	BDL	101	251
T4/1020	1020	BDL	BDL	BDL	12	BDL	133	145
T4/1040	1040	BDL	BDL	BDL	6	BDL	105	111

Ba (ppm)

sample	depth	NH_4-Ac	Na-OC	HL	NH_4-OxH	H_2O_2	residual	total
T4/020	20	BDL	BDL	4	22	5	252	283
T4/040	40	BDL	BDL	5	23	5	256	289
T4/080	80	BDL	BDL	4	12	3	291	310
T4/100	100	BDL	BDL	5	11	3	279	298
T4/120	120	BDL	BDL	4	18	4	357	383
T4/153	153	BDL	BDL	6	16	2	337	361
T4/170	170	3	3	8	3	3	325	345
T4/200	200	3	4	7	1	2	309	326
T4/300	300	6	8	10	2	2	357	385
T4/355	355	4	4	7	2	2	330	349
T4/400	400	7	11	14	3	2	406	443
T4/490	490	4	5	9	1	2	409	430
T4/591	591	4	4	8	1	2	374	393
T4/700	700	4	4	8	BDL	2	368	386
T4/795	795	7	5	10	2	2	472	498
T4/900	900	4	5	11	2	2	335	359
T4/985	985	3	3	7	1	2	378	394
T4/1010	1010	8	2	8	3	2	340	363
T4/1020	1020	13	2	4	BDL	4	123	146
T4/1040	1040	7	BDL	3	BDL	4	179	193

Sr (ppm)

sample	depth	NH_4-Ac	Na-OC	HL	NH_4-OxH	H_2O_2	residual	total
T4/020	20	BDL	BDL	1.1	6.8	0.9	161	169.8
T4/040	40	BDL	BDL	1.1	7.4	0.9	166	175.4
T4/080	80	BDL	BDL	1.5	6.6	1.2	168	177.3
T4/100	100	BDL	BDL	1.3	4.7	0.7	174	180.7
T4/120	120	1	BDL	1.6	8	1	179	190.6
T4/153	153	BDL	BDL	1.7	3.8	0.8	180	186.3
T4/170	170	1.9	BDL	1.4	1.8	0.7	176	181.8
T4/200	200	1	BDL	1.3	1.3	BDL	174	177.6
T4/300	300	2.8	BDL	1.6	2.7	0.8	177	184.9
T4/355	355	2.2	BDL	1.4	2	0.5	172	178.1
T4/400	400	3.8	0.8	2	5.7	1.3	186	199.6
T4/490	490	6.5	BDL	1.7	1.2	BDL	176	185.4
T4/591	591	4	BDL	1.3	0.9	BDL	167	173.2
T4/700	700	7.1	0.5	1.5	0.8	BDL	173	182.9
T4/795	795	6.4	BDL	1.7	1.4	0.6	165	175.1
T4/900	900	4.5	BDL	1.7	1.5	0.6	166	174.3
T4/985	985	5.7	BDL	1.3	1.3	BDL	175	183.3
T4/1010	1010	16.3	0.9	1.8	2.3	1.2	127	149.5
T4/1020	1020	15.7	0.8	BDL	0.7	1.2	110	128.4
T4/1040	1040	17	BDL	BDL	BDL	1.2	91.8	110

Ni (ppm)

sample	depth	NH_4-Ac	Na-OC	HL	NH_4-OxH	H_2O_2	residual	total
T4/020	20	BDL	BDL	BDL	BDL	BDL	23	23
T4/040	40	BDL	BDL	BDL	BDL	BDL	24	24
T4/080	80	BDL	BDL	BDL	BDL	BDL	25	25
T4/100	100	BDL	BDL	BDL	BDL	BDL	24	24
T4/120	120	BDL	BDL	BDL	BDL	BDL	30	30
T4/153	153	BDL	BDL	BDL	BDL	BDL	24	24
T4/170	170	BDL	BDL	BDL	BDL	1	26	27
T4/200	200	BDL	BDL	BDL	BDL	BDL	28	28
T4/300	300	BDL	BDL	BDL	BDL	BDL	30	30
T4/355	355	BDL	BDL	BDL	BDL	BDL	29	29
T4/400	400	2	BDL	BDL	BDL	1	32	35
T4/490	490	2	BDL	BDL	BDL	BDL	26	28
T4/591	591	BDL	BDL	BDL	BDL	BDL	28	28
T4/700	700	BDL	BDL	BDL	BDL	BDL	32	32
T4/795	795	BDL	BDL	BDL	BDL	BDL	32	32
T4/900	900	BDL	BDL	BDL	BDL	BDL	29	29
T4/985	985	BDL	BDL	BDL	BDL	BDL	31	31
T4/1010	1010	2	BDL	BDL	BDL	BDL	19	21
T4/1020	1020	BDL	BDL	BDL	BDL	BDL	5	5
T4/1040	1040	BDL	BDL	BDL	BDL	BDL	3	3

W (ppm)

sample	depth	NH_4-Ac	Na-OC	HL	NH_4-OxH	H_2O_2	residual	total
T4/020	20	BDL	BDL	BDL	BDL	BDL	BDL	BDL
T4/040	40	BDL	BDL	BDL	BDL	BDL	BDL	BDL
T4/080	80	BDL	BDL	BDL	BDL	BDL	BDL	BDL
T4/100	100	BDL	BDL	BDL	BDL	BDL	11	11
T4/120	120	BDL	BDL	BDL	BDL	BDL	13	13
T4/153	153	BDL	BDL	BDL	BDL	BDL	10	10
T4/170	170	BDL	BDL	BDL	BDL	BDL	10	10
T4/200	200	BDL	BDL	BDL	BDL	BDL	14	14
T4/300	300	BDL	BDL	BDL	BDL	BDL	11	11
T4/355	355	BDL	BDL	BDL	BDL	BDL	11	11
T4/400	400	BDL	BDL	BDL	BDL	BDL	12	12
T4/490	490	BDL	BDL	BDL	BDL	BDL	10	10
T4/591	591	BDL	BDL	BDL	BDL	BDL	11	11
T4/700	700	BDL	BDL	BDL	BDL	BDL	23	23
T4/795	795	BDL	BDL	BDL	BDL	BDL	11	11
T4/900	900	BDL	BDL	BDL	BDL	BDL	BDL	BDL
T4/985	985	BDL	BDL	BDL	BDL	BDL	11	11
T4/1010	1010	BDL	BDL	BDL	BDL	BDL	BDL	BDL
T4/1020	1020	BDL	BDL	BDL	BDL	BDL	BDL	BDL
T4/1040	1040	BDL	BDL	BDL	BDL	BDL	BDL	BDL

La (ppm)

sample	depth	NH_4-Ac	Na-OC	HL	NH_4-OxH	H_2O_2	residual	total
T4/020	20	BDL	BDL	BDL	BDL	BDL	8.1	8.1
T4/040	40	BDL	BDL	BDL	BDL	BDL	7.9	7.9
T4/080	80	BDL	BDL	BDL	BDL	BDL	7	7
T4/100	100	BDL	BDL	BDL	BDL	BDL	7	7
T4/120	120	BDL	BDL	BDL	BDL	BDL	9	9
T4/153	153	BDL	BDL	BDL	BDL	BDL	9	9
T4/170	170	BDL	BDL	BDL	BDL	BDL	7	7
T4/200	200	BDL	BDL	BDL	BDL	BDL	5	5
T4/300	300	BDL	BDL	BDL	BDL	BDL	8	8
T4/355	355	BDL	BDL	BDL	BDL	BDL	6	6
T4/400	400	BDL	BDL	BDL	BDL	BDL	9	9
T4/490	490	BDL	BDL	BDL	BDL	BDL	8	8
T4/591	591	BDL	BDL	BDL	BDL	BDL	7	7
T4/700	700	BDL	BDL	BDL	BDL	BDL	7	7
T4/795	795	BDL	BDL	BDL	BDL	BDL	10	10
T4/900	900	BDL	BDL	BDL	BDL	BDL	8	8
T4/985	985	BDL	BDL	BDL	BDL	BDL	6	6
T4/1010	1010	BDL	BDL	BDL	BDL	BDL	6	6
T4/1020	1020	BDL	BDL	BDL	BDL	BDL	5	5
T4/1040	1040	BDL	BDL	BDL	1	BDL	5	6

Y (ppm)

sample	depth	NH_4-Ac	Na-OC	HL	NH_4-OxH	H_2O_2	residual	total
T4/020	20	0.4	BDL	1.1	0.5	BDL	2.6	4.6
T4/040	40	0.3	BDL	1.1	0.3	BDL	2.6	4.3
T4/080	80	0.2	BDL	1.3	0.4	BDL	3.2	5.1
T4/100	100	0.1	BDL	1.2	0.3	BDL	2.8	4.4
T4/120	120	0.3	BDL	1.4	0.4	BDL	2.7	4.8
T4/153	153	0.1	BDL	1.5	0.3	BDL	2.6	4.5
T4/170	170	BDL	BDL	1.6	0.3	BDL	2.4	4.3
T4/200	200	BDL	BDL	1.5	0.3	BDL	2.6	4.4
T4/300	300	0.2	BDL	1.8	0.6	BDL	3	5.6
T4/355	355	0.1	BDL	1.5	0.5	BDL	2.7	4.8
T4/400	400	0.8	BDL	1.7	1	BDL	3.9	7.4
T4/490	490	1.2	BDL	1.7	0.6	BDL	2.5	6
T4/591	591	0.2	BDL	1.3	0.5	BDL	2.4	4.4
T4/700	700	0.3	BDL	1.5	0.4	BDL	3	5
T4/795	795	0.4	BDL	1.6	0.5	BDL	2.8	5
T4/900	900	0.2	BDL	1.8	0.3	BDL	2.7	5
T4/985	985	0.2	BDL	1.3	0.3	BDL	2.6	4
T4/1010	1010	0.7	BDL	0.6	1.2	BDL	3.6	6.1
T4/1020	1020	1	BDL	0.2	1	0.2	4.3	6
T4/1040	1040	1	BDL	0.1	1	0.2	4	6

Fe (%)

sample	depth	NH_4-Ac	Na-OC	HL	NH_4-OxH	H_2O_2	residual	total	bulk
E1/030	30	0.03	BDL	0.05	1.63	0.54	4.54	6.79	6.25
E1/050	50	0.09	BDL	0.06	1.66	0.63	2.87	5.31	4.74
E1/100	100	0.12	BDL	0.08	1.64	0.79	2.64	5.27	5.34
E1/170	170	0.19	BDL	0.14	2.22	0.73	2.45	5.73	5.56
E1/200	200	0.16	BDL	0.09	2.40	0.96	2.35	5.96	5.67
E1/260	260	0.17	BDL	0.07	1.79	1.04	2.51	5.58	5.40
E1/350	350	0.53	BDL	0.08	2.71	0.72	4.11	8.15	7.82
E1/482	482	0.54	BDL	0.09	2.07	1.01	4.73	8.44	8.06
E1/580	580	0.18	BDL	0.09	0.81	0.53	4.39	6.00	5.91

Al (%)

sample	depth	NH_4-Ac	Na-OC	HL	NH_4-OxH	H_2O_2	residual	total	bulk
E1/030	30	0.06	BDL	0.04	0.16	0.02	8.00	8.28	8.13
E1/050	50	0.78	BDL	0.03	0.20	0.02	7.38	8.41	8.04
E1/100	100	0.54	BDL	0.03	0.11	0.02	8.87	9.57	9.98
E1/170	170	0.49	BDL	0.04	0.10	0.02	8.80	9.45	9.79
E1/200	200	0.59	BDL	0.04	0.10	0.03	8.84	9.60	9.55
E1/260	260	0.54	BDL	0.04	0.11	0.02	9.07	9.78	9.90
E1/350	350	0.52	BDL	0.03	0.06	0.01	8.09	8.71	8.79
E1/482	482	0.52	BDL	0.04	0.08	0.02	7.73	8.39	8.38
E1/580	580	0.30	BDL	0.10	0.14	BDL	9.36	9.90	9.89

K (%)

sample	depth	NH_4-Ac	Na-OC	HL	NH_4-OxH	H_2O_2	residual	total	bulk
E1/030	30	BDL	BDL	BDL	0.15	BDL	2.29	2.44	2.38
E1/050	50	BDL	BDL	BDL	0.12	BDL	2.04	2.16	2.05
E1/100	100	0.01	0.01	BDL	0.14	BDL	2.36	2.52	2.61
E1/170	170	BDL	BDL	BDL	0.21	BDL	2.28	2.49	2.55
E1/200	200	BDL	BDL	BDL	0.25	BDL	2.16	2.41	2.43
E1/260	260	0.01	0.01	BDL	0.19	BDL	2.24	2.45	2.48
E1/350	350	BDL	BDL	BDL	0.22	BDL	1.92	2.14	2.17
E1/482	482	0.01	0.01	BDL	0.16	BDL	1.95	2.13	2.10
E1/580	580	0.03	0.03	BDL	0.05	BDL	2.31	2.42	2.37

Mg (%)

sample	depth	NH_4-Ac	Na-OC	HL	NH_4-OxH	H_2O_2	residual	total	bulk
E1/030	30	0.03	BDL	BDL	BDL	0.01	0.25	0.29	0.30
E1/050	50	0.46	BDL	BDL	BDL	BDL	0.25	0.71	0.66
E1/100	100	0.25	BDL	BDL	BDL	BDL	0.27	0.52	0.53
E1/170	170	0.22	BDL	BDL	BDL	BDL	0.29	0.51	0.51
E1/200	200	0.20	BDL	BDL	BDL	BDL	0.25	0.45	0.44
E1/260	260	0.19	BDL	BDL	BDL	BDL	0.29	0.48	0.47
E1/350	350	0.21	BDL	BDL	BDL	BDL	0.20	0.41	0.40
E1/482	482	0.23	BDL	BDL	BDL	BDL	0.23	0.46	0.44
E1/580	580	0.13	BDL	BDL	BDL	BDL	0.55	0.68	0.69

Na (%)

sample	depth	NH_4-Ac	Na-OC	HL	NH_4-OxH	H_2O_2	residual	total	bulk
E1/030	30	0.02	BDL	0.12	0.09	BDL	1.05	1.28	1.36
E1/050	50	0.01	BDL	0.09	0.15	BDL	0.89	1.14	1.19
E1/100	100	BDL	BDL	0.12	0.09	BDL	0.83	1.04	1.00
E1/170	170	BDL	BDL	0.14	0	BDL	0.78	1.01	0.99
E1/200	200	BDL	BDL	0.12	0	BDL	0.72	0.92	0.81
E1/260	260	BDL	BDL	0.11	0	BDL	0.79	0.96	0.87
E1/350	350	BDL	BDL	0.19	0	BDL	0.80	1.07	0.95
E1/482	482	BDL	BDL	0.16	0	BDL	0.91	1.13	0.97
E1/580	580	BDL	BDL	0.12	0	BDL	0.88	1.02	1.03

Ca (%)

sample	depth	NH_4-Ac	Na-OC	HL	NH_4-OxH	H_2O_2	residual	total	bulk
E1/030	30	0.33	BDL	BDL	BDL	BDL	0.15	0.48	0.48
E1/050	50	0.58	BDL	BDL	BDL	BDL	0.13	0.71	0.63
E1/100	100	0.50	BDL	BDL	BDL	BDL	0.10	0.60	0.56
E1/170	170	0.58	BDL	BDL	BDL	BDL	0.12	0.70	0.64
E1/200	200	0.45	BDL	BDL	BDL	BDL	0.10	0.55	0.49
E1/260	260	0.51	BDL	BDL	BDL	BDL	0.13	0.64	0.56
E1/350	350	0.60	BDL	BDL	BDL	BDL	0.14	0.74	0.64
E1/482	482	0.53	BDL	BDL	BDL	BDL	0.15	0.68	0.58
E1/580	580	0.46	BDL	BDL	BDL	BDL	0.07	0.53	0.52

Ti (%)

sample	depth	NH_4-Ac	Na-OC	HL	NH_4-OxH	H_2O_2	residual	total	bulk
E1/030	30	BDL	BDL	BDL	BDL	BDL	0.18	0.18	0.14
E1/050	50	BDL	BDL	BDL	BDL	BDL	0.16	0.16	0.14
E1/100	100	BDL	BDL	BDL	BDL	BDL	0.19	0.19	0.17
E1/170	170	BDL	BDL	BDL	BDL	BDL	0.19	0.19	0.18
E1/200	200	BDL	BDL	BDL	BDL	BDL	0.19	0.19	0.16
E1/260	260	BDL	BDL	BDL	BDL	BDL	0.21	0.21	0.18
E1/350	350	BDL	BDL	BDL	BDL	BDL	0.25	0.25	0.2
E1/482	482	BDL	BDL	BDL	BDL	BDL	0.25	0.25	0.2
E1/580	580	BDL	BDL	BDL	BDL	BDL	0.25	0.25	0.25

P (%)

sample	depth	NH_4-Ac	Na-OC	HL	NH_4-OxH	H_2O_2	residual	total	bulk
E1/030	30	BDL	BDL	BDL	BDL	BDL	0.06	0.06	0.05
E1/050	50	BDL	BDL	BDL	BDL	BDL	0.05	0.05	0.05
E1/100	100	BDL	BDL	BDL	BDL	BDL	0.06	0.06	0.06
E1/170	170	BDL	BDL	BDL	BDL	BDL	0.05	0.05	0.06
E1/200	200	BDL	BDL	BDL	BDL	BDL	0.05	0.05	0.06
E1/260	260	BDL	BDL	BDL	0.01	BDL	0.05	0.06	0.06
E1/350	350	BDL	BDL	BDL	0.02	BDL	0.06	0.08	0.07
E1/482	482	BDL	BDL	BDL	0.02	BDL	0.06	0.08	0.07
E1/580	580	BDL	BDL	BDL	0.02	BDL	0.05	0.07	0.07

Ba (ppm)

sample	depth	NH_4-Ac	Na-OC	HL	NH_4-OxH	H_2O_2	residual	total	bulk
E1/030	30	BDL	BDL	2	7	BDL	327	336	403
E1/050	50	BDL	BDL	1	8	BDL	283	292	411
E1/100	100	BDL	BDL	BDL	9	BDL	291	300	353
E1/170	170	BDL	BDL	1	10	BDL	290	301	402
E1/200	200	BDL	BDL	BDL	12	BDL	266	278	339
E1/260	260	BDL	BDL	1	8	BDL	289	298	288
E1/350	350	BDL	BDL	BDL	10	BDL	283	293	204
E1/482	482	BDL	BDL	1	7	BDL	281	289	295
E1/580	580	2	BDL	2	1	BDL	430	435	470

Cu (ppm)

sample	depth	NH_4-Ac	Na-OC	HL	NH_4-OxH	H_2O_2	residual	total	bulk
E1/030	30	1110	135	161	341	98	329	2174	2150
E1/050	50	14500	127	129	349	69	180	15354	14900
E1/100	100	6690	89	57	244	114	207	7401	7720
E1/170	170	5670	123	133	273	138	175	6512	6630
E1/200	200	4610	94	90	242	99	155	5290	5320
E1/260	260	4460	68	96	279	100	190	5193	5260
E1/350	350	2470	70	159	198	698	529	4124	4180
E1/482	482	2740	51	103	207	223	374	3698	3640
E1/580	580	2840	65	129	206	221	539	4000	3920

Zn (ppm)

sample	depth	NH_4-Ac	Na-OC	HL	NH_4-OxH	H_2O_2	residual	total	bulk
E1/030	30	5	BDL	BDL	BDL	BDL	17	22	17
E1/050	50	52	BDL	BDL	BDL	BDL	17	69	41
E1/100	100	24	BDL	BDL	BDL	BDL	20	44	29
E1/170	170	21	BDL	BDL	BDL	BDL	20	41	27
E1/200	200	17	BDL	BDL	BDL	BDL	17	34	23
E1/260	260	17	BDL	BDL	BDL	BDL	28	45	27
E1/350	350	13	BDL	BDL	BDL	BDL	33	47	35
E1/482	482	16	BDL	BDL	BDL	BDL	31	47	35
E1/580	580	14	BDL	BDL	1	BDL	41	56	56

Mn (ppm)

sample	depth	NH_4-Ac	Na-OC	HL	NH_4-OxH	H_2O_2	residual	total	bulk
E1/030	30	10	BDL	3	5	BDL	27	45	40
E1/050	50	140	BDL	BDL	6	BDL	31	177	153
E1/100	100	67	BDL	BDL	3	BDL	15	85	76
E1/170	170	65	BDL	2	4	BDL	23	94	89
E1/200	200	53	BDL	BDL	3	BDL	14	70	65
E1/260	260	51	BDL	BDL	3	BDL	23	77	72
E1/350	350	40	BDL	BDL	2	BDL	16	58	54
E1/482	482	48	BDL	BDL	2	BDL	20	70	65
E1/580	580	36	BDL	BDL	3	BDL	41	80	79

Cr (ppm)

sample	depth	NH_4-Ac	Na-OC	HL	NH_4-OxH	H_2O_2	residual	total	bulk
E1/030	30	BDL	BDL	BDL	5	BDL	5	10	8
E1/050	50	3	BDL	BDL	7	BDL	5	15	8
E1/100	100	2	BDL	BDL	4	BDL	5	11	9
E1/170	170	4	BDL	1	5	BDL	7	17	12
E1/200	200	2	BDL	BDL	4	BDL	6	12	9
E1/260	260	3	BDL	BDL	5	BDL	7	15	11
E1/350	350	2	BDL	BDL	4	BDL	7	13	9
E1/482	482	2	BDL	BDL	4	BDL	7	13	9
E1/580	580	1	BDL	BDL	3	BDL	8	12	9

Pb (ppm)

sample	depth	NH_4-Ac	Na-OC	HL	NH_4-OxH	H_2O_2	residual	total	bulk
T4/020	20	BDL	BDL	BDL	BDL	BDL	8	8	10
T4/040	40	BDL	BDL	BDL	BDL	BDL	5	5	7
T4/080	80	BDL	BDL	BDL	BDL	BDL	8	8	7
T4/100	100	BDL	BDL	BDL	BDL	BDL	7	7	7
T4/120	120	BDL	BDL	BDL	BDL	BDL	5	5	3
T4/153	153	BDL	BDL	BDL	BDL	BDL	5	5	3
T4/170	170	BDL	BDL	BDL	BDL	BDL	10	10	13
T4/200	200	BDL	BDL	BDL	BDL	BDL	13	13	14
T4/300	300	BDL	BDL	BDL	BDL	BDL	6	6	7

Mo (ppm)

sample	depth	NH_4-Ac	Na-OC	HL	NH_4-OxH	H_2O_2	residual	total	bulk
E1/030	30	BDL	BDL	BDL	19	83	825	927	822
E1/050	50	BDL	BDL	BDL	18	73	440	531	491
E1/100	100	BDL	BDL	BDL	23	35	268	326	329
E1/170	170	BDL	BDL	BDL	31	33	249	313	304
E1/200	200	BDL	BDL	BDL	28	28	145	201	189
E1/260	260	BDL	BDL	BDL	25	34	191	250	240
E1/350	350	BDL	BDL	BDL	14	15	226	255	247
E1/482	482	BDL	BDL	BDL	11	19	178	208	199
E1/580	580	BDL	BDL	BDL	12	11	179	202	199

V (ppm)

sample	depth	NH_4-Ac	Na-OC	HL	NH_4-OxH	H_2O_2	residual	total	bulk
E1/030	30	BDL	BDL	BDL	9	BDL	92	101	95
E1/050	50	5	BDL	BDL	13	BDL	87	105	96
E1/100	100	5	BDL	BDL	7	BDL	111	123	124
E1/170	170	5	BDL	2	10	BDL	110	127	126
E1/200	200	4	BDL	BDL	9	BDL	115	128	126
E1/260	260	3	BDL	BDL	11	BDL	118	132	131
E1/350	350	5	BDL	2	18	BDL	118	143	139
E1/482	482	4	BDL	2	15	BDL	110	131	126
E1/580	580	2	BDL	3	9	BDL	146	160	158

As (ppm)

sample	depth	NH_4-Ac	Na-OC	HL	NH_4-OxH	H_2O_2	residual	total	bulk
E1/030	30	207	3	107	297	BDL	34	648	471
E1/050	50	80	BDL	21	138	BDL	26	265	185
E1/100	100	8	BDL	BDL	40	BDL	18	66	46
E1/170	170	49	BDL	9	133	BDL	25	216	168
E1/200	200	10	BDL	BDL	91	BDL	19	120	96
E1/260	260	21	BDL	BDL	111	BDL	25	157	118
E1/350	350	BDL	BDL	BDL	47	BDL	18	65	53
E1/482	482	BDL	BDL	BDL	49	BDL	16	65	42
E1/580	580	BDL	BDL	BDL	38	BDL	3	41	34

W (ppm)

sample	depth	NH_4-Ac	Na-OC	HL	NH_4-OxH	H_2O_2	residual	total	bulk
E1/030	30	BDL	BDL	BDL	BDL	BDL	BDL	BDL	BDL
E1/050	50	BDL	BDL	BDL	BDL	BDL	BDL	BDL	BDL
E1/100	100	BDL	BDL	BDL	BDL	BDL	BDL	BDL	BDL
E1/170	170	BDL	BDL	BDL	BDL	BDL	BDL	BDL	BDL
E1/200	200	BDL	BDL	BDL	BDL	BDL	BDL	BDL	BDL
E1/260	260	BDL	BDL	BDL	BDL	BDL	BDL	BDL	BDL
E1/350	350	BDL	BDL	BDL	BDL	BDL	BDL	BDL	BDL
E1/482	482	BDL	BDL	BDL	BDL	BDL	BDL	BDL	BDL
E1/580	580	BDL	BDL	BDL	BDL	BDL	BDL	BDL	BDL

Sr (ppm)

sample	depth	NH_4-Ac	Na-OC	HL	NH_4-OxH	H_2O_2	residual	total	bulk
E1/030	30	1.6	BDL	0.8	8.6	0.9	357	368.9	350
E1/050	50	3.5	BDL	0.8	10.8	0.9	291	307	285
E1/100	100	4.6	BDL	BDL	8.1	0.6	388	401.3	411
E1/170	170	4.9	BDL	0.6	9.6	0.8	360	375.9	390
E1/200	200	3.8	BDL	BDL	10.2	0.5	347	361.5	356
E1/260	260	5.1	BDL	0.7	9.3	0.7	352	367.8	364
E1/350	350	5.6	BDL	BDL	15.3	1.3	304	326.2	317
E1/482	482	4.9	BDL	BDL	8.8	0.8	294	308.5	299
E1/580	580	3.9	BDL	BDL	4.8	BDL	277	285.7	282

Ni (ppm)

sample	depth	NH_4-Ac	Na-OC	HL	NH_4-OxH	H_2O_2	residual	total	bulk
E1/030	30	1	BDL	BDL	BDL	2	9	12	11
E1/050	50	18	BDL	BDL	BDL	2	7	27	20
E1/100	100	10	BDL	BDL	BDL	2	5	17	16
E1/170	170	9	BDL	BDL	BDL	2	5	16	14
E1/200	200	9	BDL	BDL	BDL	3	5	17	14
E1/260	260	8	BDL	BDL	BDL	3	6	17	15
E1/350	350	7	BDL	BDL	1	2	7	17	14
E1/482	482	8	BDL	BDL	BDL	3	8	19	16
E1/580	580	5	BDL	BDL	1	1	10	17	16

Zr (ppm)

sample	depth	NH_4-Ac	Na-OC	HL	NH_4-OxH	H_2O_2	residual	total	bulk
E1/030	30	BDL	BDL	BDL	BDL	BDL	5.2	5.2	21.7
E1/050	50	BDL	BDL	BDL	0.8	BDL	6.8	7.6	21.1
E1/100	100	BDL	BDL	BDL	1.1	BDL	3.6	4.7	29.3
E1/170	170	BDL	BDL	BDL	BDL	BDL	3.8	3.8	29.8
E1/200	200	BDL	BDL	BDL	BDL	BDL	6.5	6.5	29
E1/260	260	BDL	BDL	BDL	BDL	BDL	4.3	4.3	26.4
E1/350	350	BDL	BDL	BDL	2.6	BDL	3.3	5.9	25
E1/482	482	BDL	BDL	BDL	1.1	BDL	7.8	8.9	22
E1/580	580	BDL	BDL	BDL	1.1	BDL	1.8	2.9	29.3

Co (ppm)

sample	depth	NH_4-Ac	Na-OC	HL	NH_4-OxH	H_2O_2	residual	total	bulk
E1/030	30	4	BDL	BDL	1	10	46	61	56
E1/050	50	74	BDL	BDL	BDL	11	27	112	94
E1/100	100	40	BDL	BDL	BDL	13	20	73	70
E1/170	170	34	BDL	BDL	BDL	12	19	65	60
E1/200	200	32	BDL	BDL	BDL	16	16	64	57
E1/260	260	29	BDL	BDL	BDL	16	18	63	58
E1/350	350	27	BDL	BDL	BDL	12	27	66	59
E1/482	482	29	BDL	BDL	BDL	16	36	81	73
E1/580	580	15	BDL	BDL	BDL	10	45	70	68

Sn (ppm)

sample	depth	NH_4-Ac	Na-OC	HL	NH_4-OxH	H_2O_2	residual	total	bulk
E1/030	30	BDL	BDL	BDL	BDL	BDL	16	16	BDL
E1/050	50	BDL	BDL	BDL	BDL	BDL	17	17	27
E1/100	100	BDL	BDL	BDL	BDL	BDL	15	15	BDL
E1/170	170	BDL	BDL	BDL	BDL	BDL	16	16	BDL
E1/200	200	BDL	BDL	BDL	BDL	BDL	14	14	BDL
E1/260	260	BDL	BDL	BDL	BDL	BDL	14	14	BDL
E1/350	350	BDL	BDL	BDL	BDL	BDL	16	16	BDL
E1/482	482	BDL	BDL	BDL	BDL	BDL	14	14	BDL
E1/580	580	BDL	BDL	BDL	BDL	BDL	20	20	BDL

La (ppm)

sample	depth	NH_4-Ac	Na-OC	HL	NH_4-OxH	H_2O_2	residual	total	bulk
E1/030	30	BDL	BDL	BDL	BDL	BDL	12.9	12.9	21
E1/050	50	BDL	BDL	BDL	BDL	BDL	12.1	12.1	17.6
E1/100	100	BDL	BDL	BDL	BDL	BDL	13	13	16
E1/170	170	BDL	BDL	BDL	BDL	BDL	12	12	17
E1/200	200	BDL	BDL	BDL	BDL	BDL	12	12	14
E1/260	260	BDL	BDL	BDL	BDL	BDL	12	12	14
E1/350	350	BDL	BDL	BDL	0.8	BDL	12	13	13
E1/482	482	BDL	BDL	BDL	BDL	BDL	13	13	12
E1/580	580	BDL	BDL	BDL	0.7	BDL	16	17	18

Y (ppm)

sample	depth	NH_4-Ac	Na-OC	HL	NH_4-OxH	H_2O_2	residual	total	bulk
E1/030	30	0.6	BDL	BDL	BDL	BDL	5.2	5.8	6.7
E1/050	50	2.2	BDL	BDL	BDL	BDL	5.9	8.1	8.4
E1/100	100	1	BDL	BDL	BDL	BDL	5	6	7.2
E1/170	170	1	BDL	BDL	BDL	BDL	4.1	5.1	7.6
E1/200	200	0.9	BDL	BDL	BDL	BDL	4.2	5.1	7
E1/260	260	1	BDL	BDL	BDL	BDL	4.8	5.8	7.4
E1/350	350	1.2	BDL	BDL	BDL	BDL	8.2	9.4	9.9
E1/482	482	1.4	BDL	BDL	0.5	BDL	7.5	9.4	10.1
E1/580	580	0.9	BDL	BDL	BDL	BDL	13	13.9	13.5

Sc (ppm)

sample	depth	NH_4-Ac	Na-OC	HL	NH_4-OxH	H_2O_2	residual	total	bulk
E1/030	30	BDL	BDL	BDL	0.8	BDL	8.3	9.1	8.6
E1/050	50	1.7	BDL	BDL	1.1	BDL	7.8	10.6	9.5
E1/100	100	1.4	BDL	BDL	0.8	BDL	10.1	12.3	12.6
E1/170	170	1.3	BDL	BDL	0.8	BDL	10	12.1	12.5
E1/200	200	1.3	BDL	BDL	0.7	BDL	10.8	12.8	12.5
E1/260	260	1.3	BDL	BDL	1	BDL	10.8	13.1	12.8
E1/350	350	1.2	BDL	BDL	0.8	BDL	9.4	11.4	10.7
E1/482	482	1.1	BDL	BDL	0.7	BDL	8.9	10.7	10.1
E1/580	580	1	BDL	BDL	1.2	BDL	13.1	15.3	14.5

Be (ppm)

sample	depth	NH_4-Ac	Na-OC	HL	NH_4-OxH	H_2O_2	residual	total	bulk
E1/030	30	BDL	BDL	BDL	BDL	BDL	0.9	0.9	0.9
E1/050	50	BDL	BDL	BDL	BDL	BDL	0.8	0.8	0.9
E1/100	100	BDL	BDL	BDL	BDL	BDL	0.9	0.9	1.1
E1/170	170	BDL	BDL	BDL	BDL	BDL	0.8	0.8	1.1
E1/200	200	BDL	BDL	BDL	BDL	BDL	0.8	0.8	1
E1/260	260	BDL	BDL	BDL	BDL	BDL	0.9	0.9	1.1
E1/350	350	BDL	BDL	BDL	BDL	BDL	1	1	1.2
E1/482	482	BDL	BDL	BDL	BDL	BDL	1	1	1.2
E1/580	580	BDL	BDL	BDL	BDL	BDL	1.3	1.3	1.2

Ag (ppm)

sample	depth	NH_4-Ac	Na-OC	HL	NH_4-OxH	H_2O_2	residual	total	bulk
E1/030	30	BDL	BDL	0.3	BDL	BDL	0.6	0.9	0.6
E1/050	50	BDL	BDL	0.3	BDL	BDL	0.5	0.8	0.6
E1/100	100	BDL	BDL	0.2	BDL	BDL	1.3	1.5	1
E1/170	170	BDL	BDL	BDL	BDL	BDL	1.1	1.1	0.9
E1/200	200	BDL	BDL	BDL	BDL	BDL	1.3	1.3	0.7
E1/260	260	BDL	BDL	0.2	BDL	BDL	1.2	1.4	1
E1/350	350	BDL	BDL	0.3	BDL	BDL	1.2	1.5	0.8
E1/482	482	BDL	BDL	BDL	0.3	BDL	1.3	1.6	1.1
E1/580	580	BDL	BDL	BDL	BDL	BDL	1.1	1.1	0.9

Fe (%)

sample	depth	NH_4-Ac	Na-OC	HL	NH_4-OxH	H_2O_2	residual	total	bulk
O3/025	25	0.33	BDL	0.28	2.25	0.14	8.22	11.22	12.7
O3/070	70	0.25	BDL	0.28	2.19	0.09	7.92	10.73	11
O3/100	100	0.42	BDL	0.34	2.82	0.03	8.4	12.01	11.9
O3/200	200	0.37	BDL	0.49	2.8	0.05	6.59	10.3	9.68
O3/300	300	0.56	BDL	0.47	2.92	0.14	5.24	9.33	9.19
O3/400	400	0.38	BDL	0.46	3.27	0.1	6.28	10.49	10.2
O3/500	500	0.38	BDL	0.43	3.2	0.11	7.52	11.64	10.7

Al (%)

sample	depth	NH_4-Ac	Na-OC	HL	NH_4-OxH	H_2O_2	residual	total	bulk
O3/025	25	0.12	BDL	0.08	0.09	0.02	4.68	4.99	5.51
O3/070	70	0.07	BDL	0.07	0.11	0.02	5.55	5.82	5.83
O3/100	100	0.15	BDL	0.1	0.14	0.02	5.47	5.88	6.02
O3/200	200	0.11	BDL	0.09	0.17	0.03	7.31	7.71	7.79
O3/300	300	0.11	BDL	0.08	0.19	0.12	6.52	7.02	7.56
O3/400	400	0.09	BDL	0.09	0.22	0.12	7.01	7.53	7.87
O3/500	500	0.09	BDL	0.09	0.24	0.12	7.18	7.72	7.66

K (%)

sample	depth	NH_4-Ac	Na-OC	HL	NH_4-OxH	H_2O_2	residual	total	bulk
O3/025	25	0.02	BDL	0.02	BDL	BDL	2.13	2.17	2.39
O3/070	70	0.02	BDL	0.02	BDL	BDL	2.61	2.65	2.65
O3/100	100	0.03	BDL	0.02	BDL	BDL	2.24	2.29	2.36
O3/200	200	0.04	BDL	0.01	BDL	BDL	2.75	2.8	2.78
O3/300	300	0.04	BDL	BDL	BDL	0.02	2.22	2.28	2.44
O3/400	400	0.04	BDL	0.01	BDL	0.03	2.21	2.29	2.35
O3/500	500	0.04	BDL	0.01	BDL	0.03	2.11	2.19	2.19

Mg (%)

sample	depth	NH_4-Ac	Na-OC	HL	NH_4-OxH	H_2O_2	residual	total	bulk
O3/025	25	0.15	BDL	0.04	0.06	0.02	1.13	1.4	1.51
O3/070	70	0.1	0.01	0.04	0.08	0.02	1.35	1.6	1.56
O3/100	100	0.18	0.02	0.06	0.09	0.03	1.66	2.04	2
O3/200	200	0.16	0.03	0.04	0.09	0.03	1.83	2.18	2.11
O3/300	300	0.26	0.14	0.08	0.11	0.04	1.83	2.46	2.54
O3/400	400	0.14	0.03	0.04	0.11	0.03	1.6	1.95	1.94
O3/500	500	0.17	0.04	0.03	0.11	0.02	1.47	1.84	1.75

Na (%)

sample	depth	NH_4-Ac	Na-OC	HL	NH_4-OxH	H_2O_2	residual	total	bulk
O3/025	25	0.02	BDL	0.03	BDL	BDL	1.04	1.09	1.17
O3/070	70	0.02	BDL	0.03	BDL	BDL	1.22	1.27	1.24
O3/100	100	0.01	BDL	0.05	BDL	BDL	0.92	0.98	0.95
O3/200	200	0.02	BDL	0.08	BDL	BDL	0.83	0.93	0.84
O3/300	300	0.02	BDL	0.06	BDL	BDL	0.83	0.91	0.91
O3/400	400	0.02	BDL	0.1	BDL	BDL	0.85	0.97	0.88
O3/500	500	0.02	BDL	0.14	BDL	BDL	0.48	0.64	0.47

Ca (%)

sample	depth	NH_4-Ac	Na-OC	HL	NH_4-OxH	H_2O_2	residual	total	bulk
O3/025	25	3.05	0.02	0.26	BDL	0.01	0.22	3.56	3.12
O3/070	70	2.55	0.03	0.24	BDL	BDL	0.21	3.03	2.59
O3/100	100	3.63	0.04	0.37	BDL	0.01	0.17	4.22	3.61
O3/200	200	4.01	0.09	0.47	BDL	0.01	0.12	4.7	4.03
O3/300	300	4.38	0.38	0.47	BDL	BDL	0.19	5.42	4.79
O3/400	400	3.58	0.09	0.32	BDL	BDL	0.2	4.19	3.62
O3/500	500	3.15	0.12	0.29	BDL	BDL	0.11	3.67	3.07

Ti (%)

sample	depth	NH_4-Ac	Na-OC	HL	NH_4-OxH	H_2O_2	residual	total	bulk
O3/025	25	BDL	BDL	BDL	BDL	BDL	0.14	0.14	0.14
O3/070	70	BDL	BDL	BDL	BDL	BDL	0.15	0.15	0.15
O3/100	100	BDL	BDL	BDL	BDL	BDL	0.18	0.18	0.17
O3/200	200	BDL	BDL	BDL	BDL	BDL	0.22	0.22	0.23
O3/300	300	BDL	BDL	BDL	BDL	BDL	0.24	0.24	0.24
O3/400	400	BDL	BDL	BDL	BDL	BDL	0.25	0.25	0.27
O3/500	500	BDL	BDL	BDL	BDL	BDL	0.25	0.25	0.23

P (%)

sample	depth	NH_4-Ac	Na-OC	HL	NH_4-OxH	H_2O_2	residual	total	bulk
O3/025	25	BDL	BDL	0.1	0.02	BDL	BDL	0.12	0.09
O3/070	70	BDL	BDL	0.09	0.02	BDL	BDL	0.11	0.08
O3/100	100	BDL	BDL	0.11	0.05	BDL	0.01	0.17	0.12
O3/200	200	BDL	BDL	0.12	0.07	BDL	0.03	0.22	0.16
O3/300	300	BDL	BDL	0.08	0.06	BDL	0.02	0.16	0.13
O3/400	400	BDL	BDL	0.09	0.05	BDL	0.01	0.15	0.11
O3/500	500	BDL	BDL	0.06	0.06	BDL	0.02	0.14	0.1

Ba (ppm)

sample	depth	NH_4-Ac	Na-OC	HL	NH_4-OxH	H_2O_2	residual	total	bulk
O3/025	25	11	60	131	32	1	62	297	937
O3/070	70	11	48	110	31	BDL	124	324	991
O3/100	100	9	32	142	64	1	673	921	956
O3/200	200	5	22	112	53	1	664	857	860
O3/300	300	4	26	101	37	4	445	617	662
O3/400	400	4	28	118	46	4	456	656	676
O3/500	500	8	24	142	90	5	558	827	810

Sr (ppm)

sample	depth	NH_4-Ac	Na-OC	HL	NH_4-OxH	H_2O_2	residual	total	bulk
O3/025	25	18	2	5	1	1	44	70	77
O3/070	70	14	2	4	1	1	62	83	86
O3/100	100	20	3	6	1	1	53	83	85
O3/200	200	26	3	6	1	1	66	101	105
O3/300	300	24	3	4	1	1	68	100	109
O3/400	400	27	3	5	1	1	72	108	113
O3/500	500	22	3	6	2	1	61	94	92

Ni (ppm)

sample	depth	NH_4-Ac	Na-OC	HL	NH_4-OxH	H_2O_2	residual	total	bulk
O3/025	25	3	BDL	BDL	4	7	26	40	39
O3/070	70	3	BDL	1	3	6	25	38	35
O3/100	100	7	BDL	2	7	7	21	44	38
O3/200	200	10	BDL	4	9	9	21	53	44
O3/300	300	8	1	2	6	BDL	17	34	32
O3/400	400	6	BDL	2	6	BDL	13	27	22
O3/500	500	5	BDL	2	5	BDL	12	24	19

Cu (ppm)

sample	depth	NH_4-Ac	Na-OC	HL	NH_4-OxH	H_2O_2	residual	total	bulk
O3/025	25	701	28	129	49.9	270	157	1335	1410
O3/070	70	1160	55.1	240	111	342	216	2124	2110
O3/100	100	1160	42.9	295	392	303	194	2387	2400
O3/200	200	1410	59.9	515	585	121	294	2985	2980
O3/300	300	3940	94.7	560	683	37.3	258	5573	5790
O3/400	400	3030	99.3	527	524	22.7	217	4420	4500
O3/500	500	1870	74.2	568	673	40.9	480	3706	3670

Zn (ppm)

sample	depth	NH_4-Ac	Na-OC	HL	NH_4-OxH	H_2O_2	residual	total	bulk
O3/025	25	21	1	10	15	8	45	100	80
O3/070	70	36	3	30	22	10	53	155	123
O3/100	100	41	2	22	26	15	61	167	130
O3/200	200	38	3	44	29	10	69	192	154
O3/300	300	61	4	34	34	5	64	200	168
O3/400	400	33	2	17	18	2	52	125	103
O3/500	500	22	2	17	25	2	58	125	99

Mn (ppm)

sample	depth	NH_4-Ac	Na-OC	HL	NH_4-OxH	H_2O_2	residual	total	bulk
O3/025	25	611	29	54	108	56	431	1289	1250
O3/070	70	584	37	74	121	44	534	1394	1250
O3/100	100	816	60	78	211	71	575	1811	1660
O3/200	200	1060	140	111	172	54	676	2213	2020
O3/300	300	1100	242	114	195	16	554	2221	2110
O3/400	400	947	117	76	178	11	664	1993	1820
O3/500	500	1140	195	168	287	10	774	2574	2280

Cr (ppm)

sample	depth	NH_4-Ac	Na-OC	HL	NH_4-OxH	H_2O_2	residual	total	bulk
O3/025	25	BDL	BDL	1	3	BDL	9	13	23
O3/070	70	BDL	BDL	2	3	BDL	15	20	19
O3/100	100	2	BDL	BDL	4	BDL	13	19	19
O3/200	200	1	BDL	1	4	BDL	14	20	21
O3/300	300	2	BDL	1	6	1	16	26	23
O3/400	400	2	BDL	2	7	1	16	28	20
O3/500	500	1	BDL	1	4	BDL	16	22	19

Pb (ppm)

sample	depth	NH_4-Ac	Na-OC	HL	NH_4-OxH	H_2O_2	residual	total	bulk
O3/025	25	10	BDL	3	9	BDL	2	24	20
O3/070	70	22	BDL	13	14	BDL	6	55	41
O3/100	100	15	BDL	8	16	BDL	7	46	38
O3/200	200	24	BDL	19	31	BDL	19	93	74
O3/300	300	14	BDL	5	13	BDL	BDL	32	33
O3/400	400	14	BDL	9	14	BDL	23	60	48
O3/500	500	21	BDL	14	22	BDL	11	68	50

Mo (ppm)

sample	depth	NH_4-Ac	Na-OC	HL	NH_4-OxH	H_2O_2	residual	total	bulk
O3/025	25	BDL	BDL	BDL	3	BDL	4	7	7
O3/070	70	BDL	BDL	BDL	3	BDL	2	5	4
O3/100	100	BDL	BDL	BDL	3	BDL	1	4	3
O3/200	200	BDL	BDL	BDL	7	BDL	5	12	10
O3/300	300	BDL	BDL	BDL	7	3	2	12	12
O3/400	400	BDL	BDL	BDL	11	3	1	15	11
O3/500	500	BDL	BDL	BDL	9	2	2	13	11

V (ppm)

sample	depth	NH_4-Ac	Na-OC	HL	NH_4-OxH	H_2O_2	residual	total	bulk
O3/025	25	2	BDL	2	16	BDL	75	95	108
O3/070	70	BDL	BDL	3	16	BDL	82	101	102
O3/100	100	3	BDL	3	19	BDL	88	113	114
O3/200	200	BDL	BDL	5	19	BDL	106	130	128
O3/300	300	3	BDL	4	21	4	106	138	142
O3/400	400	2	BDL	5	23	3	107	140	142
O3/500	500	BDL	BDL	4	20	3	121	148	143

As (ppm)

sample	depth	NH_4-Ac	Na-OC	HL	NH_4-OxH	H_2O_2	residual	total	bulk
O3/025	25	BDL	BDL	BDL	6	BDL	BDL	6	BDL
O3/070	70	BDL	BDL	3	7	BDL	BDL	10	BDL
O3/100	100	BDL	BDL	4	30	BDL	6	40	14
O3/200	200	BDL	BDL	5	42	BDL	17	64	39
O3/300	300	BDL	BDL	BDL	31	BDL	BDL	31	16
O3/400	400	BDL	BDL	4	55	BDL	BDL	59	34
O3/500	500	BDL	BDL	BDL	55	BDL	BDL	55	38

W (ppm)

sample	depth	NH_4-Ac	Na-OC	HL	NH_4-OxH	H_2O_2	residual	total	bulk
O3/025	25	BDL	BDL	BDL	BDL	BDL	BDL	BDL	BDL
O3/070	70	BDL	BDL	BDL	BDL	BDL	BDL	BDL	BDL
O3/100	100	BDL	BDL	BDL	BDL	BDL	BDL	BDL	BDL
O3/200	200	BDL	BDL	BDL	BDL	BDL	BDL	BDL	BDL
O3/300	300	BDL	BDL	BDL	BDL	BDL	BDL	BDL	11
O3/400	400	BDL	BDL	BDL	BDL	BDL	13	13	30
O3/500	500	BDL	BDL	BDL	BDL	BDL	22	22	38

La (ppm)

sample	depth	NH_4-Ac	Na-OC	HL	NH_4-OxH	H_2O_2	residual	total	bulk
O3/025	25	4	BDL	3	1	1	39	48	57
O3/070	70	3	BDL	3	BDL	1	41	48	56
O3/100	100	4	BDL	4	1	2	64	74	76
O3/200	200	5	BDL	8	3	4	57	77	80
O3/300	300	5	BDL	6	1	1	69	83	91
O3/400	400	5	BDL	7	2	BDL	32	46	49
O3/500	500	3	BDL	3	1	BDL	31	37	38

Y (ppm)

sample	depth	NH_4-Ac	Na-OC	HL	NH_4-OxH	H_2O_2	residual	total	bulk
O3/025	25	3	BDL	2	1	BDL	5	10	11
O3/070	70	2	BDL	2	1	BDL	5	10	11
O3/100	100	3	BDL	2	1	BDL	6	12	13
O3/200	200	3	BDL	4	1	1	6	15	16
O3/300	300	5	BDL	3	1	BDL	6	16	19
O3/400	400	3	BDL	3	1	BDL	6	14	17
O3/500	500	3	BDL	3	1	BDL	8	15	17

Zr (ppm)									
sample	depth	NH_4-Ac	Na-OC	HL	NH_4-OxH	H_2O_2	residual	total	bulk
O3/025	25	BDL	BDL	BDL	4	BDL	51	55	66
O3/070	70	BDL	BDL	BDL	2	BDL	55	57	71
O3/100	100	BDL	BDL	BDL	3	BDL	54	57	69
O3/200	200	BDL	BDL	BDL	5	BDL	58	63	80
O3/300	300	BDL	BDL	BDL	4	2	59	65	88
O3/400	400	BDL	BDL	BDL	5	3	65	73	103
O3/500	500	BDL	BDL	BDL	4	3	69	76	101

Co (ppm)									
sample	depth	NH_4-Ac	Na-OC	HL	NH_4-OxH	H_2O_2	residual	total	bulk
O3/025	25	4	BDL	BDL	3	11	35	53	54
O3/070	70	5	BDL	1	4	11	32	53	48
O3/100	100	8	BDL	3	9	10	19	49	44
O3/200	200	16	2	8	11	15	15	67	55
O3/300	300	14	BDL	4	10	BDL	13	41	39
O3/400	400	12	1	4	9	BDL	8	34	29
O3/500	500	9	1	4	11	BDL	10	35	30

Sn (ppm)									
sample	depth	NH_4-Ac	Na-OC	HL	NH_4-OxH	H_2O_2	residual	total	bulk
O3/025	25	BDL	BDL	BDL	BDL	BDL	10	10	BDL
O3/070	70	BDL	BDL	BDL	BDL	BDL	10	10	BDL
O3/100	100	BDL	BDL	BDL	BDL	BDL	BDL	BDL	BDL
O3/200	200	BDL	BDL	BDL	BDL	BDL	BDL	BDL	BDL
O3/300	300	BDL	BDL	BDL	BDL	BDL	BDL	BDL	BDL
O3/400	400	BDL	BDL	BDL	BDL	BDL	BDL	BDL	BDL
O3/500	500	BDL	BDL	BDL	BDL	BDL	10	10	BDL

Sc (ppm)									
sample	depth	NH_4-Ac	Na-OC	HL	NH_4-OxH	H_2O_2	residual	total	bulk
O3/025	25	1.2	BDL	BDL	0.7	BDL	4.4	6.3	7.2
O3/070	70	1.2	BDL	BDL	0.6	BDL	5.6	7.4	7.9
O3/100	100	1.4	BDL	BDL	0.8	BDL	5.8	8	8.6
O3/200	200	1.8	BDL	BDL	1.1	BDL	7.7	10.6	11.5
O3/300	300	2.5	BDL	BDL	1.4	BDL	7.9	11.8	13.6
O3/400	400	2.1	BDL	BDL	1.6	BDL	7.6	11.3	12.7
O3/500	500	1.7	BDL	BDL	1.4	BDL	8.9	12	12.5

Be (ppm)									
sample	depth	NH_4-Ac	Na-OC	HL	NH_4-OxH	H_2O_2	residual	total	bulk
O3/025	25	BDL	BDL	BDL	BDL	BDL	0.8	0.8	1.2
O3/070	70	BDL	BDL	BDL	BDL	BDL	0.9	0.9	1.1
O3/100	100	BDL	BDL	BDL	BDL	BDL	0.8	0.8	1.3
O3/200	200	BDL	BDL	BDL	BDL	BDL	0.7	0.7	1.1
O3/300	300	BDL	BDL	BDL	BDL	BDL	0.6	0.6	1
O3/400	400	BDL	BDL	BDL	BDL	BDL	0.7	0.7	1.1
O3/500	500	BDL	BDL	BDL	BDL	BDL	0.8	0.8	1.2

Ag (ppm)									
sample	depth	NH_4-Ac	Na-OC	HL	NH_4-OxH	H_2O_2	residual	total	bulk
O3/025	25	BDL	BDL	BDL	BDL	BDL	2	2	3
O3/070	70	BDL	BDL	1	BDL	BDL	2	3	3
O3/100	100	BDL	BDL	1	BDL	BDL	3	4	3
O3/200	200	BDL	BDL	2	BDL	BDL	2	5	4
O3/300	300	BDL	BDL	3	BDL	BDL	2	5	5
O3/400	400	BDL	BDL	2	BDL	0	2	5	4
O3/500	500	BDL	BDL	1	BDL	0	3	4	3

APPENDIX. 3

Results of the extraction sequence B

Applied extraction sequence B:

The dissolved minerals in each step (Table 1) were controlled by dissolution kinetics, XRD, and DXRD control (Chapter 3 and 4).

Table 1: *Sequential extraction "B" applied in this study (abbreviations: bn: bornite; ca: calcite; cb: cinnabar; cc: chalcocite; cv: covellite; cp: chalcopyrite; dg: digenite; fh: ferrihydrite; gn: galena; gt: goethite; gy: gypsum; hm: hematite; ilm: ilmenite; jt: jarosite; Na-jt: natrojarosite; mb: molybdenite; mt: magnetite; op: orpiment; py: pyrite; sh: schwertmannite; sl: sphalerite; stb: stibnite; tn: tennantite; tt: tetrahedrite).*

Leach	Preferentially dissolved minerals	References
(1) Water soluble fraction 1.0 g sample into 50ml deionizied H_2O shake for 1 h.	secondary sulfates, e.g., bonattite, chalcanthite, gy, pickeringite, magnesioauberite	chapter 5 and 6; Ribet et al., 1995; Fanfani et al., 1997
(2) exchangeable fraction 1M NH_4-acetate pH 4.5 shake for 2 hrs	ca, vermiculite-type-mixed-layer, adsorbed and exchangeable ions	chapter 5; Gatehouse et al., 1977; Sondag, 1981; Fonseca and Martin, 1986
(3) Fe(III) oxyhydroxides 0.2 M NH_4-oxalate pH 3.0 shake for 1 h. in darkness	sh, 2-line fh, secondary jt, MnO_2	Schwertmann, 1964; Stone, 1987; chapter 4
(4) Fe(III) oxides 0.2 M NH_4-oxalate pH 3.0 heat in water bath 80°C for 2 hours	gt, jt, Na-jt, hm, mt, higher ordered fh's (e.g., 6-line fh)	chapter 3.
(5) organics and secondary Cu-sulfides 35% H_2O_2 heat in water bath for 1 hour	organics , cv, cc-dg	Sondag, 1981;, chapter 5
(6) primary sulfides Combination of $KClO_3$ and HCl, followed by 4 M HNO_3 boiling	py, cp, bn, sl, gn, mb, tt, cb, op, stb	Chao and Sanzolone, 1977; Hall et al., 1996
(7) residual HNO_3, HF, $HClO_4$, HCL digestion	Silicates, residual	Hall et al., 1996; Dold et al., 1996

Analytical conditions

Multi-element (31 elements) analyses were performed in the leach by ICP-ES. The analyses were performed by the X-Ray Assay Laboratories (XRAL) of Toronto, Canada. Of every sample a bulk analysis with the HNO_3, HF, $HCLO_4$, HCL digestion was performed to control the accuracy of the analyses.

Abbreviations:

H_2O	= 1. Step: water leach
NH_4-Ac	= 2. Step: 1 M ammonium acetate leach
NH_4-OxD	= 3. Step: 0.2M ammonium oxalate, darkness leach
NH_4-OxH	= 4. Step: 0.2M ammonium oxalate, heat leach
H_2O_2	= 5. Step: 35 % peroxide leach
sulfide	= 6. Step: $KClO_3$, HCl, 4 M HNO_3 leach
residual	= 7. Step: HNO_3, HF, $HCLO_4$, HCL leach
total	= sum of step 1 to step 7
bulk	= control analysis of a bulk sample with the HNO_3, HF, $HCLO_4$, HCL leach
BDL	= below detection limit

References

Cardoso Fonseca, E., Martin, H. (1986): The selective extraction of Pb and Zn in selected mineral and soil samples, application in geochemical exploration (Portugal). Journal of Geochemical Exploration, v. 26, p. 231-248.

Chao, T.T., (1984): Use of partial dissolution techniques in geochemical exploration. Journal of Geochemical Exploration, v. 20, p. 101-135.

Chao, T.T., Sanzolone, R.F. (1977): Chemical dissolution of sulfide minerals. Journal of Research U.S. Geol.Survey, v. 5, p. 409-412.

Dold, B., Eppinger, K.J., Kölling, M. (1996): Pyrite oxidation and the associated geochemical processes in tailings in the Atacama desert/Chile: The influence of men controlled water input after disuse. Clean technology for the mining industry, Santiago, p. 417 - 427.

Fanfani, L., Zuddas, P., Chessa, A. (1997): Heavy metals speciation analysis as a tool for studying mine tailings weathering. Journal of Geochemical Exploration, v. 58, p. 241-248.

Gatehouse, S., Roussel, D.W., Van Moort, J.C. (1977): Sequential soil analysis in exploration analysis. Journal of Geochemical Exploration, v. 8, p. 483-494.

Hall, G.E.M., Vaive, J.E., Beer, R., Hoashi, M. (1996): Selective leaches revisited, with emphasis on the amorphous Fe oxyhydroxide phase extraction. Journal of Geochemical Exploration, v. 56, p. 59-78.

Ribet, I., Ptacek, C.J., Blowes, D.W., Jambor, J.L. (1995): The potential for metal release by reductive dissolution of weathered mine tailings. Journal of Contaminant Hydrology, v. 17(3), p. 239-273.

Schwertmann, U. (1964): Differenzierung der Eisenoxide des Bodens durch Extraktion mit Ammoniumoxalat Lösung. Zeitschrift für Pflanzenernährung und Bodenkunde, v. 105, p. 194-202.

Sondag, F. (1981): Selective extraction procedures applied to geochemical prospecting in an area contaminated by old mine workings. Journal of Geochemical Exploration, v. 15, p. 645-652.

Stone, A.T. (1987) Microbial metabolites and the reductive dissolution of manganese oxides: Oxalate and pyruvate. Geochimica et Cosmochimica Acta, v. 51; p. 919-925.

Tessier, A., Campbell, P.G.C., Bisson, M. (1979): Sequential extraction procedure for speciation of particulate trace metals. Analytical Chemistry, v. 51, p. 844-851.

Fe (%)

sample	depth	H_2O	NH4-Ac	NH_4-OxD	NH_4-OxH	H_2O_2	sulfide	residual	total	bulk
A2/020	20	BDL	0.06	1.71	1.16	BDL	0.39	1.06	4.38	5.78
A2/050	50	BDL	0.06	1.68	1.82	0.03	1.03	1.68	6.3	7.87
A2/100	100	BDL	0.06	0.84	1.4	0.05	2.2	2.17	6.72	8.15
A2/150	150	BDL	0.1	0.92	1.22	0.05	0.96	1.57	4.82	6.21
A2/200	200	BDL	0.09	1.18	0.99	0.03	0.93	0.86	4.08	4.95
A2/295	295	BDL	0.09	1.2	1.18	0.03	1.68	1.51	5.69	7.3
A2/400	400	BDL	0.08	1.1	1.18	0.02	1.57	1.52	5.47	7.5
A2/500	500	BDL	0.14	1.08	1.07	0.02	1.15	0.75	4.21	5.41
A2/700	700	0.01	0.09	1.4	1.56	0.02	1.83	1.46	6.37	7.58
A2/900	900	0.01	0.1	1.64	1.75	0.07	1.61	1.36	6.54	7.42

Al (%)

sample	depth	H_2O	NH4-Ac	NH_4-OxD	NH_4-OxH	H_2O_2	sulfide	residual	total	bulk
A2/020	20	BDL	0.03	0.05	0.09	0.03	0.28	5.81	6.29	8.03
A2/050	50	BDL	0.04	0.09	0.13	0.05	0.66	5.77	6.74	8.27
A2/100	100	BDL	0.07	0.1	0.09	BDL	0.42	5.68	6.36	8.09
A2/150	150	BDL	0.1	0.15	0.11	BDL	0.43	6.03	6.82	8.33
A2/200	200	BDL	0.05	0.11	0.07	BDL	0.46	5.97	6.66	8.25
A2/295	295	BDL	0.05	0.11	0.07	BDL	0.46	5.9	6.59	8.55
A2/400	400	BDL	0.04	0.08	0.07	BDL	0.43	5.21	5.83	8.58
A2/500	500	BDL	0.04	0.08	0.07	BDL	0.52	5.47	6.18	8.18
A2/700	700	BDL	0.04	0.08	0.08	BDL	0.53	6.05	6.78	8.55
A2/900	900	0.01	0.05	0.12	0.11	BDL	0.69	6.12	7.1	8.24

K (%)

sample	depth	H_2O	NH4-Ac	NH_4-OxD	NH_4-OxH	H_2O_2	sulfide	residual	total	bulk
A2/020	20	0.02	BDL	0.24	0.03	BDL	-	3.83	4.12	5.57
A2/050	50	0.02	BDL	0.19	0.08	0.02	-	3.09	3.4	4.67
A2/100	100	0.03	BDL	0.01	0.02	BDL	-	3.2	3.26	4.59
A2/150	150	0.05	0.01	0.02	0.05	BDL	-	3.16	3.29	4.55
A2/200	200	0.03	0.01	0.02	0.01	BDL	-	3.28	3.35	4.63
A2/295	295	0.04	0.02	0.02	0.01	BDL	-	2.91	3	4.52
A2/400	400	0.03	0.02	0.02	0.01	BDL	-	3.02	3.1	4.75
A2/500	500	0.03	0.02	0.02	0.01	BDL	-	3.19	3.27	4.89
A2/700	700	0.03	0.02	0.02	0.02	BDL	-	3.35	3.44	5.01
A2/900	900	0.03	0.02	0.03	0.02	BDL	-	3.38	3.48	4.79

Mg (%)

sample	depth	H_2O	NH4-Ac	NH_4-OxD	NH_4-OxH	H_2O_2	sulfide	residual	total	bulk
A2/020	20	BDL	BDL	BDL	0.05	BDL	0.22	0.31	0.58	0.7
A2/050	50	0.02	BDL	0.01	0.07	0.01	0.52	0.35	0.98	1.14
A2/100	100	0.02	BDL	BDL	0.02	BDL	0.32	0.4	0.76	0.89
A2/150	150	0.03	BDL	BDL	0.03	BDL	0.32	0.31	0.69	0.81
A2/200	200	0.03	0.01	0.01	0.02	BDL	0.36	0.24	0.67	0.75
A2/295	295	0.02	BDL	0.02	0.03	BDL	0.36	0.33	0.76	0.93
A2/400	400	0.02	0.01	0.02	0.03	0.01	0.35	0.28	0.72	0.94
A2/500	500	BDL	0.02	0.03	0.03	BDL	0.41	0.2	0.69	0.8
A2/700	700	BDL	BDL	0.03	0.03	0.01	0.4	0.29	0.76	0.89
A2/900	900	BDL	0.01	0.03	0.04	BDL	0.53	0.31	0.92	0.99

Na (%)

sample	depth	H_2O	NH4-Ac	NH_4-OxD	NH_4-OxH	H_2O_2	sulfide	residual	total	bulk
A2/020	20	BDL	BDL	BDL	BDL	BDL	BDL	0.56	0.56	0.72
A2/050	50	BDL	BDL	BDL	BDL	BDL	BDL	0.63	0.63	0.81
A2/100	100	BDL	BDL	BDL	BDL	BDL	BDL	0.48	0.48	0.6
A2/150	150	BDL	BDL	BDL	BDL	BDL	BDL	0.79	0.79	1
A2/200	200	BDL	BDL	BDL	BDL	BDL	BDL	0.99	0.99	1.23
A2/295	295	BDL	BDL	BDL	BDL	BDL	BDL	0.67	0.67	0.86
A2/400	400	BDL	BDL	BDL	BDL	BDL	BDL	0.66	0.66	0.89
A2/500	500	BDL	BDL	BDL	BDL	BDL	BDL	0.89	0.89	1.16
A2/700	700	BDL	BDL	BDL	BDL	BDL	BDL	0.69	0.69	0.9
A2/900	900	BDL	BDL	BDL	BDL	BDL	BDL	0.72	0.72	0.86

Ca (%)

sample	depth	H_2O	NH4-Ac	NH_4-OxD	NH_4-OxH	H_2O_2	sulfide	residual	total	bulk
A2/020	20	0.02	BDL	0.01	BDL	BDL	0.06	0.09	0.18	0.22
A2/050	50	0.01	BDL	0.01	BDL	0.02	0.07	0.17	0.28	0.37
A2/100	100	0.06	BDL	0.01	BDL	0.04	0.07	0.08	0.26	0.29
A2/150	150	0.13	0.01	BDL	BDL	0.04	0.05	0.1	0.33	0.38
A2/200	200	0.13	0.03	BDL	0.01	0.05	0.06	0.09	0.37	0.41
A2/295	295	0.12	0.03	BDL	BDL	0.06	0.06	0.12	0.39	0.46
A2/400	400	0.05	0.04	BDL	BDL	0.06	0.06	0.09	0.3	0.39
A2/500	500	0.07	0.08	BDL	BDL	0.06	0.07	0.1	0.38	0.47
A2/700	700	0.04	0.05	BDL	BDL	0.08	0.07	0.08	0.32	0.37
A2/900	900	0.06	0.08	BDL	BDL	0.08	0.06	0.09	0.37	0.41

Ti (%)

sample	depth	H_2O	NH4-Ac	NH_4-OxD	NH_4-OxH	H_2O_2	sulfide	residual	total	bulk
A2/020	20	BDL	BDL	BDL	0.01	BDL	0.02	0.13	0.16	0.21
A2/050	50	BDL	BDL	BDL	0.01	BDL	0.05	0.19	0.25	0.31
A2/100	100	BDL	BDL	BDL	0.01	BDL	0.03	0.18	0.22	0.27
A2/150	150	BDL	BDL	BDL	BDL	BDL	0.03	0.15	0.18	0.23
A2/200	200	BDL	BDL	BDL	0.01	BDL	0.04	0.12	0.17	0.2
A2/295	295	BDL	BDL	BDL	0.02	BDL	0.03	0.16	0.21	0.28
A2/400	400	BDL	BDL	BDL	0.01	BDL	0.03	0.17	0.21	0.29
A2/500	500	BDL	BDL	BDL	0.01	BDL	0.04	0.13	0.18	0.24
A2/700	700	BDL	BDL	BDL	0.02	BDL	0.04	0.17	0.23	0.3
A2/900	900	BDL	BDL	BDL	0.02	BDL	0.06	0.19	0.27	0.31

P (%)

sample	depth	H_2O	NH4-Ac	NH_4-OxD	NH_4-OxH	H_2O_2	sulfide	residual	total	bulk
A2/020	20	BDL	BDL	0.03	BDL	BDL	0.02	0.01	0.06	0.07
A2/050	50	BDL	BDL	0.04	BDL	BDL	0.03	BDL	0.07	0.07
A2/100	100	BDL	BDL	0.03	BDL	BDL	0.04	0.01	0.08	0.06
A2/150	150	BDL	BDL	0.03	BDL	BDL	0.03	0.01	0.07	0.06
A2/200	200	BDL	BDL	0.03	BDL	BDL	0.03	0.01	0.07	0.05
A2/295	295	BDL	BDL	0.03	BDL	BDL	0.03	BDL	0.06	0.04
A2/400	400	BDL	BDL	0.03	BDL	BDL	0.03	0.01	0.07	0.05
A2/500	500	BDL	BDL	0.03	BDL	BDL	0.03	0.01	0.07	0.06
A2/700	700	BDL	BDL	0.03	BDL	BDL	0.03	0.01	0.07	0.06
A2/900	900	BDL	BDL	0.04	BDL	BDL	0.03	0.02	0.09	0.08

Cu (ppm)

sample	depth	H_2O	NH4-Ac	NH_4-OxD	NH_4-OxH	H_2O_2	sulfide	residual	total	bulk
A2/020	20	21.1	17.3	113	9.4	42.7	221	11.2	436	442
A2/050	50	73.3	54.2	169	24.6	260	775	13.6	1370	1360
A2/100	100	472	217	308	95.6	1550	435	103	3181	3140
A2/150	150	359	213	343	69.2	1050	217	13.1	2264	2160
A2/200	200	128	334	314	44.2	1190	382	11.5	2404	2370
A2/295	295	14.6	406	173	55.6	2440	714	60.6	3864	3850
A2/400	400	8.5	327	191	52.3	2230	1070	27.5	3906	4110
A2/500	500	5.6	206	83.3	22.5	1050	350	12.1	1730	1760
A2/700	700	18.6	368	199	59.4	1840	1030	25.6	3541	3710
A2/900	900	18.6	500	264	37.2	1090	407	12.8	2330	2250

Zn (ppm)

sample	depth	H_2O	NH4-Ac	NH_4-OxD	NH_4-OxH	H_2O_2	sulfide	residual	total	bulk
A2/020	20	1.2	BDL	2.7	5	BDL	12.1	11.9	32.9	43.8
A2/050	50	2.3	0.9	3.3	6.1	2.5	25	16.1	56.2	60.3
A2/100	100	7.1	0.7	10.8	7.6	11.3	20.7	18.2	76.4	68.2
A2/150	150	14	2.1	8.1	14.8	9.2	14.1	18.8	81.1	82.5
A2/200	200	70	28.5	97.1	40.7	38.1	23.5	27.3	325.2	321
A2/295	295	19.1	36.5	99.5	36.5	45	30.7	17.7	285	299
A2/400	400	1.1	23.7	77.9	35.1	76.7	44.5	18	277	308
A2/500	500	1.4	29.8	94.2	43.1	54.8	29.1	22	274.4	288
A2/700	700	2.4	25.8	109	48.8	66.5	40.4	18.9	311.8	333
A2/900	900	2	25.5	118	59.2	37.1	27.3	29.6	298.7	286

Mn (ppm)

sample	depth	H_2O	NH4-Ac	NH_4-OxD	NH_4-OxH	H_2O_2	sulfide	residual	total	bulk
A2/020	20	4	BDL	9	19	BDL	52	34	118	141
A2/050	50	8	2	12	24	5	104	50	205	241
A2/100	100	8	BDL	7	16	3	59	36	129	148
A2/150	150	28	3	13	21	3	44	26	138	148
A2/200	200	257	68	254	214	52	59	19	923	909
A2/295	295	111	44	207	135	77	92	30	696	750
A2/400	400	36	156	257	164	109	112	28	862	975
A2/500	500	5	128	333	211	94	82	20	873	953
A2/700	700	7	60	299	198	124	109	27	824	931
A2/900	900	5	60	275	196	70	87	28	721	727

Cr (ppm)

sample	depth	H_2O	NH4-Ac	NH_4-OxD	NH_4-OxH	H_2O_2	sulfide	residual	total	bulk
A2/020	20	BDL	BDL	3	5	BDL	6	3	17	8
A2/050	50	BDL	BDL	3	8	BDL	13	6	30	23
A2/100	100	BDL	BDL	3	6	BDL	8	8	25	16
A2/150	150	BDL	BDL	3	3	BDL	13	6	25	13
A2/200	200	BDL	BDL	3	3	BDL	10	3	19	8
A2/295	295	BDL	BDL	4	4	BDL	9	5	22	13
A2/400	400	BDL	BDL	4	4	BDL	8	5	21	14
A2/500	500	BDL	BDL	4	5	BDL	13	3	25	12
A2/700	700	BDL	BDL	4	7	BDL	10	6	27	21
A2/900	900	BDL	BDL	6	8	BDL	8	5	27	16

Pb (ppm)

sample	depth	H_2O	NH4-Ac	NH_4-OxD	NH_4-OxH	H_2O_2	sulfide	residual	total	bulk
A2/020	20	BDL	BDL	9	6	BDL	5	BDL	20	21
A2/050	50	BDL	BDL	12	BDL	BDL	3	BDL	15	25
A2/100	100	BDL	BDL	6	5	BDL	9	BDL	20	28
A2/150	150	BDL	BDL	BDL	10	BDL	8	BDL	18	33
A2/200	200	BDL	2	14	3	BDL	10	BDL	29	33
A2/295	295	BDL	3	16	5	BDL	21	BDL	45	44
A2/400	400	BDL	5	12	5	BDL	17	BDL	39	40
A2/500	500	BDL	6	8	3	BDL	9	BDL	26	34
A2/700	700	BDL	6	10	9	2	22	BDL	49	61
A2/900	900	BDL	4	17	9	BDL	26	BDL	56	50

Mo (ppm)

sample	depth	H_2O	NH4-Ac	NH_4-OxD	NH_4-OxH	H_2O_2	sulfide	residual	total	bulk
A2/020	20	BDL	BDL	37	3	27	6	3	76	80
A2/050	50	BDL	BDL	15	BDL	13	7	BDL	35	35
A2/100	100	BDL	BDL	1	BDL	BDL	32	5	38	35
A2/150	150	BDL	BDL	5	BDL	BDL	49	4	58	59
A2/200	200	BDL	BDL	4	BDL	BDL	69	7	80	58
A2/295	295	BDL	BDL	3	BDL	BDL	51	6	60	61
A2/400	400	BDL	BDL	2	BDL	BDL	64	9	75	64
A2/500	500	BDL	BDL	1	BDL	BDL	41	3	45	44
A2/700	700	BDL	BDL	1	BDL	BDL	49	7	57	62
A2/900	900	BDL	BDL	4	BDL	BDL	28	3	35	32

V (ppm)

sample	depth	H_2O	NH4-Ac	NH_4-OxD	NH_4-OxH	H_2O_2	sulfide	residual	total	bulk
A2/020	20	BDL	BDL	8	14	BDL	7	52	81	99
A2/050	50	BDL	BDL	11	19	BDL	19	70	119	149
A2/100	100	BDL	BDL	6	15	BDL	16	78	115	137
A2/150	150	BDL	BDL	6	9	BDL	13	61	89	113
A2/200	200	BDL	BDL	5	10	BDL	16	50	81	97
A2/295	295	BDL	BDL	9	14	BDL	13	68	104	133
A2/400	400	BDL	BDL	9	14	BDL	13	68	104	138
A2/500	500	BDL	BDL	9	15	BDL	17	47	88	109
A2/700	700	BDL	BDL	11	23	BDL	17	67	118	139
A2/900	900	BDL	BDL	14	24	BDL	21	66	125	141

As (ppm)

sample	depth	H_2O	NH4-Ac	NH_4-OxD	NH_4-OxH	H_2O_2	sulfide	residual	total	bulk
A2/020	20	BDL	BDL	13	BDL	BDL	BDL	BDL	13	38
A2/050	50	BDL	BDL	25	BDL	BDL	5	BDL	30	BDL
A2/100	100	BDL	BDL	15	BDL	BDL	25	BDL	40	33
A2/150	150	BDL	BDL	41	5	BDL	26	BDL	72	BDL
A2/200	200	BDL	BDL	53	BDL	BDL	51	BDL	104	105
A2/295	295	BDL	BDL	46	4	BDL	59	BDL	109	42
A2/400	400	BDL	4	33	3	BDL	89	BDL	129	44
A2/500	500	BDL	BDL	21	BDL	BDL	52	BDL	73	38
A2/700	700	BDL	5	36	4	BDL	83	BDL	128	119
A2/900	900	BDL	7	64	BDL	BDL	52	BDL	123	77

Ba (ppm)

sample	depth	H_2O	NH4-Ac	NH_4-OxD	NH_4-OxH	H_2O_2	sulfide	residual	total	bulk
A2/020	20	BDL	BDL	53	20	BDL	12	617	702	994
A2/050	50	BDL	BDL	20	34	2	22	420	498	719
A2/100	100	1	4	11	26	BDL	16	364	422	625
A2/150	150	BDL	6	10	30	BDL	22	386	454	649
A2/200	200	1	15	13	21	1	20	405	476	679
A2/295	295	BDL	15	10	16	BDL	17	367	425	633
A2/400	400	BDL	16	7	13	BDL	15	368	419	668
A2/500	500	BDL	20	8	14	BDL	19	420	481	737
A2/700	700	1	30	8	26	1	24	446	536	777
A2/900	900	BDL	22	12	14	BDL	24	458	530	732

Sr (ppm)

sample	depth	H_2O	NH4-Ac	NH_4-OxD	NH_4-OxH	H_2O_2	sulfide	residual	total	bulk
A2/020	20	BDL	BDL	3.8	6.9	0.7	15.9	73.4	101	145
A2/050	50	BDL	BDL	3.5	2.6	1.1	4.1	69.3	80.6	113
A2/100	100	0.6	BDL	1.4	2.5	1.4	3.5	52.6	62	89.1
A2/150	150	0.9	BDL	0.5	4.1	1.1	2.7	73.2	82.5	119
A2/200	200	1.1	0.7	1.2	1.3	1.7	2	81.7	89.7	131
A2/295	295	1.3	0.8	0.7	1	2.1	2.3	69	77.2	114
A2/400	400	1.3	2	0.6	0.8	1.8	1.9	59.4	67.8	113
A2/500	500	1.4	3	0.5	0.7	1.4	1.8	74.8	83.6	131
A2/700	700	1.2	2.5	0.6	1.1	2.2	2.1	59.1	68.8	99.5
A2/900	900	1	2.8	0.9	1	2.7	2.8	59.8	71	94.5

Ni (ppm)

sample	depth	H_2O	NH4-Ac	NH_4-OxD	NH_4-OxH	H_2O_2	sulfide	residual	total	bulk
A2/020	20	BDL	BDL	2	2	BDL	5	4	13	14
A2/050	50	BDL	BDL	4	BDL	BDL	13	5	22	26
A2/100	100	1	BDL	2	1	BDL	11	6	21	26
A2/150	150	1	BDL	BDL	BDL	BDL	11	5	17	20
A2/200	200	2	1	4	2	1	9	4	23	19
A2/295	295	BDL	BDL	4	2	2	10	4	22	26
A2/400	400	BDL	1	4	1	2	10	4	22	24
A2/500	500	BDL	1	4	2	2	11	4	24	22
A2/700	700	BDL	BDL	5	1	2	12	4	24	27
A2/900	900	BDL	1	6	BDL	2	11	4	24	26

Zr (ppm)

sample	depth	H_2O	NH4-Ac	NH_4-OxD	NH_4-OxH	H_2O_2	sulfide	residual	total	bulk
A2/020	20	BDL	BDL	2.8	2.3	BDL	BDL	0.9	6	11.2
A2/050	50	BDL	BDL	7.3	BDL	BDL	BDL	1.5	8.8	35
A2/100	100	BDL	BDL	2.3	0.6	BDL	0.5	2.8	6.2	18.2
A2/150	150	BDL	BDL	BDL	0.6	BDL	BDL	2.2	2.8	15.8
A2/200	200	BDL	BDL	2.5	0.5	BDL	BDL	1.9	4.9	17.4
A2/295	295	BDL	BDL	3.9	1.7	BDL	BDL	1.8	7.4	46.1
A2/400	400	BDL	BDL	3.8	BDL	BDL	BDL	1.7	5.5	51.3
A2/500	500	BDL	BDL	3.1	1.4	BDL	BDL	2	6.5	19.2
A2/700	700	BDL	BDL	4.5	BDL	BDL	0.5	1.9	6.9	45
A2/900	900	BDL	BDL	7.2	BDL	BDL	BDL	1.8	9	48.7

Co (ppm)

sample	depth	H_2O	NH4-Ac	NH_4-OxD	NH_4-OxH	H_2O_2	sulfide	residual	total	bulk
A2/020	20	BDL	BDL	BDL	BDL	BDL	BDL	BDL	BDL	3
A2/050	50	BDL	BDL	BDL	BDL	BDL	3	1	4	4
A2/100	100	1	BDL	BDL	BDL	2	12	BDL	15	14
A2/150	150	2	BDL	BDL	BDL	BDL	5	BDL	7	8
A2/200	200	3	BDL	1	BDL	1	3	1	9	11
A2/295	295	1	1	2	BDL	2	7	BDL	13	10
A2/400	400	BDL	BDL	BDL	BDL	1	5	BDL	6	10
A2/500	500	BDL	BDL	1	BDL	1	5	BDL	7	9
A2/700	700	BDL	BDL	BDL	BDL	3	8	BDL	11	11
A2/900	900	BDL	BDL	1	BDL	2	6	1	10	11

Sn (ppm)

sample	depth	H_2O	NH4-Ac	NH_4-OxD	NH_4-OxH	H_2O_2	sulfide	residual	total	bulk
A2/020	20	BDL	BDL	BDL	BDL	BDL	13	BDL	13	BDL
A2/050	50	BDL	BDL	BDL	BDL	BDL	15	BDL	15	33
A2/100	100	BDL	BDL	BDL	BDL	BDL	17	BDL	17	26
A2/150	150	BDL	BDL	BDL	BDL	BDL	18	BDL	18	BDL
A2/200	200	BDL	BDL	BDL	BDL	BDL	19	BDL	19	BDL
A2/295	295	BDL	BDL	BDL	BDL	BDL	20	BDL	20	29
A2/400	400	BDL	BDL	BDL	BDL	BDL	18	BDL	18	27
A2/500	500	BDL	BDL	BDL	BDL	BDL	20	BDL	20	14
A2/700	700	BDL	BDL	BDL	BDL	BDL	18	BDL	18	30
A2/900	900	BDL	BDL	BDL	BDL	BDL	18	BDL	18	35

W (ppm)

sample	depth	H_2O	NH4-Ac	NH_4-OxD	NH_4-OxH	H_2O_2	sulfide	residual	total	bulk
A2/020	20	BDL	BDL	BDL	11	BDL	BDL	29	40	42
A2/050	50	BDL	BDL	10	BDL	BDL	BDL	19	29	16
A2/100	100	BDL	BDL	BDL	BDL	BDL	BDL	26	26	28
A2/150	150	BDL	BDL	BDL	BDL	BDL	BDL	20	20	17
A2/200	200	BDL	BDL	BDL	BDL	BDL	BDL	14	14	BDL
A2/295	295	BDL	BDL	BDL	BDL	BDL	BDL	20	20	13
A2/400	400	BDL	BDL	BDL	BDL	BDL	BDL	19	19	29
A2/500	500	BDL	BDL	BDL	BDL	BDL	BDL	14	14	BDL
A2/700	700	BDL	BDL	11	BDL	BDL	BDL	20	31	22
A2/900	900	BDL	BDL	11	BDL	BDL	BDL	21	32	16

La (ppm)

sample	depth	H_2O	NH4-Ac	NH_4-OxD	NH_4-OxH	H_2O_2	sulfide	residual	total	bulk
A2/020	20	BDL	BDL	3.8	3.2	BDL	4.3	5.8	17.1	15.9
A2/050	50	BDL	BDL	8.9	BDL	BDL	4.4	6.1	19.4	16.9
A2/100	100	BDL	BDL	2.5	1.3	BDL	2	4.9	10.7	17.8
A2/150	150	BDL	BDL	BDL	2.6	BDL	3	7.8	13.4	18.2
A2/200	200	BDL	BDL	3.9	2.7	0.7	3.9	4.7	15.9	17.8
A2/295	295	BDL	BDL	4.7	2.6	BDL	2.6	7.5	17.4	17.9
A2/400	400	BDL	BDL	4.2	1.3	BDL	2.6	3.7	11.8	16.5
A2/500	500	BDL	BDL	3.9	2.4	0.5	3.5	4.3	14.6	17.2
A2/700	700	BDL	BDL	5.3	0.8	BDL	2.9	8.8	17.8	18.3
A2/900	900	BDL	BDL	8.6	BDL	BDL	3.4	7.6	19.6	18.3

Y (ppm)

sample	depth	H_2O	NH4-Ac	NH_4-OxD	NH_4-OxH	H_2O_2	sulfide	residual	total	bulk
A2/020	20	BDL	BDL	BDL	BDL	BDL	0.8	1.2	2	3.8
A2/050	50	BDL	BDL	BDL	BDL	BDL	1.3	1.8	3.1	5.2
A2/100	100	BDL	BDL	BDL	BDL	BDL	1.1	1.1	2.2	4.8
A2/150	150	BDL	BDL	BDL	BDL	BDL	0.9	1.4	2.3	5.5
A2/200	200	BDL	1.1	1	0.5	BDL	1.1	1.2	4.9	6.6
A2/295	295	BDL	BDL	1	BDL	BDL	1	1.1	3.1	5.9
A2/400	400	BDL	BDL	0.7	BDL	BDL	1	0.7	2.4	6.2
A2/500	500	BDL	BDL	1	BDL	BDL	1.2	1	3.2	5.7
A2/700	700	BDL	BDL	0.7	0.5	BDL	1.3	1.5	4	7.1
A2/900	900	BDL	BDL	1.4	BDL	BDL	1.3	1.4	4.1	7

Sc (ppm)

sample	depth	H_2O	NH4-Ac	NH_4-OxD	NH_4-OxH	H_2O_2	sulfide	residual	total	bulk
A2/020	20	BDL	BDL	BDL	BDL	BDL	0.5	4.1	4.6	7.1
A2/050	50	BDL	BDL	0.9	BDL	BDL	1.8	6.9	9.6	13.4
A2/100	100	BDL	BDL	BDL	BDL	BDL	0.9	6.8	7.7	11.6
A2/150	150	BDL	BDL	BDL	BDL	BDL	0.9	5.3	6.2	9.4
A2/200	200	BDL	BDL	BDL	BDL	BDL	1.1	4	5.1	7.6
A2/295	295	BDL	BDL	BDL	BDL	BDL	0.8	6.2	7	11.5
A2/400	400	BDL	BDL	BDL	BDL	BDL	0.9	5.2	6.1	11.7
A2/500	500	BDL	BDL	BDL	BDL	BDL	1.4	4.1	5.5	8.3
A2/700	700	BDL	BDL	0.5	BDL	BDL	1.4	6.5	8.4	11.6
A2/900	900	BDL	BDL	0.8	BDL	BDL	2	6.4	9.2	12.1

Be (ppm)

sample	depth	H_2O	NH4-Ac	NH_4-OxD	NH_4-OxH	H_2O_2	sulfide	residual	total	bulk
A2/020	20	BDL	BDL	BDL	BDL	BDL	BDL	0.8	0.8	1
A2/050	50	BDL	BDL	BDL	BDL	BDL	BDL	0.9	0.9	1.3
A2/100	100	BDL	BDL	BDL	BDL	BDL	BDL	1	1	1.5
A2/150	150	BDL	BDL	BDL	BDL	BDL	BDL	0.9	0.9	1.5
A2/200	200	BDL	BDL	BDL	BDL	BDL	BDL	0.9	0.9	1.5
A2/295	295	BDL	BDL	BDL	BDL	BDL	BDL	0.9	0.9	1.5
A2/400	400	BDL	BDL	BDL	BDL	BDL	BDL	0.8	0.8	1.4
A2/500	500	BDL	BDL	BDL	BDL	BDL	BDL	0.8	0.8	1.4
A2/700	700	BDL	BDL	BDL	BDL	BDL	BDL	0.9	0.9	1.4
A2/900	900	BDL	BDL	BDL	BDL	BDL	BDL	0.9	0.9	1.4

Ag (ppm)

sample	depth	H_2O	NH4-Ac	NH_4-OxD	NH_4-OxH	H_2O_2	sulfide	residual	total	bulk
A2/020	20	BDL	BDL	BDL	BDL	BDL	0.6	BDL	0.6	0.4
A2/050	50	BDL	BDL	BDL	BDL	BDL	0.8	0.3	1.1	0.7
A2/100	100	BDL	BDL	BDL	BDL	BDL	0.8	0.3	1.1	0.7
A2/150	150	BDL	BDL	BDL	BDL	BDL	0.6	BDL	0 6	0.4
A2/200	200	0.3	BDL	BDL	BDL	BDL	0.6	BDL	0.9	0.5
A2/295	295	BDL	BDL	BDL	BDL	BDL	1.2	BDL	1.2	0.7
A2/400	400	BDL	BDL	BDL	BDL	BDL	0.9	0.3	1.2	0.7
A2/500	500	BDL	BDL	BDL	BDL	BDL	0.4	BDL	0.4	0.2
A2/700	700	BDL	BDL	BDL	BDL	BDL	1.3	0.4	1.7	1.2
A2/900	900	BDL	BDL	BDL	BDL	BDL	0.8	BDL	0.8	0.7

Fe (%)

sample	depth	H_2O	NH4-Ac	NH_4-OxD	NH_4-OxH	H_2O_2	sulfide	residual	total	bulk
A3/020	20	BDL	0.06	1.49	2.02	0.03	0.63	1.13	5.36	6.19
A3/050	50	BDL	0.04	1.23	1.66	0.02	0.5	0.99	4.44	5.6
A3/070	70	0.01	0.02	0.72	1.49	BDL	0.61	1.12	3.97	4.78
A3/100	100	0.01	0.03	0.61	0.94	0.03	1.25	1.03	3.9	4.73
A3/160	160	BDL	0.04	0.62	1.15	0.02	1.54	1.14	4.51	5.55
A3/190	190	BDL	0.06	0.75	1.08	0.02	1.26	1	4.17	5.19
A3/300	300	BDL	0.08	1.06	1.4	0.08	1.28	1.2	5.1	6.37
A3/430	430	BDL	0.11	1.53	1.69	0.19	1.51	1.35	6.38	7.51
A3/490	490	BDL	0.17	1.35	1.35	0.08	1.26	0.87	5.08	6.29
A3/700	700	0.01	0.16	1.68	1.59	0.16	1.37	1.01	5.98	6.75
A3/900	900	0.02	0.14	1.75	1.51	0.11	1.53	1.06	6.12	7.17

Al (%)

sample	depth	H_2O	NH4-Ac	NH_4-OxD	NH_4-OxH	H_2O_2	sulfide	residual	total	bulk
A3/020	20	BDL	0.05	0.11	0.18	BDL	0.33	5.68	6.35	7.49
A3/050	50	BDL	0.05	0.13	0.17	BDL	0.34	4.67	5.36	7.64
A3/070	70	0.01	0.03	0.06	0.14	BDL	0.24	5.94	6.42	7.51
A3/100	100	0.02	0.04	0.08	0.08	BDL	0.31	5.52	6.05	7.26
A3/160	160	BDL	0.04	0.08	0.11	BDL	0.39	5.63	6.25	7.81
A3/190	190	BDL	0.03	0.07	0.08	BDL	0.38	5.59	6.15	7.73
A3/300	300	BDL	0.05	0.11	0.11	BDL	0.44	5.65	6.36	8.4
A3/430	430	BDL	0.06	0.15	0.12	BDL	0.55	6.32	7.2	8.71
A3/490	490	BDL	0.05	0.11	0.1	BDL	0.54	5.6	6.4	8.7
A3/700	700	BDL	0.06	0.16	0.14	BDL	0.62	6.56	7.54	8.97
A3/900	900	0.02	0.06	0.13	0.13	BDL	0.74	6.23	7.31	8.84

K (%)

sample	depth	H_2O	NH4-Ac	NH_4-OxD	NH_4-OxH	H_2O_2	sulfide	residual	total	bulk
A3/020	20	0.01	BDL	0.17	0.18	BDL	-	3.22	3.58	4.5
A3/050	50	0.02	0.01	0.17	0.15	BDL	-	2.77	3.12	4.78
A3/070	70	BDL	BDL	0.08	0.16	BDL	-	3.39	3.63	4.6
A3/100	100	0.01	BDL	0.03	0.02	BDL	-	3.11	3.17	4.32
A3/160	160	0.02	BDL	0.02	0.02	BDL	-	3.3	3.36	4.71
A3/190	190	0.02	BDL	0.02	0.01	BDL	-	3.43	3.48	5.36
A3/300	300	0.04	0.01	0.01	0.02	BDL	-	3.17	3.25	4.63
A3/430	430	0.05	0.02	0.02	0.02	BDL	-	3.35	3.46	4.83
A3/490	490	0.04	0.03	0.02	0.02	BDL	-	3.03	3.14	4.81
A3/700	700	0.04	0.03	0.03	0.03	BDL	-	3.33	3.46	4.94
A3/900	900	0.04	0.03	0.03	0.02	BDL	-	3.3	3.42	4.99

Mg (%)

sample	depth	H_2O	NH4-Ac	NH_4-OxD	NH_4-OxH	H_2O_2	sulfide	residual	total	bulk
A3/020	20	0.05	BDL	BDL	0.09	BDL	0.23	0.32	0.69	0.82
A3/050	50	0.05	BDL	0.02	0.09	BDL	0.22	0.28	0.66	0.8
A3/070	70	0.05	BDL	BDL	0.08	BDL	0.18	0.36	0.67	0.75
A3/100	100	0.04	BDL	BDL	0.03	BDL	0.25	0.34	0.66	0.77
A3/160	160	0.03	BDL	BDL	0.04	BDL	0.31	0.35	0.73	0.86
A3/190	190	0.02	BDL	BDL	0.03	BDL	0.3	0.3	0.65	0.79
A3/300	300	0.02	BDL	0.01	0.04	BDL	0.34	0.3	0.71	0.86
A3/430	430	0.03	BDL	0.03	0.05	BDL	0.42	0.36	0.89	1
A3/490	490	0.01	0.02	0.04	0.04	BDL	0.42	0.25	0.78	0.93
A3/700	700	BDL	0.02	0.04	0.05	BDL	0.47	0.31	0.89	1.01
A3/900	900	BDL	0.02	0.03	0.04	BDL	0.57	0.29	0.95	1.06

Na (%)

sample	depth	H_2O	NH4-Ac	NH_4-OxD	NH_4-OxH	H_2O_2	sulfide	residual	total	bulk
A3/020	20	BDL	BDL	BDL	BDL	BDL	BDL	0.77	0.77	0.95
A3/050	50	BDL	BDL	BDL	BDL	BDL	BDL	0.61	0.61	0.84
A3/070	70	BDL	BDL	BDL	BDL	BDL	BDL	0.64	0.64	0.78
A3/100	100	BDL	BDL	BDL	BDL	BDL	BDL	0.61	0.61	0.75
A3/160	160	BDL	BDL	BDL	BDL	BDL	BDL	0.6	0.6	0.72
A3/190	190	BDL	BDL	BDL	BDL	BDL	BDL	0.59	0.59	0.74
A3/300	300	BDL	BDL	BDL	BDL	BDL	BDL	0.78	0.78	0.99
A3/430	430	BDL	BDL	BDL	BDL	BDL	BDL	0.68	0.68	0.89
A3/490	490	BDL	BDL	BDL	BDL	BDL	BDL	0.82	0.82	1.12
A3/700	700	BDL	BDL	BDL	BDL	BDL	BDL	0.78	0.78	1
A3/900	900	0.01	BDL	BDL	BDL	BDL	BDL	0.78	0.79	0.99

Ca (%)

sample	depth	H_2O	NH4-Ac	NH_4-OxD	NH_4-OxH	H_2O_2	sulfide	residual	total	bulk
A3/020	20	0.12	BDL	0.01	0.02	0.03	0.04	0.11	0.33	0.37
A3/050	50	0.09	0.01	0.01	0.01	0.04	0.04	0.08	0.28	0.32
A3/070	70	0.05	BDL	0.01	0.01	0.03	0.04	0.11	0.25	0.28
A3/100	100	BDL	BDL	0.01	0.01	0.03	0.05	0.09	0.19	0.23
A3/160	160	0.02	BDL	0.01	0.01	0.03	0.05	0.11	0.23	0.27
A3/190	190	0.05	BDL	BDL	BDL	0.03	0.05	0.1	0.23	0.3
A3/300	300	0.03	BDL	BDL	BDL	0.06	0.06	0.09	0.24	0.29
A3/430	430	0.11	0.02	BDL	BDL	0.08	0.05	0.07	0.33	0.39
A3/490	490	0.08	0.12	BDL	BDL	0.09	0.07	0.11	0.47	0.56
A3/700	700	0.1	0.13	BDL	BDL	0.1	0.06	0.09	0.48	0.54
A3/900	900	0.07	0.11	BDL	BDL	0.09	0.06	0.09	0.42	0.48

Tl (%)

sample	depth	H_2O	NH4-Ac	NH_4-OxD	NH_4-OxH	H_2O_2	sulfide	residual	total	bulk
A3/020	20	BDL	BDL	BDL	0.02	BDL	0.02	0.15	0.19	0.21
A3/050	50	BDL	BDL	BDL	0.01	BDL	0.02	0.12	0.15	0.21
A3/070	70	BDL	BDL	BDL	0.02	BDL	0.02	0.13	0.17	0.18
A3/100	100	BDL	BDL	BDL	BDL	BDL	0.02	0.12	0.14	0.18
A3/160	160	BDL	BDL	BDL	0.01	BDL	0.03	0.13	0.17	0.2
A3/190	190	BDL	BDL	BDL	0.01	BDL	0.03	0.12	0.16	0.18
A3/300	300	BDL	BDL	BDL	0.02	BDL	0.03	0.15	0.2	0.23
A3/430	430	BDL	BDL	BDL	0.02	BDL	0.04	0.16	0.22	0.25
A3/490	490	BDL	BDL	BDL	0.02	BDL	0.04	0.15	0.21	0.25
A3/700	700	BDL	BDL	BDL	0.02	BDL	0.05	0.18	0.25	0.27
A3/900	900	BDL	BDL	BDL	0.02	BDL	0.06	0.18	0.26	0.29

P (%)

sample	depth	H-O	NH4-Ac	NH_4-OxD	NH_2-OxH	H_2O_2	sulfide	residual	total	bulk
A3/020	20	BDL	BDL	0.03	BDL	BDL	0.02	0.01	0.06	0.07
A3/050	50	BDL	BDL	0.03	BDL	BDL	0.02	0.01	0.06	0.07
A3/070	70	BDL	BDL	0.02	BDL	BDL	0.03	0.01	0.06	0.05
A3/100	100	BDL	BDL	0.02	BDL	BDL	0.03	0.01	0.06	0.04
A3/160	160	BDL	BDL	0.02	BDL	BDL	0.03	0.01	0.06	0.04
A3/190	190	BDL	BDL	0.02	BDL	BDL	0.03	0.01	0.06	0.03
A3/300	300	BDL	BDL	0.03	BDL	BDL	0.03	0.01	0.07	0.06
A3/430	430	BDL	BDL	0.05	BDL	BDL	0.03	0.01	0.09	0.08
A3/490	490	BDL	BDL	0.04	BDL	BDL	0.03	0.01	0.08	0.07
A3/700	700	BDL	BDL	0.04	BDL	BDL	0.03	0.01	0.08	0.08
A3/900	900	BDL	BDL	0.04	BDL	BDL	0.03	0.01	0.08	0.08

Cu (ppm)

sample	depth	H_2O	NH4-Ac	NH_4-OxD	NH_4-OxH	H_2O_2	sulfide	residual	total	bulk
A3/020	20	78.8	28	142	60.6	319	220	12.4	861	825
A3/050	50	59.1	41.6	135	29.2	300	442	8.8	1016	1030
A3/070	70	141	25.2	76.9	61.1	1380	292	18.1	1994	1830
A3/100	100	345	80.2	152	49.7	1530	416	33.1	2606	2580
A3/160	160	403	148	178	63.9	1900	539	86.1	3318	3230
A3/190	190	379	281	256	55.5	2000	719	49.1	3740	3950
A3/300	300	77.2	190	228	22	1330	204	18.5	2070	2070
A3/430	430	133	283	207	36	704	143	11.6	1518	1530
A3/490	490	9.8	435	144	16	732	179	8.8	1525	1540
A3/700	700	13.8	602	240	22.3	787	165	6.2	1836	1820
A3/900	900	17.5	502	156	27.3	839	194	7.4	1743	1750

Zn (ppm)

sample	depth	H_2O	NH4-Ac	NH_4-OxD	NH_4-OxH	H_2O_2	sulfide	residual	total	bulk
A3/020	20	5.6	0.5	6.6	10.2	2.5	14.4	16.9	56.7	55.7
A3/050	50	4.2	0.8	5.3	7.6	2.7	13.7	15.4	49.7	48.3
A3/070	70	5.2	BDL	2.7	6.4	4	10.3	14.2	42.8	44.8
A3/100	100	8	BDL	4.8	6.1	7.2	15.4	15	56.5	59.2
A3/160	160	8.2	0.7	5.5	7.5	6.8	16.2	14.9	59.8	61
A3/190	190	12.3	1.7	12.4	11.4	8.1	16.2	12.5	74.6	81.5
A3/300	300	37.3	16.7	40.6	24.9	13.8	16.8	18.8	168.9	177
A3/430	430	62.1	24.2	86.9	37.3	24.4	20.1	21.5	276.5	274
A3/490	490	2.1	52.6	132	56.3	52.6	28.6	25.5	349.7	364
A3/700	700	2.6	60.3	175	66.5	41	25.8	29.9	401.1	414
A3/900	900	3.1	43.2	148	54.9	37.4	25.8	26.8	339.2	362

Mn (ppm)

sample	depth	H_2O	NH4-Ac	NH_4-OxD	NH_4-OxH	H_2O_2	sulfide	residual	total	bulk
A3/020	20	31	2	13	31	5	63	39	184	200
A3/050	50	19	2	11	26	5	53	28	144	162
A3/070	70	16	BDL	6	20	3	40	38	123	132
A3/100	100	23	BDL	9	21	3	59	41	156	173
A3/160	160	25	BDL	9	24	3	58	41	160	185
A3/190	190	35	3	24	39	5	56	36	198	229
A3/300	300	125	40	98	102	16	54	26	461	499
A3/430	430	216	55	264	180	51	65	27	858	904
A3/490	490	8	184	401	241	91	82	25	1032	1120
A3/700	700	9	158	494	244	56	74	27	1062	1160
A3/900	900	9	114	386	207	63	83	25	887	973

Cr (ppm)

sample	depth	H_2O	NH4-Ac	NH_4-OxD	NH_4-OxH	H_2O_2	sulfide	residual	total	bulk
A3/020	20	BDL	BDL	4	8	BDL	6	3	21	10
A3/050	50	BDL	BDL	3	6	BDL	6	4	19	10
A3/070	70	BDL	BDL	2	6	BDL	7	4	19	8
A3/100	100	BDL	BDL	3	3	BDL	8	3	17	10
A3/160	160	BDL	BDL	2	5	BDL	10	4	21	13
A3/190	190	BDL	BDL	3	3	BDL	12	3	21	13
A3/300	300	BDL	BDL	4	3	BDL	7	4	18	14
A3/430	430	BDL	BDL	5	5	BDL	8	6	24	21
A3/490	490	BDL	1	4	6	BDL	9	3	23	18
A3/700	700	BDL	1	5	6	BDL	9	4	25	21
A3/900	900	BDL	1	6	6	BDL	8	4	25	28

Pb (ppm)

sample	depth	H_2O	NH4-Ac	NH_4-OxD	NH_4-OxH	H_2O_2	sulfide	residual	total	bulk
A3/020	20	BDL	BDL	9	14	BDL	6	BDL	29	26
A3/050	50	BDL	BDL	7	5	BDL	9	BDL	21	26
A3/070	70	BDL	BDL	BDL	11	BDL	4	BDL	15	17
A3/100	100	BDL	BDL	7	4	BDL	6	BDL	17	15
A3/160	160	BDL	BDL	5	3	BDL	6	BDL	14	17
A3/190	190	BDL	BDL	4	BDL	BDL	7	BDL	11	18
A3/300	300	BDL	BDL	13	BDL	BDL	12	BDL	25	29
A3/430	430	BDL	BDL	12	5	BDL	20	BDL	37	45
A3/490	490	BDL	8	15	4	2	16	BDL	45	47
A3/700	700	BDL	10	18	6	BDL	29	BDL	63	58
A3/900	900	BDL	6	15	9	BDL	27	BDL	57	60

Mo (ppm)

sample	depth	H_2O	NH4-Ac	NH_4-OxD	NH_4-OxH	H_2O_2	sulfide	residual	total	bulk
A3/020	20	BDL	BDL	85	15	16	55	3	174	158
A3/050	50	BDL	BDL	36	8	32	14	BDL	90	98
A3/070	70	BDL	BDL	23	11	4	64	5	107	136
A3/100	100	BDL	BDL	4	BDL	1	104	12	121	125
A3/160	160	BDL	BDL	4	BDL	BDL	100	12	116	125
A3/190	190	BDL	BDL	3	BDL	BDL	88	12	103	85
A3/300	300	BDL	BDL	3	BDL	BDL	44	7	54	59
A3/430	430	BDL	BDL	3	BDL	1	39	4	47	41
A3/490	490	BDL	BDL	2	BDL	BDL	37	1	40	33
A3/700	700	1	BDL	2	BDL	BDL	46	5	54	38
A3/900	900	BDL	BDL	3	BDL	BDL	34	2	39	38

V (ppm)

sample	depth	H_2O	NH4-Ac	NH_4-OxD	NH_4-OxH	H_2O_2	sulfide	residual	total	bulk
A3/020	20	BDL	BDL	10	22	BDL	8	53	93	107
A3/050	50	BDL	BDL	7	16	BDL	8	47	78	103
A3/070	70	BDL	BDL	3	16	BDL	6	54	79	94
A3/100	100	BDL	BDL	5	10	BDL	8	50	73	88
A3/160	160	BDL	BDL	5	14	BDL	11	55	85	102
A3/190	190	BDL	BDL	6	11	BDL	11	48	76	98
A3/300	300	BDL	BDL	7	13	BDL	13	63	96	117
A3/430	430	BDL	BDL	9	16	BDL	17	68	110	130
A3/490	490	BDL	BDL	10	19	BDL	17	54	100	121
A3/700	700	BDL	BDL	11	20	BDL	19	64	114	132
A3/900	900	BDL	BDL	14	22	BDL	23	61	120	138

As (ppm)

sample	depth	H_2O	NH4-Ac	NH_4-OxD	NH_4-OxH	H_2O_2	sulfide	residual	total	bulk
A3/020	20	BDL	BDL	27	5	BDL	5	BDL	37	42
A3/050	50	BDL	BDL	17	BDL	BDL	6	BDL	23	31
A3/070	70	BDL	BDL	16	7	BDL	14	BDL	37	59
A3/100	100	BDL	BDL	15	BDL	BDL	15	BDL	30	12
A3/160	160	BDL	BDL	10	BDL	BDL	13	BDL	23	BDL
A3/190	190	BDL	BDL	8	BDL	BDL	15	BDL	23	14
A3/300	300	BDL	BDL	27	BDL	BDL	32	BDL	59	63
A3/430	430	BDL	BDL	44	BDL	BDL	29	BDL	73	93
A3/490	490	BDL	7	51	BDL	BDL	55	BDL	113	58
A3/700	700	BDL	7	63	4	BDL	68	BDL	142	58
A3/900	900	BDL	7	55	3	BDL	51	BDL	116	98

Ba (ppm)

sample	depth	H_2O	NH4-Ac	NH_4-OxD	NH_4-OxH	H_2O_2	sulfide	residual	total	bulk
A3/020	20	BDL	2	16	59	BDL	26	453	556	779
A3/050	50	BDL	2	27	57	1	29	411	527	813
A3/070	70	BDL	1	6	50	1	14	482	554	771
A3/100	100	BDL	3	16	20	1	11	461	512	754
A3/160	160	BDL	3	18	26	2	18	475	542	792
A3/190	190	1	4	16	12	1	13	554	601	929
A3/300	300	2	14	13	23	BDL	17	370	439	672
A3/430	430	1	16	23	35	BDL	25	378	478	695
A3/490	490	BDL	27	9	15	BDL	21	394	466	725
A3/700	700	BDL	38	12	30	BDL	29	437	546	794
A3/900	900	1	32	10	19	BDL	29	437	528	765

Sr (ppm)

sample	depth	H_2O	NH4-Ac	NH_4-OxD	NH_4-OxH	H_2O_2	sulfide	residual	total	bulk
A3/020	20	0.5	BDL	2.4	6.2	1.2	7.3	75.8	93.4	124
A3/050	50	0.7	BDL	2.4	6.1	1.7	10	63.3	84.2	130
A3/070	70	BDL	BDL	1.2	6.3	1.1	5	74.1	87.7	119
A3/100	100	BDL	BDL	0.9	4.1	1.6	6.2	65.8	78.6	108
A3/160	160	0.5	BDL	1.4	9.8	2.9	13.1	69.8	97.5	128
A3/190	190	0.6	BDL	0.8	4.9	1.9	4.1	73.4	85.7	119
A3/300	300	1.1	0.7	0.9	1.5	1.6	2.5	67.7	76	112
A3/430	430	2	1	0.9	1.9	3.2	3	61.1	73.1	102
A3/490	490	1.6	4	0.8	1	2.6	2	72.3	84.3	128
A3/700	700	1.9	5	0.8	1.4	3.4	2.1	67.6	82.2	110
A3/900	900	1.5	4.3	0.6	0.9	3.1	2.1	61	73.5	104

Ni (ppm)

sample	depth	H_2O	NH4-Ac	NH_4-OxD	NH_4-OxH	H_2O_2	sulfide	residual	total	bulk
A3/020	20	2	BDL	3	2	BDL	5	3	15	16
A3/050	50	1	BDL	3	2	BDL	5	2	13	16
A3/070	70	2	BDL	2	4	BDL	6	3	17	14
A3/100	100	2	BDL	3	3	BDL	7	4	19	16
A3/160	160	1	BDL	3	3	1	9	4	21	20
A3/190	190	BDL	BDL	2	BDL	BDL	10	4	16	20
A3/300	300	1	BDL	4	BDL	1	8	5	19	23
A3/430	430	2	1	5	3	2	10	5	28	27
A3/490	490	BDL	2	6	BDL	2	9	4	23	24
A3/700	700	BDL	2	6	2	3	10	5	28	28
A3/900	900	BDL	2	6	BDL	2	11	4	25	29

Zr (ppm)

sample	depth	H_2O	NH4-Ac	NH_4-OxD	NH_4-OxH	H_2O_2	sulfide	residual	total	bulk
A3/020	20	BDL	BDL	4.5	1	BDL	BDL	2.6	8.1	14.3
A3/050	50	BDL	BDL	5	BDL	BDL	0.6	1.3	6.9	22.5
A3/070	70	BDL	BDL	2.6	4.4	BDL	BDL	1.1	8.1	8.3
A3/100	100	BDL	BDL	4.2	4.2	BDL	BDL	1.1	9.5	11.3
A3/160	160	BDL	BDL	3.8	2.3	BDL	BDL	1.7	7.8	13.5
A3/190	190	BDL	BDL	2.1	BDL	BDL	BDL	1.1	3.2	13.5
A3/300	300	BDL	BDL	4.3	BDL	BDL	BDL	3.7	8	29.4
A3/430	430	BDL	BDL	5.2	1.9	BDL	BDL	1.6	8.7	31.7
A3/490	490	BDL	BDL	5.8	BDL	BDL	BDL	1.9	7.7	23.1
A3/700	700	BDL	BDL	4.6	BDL	BDL	BDL	2.8	7.4	47.8
A3/900	900	BDL	BDL	4.4	BDL	BDL	BDL	1.4	5.8	45.5

Co (ppm)

sample	depth	H_2O	NH4-Ac	NH_4-OxD	NH_4-OxH	H_2O_2	sulfide	residual	total	bulk
A3/020	20	3	BDL	BDL	BDL	BDL	3	BDL	6	7
A3/050	50	2	BDL	BDL	BDL	BDL	1	BDL	3	6
A3/070	70	3	BDL	BDL	BDL	BDL	2	BDL	5	7
A3/100	100	3	BDL	BDL	BDL	BDL	7	BDL	10	11
A3/160	160	1	BDL	BDL	BDL	1	9	1	12	12
A3/190	190	2	BDL	BDL	BDL	BDL	6	BDL	8	9
A3/300	300	2	BDL	BDL	BDL	3	6	BDL	11	12
A3/430	430	3	BDL	BDL	BDL	4	7	BDL	14	16
A3/490	490	BDL	BDL	1	BDL	3	5	BDL	9	12
A3/700	700	BDL	1	BDL	BDL	4	6	BDL	11	14
A3/900	900	BDL	BDL	2	BDL	3	7	BDL	12	12

Sn (ppm)

sample	depth	H_2O	NH4-Ac	NH_4-OxD	NH_4-OxH	H_2O_2	sulfide	residual	total	bulk
A3/020	20	BDL	BDL	BDL	BDL	BDL	18	BDL	18	BDL
A3/050	50	BDL	BDL	BDL	BDL	BDL	26	BDL	26	BDL
A3/070	70	BDL	BDL	BDL	BDL	BDL	30	BDL	30	BDL
A3/100	100	BDL	BDL	BDL	BDL	BDL	31	BDL	31	BDL
A3/160	160	BDL	BDL	BDL	BDL	BDL	29	BDL	29	BDL
A3/190	190	BDL	BDL	BDL	BDL	BDL	26	BDL	26	BDL
A3/300	300	BDL	BDL	BDL	BDL	BDL	29	BDL	29	10
A3/430	430	BDL	BDL	BDL	BDL	BDL	29	BDL	29	14
A3/490	490	BDL	BDL	BDL	BDL	BDL	29	BDL	29	BDL
A3/700	700	BDL	BDL	BDL	BDL	BDL	27	BDL	27	23
A3/900	900	BDL	BDL	BDL	BDL	BDL	29	BDL	29	23

W (ppm)

sample	depth	H_2O	NH4-Ac	NH_4-OxD	NH_4-OxH	H_2O_2	sulfide	residual	total	bulk
A3/020	20	BDL	BDL	BDL	BDL	BDL	BDL	23	23	27
A3/050	50	BDL	BDL	11	BDL	BDL	BDL	23	34	31
A3/070	70	BDL	BDL	BDL	11	BDL	BDL	26	37	24
A3/100	100	BDL	BDL	11	13	BDL	BDL	23	47	27
A3/160	160	BDL	BDL	10	10	BDL	BDL	27	47	45
A3/190	190	BDL	BDL	11	BDL	BDL	BDL	33	44	41
A3/300	300	BDL	BDL	BDL	BDL	BDL	BDL	20	20	BDL
A3/430	430	BDL	BDL	BDL	BDL	BDL	BDL	22	22	BDL
A3/490	490	BDL	BDL	12	BDL	BDL	BDL	18	30	BDL
A3/700	700	BDL	BDL	BDL	BDL	BDL	BDL	21	21	BDL
A3/900	900	BDL	BDL	BDL	BDL	BDL	BDL	21	21	11

La (ppm)

sample	depth	H_2O	NH4-Ac	NH_4-OxD	NH_4-OxH	H_2O_2	sulfide	residual	total	bulk
A3/020	20	BDL	BDL	6.4	2.8	BDL	3.4	6.3	18.9	18.2
A3/050	50	BDL	BDL	6.6	1	BDL	6.1	4.8	18.5	17.4
A3/070	70	BDL	BDL	3.8	5.7	BDL	2.6	6.8	18.9	14.4
A3/100	100	BDL	BDL	5.4	5.1	BDL	1.7	6	18.2	14.1
A3/160	160	BDL	BDL	5.2	3.6	BDL	2	5.4	16.2	16.3
A3/190	190	BDL	BDL	3	BDL	BDL	1.8	7.8	12.6	15.5
A3/300	300	BDL	BDL	5.2	BDL	BDL	2.7	3.5	11.4	18.3
A3/430	430	BDL	BDL	6.6	3.7	1.4	4	8.5	24.2	21.4
A3/490	490	BDL	BDL	7	BDL	BDL	4.2	4.3	15.5	19.6
A3/700	700	0.6	BDL	5.7	1.5	0.9	4.1	7.6	20.4	21.5
A3/900	900	BDL	BDL	5.9	BDL	0.9	4.4	8	19.2	21.5

Y (ppm)

sample	depth	H_2O	NH4-Ac	NH_4-OxD	NH_4-OxH	H_2O_2	sulfide	residual	total	bulk
A3/020	20	BDL	BDL	1	0.5	BDL	1	1.2	3.7	4.6
A3/050	50	BDL	BDL	BDL	BDL	BDL	1	1	2	4.9
A3/070	70	BDL	BDL	BDL	BDL	BDL	0.8	1.3	2.1	3.7
A3/100	100	BDL	BDL	0.6	BDL	BDL	0.7	1.1	2.4	3.8
A3/160	160	BDL	BDL	0.5	BDL	BDL	0.9	1	2.4	4.8
A3/190	190	BDL	BDL	0.8	BDL	BDL	0.9	1.2	2.9	5
A3/300	300	BDL	BDL	BDL	BDL	BDL	0.9	0.8	1.7	5.4
A3/430	430	BDL	0.5	0.7	BDL	0.5	1.1	1.3	4.1	6.5
A3/490	490	BDL	BDL	1	0.6	BDL	1.3	0.9	3.8	6.3
A3/700	700	BDL	0.6	1.5	BDL	0.6	1.1	1.5	5.3	7.7
A3/900	900	BDL	0.6	1.7	BDL	0.6	1.3	1.5	5.7	7.8

Sc (ppm)

sample	depth	H_2O	NH4-Ac	NH_4-OxD	NH_4-OxH	H_2O_2	sulfide	residual	total	bulk
A3/020	20	BDL	BDL	0.5	BDL	BDL	0.6	4.4	5.5	7.6
A3/050	50	BDL	BDL	0.6	BDL	BDL	0.6	3.3	4.5	7.5
A3/070	70	BDL	BDL	BDL	0.8	BDL	BDL	4	4.8	7
A3/100	100	BDL	BDL	BDL	BDL	BDL	0.5	3.9	4.4	6.6
A3/160	160	BDL	BDL	BDL	BDL	BDL	0.9	4.3	5.2	7.9
A3/190	190	BDL	BDL	BDL	BDL	BDL	1	4.2	5.2	7.7
A3/300	300	BDL	BDL	BDL	BDL	BDL	0.8	5.4	6.2	9.9
A3/430	430	BDL	BDL	0.7	BDL	BDL	1.2	6	7.9	11.1
A3/490	490	BDL	BDL	0.7	BDL	BDL	1.4	4.6	6.7	9.8
A3/700	700	BDL	BDL	0.6	BDL	BDL	1.6	6.2	8.4	11.3
A3/900	900	BDL	BDL	0.6	BDL	BDL	2.1	5.6	8.3	11.8

Be (ppm)

sample	depth	H_2O	NH4-Ac	NH_4-OxD	NH_4-OxH	H_2O_2	sulfide	residual	total	bulk
A3/020	20	BDL	BDL	BDL	BDL	BDL	BDL	0.8	0.8	1.1
A3/050	50	BDL	BDL	BDL	BDL	BDL	BDL	0.7	0.7	1.2
A3/070	70	BDL	BDL	BDL	BDL	BDL	BDL	0.9	0.9	1.2
A3/100	100	BDL	BDL	BDL	BDL	BDL	BDL	0.8	0.8	1.2
A3/160	160	BDL	BDL	BDL	BDL	BDL	BDL	0.9	0.9	1.3
A3/190	190	BDL	BDL	BDL	BDL	BDL	BDL	0.8	0.8	1.2
A3/300	300	BDL	BDL	BDL	BDL	BDL	BDL	0.9	0.9	1.4
A3/430	430	BDL	BDL	BDL	BDL	BDL	BDL	1	1	1.5
A3/490	490	BDL	BDL	BDL	BDL	BDL	BDL	0.8	0.8	1.5
A3/700	700	BDL	BDL	BDL	BDL	BDL	BDL	0.9	0.9	1.6
A3/900	900	BDL	BDL	BDL	BDL	BDL	BDL	0.9	0.9	1.5

Ag (ppm)

sample	depth	H_2O	NH4-Ac	NH_4-OxD	NH_4-OxH	H_2O_2	sulfide	residual	total	bulk
A3/020	20	BDL	BDL	BDL	0.3	BDL	0.8	BDL	1.1	0.6
A3/050	50	BDL	BDL	BDL	BDL	BDL	0.7	BDL	0.7	0.4
A3/070	70	BDL	BDL	BDL	0.3	BDL	0.8	BDL	1.1	0.6
A3/100	100	BDL	BDL	BDL	BDL	BDL	0.7	BDL	0.7	0.5
A3/160	160	BDL	BDL	BDL	BDL	BDL	1	BDL	1	0.7
A3/190	190	BDL	BDL	BDL	BDL	BDL	0.8	BDL	0.8	0.9
A3/300	300	BDL	BDL	BDL	BDL	BDL	0.6	BDL	0.6	0.5
A3/430	430	BDL	BDL	BDL	BDL	BDL	0.7	BDL	0.7	0.2
A3/490	490	0.3	BDL	BDL	BDL	BDL	0.9	BDL	1.2	0.6
A3/700	700	0.3	BDL	BDL	BDL	BDL	0.9	BDL	1.2	0.8
A3/900	900	BDL	BDL	BDL	BDL	BDL	0.7	BDL	0.7	0.6

Fe (%)

sample	depth	H_2O	NH4-Ac	NH_4-OxD	NH_4-OxH	H_2O_2	sulfide	residual	total	bulk
A4/010	10	BDL	0.04	0.49	4.1	0.02	1.14	1.39	7.18	7.85
A4/035	35	BDL	0.02	1.08	2.33	0.02	0.85	1.25	5.55	6.62
A4/065	65	BDL	0.11	1.42	1.25	0.03	0.66	1.14	4.61	5.23
A4/100	100	BDL	0.04	0.73	0.85	0.04	1.06	0.97	3.69	4.74
A4/125	125	BDL	0.05	1.17	1.13	0.05	1.07	1.09	4.56	5.31
A4/200	200	BDL	0.07	0.84	1.04	0.03	1.4	1.04	4.42	5.46
A4/260	260	BDL	0.08	0.98	1.3	0.03	1.5	1.71	5.6	7.01
A4/400	400	BDL	0.14	1.39	1.67	0.2	1.33	1.25	5.98	7
A4/600	600	BDL	0.14	1.41	1.75	0.24	1.4	1.13	6.07	7.09
A4/800	800	0.01	0.16	1.72	1.37	0.14	1.32	0.91	5.63	6.51
A4/1000	1000	BDL	0.15	1.57	1.76	0.17	1.45	1.09	6.19	7.26

Al (%)

sample	depth	H_2O	NH4-Ac	NH_4-OxD	NH_4-OxH	H_2O_2	sulfide	residual	total	bulk
A4/010	10	0.01	0.03	0.14	0.47	0.14	0.73	6.8	8.32	9.16
A4/035	35	BDL	BDL	0.07	0.24	BDL	0.45	6.14	6.9	8.22
A4/065	65	BDL	0.06	0.11	0.15	BDL	0.32	5.76	6.4	7.46
A4/100	100	BDL	0.04	0.08	0.09	BDL	0.33	4.66	5.2	7.56
A4/125	125	BDL	0.03	0.09	0.14	BDL	0.35	5.87	6.48	7.66
A4/200	200	BDL	0.03	0.07	0.07	BDL	0.41	5.54	6.12	7.75
A4/260	260	BDL	0.03	0.07	0.07	BDL	0.41	6.14	6.72	8.25
A4/400	400	BDL	0.07	0.18	0.14	BDL	0.49	6.25	7.13	8.57
A4/600	600	BDL	0.06	0.15	0.14	BDL	0.55	6.19	7.09	8.7
A4/800	800	BDL	0.06	0.15	0.15	BDL	0.63	6.36	7.35	8.85
A4/1000	1000	BDL	0.06	0.15	0.16	BDL	0.66	6.2	7.23	9.04

K (%)

sample	depth	H_2O	NH4-Ac	NH_4-OxD	NH_4-OxH	H_2O_2	sulfide	residual	total	bulk
A4/010	10	BDL	0.01	BDL	0.03	0.05	-	2.2	2.29	2.78
A4/035	35	BDL	BDL	0.08	0.14	BDL	-	3.04	3.26	4.18
A4/065	65	0.04	0.01	0.17	0.07	BDL	-	3.38	3.67	4.58
A4/100	100	0.02	BDL	0.04	0.02	BDL	-	3.2	3.28	4.47
A4/125	125	0.01	BDL	0.11	0.04	BDL	-	3.34	3.5	4.52
A4/200	200	0.02	BDL	0.02	0.01	BDL	-	3.58	3.63	5.22
A4/260	260	0.03	BDL	0.01	0.01	BDL	-	3.5	3.55	4.95
A4/400	400	0.04	0.03	0.03	0.02	BDL	-	3.2	3.32	4.58
A4/600	600	0.04	0.03	0.03	0.02	BDL	-	3.26	3.38	4.68
A4/800	800	0.04	0.03	0.03	0.03	BDL	-	3.44	3.57	4.96
A4/1000	1000	0.04	0.03	0.03	0.03	BDL	-	3.43	3.56	5.04

Mg (%)

sample	depth	H_2O	NH4-Ac	NH_4-OxD	NH_4-OxH	H_2O_2	sulfide	residual	total	bulk
A4/010	10	BDL	0.03	0.03	0.23	0.01	0.5	0.3	1.1	1.17
A4/035	35	BDL	BDL	0.01	0.11	0.01	0.32	0.34	0.79	0.91
A4/065	65	0.02	BDL	BDL	0.08	BDL	0.22	0.35	0.67	0.76
A4/100	100	0.02	BDL	BDL	0.04	BDL	0.26	0.29	0.61	0.79
A4/125	125	0.02	BDL	BDL	0.07	BDL	0.27	0.36	0.72	0.83
A4/200	200	0.03	BDL	0.01	0.04	BDL	0.32	0.31	0.71	0.83
A4/260	260	0.02	BDL	0.02	0.03	BDL	0.31	0.41	0.79	0.95
A4/400	400	0.01	0.02	0.03	0.05	BDL	0.38	0.36	0.85	0.99
A4/600	600	BDL	0.02	0.03	0.06	BDL	0.43	0.33	0.87	0.97
A4/800	800	BDL	0.02	0.04	0.06	BDL	0.47	0.29	0.88	0.97
A4/1000	1000	BDL	0.02	0.04	0.06	0.01	0.5	0.32	0.95	1.08

Na (%)

sample	depth	H_2O	NH4-Ac	NH_4-OxD	NH_4-OxH	H_2O_2	sulfide	residual	total	bulk
A4/010	10	BDL	BDL	BDL	BDL	BDL	0.01	1.42	1.43	1.63
A4/035	35	BDL	BDL	BDL	BDL	BDL	BDL	0.91	0.91	1.13
A4/065	65	BDL	BDL	BDL	BDL	BDL	BDL	0.63	0.63	0.77
A4/100	100	BDL	BDL	BDL	BDL	BDL	BDL	0.61	0.61	0.75
A4/125	125	BDL	BDL	BDL	BDL	BDL	BDL	0.62	0.62	0.74
A4/200	200	BDL	BDL	BDL	BDL	BDL	BDL	0.62	0.62	0.83
A4/260	260	BDL	BDL	BDL	BDL	BDL	BDL	0.52	0.52	0.66
A4/400	400	BDL	BDL	BDL	BDL	BDL	BDL	0.67	0.67	0.93
A4/600	600	0.01	BDL	BDL	BDL	BDL	BDL	0.71	0.72	0.89
A4/800	800	0.01	BDL	BDL	BDL	BDL	BDL	0.81	0.82	1.05
A4/1000	1000	0.01	BDL	BDL	BDL	BDL	BDL	0.71	0.72	0.95

Ca (%)

sample	depth	H_2O	NH4-Ac	NH_4-OxD	NH_4-OxH	H_2O_2	sulfide	residual	total	bulk
A4/010	10	0.08	0.82	0.02	BDL	0.01	0.5	0.31	1.74	1.77
A4/035	35	0.12	0.16	0.01	0.01	0.08	0.1	0.16	0.64	0.71
A4/065	65	0.06	0.01	0.01	BDL	0.04	0.04	0.1	0.26	0.29
A4/100	100	0.01	BDL	BDL	0.01	0.03	0.04	0.08	0.17	0.22
A4/125	125	0.06	BDL	BDL	0.01	0.04	0.04	0.09	0.24	0.29
A4/200	200	0.06	BDL	BDL	0.01	0.04	0.05	0.1	0.26	0.33
A4/260	260	0.04	BDL	BDL	BDL	0.04	0.05	0.09	0.22	0.27
A4/400	400	0.08	0.07	BDL	BDL	0.08	0.06	0.07	0.36	0.44
A4/600	600	0.08	0.13	BDL	0.01	0.1	0.05	0.08	0.45	0.51
A4/800	800	0.07	0.13	BDL	0.01	0.09	0.05	0.08	0.43	0.5
A4/1000	1000	0.08	0.12	BDL	0.01	0.1	0.05	0.08	0.44	0.5

Tl (%)

sample	depth	H_2O	NH4-Ac	NH_4-OxD	NH_4-OxH	H_2O_2	sulfide	residual	total	bulk
A4/010	10	BDL	BDL	BDL	0.06	BDL	0.02	0.56	0.64	0.69
A4/035	35	BDL	BDL	BDL	0.02	BDL	0.02	0.25	0.29	0.36
A4/065	65	BDL	BDL	BDL	0.02	BDL	0.02	0.13	0.17	0.2
A4/100	100	BDL	BDL	BDL	0.01	BDL	0.02	0.12	0.15	0.19
A4/125	125	BDL	BDL	BDL	0.01	BDL	0.02	0.14	0.17	0.2
A4/200	200	BDL	BDL	BDL	0.01	BDL	0.03	0.13	0.17	0.21
A4/260	260	BDL	BDL	BDL	0.02	BDL	0.03	0.18	0.23	0.28
A4/400	400	BDL	BDL	BDL	0.02	BDL	0.03	0.15	0.2	0.26
A4/600	600	BDL	BDL	BDL	0.03	BDL	0.04	0.16	0.23	0.26
A4/800	800	BDL	BDL	BDL	0.02	BDL	0.05	0.16	0.23	0.26
A4/1000	1000	BDL	BDL	BDL	0.02	BDL	0.05	0.18	0.25	0.29

P (%)

sample	depth	H_2O	NH4-Ac	NH_4-OxD	NH_4-OxH	H_2O_2	sulfide	residual	total	bulk
A4/010	10	BDL	BDL	0.13	0.01	BDL	0.05	BDL	0.19	0.18
A4/035	35	BDL	BDL	0.05	0.01	BDL	0.04	0.01	0.11	0.1
A4/065	65	BDL	BDL	0.04	BDL	BDL	0.03	0.01	0.08	0.07
A4/100	100	BDL	BDL	0.02	BDL	BDL	0.03	0.01	0.06	0.05
A4/125	125	BDL	BDL	0.03	BDL	BDL	0.03	0.01	0.07	0.06
A4/200	200	BDL	BDL	0.02	BDL	BDL	0.03	0.01	0.06	0.04
A4/260	260	BDL	BDL	0.03	BDL	BDL	0.03	0.01	0.07	0.03
A4/400	400	BDL	BDL	0.05	BDL	BDL	0.03	0.01	0.09	0.09
A4/600	600	BDL	BDL	0.04	BDL	BDL	0.03	0.01	0.08	0.08
A4/800	800	BDL	BDL	0.04	BDL	BDL	0.03	0.01	0.08	0.07
A4/1000	1000	BDL	BDL	0.04	BDL	BDL	0.03	0.01	0.08	0.07

Cu (ppm)

sample	depth	H_2O	NH4-Ac	NH_4-OxD	NH_4-OxH	H_2O_2	sulfide	residual	total	bulk
A4/010	10	2.3	192	187	33	203	326	12.8	956	933
A4/035	35	0.6	77.5	154	79.4	311	258	12.5	893	882
A4/065	65	16.2	35.6	149	35.2	438	86.9	10.2	771	710
A4/100	100	289	120	154	60.9	1200	177	23.6	2025	2000
A4/125	125	227	107	189	58.5	970	159	14.7	1725	1750
A4/200	200	186	336	198	48.8	1840	538	56	3203	3180
A4/260	260	66.3	289	215	75.5	2690	846	61.1	4243	4390
A4/400	400	7.3	424	161	35.9	560	174	138	1500	1390
A4/600	600	8.1	472	171	14.3	490	125	5.4	1286	1280
A4/800	800	12.1	503	173	22.3	688	133	7.4	1539	1620
A4/1000	1000	10.6	582	195	23.1	734	163	6.8	1715	1810

Zn (ppm)

sample	depth	H_2O	NH4-Ac	NH_4-OxD	NH_4-OxH	H_2O_2	sulfide	residual	total	bulk
A4/010	10	0.5	9	19	81.3	1.9	76.5	35.7	223.9	225
A4/035	35	BDL	2.6	10.1	25.2	4.6	29.4	20.4	92.3	96.8
A4/065	65	2.2	0.9	5.3	7.2	2.5	11.4	14.2	43.7	43.7
A4/100	100	8.8	0.7	5.2	6.4	5.6	13.8	17.8	58.3	58.8
A4/125	125	8.4	1	6.2	8.5	4	14.6	14.5	57.2	59.2
A4/200	200	30.7	7.7	22.6	14.3	13	19.1	12.3	119.7	122
A4/260	260	35.7	16	34.2	19	23.5	23.8	15.5	167.7	180
A4/400	400	1.2	35	92.2	39.5	27.6	20.8	129	345.3	251
A4/600	600	1.5	44.5	120	54.9	28.9	21.3	27.6	298.7	312
A4/800	800	2.4	52.7	157	53.1	31.7	23.6	27.4	347.9	357
A4/1000	1000	1.7	50.6	141	59.5	31.8	23.8	27.9	336.3	361

Mn (ppm)

sample	depth	H_2O	NH4-Ac	NH_4-OxD	NH_4-OxH	H_2O_2	sulfide	residual	total	bulk
A4/010	10	7	305	2840	428	8	426	115	4129	4230
A4/035	35	28	128	691	110	33	127	57	1174	1220
A4/065	65	11	2	13	23	4	47	35	135	141
A4/100	100	32	BDL	9	21	2	55	36	155	174
A4/125	125	60	7	22	29	5	62	39	224	238
A4/200	200	109	13	61	53	17	67	36	356	387
A4/260	260	146	31	103	97	28	70	41	516	563
A4/400	400	10	91	382	208	60	62	25	838	860
A4/600	600	5	126	377	236	50	67	26	887	899
A4/800	800	7	138	463	208	48	78	25	967	1010
A4/1000	1000	7	137	405	229	53	79	27	937	996

Cr (ppm)

sample	depth	H_2O	NH4-Ac	NH_4-OxD	NH_4-OxH	H_2O_2	sulfide	residual	total	bulk
A4/010	10	BDL	BDL	2	5	BDL	3	4	14	10
A4/035	35	BDL	BDL	3	7	BDL	8	4	22	11
A4/065	65	BDL	BDL	4	4	BDL	6	4	18	8
A4/100	100	BDL	BDL	3	4	BDL	6	3	16	8
A4/125	125	BDL	1	5	5	BDL	16	5	32	15
A4/200	200	BDL	BDL	3	5	BDL	9	2	19	10
A4/260	260	BDL	BDL	4	4	BDL	11	7	26	15
A4/400	400	BDL	1	5	5	BDL	5	6	22	16
A4/600	600	BDL	1	5	6	BDL	6	5	23	11
A4/800	800	BDL	2	6	5	BDL	8	4	25	13
A4/1000	1000	BDL	1	5	8	BDL	8	5	27	15

Pb (ppm)

sample	depth	H_2O	NH4-Ac	NH_4-OxD	NH_4-OxH	H_2O_2	sulfide	residual	total	bulk
A4/010	10	BDL	BDL	14	9	BDL	17	BDL	40	48
A4/035	35	BDL	BDL	9	13	BDL	8	BDL	30	33
A4/065	65	BDL	BDL	4	BDL	BDL	6	BDL	10	25
A4/100	100	BDL	BDL	4	5	BDL	6	BDL	15	26
A4/125	125	BDL	BDL	9	4	BDL	8	BDL	21	17
A4/200	200	BDL	BDL	5	8	BDL	9	BDL	22	17
A4/260	260	BDL	BDL	7	4	BDL	7	BDL	18	22
A4/400	400	BDL	4	13	8	BDL	17	BDL	42	49
A4/600	600	BDL	8	12	9	BDL	19	BDL	48	54
A4/800	800	BDL	10	13	10	BDL	25	BDL	58	65
A4/1000	1000	BDL	8	17	11	BDL	24	BDL	60	68

Mo (ppm)

sample	depth	H_2O	NH4-Ac	NH_4-OxD	NH_4-OxH	H_2O_2	sulfide	residual	total	bulk
A4/010	10	BDL	BDL	2	BDL	12	2	BDL	16	9
A4/035	35	BDL	BDL	16	6	11	44	3	80	71
A4/065	65	BDL	BDL	38	2	3	57	2	102	99
A4/100	100	BDL	BDL	4	BDL	1	76	9	90	89
A4/125	125	BDL	BDL	14	BDL	3	79	7	103	102
A4/200	200	BDL	BDL	3	BDL	BDL	59	9	71	58
A4/260	260	BDL	BDL	2	BDL	BDL	48	9	59	56
A4/400	400	BDL	BDL	5	BDL	BDL	42	5	52	41
A4/600	600	1	BDL	4	BDL	BDL	28	1	34	60
A4/800	800	1	BDL	3	BDL	BDL	33	1	38	37
A4/1000	1000	BDL	BDL	4	BDL	BDL	34	1	39	37

V (ppm)

sample	depth	H_2O	NH4-Ac	NH_4-OxD	NH_4-OxH	H_2O_2	sulfide	residual	total	bulk
A4/010	10	BDL	BDL	9	60	3	17	101	190	205
A4/035	35	BDL	BDL	8	27	BDL	11	67	113	132
A4/065	65	BDL	BDL	9	13	BDL	8	53	83	97
A4/100	100	BDL	BDL	6	11	BDL	8	52	77	92
A4/125	125	BDL	BDL	8	12	BDL	9	55	84	101
A4/200	200	BDL	BDL	6	14	BDL	13	48	81	102
A4/260	260	BDL	BDL	8	14	BDL	13	74	109	133
A4/400	400	BDL	BDL	11	17	BDL	15	65	108	123
A4/600	600	BDL	BDL	10	20	BDL	16	63	109	126
A4/800	800	BDL	BDL	13	18	BDL	19	59	109	128
A4/1000	1000	BDL	BDL	12	23	BDL	20	65	120	136

As (ppm)

sample	depth	H_2O	NH4-Ac	NH_4-OxD	NH_4-OxH	H_2O_2	sulfide	residual	total	bulk
A4/010	10	BDL	BDL	24	21	BDL	BDL	BDL	45	89
A4/035	35	BDL	BDL	25	9	BDL	BDL	BDL	34	85
A4/065	65	BDL	BDL	18	BDL	BDL	6	BDL	24	54
A4/100	100	BDL	BDL	13	BDL	BDL	11	BDL	24	88
A4/125	125	BDL	BDL	20	BDL	BDL	8	BDL	28	10
A4/200	200	BDL	BDL	8	4	BDL	16	BDL	28	BDL
A4/260	260	BDL	BDL	13	BDL	BDL	32	BDL	45	20
A4/400	400	BDL	BDL	5	42	BDL	BDL	30	BDL	77	53
A4/600	600	BDL	BDL	7	54	BDL	BDL	38	BDL	99	86
A4/800	800	BDL	BDL	6	55	3	BDL	50	BDL	114	81
A4/1000	1000	BDL	BDL	7	57	3	BDL	49	BDL	116	9

Ba (ppm)

sample	depth	H_2O	NH4-Ac	NH_4-OxD	NH_4-OxH	H_2O_2	sulfide	residual	total	bulk
A4/010	10	2	119	103	76	7	73	264	644	706
A4/035	35	BDL	17	54	80	2	36	417	606	763
A4/065	65	BDL	4	44	52	1	25	477	603	812
A4/100	100	BDL	4	19	18	1	14	422	478	751
A4/125	125	BDL	3	35	31	1	19	464	553	797
A4/200	200	BDL	6	21	12	BDL	15	551	605	941
A4/260	260	BDL	10	12	15	1	13	436	487	729
A4/400	400	BDL	31	12	24	BDL	21	360	448	690
A4/600	600	BDL	31	11	23	BDL	24	383	472	661
A4/800	800	BDL	36	10	23	BDL	26	437	532	777
A4/1000	1000	BDL	33	12	25	BDL	26	421	517	784

Sr (ppm)

sample	depth	H_2O	NH4-Ac	NH_4-OxD	NH_4-OxH	H_2O_2	sulfide	residual	total	bulk
A4/010	10	1.7	15.1	0.7	2.3	0.6	10.6	108	139	171
A4/035	35	0.5	1.8	2.1	6.6	3	10.5	82	107	142
A4/065	65	0.7	BDL	2	6.8	2.3	8.8	73.3	93.9	122
A4/100	100	BDL	BDL	0.8	5.2	2.3	7.3	56.7	72.3	111
A4/125	125	BDL	BDL	2.1	7.6	3.3	10.8	66.6	90.4	120
A4/200	200	0.8	BDL	1	5.3	2.1	6.4	71.6	87.2	127
A4/260	260	0.7	BDL	0.7	2.3	1.7	3.3	59.6	68.3	92.8
A4/400	400	1.5	3.2	0.7	2.4	2.5	2.9	59.2	72.4	102
A4/600	600	1.5	4.9	0.6	1.8	3.1	2.7	62	76.6	107
A4/800	800	1.5	4.8	0.5	1.5	2.7	2	65.3	78.3	111
A4/1000	1000	1.4	4.4	0.7	1.7	3	2.6	58.5	72.3	103

Ni (ppm)

sample	depth	H_2O	NH4-Ac	NH_4-OxD	NH_4-OxH	H_2O_2	sulfide	residual	total	bulk
A4/010	10	BDL	BDL	9	3	BDL	7	4	23	19
A4/035	35	BDL	BDL	5	3	BDL	7	4	19	17
A4/065	65	BDL	BDL	1	BDL	BDL	6	4	11	14
A4/100	100	1	BDL	2	BDL	BDL	7	4	14	16
A4/125	125	2	BDL	4	2	BDL	11	5	24	22
A4/200	200	2	BDL	3	4	BDL	9	3	21	21
A4/260	260	1	BDL	4	2	BDL	10	6	23	25
A4/400	400	BDL	2	4	3	2	8	6	25	26
A4/600	600	BDL	2	5	2	3	9	5	26	25
A4/800	800	BDL	2	5	3	2	10	4	26	26
A4/1000	1000	BDL	2	6	2	2	9	5	26	27

Zr (ppm)

sample	depth	H_2O	NH4-Ac	NH_4-OxD	NH_4-OxH	H_2O_2	sulfide	residual	total	bulk
A4/010	10	BDL	BDL	6.2	2.5	2	1.1	51.1	62.9	68.6
A4/035	35	BDL	BDL	5.5	3.2	BDL	BDL	13.4	22.1	44.8
A4/065	65	BDL	BDL	1.3	BDL	BDL	BDL	1.9	3.2	11.3
A4/100	100	BDL	BDL	2.2	BDL	BDL	0.8	1.6	4.6	14
A4/125	125	BDL	BDL	5.5	0.7	BDL	BDL	2.1	8.3	12.8
A4/200	200	BDL	BDL	3	5.1	BDL	BDL	1.6	9.7	9.4
A4/260	260	BDL	BDL	4	2.4	BDL	BDL	2.1	8.5	34.7
A4/400	400	BDL	BDL	1.8	3.2	BDL	BDL	2	7	28.8
A4/600	600	BDL	BDL	3.3	1.7	BDL	BDL	1.4	6.4	14.1
A4/800	800	BDL	BDL	2.8	1.9	BDL	BDL	1.7	6.4	34.7
A4/1000	1000	BDL	BDL	5.1	BDL	BDL	BDL	1.4	6.5	50.1

Co (ppm)

sample	depth	H_2O	NH4-Ac	NH_4-OxD	NH_4-OxH	H_2O_2	sulfide	residual	total	bulk
A4/010	10	BDL	BDL	11	6	BDL	8	1	26	26
A4/035	35	BDL	BDL	2	2	1	5	1	11	11
A4/065	65	BDL	BDL	BDL	BDL	1	2	BDL	3	5
A4/100	100	2	BDL	BDL	1	1	6	BDL	10	10
A4/125	125	1	BDL	BDL	BDL	1	5	BDL	7	11
A4/200	200	2	BDL	BDL	BDL	BDL	7	BDL	9	12
A4/260	260	2	BDL	BDL	BDL	1	7	1	11	12
A4/400	400	BDL	1	2	BDL	4	7	BDL	14	15
A4/600	600	BDL	BDL	1	BDL	4	7	BDL	12	14
A4/800	800	BDL	BDL	2	BDL	4	6	BDL	12	13
A4/1000	1000	BDL	1	1	1	4	5	BDL	12	14

Sn (ppm)

sample	depth	H_2O	NH4-Ac	NH_4-OxD	NH_4-OxH	H_2O_2	sulfide	residual	total	bulk
A4/010	10	BDL	BDL	BDL	BDL	BDL	22	12	34	160
A4/035	35	BDL	BDL	BDL	BDL	BDL	29	BDL	29	51
A4/065	65	BDL	BDL	BDL	BDL	BDL	27	BDL	27	BDL
A4/100	100	BDL	BDL	BDL	BDL	BDL	29	BDL	29	BDL
A4/125	125	BDL	BDL	BDL	BDL	BDL	29	BDL	29	BDL
A4/200	200	BDL	BDL	BDL	BDL	BDL	28	BDL	28	BDL
A4/260	260	BDL	BDL	BDL	BDL	BDL	28	BDL	28	23
A4/400	400	BDL	BDL	BDL	BDL	BDL	27	BDL	27	22
A4/600	600	BDL	BDL	BDL	BDL	BDL	29	BDL	29	11
A4/800	800	BDL	BDL	BDL	BDL	BDL	28	BDL	28	15
A4/1000	1000	BDL	BDL	BDL	BDL	BDL	30	10	40	30

W (ppm)

sample	depth	H_2O	NH4-Ac	NH_4-OxD	NH_4-OxH	H_2O_2	sulfide	residual	total	bulk
A4/010	10	BDL	BDL	BDL	BDL	BDL	BDL	BDL	BDL	BDL
A4/035	35	BDL	BDL	10	BDL	BDL	BDL	19	29	BDL
A4/065	65	BDL	BDL	BDL	BDL	BDL	BDL	27	27	30
A4/100	100	BDL	BDL	BDL	BDL	BDL	BDL	20	20	23
A4/125	125	BDL	BDL	15	BDL	BDL	BDL	26	41	26
A4/200	200	BDL	BDL	16	18	BDL	BDL	30	64	42
A4/260	260	BDL	BDL	BDL	BDL	BDL	BDL	27	27	17
A4/400	400	BDL	BDL	BDL	BDL	BDL	BDL	19	19	11
A4/600	600	BDL	BDL	BDL	BDL	BDL	BDL	20	20	BDL
A4/800	800	BDL	BDL	BDL	BDL	BDL	BDL	20	20	BDL
A4/1000	1000	BDL	BDL	BDL	BDL	BDL	BDL	22	22	24

La (ppm)

sample	depth	H_2O	NH4-Ac	NH_4-OxD	NH_4-OxH	H_2O_2	sulfide	residual	total	bulk
A4/010	10	BDL	2.6	6.5	BDL	BDL	16.2	4.7	30	27.4
A4/035	35	BDL	BDL	7.2	3.5	BDL	7.2	7	24.9	20.2
A4/065	65	BDL	BDL	1.9	BDL	BDL	4.9	6	12.8	15.4
A4/100	100	BDL	BDL	2.6	BDL	BDL	2.3	1.8	6.7	14.9
A4/125	125	BDL	BDL	7.3	1.8	0.7	2.5	8.2	20.5	16.6
A4/200	200	BDL	BDL	3.9	6	BDL	2	7.5	19.4	13.8
A4/260	260	BDL	BDL	4.8	3.3	BDL	1.8	9.2	19.1	16.6
A4/400	400	BDL	BDL	2.8	5	0.9	4.3	8.8	21.8	23.2
A4/600	600	BDL	BDL	4	3.5	1	4.6	6.8	19.9	19.4
A4/800	800	BDL	BDL	3.4	3.6	0.8	5	7	19.8	21.1
A4/1000	1000	BDL	BDL	6	1.2	0.6	4.7	5.1	17.6	23.3

Y (ppm)

sample	depth	H_2O	NH4-Ac	NH_4-OxD	NH_4-OxH	H_2O_2	sulfide	residual	total	bulk
A4/010	10	BDL	4.5	10.9	2	BDL	8.3	4	29.7	25.5
A4/035	35	BDL	1.1	3.3	0.8	BDL	2.4	2	9.6	11.1
A4/065	65	BDL	BDL	0.6	BDL	BDL	0.8	1.2	2.6	4.4
A4/100	100	BDL	BDL	0.7	0.6	BDL	0.7	BDL	2	10.7
A4/125	125	BDL	BDL	0.8	BDL	BDL	0.8	1.3	2.9	6.3
A4/200	200	BDL	0.6	0.9	0.5	BDL	0.9	1.3	4.2	5.7
A4/260	260	BDL	BDL	0.7	BDL	BDL	0.8	1.4	2.9	7.2
A4/400	400	BDL	BDL	1.6	0.6	0.5	1	1.4	5.1	6.1
A4/600	600	BDL	BDL	1.4	0.5	BDL	1	1.3	4.2	6.4
A4/800	800	BDL	0.6	1.9	BDL	0.5	1.1	1.3	5.4	7.6
A4/1000	1000	BDL	0.6	2	0.9	BDL	1.1	1.2	5.8	7.8

Sc (ppm)

sample	depth	H_2O	NH4-Ac	NH_4-OxD	NH_4-OxH	H_2O_2	sulfide	residual	total	bulk
A4/010	10	BDL	1.5	4	3.5	BDL	1.5	10.8	21.3	25
A4/035	35	BDL	BDL	1.7	1.2	BDL	0.9	5.7	9.5	12.3
A4/065	65	BDL	BDL	BDL	BDL	BDL	0.6	3.9	4.5	6.9
A4/100	100	BDL	BDL	BDL	BDL	BDL	0.6	3.1	3.7	6.8
A4/125	125	BDL	BDL	0.7	BDL	BDL	0.6	4.3	5.6	7.8
A4/200	200	BDL	BDL	BDL	0.6	BDL	1	4.1	5.7	8
A4/260	260	BDL	BDL	BDL	BDL	BDL	0.9	7.1	8	12
A4/400	400	BDL	BDL	BDL	BDL	BDL	1.1	5.7	6.8	10.3
A4/600	600	BDL	BDL	BDL	BDL	BDL	1.2	5.5	6.7	10
A4/800	800	BDL	BDL	BDL	BDL	BDL	1.5	5.4	6.9	10.7
A4/1000	1000	BDL	BDL	0.6	BDL	BDL	1.7	5.6	7.9	11.8

Be (ppm)

sample	depth	H_2O	NH4-Ac	NH_4-OxD	NH_4-OxH	H_2O_2	sulfide	residual	total	bulk
A4/010	10	BDL	BDL	BDL	0.7	BDL	BDL	0.9	1.6	2.1
A4/035	35	BDL	BDL	BDL	BDL	BDL	BDL	0.9	0.9	1.5
A4/065	65	BDL	BDL	BDL	BDL	BDL	BDL	0.9	0.9	1.2
A4/100	100	BDL	BDL	BDL	BDL	BDL	BDL	0.8	0.8	1.3
A4/125	125	BDL	BDL	BDL	BDL	BDL	BDL	0.9	0.9	1.3
A4/200	200	BDL	BDL	BDL	BDL	BDL	BDL	0.8	0.8	1.3
A4/260	260	BDL	BDL	BDL	BDL	BDL	BDL	1	1	1.4
A4/400	400	BDL	BDL	BDL	BDL	BDL	BDL	0.9	0.9	1.5
A4/600	600	BDL	BDL	BDL	BDL	BDL	BDL	0.9	0.9	1.5
A4/800	800	BDL	BDL	BDL	BDL	BDL	BDL	0.9	0.9	1.5
A4/1000	1000	BDL	BDL	BDL	BDL	BDL	BDL	0.9	0.9	1.5

Ag (ppm)

sample	depth	H_2O	NH4-Ac	NH_4-OxD	NH_4-OxH	H_2O_2	sulfide	residual	total	bulk
A4/010	10	BDL	BDL	1.7	BDL	BDL	0.6	BDL	2.3	0.3
A4/035	35	BDL	BDL	BDL	BDL	BDL	0.6	BDL	0.6	0.3
A4/065	65	BDL	BDL	BDL	BDL	BDL	0.7	BDL	0.7	0.2
A4/100	100	BDL	BDL	BDL	0.6	BDL	0.6	BDL	1.2	0.4
A4/125	125	0.3	BDL	BDL	BDL	BDL	0.6	BDL	0.9	0.4
A4/200	200	BDL	BDL	BDL	0.4	BDL	1	BDL	1.4	0.6
A4/260	260	BDL	BDL	BDL	BDL	BDL	0.9	BDL	0.9	1.1
A4/400	400	BDL	BDL	BDL	BDL	BDL	0.6	BDL	0.6	0.4
A4/600	600	BDL	BDL	BDL	BDL	BDL	0.7	BDL	0.7	0.8
A4/800	800	BDL	BDL	BDL	BDL	BDL	0.6	BDL	0.6	0.5
A4/1000	1000	BDL	BDL	BDL	0.2	BDL	0.7	BDL	0.9	0.2

Table A3.1.4: *Drill core A5 from Piuquenes/Andina* *sequnece B*

Fe (%)

sample	depth	H_2O	NH4-Ac	NH_4-OxD	NH_4-OxH	H_2O_2	sulfide	residual	total	bulk
A5/020	20	BDL	0.25	1.4	1.46	0.01	0.58	1.02	4.72	5.55
A5/050	50	BDL	0.05	0.75	1.1	0.1	1.27	1.1	4.37	5.08
A5/140	140	BDL	0.06	0.89	1.24	BDL	1.53	1.2	4.92	5.89
A5/500	500	BDL	0.11	1.13	1.42	0.09	1.39	1.1	5.24	6.3
A5/900	900	0.02	0.25	1.76	1.39	0.08	1.39	0.93	5.82	6.82

Al (%)

sample	depth	H_2O	NH4-Ac	NH_4-OxD	NH_4-OxH	H_2O_2	sulfide	residual	total	bulk
A5/020	20	BDL	0.14	0.28	0.29	BDL	0.4	5.42	6.53	7.8
A5/050	50	BDL	0.05	0.11	0.14	BDL	0.4	6.01	6.71	7.42
A5/140	140	BDL	0.05	0.1	0.12	BDL	0.49	5.88	6.64	7.45
A5/500	500	BDL	0.04	0.08	0.09	BDL	0.45	5.42	6.08	7.94
A5/900	900	0.02	0.14	0.3	0.15	BDL	0.63	5.8	7.04	8.19

K (%)

sample	depth	H_2O	NH4-Ac	NH_4-OxD	NH_4-OxH	H_2O_2	sulfide	residual	total	bulk
A5/020	20	0.08	0.06	0.17	0.11	BDL	-	3.45	3.87	4.76
A5/050	50	0.01	BDL	0.06	0.05	BDL	-	3.55	3.67	4.51
A5/140	140	0.02	BDL	0.05	0.03	BDL	-	3.28	3.38	4.28
A5/500	500	0.03	0.02	0.02	0.01	BDL	-	2.79	2.87	4.28
A5/900	900	0.07	0.09	0.05	0.03	BDL	-	3.08	3.32	4.55

Mg (%)

sample	depth	H_2O	NH4-Ac	NH_4-OxD	NH_4-OxH	H_2O_2	sulfide	residual	total	bulk
A5/020	20	0.03	0.03	0.04	0.14	0.01	0.23	0.29	0.77	0.83
A5/050	50	0.03	BDL	BDL	0.06	BDL	0.31	0.37	0.77	0.81
A5/140	140	0.02	BDL	BDL	0.05	BDL	0.38	0.38	0.83	0.9
A5/500	500	0.01	0.02	0.03	0.03	0.01	0.36	0.27	0.73	0.87
A5/900	900	BDL	0.03	0.05	0.04	0.01	0.45	0.25	0.83	0.94

Na (%)

sample	depth	H_2O	NH4-Ac	NH_4-OxD	NH_4-OxH	H_2O_2	sulfide	residual	total	bulk
A5/020	20	0.01	BDL	BDL	BDL	BDL	BDL	0.74	0.75	0.87
A5/050	50	BDL	BDL	BDL	BDL	BDL	BDL	0.64	0.64	0.71
A5/140	140	BDL	BDL	BDL	BDL	BDL	BDL	0.58	0.58	0.66
A5/500	500	BDL	BDL	BDL	BDL	BDL	BDL	0.72	0.72	0.99
A5/900	900	0.01	BDL	BDL	BDL	BDL	BDL	0.83	0.84	1.06

Ca (%)

sample	depth	H_2O	NH4-Ac	NH_4-OxD	NH_4-OxH	H_2O_2	sulfide	residual	total	bulk
A5/020	20	BDL	BDL	0.01	0.01	0.04	0.03	0.09	0.18	0.22
A5/050	50	0.07	BDL	0.01	0.01	0.04	0.05	0.09	0.27	0.29
A5/140	140	0.03	BDL	0.01	0.01	BDL	0.05	0.14	0.24	0.3
A5/500	500	0.07	0.09	BDL	0.01	0.08	0.06	0.1	0.41	0.46
A5/900	900	0.04	0.09	BDL	BDL	0.1	0.06	0.1	0.39	0.46

Ti (%)

sample	depth	H_2O	NH4-Ac	NH_4-OxD	NH_4-OxH	H_2O_2	sulfide	residual	total	bulk
A5/020	20	BDL	BDL	BDL	0.02	BDL	0.02	0.15	0.19	0.23
A5/050	50	BDL	BDL	BDL	0.01	BDL	0.02	0.14	0.17	0.2
A5/140	140	BDL	BDL	BDL	0.01	BDL	0.03	0.15	0.19	0.23
A5/500	500	BDL	BDL	BDL	0.02	BDL	0.03	0.14	0.19	0.23
A5/900	900	BDL	BDL	BDL	0.02	BDL	0.05	0.16	0.23	0.27

P (%)

sample	depth	H_2O	NH4-Ac	NH_4-OxD	NH_4-OxH	H_2O_2	sulfide	residual	total	bulk
A5/020	20	BDL	BDL	0.04	BDL	BDL	0.02	0.01	0.07	0.07
A5/050	50	BDL	BDL	0.03	BDL	BDL	0.03	0.01	0.07	0.06
A5/140	140	BDL	BDL	0.03	BDL	BDL	0.03	0.01	0.07	0.04
A5/500	500	BDL	BDL	0.03	BDL	BDL	0.03	BDL	0.06	0.06
A5/900	900	BDL	BDL	0.04	BDL	BDL	0.03	0.01	0.08	0.07

Ba (ppm)

sample	depth	H_2O	NH4-Ac	NH_4-OxD	NH_4-OxH	H_2O_2	sulfide	residual	total	bulk
A5/020	20	BDL	4	43	56	1	20	481	605	782
A5/050	50	BDL	4	27	35	BDL	20	497	583	772
A5/140	140	BDL	3	19	22	BDL	17	457	518	679
A5/500	500	BDL	21	9	16	1	18	347	412	672
A5/900	900	2	54	13	22	1	25	419	536	774

Sr (ppm)

sample	depth	H_2O	NH4-Ac	NH_4-OxD	NH_4-OxH	H_2O_2	sulfide	residual	total	bulk
A5/020	20	BDL	0.8	1.8	4.4	2.5	5.3	73	87.8	120
A5/050	50	0.6	BDL	1.2	5.8	1.6	8.4	71.2	88.8	111
A5/140	140	BDL	BDL	2.3	4.2	0.6	6.3	67.8	81.2	102
A5/500	500	1.6	3.6	0.7	0.9	3	2.1	67.1	79	114
A5/900	900	0.8	4.1	BDL	1.1	2.8	1.8	64.3	74.9	103

Ni (ppm)

sample	depth	H_2O	NH4-Ac	NH_4-OxD	NH_4-OxH	H_2O_2	sulfide	residual	total	bulk
A5/020	20	BDL	BDL	3	3	BDL	5	3	14	15
A5/050	50	1	BDL	2	2	2	8	3	18	16
A5/140	140	1	BDL	BDL	2	BDL	11	5	19	23
A5/500	500	BDL	1	4	BDL	2	8	4	19	22
A5/900	900	BDL	2	4	3	2	10	3	24	25

Zr (ppm)

sample	depth	H_2O	NH4-Ac	NH_4-OxD	NH_4-OxH	H_2O_2	sulfide	residual	total	bulk
A5/020	20	BDL	BDL	3.6	BDL	BDL	BDL	1.2	4.8	12.9
A5/050	50	BDL	BDL	3.9	BDL	BDL	BDL	1.3	5.2	5.7
A5/140	140	BDL	BDL	BDL	BDL	BDL	BDL	1.2	1.2	12.2
A5/500	500	BDL	BDL	2.4	BDL	BDL	BDL	2.7	5.1	24.9
A5/900	900	BDL	BDL	1.6	2.7	BDL	BDL	1.6	5.9	35.4

Co (ppm)

sample	depth	H_2O	NH4-Ac	NH_4-OxD	NH_4-OxH	H_2O_2	sulfide	residual	total	bulk
A5/020	20	BDL	BDL	BDL	2	BDL	2	BDL	4	5
A5/050	50	1	BDL	BDL	BDL	3	7	BDL	11	12
A5/140	140	2	BDL	BDL	BDL	BDL	8	BDL	10	11
A5/500	500	BDL	BDL	BDL	BDL	3	5	BDL	8	11
A5/900	900	BDL	BDL	2	BDL	3	6	BDL	11	12

Sn (ppm)

sample	depth	H_2O	NH4-Ac	NH_4-OxD	NH_4-OxH	H_2O_2	sulfide	residual	total	bulk
A5/020	20	BDL	BDL	BDL	BDL	BDL	30	BDL	30	BDL
A5/050	50	BDL	BDL	BDL	BDL	BDL	30	BDL	30	BDL
A5/140	140	BDL	BDL	BDL	BDL	BDL	29	BDL	29	BDL
A5/500	500	BDL	BDL	BDL	BDL	BDL	21	BDL	21	BDL
A5/900	900	BDL	BDL	BDL	BDL	BDL	24	BDL	24	18

Cu (ppm)

sample	depth	H2O	NH4-Ac	NH4-OxD	NH4-OxH	H2O2	sulfide	residual	total	bulk
A5/020	20	0.6	41.1	151	14.8	478	381	8.6	1075	1020
A5/050	50	213	87.7	142	47.5	806	195	16.2	1507	1400
A5/140	140	225	167	235	46.9	485	391	65.8	1616	2810
A5/500	500	4.2	315	145	25.2	1680	361	22.2	2553	1840
A5/900	900	17.2	352	128	40.4	1480	171	8.9	2198	2180

Zn (ppm)

sample	depth	H_2O	NH4-Ac	NH_4-OxD	NH_4-OxH	H_2O_2	sulfide	residual	total	bulk
A5/020	20	BDL	2.9	9.5	11.2	2.7	12.5	12.4	51.2	52.6
A5/050	50	6.8	0.8	5.8	8.2	5.9	16.3	14	57.8	59.1
A5/140	140	6.7	1.2	5.6	8.2	2.5	20.3	15	59.5	71.6
A5/500	500	0.8	33.2	95.1	39.9	54.8	28.2	20.5	272.5	293
A5/900	900	4.2	56.4	167	51.7	53.3	20	29.1	381.7	400

Mn (ppm)

sample	depth	H_2O	NH4-Ac	NH_4-OxD	NH_4-OxH	H_2O_2	sulfide	residual	total	bulk
A5/020	20	8	11	20	42	5	53	30	169	175
A5/050	50	16	BDL	10	25	3	65	36	155	160
A5/140	140	22	2	14	31	BDL	82	45	196	212
A5/500	500	7	152	324	183	93	80	23	862	950
A5/900	900	10	140	459	196	74	60	21	960	1050

Cr (ppm)

sample	depth	H_2O	NH4-Ac	NH_4-OxD	NH_4-OxH	H_2O_2	sulfide	residual	total	bulk
A5/020	20	BDL	1	5	8	BDL	5	3	22	9
A5/050	50	BDL	2	5	6	BDL	9	3	25	11
A5/140	140	BDL	BDL	4	6	BDL	12	4	26	15
A5/500	500	BDL	BDL	3	5	BDL	6	4	18	15
A5/900	900	BDL	1	6	6	BDL	7	3	23	18

Pb (ppm)

sample	depth	H_2O	NH4-Ac	NH_4-OxD	NH_4-OxH	H_2O_2	sulfide	residual	total	bulk
A5/020	20	BDL	BDL	7	7	BDL	8	BDL	22	30
A5/050	50	BDL	BDL	8	5	BDL	9	BDL	22	20
A5/140	140	BDL	BDL	6	2	BDL	6	BDL	14	17
A5/500	500	BDL	6	12	4	3	10	BDL	35	38
A5/900	900	BDL	7	8	5	2	18	BDL	40	46

Mo (ppm)

sample	depth	H_2O	NH4-Ac	NH_4-OxD	NH_4-OxH	H_2O_2	sulfide	residual	total	bulk
A5/020	20	BDL	BDL	28	3	17	59	BDL	107	106
A5/050	50	BDL	BDL	6	1	1	59	4	71	60
A5/140	140	BDL	BDL	5	BDL	BDL	81	9	95	84
A5/500	500	BDL	BDL	2	BDL	BDL	40	5	47	41
A5/900	900	BDL	BDL	2	BDL	BDL	38	2	42	41

V (ppm)

sample	depth	H_2O	NH4-Ac	NH_4-OxD	NH_4-OxH	H_2O_2	sulfide	residual	total	bulk
A5/020	20	BDL	BDL	12	21	BDL	8	52	93	103
A5/050	50	BDL	BDL	6	14	BDL	11	55	86	94
A5/140	140	BDL	BDL	7	14	BDL	14	59	94	107
A5/500	500	BDL	BDL	7	16	BDL	14	54	91	115
A5/900	900	BDL	BDL	16	20	BDL	19	54	109	128

As (ppm)

sample	depth	H_2O	NH4-Ac	NH_4-OxD	NH_4-OxH	H_2O_2	sulfide	residual	total	bulk
A5/020	20	BDL	BDL	28	BDL	BDL	6	BDL	34	41
A5/050	50	BDL	BDL	12	BDL	BDL	11	3	26	52
A5/140	140	BDL	BDL	11	BDL	BDL	15	BDL	26	21
A5/500	500	BDL	5	41	3	BDL	49	BDL	98	47
A5/900	900	BDL	6	46	3	BDL	77	BDL	132	7

W (ppm)

sample	depth	H_2O	NH4-Ac	NH_4-OxD	NH_4-OxH	H_2O_2	sulfide	residual	total	bulk
A5/020	20	BDL	BDL	BDL	BDL	BDL	BDL	27	27	22
A5/050	50	BDL	BDL	BDL	BDL	BDL	BDL	29	29	27
A5/140	140	BDL	BDL	BDL	BDL	BDL	BDL	23	23	16
A5/500	500	BDL	BDL	BDL	BDL	BDL	BDL	15	15	BDL
A5/900	900	BDL	BDL	BDL	BDL	BDL	BDL	19	19	13

La (ppm)

sample	depth	H_2O	NH4-Ac	NH_4-OxD	NH_4-OxH	H_2O_2	sulfide	residual	total	bulk
A5/020	20	BDL	BDL	5.1	2.1	BDL	6.1	2.6	15.9	15.7
A5/050	50	BDL	BDL	5.3	1.8	0.6	3.2	7.4	18.3	14.6
A5/140	140	BDL	BDL	BDL	1.1	BDL	1.9	7.8	10.8	13.7
A5/500	500	BDL	BDL	3	0.5	0.7	2.9	5.9	13	18.7
A5/900	900	BDL	BDL	1.8	3.9	0.7	3.7	8.2	18.3	20.2

Y (ppm)

sample	depth	H_2O	NH4-Ac	NH_4-OxD	NH_4-OxH	H_2O_2	sulfide	residual	total	bulk
A5/020	20	BDL	BDL	1.2	0.6	BDL	0.7	0.8	3.3	4.5
A5/050	50	BDL	BDL	1.1	BDL	BDL	0.8	1.3	3.2	4.3
A5/140	140	BDL	BDL	0.6	BDL	BDL	0.9	1.6	3.1	4.4
A5/500	500	BDL	BDL	0.9	BDL	BDL	0.9	1	2.8	5.2
A5/900	900	BDL	BDL	0.6	1.7	BDL	0.6	1.1	5.3	7

Sc (ppm)

sample	depth	H_2O	NH4-Ac	NH_4-OxD	NH_4-OxH	H_2O_2	sulfide	residual	total	bulk
A5/020	20	BDL	BDL	0.8	0.5	BDL	0.6	3.8	5.7	7.9
A5/050	50	BDL	BDL	0.5	BDL	BDL	0.7	4.1	5.3	7
A5/140	140	BDL	BDL	BDL	BDL	BDL	1.1	5.3	6.4	8.5
A5/500	500	BDL	BDL	BDL	BDL	BDL	1	5.1	6.1	9.7
A5/900	900	BDL	BDL	BDL	BDL	BDL	1.8	5.2	7	10.7

Be (ppm)

sample	depth	H_2O	NH4-Ac	NH_4-OxD	NH_4-OxH	H_2O_2	sulfide	residual	total	bulk
A5/020	20	BDL	BDL	BDL	BDL	BDL	BDL	0.8	0.8	1.2
A5/050	50	BDL	BDL	BDL	BDL	BDL	BDL	0.9	0.9	1.2
A5/140	140	BDL	BDL	BDL	BDL	BDL	BDL	0.9	0.9	1.2
A5/500	500	BDL	BDL	BDL	BDL	BDL	BDL	0.8	0.8	1.4
A5/900	900	BDL	BDL	BDL	BDL	BDL	BDL	0.8	0.8	1.4

Ag (ppm)

sample	depth	H_2O	NH4-Ac	NH_4-OxD	NH_4-OxH	H_2O_2	sulfide	residual	total	bulk
A5/020	20	BDL	BDL	BDL	0.2	BDL	0.4	BDL	0.6	0.6
A5/050	50	BDL	BDL	BDL	BDL	BDL	0.6	BDL	0.6	0.3
A5/140	140	BDL	BDL	BDL	BDL	BDL	BDL	0.8	BDL	0.8	0.4
A5/500	500	BDL	BDL	BDL	BDL	BDL	BDL	0.7	BDL	0.7	0.7
A5/900	900	BDL	BDL	BDL	BDL	BDL	BDL	1	BDL	1	0.8

Fe (%)										
sample	depth	H_2O	NH4-Ac	NH_4-OxD	NH_4-OxH	H_2O_2	sulfide	residual	total	bulk
AS3/002	2	BDL	0.07	0.56	4.83	0.07	0.93	0.99	7.45	8.07
AS3/010	10	BDL	0.04	1.36	1.47	0.04	0.42	1.09	4.42	5.14
AS3/016	16	BDL	0.12	2.33	1.12	0.02	0.61	1.16	5.36	6.45
Al (%)										
sample	depth	H_2O	NH4-Ac	NH_4-OxD	NH_4-OxH	H_2O_2	sulfide	residual	total	bulk
AS3/002	2	BDL	0.07	0.18	0.58	0.3	0.68	7.28	9.09	10.1
AS3/010	10	BDL	BDL	0.04	0.15	0.03	0.26	5.35	5.83	6.43
AS3/016	16	BDL	0.02	0.05	0.18	0.06	0.45	6.22	6.98	7.86
K (%)										
sample	depth	H_2O	NH4-Ac	NH_4-OxD	NH_4-OxH	H_2O_2	sulfide	residual	total	bulk
AS3/002	2	0.01	0.02	0.01	0.12	0.1	-	2.75	3.01	3.82
AS3/010	10	BDL	BDL	0.17	0.1	BDL	-	3.17	3.44	4.13
AS3/016	16	BDL	BDL	0.3	0.05	0.01	-	3.55	3.91	4.73
Mg (%)										
sample	depth	H_2O	NH4-Ac	NH_4-OxD	NH_4-OxH	H_2O_2	sulfide	residual	total	bulk
AS3/002	2	BDL	0.03	0.03	0.25	0.02	0.42	0.28	1.03	1.09
AS3/010	10	BDL	BDL	BDL	0.07	BDL	0.2	0.29	0.56	0.59
AS3/016	16	BDL	BDL	0.01	0.12	BDL	0.36	0.37	0.86	0.95
Na (%)										
sample	depth	H_2O	NH4-Ac	NH_4-OxD	NH_4-OxH	H_2O_2	sulfide	residual	total	bulk
AS3/002	2	BDL	BDL	BDL	BDL	0.01	0.01	1.19	1.21	1.53
AS3/010	10	BDL	BDL	BDL	BDL	BDL	BDL	0.81	0.81	0.94
AS3/016	16	BDL	BDL	BDL	BDL	BDL	BDL	0.76	0.76	0.91
Ca (%)										
sample	depth	H_2O	NH4-Ac	NH_4-OxD	NH_4-OxH	H_2O_2	sulfide	residual	total	bulk
AS3/002	2	0.08	0.52	0.02	0.01	BDL	0.45	0.17	1.25	1.31
AS3/010	10	0.02	0.02	0.02	0.01	0.01	0.06	0.11	0.25	0.25
AS3/016	16	0.02	0.02	BDL	0.01	BDL	0.07	0.09	0.21	0.25
Ti (%)										
sample	depth	H_2O	NH4-Ac	NH_4-OxD	NH_4-OxH	H_2O_2	sulfide	residual	total	bulk
AS3/002	2	BDL	BDL	BDL	0.05	0.01	0.02	0.44	0.52	0.62
AS3/010	10	BDL	BDL	BDL	0.02	BDL	0.02	0.14	0.18	0.18
AS3/016	16	BDL	BDL	BDL	0.02	BDL	0.02	0.16	0.2	0.25
Na (%)										
sample	depth	H_2O	NH4-Ac	NH_4-OxD	NH_4-OxH	H_2O_2	sulfide	residual	total	bulk
AS3/002	2	BDL	BDL	0.1	0.04	BDL	0.02	BDL	0.16	0.16
AS3/010	10	BDL	BDL	0.03	BDL	BDL	0.02	0.01	0.06	0.06
AS3/016	16	BDL	BDL	0.05	BDL	BDL	0.02	0.01	0.08	0.09
Ba (ppm)										
sample	depth	H_2O	NH4-Ac	NH_4-OxD	NH_4-OxH	H_2O_2	sulfide	residual	total	bulk
AS3/002	2	2	101	106	149	13	81	299	751	853
AS3/010	10	BDL	3	28	47	1	18	460	557	700
AS3/016	16	BDL	BDL	90	39	2	22	464	617	785
Sr (ppm)										
sample	depth	H_2O	NH4-Ac	NH_4-OxD	NH_4-OxH	H_2O_2	sulfide	residual	total	bulk
AS3/002	2	0.9	9.1	1.2	5	0.8	14	79.2	110	134
AS3/010	10	BDL	BDL	4.6	5.1	1.2	6.6	76.9	94.4	115
AS3/016	16	BDL	BDL	3	7.3	1.1	18.2	71	101	121
Ni (ppm)										
sample	depth	H_2O	NH4-Ac	NH_4-OxD	NH_4-OxH	H_2O_2	sulfide	residual	total	bulk
AS3/002	2	BDL	2	11	12	BDL	6	3	34	17
AS3/010	10	BDL	BDL	3	2	BDL	3	3	11	10
AS3/016	16	BDL	BDL	2	2	BDL	6	4	14	16
Zr (ppm)										
sample	depth	H_2O	NH4-Ac	NH_4-OxD	NH_4-OxH	H_2O_2	sulfide	residual	total	bulk
AS3/002	2	BDL	BDL	5.3	17.7	5.6	0.9	44.9	74.4	68
AS3/010	10	BDL	BDL	4.9	1.2	BDL	BDL	2.6	8.7	5
AS3/016	16	BDL	BDL	4.2	BDL	BDL	BDL	2.2	6.4	5.8
Co (ppm)										
sample	depth	H_2O	NH4-Ac	NH_4-OxD	NH_4-OxH	H_2O_2	sulfide	residual	total	bulk
AS3/002	2	BDL	BDL	11	6	BDL	7	BDL	24	25
AS3/010	10	BDL	BDL	BDL	BDL	BDL	BDL	1	1	1
AS3/016	16	BDL	BDL	BDL	BDL	BDL	2	BDL	2	3
Sn (ppm)										
sample	depth	H_2O	NH4-Ac	NH_4-OxD	NH_4-OxH	H_2O_2	sulfide	residual	total	bulk
AS3/002	2	BDL	BDL	BDL	BDL	BDL	14	BDL	14	138
AS3/010	10	BDL	BDL	BDL	BDL	BDL	21	BDL	21	BDL
AS3/016	16	BDL	BDL	BDL	BDL	BDL	11	BDL	11	18

Cu (ppm)										
sample	depth	H_2O	NH4-Ac	NH_4-OxD	NH_4-OxH	H_2O_2	sulfide	residual	total	bulk
AS3/002	2	9	513	385	322	66	52.8	8	1356	1240
AS3/010	10	9	15	124	35	140	327	14.7	665	676
AS3/016	16	10	14	183	7	34	237	7	493	486
Zn (ppm)										
sample	depth	H_2O	NH4-Ac	NH_4-OxD	NH_4-OxH	H_2O_2	sulfide	residual	total	bulk
AS3/002	2	0.8	25.2	26.6	81.9	3.7	60.8	26.4	225.4	219
AS3/010	10	BDL	BDL	3.6	7.4	1.6	13.5	15.3	41.4	44.8
AS3/016	16	BDL	BDL	6.5	9.6	1.2	21.2	16.1	54.6	61.8
Mn (ppm)										
sample	depth	H_2O	NH4-Ac	NH_4-OxD	NH_4-OxH	H_2O_2	sulfide	residual	total	bulk
AS3/002	2	12	333	3030	1020	16	408	69	4888	5170
AS3/010	10	BDL	BDL	9	25	3	58	33	128	139
AS3/016	16	2	BDL	17	36	BDL	91	38	184	198
Cr (ppm)										
sample	depth	H_2O	NH4-Ac	NH_4-OxD	NH_4-OxH	H_2O_2	sulfide	residual	total	bulk
AS3/002	2	BDL	BDL	1	5	BDL	3	3	12	9
AS3/010	10	BDL	BDL	4	8	BDL	2	4	18	8
AS3/016	16	BDL	BDL	6	5	BDL	4	4	19	11
Pb (ppm)										
sample	depth	H_2O	NH4-Ac	NH_4-OxD	NH_4-OxH	H_2O_2	sulfide	residual	total	bulk
AS3/002	2	BDL	BDL	7	25	BDL	15	BDL	47	48
AS3/010	10	BDL	BDL	9	5	BDL	4	BDL	18	27
AS3/016	16	BDL	BDL	12	6	BDL	9	BDL	27	35
Mo (ppm)										
sample	depth	H_2O	NH4-Ac	NH_4-OxD	NH_4-OxH	H_2O_2	sulfide	residual	total	bulk
AS3/002	2	BDL	BDL	2	4	7	BDL	BDL	13	7
AS3/010	10	BDL	BDL	29	4	39	4	2	78	70
AS3/016	16	BDL	BDL	58	5	6	5	BDL	74	76
V (ppm)										
sample	depth	H_2O	NH4-Ac	NH_4-OxD	NH_4-OxH	H_2O_2	sulfide	residual	total	bulk
AS3/002	2	BDL	BDL	6	51	6	13	82	158	174
AS3/010	10	BDL	BDL	8	19	BDL	6	48	81	87
AS3/016	16	BDL	BDL	13	16	BDL	12	61	102	116
As (ppm)										
sample	depth	H_2O	NH4-Ac	NH_4-OxD	NH_4-OxH	H_2O_2	sulfide	residual	total	bulk
AS3/002	2	BDL	BDL	21	43	BDL	BDL	BDL	64	78
AS3/010	10	BDL	BDL	17	BDL	BDL	BDL	BDL	17	28
AS3/016	16	BDL	BDL	29	BDL	BDL	BDL	BDL	29	61
W (ppm)										
sample	depth	H_2O	NH4-Ac	NH_4-OxD	NH_4-OxH	H_2O_2	sulfide	residual	total	bulk
AS3/002	2	BDL	BDL	BDL	30	BDL	BDL	BDL	30	BDL
AS3/010	10	BDL	BDL	11	BDL	BDL	BDL	23	34	17
AS3/016	16	BDL	BDL	BDL	BDL	BDL	BDL	27	27	12
La (ppm)										
sample	depth	H_2O	NH4-Ac	NH_4-OxD	NH_4-OxH	H_2O_2	sulfide	residual	total	bulk
AS3/002	2	BDL	2	5.7	16.5	BDL	16.9	5.8	46.9	29.9
AS3/010	10	BDL	BDL	6.6	2.3	BDL	4.4	5	18.3	13.1
AS3/016	16	BDL	BDL	5.8	1.8	BDL	7.2	4.9	19.7	19.2
Y (ppm)										
sample	depth	H_2O	NH4-Ac	NH_4-OxD	NH_4-OxH	H_2O_2	sulfide	residual	total	bulk
AS3/002	2	BDL	4.6	8.9	2.4	BDL	7.1	4	27	25.2
AS3/010	10	BDL	BDL	0.8	BDL	BDL	0.8	1.1	2.7	3.5
AS3/016	16	BDL	BDL	0.7	BDL	BDL	1.1	1.2	3	4.5
Sc (ppm)										
sample	depth	H_2O	NH4-Ac	NH_4-OxD	NH_4-OxH	H_2O_2	sulfide	residual	total	bulk
AS3/002	2	BDL	1.5	3.4	5.9	0.6	1.5	10	22.9	24.6
AS3/010	10	BDL	BDL	0.6	BDL	BDL	BDL	3.9	4.5	6.3
AS3/016	16	BDL	BDL	BDL	BDL	BDL	0.8	5	5.8	8.4
Be (ppm)										
sample	depth	H_2O	NH4-Ac	NH_4-OxD	NH_4-OxH	H_2O_2	sulfide	residual	total	bulk
AS3/002	2	BDL	BDL	BDL	0.9	BDL	BDL	0.9	1.8	2.2
AS3/010	10	BDL	BDL	BDL	BDL	BDL	BDL	0.8	0.8	1
AS3/016	16	BDL	BDL	BDL	BDL	BDL	BDL	0.9	0.9	1.2
Ag (ppm)										
sample	depth	H_2O	NH4-Ac	NH_4-OxD	NH_4-OxH	H_2O_2	sulfide	residual	total	bulk
AS3/002	2	BDL	BDL	BDL	BDL	BDL	0.5	0.4	0.9	BDL
AS3/010	10	BDL	BDL	BDL	BDL	BDL	0.2	BDL	0.2	0.3
AS3/016	16	BDL	BDL	BDL	BDL	BDL	0.7	BDL	0.7	0.8

Fe (%)

sample	depth	H_2O	NH4-Ac	NH_4-OxD	NH_4-OxH	H_2O_2	sulfide	residual	total	bulk
T1/010	10	BDL	0.25	0.46	0.96	0.03	1.09	0.91	3.7	4.3
T1/040	40	0.01	0.11	0.42	1.41	0.01	1.03	1.01	4	5.4
T1/100	100	BDL	0.04	0.31	0.67	BDL	1.61	0.93	3.56	5.03
T1/105	105	BDL	0.13	0.5	1.46	0.04	1.14	0.84	4.11	5.72
T1/200	200	BDL	0.05	0.31	0.51	BDL	1.93	0.93	3.73	5.5
T1/290	290	BDL	0.05	0.4	0.55	BDL	1.98	0.9	3.88	5.57
T1/400	400	BDL	0.09	0.51	0.52	BDL	1.75	1.01	3.88	5.42
T1/580	580	BDL	0.07	0.49	0.39	BDL	1.71	0.84	3.5	4.87
T1/800	800	BDL	0.1	0.42	0.5	BDL	1.79	0.85	3.66	5.18
T1/890	890	BDL	0.07	0.36	0.49	BDL	1.83	0.91	3.66	5.06

Al (%)

sample	depth	H_2O	NH4-Ac	NH_4-OxD	NH_4-OxH	H_2O_2	sulfide	residual	total	bulk
T1/010	10	BDL	0.32	0.37	0.34	0.03	1.2	6.44	8.7	8.31
T1/040	40	0.01	0.13	0.23	0.33	0.07	1.13	6.43	8.33	10.3
T1/100	100	0.01	0.09	0.19	0.21	BDL	1.25	5.62	7.37	9.85
T1/105	105	BDL	0.09	0.17	0.24	0.02	1.16	5.2	6.88	9.73
T1/200	200	BDL	0.07	0.16	0.19	BDL	1.28	5.49	7.19	10.2
T1/290	290	BDL	0.07	0.15	0.18	BDL	1.18	5.56	7.14	9.76
T1/400	400	BDL	0.09	0.21	0.23	BDL	1.27	5.6	7.4	10.1
T1/580	580	BDL	0.07	0.18	0.2	BDL	1.19	5.43	7.07	9.61
T1/800	800	BDL	0.09	0.28	0.31	BDL	1.54	5.15	7.37	10.2
T1/890	890	BDL	0.08	0.21	0.24	BDL	1.31	5.52	7.36	9.85

K (%)

sample	depth	H_2O	NH4-Ac	NH_4-OxD	NH_4-OxH	H_2O_2	sulfide	residual	total	bulk
T1/010	10	0.15	0.05	0.04	0.13	BDL	-	2.31	2.68	2.26
T1/040	40	0.05	0.01	0.05	0.17	0.02	-	2.23	2.53	3.73
T1/100	100	0.03	BDL	0.01	0.03	BDL	-	1.83	1.9	3.42
T1/105	105	0.06	0.02	0.06	0.18	BDL	-	1.81	2.13	3.6
T1/200	200	0.04	BDL	0.01	0.02	BDL	-	1.83	1.9	3.62
T1/290	290	0.03	BDL	BDL	0.02	BDL	-	1.84	1.89	3.48
T1/400	400	0.05	0.01	0.01	0.02	BDL	-	1.96	2.05	3.57
T1/580	580	0.03	0.02	BDL	0.01	BDL	-	1.86	1.92	3.47
T1/800	800	0.04	0.02	BDL	0.02	BDL	-	1.83	1.91	3.82
T1/890	890	0.04	0.02	0.01	0.02	BDL	-	1.86	1.95	3.51

Mg (%)

sample	depth	H_2O	NH4-Ac	NH_4-OxD	NH_4-OxH	H_2O_2	sulfide	residual	total	bulk
T1/010	10	0.15	0.04	0.05	0.13	0.02	0.94	0.61	1.94	2.4
T1/040	40	0.06	0.01	0.02	0.13	BDL	0.9	0.7	1.82	2.25
T1/100	100	0.04	BDL	0.02	0.09	BDL	0.96	0.69	1.8	2.24
T1/105	105	0.05	0.01	0.03	0.11	0.02	0.9	0.59	1.71	2.17
T1/200	200	0.03	BDL	0.02	0.08	BDL	0.99	0.65	1.77	2.3
T1/290	290	0.04	BDL	0.01	0.07	BDL	0.91	0.63	1.66	2.1
T1/400	400	0.04	0.02	0.02	0.09	0.01	0.98	0.71	1.87	2.38
T1/580	580	0.01	0.02	0.02	0.07	BDL	0.94	0.58	1.64	2
T1/800	800	0.01	0.02	0.03	0.11	0.01	1.22	0.64	2.04	2.55
T1/890	890	0.02	0.02	0.02	0.09	BDL	1.08	0.69	1.92	2.34

Na (%)

sample	depth	H_2O	NH4-Ac	NH_4-OxD	NH_4-OxH	H_2O_2	sulfide	residual	total	bulk
T1/010	10	0.01	BDL	BDL	0.02	BDL	0.03	0.86	0.92	0.96
T1/040	40	BDL	BDL	BDL	0.01	BDL	0.03	0.87	0.91	1.11
T1/100	100	BDL	BDL	BDL	0.01	BDL	0.03	0.83	0.87	1.2
T1/105	105	BDL	BDL	BDL	BDL	BDL	0.03	0.78	0.81	1.13
T1/200	200	BDL	BDL	BDL	BDL	BDL	0.03	0.85	0.88	1.28
T1/290	290	BDL	BDL	BDL	BDL	BDL	0.03	0.8	0.83	1.22
T1/400	400	BDL	BDL	BDL	BDL	BDL	0.03	0.8	0.83	1.15
T1/580	580	BDL	BDL	BDL	BDL	BDL	0.02	0.93	0.95	1.3
T1/800	800	BDL	BDL	BDL	BDL	BDL	0.03	0.72	0.75	1.13
T1/890	890	BDL	BDL	BDL	BDL	BDL	0.03	0.86	0.89	1.19

Ca (%)

sample	depth	H_2O	NH4-Ac	NH_4-OxD	NH_4-OxH	H_2O_2	sulfide	residual	total	bulk
T1/010	10	0.25	0.02	0.01	0.02	0.02	0.12	0.43	0.87	1.04
T1/040	40	0.21	0.01	0.01	0.02	BDL	0.15	0.47	0.87	1.09
T1/100	100	0.11	BDL	0.01	0.02	0.07	0.14	0.48	0.83	1.11
T1/105	105	0.11	0.01	BDL	0.01	0.04	0.13	0.46	0.76	1.08
T1/200	200	0.05	BDL	0.02	0.01	0.05	0.14	0.52	0.79	1.12
T1/290	290	0.07	BDL	BDL	0.01	0.05	0.13	0.47	0.73	1.05
T1/400	400	0.13	0.01	BDL	BDL	0.08	0.14	0.45	0.81	1.1
T1/580	580	0.12	0.04	BDL	BDL	0.06	0.11	0.46	0.79	1.08
T1/800	800	0.14	0.05	BDL	0.01	0.09	0.14	0.4	0.83	1.13
T1/890	890	0.12	0.02	BDL	0.01	0.06	0.12	0.44	0.77	1.01

Ti (%)

sample	depth	H_2O	NH4-Ac	NH_4-OxD	NH_4-OxH	H_2O_2	sulfide	residual	total	bulk
T1/010	10	BDL	BDL	BDL	BDL	BDL	0.07	0.2	0.27	0.36
T1/040	40	BDL	BDL	BDL	BDL	BDL	0.07	0.19	0.26	0.34
T1/100	100	BDL	BDL	BDL	BDL	BDL	0.08	0.14	0.22	0.31
T1/105	105	BDL	BDL	BDL	BDL	BDL	0.07	0.16	0.23	0.33
T1/200	200	BDL	BDL	BDL	BDL	BDL	0.08	0.14	0.22	0.32
T1/290	290	BDL	BDL	BDL	BDL	BDL	0.07	0.13	0.2	0.3
T1/400	400	BDL	BDL	BDL	BDL	BDL	0.08	0.16	0.24	0.32
T1/580	580	BDL	BDL	BDL	BDL	BDL	0.09	0.13	0.22	0.31
T1/800	800	BDL	BDL	BDL	BDL	BDL	0.11	0.15	0.26	0.34
T1/890	890	BDL	BDL	BDL	BDL	BDL	0.08	0.15	0.23	0.3

P (%)

sample	depth	H_2O	NH4-Ac	NH_4-OxD	NH_4-OxH	H_2O_2	sulfide	residual	total	bulk
T1/010	10	BDL	BDL	0.04	0.03	BDL	0.02	0.01	0.1	0.1
T1/040	40	BDL	BDL	0.04	0.03	BDL	0.02	0.01	0.1	0.12
T1/100	100	BDL	BDL	0.05	BDL	BDL	0.04	BDL	0.09	0.09
T1/105	105	BDL	BDL	0.04	0.02	BDL	0.03	BDL	0.09	0.09
T1/200	200	BDL	BDL	0.04	BDL	BDL	0.03	BDL	0.07	0.04
T1/290	290	BDL	BDL	0.03	BDL	BDL	0.03	BDL	0.06	0.05
T1/400	400	BDL	BDL	0.06	BDL	BDL	0.03	BDL	0.09	0.1
T1/580	580	BDL	BDL	0.04	BDL	BDL	0.03	BDL	0.07	0.08
T1/800	800	BDL	0.01	0.06	BDL	BDL	0.03	BDL	0.1	0.11
T1/890	890	BDL	BDL	0.05	BDL	BDL	0.03	BDL	0.08	0.09

Cu (ppm)

sample	depth	H2O	NH4-Ac	NH4-OxD	NH4-OxH	H2O2	sulfide	residual	total	bulk
T1/010	10	298	939	510	377	212	214	14.2	2564	2330
T1/040	40	593	309	332	370	14.5	155	16.3	1790	1930
T1/100	100	847	265	260	96.1	870	175	13.8	2527	2570
T1/105	105	128	198	251	218	266	172	16	1249	1340
T1/200	200	505	463	483	189	2100	1930	62.1	5732	5970
T1/290	290	1230	414	481	145	1740	1080	40.1	5130	5240
T1/400	400	114	1300	508	99.7	778	345	16.4	3161	3260
T1/580	580	6.2	692	348	105	835	183	18.4	2188	2250
T1/800	800	3.7	882	605	123	532	378	19	2543	2650
T1/890	890	6.2	443	430	108	1060	764	27.2	2838	2830

Zn (ppm)

sample	depth	H_2O	NH4-Ac	NH_4-OxD	NH_4-OxH	H_2O_2	sulfide	residual	total	bulk
T1/010	10	31.9	28.8	7.7	8.7	1	20.7	16.2	115	104
T1/040	40	15.2	2 7	3.1	8.2	BDL	21.3	16.2	66.7	82.4
T1/100	100	25	4.2	2.2	5.7	2.1	22.3	15.8	77.3	94.6
T1/105	105	13.9	14.3	5.8	6	1.6	20.9	14.7	77.2	95.7
T1/200	200	14.6	3.2	2.9	5.3	4.5	26.9	16.3	73.7	82.5
T1/290	290	22.3	3.2	2.5	5	3.5	23.2	15.8	75.5	82.8
T1/400	400	19.5	28.5	12.6	7.8	3	24.5	18.6	114.5	139
T1/580	580	BDL	16.3	6.9	5.7	1.8	23.1	18.4	72.2	87.5
T1/800	800	BDL	23.8	6.9	7.5	1.8	25.4	17.6	83	86.7
T1/890	890	1.2	18.9	5.5	5.9	2	23.1	16	72.6	74.2

Mn (ppm)

sample	depth	H_2O	NH4-Ac	NH_4-OxD	NH_4-OxH	H_2O_2	sulfide	residual	total	bulk
T1/010	10	51	9	10	22	3	108	65	268	344
T1/040	40	27	3	6	26	BDL	111	77	250	313
T1/100	100	22	BDL	5	18	4	127	76	252	316
T1/105	105	14	3	7	21	6	115	63	229	302
T1/200	200	19	2	5	16	3	131	74	250	326
T1/290	290	31	BDL	4	16	3	127	71	252	326
T1/400	400	95	19	18	25	6	140	80	383	473
T1/580	580	6	17	18	19	3	126	66	255	318
T1/800	800	4	16	14	24	5	135	63	261	333
T1/890	890	10	7	8	19	3	123	70	240	294

Cr (ppm)

sample	depth	H_2O	NH4-Ac	NH_4-OxD	NH_4-OxH	H_2O_2	sulfide	residual	total	bulk
T1/010	10	BDL	3	1	11	BDL	20	8	43	28
T1/040	40	BDL	2	4	13	BDL	21	7	47	34
T1/100	100	BDL	1	4	10	BDL	22	7	44	26
T1/105	105	BDL	1	3	15	BDL	30	6	55	38
T1/200	200	BDL	BDL	6	7	BDL	25	8	46	29
T1/290	290	BDL	BDL	2	7	BDL	21	5	35	30
T1/400	400	BDL	1	5	7	BDL	20	7	40	30
T1/580	580	BDL	1	4	6	BDL	21	5	37	25
T1/800	800	BDL	2	3	7	BDL	28	5	45	29
T1/890	890	BDL	1	5	8	BDL	27	7	48	25

Pb (ppm)

sample	depth	H_2O	NH4-Ac	NH_4-OxD	NH_4-OxH	H_2O_2	sulfide	residual	total	bulk
T1/010	10	BDL	BDL	BDL	7	BDL	9	BDL	16	29
T1/040	40	BDL	BDL	BDL	11	BDL	4	BDL	15	27
T1/100	100	BDL	BDL	4	11	BDL	5	BDL	20	22
T1/105	105	BDL	BDL	3	5	BDL	3	BDL	11	20
T1/200	200	BDL	BDL	19	BDL	BDL	6	BDL	25	12
T1/290	290	BDL	BDL	BDL	BDL	BDL	4	BDL	4	19
T1/400	400	BDL	BDL	BDL	2	BDL	5	BDL	7	20
T1/580	580	BDL	BDL	BDL	7	BDL	6	BDL	13	14
T1/800	800	BDL	2	BDL	5	BDL	5	BDL	12	24
T1/890	890	BDL	BDL	3	3	BDL	4	BDL	10	13

Mo (ppm)

sample	depth	H_2O	NH4-Ac	NH_4-OxD	NH_4-OxH	H_2O_2	sulfide	residual	total	bulk
T1/010	10	BDL	2	37	37	27	2	BDL	105	92
T1/040	40	BDL	2	33	53	29	6	BDL	123	139
T1/100	100	BDL	BDL	17	12	BDL	48	BDL	77	87
T1/105	105	BDL	2	32	35	49	32	1	151	155
T1/200	200	BDL	1	20	6	BDL	82	10	119	143
T1/290	290	BDL	1	21	5	BDL	74	9	110	122
T1/400	400	BDL	1	22	2	BDL	32	4	61	67
T1/580	580	3	BDL	17	2	BDL	32	4	58	85
T1/800	800	8	2	42	7	BDL	20	BDL	79	84
T1/890	890	2	1	23	7	BDL	61	5	99	111

V (ppm)

sample	depth	H_2O	NH4-Ac	NH_4-OxD	NH_4-OxH	H_2O_2	sulfide	residual	total	bulk
T1/010	10	BDL	4	13	18	BDL	48	105	188	184
T1/040	40	BDL	BDL	7	21	BDL	46	107	181	222
T1/100	100	BDL	BDL	6	19	BDL	54	88	167	209
T1/105	105	BDL	BDL	7	25	BDL	47	89	168	221
T1/200	200	BDL	BDL	10	13	BDL	57	90	170	221
T1/290	290	BDL	BDL	4	13	BDL	50	83	150	204
T1/400	400	BDL	BDL	8	12	BDL	54	92	166	216
T1/580	580	BDL	BDL	7	11	BDL	54	76	148	190
T1/800	800	BDL	BDL	4	13	BDL	66	80	163	211
T1/890	890	BDL	BDL	7	13	BDL	58	88	166	211

As (ppm)

sample	depth	H_2O	NH4-Ac	NH_4-OxD	NH_4-OxH	H_2O_2	sulfide	residual	total	bulk
T1/010	10	BDL	6	37	25	BDL	BDL	BDL	68	72
T1/040	40	BDL	7	44	38	BDL	BDL	BDL	89	134
T1/100	100	BDL	7	52	17	BDL	BDL	BDL	76	96
T1/105	105	BDL	BDL	26	28	BDL	BDL	BDL	54	112
T1/200	200	BDL	4	41	4	BDL	8	BDL	57	83
T1/290	290	BDL	4	20	4	BDL	7	BDL	35	43
T1/400	400	BDL	4	36	5	BDL	BDL	BDL	45	59
T1/580	580	BDL	6	40	10	BDL	BDL	BDL	56	25
T1/800	800	BDL	19	134	22	BDL	BDL	BDL	175	202
T1/890	890	BDL	8	61	12	BDL	BDL	BDL	81	103

Ba (ppm)

sample	depth	H_2O	NH4-Ac	NH_4-OxD	NH_4-OxH	H_2O_2	sulfide	residual	total	bulk
T1/010	10	BDL	1	7	37	1	39	263	348	503
T1/040	40	BDL	BDL	2	44	2	35	256	339	465
T1/100	100	BDL	2	13	19	1	40	226	301	454
T1/105	105	BDL	BDL	9	36	2	39	205	291	437
T1/200	200	BDL	3	18	11	1	39	223	295	477
T1/290	290	BDL	2	16	13	1	35	225	292	470
T1/400	400	1	8	10	13	1	41	251	325	502
T1/580	580	BDL	11	8	11	1	42	241	314	472
T1/800	800	BDL	12	8	10	1	51	226	308	517
T1/890	890	BDL	8	8	8	1	36	208	269	406

Sr (ppm)

sample	depth	H_2O	NH4-Ac	NH_4-OxD	NH_4-OxH	H_2O_2	sulfide	residual	total	bulk
T1/010	10	1.2	0.6	1.7	10.7	3	22.8	152	192	201
T1/040	40	1.6	BDL	2.3	15.9	2	21.1	144	187	272
T1/100	100	2.8	BDL	2.6	9	5.8	14.8	135	170	275
T1/105	105	1.3	BDL	2.6	11.7	4.2	14.8	115	150	249
T1/200	200	1.4	BDL	1.6	2.6	2.5	11.6	125	145	247
T1/290	290	1.4	BDL	1	2.9	3.4	11.4	120	140	240
T1/400	400	7.8	2.1	0.8	4.1	4.7	15.6	130	165	263
T1/580	580	3.2	2.7	0.8	2.9	2.7	9.8	130	152	247
T1/800	800	4	4.4	1	4.6	5.2	15.3	113	148	242
T1/890	890	3.1	1.8	1.6	4.3	4.2	10.4	111	136	219

Ni (ppm)

sample	depth	H_2O	NH4-Ac	NH_4-OxD	NH_4-OxH	H_2O_2	sulfide	residual	total	bulk
T1/010	10	3	2	4	BDL	BDL	13	8	30	39
T1/040	40	2	BDL	1	6	BDL	14	9	32	38
T1/100	100	2	BDL	2	3	BDL	16	8	31	38
T1/105	105	1	BDL	3	1	BDL	18	7	30	42
T1/200	200	1	BDL	7	1	BDL	18	8	35	42
T1/290	290	2	BDL	BDL	1	BDL	17	8	28	40
T1/400	400	BDL	1	2	3	BDL	15	9	30	39
T1/580	580	BDL	BDL	3	5	BDL	15	7	30	34
T1/800	800	BDL	BDL	3	4	BDL	19	8	34	40
T1/890	890	BDL	BDL	2	2	BDL	19	10	33	39

Zr (ppm)

sample	depth	H_2O	NH4-Ac	NH_4-OxD	NH_4-OxH	H_2O_2	sulfide	residual	total	bulk
T1/010	10	BDL	BDL	BDL	BDL	BDL	BDL	7	7	10
T1/040	40	BDL	BDL	BDL	6.4	BDL	BDL	4	10.4	55.5
T1/100	100	BDL	BDL	3.2	2.4	BDL	BDL	3.2	8.8	60.4
T1/105	105	BDL	BDL	3	BDL	BDL	BDL	2.1	5.1	57.5
T1/200	200	BDL	BDL	12.3	BDL	BDL	BDL	1.7	14	49
T1/290	290	BDL	BDL	BDL	BDL	BDL	BDL	4.1	4.1	55.1
T1/400	400	BDL	BDL	BDL	3.1	BDL	BDL	1.9	5	46.1
T1/580	580	BDL	BDL	4.1	6.1	BDL	BDL	4.7	14.9	57
T1/800	800	BDL	BDL	4.5	3.4	BDL	BDL	2.1	10	51.8
T1/890	890	BDL	BDL	2.4	1.1	BDL	BDL	6.6	10.1	27.8

Co (ppm)

sample	depth	H_2O	NH4-Ac	NH_4-OxD	NH_4-OxH	H_2O_2	sulfide	residual	total	bulk
T1/010	10	5	2	BDL	2	BDL	5	2	16	14
T1/040	40	4	BDL	BDL	BDL	BDL	5	2	11	13
T1/100	100	3	BDL	BDL	2	2	10	3	20	19
T1/105	105	2	BDL	BDL	2	1	5	1	11	12
T1/200	200	2	BDL	2	BDL	1	15	2	22	25
T1/290	290	4	BDL	BDL	BDL	2	16	2	24	28
T1/400	400	4	2	BDL	BDL	3	11	2	22	25
T1/580	580	BDL	BDL	BDL	BDL	2	11	2	15	18
T1/800	800	BDL	BDL	BDL	BDL	2	10	2	14	19
T1/890	890	BDL	BDL	BDL	BDL	1	12	2	15	17

Sn (ppm)

sample	depth	H_2O	NH4-Ac	NH_4-OxD	NH_4-OxH	H_2O_2	sulfide	residual	total	bulk
T1/010	10	BDL	BDL	BDL	BDL	BDL	17	BDL	17	50
T1/040	40	BDL	BDL	BDL	BDL	BDL	11	BDL	11	42
T1/100	100	BDL	BDL	BDL	BDL	BDL	17	BDL	17	34
T1/105	105	BDL	BDL	BDL	BDL	BDL	16	BDL	16	39
T1/200	200	BDL	BDL	BDL	BDL	BDL	17	BDL	17	37
T1/290	290	BDL	BDL	BDL	BDL	BDL	17	BDL	17	32
T1/400	400	BDL	BDL	BDL	BDL	BDL	17	BDL	17	32
T1/580	580	BDL	BDL	BDL	BDL	BDL	17	BDL	17	26
T1/800	800	BDL	BDL	BDL	BDL	BDL	17	BDL	17	38
T1/890	890	BDL	BDL	BDL	BDL	BDL	17	BDL	17	28

W (ppm)

sample	depth	H_2O	NH4-Ac	NH_4-OxD	NH_4-OxH	H_2O_2	sulfide	residual	total	bulk
T1/010	10	BDL	BDL	BDL	BDL	BDL	BDL	18	18	16
T1/040	40	BDL	BDL	BDL	14	BDL	BDL	17	31	11
T1/100	100	BDL	BDL	BDL	10	BDL	BDL	BDL	12	22	BDL
T1/105	105	BDL	BDL	BDL	BDL	BDL	BDL	17	17	BDL
T1/200	200	BDL	BDL	27	BDL	BDL	BDL	14	41	BDL
T1/290	290	BDL	BDL	BDL	BDL	BDL	BDL	15	15	BDL
T1/400	400	BDL	BDL	BDL	BDL	BDL	BDL	13	13	BDL
T1/580	580	BDL	BDL	11	14	BDL	BDL	10	35	BDL
T1/800	800	BDL	BDL	BDL	12	BDL	BDL	13	25	11
T1/890	890	BDL	BDL	BDL	BDL	BDL	BDL	13	13	BDL

La (ppm)

sample	depth	H_2O	NH4-Ac	NH_4-OxD	NH_4-OxH	H_2O_2	sulfide	residual	total	bulk
T1/010	10	BDL	BDL	4.9	BDL	BDL	3.7	6.8	15.4	17.9
T1/040	40	BDL	BDL	BDL	7.6	BDL	3.2	7.5	18.3	15.1
T1/100	100	0.5	BDL	3.7	3	BDL	2.2	7.1	16.5	15.2
T1/105	105	BDL	BDL	3.4	BDL	BDL	2.5	3.8	9.7	12.6
T1/200	200	BDL	BDL	14.9	BDL	BDL	1.3	5.9	22.1	14.2
T1/290	290	BDL	BDL	BDL	BDL	BDL	1.5	7	8.5	14.9
T1/400	400	BDL	BDL	0.6	3.7	BDL	2	6.5	12.8	17
T1/580	580	BDL	BDL	5	6.7	BDL	1.7	4.9	18.3	14.7
T1/800	800	BDL	BDL	5.4	3.8	BDL	2.2	6.5	17.9	18.5
T1/890	890	BDL	BDL	2.8	1.7	BDL	1.4	5.1	11	13.5

Y (ppm)

sample	depth	H_2O	NH4-Ac	NH_4-OxD	NH_4-OxH	H_2O_2	sulfide	residual	total	bulk
T1/010	10	BDL	0.6	3.1	1.7	BDL	1.5	2.2	9.1	6.2
T1/040	40	BDL	BDL	0.8	BDL	BDL	1.6	1.9	4.3	7.8
T1/100	100	BDL	BDL	1	0.9	BDL	1.6	1.6	5.1	7
T1/105	105	BDL	BDL	BDL	1.1	BDL	1.4	1.1	3.6	6.3
T1/200	200	BDL	BDL	2.4	BDL	BDL	1.3	1.2	4.9	6.3
T1/290	290	BDL	BDL	BDL	BDL	BDL	1.2	1.3	2.5	7.6
T1/400	400	BDL	BDL	0.7	BDL	BDL	1.4	1.2	3.3	7.2
T1/580	580	BDL	BDL	BDL	BDL	BDL	1.3	1.1	2.4	6.4
T1/800	800	BDL	BDL	BDL	BDL	0.5	1.4	1.3	3.2	7
T1/890	890	BDL	BDL	0.9	BDL	BDL	1.2	1	3.1	5.7

Sc (ppm)

sample	depth	H_2O	NH4-Ac	NH_4-OxD	NH_4-OxH	H_2O_2	sulfide	residual	total	bulk
T1/010	10	BDL	0.7	1	BDL	BDL	4.5	10	16.2	17.2
T1/040	40	BDL	BDL	BDL	1.3	BDL	4.4	9.3	15	20.8
T1/100	100	BDL	BDL	0.5	0.6	BDL	4.7	7.8	13.6	19.3
T1/105	105	BDL	BDL	0.5	BDL	BDL	4.3	7.7	12.5	20.1
T1/200	200	BDL	BDL	1.4	BDL	BDL	4.8	7.9	14.1	21.3
T1/290	290	BDL	BDL	BDL	BDL	BDL	4.2	7.6	11.8	18.5
T1/400	400	BDL	BDL	BDL	0.6	BDL	4.5	7.3	12.4	19.7
T1/580	580	BDL	BDL	0.6	0.9	BDL	4.7	6.6	12.8	17.3
T1/800	800	BDL	BDL	0.7	0.7	BDL	5.9	6.5	13.8	20.1
T1/890	890	BDL	BDL	BDL	BDL	BDL	5.1	8.1	13.2	20

Be (ppm)

sample	depth	H_2O	NH4-Ac	NH_4-OxD	NH_4-OxH	H_2O_2	sulfide	residual	total	bulk
T1/010	10	BDL	BDL	BDL	BDL	BDL	BDL	0.7	0.7	1.1
T1/040	40	BDL	BDL	BDL	BDL	BDL	BDL	0.7	0.7	1.1
T1/100	100	BDL	BDL	BDL	BDL	BDL	BDL	0.6	0.6	1
T1/105	105	BDL	BDL	BDL	BDL	BDL	BDL	0.7	0.7	1.1
T1/200	200	BDL	BDL	BDL	BDL	BDL	BDL	0.7	0.7	1.1
T1/290	290	BDL	BDL	BDL	BDL	BDL	BDL	0.6	0.6	1
T1/400	400	BDL	BDL	BDL	BDL	BDL	BDL	0.6	0.6	1.1
T1/580	580	BDL	BDL	BDL	BDL	BDL	BDL	0.6	0.6	1
T1/800	800	BDL	BDL	BDL	BDL	BDL	BDL	0.6	0.6	1
T1/890	890	BDL	BDL	BDL	BDL	BDL	BDL	0.7	0.7	1.1

Ag (ppm)

sample	depth	H_2O	NH4-Ac	NH_4-OxD	NH_4-OxH	H_2O_2	sulfide	residual	total	bulk
T1/010	10	BDL	BDL	BDL	2.2	BDL	0.4	BDL	2.6	0.2
T1/040	40	BDL	BDL	BDL	BDL	BDL	0.3	BDL	0.3	0.3
T1/100	100	BDL	BDL	0.2	1.3	BDL	0.4	0.4	2.3	BDL
T1/105	105	BDL	BDL	BDL	1.8	BDL	0.3	BDL	2.1	BDL
T1/200	200	BDL	BDL	2.9	BDL	BDL	0.5	BDL	3.4	0.2
T1/290	290	BDL	BDL	BDL	BDL	BDL	0.4	BDL	0.4	0.3
T1/400	400	0.2	BDL	BDL	BDL	BDL	0.2	BDL	0.4	0.8
T1/580	580	BDL	BDL	BDL	BDL	BDL	0.3	BDL	0.3	BDL
T1/800	800	BDL	BDL	BDL	BDL	BDL	0.2	BDL	0.2	0.3
T1/890	890	BDL	BDL	BDL	BDL	BDL	0.4	BDL	0.4	BDL

Table A3.2.2: Drill core T2 from Cauquenes/Teniente *sequence B*

Fe (%)

sample	depth	H_2O	NH4-Ac	NH_4-OxD	NH_4-OxH	H_2O_2	sulfide	residual	total	bulk
T2/020	20	BDL	0.05	0.41	1.24	0.02	1.36	0.95	4.03	5.53
T2/070	70	BDL	0.17	0.53	1.06	0.01	1.62	0.97	4.36	5.51
T2/100	100	BDL	0.12	0.47	1.12	0.01	1.41	0.94	4.07	4.93
T2/160	160	BDL	0.14	0.61	1.04	0.01	1.48	0.93	4.21	5.75
T2/190	190	BDL	0.05	0.3	0.53	BDL	1.62	0.84	3.34	4.77
T2/220	220	BDL	0.12	0.5	0.66	0.03	1.61	0.97	3.89	5.47
T2/300	300	BDL	0.11	0.57	0.45	0.02	1.63	1.08	3.86	5.64
T2/400	400	BDL	0.07	0.5	0.42	BDL	1.73	0.98	3.7	5.07
T2/580	580	BDL	0.09	0.48	0.45	BDL	1.81	0.9	3.73	4.93
T2/800	800	BDL	0.19	0.53	0.71	0.03	1.98	1.02	4.46	5.69
T2/1000	1000	BDL	0.09	0.47	0.93	BDL	1.62	1.03	4.14	5.29

Al (%)

sample	depth	H_2O	NH4-Ac	NH_4-OxD	NH_4-OxH	H_2O_2	sulfide	residual	total	bulk
T2/020	20	0.02	0.08	0.27	0.54	0.1	1.46	7.01	9.48	12.2
T2/070	70	BDL	0.2	0.4	0.47	0.06	1.67	6.3	9.1	11.4
T2/100	100	BDL	0.11	0.23	0.34	0.06	1.47	5.64	7.85	9
T2/160	160	BDL	0.13	0.3	0.4	0.06	1.53	6.04	8.46	11.2
T2/190	190	BDL	0.07	0.19	0.23	BDL	1.29	5.39	7.17	10.2
T2/220	220	BDL	0.13	0.35	0.35	BDL	1.54	6.16	8.53	11.6
T2/300	300	BDL	0.11	0.27	0.29	0.01	1.3	6.33	8.31	11.4
T2/400	400	BDL	0.07	0.21	0.22	BDL	1.21	5.93	7.64	9.92
T2/580	580	BDL	0.09	0.21	0.24	BDL	1.34	5.12	7	9.61
T2/800	800	BDL	0.19	0.57	0.53	BDL	1.97	6.64	9.9	12
T2/1000	1000	BDL	0.08	0.23	0.27	BDL	1.48	4.94	7	9.46

K (%)

sample	depth	H_2O	NH4-Ac	NH_4-OxD	NH_4-OxH	H_2O_2	sulfide	residual	total	bulk
T2/020	20	0.03	0.02	0.04	0.2	0.02	-	2.68	2.99	4.81
T2/070	70	0.08	0.03	0.03	0.12	0.02	-	2.54	2.82	4.41
T2/100	100	0.05	0.02	0.04	0.13	0.01	-	2.05	2.3	3.84
T2/160	160	0.06	0.02	0.03	0.11	0.01	-	2.18	2.41	4.15
T2/190	190	0.03	BDL	0.01	0.02	BDL	-	1.81	1.87	3.55
T2/220	220	0.06	0.02	0.02	0.05	BDL	-	2.23	2.38	4.26
T2/300	300	0.05	0.02	0.01	0.02	BDL	-	2.25	2.35	4.13
T2/400	400	0.04	0.02	BDL	0.02	BDL	-	2.05	2.13	3.66
T2/580	580	0.04	0.02	0.01	0.02	BDL	-	1.93	2.02	3.51
T2/800	800	0.07	0.05	0.02	0.04	BDL	-	2.62	2.8	4.62
T2/1000	1000	0.04	0.02	0.04	0.09	BDL	-	1.95	2.14	3.5

Mg (%)

sample	depth	H_2O	NH4-Ac	NH_4-OxD	NH_4-OxH	H_2O_2	sulfide	residual	total	bulk
T2/020	20	0.11	BDL	0.02	0.18	0.01	1.24	0.69	2.25	2.71
T2/070	70	0.05	0.03	0.05	0.22	0.02	1.38	0.66	2.41	2.81
T2/100	100	0.03	0.01	0.02	0.16	BDL	1.18	0.66	2.06	2.5
T2/160	160	0.04	0.02	0.03	0.19	BDL	1.24	0.66	2.18	2.71
T2/190	190	0.02	BDL	0.02	0.09	BDL	1	0.6	1.73	2.19
T2/220	220	0.03	0.02	0.03	0.15	0.01	1.22	0.69	2.15	2.66
T2/300	300	0.03	0.02	0.02	0.12	0.01	1.01	0.78	1.99	2.54
T2/400	400	0.02	0.01	0.02	0.09	BDL	0.95	0.7	1.79	2.21
T2/580	580	0.01	0.03	0.02	0.08	BDL	1.07	0.6	1.81	2.2
T2/800	800	0.03	0.05	0.06	0.21	0.04	1.61	0.75	2.75	3.09
T2/1000	1000	0.02	0.02	0.02	0.13	0.01	1.24	0.72	2.16	2.53

Na (%)

sample	depth	H_2O	NH4-Ac	NH_4-OxD	NH_4-OxH	H_2O_2	sulfide	residual	total	bulk
T2/020	20	0.01	BDL	BDL	BDL	BDL	0.03	0.69	0.73	1.05
T2/070	70	BDL	BDL	BDL	BDL	BDL	0.03	0.68	0.71	0.89
T2/100	100	BDL	BDL	BDL	BDL	BDL	0.03	0.72	0.75	1.01
T2/160	160	BDL	BDL	BDL	BDL	BDL	0.03	0.7	0.73	1.03
T2/190	190	BDL	BDL	BDL	BDL	BDL	0.03	0.87	0.9	1.29
T2/220	220	BDL	BDL	BDL	BDL	BDL	0.03	0.74	0.77	1.13
T2/300	300	BDL	BDL	BDL	BDL	BDL	0.03	0.81	0.84	1.21
T2/400	400	BDL	BDL	BDL	BDL	BDL	0.02	0.85	0.87	1.18
T2/580	580	BDL	BDL	BDL	BDL	BDL	0.02	0.93	0.95	1.23
T2/800	800	0.01	BDL	BDL	BDL	BDL	0.04	0.58	0.63	0.86
T2/1000	1000	BDL	BDL	BDL	BDL	BDL	0.02	0.78	0.8	0.99

Ca (%)

sample	depth	H_2O	NH4-Ac	NH_4-OxD	NH_4-OxH	H_2O_2	sulfide	residual	total	bulk
T2/020	20	0.32	0.02	0.01	0.01	BDL	0.1	0.28	0.74	0.92
T2/070	70	0.22	0.02	0.01	0.02	BDL	0.16	0.3	0.73	0.84
T2/100	100	0.2	0.02	BDL	0.01	BDL	0.18	0.38	0.79	1.01
T2/160	160	0.24	0.03	BDL	0.01	BDL	0.18	0.36	0.82	1.04
T2/190	190	0.08	BDL	0.01	BDL	0.06	0.14	0.47	0.76	1.1
T2/220	220	0.1	0.01	BDL	0.01	0.06	0.12	0.37	0.67	0.93
T2/300	300	0.2	0.02	BDL	0.01	0.08	0.11	0.42	0.84	1.13
T2/400	400	0.07	0.02	BDL	0.01	0.05	0.1	0.41	0.66	0.9
T2/580	580	0.12	0.07	BDL	BDL	0.07	0.12	0.46	0.84	1.11
T2/800	800	0.17	0.07	0.01	0.01	0.1	0.12	0.26	0.74	0.88
T2/1000	1000	0.12	0.04	BDL	0.01	0.06	0.1	0.33	0.66	0.85

Tl (%)

sample	depth	H_2O	NH4-Ac	NH_4-OxD	NH_4-OxH	H_2O_2	sulfide	residual	total	bulk
T2/020	20	BDL	BDL	BDL	BDL	BDL	0.08	0.2	0.28	0.35
T2/070	70	BDL	BDL	BDL	BDL	BDL	0.09	0.18	0.27	0.35
T2/100	100	BDL	BDL	BDL	BDL	BDL	0.09	0.17	0.26	0.28
T2/160	160	BDL	BDL	BDL	BDL	BDL	0.09	0.17	0.26	0.34
T2/190	190	BDL	BDL	BDL	BDL	BDL	0.08	0.15	0.23	0.31
T2/220	220	BDL	BDL	BDL	BDL	BDL	0.09	0.16	0.25	0.35
T2/300	300	BDL	BDL	BDL	BDL	BDL	0.08	0.16	0.24	0.34
T2/400	400	BDL	BDL	BDL	BDL	BDL	0.09	0.14	0.23	0.31
T2/580	580	BDL	BDL	BDL	BDL	BDL	0.1	0.15	0.25	0.32
T2/800	800	BDL	BDL	BDL	BDL	BDL	0.11	0.18	0.29	0.36
T2/1000	1000	BDL	BDL	BDL	BDL	BDL	0.09	0.18	0.27	0.32

P (%)

sample	depth	H_2O	NH4-Ac	NH_4-OxD	NH_4-OxH	H_2O_2	sulfide	residual	total	bulk
T2/020	20	BDL	0.01	0.06	0.03	BDL	0.01	0.02	0.13	0.1
T2/070	70	BDL	0.01	0.08	0.02	BDL	0.02	0.01	0.14	0.13
T2/100	100	BDL	BDL	0.06	0.02	BDL	0.02	BDL	0.1	0.11
T2/160	160	BDL	0.01	0.07	0.02	BDL	0.02	BDL	0.12	0.14
T2/190	190	BDL	BDL	0.04	BDL	BDL	0.03	BDL	0.07	0.09
T2/220	220	BDL	0.01	0.08	BDL	BDL	0.02	BDL	0.11	0.13
T2/300	300	BDL	0.01	0.06	BDL	BDL	0.03	0.01	0.11	0.12
T2/400	400	BDL	BDL	0.05	BDL	BDL	0.03	BDL	0.08	0.08
T2/580	580	BDL	0.01	0.05	BDL	BDL	0.03	BDL	0.09	0.08
T2/800	800	BDL	0.01	0.1	0.02	BDL	0.02	BDL	0.15	0.15
T2/1000	1000	BDL	BDL	0.06	0.02	BDL	0.03	BDL	0.11	0.12

Cu (ppm)

sample	depth	H_2O	NH4-Ac	NH_4-OxD	NH_4-OxH	H_2O_2	sulfide	residual	total	bulk
T2/020	20	4560	623	516	445	94	417	14.5	6670	6720
T2/070	70	336	654	529	247	208	373	12.1	2359	2210
T2/100	100	204	271	277	229	15.3	212	12.2	1221	1130
T2/160	160	189	318	341	196	39	252	13	1348	1430
T2/190	190	106	231	365	123	896	598	18	2337	2310
T2/220	220	213	341	366	136	360	456	15.9	1888	1970
T2/300	300	153	1120	610	107	565	242	21.3	2818	3110
T2/400	400	7.6	724	670	131	1120	1010	24.9	3688	3540
T2/580	580	6.1	689	526	97	958	483	20.5	2780	2620
T2/800	800	5.5	1140	1170	190	288	1020	23.7	3837	3860
T2/1000	1000	2.2	222	331	108	493	177	16.4	1350	1290

Zn (ppm)

sample	depth	H_2O	NH4-Ac	NH_4-OxD	NH_4-OxH	H_2O_2	sulfide	residual	total	bulk
T2/020	20	85.4	7.7	3.4	11.3	1.1	28.1	19.3	156.3	125
T2/070	70	9.6	12.7	4.9	11.9	0.7	32.1	17.5	89.4	114
T2/100	100	6.4	5.3	3	8.7	0.7	27.5	18.5	70.1	72.7
T2/160	160	19.4	34.9	8.3	11.1	0.6	29	16.7	120	96.9
T2/190	190	10.2	27.4	4.2	5.4	2.3	23.8	15	88.3	75.7
T2/220	220	12.9	12.1	4.6	8.7	1.5	28	18.5	86.3	92.6
T2/300	300	6.5	9.4	5.8	7	1.7	24.2	27.3	81.9	91.4
T2/400	400	1.6	22.1	12.9	8.7	3.4	26.4	19.5	94.6	112
T2/580	580	BDL	22.3	7.6	7	2.7	26.1	20.2	85.9	83.1
T2/800	800	BDL	9.8	7.7	10.9	2.9	35	16.2	82.5	90.8
T2/1000	1000	BDL	4.3	3.5	7	2.2	26.6	16.7	60.3	73.4

Mn (ppm)

sample	depth	H_2O	NH4-Ac	NH_4-OxD	NH_4-OxH	H_2O_2	sulfide	residual	total	bulk
T2/020	20	57	3	5	32	BDL	147	63	307	371
T2/070	70	15	5	9	37	3	173	67	309	354
T2/100	100	9	2	6	28	BDL	154	71	270	337
T2/160	160	11	3	7	33	BDL	162	67	283	360
T2/190	190	5	BDL	4	17	3	132	65	226	294
T2/220	220	9	3	7	27	4	157	73	280	350
T2/300	300	11	4	9	24	4	142	87	281	364
T2/400	400	23	19	15	21	4	131	77	290	360
T2/580	580	BDL	19	19	21	4	133	69	265	317
T2/800	800	3	13	14	35	11	180	69	325	375
T2/1000	1000	6	6	8	23	4	143	73	263	308

Cr (ppm)

sample	depth	H_2O	NH4-Ac	NH_4-OxD	NH_4-OxH	H_2O_2	sulfide	residual	total	bulk
T2/020	20	BDL	2	4	10	BDL	24	7	47	32
T2/070	70	BDL	4	8	10	BDL	28	7	57	31
T2/100	100	BDL	1	5	10	BDL	25	7	48	33
T2/160	160	BDL	2	5	9	BDL	26	7	49	35
T2/190	190	BDL	1	4	5	BDL	22	5	37	27
T2/220	220	BDL	2	6	6	BDL	28	7	49	41
T2/300	300	BDL	2	6	6	BDL	22	6	42	31
T2/400	400	BDL	1	5	7	BDL	24	7	44	26
T2/580	580	BDL	1	6	6	BDL	25	4	42	24
T2/800	800	BDL	3	7	6	BDL	35	9	60	34
T2/1000	1000	BDL	1	5	11	BDL	33	6	56	33

Pb (ppm)

sample	depth	H_2O	NH4-Ac	NH_4-OxD	NH_4-OxH	H_2O_2	sulfide	residual	total	bulk
T2/020	20	BDL	BDL	BDL	15	BDL	10	BDL	25	40
T2/070	70	BDL	BDL	3	16	BDL	8	BDL	27	32
T2/100	100	BDL	BDL	2	8	BDL	7	BDL	17	25
T2/160	160	BDL	BDL	BDL	10	BDL	7	BDL	17	32
T2/190	190	BDL	BDL	4	BDL	BDL	3	BDL	7	18
T2/220	220	BDL	BDL	2	2	BDL	7	BDL	11	26
T2/300	300	BDL	BDL	BDL	4	BDL	7	BDL	11	22
T2/400	400	BDL	BDL	BDL	9	BDL	5	BDL	14	21
T2/580	580	BDL	2	10	2	BDL	5	BDL	19	25
T2/800	800	BDL	BDL	BDL	BDL	BDL	10	BDL	10	23
T2/1000	1000	BDL	BDL	7	12	BDL	5	BDL	24	51

Mo (ppm)

sample	depth	H_2O	NH4-Ac	NH_4-OxD	NH_4-OxH	H_2O_2	sulfide	residual	total	bulk
T2/020	20	BDL	1	48	70	10	2	BDL	131	140
T2/070	70	BDL	2	47	50	14	3	BDL	116	112
T2/100	100	BDL	1	28	33	15	5	BDL	82	80
T2/160	160	BDL	1	36	33	17	4	BDL	91	96
T2/190	190	BDL	1	24	9	BDL	44	3	81	89
T2/220	220	BDL	2	36	21	8	17	BDL	84	87
T2/300	300	BDL	2	36	4	BDL	36	2	80	82
T2/400	400	2	1	30	4	BDL	53	6	96	91
T2/580	580	4	1	27	3	BDL	31	4	70	64
T2/800	800	16	4	67	61	7	12	BDL	167	171
T2/1000	1000	3	2	43	33	1	54	4	140	143

V (ppm)

sample	depth	H_2O	NH4-Ac	NH_4-OxD	NH_4-OxH	H_2O_2	sulfide	residual	total	bulk
T2/020	20	BDL	BDL	3	12	2	57	116	190	245
T2/070	70	BDL	BDL	7	16	BDL	68	113	204	249
T2/100	100	BDL	BDL	6	19	BDL	60	95	180	200
T2/160	160	BDL	BDL	5	18	BDL	62	100	185	244
T2/190	190	BDL	BDL	6	11	BDL	56	85	158	207
T2/220	220	BDL	BDL	6	12	BDL	65	101	184	239
T2/300	300	BDL	BDL	7	12	BDL	56	100	175	228
T2/400	400	BDL	BDL	7	11	BDL	55	87	160	204
T2/580	580	BDL	BDL	10	12	BDL	60	82	164	196
T2/800	800	BDL	BDL	4	10	BDL	77	108	199	241
T2/1000	1000	BDL	BDL	6	18	BDL	61	98	183	210

As (ppm)

sample	depth	H_2O	NH4-Ac	NH_4-OxD	NH_4-OxH	H_2O_2	sulfide	residual	total	bulk
T2/020	20	BDL	9	76	46	BDL	BDL	BDL	131	106
T2/070	70	BDL	9	82	30	BDL	BDL	BDL	121	153
T2/100	100	BDL	5	53	23	BDL	BDL	BDL	81	56
T2/160	160	BDL	6	61	24	BDL	BDL	BDL	91	132
T2/190	190	BDL	4	39	6	BDL	BDL	BDL	49	77
T2/220	220	BDL	6	63	9	BDL	BDL	BDL	78	35
T2/300	300	BDL	6	48	5	BDL	3	BDL	62	95
T2/400	400	BDL	6	49	9	BDL	5	BDL	69	67
T2/580	580	BDL	12	80	11	BDL	4	BDL	107	133
T2/800	800	BDL	26	242	40	BDL	BDL	BDL	308	335
T2/1000	1000	BDL	10	86	29	BDL	BDL	BDL	125	154

Ba (ppm)

sample	depth	H_2O	NH4-Ac	NH_4-OxD	NH_4-OxH	H_2O_2	sulfide	residual	total	bulk
T2/020	20	BDL	BDL	2	49	3	41	277	372	592
T2/070	70	BDL	2	11	41	2	50	271	377	531
T2/100	100	BDL	BDL	7	37	2	45	238	329	481
T2/160	160	BDL	1	10	39	1	45	249	345	526
T2/190	190	BDL	3	12	11	1	40	228	295	471
T2/220	220	BDL	4	17	23	BDL	48	260	352	556
T2/300	300	1	11	9	12	1	42	273	349	560
T2/400	400	BDL	12	10	9	BDL	41	253	325	503
T2/580	580	BDL	13	9	11	BDL	50	234	317	482
T2/800	800	BDL	16	9	13	BDL	55	297	390	617
T2/1000	1000	BDL	2	12	23	2	39	219	297	425

Sr (ppm)

sample	depth	H_2O	NH4-Ac	NH_4-OxD	NH_4-OxH	H_2O_2	sulfide	residual	total	bulk
T2/020	20	BDL	BDL	2	22.7	3.1	31.9	146	206	316
T2/070	70	1.5	0.7	2.9	18.6	2.8	31.6	132	190	274
T2/100	100	1.4	BDL	4.7	14.2	1.7	25.1	122	169	209
T2/160	160	2.7	0.7	2.6	13.8	1.7	27.4	118	167	268
T2/190	190	1.1	BDL	1	3.6	2.8	13.7	127	149	258
T2/220	220	1.4	0.7	2	8.4	4.1	21.8	121	159	266
T2/300	300	4.5	1.4	0.6	4.6	5.7	16.3	138	171	281
T2/400	400	2.2	1.8	0.6	3.8	2.7	10.6	128	150	242
T2/580	580	3.6	5.1	1	3.2	3.1	11.4	126	153	236
T2/800	800	4.5	4.8	1.3	7	7.1	26.3	105	156	230
T2/1000	1000	1.2	1.2	3.5	9.8	6.1	12.2	89.8	124	182

Ni (ppm)

sample	depth	H_2O	NH4-Ac	NH_4-OxD	NH_4-OxH	H_2O_2	sulfide	residual	total	bulk
T2/020	20	4	BDL	3	3	BDL	17	9	36	44
T2/070	70	BDL	BDL	3	6	BDL	19	9	37	42
T2/100	100	BDL	BDL	2	3	BDL	17	9	31	32
T2/160	160	BDL	BDL	BDL	4	BDL	17	8	29	40
T2/190	190	BDL	BDL	2	2	BDL	16	8	28	36
T2/220	220	1	BDL	2	BDL	BDL	18	9	30	41
T2/300	300	BDL	BDL	BDL	BDL	BDL	14	10	24	40
T2/400	400	BDL	1	1	3	BDL	17	9	31	38
T2/580	580	BDL	BDL	5	2	BDL	17	9	33	37
T2/800	800	BDL	2	4	3	BDL	23	11	43	45
T2/1000	1000	BDL	BDL	4	5	BDL	21	11	41	41

Zr (ppm)

sample	depth	H_2O	NH4-Ac	NH_4-OxD	NH_4-OxH	H_2O_2	sulfide	residual	total	bulk
T2/020	20	BDL	BDL	4.2	BDL	BDL	BDL	4.7	8.9	31.8
T2/070	70	BDL	BDL	3	5	BDL	0.6	4.2	12.8	22.6
T2/100	100	BDL	BDL	1.9	0.6	BDL	BDL	2.1	4.6	12.8
T2/160	160	BDL	BDL	BDL	2.2	BDL	BDL	2.3	4.5	29.1
T2/190	190	BDL	BDL	2.6	BDL	BDL	BDL	1.7	4.3	65.6
T2/220	220	BDL	BDL	1.4	BDL	BDL	BDL	2	3.4	60.7
T2/300	300	BDL	BDL	BDL	BDL	BDL	BDL	2.5	2.5	61
T2/400	400	BDL	BDL	BDL	3.9	BDL	BDL	2.7	6.6	52.9
T2/580	580	1.2	BDL	8.1	0.5	BDL	BDL	4.1	13.9	62.7
T2/800	800	BDL	BDL	3.7	BDL	BDL	BDL	2.3	6	24.3
T2/1000	1000	BDL	BDL	5.9	4.2	BDL	BDL	1.5	11.6	46.3

Co (ppm)

sample	depth	H_2O	NH4-Ac	NH_4-OxD	NH_4-OxH	H_2O_2	sulfide	residual	total	bulk
T2/020	20	10	BDL	BDL	BDL	BDL	6	1	17	20
T2/070	70	BDL	BDL	BDL	2	BDL	9	2	13	14
T2/100	100	2	BDL	BDL	2	BDL	7	2	13	10
T2/160	160	1	BDL	BDL	1	BDL	9	2	13	13
T2/190	190	BDL	BDL	BDL	BDL	1	10	2	13	15
T2/220	220	BDL	BDL	BDL	BDL	1	8	2	11	16
T2/300	300	BDL	BDL	BDL	BDL	3	10	1	14	20
T2/400	400	1	2	BDL	BDL	2	12	3	20	22
T2/580	580	BDL	BDL	1	BDL	2	12	2	17	18
T2/800	800	BDL	BDL	BDL	BDL	2	9	2	13	14
T2/1000	1000	BDL	BDL	BDL	2	2	8	2	14	10

Sn (ppm)

sample	depth	H_2O	NH4-Ac	NH_4-OxD	NH_4-OxH	H_2O_2	sulfide	residual	total	bulk
T2/020	20	BDL	BDL	BDL	BDL	BDL	13	BDL	13	47
T2/070	70	BDL	BDL	BDL	BDL	BDL	14	BDL	14	52
T2/100	100	BDL	BDL	BDL	BDL	BDL	11	BDL	11	34
T2/160	160	BDL	BDL	BDL	BDL	BDL	13	BDL	13	45
T2/190	190	BDL	BDL	BDL	BDL	BDL	17	BDL	17	27
T2/220	220	BDL	BDL	BDL	BDL	BDL	15	BDL	15	42
T2/300	300	BDL	BDL	BDL	BDL	BDL	17	BDL	17	45
T2/400	400	BDL	BDL	BDL	BDL	BDL	16	BDL	16	33
T2/580	580	BDL	BDL	BDL	BDL	BDL	11	BDL	11	33
T2/800	800	BDL	BDL	BDL	BDL	BDL	17	BDL	17	46
T2/1000	1000	BDL	BDL	BDL	BDL	BDL	16	BDL	16	66

W (ppm)

sample	depth	H_2O	NH4-Ac	NH_4-OxD	NH_4-OxH	H_2O_2	sulfide	residual	total	bulk
T2/020	20	BDL	BDL	14	BDL	BDL	BDL	20	34	21
T2/070	70	BDL	BDL	13	13	BDL	BDL	16	42	13
T2/100	100	BDL	BDL	BDL	BDL	BDL	BDL	14	14	BDL
T2/160	160	BDL	BDL	BDL	BDL	BDL	BDL	15	15	35
T2/190	190	BDL	BDL	BDL	BDL	BDL	BDL	11	11	BDL
T2/220	220	BDL	BDL	BDL	BDL	BDL	BDL	12	12	11
T2/300	300	BDL	BDL	BDL	BDL	BDL	BDL	13	13	12
T2/400	400	BDL	BDL	BDL	BDL	BDL	BDL	10	10	BDL
T2/580	580	BDL	BDL	19	BDL	BDL	BDL	BDL	19	BDL
T2/800	800	BDL	BDL	13	BDL	BDL	BDL	15	28	13
T2/1000	1000	BDL	BDL	16	BDL	BDL	BDL	14	30	10

La (ppm)

sample	depth	H_2O	NH4-Ac	NH_4-OxD	NH_4-OxH	H_2O_2	sulfide	residual	total	bulk
T2/020	20	BDL	BDL	5.5	1.3	BDL	5.6	6	18.4	22.3
T2/070	70	BDL	BDL	4.2	6.3	BDL	5.7	3.3	19.5	18.2
T2/100	100	BDL	BDL	2.9	1.6	BDL	3.9	5.5	13.9	15.5
T2/160	160	BDL	BDL	BDL	3.5	BDL	4.5	6.1	14.1	17.1
T2/190	190	BDL	BDL	3.4	0.9	BDL	2.1	5.5	11.9	14.2
T2/220	220	BDL	BDL	2	BDL	BDL	3.7	5.6	11.3	18.8
T2/300	300	BDL	BDL	BDL	BDL	BDL	2.6	6.4	9	18.6
T2/400	400	BDL	BDL	BDL	4.8	BDL	1.8	7.2	13.8	15.3
T2/580	580	1	BDL	9.9	1.2	BDL	2.2	2.5	16.8	16.3
T2/800	800	BDL	BDL	4.5	BDL	BDL	5.1	6.3	15.9	20.8
T2/1000	1000	BDL	BDL	6.8	4.9	BDL	2.9	2.8	17.4	14.4

Y (ppm)

sample	depth	H_2O	NH4-Ac	NH_4-OxD	NH_4-OxH	H_2O_2	sulfide	residual	total	bulk
T2/020	20	1	BDL	1	BDL	BDL	1.6	2.1	5.7	9.9
T2/070	70	BDL	BDL	1.4	1.1	BDL	2	1.3	5.8	8.3
T2/100	100	BDL	BDL	1.1	0.9	BDL	1.9	1.5	5.4	6.8
T2/160	160	BDL	BDL	BDL	0.6	BDL	2.1	1.7	4.4	8.3
T2/190	190	BDL	BDL	0.9	BDL	BDL	1.5	1.2	3.6	6.8
T2/220	220	BDL	BDL	1.5	BDL	BDL	1.8	1.5	4.8	7.9
T2/300	300	BDL	0.5	1	BDL	0.6	1.3	1.7	5.1	9.9
T2/400	400	BDL	BDL	0.9	0.5	BDL	1.2	1.3	3.9	6.7
T2/580	580	BDL	BDL	1.6	BDL	BDL	1.5	0.7	3.8	7.5
T2/800	800	BDL	BDL	1.3	BDL	BDL	1.4	1.7	4.4	6.7
T2/1000	1000	BDL	BDL	1.2	1.3	BDL	1.4	0.7	4.6	5.5

Sc (ppm)

sample	depth	H_2O	NH4-Ac	NH_4-OxD	NH_4-OxH	H_2O_2	sulfide	residual	total	bulk
T2/020	20	BDL	BDL	0.9	0.7	BDL	5.2	10.1	16.9	24
T2/070	70	BDL	BDL	0.8	1.2	BDL	6.1	9.1	17.2	23.9
T2/100	100	BDL	BDL	BDL	0.7	BDL	5.4	7.7	13.8	20.6
T2/160	160	BDL	BDL	BDL	0.9	BDL	5.4	8.5	14.8	23.1
T2/190	190	BDL	BDL	BDL	BDL	BDL	4.9	7.1	12	20
T2/220	220	BDL	BDL	0.6	BDL	BDL	5.6	8.4	14.6	22.8
T2/300	300	BDL	BDL	BDL	BDL	BDL	4.7	8.8	13.5	21.5
T2/400	400	BDL	BDL	BDL	0.7	BDL	4.6	7.5	12.8	19
T2/580	580	BDL	BDL	1	BDL	BDL	5.3	6.1	12.4	18.4
T2/800	800	BDL	BDL	0.9	0.5	BDL	6.8	9.3	17.5	23.8
T2/1000	1000	BDL	BDL	0.9	0.8	BDL	5.3	6.8	13.8	20.5

Be (ppm)

sample	depth	H_2O	NH4-Ac	NH_4-OxD	NH_4-OxH	H_2O_2	sulfide	residual	total	bulk
T2/020	20	BDL	BDL	BDL	BDL	BDL	BDL	0.7	0.7	1.2
T2/070	70	BDL	BDL	BDL	BDL	BDL	BDL	0.7	0.7	1.1
T2/100	100	BDL	BDL	BDL	BDL	BDL	BDL	0.6	0.6	1
T2/160	160	BDL	BDL	BDL	BDL	BDL	BDL	0.7	0.7	1.2
T2/190	190	BDL	BDL	BDL	BDL	BDL	BDL	0.7	0.7	1.1
T2/220	220	BDL	BDL	BDL	BDL	BDL	BDL	0.7	0.7	1.1
T2/300	300	BDL	BDL	BDL	BDL	BDL	BDL	0.7	0.7	1.1
T2/400	400	BDL	BDL	BDL	BDL	BDL	BDL	0.7	0.7	1.1
T2/580	580	BDL	BDL	BDL	BDL	BDL	BDL	0.7	0.7	1
T2/800	800	BDL	BDL	BDL	BDL	BDL	BDL	0.7	0.7	1.1
T2/1000	1000	BDL	BDL	BDL	BDL	BDL	BDL	0.6	0.6	1

Ag (ppm)

sample	depth	H_2O	NH4-Ac	NH_4-OxD	NH_4-OxH	H_2O_2	sulfide	residual	total	bulk
T2/020	20	0.4	BDL	BDL	BDL	BDL	0.6	BDL	1	0.4
T2/070	70	0.5	BDL	BDL	1	BDL	0.4	BDL	1.9	0.3
T2/100	100	BDL	BDL	BDL	0.9	BDL	0.2	BDL	1.1	BDL
T2/160	160	0.4	BDL	BDL	BDL	BDL	0.3	BDL	0.7	BDL
T2/190	190	0.4	BDL	BDL	BDL	BDL	0.3	BDL	0.7	BDL
T2/220	220	BDL	BDL	BDL	BDL	BDL	0.3	BDL	0.3	BDL
T2/300	300	BDL	BDL	BDL	BDL	BDL	0.3	BDL	0.3	BDL
T2/400	400	BDL	BDL	BDL	0.3	BDL	0.5	BDL	0.8	0.4
T2/580	580	0.3	BDL	0.7	BDL	BDL	0.4	BDL	1.4	BDL
T2/800	800	BDL	BDL	BDL	BDL	BDL	0.5	0.5	1	0.4
T2/1000	1000	0.4	BDL	0.2	2.3	BDL	0.3	BDL	3.2	BDL

Fe (%)										
sample	depth	H_2O	NH4-Ac	NH_4-OxD	NH_4-OxH	H_2O_2	sulfide	residual	total	bulk
T3/020	20	BDL	0.26	0.72	1.07	0.01	1.43	0.81	4.3	5.78
T3/060	60	BDL	0.13	0.53	0.91	BDL	1.61	0.93	4.11	5.28
T3/100	100	BDL	0.16	0.49	1.02	0.03	1.35	0.66	3.71	4.78
T3/150	150	BDL	0.11	0.51	1.07	0.04	1.39	0.84	3.96	5.14
T3/170	170	BDL	0.05	0.35	0.68	BDL	2.31	0.88	4.27	5.38
T3/300	300	BDL	0.1	0.31	0.68	0.02	1.88	0.91	3.9	5.26
T3/400	400	BDL	0.1	0.62	0.5	0.02	1.59	0.77	3.6	4.59
T3/595	595	BDL	0.13	0.48	0.59	0.03	1.94	0.75	3.92	4.7
T3/800	800	BDL	0.21	0.96	0.57	BDL	2.12	0.83	4.69	5.55
T3/1000	1000	BDL	0.28	0.58	0.7	BDL	1.89	0.9	4.35	5.13

Al (%)										
sample	depth	H_2O	NH4-Ac	NH_4-OxD	NH_4-OxH	H_2O_2	sulfide	residual	total	bulk
T3/020	20	BDL	0.31	0.85	0.62	0.07	1.48	6.37	9.7	12.7
T3/060	60	BDL	0.14	0.39	0.48	0.04	1.64	6.12	8.81	10.6
T3/100	100	BDL	0.15	0.37	0.35	0.01	1.24	4.94	7.06	9.07
T3/150	150	BDL	0.1	0.26	0.28	0.01	1.39	5.55	7.59	8.4
T3/170	170	BDL	0.07	0.21	0.23	BDL	1.37	5.7	7.58	9.13
T3/300	300	BDL	0.12	0.32	0.34	0.01	1.55	5.81	8.15	10.7
T3/400	400	BDL	0.1	0.28	0.33	BDL	1.2	5.14	7.05	9.09
T3/595	595	BDL	0.12	0.29	0.35	0.01	1.52	5.38	7.67	9.19
T3/800	800	BDL	0.2	0.64	0.53	BDL	2.02	6.01	9.4	11.1
T3/1000	1000	BDL	0.33	0.73	0.42	BDL	1.89	5.64	9.01	10.3

K (%)										
sample	depth	H_2O	NH4-Ac	NH_4-OxD	NH_4-OxH	H_2O_2	sulfide	residual	total	bulk
T3/020	20	0.13	0.08	0.06	0.15	0.02	-	2.59	3.03	4.94
T3/060	60	0.06	0.02	0.03	0.09	0.01	-	2.21	2.42	3.89
T3/100	100	0.08	0.05	0.05	0.1	BDL	-	1.77	2.05	3.23
T3/150	150	0.05	0.02	0.05	0.12	BDL	-	1.99	2.23	3.58
T3/170	170	0.04	0.01	0.01	0.03	BDL	-	1.91	2	3.27
T3/300	300	0.05	0.03	0.01	0.04	BDL	-	2.12	2.25	3.97
T3/400	400	0.05	0.03	0.02	0.03	BDL	-	1.82	1.95	3.29
T3/595	595	0.05	0.04	0.02	0.04	0.01	-	1.89	2.05	3.46
T3/800	800	0.07	0.05	0.03	0.05	0.01	-	2.24	2.45	4.28
T3/1000	1000	0.09	0.07	0.04	0.06	BDL	-	2.1	2.36	3.93

Mg (%)										
sample	depth	H_2O	NH4-Ac	NH_4-OxD	NH_4-OxH	H_2O_2	sulfide	residual	total	bulk
T3/020	20	0.14	0.07	0.14	0.3	0.05	1.23	0.51	2.44	2.96
T3/060	60	0.05	0.02	0.05	0.26	0.02	1.34	0.65	2.39	2.7
T3/100	100	0.04	0.05	0.08	0.19	0.03	0.93	0.42	1.74	2.05
T3/150	150	0.04	0.02	0.04	0.14	0.02	1.09	0.57	1.92	2.31
T3/170	170	0.02	0.01	0.03	0.1	BDL	1.05	0.63	1.84	2.03
T3/300	300	0.02	0.03	0.04	0.16	0.02	1.22	0.62	2.11	2.51
T3/400	400	0.01	0.03	0.04	0.15	BDL	0.94	0.51	1.68	2.12
T3/595	595	0.01	0.04	0.04	0.15	0.01	1.21	0.52	1.98	2.13
T3/800	800	0.02	0.05	0.08	0.21	0.02	1.63	0.57	2.58	2.83
T3/1000	1000	0.06	0.09	0.12	0.19	0.01	1.51	0.67	2.65	2.95

Na (%)										
sample	depth	H_2O	NH4-Ac	NH_4-OxD	NH_4-OxH	H_2O_2	sulfide	residual	total	bulk
T3/020	20	0.02	BDL	BDL	BDL	BDL	0.03	0.59	0.64	0.91
T3/060	60	BDL	BDL	BDL	BDL	BDL	0.03	0.7	0.73	0.93
T3/100	100	BDL	BDL	BDL	BDL	BDL	0.04	0.77	0.81	1.06
T3/150	150	BDL	BDL	BDL	BDL	BDL	0.03	0.74	0.77	0.92
T3/170	170	BDL	BDL	BDL	BDL	BDL	0.03	0.78	0.81	1.06
T3/300	300	BDL	BDL	BDL	BDL	BDL	0.03	0.75	0.78	1.19
T3/400	400	BDL	BDL	BDL	BDL	BDL	0.02	0.79	0.81	1.12
T3/595	595	BDL	BDL	BDL	BDL	BDL	0.03	0.79	0.82	1.06
T3/800	800	0.01	BDL	BDL	BDL	BDL	0.04	0.72	0.77	1.06
T3/1000	1000	0.01	BDL	BDL	BDL	BDL	0.04	0.68	0.73	0.93

Ca (%)										
sample	depth	H_2O	NH4-Ac	NH_4-OxD	NH_4-OxH	H_2O_2	sulfide	residual	total	bulk
T3/020	20	0.07	0.02	0.01	0.01	BDL	0.12	0.26	0.49	0.65
T3/060	60	0.03	BDL	BDL	0.02	BDL	0.18	0.37	0.6	0.76
T3/100	100	0.06	0.03	0.01	0.01	0.08	0.13	0.41	0.73	0.95
T3/150	150	0.1	0.02	0.01	0.01	0.06	0.12	0.4	0.72	0.94
T3/170	170	0.07	0.01	0.01	0.01	0.07	0.15	0.47	0.79	1.02
T3/300	300	0.06	0.03	BDL	0.01	0.1	0.12	0.37	0.69	0.96
T3/400	400	0.06	0.04	BDL	0.01	0.08	0.09	0.37	0.65	0.86
T3/595	595	0.1	0.09	BDL	0.01	0.09	0.11	0.37	0.77	0.94
T3/800	800	0.13	0.1	0.01	BDL	0.1	0.12	0.35	0.81	1.04
T3/1000	1000	0.24	0.07	BDL	BDL	0.08	0.14	0.33	0.86	1.03

Ti (%)										
sample	depth	H_2O	NH4-Ac	NH_4-OxD	NH_4-OxH	H_2O_2	sulfide	residual	total	bulk
T3/020	20	BDL	BDL	BDL	0.01	BDL	0.07	0.21	0.29	0.39
T3/060	60	BDL	BDL	BDL	0.01	BDL	0.09	0.18	0.28	0.35
T3/100	100	BDL	BDL	BDL	BDL	BDL	0.07	0.15	0.22	0.28
T3/150	150	BDL	BDL	BDL	BDL	BDL	0.08	0.16	0.24	0.31
T3/170	170	BDL	BDL	BDL	BDL	BDL	0.08	0.16	0.24	0.28
T3/300	300	BDL	BDL	BDL	BDL	BDL	0.09	0.18	0.27	0.35
T3/400	400	BDL	BDL	BDL	BDL	BDL	0.07	0.14	0.21	0.28
T3/595	595	BDL	BDL	BDL	BDL	BDL	0.1	0.14	0.24	0.3
T3/800	800	BDL	BDL	BDL	BDL	BDL	0.13	0.19	0.32	0.37
T3/1000	1000	BDL	BDL	BDL	BDL	BDL	0.12	0.2	0.32	0.35

P (%)										
sample	depth	H_2O	NH4-Ac	NH_4-OxD	NH_4-OxH	H_2O_2	sulfide	residual	total	bulk
T3/020	20	BDL	BDL	0.08	0.02	BDL	0.01	0.01	0.12	0.14
T3/060	60	BDL	0.01	0.08	0.01	BDL	0.02	0.01	0.13	0.13
T3/100	100	BDL	BDL	0.06	0.01	BDL	0.02	BDL	0.09	0.11
T3/150	150	BDL	BDL	0.05	0.01	BDL	0.02	BDL	0.08	0.09
T3/170	170	BDL	BDL	0.05	BDL	BDL	0.03	BDL	0.08	0.06
T3/300	300	BDL	BDL	0.07	0.01	BDL	0.03	BDL	0.11	0.13
T3/400	400	BDL	BDL	0.06	BDL	BDL	0.02	BDL	0.08	0.1
T3/595	595	BDL	0.01	0.06	BDL	BDL	0.03	BDL	0.1	0.09
T3/800	800	BDL	0.01	0.12	BDL	BDL	0.02	0.01	0.16	0.13
T3/1000	1000	BDL	0.01	0.11	0.01	BDL	0.02	BDL	0.15	0.13

Cu (ppm)										
sample	depth	H2O	NH4-Ac	NH4-OxD	NH4-OxH	H2O2	sulfide	residual	total	bulk
T3/020	20	7.2	804	769	190	45.2	515	12.9	2343	2500
T3/060	60	120	344	342	176	62.5	118	11.6	1174	1150
T3/100	100	0.6	168	252	64.2	432	87.3	11.9	1016	998
T3/150	150	47.6	214	244	112	220	133	15.2	986	864
T3/170	170	30.8	388	524	130	2030	1090	24.5	4217	3990
T3/300	300	2.8	393	490	74.6	672	89	12.6	1734	1750
T3/400	400	5.3	683	547	96.8	862	141	13.5	2349	2120
T3/595	595	5.8	810	608	79.3	800	133	12.8	2449	2200
T3/800	800	6.7	1380	1190	112	600	552	20	3861	3620
T3/1000	1000	3.3	814	899	144	374	784	18.3	3037	2650

Zn (ppm)										
sample	depth	H_2O	NH4-Ac	NH_4-OxD	NH_4-OxH	H_2O_2	sulfide	residual	total	bulk
T3/020	20	3.1	23.1	15.2	13.2	BDL	31.2	13.7	99.5	131
T3/060	60	6.2	4.8	4.8	11.8	BDL	30.8	20	78.4	83.5
T3/100	100	BDL	21	12.9	9	2.6	19.9	12.4	77.8	95.4
T3/150	150	4	3.7	3.8	6.6	1.4	24.8	15.2	59.5	70.5
T3/170	170	2.6	4.1	3.2	5.9	4.6	26.4	15.9	62.7	64.7
T3/300	300	BDL	7.4	4.7	8.7	2.2	27.2	15.5	65.7	72.7
T3/400	400	BDL	11.1	9.2	8.5	2.4	24.3	15.3	70.8	80.2
T3/595	595	BDL	14	10.5	10.6	2.9	28.1	15.1	81.2	86
T3/800	800	BDL	16.4	16.8	11.8	2.1	33.9	14.2	95.2	104
T3/1000	1000	BDL	9.2	7.3	7.2	1.4	31.4	13.8	70.3	113

Mn (ppm)										
sample	depth	H_2O	NH4-Ac	NH_4-OxD	NH_4-OxH	H_2O_2	sulfide	residual	total	bulk
T3/020	20	40	24	24	46	BDL	158	47	339	407
T3/060	60	20	6	11	41	4	172	67	321	371
T3/100	100	5	12	15	30	8	116	44	230	281
T3/150	150	14	4	8	24	4	139	61	254	273
T3/170	170	9	3	7	20	3	139	66	247	281
T3/300	300	2	8	10	30	5	165	65	285	347
T3/400	400	2	17	17	31	4	131	56	258	319
T3/595	595	BDL	27	27	33	6	150	52	295	324
T3/800	800	BDL	23	26	36	5	178	52	320	360
T3/1000	1000	6	28	22	30	4	170	64	324	360

Cr (ppm)										
sample	depth	H_2O	NH4-Ac	NH_4-OxD	NH_4-OxH	H_2O_2	sulfide	residual	total	bulk
T3/020	20	BDL	4	8	9	BDL	25	9	55	40
T3/060	60	BDL	2	6	11	BDL	28	9	56	35
T3/100	100	BDL	2	4	12	BDL	21	5	44	51
T3/150	150	BDL	2	4	10	BDL	27	6	49	26
T3/170	170	BDL	1	5	11	BDL	26	7	50	40
T3/300	300	BDL	2	3	8	BDL	24	6	43	36
T3/400	400	BDL	2	7	7	BDL	21	5	42	26
T3/595	595	BDL	2	5	8	BDL	27	5	47	26
T3/800	800	BDL	3	9	5	BDL	34	6	57	43
T3/1000	1000	BDL	4	6	5	BDL	35	7	57	33

Pb (ppm)										
sample	depth	H_2O	NH4-Ac	NH_4-OxD	NH_4-OxH	H_2O_2	sulfide	residual	total	bulk
T3/020	20	BDL	BDL	8	9	BDL	13	BDL	30	35
T3/060	60	BDL	BDL	BDL	12	BDL	5	BDL	17	21
T3/100	100	BDL	BDL	2	9	BDL	6	BDL	17	15
T3/150	150	BDL	BDL	3	5	BDL	7	BDL	15	23
T3/170	170	BDL	7	70	13	BDL	30	BDL	120	180
T3/300	300	BDL	BDL	BDL	8	BDL	9	BDL	17	27
T3/400	400	BDL	BDL	3	BDL	BDL	6	BDL	9	19
T3/595	595	BDL	3	7	8	BDL	9	BDL	27	25
T3/800	800	BDL	BDL	5	BDL	BDL	10	BDL	15	28
T3/1000	1000	BDL	4	BDL	BDL	BDL	6	BDL	10	15

Mo (ppm)										
sample	depth	H_2O	NH4-Ac	NH_4-OxD	NH_4-OxH	H_2O_2	sulfide	residual	total	bulk
T3/020	20	2	2	60	48	15	1	BDL	128	130
T3/060	60	BDL	2	40	29	13	2	BDL	86	75
T3/100	100	2	1	27	20	BDL	45	1	96	98
T3/150	150	BDL	1	31	25	43	9	1	110	109
T3/170	170	BDL	BDL	19	10	BDL	109	5	143	150
T3/300	300	6	1	24	18	BDL	24	BDL	73	76
T3/400	400	7	1	34	2	BDL	31	BDL	75	72
T3/595	595	9	2	29	6	BDL	23	BDL	69	63
T3/800	800	21	4	94	6	BDL	19	BDL	144	124
T3/1000	1000	8	3	64	39	3	18	BDL	135	122

V (ppm)										
sample	depth	H_2O	NH4-Ac	NH_4-OxD	NH_4-OxH	H_2O_2	sulfide	residual	total	bulk
T3/020	20	BDL	2	14	16	BDL	57	113	202	266
T3/060	60	BDL	BDL	6	20	BDL	67	104	197	234
T3/100	100	BDL	2	9	23	BDL	48	80	162	192
T3/150	150	BDL	BDL	8	18	BDL	55	92	173	213
T3/170	170	BDL	BDL	7	19	BDL	58	92	176	197
T3/300	300	BDL	BDL	3	17	BDL	64	99	183	225
T3/400	400	BDL	BDL	10	13	BDL	50	74	147	190
T3/595	595	BDL	BDL	7	15	BDL	66	77	165	189
T3/800	800	BDL	BDL	2	10	BDL	83	92	197	228
T3/1000	1000	BDL	BDL	3	8	11	BDL	77	93	192	222

As (ppm)										
sample	depth	H_2O	NH4-Ac	NH_4-OxD	NH_4-OxH	H_2O_2	sulfide	residual	total	bulk
T3/020	20	BDL	7	100	27	BDL	BDL	BDL	134	150
T3/060	60	BDL	9	78	22	BDL	BDL	BDL	109	67
T3/100	100	BDL	4	37	18	BDL	BDL	BDL	59	41
T3/150	150	BDL	6	47	20	BDL	BDL	BDL	73	57
T3/170	170	BDL	4	36	11	BDL	14	BDL	65	55
T3/300	300	BDL	5	40	13	BDL	BDL	BDL	58	59
T3/400	400	BDL	6	48	3	BDL	BDL	BDL	57	87
T3/595	595	BDL	13	77	13	BDL	5	BDL	108	170
T3/800	800	BDL	31	282	16	BDL	BDL	BDL	329	328
T3/1000	1000	BDL	27	219	19	BDL	BDL	BDL	265	250

Ba (ppm)

sample	depth	H_2O	NH4-Ac	NH_4-OxD	NH_4-OxH	H_2O_2	sulfide	residual	total	bulk
T3/020	20	BDL	2	16	47	2	43	266	376	597
T3/060	60	BDL	2	17	34	1	48	249	351	474
T3/100	100	BDL	4	23	33	1	36	211	308	449
T3/150	150	BDL	1	13	35	2	41	229	321	427
T3/170	170	1	15	14	19	1	41	229	320	469
T3/300	300	BDL	20	9	13	2	44	261	349	606
T3/400	400	BDL	19	9	9	BDL	36	227	300	502
T3/595	595	BDL	24	9	14	1	52	239	339	490
T3/800	800	BDL	25	14	10	2	65	266	382	590
T3/1000	1000	BDL	10	15	23	1	58	247	354	515

Sr (ppm)

sample	depth	H_2O	NH4-Ac	NH_4-OxD	NH_4-OxH	H_2O_2	sulfide	residual	total	bulk
T3/020	20	1	0.8	4.7	21.6	2	35.6	130	196	305
T3/060	60	BDL	BDL	2.5	10.4	2	24.1	121	160	230
T3/100	100	0.7	1.2	2.3	8.1	5.4	17.9	119	155	230
T3/150	150	0.8	BDL	2.9	10.8	4	18.1	117	154	169
T3/170	170	1.9	0.9	1.1	4.2	3.2	14.7	124	150	218
T3/300	300	1.4	2.2	1.1	6.9	4.5	20.1	121	157	250
T3/400	400	1.6	3.1	0.8	4.9	3.6	13.4	121	148	226
T3/595	595	2.8	6.4	1.1	5.1	4	15	114	148	217
T3/800	800	2.9	6.2	1.3	5.9	5.8	23.7	119	165	244
T3/1000	1000	4.4	4.6	3.9	11.6	8	22.2	104	159	217

Ni (ppm)

sample	depth	H_2O	NH4-Ac	NH_4-OxD	NH_4-OxH	H_2O_2	sulfide	residual	total	bulk
T3/020	20	1	2	8	5	BDL	17	6	39	45
T3/060	60	1	BDL	3	6	BDL	19	9	38	41
T3/100	100	BDL	BDL	2	6	1	14	6	29	33
T3/150	150	BDL	BDL	3	3	BDL	18	7	31	37
T3/170	170	BDL	BDL	2	4	BDL	21	8	35	38
T3/300	300	BDL	BDL	1	3	1	17	8	30	36
T3/400	400	BDL	1	3	1	BDL	14	6	25	33
T3/595	595	BDL	1	5	4	1	18	8	37	34
T3/800	800	BDL	2	6	2	BDL	23	8	41	43
T3/1000	1000	BDL	2	4	BDL	BDL	22	8	36	42

Zr (ppm)

sample	depth	H_2O	NH4-Ac	NH_4-OxD	NH_4-OxH	H_2O_2	sulfide	residual	total	bulk
T3/020	20	BDL	BDL	8	BDL	BDL	BDL	3.7	11.7	17.2
T3/060	60	BDL	BDL	3.6	2.9	BDL	BDL	4.5	11	13.3
T3/100	100	BDL	BDL	BDL	5.8	BDL	BDL	3.7	9.5	49.8
T3/150	150	BDL	BDL	3.6	0.7	BDL	BDL	2.7	7	13.8
T3/170	170	BDL	BDL	2.1	2.7	BDL	BDL	2.3	7.1	55.4
T3/300	300	BDL	BDL	BDL	0.6	BDL	0.5	1.6	2.7	46
T3/400	400	BDL	BDL	2.5	BDL	BDL	BDL	2.7	5.2	52.2
T3/595	595	BDL	BDL	6.1	2.9	BDL	BDL	1.8	10.8	49
T3/800	800	BDL	BDL	5.5	BDL	BDL	BDL	1.7	7.2	35.5
T3/1000	1000	BDL	BDL	2	BDL	BDL	BDL	1.9	3.9	48.8

Co (ppm)

sample	depth	H_2O	NH4-Ac	NH_4-OxD	NH_4-OxH	H_2O_2	sulfide	residual	total	bulk
T3/020	20	1	2	2	1	BDL	7	1	14	18
T3/060	60	2	BDL	BDL	3	BDL	8	2	15	15
T3/100	100	BDL	BDL	BDL	1	3	6	1	11	14
T3/150	150	BDL	BDL	BDL	1	1	7	2	11	12
T3/170	170	BDL	BDL	BDL	BDL	2	20	2	24	25
T3/300	300	BDL	BDL	BDL	1	3	10	3	17	17
T3/400	400	BDL	BDL	BDL	BDL	2	10	2	14	17
T3/595	595	BDL	BDL	BDL	BDL	3	12	2	17	17
T3/800	800	BDL	BDL	2	BDL	3	10	1	16	18
T3/1000	1000	BDL	BDL	BDL	BDL	2	9	2	13	14

Sn (ppm)

sample	depth	H_2O	NH4-Ac	NH_4-OxD	NH_4-OxH	H_2O_2	sulfide	residual	total	bulk
T3/020	20	BDL	BDL	BDL	BDL	BDL	13	BDL	13	58
T3/060	60	BDL	BDL	BDL	BDL	BDL	14	BDL	14	43
T3/100	100	BDL	BDL	BDL	BDL	BDL	17	BDL	17	26
T3/150	150	BDL	BDL	BDL	BDL	BDL	19	BDL	19	37
T3/170	170	BDL	BDL	52	BDL	BDL	19	BDL	71	165
T3/300	300	BDL	BDL	BDL	BDL	BDL	16	BDL	16	39
T3/400	400	BDL	BDL	BDL	BDL	BDL	17	BDL	17	22
T3/595	595	BDL	BDL	BDL	BDL	BDL	17	BDL	17	30
T3/800	800	BDL	BDL	BDL	BDL	BDL	16	BDL	16	44
T3/1000	1000	BDL	BDL	BDL	BDL	BDL	16	BDL	16	35

W (ppm)

sample	depth	H_2O	NH4-Ac	NH_4-OxD	NH_4-OxH	H_2O_2	sulfide	residual	total	bulk
T3/020	20	BDL	BDL	27	BDL	BDL	BDL	17	44	17
T3/060	60	BDL	BDL	11	BDL	BDL	BDL	14	25	BDL
T3/100	100	BDL	BDL	BDL	13	BDL	BDL	12	25	BDL
T3/150	150	BDL	BDL	BDL	BDL	BDL	BDL	11	11	12
T3/170	170	BDL	BDL	BDL	BDL	BDL	BDL	16	16	BDL
T3/300	300	BDL	BDL	BDL	BDL	BDL	BDL	16	16	15
T3/400	400	BDL	BDL	BDL	BDL	BDL	BDL	11	11	11
T3/595	595	BDL	BDL	18	BDL	BDL	BDL	12	30	11
T3/800	800	BDL	BDL	18	BDL	BDL	BDL	16	34	BDL
T3/1000	1000	BDL	BDL	11	BDL	BDL	BDL	14	25	13

La (ppm)

sample	depth	H_2O	NH4-Ac	NH_4-OxD	NH_4-OxH	H_2O_2	sulfide	residual	total	bulk
T3/020	20	BDL	BDL	10.1	1.9	BDL	5.6	3.7	21.3	20
T3/060	60	BDL	BDL	4.5	4	BDL	4.3	5.5	18.3	15.5
T3/100	100	BDL	BDL	BDL	6.6	BDL	3.4	3.3	13.3	16.4
T3/150	150	BDL	BDL	4.7	1.7	BDL	3.3	4.7	14.4	12.5
T3/170	170	BDL	BDL	2.9	3.3	0.7	1.9	6	14.8	15
T3/300	300	BDL	BDL	BDL	1.5	0.7	3.4	6.3	11.9	22.9
T3/400	400	BDL	BDL	3.2	BDL	BDL	2.6	5.2	11	16.6
T3/595	595	BDL	BDL	7.5	3.8	BDL	3.1	7	21.4	16.4
T3/800	800	BDL	BDL	6.6	BDL	BDL	4.4	6.6	17.6	20.8
T3/1000	1000	BDL	BDL	2.7	BDL	BDL	3.8	6.8	13.3	18.4

Y (ppm)

sample	depth	H_2O	NH4-Ac	NH_4-OxD	NH_4-OxH	H_2O_2	sulfide	residual	total	bulk
T3/020	20	BDL	BDL	1.6	BDL	BDL	1.6	2	5.2	8.7
T3/060	60	BDL	BDL	1	1.2	BDL	2.1	1.8	6.1	7
T3/100	100	BDL	BDL	1.3	BDL	BDL	1.4	1.1	3.8	6.7
T3/150	150	BDL	BDL	1.3	BDL	BDL	1.5	1.4	4.2	5.6
T3/170	170	BDL	BDL	0.9	0.7	BDL	1.3	1.5	4.4	6.1
T3/300	300	BDL	BDL	0.6	0.7	0.7	1.5	1.5	5	7.4
T3/400	400	BDL	BDL	1	BDL	0.5	1.1	1.2	3.8	9.1
T3/595	595	BDL	BDL	1.2	BDL	0.8	1.4	1.3	4.7	6.8
T3/800	800	BDL	0.6	2.3	BDL	0.6	1.7	1.8	7	11.2
T3/1000	1000	BDL	BDL	0.7	BDL	BDL	1.5	1.5	3.7	7.1

Sc (ppm)

sample	depth	H_2O	NH4-Ac	NH_4-OxD	NH_4-OxH	H_2O_2	sulfide	residual	total	bulk
T3/020	20	BDL	0.6	1.9	1	BDL	5	9.3	17.8	25.8
T3/060	60	BDL	BDL	0.8	1.2	BDL	5.8	9.3	17.1	21.8
T3/100	100	BDL	BDL	BDL	1.3	BDL	4.2	7	12.5	17.9
T3/150	150	BDL	BDL	0.7	0.6	BDL	4.8	7.8	13.9	17.7
T3/170	170	BDL	BDL	BDL	0.6	BDL	4.8	8.7	14.1	18.3
T3/300	300	BDL	BDL	BDL	0.6	BDL	5.3	7.9	13.8	21.3
T3/400	400	BDL	BDL	0.5	BDL	BDL	4.1	6.5	11.1	17.4
T3/595	595	BDL	BDL	0.9	0.8	BDL	5.6	6.4	13.7	17.4
T3/800	800	BDL	BDL	1	BDL	BDL	7.3	8	16.3	22.2
T3/1000	1000	BDL	0.5	0.9	BDL	BDL	6.9	7.8	16.1	22.6

Be (ppm)

sample	depth	H_2O	NH4-Ac	NH_4-OxD	NH_4-OxH	H_2O_2	sulfide	residual	total	bulk
T3/020	20	BDL	BDL	BDL	BDL	BDL	BDL	0.6	0.6	1.3
T3/060	60	BDL	BDL	BDL	BDL	BDL	BDL	0.6	0.6	1.1
T3/100	100	BDL	BDL	BDL	BDL	BDL	BDL	0.6	0.6	0.9
T3/150	150	BDL	BDL	BDL	BDL	BDL	BDL	0.6	0.6	1
T3/170	170	BDL	BDL	BDL	BDL	BDL	BDL	0.7	0.7	1
T3/300	300	BDL	BDL	BDL	BDL	BDL	BDL	0.6	0.6	1
T3/400	400	BDL	BDL	BDL	BDL	BDL	BDL	0.6	0.6	1
T3/595	595	BDL	BDL	BDL	BDL	BDL	BDL	0.6	0.6	1
T3/800	800	BDL	BDL	BDL	BDL	BDL	BDL	0.6	0.6	1.1
T3/1000	1000	BDL	BDL	BDL	BDL	BDL	BDL	0.6	0.6	1

Ag (ppm)

sample	depth	H_2O	NH4-Ac	NH_4-OxD	NH_4-OxH	H_2O_2	sulfide	residual	total	bulk
T3/020	20	BDL	BDL	BDL	BDL	BDL	1	BDL	1	1.1
T3/060	60	BDL	BDL	BDL	1.3	BDL	BDL	0.2	1.5	BDL
T3/100	100	BDL	BDL	BDL	BDL	BDL	0.3	BDL	0.3	BDL
T3/150	150	BDL	BDL	BDL	BDL	BDL	0.4	BDL	0.4	BDL
T3/170	170	0.3	BDL	BDL	0.7	BDL	0.3	BDL	1.3	0.3
T3/300	300	BDL	BDL	BDL	0.7	BDL	0.2	0.2	1.1	BDL
T3/400	400	BDL	BDL	BDL	BDL	BDL	0.3	BDL	0.3	BDL
T3/595	595	BDL	BDL	BDL	BDL	BDL	0.3	BDL	0.3	0.3
T3/800	800	BDL	BDL	BDL	BDL	BDL	0.5	BDL	0.5	0.2
T3/1000	1000	0.2	BDL	BDL	BDL	BDL	0.4	BDL	0.6	BDL

Table A3.2.4: *Drill core T4 from Cauquenes/Teniente* *sequence B*

Fe (%)

sample	depth	H_2O	NH4-Ac	NH_4-OxD	NH_4-OxH	H_2O_2	sulfide	residual	total	bulk
T4/010	10	BDL	0.05	0.36	0.9	BDL	0.9	0.75	2.96	3.99
T4/040	40	BDL	0.08	0.62	1.05	0.01	1.01	0.67	3.44	4.42
T4/100	100	BDL	0.15	0.81	0.98	0.01	1.24	0.75	3.94	4.84
T4/153	153	BDL	0.1	0.69	0.8	BDL	1.11	0.82	3.52	4.62
T4/490	490	BDL	0.1	0.56	0.41	0.01	1.8	0.8	3.68	4.73
T4/795	795	BDL	0.12	0.51	0.59	0.01	2.11	0.8	4.14	5.1

Al (%)

sample	depth	H_2O	NH4-Ac	NH_4-OxD	NH_4-OxH	H_2O_2	sulfide	residual	total	bulk
T4/010	10	BDL	0.05	0.14	0.25	0.06	1.04	5.73	7.27	9.49
T4/040	40	BDL	0.05	0.16	0.25	0.06	1.15	5.48	7.15	9.25
T4/100	100	BDL	0.09	0.22	0.32	0.05	1.33	5.42	7.43	8.91
T4/153	153	BDL	0.07	0.18	0.26	0.05	1.19	5.26	7.01	9.03
T4/490	490	BDL	0.08	0.19	0.26	BDL	1.27	5.52	7.32	9.08
T4/795	795	BDL	0.12	0.31	0.34	0.01	1.67	5.5	7.95	8.18

K (%)

sample	depth	H_2O	NH4-Ac	NH_4-OxD	NH_4-OxH	H_2O_2	sulfide	residual	total	bulk
T4/010	10	0.03	0.02	0.03	0.11	0.01	-	1.96	2.16	3.33
T4/040	40	0.03	0.02	0.07	0.13	0.01	-	1.73	1.99	3.18
T4/100	100	0.06	0.04	0.1	0.12	0.01	-	1.76	2.09	3.15
T4/153	153	0.05	0.02	0.07	0.08	0.01	-	1.83	2.06	3.18
T4/490	490	0.05	0.01	0.01	0.02	BDL	-	1.88	1.97	3.28
T4/795	795	0.05	0.03	0.01	0.03	0.01	-	2.03	2.16	3.66

Mg (%)

sample	depth	H_2O	NH4-Ac	NH_4-OxD	NH_4-OxH	H_2O_2	sulfide	residual	total	bulk
T4/010	10	BDL	0.01	0.02	0.12	BDL	0.84	0.57	1.56	1.95
T4/040	40	BDL	0.02	0.03	0.13	BDL	0.99	0.52	1.69	2.04
T4/100	100	0.02	0.04	0.04	0.18	BDL	1.04	0.51	1.83	2.08
T4/153	153	0.02	0.02	0.03	0.14	BDL	0.94	0.55	1.7	2.05
T4/490	490	0.03	0.01	0.02	0.11	BDL	1.02	0.56	1.75	2.01
T4/795	795	0.01	0.03	0.03	0.14	0.01	1.35	0.56	2.13	2.42

Na (%)

sample	depth	H_2O	NH4-Ac	NH_4-OxD	NH_4-OxH	H_2O_2	sulfide	residual	total	bulk
T4/010	10	BDL	BDL	BDL	BDL	BDL	0.02	1.15	1.17	1.51
T4/040	40	BDL	BDL	BDL	BDL	BDL	0.02	1.09	1.11	1.48
T4/100	100	BDL	BDL	BDL	BDL	BDL	0.04	0.87	0.91	1.1
T4/153	153	BDL	BDL	BDL	BDL	BDL	0.03	0.86	0.89	1.1
T4/490	490	BDL	BDL	BDL	BDL	BDL	0.02	0.96	0.98	1.23
T4/795	795	0.01	BDL	BDL	BDL	BDL	0.03	0.78	0.82	1

Ca (%)

sample	depth	H_2O	NH4-Ac	NH_4-OxD	NH_4-OxH	H_2O_2	sulfide	residual	total	bulk
T4/010	10	BDL	0.02	0.01	0.01	BDL	0.12	0.46	0.62	0.86
T4/040	40	BDL	0.02	0.01	0.01	BDL	0.15	0.5	0.69	0.95
T4/100	100	0.04	0.03	0.01	0.01	BDL	0.2	0.55	0.84	1.03
T4/153	153	0.05	0.02	0.01	0.01	BDL	0.21	0.46	0.76	0.97
T4/490	490	0.11	0.01	0.01	0.01	0.07	0.1	0.45	0.76	0.95
T4/795	795	0.07	0.08	BDL	0.01	0.09	0.12	0.41	0.78	0.95

Ti (%)

sample	depth	H_2O	NH4-Ac	NH_4-OxD	NH_4-OxH	H_2O_2	sulfide	residual	total	bulk
T4/010	10	BDL	BDL	BDL	BDL	BDL	0.06	0.14	0.2	0.28
T4/040	40	BDL	BDL	BDL	BDL	BDL	0.07	0.14	0.21	0.3
T4/100	100	BDL	BDL	BDL	BDL	BDL	0.08	0.16	0.25	0.31
T4/153	153	BDL	BDL	BDL	BDL	BDL	0.07	0.17	0.24	0.3
T4/490	490	BDL	BDL	BDL	BDL	BDL	0.09	0.15	0.24	0.3
T4/795	795	BDL	BDL	BDL	BDL	BDL	0.11	0.16	0.27	0.28

P (%)

sample	depth	H_2O	NH4-Ac	NH_4-OxD	NH_4-OxH	H_2O_2	sulfide	residual	total	bulk
T4/010	10	BDL	BDL	0.03	0.02	BDL	0.02	BDL	0.07	0.09
T4/040	40	BDL	BDL	0.04	0.02	BDL	0.02	BDL	0.08	0.1
T4/100	100	BDL	BDL	0.04	0.01	BDL	0.02	BDL	0.07	0.09
T4/153	153	BDL	BDL	0.05	BDL	BDL	0.03	BDL	0.08	0.11
T4/490	490	BDL	BDL	0.05	BDL	BDL	0.03	BDL	0.08	0.07
T4/795	795	BDL	0.01	0.07	BDL	BDL	0.03	BDL	0.11	0.09

Ba (ppm)

sample	depth	H_2O	NH4-Ac	NH_4-OxD	NH_4-OxH	H_2O_2	sulfide	residual	total	bulk
T4/010	10	BDL	BDL	9	37	1	28	206	281	428
T4/040	40	BDL	BDL	18	43	1	31	188	281	384
T4/100	100	BDL	1	13	30	1	36	209	290	379
T4/153	153	BDL	BDL	17	32	1	33	222	305	421
T4/490	490	2	11	10	11	BDL	42	239	315	439
T4/795	795	BDL	21	12	9	1	56	252	351	485

Sr (ppm)

sample	depth	H_2O	NH4-Ac	NH_4-OxD	NH_4-OxH	H_2O_2	sulfide	residual	total	bulk
T4/010	10	BDL	0.5	2.4	9.1	1	15.6	124	153	234
T4/040	40	BDL	BDL	3.7	7.5	0.9	16	124	152	234
T4/100	100	BDL	0.5	2.9	4.3	0.9	18	135	162	224
T4/153	153	BDL	BDL	2.8	5.5	1.2	20.8	138	168	246
T4/490	490	6.7	1.4	0.7	3.1	3	11.3	137	163	236
T4/795	795	2	5.7	1	4.4	3.9	16.7	119	153	167

Ni (ppm)

sample	depth	H_2O	NH4-Ac	NH_4-OxD	NH_4-OxH	H_2O_2	sulfide	residual	total	bulk
T4/010	10	BDL	BDL	2	4	BDL	12	9	27	28
T4/040	40	BDL	BDL	5	BDL	BDL	15	8	28	31
T4/100	100	BDL	BDL	2	1	BDL	16	7	26	32
T4/153	153	BDL	BDL	3	3	BDL	14	8	28	31
T4/490	490	3	1	2	1	BDL	17	8	32	36
T4/795	795	BDL	1	4	4	BDL	21	7	37	39

Zr (ppm)

sample	depth	H_2O	NH4-Ac	NH_4-OxD	NH_4-OxH	H_2O_2	sulfide	residual	total	bulk
T4/010	10	BDL	BDL	3.2	3.6	BDL	BDL	6	12.8	49.9
T4/040	40	BDL	BDL	8.2	BDL	BDL	BDL	1.3	9.5	67.1
T4/100	100	BDL	BDL	2.5	BDL	BDL	BDL	2.2	4.7	58.5
T4/153	153	BDL	BDL	3.4	1.1	BDL	BDL	3.7	8.2	63.1
T4/490	490	2.2	BDL	1.8	BDL	BDL	BDL	1.7	5.7	66.5
T4/795	795	BDL	BDL	2.2	2.9	BDL	BDL	2.2	7.3	13.8

Cu (ppm)

sample	depth	H2O	NH4-Ac	NH4-OxD	NH4-OxH	H2O2	sulfide	residual	total	bulk
T4/010	10	0.9	31	90.2	137	1.5	41.8	12.8	315	323
T4/040	40	1.1	31.3	132	110	2.4	59.7	13.3	350	351
T4/100	100	BDL	19.1	103	50.7	2.8	87.2	12.6	275	275
T4/153	153	1	38.4	113	41.3	2.3	65	11.5	273	294
T4/490	490	488	1580	535	108	964	149	22.4	3846	3820
T4/795	795	12.2	1020	683	96.2	998	654	21	3484	3280

Zn (ppm)

sample	depth	H_2O	NH4-Ac	NH_4-OxD	NH_4-OxH	H_2O_2	sulfide	residual	total	bulk
T4/010	10	BDL	0.8	1.7	5.8	0.6	18.9	21.2	49	60.3
T4/040	40	BDL	12.1	5	6.1	0.7	20.3	16.3	60.5	69.3
T4/100	100	BDL	2.2	3.8	6.4	BDL	23.8	13.2	49.4	57
T4/153	153	0.7	4.2	3.7	5.6	BDL	21.2	15.4	50.8	58.9
T4/490	490	24.9	13.9	10.3	8.9	3.9	26.2	20	108.1	114
T4/795	795	BDL	9.5	5.8	9.6	2.7	31.1	15.4	74.1	81.7

Mn (ppm)

sample	depth	H_2O	NH4-Ac	NH_4-OxD	NH_4-OxH	H_2O_2	sulfide	residual	total	bulk
T4/010	10	BDL	3	5	19	BDL	100	61	188	236
T4/040	40	BDL	4	7	20	BDL	109	51	191	233
T4/100	100	3	6	10	28	BDL	133	56	236	278
T4/153	153	3	3	8	24	BDL	123	62	223	274
T4/490	490	35	6	17	26	4	138	63	289	324
T4/795	795	BDL	22	17	29	5	151	53	277	311

Cr (ppm)

sample	depth	H_2O	NH4-Ac	NH_4-OxD	NH_4-OxH	H_2O_2	sulfide	residual	total	bulk
T4/010	10	BDL	BDL	2	8	BDL	17	8	35	22
T4/040	40	BDL	BDL	4	10	BDL	22	4	40	21
T4/100	100	BDL	BDL	5	10	BDL	23	6	44	27
T4/153	153	BDL	BDL	5	9	BDL	20	7	41	22
T4/490	490	BDL	1	7	6	BDL	24	7	45	22
T4/795	795	BDL	2	5	7	BDL	29	6	49	25

Pb (ppm)

sample	depth	H_2O	NH4-Ac	NH_4-OxD	NH_4-OxH	H_2O_2	sulfide	residual	total	bulk
T4/010	10	BDL	BDL	3	15	BDL	10	BDL	28	31
T4/040	40	BDL	BDL	10	9	BDL	8	BDL	27	22
T4/100	100	BDL	BDL	BDL	BDL	BDL	3	BDL	3	15
T4/153	153	BDL	BDL	7	4	BDL	8	BDL	19	30
T4/490	490	2	BDL	3	2	BDL	6	BDL	13	16
T4/795	795	BDL	BDL	3	6	BDL	8	BDL	17	17

Mo (ppm)

sample	depth	H_2O	NH4-Ac	NH_4-OxD	NH_4-OxH	H_2O_2	sulfide	residual	total	bulk
T4/010	10	1	2	36	42	24	2	BDL	107	106
T4/040	40	1	2	45	30	30	6	BDL	114	110
T4/100	100	BDL	1	36	14	57	7	BDL	115	113
T4/153	153	BDL	BDL	30	9	31	5	BDL	75	71
T4/490	490	1	BDL	21	3	BDL	38	2	65	64
T4/795	795	14	2	46	9	BDL	32	1	104	100

V (ppm)

sample	depth	H_2O	NH4-Ac	NH_4-OxD	NH_4-OxH	H_2O_2	sulfide	residual	total	bulk
T4/010	10	BDL	BDL	5	16	BDL	41	86	148	187
T4/040	40	BDL	BDL	11	19	BDL	47	78	155	190
T4/100	100	BDL	BDL	13	21	BDL	54	84	172	201
T4/153	153	BDL	BDL	10	17	BDL	48	87	162	200
T4/490	490	BDL	BDL	11	13	BDL	58	78	160	187
T4/795	795	BDL	BDL	6	14	BDL	71	85	176	180

As (ppm)

sample	depth	H_2O	NH4-Ac	NH_4-OxD	NH_4-OxH	H_2O_2	sulfide	residual	total	bulk
T4/010	10	BDL	6	51	38	BDL	BDL	BDL	95	124
T4/040	40	BDL	6	60	40	BDL	BDL	BDL	106	121
T4/100	100	BDL	BDL	38	14	BDL	BDL	BDL	52	85
T4/153	153	BDL	6	60	14	BDL	BDL	BDL	80	97
T4/490	490	BDL	5	32	4	BDL	BDL	BDL	41	64
T4/795	795	3	23	148	17	BDL	5	BDL	196	173

W (ppm)

sample	depth	H_2O	NH4-Ac	NH_4-OxD	NH_4-OxH	H_2O_2	sulfide	residual	total	bulk
T4/010	10	BDL	BDL	BDL	BDL	BDL	BDL	12	12	BDL
T4/040	40	BDL	BDL	19	BDL	BDL	BDL	12	31	BDL
T4/100	100	BDL	BDL	BDL	BDL	BDL	BDL	11	11	BDL
T4/153	153	BDL	BDL	12	BDL	BDL	BDL	12	24	BDL
T4/490	490	BDL	BDL	BDL	BDL	BDL	BDL	12	12	BDL
T4/795	795	BDL	BDL	16	BDL	BDL	BDL	15	31	12

La (ppm)

sample	depth	H_2O	NH4-Ac	NH_4-OxD	NH_4-OxH	H_2O_2	sulfide	residual	total	bulk
T4/010	10	BDL	BDL	4.3	4.6	BDL	2.9	2.2	14	14.9
T4/040	40	BDL	BDL	9.8	BDL	BDL	3.2	6	19	14.4
T4/100	100	BDL	BDL	3.3	BDL	BDL	2.8	5	11.1	10.7
T4/153	153	BDL	BDL	4.7	1.8	BDL	3	4.4	13.9	14.5
T4/490	490	1.8	BDL	2.4	BDL	BDL	2.3	5.9	12.4	13.2
T4/795	795	BDL	BDL	6.7	3.6	0.5	2.8	6	19.6	14.4

Y (ppm)

sample	depth	H_2O	NH4-Ac	NH_4-OxD	NH_4-OxH	H_2O_2	sulfide	residual	total	bulk
T4/010	10	BDL	BDL	BDL	0.8	BDL	1.3	0.9	3	6.3
T4/040	40	BDL	BDL	1.1	0.9	BDL	1.6	1.3	4.9	7.4
T4/100	100	BDL	BDL	0.5	BDL	BDL	1.3	1.4	3.2	5.7
T4/153	153	BDL	BDL	0.8	BDL	BDL	1.9	1.3	4	7.6
T4/490	490	BDL	1	1.4	0.8	0.6	1.3	1.2	6.3	7.9
T4/795	795	BDL	BDL	1.2	BDL	0.5	1.3	1.5	4.5	5.6

Sc (ppm)

sample	depth	H_2O	NH4-Ac	NH_4-OxD	NH_4-OxH	H_2O_2	sulfide	residual	total	bulk
T4/010	10	BDL	BDL	0.5	0.9	BDL	3.9	7.9	13.2	18.2
T4/040	40	BDL	BDL	1.1	BDL	BDL	4.5	7.1	12.7	18.5
T4/100	100	BDL	BDL	0.6	BDL	BDL	4.9	7.7	13.2	18.6
T4/153	153	BDL	BDL	0.7	0.7	BDL	4.3	7.4	13.1	18.5
T4/490	490	BDL	BDL	BDL	BDL	BDL	4.8	6.7	11.5	17
T4/795	795	BDL	BDL	0.8	0.7	BDL	6	7.4	14.9	16.8

Co (ppm)

sample	depth	H_2O	NH4-Ac	NH_4-OxD	NH_4-OxH	H_2O_2	sulfide	residual	total	bulk
T4/010	10	BDL	BDL	BDL	1	BDL	5	2	8	7
T4/040	40	BDL	BDL	BDL	2	BDL	5	2	9	8
T4/100	100	BDL	BDL	BDL	BDL	BDL	7	1	8	9
T4/153	153	BDL	BDL	BDL	BDL	BDL	6	2	8	9
T4/490	490	4	BDL	BDL	BDL	3	13	2	22	22
T4/795	795	BDL	BDL	BDL	BDL	2	13	2	17	19

Sn (ppm)

sample	depth	H_2O	NH4-Ac	NH_4-OxD	NH_4-OxH	H_2O_2	sulfide	residual	total	bulk
T4/010	10	BDL	BDL	BDL	BDL	BDL	BDL	BDL	BDL	21
T4/040	40	BDL	BDL	BDL	BDL	BDL	BDL	BDL	BDL	29
T4/100	100	BDL	BDL	BDL	BDL	BDL	BDL	BDL	BDL	31
T4/153	153	BDL	BDL	BDL	BDL	BDL	BDL	BDL	BDL	28
T4/490	490	BDL	BDL	BDL	BDL	BDL	16	BDL	16	28
T4/795	795	BDL	BDL	BDL	BDL	BDL	17	BDL	17	36

Be (ppm)

sample	depth	H_2O	NH4-Ac	NH_4-OxD	NH_4-OxH	H_2O_2	sulfide	residual	total	bulk
T4/010	10	BDL	BDL	BDL	BDL	BDL	BDL	0.7	0.7	1
T4/040	40	BDL	BDL	BDL	BDL	BDL	BDL	0.6	0.6	0.9
T4/100	100	BDL	BDL	BDL	BDL	BDL	BDL	0.6	0.6	1
T4/153	153	BDL	BDL	BDL	BDL	BDL	BDL	0.6	0.6	1
T4/490	490	BDL	BDL	BDL	BDL	BDL	BDL	0.6	0.6	1
T4/795	795	BDL	BDL	BDL	BDL	BDL	BDL	0.7	0.7	1.1

Ag (ppm)

sample	depth	H_2O	NH4-Ac	NH_4-OxD	NH_4-OxH	H_2O_2	sulfide	residual	total	bulk
T4/010	10	0.3	BDL	BDL	0.6	BDL	BDL	BDL	0.9	BDL
T4/040	40	BDL	BDL	BDL	1.2	BDL	0.3	0.2	1.7	BDL
T4/100	100	BDL	BDL	BDL	BDL	BDL	0.3	BDL	0.3	BDL
T4/153	153	BDL	BDL	BDL	BDL	BDL	0.2	0.2	0.4	0.4
T4/490	490	1.2	BDL	BDL	0.8	BDL	0.3	BDL	2.3	BDL
T4/795	795	0.5	BDL	BDL	BDL	BDL	0.6	0.2	1.3	0.9

Fe (%)										
sample	depth	H_2O	NH4-Ac	NH_4-OxD	NH_4-OxH	H_2O_2	sulfide	residual	total	bulk
E1/010	10	BDL	0.04	0.2	2.36	1.25	2.73	0.31	6.89	8.32
E1/030	30	BDL	0.03	0.34	1.92	1.03	3.41	0.36	7.09	8.54
E1/050	50	0.03	0.03	0.18	2.1	1.38	1.47	0.34	5.53	6.87
E1/100	100	0.04	0.02	0.33	1.96	1.51	1.21	0.36	5.43	6.95
E1/170	170	0.05	0.05	1.59	1.43	1.38	1.25	0.39	6.14	7.16
E1/200	200	0.05	0.03	0.47	2.58	1.54	1.24	0.36	6.27	7.39
E1/260	260	0.03	0.04	0.35	2.16	1.5	1.51	0.39	5.98	7.18
E1/350	350	0.2	0.09	0.77	3.54	0.99	2.45	0.47	8.51	10.3
E1/482	482	0.09	0.12	0.77	2.72	1.76	3.04	0.44	8.94	10.8

Al (%)										
sample	depth	H_2O	NH4-Ac	NH_4-OxD	NH_4-OxH	H_2O_2	sulfide	residual	total	bulk
E1/010	10	BDL	0.03	0.06	0.22	0.02	0.11	3.37	3.81	7.69
E1/030	30	0.01	0.04	0.07	0.23	0.02	0.1	5.87	6.34	7.46
E1/050	50	0.57	0.05	0.06	0.3	0.02	0.11	5.29	6.4	7.72
E1/100	100	0.38	0.06	0.08	0.18	0.02	0.14	6.56	7.42	8.78
E1/170	170	0.33	0.07	0.09	0.16	0.03	0.14	6.64	7.46	8.52
E1/200	200	0.42	0.08	0.07	0.15	0.03	0.12	6.75	7.62	8.52
E1/260	260	0.36	0.07	0.09	0.2	0.02	0.15	6.49	7.38	8.85
E1/350	350	0.39	0.06	0.06	0.12	0.01	0.12	5.8	6.56	7.99
E1/482	482	0.3	0.14	0.27	0.28	0.02	0.19	5.38	6.58	7.67

K (%)										
sample	depth	H_2O	NH4-Ac	NH_4-OxD	NH_4-OxH	H_2O_2	sulfide	residual	total	bulk
E1/010	10	BDL	BDL	0.02	0.24	BDL	-	1.72	1.98	2.48
E1/030	30	BDL	BDL	0.02	0.19	BDL	-	1.73	1.94	2.4
E1/050	50	BDL	BDL	BDL	0.15	BDL	-	1.57	1.72	2.16
E1/100	100	BDL	BDL	0.03	0.18	BDL	-	1.83	2.04	2.56
E1/170	170	BDL	BDL	0.14	0.14	BDL	-	1.81	2.09	2.45
E1/200	200	BDL	BDL	0.03	0.29	BDL	-	1.71	2.03	2.38
E1/260	260	BDL	BDL	0.02	0.24	BDL	-	1.72	1.98	2.46
E1/350	350	BDL	BDL	0.02	0.32	BDL	-	1.4	1.74	2.18
E1/482	482	BDL	BDL	0.04	0.26	BDL	-	1.41	1.71	2.15

Mg (%)										
sample	depth	H_2O	NH4-Ac	NH_4-OxD	NH_4-OxH	H_2O_2	sulfide	residual	total	bulk
E1/010	10	0.03	BDL	BDL	0.01	BDL	0.03	0.13	0.2	0.33
E1/030	30	0.02	BDL	BDL	0.01	BDL	0.03	0.17	0.23	0.29
E1/050	50	0.4	BDL	BDL	0.01	BDL	0.03	0.16	0.6	0.72
E1/100	100	0.23	BDL	BDL	BDL	BDL	0.03	0.19	0.45	0.55
E1/170	170	0.19	BDL	BDL	0.01	BDL	0.04	0.2	0.44	0.53
E1/200	200	0.18	0.01	BDL	BDL	BDL	0.02	0.19	0.4	0.48
E1/260	260	0.18	BDL	BDL	0.01	BDL	0.04	0.18	0.41	0.52
E1/350	350	0.19	BDL	BDL	BDL	BDL	0.02	0.14	0.35	0.43
E1/482	482	0.19	BDL	BDL	0.02	BDL	0.03	0.13	0.37	0.48

Na (%)										
sample	depth	H_2O	NH4-Ac	NH_4-OxD	NH_4-OxH	H_2O_2	sulfide	residual	total	bulk
E1/010	10	0.03	BDL	0.01	0.12	BDL	BDL	0.77	0.93	1.17
E1/030	30	0.02	BDL	0.02	0.1	BDL	BDL	0.78	0.92	1.16
E1/050	50	0.01	BDL	0.02	0.19	BDL	BDL	0.65	0.87	1.09
E1/100	100	BDL	BDL	BDL	0.12	BDL	BDL	0.61	0.73	0.99
E1/170	170	BDL	BDL	0.06	0.06	BDL	BDL	0.6	0.72	0.89
E1/200	200	BDL	BDL	BDL	0.08	BDL	BDL	0.53	0.61	0.89
E1/260	260	BDL	BDL	BDL	0.07	BDL	BDL	0.58	0.65	0.96
E1/350	350	BDL	BDL	BDL	0.11	BDL	BDL	0.58	0.69	0.94
E1/482	482	BDL	BDL	BDL	0.09	BDL	BDL	0.65	0.74	1.05

Ca (%)										
sample	depth	H_2O	NH4-Ac	NH_4-OxD	NH_4-OxH	H_2O_2	sulfide	residual	total	bulk
E1/010	10	0.38	0.05	0.02	0.02	BDL	BDL	0.07	0.54	0.64
E1/030	30	0.36	0.02	0.02	0.02	BDL	BDL	0.12	0.54	0.58
E1/050	50	0.61	0.01	0.01	0.03	BDL	BDL	0.1	0.76	0.84
E1/100	100	0.54	0.01	BDL	0.01	BDL	BDL	0.09	0.65	0.72
E1/170	170	0.63	0.02	0.02	0.02	BDL	BDL	0.1	0.79	0.79
E1/200	200	0.49	0.03	BDL	0.01	BDL	BDL	0.09	0.62	0.68
E1/260	260	0.56	0.03	0.01	0.02	BDL	BDL	0.11	0.73	0.77
E1/350	350	0.66	0.02	BDL	BDL	BDL	BDL	0.11	0.79	0.87
E1/482	482	0.56	0.02	BDL	0.01	BDL	BDL	0.14	0.73	0.82

Tl (%)										
sample	depth	H_2O	NH4-Ac	NH_4-OxD	NH_4-OxH	H_2O_2	sulfide	residual	total	bulk
E1/010	10	BDL	BDL	BDL	BDL	BDL	BDL	0.17	0.17	0.18
E1/030	30	BDL	BDL	BDL	BDL	BDL	BDL	0.17	0.17	0.16
E1/050	50	BDL	BDL	BDL	BDL	BDL	BDL	0.16	0.16	0.17
E1/100	100	BDL	BDL	BDL	BDL	BDL	BDL	0.19	0.19	0.19
E1/170	170	BDL	BDL	BDL	BDL	BDL	BDL	0.2	0.2	0.2
E1/200	200	BDL	BDL	BDL	BDL	BDL	BDL	0.21	0.21	0.18
E1/260	260	BDL	BDL	BDL	BDL	BDL	BDL	0.2	0.2	0.21
E1/350	350	BDL	BDL	BDL	BDL	BDL	BDL	0.22	0.22	0.22
E1/482	482	BDL	BDL	BDL	BDL	BDL	BDL	0.21	0.21	0.22

P (%)										
sample	depth	H_2O	NH4-Ac	NH_4-OxD	NH_4-OxH	H_2O_2	sulfide	residual	total	bulk
E1/010	10	BDL	BDL	BDL	BDL	BDL	BDL	0.05	0.05	0.06
E1/030	30	BDL	BDL	BDL	BDL	BDL	BDL	0.05	0.05	0.06
E1/050	50	BDL	BDL	BDL	BDL	BDL	BDL	0.04	0.04	BDL
E1/100	100	BDL	BDL	BDL	BDL	BDL	BDL	0.05	0.05	0.03
E1/170	170	BDL	BDL	BDL	BDL	BDL	BDL	0.05	0.05	0.03
E1/200	200	BDL	BDL	BDL	BDL	BDL	BDL	0.05	0.05	0.03
E1/260	260	BDL	BDL	BDL	BDL	BDL	BDL	0.05	0.05	0.05
E1/350	350	BDL	BDL	BDL	0.02	BDL	BDL	0.05	0.07	0.06
E1/482	482	BDL	BDL	BDL	0.02	BDL	BDL	0.04	0.06	0.07

Ba (ppm)										
sample	depth	H_2O	NH4-Ac	NH_4-OxD	NH_4-OxH	H_2O_2	sulfide	residual	total	bulk
E1/010	10	BDL	BDL	1	24	BDL	11	199	235	443
E1/030	30	BDL	BDL	BDL	24	BDL	11	231	266	426
E1/050	50	BDL	BDL	BDL	20	BDL	10	196	226	379
E1/100	100	BDL	BDL	BDL	21	BDL	11	206	238	428
E1/170	170	BDL	BDL	4	24	BDL	11	207	246	397
E1/200	200	BDL	BDL	BDL	23	BDL	9	192	224	459
E1/260	260	1	BDL	BDL	27	BDL	11	197	236	451
E1/350	350	BDL	BDL	BDL	30	BDL	14	189	233	414
E1/482	482	BDL	BDL	BDL	27	BDL	12	192	231	418

Cu (ppm)										
sample	depth	H_2O	NH4-Ac	NH_4-OxD	NH_4-OxH	H_2O_2	sulfide	residual	total	bulk
E1/010	10	1320	471	235	433	51.7	82.5	51.2	2644	2610
E1/030	30	786	335	268	379	89.3	123	54.9	2035	2040
E1/050	50	12910	377	98.5	389	37.9	43.4	32.2	13888	14890
E1/100	100	6190	211	63.7	384	23.5	38.1	37.6	6948	7060
E1/170	170	5220	229	156	275	32.3	44.2	43.2	6000	5880
E1/200	200	4270	319	64.3	283	21.9	38.6	40.4	5037	4820
E1/260	260	4030	283	101	356	34.9	55.8	46.6	4907	4880
E1/350	350	2820	154	132	302	246	205	61.2	3920	3860
E1/482	482	2060	212	275	301	92.5	104	51.6	3096	3190

Zn (ppm)										
sample	depth	H_2O	NH4-Ac	NH_4-OxD	NH_4-OxH	H_2O_2	sulfide	residual	total	bulk
E1/010	10	4	0.5	BDL	1.5	0.5	4.4	13.5	24.4	26.2
E1/030	30	3.6	BDL	1.7	1.7	0.6	4.6	13	25.2	26.5
E1/050	50	33.9	0.8	BDL	1.6	0.6	3.6	13.6	54.1	49
E1/100	100	16.5	BDL	BDL	0.9	BDL	3	14.4	34.8	34.4
E1/170	170	14.5	BDL	BDL	1.2	BDL	4.3	14.7	34.7	32.4
E1/200	200	11.7	0.6	BDL	1.1	BDL	2.5	13.8	29.7	27.9
E1/260	260	12.1	BDL	BDL	1.3	BDL	3.8	17.3	34.5	34.4
E1/350	350	11.6	BDL	BDL	1.6	0.5	4.6	24.7	43	46.5
E1/482	482	14.7	0.5	0.8	3.6	0.7	5.8	25	51.1	48.9

Mn (ppm)										
sample	depth	H_2O	NH4-Ac	NH_4-OxD	NH_4-OxH	H_2O_2	sulfide	residual	total	bulk
E1/010	10	16	BDL	2	8	BDL	8	9	43	52
E1/030	30	10	BDL	3	7	BDL	8	11	39	38
E1/050	50	143	3	BDL	9	BDL	8	13	176	188
E1/100	100	70	BDL	BDL	3	BDL	3	8	84	77
E1/170	170	68	2	4	4	BDL	6	11	95	86
E1/200	200	55	3	BDL	3	BDL	3	7	71	68
E1/260	260	54	3	BDL	5	BDL	9	11	82	83
E1/350	350	42	BDL	BDL	3	BDL	4	9	58	58
E1/482	482	43	BDL	BDL	4	BDL	6	9	62	67

Cr (ppm)										
sample	depth	H_2O	NH4-Ac	NH_4-OxD	NH_4-OxH	H_2O_2	sulfide	residual	total	bulk
E1/010	10	BDL	BDL	2	5	BDL	BDL	BDL	7	4
E1/030	30	BDL	BDL	1	4	BDL	BDL	BDL	5	1
E1/050	50	2	BDL	1	5	BDL	BDL	1	9	8
E1/100	100	1	BDL	2	1	BDL	BDL	BDL	4	5
E1/170	170	2	1	5	2	BDL	1	BDL	11	5
E1/200	200	2	BDL	1	4	BDL	1	BDL	8	5
E1/260	260	1	BDL	1	3	BDL	2	BDL	7	9
E1/350	350	1	BDL	1	2	BDL	1	BDL	5	6
E1/482	482	BDL	BDL	1	2	BDL	1	BDL	4	3

Pb (ppm)										
sample	depth	H_2O	NH4-Ac	NH_4-OxD	NH_4-OxH	H_2O_2	sulfide	residual	total	bulk
E1/010	10	BDL	BDL	13	4	BDL	2	10	29	20
E1/030	30	4	BDL	4	3	BDL	4	7	22	29
E1/050	50	BDL	BDL	5	BDL	BDL	BDL	3	8	12
E1/100	100	BDL	BDL	4	BDL	BDL	3	4	11	17
E1/170	170	BDL	BDL	BDL	2	BDL	4	BDL	6	22
E1/200	200	BDL	BDL	3	5	BDL	2	2	12	15
E1/260	260	6	BDL	BDL	BDL	BDL	3	2	11	23
E1/350	350	BDL	BDL	BDL	3	BDL	5	8	16	30
E1/482	482	BDL	BDL	4	BDL	BDL	4	8	16	30

Mo (ppm)										
sample	depth	H_2O	NH4-Ac	NH_4-OxD	NH_4-OxH	H_2O_2	sulfide	residual	total	bulk
E1/010	10	BDL	1	7	21	167	575	128	899	881
E1/030	30	BDL	BDL	7	20	138	620	181	966	989
E1/050	50	BDL	BDL	3	21	168	312	84	588	587
E1/100	100	BDL	BDL	5	26	107	206	20	364	374
E1/170	170	BDL	BDL	14	22	91	195	18	340	333
E1/200	200	BDL	BDL	7	27	64	84	29	211	208
E1/260	260	BDL	BDL	5	28	66	137	26	262	254
E1/350	350	BDL	BDL	5	13	52	170	30	270	273
E1/482	482	BDL	BDL	8	11	80	115	12	226	224

V (ppm)										
sample	depth	H_2O	NH4-Ac	NH_4-OxD	NH_4-OxH	H_2O_2	sulfide	residual	total	bulk
E1/010	10	BDL	BDL	6	10	BDL	BDL	75	91	116
E1/030	30	BDL	BDL	4	8	BDL	BDL	72	84	106
E1/050	50	BDL	BDL	4	13	BDL	BDL	68	85	114
E1/100	100	BDL	BDL	6	5	BDL	BDL	86	97	130
E1/170	170	BDL	BDL	11	5	BDL	BDL	87	103	133
E1/200	200	BDL	BDL	6	8	BDL	3	92	109	135
E1/260	260	BDL	BDL	7	8	BDL	4	90	109	139
E1/350	350	BDL	BDL	13	12	BDL	4	83	112	149
E1/482	482	BDL	BDL	13	12	BDL	6	74	105	135

As (ppm)										
sample	depth	H_2O	NH4-Ac	NH_4-OxD	NH_4-OxH	H_2O_2	sulfide	residual	total	bulk
E1/010	10	3	132	393	132	BDL	11	16	687	703
E1/030	30	14	108	337	124	BDL	13	13	609	654
E1/050	50	6	35	107	100	BDL	11	BDL	259	323
E1/100	100	BDL	BDL	30	25	BDL	4	BDL	59	122
E1/170	170	BDL	15	150	43	BDL	6	4	218	190
E1/200	200	BDL	BDL	64	53	BDL	6	BDL	123	140
E1/260	260	7	6	80	62	BDL	8	BDL	163	213
E1/350	350	BDL	BDL	19	41	BDL	BDL	BDL	60	83
E1/482	482	BDL	BDL	30	28	BDL	BDL	BDL	58	66

W (ppm)										
sample	depth	H_2O	NH4-Ac	NH_4-OxD	NH_4-OxH	H_2O_2	sulfide	residual	total	bulk
E1/010	10	BDL	BDL	18	BDL	BDL	BDL	BDL	18	BDL
E1/030	30	12	BDL	BDL	BDL	BDL	BDL	BDL	12	BDL
E1/050	50	BDL	BDL	15	BDL	BDL	BDL	BDL	15	BDL
E1/100	100	BDL	BDL	11	BDL	BDL	BDL	BDL	11	BDL
E1/170	170	BDL	BDL	BDL	BDL	BDL	BDL	BDL	BDL	BDL
E1/200	200	BDL	BDL	10	BDL	BDL	BDL	BDL	10	BDL
E1/260	260	20	BDL	BDL	BDL	BDL	BDL	BDL	20	BDL
E1/350	350	BDL	BDL	BDL	BDL	BDL	BDL	BDL	BDL	BDL
E1/482	482	BDL	BDL	BDL	BDL	BDL	BDL	BDL	BDL	BDL

Sr (ppm)										
sample	depth	H_2O	NH4-Ac	NH_4-OxD	NH_4-OxH	H_2O_2	sulfide	residual	total	bulk
E1/010	10	0.5	BDL	2.9	19.7	2.7	9.8	162	198	396
E1/030	30	0.7	BDL	2.6	17.3	2.8	9.2	257	290	395
E1/050	50	1.6	0.6	2.2	21.1	1.8	10.6	202	240	329
E1/100	100	2.8	BDL	2.1	15.8	1.2	12.4	280	314	436
E1/170	170	3.2	0.5	8.2	12.8	1.2	10.6	268	305	399
E1/200	200	2.5	0.5	2.4	17	0.8	8.3	263	295	380
E1/260	260	3.7	0.6	2.3	18.3	1.2	12.6	246	285	391
E1/350	350	4.3	0.5	1.9	31.8	1.3	11.1	206	257	353
E1/482	482	2.9	0.7	3.4	20.1	1.3	11.2	206	246	329

Ni (ppm)										
sample	depth	H_2O	NH4-Ac	NH_4-OxD	NH_4-OxH	H_2O_2	sulfide	residual	total	bulk
E1/010	10	BDL	BDL	5	BDL	3	6	2	16	16
E1/030	30	4	BDL	3	BDL	2	8	1	18	17
E1/050	50	19	BDL	4	BDL	4	4	2	33	29
E1/100	100	11	BDL	3	BDL	4	2	2	22	21
E1/170	170	10	BDL	1	BDL	3	3	2	19	20
E1/200	200	10	BDL	3	1	3	2	2	21	20
E1/260	260	15	BDL	2	BDL	3	4	2	26	20
E1/350	350	7	BDL	2	1	2	5	3	20	22
E1/482	482	7	BDL	3	BDL	3	6	2	21	25

Zr (ppm)										
sample	depth	H_2O	NH4-Ac	NH_4-OxD	NH_4-OxH	H_2O_2	sulfide	residual	total	bulk
E1/010	10	BDL	BDL	9.1	3	BDL	BDL	3.5	15.6	21.7
E1/030	30	4.9	BDL	4.5	1.4	BDL	0.8	4.5	16.1	BDL
E1/050	50	BDL	BDL	7.3	2.2	BDL	BDL	4.8	14.3	24
E1/100	100	BDL	BDL	4.8	BDL	BDL	BDL	4.7	9.5	24.9
E1/170	170	BDL	BDL	2.7	2	BDL	BDL	4	8.7	38.4
E1/200	200	BDL	BDL	5.7	3.6	BDL	BDL	4.1	13.4	26.4
E1/260	260	9.5	BDL	1.7	1.3	BDL	BDL	3.3	15.8	15.5
E1/350	350	BDL	BDL	3	5.2	BDL	0.5	2.8	11.5	25.2
E1/482	482	BDL	BDL	5.5	BDL	BDL	0.8	3.9	10.2	31.3

Co (ppm)										
sample	depth	H_2O	NH4-Ac	NH_4-OxD	NH_4-OxH	H_2O_2	sulfide	residual	total	bulk
E1/010	10	6	BDL	BDL	BDL	19	40	BDL	65	63
E1/030	30	4	BDL	BDL	BDL	16	50	BDL	70	68
E1/050	50	81	1	BDL	BDL	22	21	BDL	125	120
E1/100	100	45	BDL	BDL	BDL	22	17	BDL	84	79
E1/170	170	38	1	BDL	BDL	21	15	BDL	75	69
E1/200	200	35	2	BDL	BDL	22	14	BDL	73	67
E1/260	260	33	2	BDL	BDL	23	17	BDL	75	70
E1/350	350	30	BDL	BDL	BDL	14	30	BDL	74	70
E1/482	482	27	BDL	BDL	BDL	23	38	BDL	88	87

Sn (ppm)										
sample	depth	H_2O	NH4-Ac	NH_4-OxD	NH_4-OxH	H_2O_2	sulfide	residual	total	bulk
E1/010	10	BDL	BDL	BDL	BDL	BDL	20	BDL	20	BDL
E1/030	30	BDL	BDL	BDL	BDL	BDL	21	BDL	21	BDL
E1/050	50	BDL	BDL	BDL	BDL	BDL	22	BDL	22	BDL
E1/100	100	BDL	BDL	BDL	BDL	BDL	21	BDL	21	BDL
E1/170	170	BDL	BDL	BDL	BDL	BDL	21	BDL	21	BDL
E1/200	200	BDL	BDL	BDL	BDL	BDL	20	BDL	20	BDL
E1/260	260	BDL	BDL	BDL	BDL	BDL	21	BDL	21	BDL
E1/350	350	BDL	BDL	BDL	BDL	BDL	21	BDL	21	BDL
E1/482	482	BDL	BDL	BDL	BDL	BDL	21	BDL	21	BDL

La (ppm)										
sample	depth	H_2O	NH4-Ac	NH_4-OxD	NH_4-OxH	H_2O_2	sulfide	residual	total	bulk
E1/010	10	BDL	BDL	10.9	3.7	BDL	1.5	2.9	19	20.9
E1/030	30	3.7	BDL	5.4	2.2	BDL	1.7	11	24	20.3
E1/050	50	BDL	BDL	8.7	3.3	BDL	1.2	8.2	21.4	18.1
E1/100	100	BDL	BDL	5.9	BDL	BDL	1.8	10.8	18.5	22.5
E1/170	170	BDL	BDL	3.4	3	BDL	1.7	10.2	18.3	19.6
E1/200	200	BDL	BDL	6.7	4.6	BDL	1.1	10.2	22.6	24.1
E1/260	260	7.1	BDL	2	2.6	BDL	1.7	8.8	22.2	24.2
E1/350	350	BDL	BDL	3.5	6.5	BDL	1.6	8.6	20.2	20.5
E1/482	482	BDL	BDL	6.8	1.6	BDL	2	10.1	20.5	22.8

Y (ppm)										
sample	depth	H_2O	NH4-Ac	NH_4-OxD	NH_4-OxH	H_2O_2	sulfide	residual	total	bulk
E1/010	10	BDL	BDL	1.1	BDL	BDL	1.6	0.8	3.5	7.5
E1/030	30	BDL	BDL	BDL	BDL	BDL	1.4	2.7	4.1	7.8
E1/050	50	2.1	BDL	BDL	BDL	BDL	2.1	2.6	6.8	10
E1/100	100	1	BDL	BDL	BDL	BDL	1.8	2.4	5.2	7.4
E1/170	170	1.1	BDL	BDL	BDL	BDL	1.4	2.3	4.8	8.2
E1/200	200	0.9	BDL	BDL	BDL	BDL	1.2	2.6	4.7	6.4
E1/260	260	1	BDL	BDL	BDL	BDL	1.7	2.2	4.9	6.8
E1/350	350	1.2	BDL	BDL	BDL	BDL	2.8	3.3	7.3	10.9
E1/482	482	1.3	BDL	BDL	BDL	BDL	2.3	3.4	7	10.6

Sc (ppm)										
sample	depth	H_2O	NH4-Ac	NH_4-OxD	NH_4-OxH	H_2O_2	sulfide	residual	total	bulk
E1/010	10	BDL	BDL	1.4	1.1	BDL	BDL	3.3	5.8	10.9
E1/030	30	BDL	BDL	0.9	0.8	BDL	BDL	6.2	7.9	9.7
E1/050	50	1	BDL	1.2	1.2	BDL	BDL	5.6	9	11.8
E1/100	100	0.7	BDL	1.2	BDL	BDL	BDL	7.5	9.4	13.5
E1/170	170	0.6	BDL	1	0.8	BDL	BDL	7.7	10.1	13.7
E1/200	200	0.7	BDL	1.2	0.9	BDL	BDL	8.5	11.3	13.9
E1/260	260	1.5	BDL	0.9	0.9	BDL	BDL	7.7	11	14.2
E1/350	350	0.8	BDL	0.9	0.9	BDL	BDL	6.6	9.2	12.6
E1/482	482	BDL	BDL	1.5	0.5	BDL	BDL	6.4	8.4	11.6

Be (ppm)										
sample	depth	H_2O	NH4-Ac	NH_4-OxD	NH_4-OxH	H_2O_2	sulfide	residual	total	bulk
E1/010	10	BDL	BDL	BDL	BDL	BDL	BDL	0.6	0.6	1
E1/030	30	BDL	BDL	BDL	BDL	BDL	BDL	0.6	0.6	0.9
E1/050	50	BDL	BDL	BDL	BDL	BDL	BDL	0.6	0.6	1
E1/100	100	BDL	BDL	BDL	BDL	BDL	BDL	0.7	0.7	1
E1/170	170	BDL	BDL	BDL	BDL	BDL	BDL	0.7	0.7	1
E1/200	200	BDL	BDL	BDL	BDL	BDL	BDL	0.7	0.7	1
E1/260	260	BDL	BDL	BDL	BDL	BDL	BDL	0.7	0.7	1
E1/350	350	BDL	BDL	BDL	BDL	BDL	BDL	0.7	0.7	1.1
E1/482	482	BDL	BDL	BDL	BDL	BDL	BDL	0.7	0.7	1.1

Ag (ppm)										
sample	depth	H_2O	NH4-Ac	NH_4-OxD	NH_4-OxH	H_2O_2	sulfide	residual	total	bulk
E1/010	10	0.3	BDL	1.6	BDL	BDL	0.6	BDL	2.5	BDL
E1/030	30	0.3	BDL	BDL	BDL	BDL	0.6	BDL	0.9	BDL
E1/050	50	0.3	BDL	BDL	BDL	BDL	0.6	BDL	0.9	0.3
E1/100	100	0.3	BDL	BDL	BDL	BDL	0.6	BDL	0.9	0.3
E1/170	170	0.6	BDL	BDL	BDL	BDL	0.9	BDL	1.5	BDL
E1/200	200	0.2	BDL	BDL	BDL	BDL	0.6	BDL	0.8	0.5
E1/260	260	0.3	BDL	BDL	BDL	BDL	0.8	BDL	1.1	0.2
E1/350	350	0.4	BDL	BDL	BDL	BDL	0.7	BDL	1.1	BDL
E1/482	482	0.5	BDL	BDL	BDL	BDL	0.7	BDL	1.2	BDL

Fe (%)

sample	depth	H_2O	NH4-Ac	NH_4-OxD	NH_4-OxH	H_2O_2	sulfide	residual	total	bulk
E2/010	10	0.17	0.06	0.34	0.88	0.73	0.23	0.07	2.48	2.89
E2/030	30	0.03	0.01	0.29	2.16	1.63	1.44	0.22	5.78	6.72
E2/050	50	0.05	0.02	0.26	2.44	1.58	1.49	0.28	6.12	6.93
E2/070	70	0.03	0.04	0.2	2.73	1.43	1.89	0.34	6.66	7.8
E2/100	100	0.04	0.06	0.2	2.45	1.46	1.58	0.35	6.14	7.23
E2/155	155	0.04	0.05	0.26	2.45	1.48	1.06	0.34	5.68	6.81
E2/190	190	0.03	0.04	1.88	1.47	1.1	1.41	0.37	6.3	7.49
E2/280	280	0.04	0.03	0.16	3.94	1.26	0.96	0.36	6.75	8.03
E2/300	300	0.05	0.05	0.18	3.96	1.13	1.07	0.39	6.83	8.36
E2/390	390	0.06	0.03	0.21	2.89	1.69	1.09	0.4	6.37	8.33
E2/500	500	0.03	0.06	0.25	1.89	1.18	2.43	0.57	6.41	8.24

Al (%)

sample	depth	H_2O	NH4-Ac	NH_4-OxD	NH_4-OxH	H_2O_2	sulfide	residual	total	bulk
E2/010	10	3.09	0.06	0.04	0.12	BDL	0.03	1.44	4.78	5.27
E2/030	30	1.1	0.09	0.18	0.41	0.02	0.12	4.39	6.31	7.17
E2/050	50	0.88	0.06	0.12	0.38	0.01	0.09	5.22	6.76	7.55
E2/070	70	0.25	0.06	0.1	0.33	0.01	0.11	6.36	7.22	8.9
E2/100	100	0.28	0.1	0.14	0.29	0.02	0.14	6.58	7.55	8.77
E2/155	155	0.32	0.07	0.1	0.21	0.01	0.12	6.66	7.49	8.67
E2/190	190	0.33	0.09	0.13	0.24	0.02	0.15	6.69	7.65	8.63
E2/280	280	0.39	0.13	0.19	0.34	0.03	0.18	6.21	7.47	8.68
E2/300	300	0.41	0.1	0.13	0.2	0.03	0.15	6.17	7.19	8.01
E2/390	390	0.5	0.07	0.1	0.2	0.02	0.13	6.18	7.2	8.33
E2/500	500	0.2	0.09	0.16	0.33	0.02	0.31	6.79	7.9	9.46

K (%)

sample	depth	H_2O	NH4-Ac	NH_4-OxD	NH_4-OxH	H_2O_2	sulfide	residual	total	bulk
E2/010	10	BDL	BDL	0.01	0.04	BDL	-	0.4	0.45	0.55
E2/030	30	BDL	BDL	0.02	0.13	BDL	-	1.32	1.47	1.83
E2/050	50	BDL	BDL	0.02	0.15	BDL	-	1.58	1.75	2.11
E2/070	70	BDL	BDL	0.01	0.19	BDL	-	2.02	2.22	2.84
E2/100	100	BDL	BDL	0.02	0.18	BDL	-	1.95	2.15	2.68
E2/155	155	BDL	BDL	0.02	0.19	BDL	-	1.83	2.04	2.48
E2/190	190	BDL	BDL	0.17	0.12	BDL	-	1.73	2.02	2.35
E2/280	280	BDL	BDL	0.02	0.44	BDL	-	1.48	1.94	2.35
E2/300	300	BDL	BDL	0.02	0.42	BDL	-	1.42	1.86	2.2
E2/390	390	BDL	BDL	0.02	0.27	BDL	-	1.56	1.85	2.28
E2/500	500	BDL	BDL	0.02	0.21	BDL	-	1.67	1.9	2.47

Mg (%)

sample	depth	H_2O	NH4-Ac	NH_4-OxD	NH_4-OxH	H_2O_2	sulfide	residual	total	bulk
E2/010	10	1.45	0.02	BDL	BDL	BDL	BDL	0.04	1.51	1.63
E2/030	30	0.57	0.02	BDL	BDL	BDL	BDL	0.11	0.7	0.79
E2/050	50	0.47	0.01	BDL	BDL	BDL	BDL	0.14	0.62	0.63
E2/070	70	0.14	BDL	BDL	BDL	BDL	0.01	0.18	0.33	0.45
E2/100	100	0.16	BDL	BDL	BDL	BDL	0.02	0.18	0.36	0.47
E2/155	155	0.18	BDL	BDL	BDL	BDL	0.02	0.17	0.37	0.46
E2/190	190	0.2	0.01	BDL	BDL	BDL	0.02	0.18	0.41	0.47
E2/280	280	0.24	BDL	BDL	0.01	BDL	0.02	0.16	0.43	0.5
E2/300	300	0.23	BDL	BDL	BDL	BDL	0.01	0.15	0.39	0.43
E2/390	390	0.24	BDL	BDL	BDL	BDL	0.02	0.15	0.41	0.5
E2/500	500	0.17	BDL	BDL	0.07	BDL	0.17	0.2	0.61	0.71

Na (%)

sample	depth	H_2O	NH4-Ac	NH_4-OxD	NH_4-OxH	H_2O_2	sulfide	residual	total	bulk
E2/010	10	BDL	BDL	0.02	0.09	BDL	BDL	0.17	0.28	0.32
E2/030	30	0.25	0.01	0.03	0.25	BDL	0.01	0.53	1.08	1.37
E2/050	50	0.11	BDL	0.03	0.27	BDL	BDL	0.6	1.01	1.22
E2/070	70	0.01	BDL	0.01	0.27	BDL	BDL	0.69	0.98	1.4
E2/100	100	0.01	BDL	BDL	0.22	BDL	BDL	0.63	0.86	1.24
E2/155	155	0.01	BDL	0.01	0.19	BDL	BDL	0.54	0.75	0.98
E2/190	190	0.01	BDL	0.13	0.09	BDL	BDL	0.55	0.78	0.89
E2/280	280	0.01	BDL	BDL	0.12	BDL	BDL	0.54	0.67	0.82
E2/300	300	BDL	BDL	BDL	0.09	BDL	BDL	0.54	0.63	0.8
E2/390	390	BDL	BDL	0.02	0.14	BDL	BDL	0.55	0.71	0.94
E2/500	500	BDL	BDL	BDL	0.06	BDL	BDL	0.63	0.69	0.93

Ca (%)

sample	depth	H_2O	NH4-Ac	NH_4-OxD	NH_4-OxH	H_2O_2	sulfide	residual	total	bulk
E2/010	10	0.18	BDL	BDL	BDL	BDL	BDL	0.02	0.2	0.24
E2/030	30	0.93	0.03	BDL	0.02	BDL	BDL	0.06	1.04	1.1
E2/050	50	0.59	0.01	BDL	0.01	BDL	BDL	0.07	0.68	0.66
E2/070	70	0.49	0.02	BDL	0.01	BDL	BDL	0.09	0.61	0.71
E2/100	100	0.77	0.03	BDL	0.01	BDL	BDL	0.09	0.9	0.93
E2/155	155	0.91	0.04	BDL	BDL	BDL	BDL	0.09	1.04	1.09
E2/190	190	0.53	0.03	0.01	BDL	BDL	BDL	0.09	0.66	0.68
E2/280	280	0.46	0.02	BDL	0.01	BDL	BDL	0.09	0.58	0.61
E2/300	300	0.37	0.01	BDL	BDL	BDL	BDL	0.09	0.47	0.5
E2/390	390	0.53	0.02	BDL	0.01	BDL	BDL	0.1	0.66	0.78
E2/500	500	0.39	0.02	0.01	0.01	BDL	BDL	0.1	0.53	0.63

Ti (%)

sample	depth	H_2O	NH4-Ac	NH_4-OxD	NH_4-OxH	H_2O_2	sulfide	residual	total	bulk
E2/010	10	BDL	BDL	BDL	BDL	BDL	BDL	0.04	0.04	0.05
E2/030	30	BDL	BDL	BDL	BDL	BDL	BDL	0.13	0.13	0.12
E2/050	50	BDL	BDL	BDL	BDL	BDL	BDL	0.15	0.15	0.14
E2/070	70	BDL	BDL	BDL	BDL	BDL	BDL	0.19	0.19	0.17
E2/100	100	BDL	BDL	BDL	BDL	BDL	BDL	0.2	0.2	0.18
E2/155	155	BDL	BDL	BDL	BDL	BDL	BDL	0.18	0.18	0.18
E2/190	190	BDL	BDL	BDL	BDL	BDL	BDL	0.2	0.2	0.19
E2/280	280	BDL	BDL	BDL	BDL	BDL	BDL	0.2	0.2	0.2
E2/300	300	BDL	BDL	BDL	BDL	BDL	BDL	0.22	0.22	0.2
E2/390	390	BDL	BDL	BDL	BDL	BDL	BDL	0.2	0.2	0.21
E2/500	500	BDL	BDL	BDL	BDL	BDL	BDL	0.01	0.25	0.26	0.28

P (%)

sample	depth	H_2O	NH4-Ac	NH_4-OxD	NH_4-OxH	H_2O_2	sulfide	residual	total	bulk
E2/010	10	BDL	BDL	BDL	BDL	BDL	BDL	0.01	0.01	BDL
E2/030	30	BDL	BDL	BDL	BDL	BDL	BDL	0.04	0.04	BDL
E2/050	50	BDL	BDL	BDL	BDL	BDL	BDL	0.04	0.04	BDL
E2/070	70	BDL	BDL	BDL	BDL	BDL	BDL	0.05	0.05	0.05
E2/100	100	BDL	BDL	BDL	BDL	BDL	BDL	0.05	0.05	0.04
E2/155	155	BDL	BDL	BDL	BDL	BDL	BDL	0.05	0.05	0.04
E2/190	190	BDL	BDL	BDL	BDL	BDL	BDL	0.05	0.05	0.04
E2/280	280	BDL	BDL	BDL	0.01	BDL	BDL	0.05	0.06	0.03
E2/300	300	BDL	BDL	BDL	0.01	BDL	BDL	0.05	0.06	0.03
E2/390	390	BDL	BDL	BDL	0.01	BDL	BDL	0.05	0.06	0.05
E2/500	500	BDL	BDL	BDL	0.02	BDL	BDL	0.05	0.07	0.06

Cu (ppm)

sample	depth	H_2O	NH4-Ac	NH_4-OxD	NH_4-OxH	H_2O_2	sulfide	residual	total	bulk
E2/010	10	50386	592	40.9	138	8.5	5.5	12.7	51184	48918
E2/030	30	17430	617	125	554	26	42.3	34.5	18829	20120
E2/050	50	12330	347	95.8	605	27.3	24.9	32.5	13463	12140
E2/070	70	2900	160	138	738	42	35.1	38.6	4052	3980
E2/100	100	3420	291	194	710	48.2	49.1	43.2	4756	4540
E2/155	155	3780	225	70.1	459	22.1	38.2	44.1	4639	4740
E2/190	190	4030	306	113	406	71.9	48.1	46.2	5021	5230
E2/280	280	5040	294	81	421	23.3	42.3	53.3	5955	6250
E2/300	300	5220	245	76.1	266	28.8	48.4	57.6	5942	5690
E2/390	390	4380	164	61.1	347	22.8	38.3	51.5	5065	5160
E2/500	500	3870	283	175	346	117	101	64.7	4957	5140

Zn (ppm)

sample	depth	H_2O	NH4-Ac	NH_4-OxD	NH_4-OxH	H_2O_2	sulfide	residual	total	bulk
E2/010	10	112	1.2	BDL	0.8	BDL	0.8	3.5	118.3	101
E2/030	30	41.1	1.1	BDL	1.6	BDL	2.1	9.2	55.1	51.5
E2/050	50	32.6	0.7	BDL	1.2	0.8	2.2	12.2	49.7	39.5
E2/070	70	10.1	BDL	BDL	1.3	BDL	2.2	14.4	28	26.2
E2/100	100	11.7	BDL	BDL	1.2	BDL	2.4	12.8	28.1	30.5
E2/155	155	12.3	BDL	BDL	0.8	BDL	3.7	14	30.8	27.9
E2/190	190	13.6	0.7	BDL	1.6	0.5	3.2	16	35.6	43.6
E2/280	280	17.2	0.5	BDL	2.1	BDL	4.2	16.7	40.7	52.1
E2/300	300	15.5	BDL	BDL	1.5	BDL	4	18.4	39.4	39.3
E2/390	390	15.5	BDL	0.5	1.8	0.5	4.5	19.4	42.2	44.6
E2/500	500	13.3	0.5	0.6	5	0.9	8.6	37.4	66.3	79.2

Mn (ppm)

sample	depth	H_2O	NH4-Ac	NH_4-OxD	NH_4-OxH	H_2O_2	sulfide	residual	total	bulk
E2/010	10	539	6	BDL	2	BDL	BDL	BDL	547	620
E2/030	30	161	4	BDL	7	BDL	BDL	4	176	189
E2/050	50	127	3	BDL	7	BDL	BDL	5	142	128
E2/070	70	39	BDL	BDL	4	BDL	2	7	52	52
E2/100	100	45	BDL	BDL	3	BDL	3	7	58	57
E2/155	155	50	BDL	BDL	2	BDL	3	6	61	62
E2/190	190	53	3	5	3	BDL	3	7	74	71
E2/280	280	62	BDL	BDL	4	BDL	2	7	75	73
E2/300	300	55	BDL	BDL	3	BDL	BDL	7	65	60
E2/390	390	59	BDL	BDL	2	BDL	2	7	70	73
E2/500	500	42	BDL	BDL	9	BDL	19	13	83	90

Cr (ppm)

sample	depth	H_2O	NH4-Ac	NH_4-OxD	NH_4-OxH	H_2O_2	sulfide	residual	total	bulk
E2/010	10	23	3	6	5	BDL	BDL	BDL	37	42
E2/030	30	5	BDL	BDL	7	BDL	1	BDL	13	6
E2/050	50	4	BDL	2	5	BDL	BDL	BDL	11	5
E2/070	70	1	1	BDL	6	BDL	BDL	BDL	8	7
E2/100	100	1	1	1	5	BDL	BDL	1	9	8
E2/155	155	BDL	1	1	4	BDL	BDL	BDL	6	6
E2/190	190	1	1	4	3	BDL	BDL	2	11	10
E2/280	280	1	1	BDL	8	BDL	BDL	2	12	11
E2/300	300	2	BDL	BDL	3	BDL	BDL	BDL	5	7
E2/390	390	2	1	3	5	BDL	1	BDL	12	9
E2/500	500	BDL	1	1	BDL	BDL	4	2	8	10

Pb (ppm)

sample	depth	H_2O	NH4-Ac	NH_4-OxD	NH_4-OxH	H_2O_2	sulfide	residual	total	bulk
E2/010	10	BDL	BDL	3	BDL	BDL	BDL	BDL	3	BDL
E2/030	30	BDL	BDL	2	BDL	BDL	3	5	10	8
E2/050	50	BDL	BDL	BDL	BDL	BDL	3	3	6	10
E2/070	70	BDL	BDL	BDL	BDL	BDL	4	6	10	30
E2/100	100	BDL	BDL	5	4	BDL	3	4	16	24
E2/155	155	BDL	BDL	9	BDL	BDL	4	4	17	16
E2/190	190	BDL	BDL	4	3	BDL	BDL	2	9	16
E2/280	280	BDL	BDL	3	BDL	BDL	BDL	BDL	3	21
E2/300	300	BDL	BDL	4	BDL	BDL	3	3	10	25
E2/390	390	BDL	BDL	26	2	BDL	3	6	37	21
E2/500	500	BDL	BDL	7	BDL	BDL	4	3	14	27

Mo (ppm)

sample	depth	H_2O	NH4-Ac	NH_4-OxD	NH_4-OxH	H_2O_2	sulfide	residual	total	bulk
E2/010	10	BDL	BDL	1	5	129	40	6	181	178
E2/030	30	3	1	10	24	268	176	28	510	502
E2/050	50	BDL	BDL	8	26	239	230	36	539	505
E2/070	70	BDL	BDL	2	33	59	108	28	230	232
E2/100	100	BDL	BDL	6	38	94	127	25	290	274
E2/155	155	BDL	BDL	4	28	63	92	11	198	197
E2/190	190	BDL	BDL	19	28	96	165	13	321	311
E2/280	280	BDL	BDL	4	33	77	88	7	209	206
E2/300	300	BDL	BDL	5	27	81	117	9	239	228
E2/390	390	BDL	BDL	6	22	89	105	8	230	229
E2/500	500	BDL	BDL	4	15	46	112	19	196	200

V (ppm)

sample	depth	H_2O	NH4-Ac	NH_4-OxD	NH_4-OxH	H_2O_2	sulfide	residual	total	bulk
E2/010	10	9	15	13	8	BDL	BDL	18	63	68
E2/030	30	3	BDL	7	17	BDL	BDL	57	84	102
E2/050	50	BDL	BDL	8	12	BDL	BDL	66	86	107
E2/070	70	BDL	BDL	2	11	BDL	2	80	95	124
E2/100	100	BDL	BDL	5	12	BDL	3	85	105	134
E2/155	155	BDL	BDL	6	12	BDL	3	88	109	141
E2/190	190	BDL	BDL	15	10	BDL	3	91	119	144
E2/280	280	BDL	BDL	7	15	BDL	3	84	109	140
E2/300	300	BDL	BDL	8	9	BDL	3	84	104	132
E2/390	390	BDL	BDL	11	13	BDL	3	86	113	138
E2/500	500	BDL	BDL	7	10	BDL	12	99	128	166

As (ppm)

sample	depth	H_2O	NH4-Ac	NH_4-OxD	NH_4-OxH	H_2O_2	sulfide	residual	total	bulk
E2/010	10	BDL	BDL	25	15	BDL	BDL	BDL	54	35
E2/030	30	BDL	BDL	14	37	BDL	3	BDL	54	57
E2/050	50	BDL	BDL	17	56	BDL	4	BDL	77	74
E2/070	70	BDL	7	40	131	BDL	5	BDL	183	204
E2/100	100	BDL	17	68	151	BDL	11	4	251	223
E2/155	155	BDL	10	59	127	BDL	9	5	210	229
E2/190	190	BDL	4	54	37	BDL	5	BDL	100	112
E2/280	280	BDL	BDL	23	36	BDL	5	BDL	64	51
E2/300	300	BDL	BDL	16	20	BDL	4	BDL	40	77
E2/390	390	BDL	BDL	40	44	BDL	4	BDL	88	129
E2/500	500	BDL	BDL	18	14	BDL	BDL	BDL	32	65

Ba (ppm)

sample	depth	H_2O	NH4-Ac	NH_4-OxD	NH_4-OxH	H_2O_2	sulfide	residual	total	bulk
E2/010	10	BDL	BDL	BDL	8	BDL	2	51	61	95
E2/030	30	BDL	BDL	BDL	18	BDL	9	162	189	359
E2/050	50	BDL	BDL	BDL	22	BDL	8	187	217	383
E2/070	70	BDL	BDL	BDL	24	BDL	10	226	260	569
E2/100	100	BDL	BDL	BDL	21	BDL	10	213	244	526
E2/155	155	BDL	BDL	2	21	BDL	9	202	234	432
E2/190	190	BDL	BDL	5	21	BDL	10	199	235	353
E2/280	280	BDL	BDL	BDL	27	BDL	16	182	225	341
E2/300	300	BDL	BDL	BDL	25	BDL	26	183	234	360
E2/390	390	BDL	BDL	5	22	BDL	14	190	231	382
E2/500	500	BDL	BDL	1	17	BDL	10	216	244	383

Sr (ppm)

sample	depth	H_2O	NH4-Ac	NH_4-OxD	NH_4-OxH	H_2O_2	sulfide	residual	total	bulk
E2/010	10	BDL	BDL	0.9	7.1	BDL	3.4	57.6	69	92
E2/030	30	1.5	0.9	2.7	26.6	1.1	10.5	186	229	294
E2/050	50	1.3	0.7	1.9	28	1.2	9.1	207	249	326
E2/070	70	2.6	0.7	2.6	36.4	1.4	12	272	328	460
E2/100	100	4.4	0.9	2.6	31	1.2	10.9	284	335	442
E2/155	155	6.1	1.1	4	24.4	0.8	10.7	248	295	385
E2/190	190	2.3	0.6	12.5	14.5	0.8	11.2	251	293	370
E2/280	280	1.9	0.6	1.7	19.6	0.8	12.6	243	280	374
E2/300	300	1.7	BDL	1.7	21.4	1.2	12.1	230	268	349
E2/390	390	3	0.6	3.2	20	1.3	10.7	229	268	357
E2/500	500	2.3	BDL	2.1	17	1.1	13.9	186	222	312

Ni (ppm)

sample	depth	H_2O	NH4-Ac	NH_4-OxD	NH_4-OxH	H_2O_2	sulfide	residual	total	bulk
E2/010	10	76	BDL	2	BDL	1	BDL	BDL	79	76
E2/030	30	28	BDL	4	BDL	4	3	1	40	37
E2/050	50	23	BDL	BDL	BDL	3	4	2	32	29
E2/070	70	7	BDL	2	BDL	3	4	1	17	18
E2/100	100	7	BDL	2	BDL	3	2	3	17	18
E2/155	155	10	BDL	5	BDL	3	2	2	22	18
E2/190	190	10	BDL	2	1	3	2	2	20	22
E2/280	280	11	BDL	4	BDL	3	2	3	23	21
E2/300	300	11	BDL	3	BDL	2	1	2	19	19
E2/390	390	12	BDL	13	BDL	3	2	3	33	23
E2/500	500	8	BDL	4	BDL	3	6	3	24	26

Zr (ppm)

sample	depth	H_2O	NH4-Ac	NH_4-OxD	NH_4-OxH	H_2O_2	sulfide	residual	total	bulk
E2/010	10	BDL	BDL	4	1.4	BDL	BDL	1.4	6.8	1.4
E2/030	30	BDL	BDL	7.7	2.6	BDL	BDL	1.8	12.1	5.6
E2/050	50	BDL	BDL	BDL	0.9	BDL	BDL	2.9	3.8	18.3
E2/070	70	BDL	BDL	4.1	BDL	BDL	BDL	2.1	6.2	24.8
E2/100	100	BDL	BDL	3.9	2	BDL	BDL	3.2	9.1	29.9
E2/155	155	0.7	BDL	11.2	BDL	BDL	BDL	4.2	16.1	24.2
E2/190	190	BDL	BDL	5.2	3.3	BDL	BDL	6.6	15.1	38.2
E2/280	280	BDL	BDL	7.6	2.8	BDL	BDL	3.1	13.5	24.4
E2/300	300	BDL	BDL	5	2.7	BDL	0.6	3.6	11.9	23.5
E2/390	390	BDL	BDL	25.7	2.8	BDL	BDL	3.2	31.7	29
E2/500	500	BDL	BDL	8.1	BDL	BDL	0.6	3.6	12.3	30.2

Co (ppm)

sample	depth	H_2O	NH4-Ac	NH_4-OxD	NH_4-OxH	H_2O_2	sulfide	residual	total	bulk
E2/010	10	288	3	BDL	BDL	11	2	BDL	304	292
E2/030	30	119	3	BDL	BDL	26	19	BDL	167	157
E2/050	50	99	2	BDL	BDL	24	23	BDL	148	122
E2/070	70	28	BDL	BDL	BDL	20	26	BDL	74	69
E2/100	100	33	BDL	BDL	BDL	21	20	BDL	74	67
E2/155	155	36	1	BDL	BDL	21	12	BDL	70	66
E2/190	190	38	2	BDL	BDL	16	17	BDL	73	68
E2/280	280	46	1	BDL	BDL	20	9	BDL	76	71
E2/300	300	43	1	BDL	BDL	17	11	BDL	72	62
E2/390	390	43	BDL	1	BDL	23	11	BDL	78	76
E2/500	500	28	1	BDL	BDL	22	36	BDL	87	89

Sn (ppm)

sample	depth	H_2O	NH4-Ac	NH_4-OxD	NH_4-OxH	H_2O_2	sulfide	residual	total	bulk
E2/010	10	BDL	BDL	BDL	BDL	BDL	23	BDL	23	BDL
E2/030	30	BDL	BDL	BDL	BDL	BDL	21	BDL	21	BDL
E2/050	50	BDL	BDL	BDL	BDL	BDL	18	BDL	18	BDL
E2/070	70	BDL	BDL	BDL	BDL	BDL	22	BDL	22	BDL
E2/100	100	BDL	BDL	BDL	BDL	BDL	19	11	30	BDL
E2/155	155	BDL	BDL	BDL	BDL	BDL	22	BDL	22	BDL
E2/190	190	BDL	BDL	BDL	BDL	BDL	20	BDL	20	BDL
E2/280	280	BDL	BDL	BDL	BDL	BDL	20	BDL	20	BDL
E2/300	300	BDL	BDL	BDL	BDL	BDL	21	BDL	21	BDL
E2/390	390	BDL	BDL	10	BDL	BDL	21	10	41	BDL
E2/500	500	BDL	BDL	BDL	BDL	BDL	21	BDL	21	19

W (ppm)

sample	depth	H_2O	NH4-Ac	NH_4-OxD	NH_4-OxH	H_2O_2	sulfide	residual	total	bulk
E2/010	10	BDL	BDL	BDL	BDL	BDL	BDL	BDL	BDL	BDL
E2/030	30	BDL	BDL	18	BDL	BDL	BDL	BDL	18	BDL
E2/050	50	BDL	BDL	BDL	BDL	BDL	BDL	BDL	BDL	BDL
E2/070	70	BDL	BDL	BDL	BDL	BDL	BDL	BDL	BDL	BDL
E2/100	100	BDL	BDL	BDL	BDL	BDL	BDL	BDL	BDL	BDL
E2/155	155	BDL	BDL	22	BDL	BDL	BDL	BDL	22	BDL
E2/190	190	BDL	BDL	BDL	BDL	BDL	BDL	BDL	BDL	BDL
E2/280	280	BDL	BDL	15	BDL	BDL	BDL	BDL	15	BDL
E2/300	300	BDL	BDL	11	BDL	BDL	BDL	BDL	11	BDL
E2/390	390	BDL	BDL	54	BDL	BDL	BDL	BDL	54	BDL
E2/500	500	BDL	BDL	17	BDL	BDL	BDL	BDL	17	BDL

La (ppm)

sample	depth	H_2O	NH4-Ac	NH_4-OxD	NH_4-OxH	H_2O_2	sulfide	residual	total	bulk
E2/010	10	BDL	BDL	4.8	2.1	BDL	BDL	2.3	9.2	4.8
E2/030	30	BDL	BDL	9.6	3.4	BDL	1.2	7.5	21.7	18.6
E2/050	50	BDL	BDL	BDL	1.9	BDL	1	9.3	12.2	19
E2/070	70	BDL	BDL	5	BDL	BDL	1.4	8.9	15.3	30.1
E2/100	100	BDL	BDL	4.7	3.5	BDL	1.1	11.4	20.7	28.2
E2/155	155	0.6	BDL	13.4	1.1	BDL	1.5	8.9	25.5	21.8
E2/190	190	BDL	BDL	6.1	4.2	BDL	1.5	9.6	21.4	16.9
E2/280	280	BDL	BDL	9.3	4.5	BDL	1.8	9.7	25.3	16.6
E2/300	300	BDL	BDL	5.9	4.1	BDL	1.8	9.8	21.6	17.8
E2/390	390	BDL	BDL	30.9	4	BDL	1.3	9.9	46.1	19.1
E2/500	500	BDL	BDL	9.7	BDL	BDL	1.7	10.4	21.8	17.6

Y (ppm)

sample	depth	H_2O	NH4-Ac	NH_4-OxD	NH_4-OxH	H_2O_2	sulfide	residual	total	bulk
E2/010	10	7	BDL	BDL	BDL	BDL	BDL	0.6	7.6	10.1
E2/030	30	3.2	BDL	BDL	BDL	BDL	1.6	2.2	7	7.5
E2/050	50	2.1	BDL	BDL	BDL	BDL	1.7	2.7	6.5	8.4
E2/070	70	0.8	BDL	BDL	BDL	BDL	1.6	2.4	4.8	7.6
E2/100	100	0.9	BDL	BDL	BDL	BDL	1.3	2.6	4.8	6.3
E2/155	155	0.8	BDL	BDL	BDL	BDL	1.3	2	4.1	6.6
E2/190	190	0.9	BDL	BDL	BDL	BDL	1.5	2.4	4.8	7.3
E2/280	280	1.1	BDL	BDL	BDL	BDL	1.5	2.4	5	8.2
E2/300	300	1.1	BDL	BDL	BDL	BDL	1.8	2.5	5.4	8
E2/390	390	1.2	BDL	0.9	BDL	BDL	1.9	2.9	6.9	8.9
E2/500	500	1.1	BDL	BDL	BDL	BDL	4.1	5.8	11	16.3

Sc (ppm)

sample	depth	H_2O	NH4-Ac	NH_4-OxD	NH_4-OxH	H_2O_2	sulfide	residual	total	bulk
E2/010	10	6.9	BDL	0.7	0.7	BDL	BDL	1.5	9.8	12.4
E2/030	30	1.7	BDL	1.5	1.1	BDL	BDL	4.8	9.1	11.2
E2/050	50	1.4	BDL	BDL	0.8	BDL	BDL	5.4	7.6	10.5
E2/070	70	BDL	BDL	1.1	0.8	BDL	BDL	6.4	8.3	12
E2/100	100	BDL	BDL	1.1	1.3	BDL	BDL	7.7	10.1	13.7
E2/155	155	0.6	BDL	1.9	1.1	BDL	BDL	8	11.6	14.4
E2/190	190	BDL	BDL	1.4	1.4	BDL	BDL	8.3	11.1	14.4
E2/280	280	BDL	BDL	1.7	1.3	BDL	BDL	7.6	10.6	14
E2/300	300	0.5	BDL	1.3	1	BDL	BDL	7.3	10.1	13
E2/390	390	0.7	BDL	3.3	1	BDL	BDL	7.2	12.2	13.1
E2/500	500	BDL	0.5	1.9	1.1	BDL	0.8	8.6	12.9	17

Be (ppm)

sample	depth	H_2O	NH4-Ac	NH_4-OxD	NH_4-OxH	H_2O_2	sulfide	residual	total	bulk
E2/010	10	0.7	BDL	BDL	BDL	BDL	BDL	BDL	0.7	1.1
E2/030	30	BDL	BDL	BDL	BDL	BDL	BDL	0.5	0.5	1
E2/050	50	BDL	BDL	BDL	BDL	BDL	BDL	0.6	0.6	1
E2/070	70	BDL	BDL	BDL	BDL	BDL	BDL	0.7	0.7	1
E2/100	100	BDL	BDL	BDL	BDL	BDL	BDL	0.7	0.7	1
E2/155	155	BDL	BDL	BDL	BDL	BDL	BDL	0.7	0.7	1
E2/190	190	BDL	BDL	BDL	BDL	BDL	BDL	0.7	0.7	1
E2/280	280	BDL	BDL	BDL	BDL	BDL	BDL	0.7	0.7	1
E2/300	300	BDL	BDL	BDL	BDL	BDL	BDL	0.7	0.7	1
E2/390	390	BDL	BDL	BDL	BDL	BDL	BDL	0.7	0.7	1
E2/500	500	BDL	BDL	BDL	BDL	BDL	BDL	0.8	0.8	1.1

Ag (ppm)

sample	depth	H_2O	NH4-Ac	NH_4-OxD	NH_4-OxH	H_2O_2	sulfide	residual	total	bulk
E2/010	10	0.3	BDL	BDL	BDL	BDL	BDL	BDL	0.3	BDL
E2/030	30	1.4	BDL	BDL	BDL	BDL	0.2	BDL	1.6	BDL
E2/050	50	0.4	BDL	BDL	BDL	BDL	0.6	BDL	1	0.2
E2/070	70	0.4	BDL	BDL	BDL	BDL	0.6	BDL	1	BDL
E2/100	100	0.7	BDL	BDL	BDL	BDL	0.6	BDL	1.3	0.3
E2/155	155	BDL	BDL	BDL	BDL	BDL	0.6	BDL	0.6	BDL
E2/190	190	BDL	BDL	BDL	BDL	BDL	0.7	BDL	0.7	BDL
E2/280	280	0.2	BDL	BDL	BDL	BDL	BDL	BDL	0.2	BDL
E2/300	300	0.3	BDL	BDL	BDL	BDL	0.6	BDL	0.9	0.3
E2/390	390	BDL	BDL	1.6	BDL	BDL	0.4	BDL	2	BDL
E2/500	500	BDL	BDL	BDL	BDL	BDL	0.8	BDL	0.8	0.4

Fe (%)

sample	depth	H_2O	NH4-Ac	NH_4-OxD	NH_4-OxH	H_2O_2	sulfide	residual	total	bulk
E3/010	10	0.02	0.03	0.21	1.96	2.07	1.88	0.37	6.54	7.93
E3/030	30	BDL	0.08	0.19	1.58	2.23	1.89	0.36	6.33	7.75
E3/100	100	0.02	0.04	1.28	0.69	1.44	1.65	0.34	5.46	6.82
E3/150	150	0.03	0.04	1.01	0.93	1.84	2.01	0.33	6.19	7.58
E3/170	170	0.07	0.04	0.53	2.29	1.7	1.77	0.25	6.65	7.93
E3/200	200	0.02	0.03	0.35	2.72	1.2	1.85	0.35	6.52	7.66
E3/250	250	0.03	0.04	0.55	3.29	1.12	1.62	0.35	7	8.01
E3/270	270	0.07	0.11	0.28	3.76	1.41	1.8	0.42	7.85	9.05
E3/300	300	0.05	0.24	0.31	3.52	1.89	2.54	0.45	9	10.4
E3/386	386	0.04	0.14	0.61	2.96	2.37	1.96	0.51	8.59	10.6
E3/400	400	BDL	0.06	0.45	2.08	0.08	0.92	2.17	5.76	7.32

Al (%)

sample	depth	H_2O	NH4-Ac	NH_4-OxD	NH_4-OxH	H_2O_2	sulfide	residual	total	bulk
E3/010	10	0.03	0.02	0.05	0.25	0.01	0.1	7.24	7.7	8.91
E3/030	30	0.02	0.14	0.19	0.31	0.02	0.12	6.96	7.76	8.92
E3/100	100	0.33	0.11	0.2	0.21	0.03	0.19	6.39	7.46	8.61
E3/150	150	0.52	0.11	0.16	0.22	0.03	0.15	5.56	6.75	8.09
E3/170	170	1.19	0.1	0.13	0.17	0.04	0.16	4.59	6.38	7.23
E3/200	200	0.64	0.1	0.1	0.17	0.03	0.2	5.65	6.89	8.38
E3/250	250	0.68	0.07	0.08	0.16	0.03	0.17	5.45	6.64	8.27
E3/270	270	0.63	0.07	0.07	0.12	0.03	0.15	5.39	6.46	7.24
E3/300	300	0.59	0.1	0.13	0.15	0.04	0.21	5.24	6.46	7.21
E3/386	386	0.35	0.09	0.12	0.18	0.03	0.21	5.85	6.83	8.1
E3/400	400	BDL	0.09	0.19	0.24	0.05	0.8	4.82	6.19	7.86

K (%)

sample	depth	H_2O	NH4-Ac	NH_4-OxD	NH_4-OxH	H_2O_2	sulfide	residual	total	bulk
E3/010	10	BDL	BDL	0.01	0.16	BDL	-	2.07	2.24	2.77
E3/030	30	0.02	0.01	0.02	0.14	BDL	-	1.95	2.14	2.74
E3/100	100	BDL	BDL	0.13	0.06	BDL	-	1.81	2	2.5
E3/150	150	BDL	BDL	0.11	0.09	BDL	-	1.63	1.83	2.31
E3/170	170	BDL	BDL	0.05	0.25	BDL	-	1.16	1.46	1.76
E3/200	200	BDL	BDL	0.01	0.31	BDL	-	1.41	1.73	2.22
E3/250	250	BDL	BDL	0.02	0.35	BDL	-	1.46	1.83	2.26
E3/270	270	BDL	BDL	0.02	0.36	BDL	-	1.25	1.63	2.02
E3/300	300	BDL	BDL	0.03	0.37	BDL	-	1.13	1.53	1.94
E3/386	386	BDL	BDL	0.06	0.33	BDL	-	1.4	1.79	2.33
E3/400	400	0.04	0.03	0.01	0.04	BDL	-	1.22	1.34	1.75

Mg (%)

sample	depth	H_2O	NH4-Ac	NH_4-OxD	NH_4-OxH	H_2O_2	sulfide	residual	total	bulk
E3/010	10	0.01	BDL	BDL	BDL	BDL	0.03	0.19	0.23	0.32
E3/030	30	0.02	BDL	BDL	BDL	BDL	0.03	0.19	0.24	0.32
E3/100	100	0.42	0.01	BDL	0.02	BDL	0.04	0.19	0.68	0.79
E3/150	150	0.3	0.01	BDL	0.01	BDL	0.03	0.16	0.51	0.63
E3/170	170	0.5	0.01	BDL	BDL	BDL	0.02	0.12	0.65	0.73
E3/200	200	0.26	0.01	BDL	BDL	BDL	0.02	0.14	0.43	0.53
E3/250	250	0.26	BDL	BDL	BDL	BDL	0.02	0.14	0.42	0.54
E3/270	270	0.25	BDL	BDL	BDL	BDL	BDL	0.12	0.37	0.44
E3/300	300	0.24	BDL	BDL	BDL	BDL	0.02	0.11	0.37	0.45
E3/386	386	0.17	BDL	BDL	0.01	BDL	0.05	0.14	0.37	0.49
E3/400	400	0.06	0.03	0.02	0.08	0.01	0.49	0.56	1.25	1.48

Na (%)

sample	depth	H_2O	NH4-Ac	NH_4-OxD	NH_4-OxH	H_2O_2	sulfide	residual	total	bulk
E3/010	10	BDL	BDL	BDL	0.16	BDL	BDL	0.77	0.93	1.27
E3/030	30	0.01	BDL	0.01	0.14	BDL	BDL	0.76	0.92	1.22
E3/100	100	BDL	BDL	0.07	0.03	BDL	BDL	0.57	0.67	0.94
E3/150	150	BDL	BDL	0.04	0.04	BDL	BDL	0.57	0.65	0.86
E3/170	170	BDL	BDL	BDL	0.04	BDL	BDL	0.38	0.42	0.55
E3/200	200	BDL	BDL	BDL	0.08	BDL	0.01	0.52	0.61	0.8
E3/250	250	BDL	BDL	BDL	0.08	BDL	BDL	0.53	0.61	0.83
E3/270	270	BDL	BDL	BDL	0.16	BDL	0.02	0.51	0.69	0.96
E3/300	300	BDL	BDL	BDL	0.14	BDL	0.04	0.53	0.71	0.96
E3/386	386	BDL	BDL	0.02	0.13	BDL	BDL	0.65	0.8	1.17
E3/400	400	0.02	BDL	BDL	BDL	BDL	0.03	1.41	1.46	1.73

Ca (%)

sample	depth	H_2O	NH4-Ac	NH_4-OxD	NH_4-OxH	H_2O_2	sulfide	residual	total	bulk
E3/010	10	0.43	0.02	0.01	0.02	BDL	BDL	0.09	0.57	0.66
E3/030	30	0.7	0.03	0.01	0.02	BDL	BDL	0.09	0.85	0.94
E3/100	100	0.62	0.02	0.02	0.01	BDL	BDL	0.08	0.75	0.88
E3/150	150	0.47	0.02	0.02	0.01	BDL	BDL	0.08	0.6	0.67
E3/170	170	0.4	0.01	0.01	0.01	BDL	BDL	0.06	0.49	0.56
E3/200	200	0.31	0.01	BDL	BDL	BDL	BDL	0.09	0.41	0.51
E3/250	250	0.44	0.01	BDL	BDL	BDL	BDL	0.08	0.53	0.66
E3/270	270	0.5	0.02	BDL	BDL	BDL	BDL	0.1	0.62	0.75
E3/300	300	0.43	0.02	BDL	BDL	BDL	BDL	0.11	0.56	0.68
E3/386	386	0.44	0.02	BDL	0.01	BDL	BDL	0.12	0.59	0.76
E3/400	400	0.24	0.11	0.01	0.01	0.05	0.27	1.27	1.96	2.42

Ti (%)

sample	depth	H_2O	NH4-Ac	NH_4-OxD	NH_4-OxH	H_2O_2	sulfide	residual	total	bulk
E3/010	10	BDL	BDL	BDL	BDL	BDL	BDL	0.2	0.2	0.19
E3/030	30	BDL	BDL	BDL	BDL	BDL	BDL	0.19	0.19	0.19
E3/100	100	BDL	BDL	BDL	BDL	BDL	BDL	0.18	0.18	0.18
E3/150	150	BDL	BDL	BDL	BDL	BDL	BDL	0.16	0.16	0.18
E3/170	170	BDL	BDL	BDL	BDL	BDL	BDL	0.14	0.14	0.14
E3/200	200	BDL	BDL	BDL	BDL	BDL	BDL	0.19	0.19	0.2
E3/250	250	BDL	BDL	BDL	BDL	BDL	BDL	0.19	0.19	0.19
E3/270	270	BDL	BDL	BDL	BDL	BDL	BDL	0.2	0.2	0.18
E3/300	300	BDL	BDL	BDL	BDL	BDL	BDL	0.19	0.19	0.19
E3/386	386	BDL	BDL	BDL	BDL	BDL	BDL	0.22	0.22	0.24
E3/400	400	BDL	BDL	BDL	0.03	0.01	0.03	0.49	0.56	0.69

P (%)

sample	depth	H_2O	NH4-Ac	NH_4-OxD	NH_4-OxH	H_2O_2	sulfide	residual	total	bulk
E3/010	10	BDL	BDL	BDL	BDL	BDL	BDL	0.06	0.06	0.08
E3/030	30	BDL	BDL	BDL	BDL	BDL	BDL	0.06	0.06	0.08
E3/100	100	BDL	BDL	BDL	BDL	BDL	BDL	0.05	0.05	BDL
E3/150	150	BDL	BDL	BDL	BDL	BDL	BDL	0.05	0.05	BDL
E3/170	170	BDL	BDL	BDL	BDL	BDL	BDL	0.04	0.04	BDL
E3/200	200	BDL	BDL	BDL	BDL	BDL	BDL	0.01	0.05	0.06	0.03
E3/250	250	BDL	BDL	BDL	0.01	BDL	0.01	0.05	0.07	0.05
E3/270	270	BDL	BDL	BDL	0.01	BDL	0.01	0.05	0.07	0.05
E3/300	300	BDL	BDL	BDL	0.01	BDL	0.02	0.04	0.07	0.06
E3/386	386	BDL	BDL	BDL	0.02	BDL	0.01	0.05	0.08	0.09
E3/400	400	BDL	BDL	0.04	BDL	BDL	0.03	BDL	0.07	0.09

Cu (ppm)

sample	depth	H_2O	NH4-Ac	NH_4-OxD	NH_4-OxH	H_2O_2	sulfide	residual	total	bulk
E3/010	10	564	37.5	25.8	528	24.4	37.2	41.2	1258	1100
E3/030	30	674	157	90.4	489	25.7	39.3	40.1	1516	1520
E3/100	100	17310	782	388	403	68.5	55.5	43.6	19051	20270
E3/150	150	11450	559	208	315	41.4	47.8	38.6	12660	12800
E3/170	170	16200	520	91	264	25.4	47	37.4	17185	18090
E3/200	200	5290	295	85.8	290	27.1	97.1	52.5	6138	6240
E3/250	250	3960	161	94.2	312	24	84.7	53.5	4689	4850
E3/270	270	2790	122	35	339	23.9	89.3	62	3461	3430
E3/300	300	2320	117	53.8	244	30	115	56.4	2936	2970
E3/386	386	1560	88.4	68.9	337	25.7	69.4	63	2212	2340
E3/400	400	250	431	390	228	5.6	50.8	26.7	1382	1380

Zn (ppm)

sample	depth	H_2O	NH4-Ac	NH_4-OxD	NH_4-OxH	H_2O_2	sulfide	residual	total	bulk
E3/010	10	1.5	BDL	BDL	1.5	BDL	3.8	15.8	22.6	27.9
E3/030	30	3.3	BDL	0.7	1.6	BDL	2.5	14.8	22.9	24.3
E3/100	100	43.7	1.3	BDL	1.2	BDL	3.1	13.7	63	56.4
E3/150	150	24.6	0.9	BDL	1	0.6	3.6	13.4	44.1	39.6
E3/170	170	34.1	0.9	0.7	1	0.5	2.5	9.2	48.9	42.1
E3/200	200	17.3	0.7	BDL	1.4	0.6	3.7	15.7	39.4	40
E3/250	250	15.3	BDL	BDL	1.3	0.5	3.6	17.5	38.2	41.7
E3/270	270	12.5	BDL	BDL	1.7	0.6	4.2	20.7	39.7	41.8
E3/300	300	12.5	BDL	BDL	2.5	0.9	6.5	23.4	45.8	51
E3/386	386	9	BDL	BDL	2.2	0.9	6	23.1	41.2	49.9
E3/400	400	2.4	1.6	2.2	17.4	1.3	36.7	37.7	99.3	115

Mn (ppm)

sample	depth	H_2O	NH4-Ac	NH_4-OxD	NH_4-OxH	H_2O_2	sulfide	residual	total	bulk
E3/010	10	3	BDL	BDL	3	BDL	3	7	16	14
E3/030	30	4	BDL	BDL	3	BDL	3	8	18	15
E3/100	100	154	4	8	3	BDL	5	7	181	177
E3/150	150	91	3	4	3	BDL	4	6	111	112
E3/170	170	139	4	BDL	2	BDL	2	5	152	156
E3/200	200	64	3	BDL	2	BDL	3	6	78	71
E3/250	250	53	BDL	BDL	2	BDL	2	6	63	59
E3/270	270	44	BDL	BDL	2	BDL	BDL	6	52	55
E3/300	300	45	BDL	BDL	2	BDL	3	6	56	57
E3/386	386	62	BDL	3	4	BDL	7	9	85	93
E3/400	400	62	26	24	94	10	167	350	733	865

Cr (ppm)

sample	depth	H_2O	NH4-Ac	NH_4-OxD	NH_4-OxH	H_2O_2	sulfide	residual	total	bulk
E3/010	10	BDL	BDL	BDL	3	BDL	BDL	BDL	3	4
E3/030	30	BDL	BDL	BDL	3	BDL	BDL	BDL	3	3
E3/100	100	BDL	1	5	1	BDL	1	BDL	8	8
E3/150	150	2	1	4	BDL	BDL	1	BDL	8	7
E3/170	170	3	BDL	4	4	BDL	BDL	BDL	11	10
E3/200	200	BDL	BDL	BDL	4	BDL	2	2	8	6
E3/250	250	1	BDL	2	4	BDL	BDL	BDL	7	6
E3/270	270	BDL	BDL	BDL	2	BDL	1	BDL	3	5
E3/300	300	BDL	BDL	BDL	2	BDL	3	BDL	5	2
E3/386	386	BDL	BDL	4	2	BDL	3	BDL	9	6
E3/400	400	BDL	BDL	BDL	6	BDL	6	9	21	14

Pb (ppm)

sample	depth	H_2O	NH4-Ac	NH_4-OxD	NH_4-OxH	H_2O_2	sulfide	residual	total	bulk
E3/010	10	BDL	BDL	BDL	BDL	BDL	3	3	6	28
E3/030	30	BDL	BDL	BDL	2	BDL	3	4	9	24
E3/100	100	BDL	BDL	8	2	BDL	4	4	18	12
E3/150	150	BDL	BDL	9	BDL	BDL	3	4	16	9
E3/170	170	BDL	BDL	7	BDL	BDL	4	2	13	6
E3/200	200	BDL	BDL	BDL	BDL	BDL	2	BDL	2	17
E3/250	250	BDL	BDL	7	2	BDL	6	5	20	22
E3/270	270	BDL	BDL	BDL	BDL	BDL	5	6	11	22
E3/300	300	BDL	BDL	BDL	BDL	BDL	7	6	13	28
E3/386	386	BDL	BDL	4	BDL	BDL	5	8	17	32
E3/400	400	BDL	BDL	4	6	BDL	6	BDL	16	37

Mo (ppm)

sample	depth	H_2O	NH4-Ac	NH_4-OxD	NH_4-OxH	H_2O_2	sulfide	residual	total	bulk
E3/010	10	BDL	BDL	6	29	174	343	112	664	631
E3/030	30	BDL	2	11	27	234	301	82	657	666
E3/100	100	BDL	BDL	22	15	79	163	41	320	327
E3/150	150	BDL	BDL	15	14	124	211	53	417	435
E3/170	170	BDL	BDL	8	19	106	131	21	285	270
E3/200	200	BDL	BDL	8	25	86	174	21	314	310
E3/250	250	BDL	BDL	10	24	72	152	12	270	264
E3/270	270	BDL	BDL	4	15	65	114	12	210	199
E3/300	300	BDL	BDL	2	10	77	125	5	219	210
E3/386	386	BDL	BDL	5	11	73	105	16	210	216
E3/400	400	BDL	BDL	BDL	1	7	BDL	BDL	8	6

V (ppm)

sample	depth	H_2O	NH4-Ac	NH_4-OxD	NH_4-OxH	H_2O_2	sulfide	residual	total	bulk
E3/010	10	BDL	BDL	BDL	6	BDL	BDL	92	98	127
E3/030	30	BDL	BDL	3	7	BDL	BDL	87	97	129
E3/100	100	BDL	BDL	10	4	BDL	4	82	100	125
E3/150	150	BDL	BDL	12	3	BDL	3	74	92	130
E3/170	170	BDL	4	20	8	BDL	4	64	100	120
E3/200	200	BDL	BDL	14	9	BDL	5	80	108	139
E3/250	250	BDL	BDL	23	11	BDL	5	81	120	148
E3/270	270	BDL	BDL	10	9	BDL	6	78	103	123
E3/300	300	BDL	3	8	9	BDL	8	77	105	127
E3/386	386	BDL	BDL	10	8	2	8	81	109	139
E3/400	400	BDL	BDL	10	48	3	18	102	181	211

As (ppm)

sample	depth	H_2O	NH4-Ac	NH_4-OxD	NH_4-OxH	H_2O_2	sulfide	residual	total	bulk
E3/010	10	BDL	BDL	6	30	BDL	8	BDL	44	82
E3/030	30	BDL	BDL	14	31	BDL	9	BDL	54	102
E3/100	100	BDL	16	110	24	BDL	6	BDL	156	240
E3/150	150	BDL	19	94	22	BDL	7	BDL	142	166
E3/170	170	4	35	122	45	BDL	6	BDL	212	226
E3/200	200	BDL	BDL	15	24	BDL	12	BDL	51	76
E3/250	250	BDL	BDL	23	39	BDL	11	BDL	73	131
E3/270	270	BDL	BDL	14	17	BDL	7	BDL	38	53
E3/300	300	BDL	BDL	11	8	BDL	5	BDL	24	49
E3/386	386	BDL	BDL	25	12	BDL	4	BDL	41	45
E3/400	400	BDL	BDL	3	5	BDL	BDL	BDL	8	44

Ba (ppm)

sample	depth	H_2O	NH4-Ac	NH_4-OxD	NH_4-OxH	H_2O_2	sulfide	residual	total	bulk
E3/010	10	BDL	BDL	BDL	21	BDL	9	248	278	504
E3/030	30	BDL	BDL	BDL	23	BDL	9	243	275	471
E3/100	100	BDL	BDL	3	13	BDL	11	202	229	400
E3/150	150	BDL	BDL	3	17	BDL	10	191	221	382
E3/170	170	BDL	BDL	BDL	22	BDL	11	138	171	254
E3/200	200	BDL	BDL	BDL	24	BDL	17	178	219	366
E3/250	250	BDL	BDL	BDL	29	BDL	17	176	222	389
E3/270	270	BDL	BDL	BDL	29	BDL	28	176	233	417
E3/300	300	BDL	BDL	BDL	27	BDL	33	160	220	395
E3/386	386	BDL	BDL	BDL	27	BDL	15	198	240	421
E3/400	400	2	51	24	36	3	28	251	395	488

Sr (ppm)

sample	depth	H_2O	NH4-Ac	NH_4-OxD	NH_4-OxH	H_2O_2	sulfide	residual	total	bulk
E3/010	10	2.2	0.5	2	24.6	2.8	11.3	280	323	428
E3/030	30	3.9	0.8	3.4	26.3	2	8.8	279	324	428
E3/100	100	4.9	0.7	8	10.5	1.4	11.5	264	301	399
E3/150	150	3	0.6	6.4	12	1.2	9.4	240	273	371
E3/170	170	2.6	BDL	3.3	11.8	0.5	8.7	187	214	280
E3/200	200	1.4	BDL	1.3	18.2	0.6	16.8	212	250	346
E3/250	250	2.6	BDL	2.1	19	0.5	18.4	210	253	351
E3/270	270	3.8	0.7	2	27.4	1.6	19.1	197	252	317
E3/300	300	3.9	0.6	2.2	20.5	1.5	22.3	198	249	315
E3/386	386	3.8	0.6	3.7	20.2	0.7	13.1	200	242	325
E3/400	400	5.4	6.5	2	7.1	3.4	24.7	209	258	331

Ni (ppm)

sample	depth	H_2O	NH4-Ac	NH_4-OxD	NH_4-OxH	H_2O_2	sulfide	residual	total	bulk
E3/010	10	BDL	1	BDL	BDL	5	5	2	13	16
E3/030	30	BDL	BDL	2	BDL	5	4	2	13	16
E3/100	100	22	BDL	4	2	3	3	2	36	35
E3/150	150	15	BDL	5	BDL	5	5	1	31	29
E3/170	170	27	BDL	3	BDL	4	3	2	39	38
E3/200	200	12	BDL	BDL	BDL	2	2	2	18	22
E3/250	250	11	BDL	3	BDL	3	2	2	21	22
E3/270	270	10	BDL	BDL	BDL	3	1	2	16	21
E3/300	300	9	BDL	BDL	BDL	4	4	2	19	24
E3/386	386	6	BDL	4	BDL	5	5	2	22	24
E3/400	400	BDL	BDL	3	3	BDL	6	5	17	21

Zr (ppm)

sample	depth	H_2O	NH4-Ac	NH_4-OxD	NH_4-OxH	H_2O_2	sulfide	residual	total	bulk
E3/010	10	BDL	BDL	BDL	BDL	BDL	0.5	2.3	2.8	9.8
E3/030	30	BDL	BDL	3.2	2.4	BDL	BDL	2.6	8.2	23.5
E3/100	100	BDL	BDL	7.9	3	BDL	BDL	4.9	15.8	13.2
E3/150	150	BDL	BDL	9.5	BDL	BDL	BDL	2	11.5	23.4
E3/170	170	BDL	BDL	5.1	0.7	BDL	BDL	3.7	9.5	24.1
E3/200	200	BDL	BDL	BDL	BDL	BDL	BDL	2.5	2.5	23.8
E3/250	250	BDL	BDL	6.2	2.7	BDL	0.6	2.6	12.1	18.7
E3/270	270	BDL	BDL	BDL	2.5	BDL	BDL	2.7	5.2	20.3
E3/300	300	BDL	BDL	0.9	BDL	BDL	1	4	5.9	25.3
E3/386	386	BDL	BDL	4.3	BDL	BDL	BDL	3.6	7.9	26.1
E3/400	400	BDL	BDL	10.3	4.7	BDL	2.4	55	72.4	108

Co (ppm)

sample	depth	H_2O	NH4-Ac	NH_4-OxD	NH_4-OxH	H_2O_2	sulfide	residual	total	bulk
E3/010	10	3	BDL	BDL	BDL	32	29	BDL	64	63
E3/030	30	5	BDL	BDL	BDL	35	28	BDL	68	68
E3/100	100	91	2	BDL	BDL	21	21	BDL	135	135
E3/150	150	64	2	BDL	BDL	28	27	BDL	121	119
E3/170	170	105	2	BDL	BDL	25	22	BDL	154	151
E3/200	200	48	2	BDL	BDL	20	13	BDL	83	82
E3/250	250	47	1	1	BDL	19	14	BDL	82	82
E3/270	270	42	1	BDL	BDL	22	12	BDL	77	70
E3/300	300	38	1	BDL	BDL	29	15	BDL	83	81
E3/386	386	25	BDL	BDL	BDL	31	20	BDL	76	78
E3/400	400	3	2	BDL	2	BDL	7	3	17	19

Sn (ppm)

sample	depth	H_2O	NH4-Ac	NH_4-OxD	NH_4-OxH	H_2O_2	sulfide	residual	total	bulk
E3/010	10	BDL	BDL	BDL	BDL	BDL	21	BDL	21	BDL
E3/030	30	BDL	BDL	BDL	BDL	BDL	20	BDL	20	BDL
E3/100	100	BDL	BDL	BDL	BDL	BDL	22	10	32	BDL
E3/150	150	BDL	BDL	BDL	BDL	BDL	21	12	33	BDL
E3/170	170	BDL	BDL	BDL	BDL	BDL	26	11	37	BDL
E3/200	200	BDL	BDL	BDL	BDL	BDL	29	10	39	BDL
E3/250	250	BDL	BDL	BDL	BDL	BDL	27	BDL	27	BDL
E3/270	270	BDL	BDL	BDL	BDL	BDL	26	10	36	BDL
E3/300	300	BDL	BDL	BDL	BDL	BDL	25	10	35	BDL
E3/386	386	BDL	BDL	BDL	BDL	BDL	24	11	35	13
E3/400	400	BDL	BDL	BDL	BDL	BDL	20	BDL	20	161

W (ppm)

sample	depth	H_2O	NH4-Ac	NH_4-OxD	NH_4-OxH	H_2O_2	sulfide	residual	total	bulk
E3/010	10	BDL	BDL	BDL	BDL	BDL	BDL	BDL	BDL	BDL
E3/030	30	BDL	BDL	BDL	BDL	BDL	BDL	BDL	BDL	BDL
E3/100	100	BDL	BDL	BDL	BDL	BDL	BDL	BDL	BDL	BDL
E3/150	150	BDL	BDL	18	BDL	BDL	BDL	BDL	18	BDL
E3/170	170	BDL	BDL	BDL	BDL	BDL	BDL	BDL	BDL	BDL
E3/200	200	BDL	BDL	BDL	BDL	BDL	BDL	BDL	BDL	BDL
E3/250	250	BDL	BDL	14	BDL	BDL	BDL	BDL	14	BDL
E3/270	270	BDL	BDL	BDL	BDL	BDL	BDL	BDL	BDL	BDL
E3/300	300	BDL	BDL	BDL	BDL	BDL	BDL	BDL	BDL	BDL
E3/386	386	BDL	BDL	BDL	BDL	BDL	BDL	BDL	BDL	BDL
E3/400	400	BDL	BDL	BDL	BDL	BDL	BDL	BDL	BDL	BDL

La (ppm)

sample	depth	H_2O	NH4-Ac	NH_4-OxD	NH_4-OxH	H_2O_2	sulfide	residual	total	bulk
E3/010	10	BDL	BDL	BDL	BDL	BDL	1.6	9.6	11.2	24.6
E3/030	30	BDL	BDL	4.2	3.4	BDL	1.1	11.7	20.4	22.8
E3/100	100	BDL	BDL	9.6	3.9	BDL	1.5	10.7	25.7	21.2
E3/150	150	BDL	BDL	11.8	0.8	BDL	1	8.8	22.4	19.3
E3/170	170	BDL	BDL	6.5	1.7	BDL	1.3	7.8	17.3	13.4
E3/200	200	BDL	BDL	BDL	1.2	BDL	1.7	7.3	10.2	17.4
E3/250	250	BDL	BDL	7.5	3.9	BDL	2.5	6.5	20.4	19.8
E3/270	270	BDL	BDL	BDL	3.7	BDL	2.5	9.2	15.4	21.4
E3/300	300	BDL	BDL	1.3	1.5	BDL	3.2	9	15	20.6
E3/386	386	BDL	BDL	4.9	1	BDL	1.8	10.7	18.4	25.6
E3/400	400	BDL	1.3	7.2	1.8	BDL	9.2	5.8	25.3	26.5

Y (ppm)

sample	depth	H_2O	NH4-Ac	NH_4-OxD	NH_4-OxH	H_2O_2	sulfide	residual	total	bulk
E3/010	10	BDL	BDL	BDL	BDL	BDL	2.1	3.3	5.4	8
E3/030	30	BDL	BDL	BDL	BDL	BDL	1.6	3.9	5.5	8.9
E3/100	100	2.3	BDL	BDL	BDL	BDL	1.4	2.3	6	8.6
E3/150	150	1.3	BDL	BDL	BDL	BDL	1.4	2.2	4.9	7.9
E3/170	170	2.3	BDL	BDL	BDL	BDL	1	1.5	4.8	6.9
E3/200	200	1.1	BDL	BDL	BDL	BDL	2.1	1.7	4.9	8.9
E3/250	250	1.3	BDL	0.8	BDL	BDL	2.1	1.6	5.8	7.8
E3/270	270	1.3	BDL	BDL	BDL	BDL	3.1	2.7	7.1	9
E3/300	300	1.3	BDL	BDL	BDL	BDL	4.4	3	8.7	11.3
E3/386	386	0.9	BDL	BDL	BDL	BDL	3.4	3.2	7.5	12.1
E3/400	400	BDL	1.8	2.5	0.7	BDL	3.6	6.1	14.7	21.1

Sc (ppm)

sample	depth	H_2O	NH4-Ac	NH_4-OxD	NH_4-OxH	H_2O_2	sulfide	residual	total	bulk
E3/010	10	BDL	BDL	BDL	0.8	BDL	BDL	7.8	8.6	11.7
E3/030	30	BDL	BDL	0.8	1.1	BDL	BDL	7.6	9.5	11.9
E3/100	100	0.7	BDL	1.8	0.9	BDL	BDL	7.6	11	13.8
E3/150	150	0.8	0.5	1.7	0.6	BDL	BDL	6.4	10	13.1
E3/170	170	2	0.7	1.3	0.5	BDL	BDL	5.9	10.4	12.8
E3/200	200	1.1	0.6	0.5	0.6	BDL	BDL	7	9.8	14.1
E3/250	250	1	BDL	1.1	0.8	BDL	BDL	6.5	9.4	13.5
E3/270	270	1.1	BDL	BDL	0.6	BDL	BDL	6.4	8.1	11
E3/300	300	0.9	BDL	1	BDL	BDL	BDL	6.4	8.3	11.8
E3/386	386	BDL	BDL	1.4	0.6	BDL	BDL	6.4	8.4	12.4
E3/400	400	BDL	0.6	1.2	0.8	BDL	1.5	8.7	12.8	17.6

Be (ppm)

sample	depth	H_2O	NH4-Ac	NH_4-OxD	NH_4-OxH	H_2O_2	sulfide	residual	total	bulk
E3/010	10	BDL	BDL	BDL	BDL	BDL	BDL	0.8	0.8	1
E3/030	30	BDL	BDL	BDL	BDL	BDL	BDL	0.8	0.8	1
E3/100	100	BDL	BDL	BDL	BDL	BDL	BDL	0.7	0.7	1.1
E3/150	150	BDL	BDL	BDL	BDL	BDL	BDL	0.6	0.6	1
E3/170	170	BDL	BDL	BDL	BDL	BDL	BDL	BDL	BDL	0.9
E3/200	200	BDL	BDL	BDL	BDL	BDL	BDL	0.6	0.6	1
E3/250	250	BDL	BDL	BDL	BDL	BDL	BDL	0.6	0.6	1.1
E3/270	270	BDL	BDL	BDL	BDL	BDL	BDL	0.7	0.7	1
E3/300	300	BDL	BDL	BDL	BDL	BDL	BDL	0.7	0.7	1
E3/386	386	BDL	BDL	BDL	BDL	BDL	BDL	0.7	0.7	1.1
E3/400	400	BDL	BDL	BDL	BDL	BDL	BDL	0.9	0.9	1.4

Ag (ppm)

sample	depth	H_2O	NH4-Ac	NH_4-OxD	NH_4-OxH	H_2O_2	sulfide	residual	total	bulk
E3/010	10	BDL	BDL	BDL	BDL	BDL	0.4	BDL	0.4	BDL
E3/030	30	BDL	BDL	BDL	BDL	BDL	0.4	BDL	0.4	BDL
E3/100	100	BDL	BDL	BDL	BDL	BDL	0.6	BDL	0.6	0.4
E3/150	150	BDL	BDL	BDL	BDL	BDL	0.6	BDL	0.6	BDL
E3/170	170	BDL	BDL	BDL	BDL	BDL	0.6	BDL	0.6	BDL
E3/200	200	BDL	BDL	BDL	BDL	BDL	0.4	BDL	0.4	BDL
E3/250	250	BDL	BDL	1.4	BDL	BDL	0.8	BDL	2.2	BDL
E3/270	270	BDL	BDL	BDL	BDL	BDL	0.6	BDL	0.6	BDL
E3/300	300	BDL	BDL	BDL	BDL	BDL	0.4	BDL	0.4	BDL
E3/386	386	BDL	BDL	BDL	BDL	BDL	0.6	BDL	0.6	0.3
E3/400	400	BDL	BDL	BDL	BDL	BDL	BDL	BDL	BDL	BDL

Fe (%)										
sample	depth	H_2O	NH4-Ac	NH_4-OxD	NH_4-OxH	H_2O_2	sulfide	residual	total	bulk
E4/010	10	0.18	0.27	0.54	1.62	1.43	0.6	0.19	4.83	5.51
E4/040	40	0.22	0.28	0.52	2.03	1.44	1.12	0.24	5.85	7.03
E4/080	80	0.13	0.36	0.39	2.46	1.44	1.25	0.36	6.39	7.2
E4/100	100	0.16	0.33	0.4	2.67	1.21	1.01	0.35	6.13	6.85
E4/120	120	0.11	0.29	0.45	2.58	0.81	1.17	0.33	5.74	6.51
E4/140	140	0.11	0.24	0.33	2.78	1.7	1.45	0.34	6.95	7.44
E4/200	200	0.04	0.11	0.2	2.67	1.84	1.78	0.36	7	7.92
E4/250	250	0.03	0.09	0.59	3.14	1.35	1.57	0.45	7.22	8.3
E4/270	270	BDL	0.04	0.39	1.93	0.07	0.95	1.67	5.05	6.03
Al (%)										
sample	depth	H_2O	NH4-Ac	NH_4-OxD	NH_4-OxH	H_2O_2	sulfide	residual	total	bulk
E4/010	10	1.38	0.09	0.06	0.27	0.02	0.11	3.97	5.9	6.59
E4/040	40	0.89	0.05	0.09	0.28	0.02	0.15	5.01	6.49	7.61
E4/080	80	0.33	0.05	0.08	0.18	0.02	0.18	6.83	7.67	8.64
E4/100	100	0.31	0.04	0.06	0.19	0.02	0.18	6.71	7.51	8.75
E4/120	120	0.42	0.06	0.1	0.24	0.02	0.23	6.77	7.84	8.71
E4/140	140	0.28	0.05	0.1	0.22	0.03	0.21	7.15	8.04	8.51
E4/200	200	0.31	0.1	0.14	0.2	0.04	0.25	6.96	8	8.71
E4/250	250	0.42	0.09	0.12	0.15	0.03	0.19	6.44	7.44	8.15
E4/270	270	0.06	0.13	0.16	0.28	BDL	0.78	5.34	6.75	7.47
K (%)										
sample	depth	H_2O	NH4-Ac	NH_4-OxD	NH_4-OxH	H_2O_2	sulfide	residual	total	bulk
E4/010	10	BDL	BDL	0.02	0.1	BDL	-	1.09	1.21	1.44
E4/040	40	BDL	BDL	0.04	0.15	BDL	-	1.39	1.58	1.99
E4/080	80	BDL	BDL	0.04	0.25	BDL	-	1.98	2.27	2.72
E4/100	100	BDL	BDL	0.04	0.24	BDL	-	2.01	2.29	2.71
E4/120	120	BDL	BDL	0.04	0.22	BDL	-	1.83	2.09	2.56
E4/140	140	BDL	BDL	0.03	0.25	BDL	-	1.86	2.14	2.42
E4/200	200	BDL	BDL	0.02	0.32	BDL	-	1.7	2.04	2.42
E4/250	250	BDL	BDL	0.02	0.32	BDL	-	1.55	1.89	2.26
E4/270	270	0.01	BDL	0.01	0.09	BDL	-	1.42	1.53	1.74
Mg (%)										
sample	depth	H_2O	NH4-Ac	NH_4-OxD	NH_4-OxH	H_2O_2	sulfide	residual	total	bulk
E4/010	10	1.13	0.05	BDL	BDL	BDL	BDL	0.1	1.28	1.43
E4/040	40	0.6	0.02	BDL	BDL	BDL	BDL	0.12	0.74	0.88
E4/080	80	0.13	BDL	BDL	BDL	BDL	0.02	0.19	0.34	0.42
E4/100	100	0.11	BDL	BDL	BDL	BDL	0.02	0.18	0.31	0.39
E4/120	120	0.22	0.01	BDL	BDL	BDL	0.02	0.18	0.43	0.52
E4/140	140	0.12	BDL	BDL	BDL	BDL	0.02	0.18	0.32	0.4
E4/200	200	0.15	BDL	BDL	BDL	BDL	0.04	0.18	0.37	0.46
E4/250	250	0.17	BDL	BDL	BDL	BDL	0.03	0.17	0.37	0.44
E4/270	270	0.08	BDL	0.01	0.11	0.01	0.61	0.39	1.21	1.26
Na (%)										
sample	depth	H_2O	NH4-Ac	NH_4-OxD	NH_4-OxH	H_2O_2	sulfide	residual	total	bulk
E4/010	10	BDL	BDL	0.02	0.19	BDL	0.01	0.4	0.62	0.7
E4/040	40	BDL	BDL	0.03	0.2	BDL	0.02	0.52	0.77	0.93
E4/080	80	BDL	BDL	BDL	0.11	BDL	BDL	0.68	0.79	1.03
E4/100	100	BDL	BDL	BDL	0.14	BDL	BDL	0.65	0.79	0.97
E4/120	120	BDL	BDL	0.01	0.18	BDL	0.02	0.53	0.74	1.04
E4/140	140	BDL	BDL	BDL	0.15	BDL	BDL	0.54	0.69	0.9
E4/200	200	BDL	BDL	BDL	0.08	BDL	BDL	0.52	0.6	0.88
E4/250	250	BDL	BDL	BDL	0.08	BDL	0.01	0.57	0.66	0.87
E4/270	270	BDL	BDL	BDL	0.05	BDL	0.01	1.53	1.59	1.83
Ca (%)										
sample	depth	H_2O	NH4-Ac	NH_4-OxD	NH_4-OxH	H_2O_2	sulfide	residual	total	bulk
E4/010	10	0.6	0.03	BDL	0.01	BDL	BDL	0.05	0.69	0.81
E4/040	40	0.66	0.02	BDL	0.01	BDL	BDL	0.06	0.75	0.9
E4/080	80	0.42	0.02	BDL	0.01	BDL	BDL	0.09	0.54	0.63
E4/100	100	0.47	0.03	BDL	0.01	BDL	BDL	0.08	0.59	0.66
E4/120	120	0.51	0.03	BDL	0.01	BDL	BDL	0.07	0.62	0.74
E4/140	140	0.53	0.02	BDL	0.01	BDL	BDL	0.08	0.64	0.71
E4/200	200	0.4	0.01	BDL	BDL	BDL	BDL	0.09	0.5	0.62
E4/250	250	0.34	0.01	BDL	BDL	BDL	BDL	0.11	0.46	0.56
E4/270	270	0.7	0.04	0.01	0.01	0.05	0.16	0.83	1.8	2.04
Ti (%)										
sample	depth	H_2O	NH4-Ac	NH_4-OxD	NH_4-OxH	H_2O_2	sulfide	residual	total	bulk
E4/010	10	BDL	BDL	BDL	BDL	BDL	BDL	0.11	0.11	0.12
E4/040	40	BDL	BDL	BDL	BDL	BDL	BDL	0.13	0.13	0.16
E4/080	80	BDL	BDL	BDL	BDL	BDL	BDL	0.2	0.2	0.19
E4/100	100	BDL	BDL	BDL	BDL	BDL	BDL	0.2	0.2	0.2
E4/120	120	BDL	BDL	BDL	BDL	BDL	BDL	0.21	0.21	0.18
E4/140	140	BDL	BDL	BDL	BDL	BDL	BDL	0.19	0.19	0.19
E4/200	200	BDL	BDL	BDL	BDL	BDL	BDL	0.21	0.21	0.18
E4/250	250	BDL	BDL	BDL	BDL	BDL	BDL	0.22	0.22	0.2
E4/270	270	BDL	BDL	0.01	0.02	BDL	0.02	0.33	0.38	0.44
P (%)										
sample	depth	H_2O	NH4-Ac	NH_4-OxD	NH_4-OxH	H_2O_2	sulfide	residual	total	bulk
E4/010	10	BDL	BDL	BDL	BDL	BDL	BDL	0.03	0.03	BDL
E4/040	40	BDL	BDL	BDL	BDL	BDL	BDL	0.04	0.04	BDL
E4/080	80	BDL	BDL	BDL	BDL	BDL	BDL	0.06	0.06	0.06
E4/100	100	BDL	BDL	BDL	BDL	BDL	BDL	0.06	0.06	0.06
E4/120	120	BDL	BDL	BDL	BDL	BDL	0.01	0.05	0.06	BDL
E4/140	140	BDL	BDL	BDL	BDL	BDL	BDL	0.05	0.05	0.04
E4/200	200	BDL	BDL	BDL	BDL	BDL	BDL	0.06	0.06	0.04
E4/250	250	BDL	BDL	BDL	0.01	BDL	0.01	0.05	0.07	0.07
E4/270	270	BDL	BDL	0.03	0.01	BDL	0.03	0.01	0.08	0.08
Ba (ppm)										
sample	depth	H_2O	NH4-Ac	NH_4-OxD	NH_4-OxH	H_2O_2	sulfide	residual	total	bulk
E4/010	10	BDL	BDL	BDL	14	BDL	9	129	152	215
E4/040	40	BDL	BDL	BDL	19	BDL	14	167	200	301
E4/080	80	BDL	BDL	BDL	26	BDL	19	230	275	458
E4/100	100	BDL	BDL	BDL	28	BDL	12	218	258	442
E4/120	120	BDL	BDL	BDL	20	BDL	15	203	238	470
E4/140	140	BDL	BDL	BDL	27	BDL	11	197	235	429
E4/200	200	BDL	BDL	BDL	22	BDL	14	191	227	439
E4/250	250	BDL	BDL	BDL	27	BDL	19	194	240	380
E4/270	270	BDL	4	9	57	1	36	248	355	426

Cu (ppm)										
sample	depth	H_2O	NH4-Ac	NH_4-OxD	NH_4-OxH	H_2O_2	sulfide	residual	total	bulk
E4/010	10	45529	1770	57.4	405	20.4	35.1	28.5	47845	43056
E4/040	40	19260	644	69.6	394	22.7	56.2	30.3	20477	23120
E4/080	80	2880	187	36.5	286	22.5	47.8	32.3	3492	3490
E4/100	100	2770	167	33.3	370	19.3	38.5	37	3435	3400
E4/120	120	9290	573	76.6	494	24.4	76.2	43.1	10577	10520
E4/140	140	3410	156	52.1	406	25.7	57.8	47.7	4155	3980
E4/200	200	3660	171	61.6	299	32.1	59.8	40.1	4324	4350
E4/250	250	2170	133	84.9	218	23.8	76.3	56.3	2762	2720
E4/270	270	648	132	202	143	42.3	69.7	23.8	1261	1170
Zn (ppm)										
sample	depth	H_2O	NH4-Ac	NH_4-OxD	NH_4-OxH	H_2O_2	sulfide	residual	total	bulk
E4/010	10	115	4.7	BDL	1.4	BDL	1.8	13	135.9	124
E4/040	40	54.3	1.4	BDL	1.3	BDL	2.4	13	72.4	68.2
E4/080	80	9.6	BDL	BDL	0.8	BDL	2.3	14.3	27	28.4
E4/100	100	8	BDL	BDL	0.8	BDL	2.3	55.3	66.4	26.6
E4/120	120	19.7	0.9	BDL	1.1	BDL	2.9	12.5	37.1	33.6
E4/140	140	9.1	BDL	BDL	1	BDL	2.9	13.7	26.7	28.3
E4/200	200	10.2	0.6	BDL	0.8	0.5	3.1	16	31.2	78.5
E4/250	250	9.5	BDL	BDL	1.3	0.6	4	19.9	35.3	38.1
E4/270	270	4.7	BDL	1	11.3	1.4	36.1	27.7	82.2	85.8
Mn (ppm)										
sample	depth	H_2O	NH4-Ac	NH_4-OxD	NH_4-OxH	H_2O_2	sulfide	residual	total	bulk
E4/010	10	397	17	2	6	BDL	BDL	3	425	438
E4/040	40	190	6	BDL	4	BDL	BDL	5	205	230
E4/080	80	42	2	BDL	BDL	BDL	2	6	52	48
E4/100	100	37	BDL	BDL	2	BDL	2	6	47	49
E4/120	120	70	4	BDL	3	BDL	3	6	86	88
E4/140	140	37	BDL	BDL	2	BDL	2	6	47	49
E4/200	200	42	BDL	BDL	3	BDL	4	6	55	56
E4/250	250	38	BDL	BDL	3	BDL	5	9	55	55
E4/270	270	63	5	14	71	9	241	193	596	628
Cr (ppm)										
sample	depth	H_2O	NH4-Ac	NH_4-OxD	NH_4-OxH	H_2O_2	sulfide	residual	total	bulk
E4/010	10	5	3	1	5	BDL	BDL	BDL	14	10
E4/040	40	5	2	6	5	BDL	1	BDL	19	9
E4/080	80	2	2	BDL	2	BDL	BDL	BDL	6	5
E4/100	100	1	2	BDL	BDL	BDL	BDL	BDL	3	7
E4/120	120	1	2	BDL	2	BDL	BDL	3	8	8
E4/140	140	BDL	2	BDL	2	BDL	BDL	BDL	4	5
E4/200	200	BDL	1	1	2	BDL	BDL	BDL	4	8
E4/250	250	BDL	BDL	BDL	3	BDL	BDL	BDL	3	6
E4/270	270	BDL	BDL	BDL	1	BDL	45	3	49	10
Pb (ppm)										
sample	depth	H_2O	NH4-Ac	NH_4-OxD	NH_4-OxH	H_2O_2	sulfide	residual	total	bulk
E4/010	10	BDL	BDL	5	3	BDL	3	4	15	BDL
E4/040	40	BDL	BDL	6	BDL	BDL	4	3	13	4
E4/080	80	BDL	BDL	BDL	BDL	BDL	5	3	8	24
E4/100	100	BDL	BDL	BDL	BDL	BDL	4	6	10	20
E4/120	120	BDL	BDL	3	BDL	BDL	4	BDL	7	18
E4/140	140	BDL	BDL	4	BDL	BDL	3	BDL	7	19
E4/200	200	BDL	BDL	6	BDL	BDL	6	BDL	12	17
E4/250	250	BDL	BDL	2	BDL	BDL	3	2	7	18
E4/270	270	BDL	BDL	BDL	BDL	BDL	2	BDL	2	23
Mo (ppm)										
sample	depth	H_2O	NH4-Ac	NH_4-OxD	NH_4-OxH	H_2O_2	sulfide	residual	total	bulk
E4/010	10	BDL	BDL	3	18	132	130	24	307	307
E4/040	40	BDL	BDL	8	22	178	195	17	420	419
E4/080	80	BDL	BDL	5	22	174	255	45	501	488
E4/100	100	BDL	BDL	4	28	90	146	35	303	286
E4/120	120	BDL	BDL	4	27	32	102	12	177	163
E4/140	140	BDL	BDL	4	32	46	93	21	196	176
E4/200	200	BDL	BDL	4	27	51	113	17	212	191
E4/250	250	BDL	BDL	7	21	45	92	9	174	165
E4/270	270	BDL	BDL	BDL	1	10	11	BDL	22	16
V (ppm)										
sample	depth	H_2O	NH4-Ac	NH_4-OxD	NH_4-OxH	H_2O_2	sulfide	residual	total	bulk
E4/010	10	2	9	10	11	BDL	BDL	51	83	98
E4/040	40	BDL	5	12	12	BDL	BDL	64	93	116
E4/080	80	BDL	3	3	5	BDL	BDL	88	99	129
E4/100	100	BDL	3	4	5	BDL	BDL	90	102	130
E4/120	120	BDL	3	4	8	BDL	5	89	109	132
E4/140	140	BDL	BDL	4	8	BDL	5	97	114	140
E4/200	200	BDL	BDL	7	8	BDL	6	96	117	141
E4/250	250	BDL	BDL	20	10	BDL	7	89	126	143
E4/270	270	BDL	BDL	10	25	BDL	16	81	132	145
As (ppm)										
sample	depth	H_2O	NH4-Ac	NH_4-OxD	NH_4-OxH	H_2O_2	sulfide	residual	total	bulk
E1/010	10	3	132	393	132	BDL	11	16	687	703
E1/030	30	14	108	337	124	BDL	13	13	609	654
E1/050	50	6	35	107	100	BDL	11	BDL	259	323
E1/100	100	BDL	BDL	30	25	BDL	4	BDL	59	122
E1/170	170	BDL	15	150	43	BDL	6	4	218	190
E1/200	200	BDL	BDL	64	53	BDL	6	BDL	123	140
E1/260	260	7	6	80	62	BDL	8	BDL	163	213
E1/350	350	BDL	BDL	19	41	BDL	BDL	BDL	60	83
E1/482	482	BDL	BDL	30	28	BDL	BDL	BDL	58	66
W (ppm)										
sample	depth	H_2O	NH4-Ac	NH_4-OxD	NH_4-OxH	H_2O_2	sulfide	residual	total	bulk
E4/010	10	BDL	BDL	15	BDL	BDL	BDL	BDL	15	BDL
E4/040	40	BDL	BDL	12	BDL	BDL	BDL	BDL	12	BDL
E4/080	80	BDL	BDL	BDL	BDL	BDL	BDL	12	12	BDL
E4/100	100	BDL	BDL	BDL	BDL	BDL	BDL	BDL	BDL	BDL
E4/120	120	BDL	BDL	15	BDL	BDL	BDL	BDL	15	BDL
E4/140	140	BDL	BDL	11	BDL	BDL	BDL	BDL	11	BDL
E4/200	200	BDL	BDL	13	BDL	BDL	BDL	BDL	13	BDL
E4/250	250	BDL	BDL	BDL	BDL	BDL	BDL	BDL	BDL	BDL
E4/270	270	BDL	BDL	BDL	BDL	BDL	BDL	BDL	BDL	BDL

Sr (ppm)

sample	depth	H_2O	NH4-Ac	NH_4-OxD	NH_4-OxH	H_2O_2	sulfide	residual	total	bulk
E4/010	10	1.3	0.7	1.7	19.6	0.6	13.5	153	190	235
E4/040	40	2.1	0.8	2.7	22	0.8	16.1	197	242	316
E4/080	80	3.1	0.7	2.5	23.2	1.1	19.8	291	341	436
E4/100	100	3.4	0.7	2.4	25.6	0.8	19.3	284	336	439
E4/120	120	2.7	0.9	3.1	20.1	BDL	20	250	297	373
E4/140	140	2.9	0.7	2.4	19.4	BDL	17.3	257	300	357
E4/200	200	2.7	BDL	1.9	16.2	0.6	15.7	269	306	381
E4/250	250	2.2	BDL	2.1	24.1	1.1	16.3	243	289	358
E4/270	270	6.2	1	1.4	10	3.2	13.5	205	240	289

Ni (ppm)

sample	depth	H_2O	NH4-Ac	NH_4-OxD	NH_4-OxH	H_2O_2	sulfide	residual	total	bulk
E4/010	10	54	2	4	2	4	BDL	2	68	64
E4/040	40	29	BDL	4	BDL	4	2	2	41	41
E4/080	80	7	BDL	3	BDL	4	1	2	17	16
E4/100	100	7	BDL	1	BDL	3	2	3	16	16
E4/120	120	11	BDL	4	BDL	3	BDL	2	20	19
E4/140	140	7	BDL	3	BDL	4	2	2	18	18
E4/200	200	8	BDL	4	BDL	5	4	2	23	20
E4/250	250	8	BDL	2	BDL	4	2	3	19	18
E4/270	270	3	BDL	BDL	BDL	BDL	23	3	29	15

Zr (ppm)

sample	depth	H_2O	NH4-Ac	NH_4-OxD	NH_4-OxH	H_2O_2	sulfide	residual	total	bulk
E4/010	10	BDL	BDL	7.4	3.5	BDL	BDL	2.5	13.4	6.6
E4/040	40	BDL	BDL	6.7	0.9	BDL	BDL	5.3	12.9	13.2
E4/080	80	BDL	BDL	4.6	BDL	BDL	BDL	2.7	7.3	10.1
E4/100	100	BDL	BDL	2	1.1	BDL	BDL	2.7	5.8	17.1
E4/120	120	BDL	BDL	7.5	2	BDL	BDL	3.1	12.6	11.1
E4/140	140	BDL	BDL	5.5	0.6	BDL	BDL	4.8	10.9	25.6
E4/200	200	BDL	BDL	6.7	BDL	BDL	0.8	2.8	10.3	46.6
E4/250	250	BDL	BDL	4.1	BDL	BDL	BDL	4.9	9	20.9
E4/270	270	BDL	BDL	3.2	BDL	BDL	1.4	44.8	49.4	71.6

Co (ppm)

sample	depth	H_2O	NH4-Ac	NH_4-OxD	NH_4-OxH	H_2O_2	sulfide	residual	total	bulk
E4/010	10	233	9	BDL	BDL	24	5	BDL	271	280
E4/040	40	137	4	BDL	BDL	25	11	BDL	177	184
E4/080	80	28	2	BDL	BDL	24	12	BDL	66	62
E4/100	100	26	1	BDL	BDL	19	8	BDL	54	51
E4/120	120	50	2	BDL	BDL	17	6	BDL	75	72
E4/140	140	27	BDL	BDL	BDL	26	15	BDL	68	63
E4/200	200	30	BDL	BDL	BDL	29	19	BDL	78	73
E4/250	250	32	BDL	BDL	BDL	23	13	BDL	68	61
E4/270	270	10	BDL	BDL	BDL	2	6	1	19	20

Sn (ppm)

sample	depth	H_2O	NH4-Ac	NH_4-OxD	NH_4-OxH	H_2O_2	sulfide	residual	total	bulk
E4/010	10	BDL	BDL	BDL	BDL	BDL	28	BDL	28	BDL
E4/040	40	BDL	BDL	BDL	BDL	BDL	28	11	39	BDL
E4/080	80	BDL	BDL	BDL	BDL	BDL	26	12	38	BDL
E4/100	100	BDL	BDL	BDL	BDL	BDL	24	11	35	BDL
E4/120	120	BDL	BDL	BDL	BDL	BDL	27	BDL	27	BDL
E4/140	140	BDL	BDL	BDL	BDL	BDL	30	BDL	30	BDL
E4/200	200	BDL	BDL	BDL	BDL	BDL	28	10	38	BDL
E4/250	250	BDL	BDL	BDL	BDL	BDL	24	12	36	BDL
E4/270	270	BDL	BDL	BDL	BDL	BDL	25	BDL	25	73

La (ppm)

sample	depth	H_2O	NH4-Ac	NH_4-OxD	NH_4-OxH	H_2O_2	sulfide	residual	total	bulk
E4/010	10	BDL	BDL	9.4	4.3	BDL	1.6	6.3	21.6	10.4
E4/040	40	BDL	BDL	7.8	1.7	BDL	1.9	8	19.4	14.4
E4/080	80	BDL	BDL	5.7	1.2	BDL	2	10.6	19.5	22.3
E4/100	100	BDL	BDL	2.2	2.4	BDL	1.9	7.3	13.8	25.4
E4/120	120	BDL	BDL	8.6	3	BDL	2.1	9.7	23.4	24
E4/140	140	BDL	BDL	6.9	2	BDL	2.3	9.5	20.7	23
E4/200	200	BDL	BDL	8.2	1.3	BDL	2.1	9.9	21.5	23.2
E4/250	250	BDL	BDL	4.8	0.6	BDL	1.8	10.4	17.6	18.4
E4/270	270	BDL	BDL	0.8	BDL	0.6	7.4	4.6	13.4	17.8

Y (ppm)

sample	depth	H_2O	NH4-Ac	NH_4-OxD	NH_4-OxH	H_2O_2	sulfide	residual	total	bulk
E4/010	10	5.2	BDL	BDL	BDL	BDL	1.9	1.7	8.8	11.3
E4/040	40	2.9	BDL	BDL	BDL	BDL	2.3	2.1	7.3	10.5
E4/080	80	0.6	BDL	BDL	BDL	BDL	3	2.6	6.2	8.7
E4/100	100	0.6	BDL	BDL	BDL	BDL	1.9	1.8	4.3	6.5
E4/120	120	1	BDL	BDL	BDL	BDL	2.1	2	5.1	6.3
E4/140	140	0.6	BDL	BDL	BDL	BDL	1.6	1.9	4.1	6.4
E4/200	200	0.7	BDL	BDL	BDL	BDL	2.2	2.3	5.2	7.5
E4/250	250	0.8	BDL	BDL	BDL	BDL	2.4	2.9	6.1	8.1
E4/270	270	1.1	0.6	1.2	BDL	BDL	2.9	4.5	10.3	14

Sc (ppm)

sample	depth	H_2O	NH4-Ac	NH_4-OxD	NH_4-OxH	H_2O_2	sulfide	residual	total	bulk
E4/010	10	3.8	BDL	1.1	1.2	BDL	BDL	4.3	10.4	12.5
E4/040	40	2.3	BDL	1	0.9	BDL	BDL	5.5	9.7	12.1
E4/080	80	0.6	BDL	0.9	BDL	BDL	BDL	7.4	8.9	12
E4/100	100	0.6	BDL	0.6	0.6	BDL	BDL	7.8	9.6	12.4
E4/120	120	0.8	BDL	1.3	0.8	BDL	BDL	8	10.9	13.6
E4/140	140	BDL	BDL	1.3	0.8	BDL	BDL	8.9	11	14.1
E4/200	200	BDL	BDL	1.5	0.8	BDL	BDL	8.8	11.1	14.8
E4/250	250	BDL	BDL	1.1	0.6	BDL	BDL	7.8	9.5	13.6
E4/270	270	BDL	BDL	BDL	0.6	BDL	1.5	7.7	9.8	13.5

Be (ppm)

sample	depth	H_2O	NH4-Ac	NH_4-OxD	NH_4-OxH	H_2O_2	sulfide	residual	total	bulk
E4/010	10	0.5	BDL	BDL	BDL	BDL	BDL	BDL	0.5	1.3
E4/040	40	BDL	BDL	BDL	BDL	BDL	BDL	0.5	0.5	1.1
E4/080	80	BDL	BDL	BDL	BDL	BDL	BDL	0.7	0.7	1
E4/100	100	BDL	BDL	BDL	BDL	BDL	BDL	0.7	0.7	1
E4/120	120	BDL	BDL	BDL	BDL	BDL	BDL	0.7	0.7	1
E4/140	140	BDL	BDL	BDL	BDL	BDL	BDL	0.7	0.7	1
E4/200	200	BDL	BDL	BDL	BDL	BDL	BDL	0.7	0.7	1
E4/250	250	BDL	BDL	BDL	BDL	BDL	BDL	0.7	0.7	1
E4/270	270	BDL	BDL	BDL	BDL	BDL	BDL	0.9	0.9	1.3

Ag (ppm)

sample	depth	H_2O	NH4-Ac	NH_4-OxD	NH_4-OxH	H_2O_2	sulfide	residual	total	bulk
E4/010	10	BDL	BDL	BDL	BDL	BDL	0.4	BDL	0.4	BDL
E4/040	40	BDL	BDL	BDL	BDL	BDL	0.5	BDL	0.5	BDL
E4/080	80	BDL	BDL	BDL	BDL	BDL	0.8	BDL	0.8	0.4
E4/100	100	BDL	BDL	BDL	BDL	BDL	BDL	BDL	BDL	0.3
E4/120	120	BDL	BDL	BDL	BDL	BDL	0.7	BDL	0.7	0.3
E4/140	140	BDL	BDL	BDL	BDL	BDL	0.6	BDL	0.6	BDL
E4/200	200	BDL	BDL	0.5	BDL	BDL	0.8	BDL	1.3	0.3
E4/250	250	BDL	BDL	BDL	BDL	BDL	0.6	BDL	0.6	BDL
E4/270	270	BDL	BDL	BDL	BDL	BDL	BDL	BDL	BDL	BDL

APPENDIX. 4

Results of bulk analyses of the drill cores S1, S2, S3, S6, S7, S8, and S9 from the Ojancos tailings impoundment No.2

Results of ICP-MS analyses:

Table A4.1: In a prelimary phase of the study (Dold, 1994; Dold et al., 1996), samples from the drill cores S2, S7, and S8 were subjected to HNO_3, HF, $HCLO_4$, HCL bulk digestion and analyzed with a FINNIGAN MAT SOLA® ICP-MS at the Geoscience Department of the University of Bremen, Germany for the element Ag, Al, As, Ba, Co, Cd, Cr, Cu, Fe, Mg, Ni, Pb, and Zn.

Analyses performed by the laboratory of SERNAGEOMIN:

Table A4.2: Samples from the drill cores S7, S8, and S9 were analyzed by the laboratory of the geological survey of Chile (SERNAGEOMIN), Santiago, Chile. For Ca, K, Mn, and Si determination a sinteration with sodic peroxide and following attack by HCl and H_2O_2 was used as dissolution technique. The solutions were measured by ICP-AES Jobin Yvon® JY-70. Total sulfur was measured by a LECO® furnace. Sulfates were dissolved by HCl and determined turbidometrically. Hg was analyzed by atomic absorption spectroscopy (AAS) cold vapor technique.

Analyses performed by the X-Ray Assay Laboratories (XRAL), of Toronto, Canada.

Table A4.3: Samples from the drill cores S1, S3, S6, and S9 were subjected to HNO_3, HF, $HCLO_4$, HCL bulk digestion and analyzed with ICP-ES multi-element analysis.

References

Dold, B. (1994): Geochemische Untersuchungen einer Flotationshalde in Copiapó/Region Atacama/Nordchile. - unpublished Diplomarbeit (Teil 2) Universität Bremen, Bremen, 91 p.

Dold, B., Eppinger, K.J., Kölling, M. (1996): Pyrite oxidation and the associated geochemical processes in tailings in the Atacama desert/Chile: The influence of men controlled water input after disuse. Clean technology for the mining industry, Santiago, p. 417 - 427.

Table A4.1: Results of ICP-MS analyses, University Bremen, Germany

depth [cm]	S2-Fe [%]	S2-Mg [%]	S2-Al [%]	S2-Ag [mg/kg]	S2-As [mg/kg]	S2-Ba [mg/kg]	S2-Cd [mg/kg]	S2-Co [mg/kg]	S2-Cr [mg/kg]	S2-Cu [mg/kg]	S2-Ni [mg/kg]	S2-Pb [mg/kg]	S2-Zn [mg/kg]
10	16.51	1.85	3.64	3.80	44.56	128.65	1.87	312.61	26.94	1763.42	1007.71	12.72	61.92
100	18.58	1.31	3.17	4.62	55.43	380.58	2.17	217.05	32.07	2389.51	1174.69	15.20	62.13
200	19.17	1.19	2.69	6.86	68.58	47.68	1.76	199.66	33.40	3396.41	1245.83	15.61	54.17
300	12.95	1.07	3.50	5.48	181.37	193.09	3.40	138.03	37.28	2824.23	775.78	35.89	93.30
400	8.41	0.96	3.19	12.19	411.58	789.45	3.16	133.76	44.29	3780.20	547.51	129.75	381.23
490	7.10	0.78	4.04	12.54	653.57	991.73	3.05	86.06	33.46	7254.80	467.45	138.59	338.09
500	7.59	1.14	5.32	17.41	555.20	1404.16	7.56	88.49	31.09	8041.83	491.17	324.05	675.71
600	9.97	0.64	4.55	14.52	633.96	1285.99	3.01	57.80	25.40	2809.39	630.67	189.09	298.96
700	10.06	0.74	4.40	12.91	417.05	1069.49	3.17	111.64	21.37	5333.07	660.11	91.40	137.42
800	10.13	0.78	4.57	17.42	326.06	1233.20	2.64	91.68	20.71	4253.22	640.97	125.86	204.26

depth [cm]	S7-Fe [%]	S7-Mg [%]	S7-Al [%]	S7-Ag [mg/kg]	S7-As [mg/kg]	S7-Ba [mg/kg]	S7-Cd [mg/kg]	S7-Co [mg/kg]	S7-Cr [mg/kg]	S7-Cu [mg/kg]	S7-Ni [mg/kg]	S7-Pb [mg/kg]	S7-Zn [mg/kg]
10	13.10	1.52	3.64	3.19	94.62	67.39	2.18	357.66	20.23	5981.89	891.89	13.29	40.11
100	13.45	0.99	3.36	8.23	145.02	121.15	2.09	174.02	25.30	2910.62	882.52	16.04	52.31
200	9.99	0.68	2.88	11.75	558.17	1331.56	2.61	104.49	32.55	3821.22	649.10	150.92	387.18
300	7.05	0.65	4.99	11.12	332.59	1219.20	3.04	62.31	24.66	5909.86	436.11	113.77	158.19
400	8.12	0.77	5.09	16.90	1043.32	1082.89	5.14	107.33	24.71	5089.65	527.94	133.19	531.88
500	8.98	0.91	5.53	21.93	686.86	1127.60	2.74	107.29	55.90	7200.81	592.00	437.07	290.02
600	10.27	0.84	4.82	13.81	507.26	1297.13	2.62	121.94	25.26	4196.82	655.57	178.44	148.63
700	9.72	0.97	5.34	18.34	461.47	846.67	3.11	117.39	27.24	4195.33	626.23	171.05	179.09
800	10.39	1.09	5.83	21.39	591.75	1206.98	3.64	135.65	38.87	4771.74	674.59	268.58	226.96

depth [cm]	S8-Fe [%]	S8-Mg [%]	S8-Al [%]	S8-Ag [mg/kg]	S8-As [mg/kg]	S8-Ba [mg/kg]	S8-Cd [mg/kg]	S8-Co [mg/kg]	S8-Cr [mg/kg]	S8-Cu [mg/kg]	S8-Ni [mg/kg]	S8-Pb [mg/kg]	S8-Zn [mg/kg]
10	16.43	1.22	3.73	3.98	63.89	616.05	2.03	336.59	28.71	2881.32	960.88	12.56	100.96
100	15.40	1.36	3.44	4.72	105.09	107.58	2.40	266.32	34.90	1688.61	925.14	15.17	56.17
200	8.78	1.20	3.80	5.50	152.58	208.60	2.79	128.39	41.13	2068.44	490.43	133.73	153.73
300	5.43	1.00	2.83	10.66	100.29	205.64	2.53	65.86	40.85	3579.46	324.79	59.05	209.70
400	6.76	0.91	3.77	22.37	854.21	3749.07	9.40	97.88	49.12	5490.86	417.64	1156.21	1231.65
500	8.58	1.00	6.06	24.69	1704.87	920.38	7.96	89.10	60.24	6266.11	492.58	302.78	984.61
555	10.58	0.86	4.14	24.11	604.70	1414.79	2.75	58.61	94.82	2561.16	605.78	1141.20	387.96
600	9.09	1.14	5.51	23.64	412.85	1138.37	0.87	116.26	60.57	3816.90	534.87	185.51	181.18
700	9.12	1.09	5.50	18.82	293.98	894.62	2.74	92.32	47.22	4443.27	523.32	220.84	173.66
800	8.80	1.12	5.48	16.21	514.36	608.18	2.70	101.94	73.36	4145.74	487.16	266.73	231.77

Table A4.2: Results of analyses performed at the laboratory of SERNAGEOMIN, Santiago de Chile

depth [cm]	S7-CaO [%]	S7-K2O [%]	S7-MnO [%]	S7-SIO2 [%]	S7-S [%]	S7-SO4 [%]	S7-Hg [mg/kg]
10	8.8	0.4	0.13	39.9	3.15	2.55	0.13
100	12.6	0.5	0.13	36.8	1.4	1.93	0.23
200	19.5	0.6	0.21	30	0.7	1.36	0.64
300	8.8	2	0.09	48.4	1.01	4.46	0.58
400	4.1	2.2	0.18	18.1	2.13	4.1	1.48
500	3.9	2.4	0.05	46.8	0.69	5.88	1.82
600	3.4	2.3	0.06	49.4	0.03	4.09	1.48
700	4.2	2.4	0.07	50	0.13	5.39	1.75
800	5	2.4	0.08	46.6	0.02	6.8	1.2

depth [cm]	S8-CaO [%]	S8-K2O [%]	S8-MnO [%]	S8-SIO2 [%]	S8-S [%]	S8-SO4 [%]	S8-Hg [mg/kg]
10	8.7	1.3	0.12	39.3	2.32	2.35	0.01
100	14.2	0.5	0.16	38.1	2.02	0.74	0.05
200	19.8	1	0.21	42	1.1	1.66	0.17
300	28.5	0.4	0.27	27.7	0.35	0.6	1.46
400	20.8	1.2	0.27	31.9	0.3	5.42	1.68
500	6.3	2.4	0.18	39.5	1.58	9.2	3.89
555	7.2	2.5	0.07	35.8	0.67	11.94	3.54
600	5.4	2.6	0.07	45.2	0.02	6.9	1.48
700	5.6	2.5	0.07	44.4	0.02	8.4	1.7
800	7.5	2.4	0.08	40.7	0.02	9.29	1.8

depth [cm]	S9-CaO [%]	S9-K2O [%]	S9-MnO [%]	S9-SIO2 [%]	S9-S [%]	S9-SO4 [%]	S9-Hg [mg/kg]
10	9.2	0.8	0.13	34.3	3.18	2.92	0.02
100	10.9	0.6	0.14	39.5	2.11	1.22	0.07
200	24.2	0.4	0.22	29.3	0.5	2.56	0.16
300	22.1	0.6	0.19	30.9	0.72	0.68	0.15
400	28.8	0.6	0.26	23.9	0.29	5.56	0.94
500	4.8	2.4	0.13	42.2	1.58	7.01	1.32
600	6.9	2.4	0.05	42.8	0.55	10.26	2.3
700	5.2	2.6	0.06	43.7	0.02	8.2	1.67
800	5.1	2.4	0.06	42.4	0.02	7.5	1.73

Table A4.3: ICP-ES results of S1, S3, S6, and S9 performed by the X-Ray Assay Laboratories (XRAL) of Toronto, Canada

Sample Ident	Be	Na	Mg	Al	P	K	Ca	Sc	Ti	V	Cr	Mn	Fe	Co	Ni	Cu	Zn	As	Sr	Y	Zr	Mo	Ag	Cd	Sb	Ba	La	Pb
Analysis Unit	ppm	%	%	%	%	%	%	ppm	%	ppm	ppm	ppm	%	ppm	ppm	ppm	ppm	ppm	ppm	ppm	ppm	ppm	ppm	ppm	ppm	ppm	ppm	ppm
Detection Limit	0.5	0.01	0.01	0.01	0.01	0.01	0.01	0.5	0.01	2	1	2	0.01	1	1	0.5	0.5	3	0.5	0.5	0.5	1	0.2	1	5	1	0.5	2
S1/010	1.7	1.65	1.6	3.75	0.15	0.5	7.72	8.1	0.17	103	53	1140	17	361	98	1830	32.6	57	93.9	9.2	51	3	2	6	-5	110	23.9	8
S1/100	1.9	1.83	1.19	3.3	0.12	0.23	6.81	6.1	0.15	131	53	872	19.7	172	84	2410	29.6	-3	90.4	9.6	46.6	2	2.5	7	-5	65	29.9	8
S1/200	1.4	1.53	0.98	2.82	0.11	0.19	12.5	5.9	0.14	115	54	1440	15.1	119	58	4270	45.7	46	86.1	10.2	41.6	9	6.8	5	8	40	27.2	16
S1/300	1.7	1.59	0.87	3.92	0.14	1.02	7.81	8.1	0.22	122	61	984	19.9	183	44	1790	47.1	27	151	12.2	55.2	4	2.4	7	6	344	27.2	19
S1/400	0.7	1.14	0.71	2.64	0.1	0.39	17.7	6.8	0.13	84	66	1940	7.92	85	32	5140	114	125	128	8.3	36	45	8.3	2	12	417	17.3	45
S1/500	1.1	1.05	0.85	5.48	0.1	1.79	4.8	10.6	0.18	125	60	1290	9.73	90	42	5610	417	462	158	13.7	44.1	121	9.5	4	61	405	40.6	153
S1/600	1.6	1.1	0.92	6.21	0.11	1.96	3.52	10.4	0.21	123	64	1150	10.4	89	52	4450	646	522	260	13.2	58	284	29.7	6	70	359	37.1	332
S1/670-690	1.6	0.98	0.89	5.28	0.16	1.71	3.04	10.7	0.2	140	68	521	12.5	102	50	4330	169	372	161	15.3	52.1	76	15.7	3	48	1020	56.5	147
S1/800	1.5	1.08	0.89	5.26	0.14	1.92	2.65	10	0.21	140	49	555	12.3	119	48	4040	177	381	155	13.9	57.4	83	15	3	57	999	53.6	120
S3/010	1.5	1.57	1.19	3.31	0.13	0.34	9.57	6.9	0.16	105	49	1280	16.1	239	76	2390	32.9	23	93	8.4	43.7	3	2.7	4	-5	79	21.2	5
S3/100	2.1	1.72	1.18	3.33	0.13	0.34	6.05	6	0.15	133	52	839	20.8	195	86	1700	36.3	-3	79	9.6	48.7	2	1.7	7	5	98	31.5	10
S3/200	1.7	1.72	0.79	3.98	0.13	0.89	4.38	7.1	0.21	112	52	611	20.3	153	34	1090	26.1	-3	156	10.8	54.3	1	0.8	6	-5	284	20.7	4
S3/300	0.6	1.39	0.68	2.99	0.1	0.47	17.2	7.1	0.16	83	55	2300	8.05	77	32	5180	701	249	173	10.2	38.7	20	12.8	5	41	1320	13.2	198
S3/400	0.9	1.16	0.76	3.78	0.11	0.96	12.8	7.8	0.15	97	65	1530	7.91	70	36	5880	201	157	145	10.4	40.8	75	7.6	2	19	567	27.4	94
S3/500	1.2	1.35	1.06	6.12	0.1	1.79	2.86	11.1	0.2	129	52	1680	9.3	122	57	5980	663	469	219	11.5	55.5	203	10.6	6	77	479	38.6	335
S3/600	1.5	1.06	0.79	5.2	0.1	1.84	2.46	8	0.17	110	47	604	11.4	92	39	3360	324	305	199	11.7	57.1	267	22	4	44	316	42.1	285
S3/700	1.5	0.85	0.93	5.84	0.18	1.93	2.83	10.6	0.21	138	60	526	10.6	92	47	6080	195	377	203	15.2	54.4	126	19	3	50	584	64.4	166
S3/800	1.4	1	0.82	5.1	0.12	1.85	2.28	9.3	0.2	127	53	676	11.5	128	54	3540	259	426	167	13.8	51.5	134	16.5	3	60	425	46.9	192
S6/010	1.5	1.68	1.19	4.01	0.16	0.51	9.3	7.1	0.18	97	48	1490	14.9	199	72	1030	30.5	26	88.7	9.4	50.6	3	1	3	-5	122	23.1	2
S6/100	1.9	1.69	1.08	3.36	0.13	0.27	7.28	6.4	0.17	127	53	971	19.2	209	79	1850	33.2	-3	92.2	9.9	46.1	1	2.1	5	-5	75	27.9	4
S6/200	1.4	1.59	0.73	3.61	0.12	0.86	8.46	6.5	0.18	102	54	983	16.6	137	33	1960	35.2	-3	126	9.4	53.1	4	2.7	5	-5	267	23.1	3
S6/300	-0.5	1.19	0.58	2.57	0.09	0.3	20.9	6.1	0.12	68	62	2110	3.34	44	25	6480	73.1	154	128	7.6	31.1	67	9	1	8	157	15.4	24
S6/400	1.2	1.59	0.67	5.23	0.08	1.65	2.03	7.8	0.15	99	47	1010	11	95	38	4550	192	115	151	10.2	60.5	185	5.5	3	19	367	46.4	84
S6/500	1.5	0.96	0.86	6.39	0.11	2.01	3.09	10.5	0.2	124	58	1220	10.1	82	50	4320	656	633	278	12.3	48	395	27.2	5	84	182	28.9	336
S6/600	1.3	0.79	1.07	5.85	0.2	1.82	3.18	11.9	0.21	139	76	466	10.2	101	50	4290	152	348	172	16.6	62.2	85	21.2	2	58	504	65.6	164
S6/700	1.3	0.79	1.03	5.67	0.19	1.8	3.5	12.1	0.21	151	67	535	10.7	89	43	4110	210	396	155	16.7	58.2	85	17.2	3	49	675	59.3	204
S9/010	1.9	1.42	1.11	3.23	0.17	0.7	6.51	6.8	0.19	109	57	1130	20.2	320	87	2600	34	7	80.7	8.5	54	2	1.2	6	8	189	27.9	8
S9/100	1.7	1.56	1.1	3.61	0.14	0.5	7.35	6.4	0.17	111	46	1130	17.2	205	66	1420	32	13	86.8	9.1	49.2	-1	1.7	5	-5	125	28.2	8
S9/200	0.8	1.24	0.9	2.59	0.11	0.26	15.8	6.8	0.13	86	38	1690	8.33	86	44	2580	74.5	93	95.3	8.8	36.7	10	5	2	6	100	15.2	39
S9/300	0.9	1.56	0.86	3.23	0.1	0.42	15	7.7	0.17	89	57	1560	9.8	67	25	3430	73.9	66	120	8.8	43	4	5.2	2	11	105	9.5	7
S9/400	-0.5	0.9	0.63	2.61	0.1	0.42	18.2	6.8	0.11	82	78	1920	4.41	60	35	4920	257	326	125	9.2	33.2	31	10.1	2	28	436	23.3	189
S9/500	1.3	1.12	1.05	6.21	0.1	1.89	3.31	11.6	0.21	130	71	1130	9.63	85	46	6710	560	844	195	12.9	54.4	232	12.7	5	99	360	44.1	231
S9/600	1.2	0.78	0.98	5.49	0.19	1.87	4.67	12	0.19	127	72	385	9.46	67	39	3650	177	362	172	14.2	54.5	57	17	2	73	302	50.5	363
S9/700	1.3	0.74	1.07	5.93	0.21	1.91	3.36	12.8	0.21	148	77	471	10.4	100	48	3760	143	408	162	16.6	59.4	57	21.4	2	72	580	61.3	188
S9/800	1.2	0.83	1.03	5.85	0.23	1.87	3.49	13	0.22	155	81	531	11.1	92	47	4560	177	393	158	16.7	59.5	94	17.9	3	52	450	58.9	169

SX/YYY = drill core number/depth in cm

APPENDIX. 5

Climatic data

Representative climatic data (the year 1995) from the Saladillo (1580 m a.s.l) and Lagunitas (2765 m a.s.l.) meteorological stations nearby the Piuquenes tailings impoundment (2100 m a.sl.), Andina:

Table A4.1: *Climatic data Saladillo 1995 (1580 a.s.l.)*

Month	J	F	M	A	M	J	J	A	S	O	N	D
Evaporation (mm)	10.4	8.8	8.1	6.2	4.5	2.8	2.1	3.1	4.9	6.6	8.6	9.3
Precipitation (mm)	57.9	1.1	1.2	34.9	31.1	105.1	60	45.2	40.8	2.9	0	1.8
Tmax (°C)	30.3	28	27.2	28.3	26.2	24.5	21.6	25.4	28.2	26.5	28.6	29.1
Tmin (°C)	8.6	7.4	8.3	5.9	4.9	0.5	-1.5	-4.2	1.5	3.2	6.4	6.7
Tmed (°C)	15.6	15.3	14.8	12.8	11.6	7	2.2	5.2	8.6	10.6	14.1	17.1

Table A4.2: *Climatic data Lagunitas 1995 (2765 a.s.l.)*

Month	J	F	M	A	M	J	J	A	S	O	N	D
Precipitation (mm)	67.2	0	0	0	47.3	159.4	142.9	147.1	48.6	5.8	4.7	23.3
Tmax (°C)	19.8	19.4	18.9	19.2	16.7	14.7	14.7	12.5	15.7	17.5	17	24
Tmin (°C)	1.6	1.2	0	-0.1	-3	-7	-11.8	-11.1	-7.2	-2.8	0	5.4
Tmed (°C)	12.8	11.7	11.3	9.3	7.2	2.4	-2.2	0.2	3.7	6.5	9.6	11.6

Representative climatic data (the year 1989) from the Parron meteorological station nearby the Cauquenes tailings impoundment (725 m a.sl.), Teniente:

Table A4.3: *Climatic data Parron 1989 (700 m a.s.l.)*

Month	J	F	M	A	M	J	J	A	S	O	N	D
Precipitation (mm)	0	0	0	0	38.6	42.9	134.1	277	28.6	11.2	1.2	0
Tmax (°C)	33	32	29	26	19.8	25	26.3	21.8	25.2	30	31	31.9
Tmin (°C)	6.6	6	2.2	-0.8	-2.4	-0.4	-4.5	-1.6	-2.8	-1.6	2	5.4